PREDICTING THE GEOGRAPHIC DISTRIBUTION OF ANCIENT SOILS WITH SPECIAL REFERENCE TO THE CRETACEOUS

by

ARGHYA GOSWAMI

Presented to the Faculty of the Graduate School of
The University of Texas at Arlington in Partial Fulfillment
of the Requirements
for the Degree of

DOCTOR OF PHILOSOPHY

THE UNIVERSITY OF TEXAS AT ARLINGTON
December 2011

ACKNOWLEDGEMENTS

I would like to acknowledge all of the people who have helped me succeed in completing this dissertation. First of all, this dissertation would not be possible without the direction and assistance of my advisor, Christopher R. Scotese, the best adviser a student can have, for his continuous support and guidance. In addition, the assistance of my committee members John Holbrook, Arne Winguth, Marline Sattler, and Thomas L. Moore are greatly appreciated. Moreover, special thanks to “Paleoterra” for the guidance and support related to FOAM and “GANDOLPH Project” and “PALEOMAP Project” for allowing me to use the results of Fast Ocean Atmospheric Model simulations. I would also like to thank Josh Been, the GIS librarian at University of Texas at Arlington, for his continuous support regarding GIS and scripting help.

Funding and Scholarships were provided by Christopher R. Scotese, John Wickham, Chair of the Department of Earth and Environmental Sciences, and the Graduate School, University of Texas at Arlington. I am grateful for their support, without which this research would not have been possible.

I like to thank my good friend, Dr. Sharmistha Basu, for helping me with my proofreading at a very short notice. I would also like to thank my friends and fellow graduate students for their support and camaraderie, including Amira Yamusha and Derek Main for all of their help and encouragement.

Finally, I thank my wife, Soma, and my parents, and other family members for their continuous support and belief in me throughout my time here at University of Texas at Arlington.

November 18, 2011

ABSTRACT

PREDICTING THE GEOGRAPHIC DISTRIBUTION
OF ANCIENT SOILS WITH SPECIAL
REFERENCE TO THE
CRETACEOUS

Arghya Goswami, PhD

The University of Texas at Arlington, 2011

Supervising Professor: Christopher R. Scotese

Different kinds of soils form in different climatic regimes. Soils closely match climatic conditions. Therefore, they are one of the best indicators of past climates. This study uses the "climate envelope" technique developed by Moore (2007) to build a "paleo-soil prediction program". Though factors controlling soil formation are complex (Retallack, 1990), the best fit between a given soil type (Zobler 1999) and the annual range of rainfall and temperature (Legates and Wilmott 1990) are thought to be the primary factors. Each modern soil type has a unique climatic "fingerprint" or "climate envelope" defined by the range of rainfall and temperature values. Assuming similar types of soil formed under similar temperature-precipitation regimes in the past, paleoclimate simulations (Fast Ocean and Atmosphere Model) can be used to predict the ancient geographic distribution of different soil types.

The earth's pole-to-equator temperature gradient represents a fundamental climatological property related to equator-to-pole heat transport efficiency, hydrological cycling, and atmospheric chemistry (Cronin, 2009). On the other hand, one of the major challenges of

paleoclimate research is that climate models, both coupled and uncoupled ocean-atmosphere models, often underestimate the warm polar temperatures that are indicated by fossil and geochemical data (e.g., DeConto et al., 2000). To test the validity of the four Cretaceous paleoclimate simulations (Early Maastrichtian (70 Ma), Cenomanian-Turonian (90 Ma), Early Aptian (120 Ma) and Valanginian – Berriasian (140 Ma)), seven Cretaceous stages were studied by constructing detailed pole-to-equator temperature gradients based on paleotemperature estimates from plant and animal fossils, as well as isotopic data.

In the final part of this study, the pole-to-equator temperature gradients derived from fossils and isotopic data and the pole-to-equator temperature gradients estimated by FOAM were compared. The FOAM temperatures were adjusted to conform to the geological evidence for the Cretaceous. With this new adjusted temperature and global precipitation data, the ancient soil prediction program was rerun for the four Cretaceous time intervals. The revised ancient soil maps are in better agreement with the geologic and climatic conditions known to have existed during the Cretaceous.

TABLE OF CONTENTS

LIST OF ILLUSTRATIONS

Figure Page

LIST OF TABLES

CHAPTER 1

METHODOLOGY USED TO MAP ANCIENT SOILS USING RESULTS FROM PALEOCLIMATE SIMULATIONS

Different kinds of soils form in different climate regimes. For example, organic-rich histosols often form in the low-lying, permanently waterlogged landscapes typical of tropical, everwet climates. Vertisols have thick uniform, clayey profiles that are cut by deep cracks for at least part of the year. These soils are found in sub-humid to semi-arid climates with a pronounced dry season. Aridisols, as the name suggests, are found in arid to semi-arid regions. Rainfall in these regions is sufficient to dissolve soluble salts in the soil, but is not sufficient to carry the dissolved salts into the water table. Therefore, aridisols commonly have calcareous, gypsiferous, or salty horizons. Soils are one of the best indicators of past climates primarily because they closely match climate regimes.

In this chapter, the associations between modern soil types and climate are used to build a “paleo-soil prediction program”. The paleo-soil prediction program uses the “climate envelope” technique pioneered by Moore et al., (2007).There are two principal inputs for the paleo-soil prediction program, 1) a present-day, digital map of the world’s soil types (Zobler 1999) and 2) a dataset that describes global modern rainfall and temperature patterns (Legates and Wilmott, 1990). Though factors controlling soil formation are complex (Retallack, 1990), using a best match between a given soil type and the range of rainfall and temperature is determined using a bi-variate approach.

Each soil type has a unique climatic “fingerprint” or “climate envelope” defined by the range of rainfall and temperature values. Assuming similar types of soil formed under the same temperature-precipitation regimes in the past, paleoclimate simulations using the Fast Ocean

and Atmosphere Model (FOAM) can be used to map the ancient geographic distribution for that soil type.

Table 1.1 Geologic Time Intervals

No	Period	Time Intervals	Age (Ma)
1	Neogene	Miocene	10
2	Paleogene	Oligocene	30
3		Eocene	45
4	Cretaceous	Maastrichtian	70
5		Cenomanian	90
6		Aptian	120
7		Berriasian- Valanginian	140
8	Jurassic	Oxfordian	160
9		Toarcian	180
10	Triassic	Carnian	220
11		Induan	250
12	Permian	Artinskian	280
13	Carboniferous	Tournaisian	340
14	Devonian	Famennian	360
15		Emsian	400
16	Silurian	Llandovery	430
17	Ordovician	Tremadocian	480

Using paleo-temperature and paleo-precipitation data obtained from FOAM simulations produced by the GANDOLPH Project (Scotese et al. 2007, 2008, 2009, and 2011) and paleogeographic maps provided by the PALEOMAP Project, the ancient geographic distribution of ten soil types were mapped for seventeen time intervals. The time intervals are listed in Table 1.1.

1.1 Previous Work

The concept of fossils soils can be traced back to Scottish physician James Hutton (1795) (Retallack, 1990). Hutton described the red beds that were found along the unconformities at Siccar Point as ancient soil surfaces comparable to modern soils. The term 'paleosol' refers to a past soil preserved by burial beneath sediments (alluvium or loess) or volcanic deposits (volcanic ash), which in the case of older deposits have become lithified (www.wikipedia.com). Typically paleosols reflect a climate significantly different from the climate now prevalent in the area where the soil is found.

In his book "Soils of the Past", Retallack (1990) describes the development of the science of paleopedology which is the study of paleosols. One of the oldest records of buried soils within consolidated sedimentary rocks are the 'dirt beds' and fossil stumps reported in latest Jurassic limestones of the Dorset coast by Webster (1826) and popularized by Buckland (1837) in a volume widely known as the "Bridgewater Treatise". A summary of early discoveries of pre-Quaternary paleosols was given in Albert C. Seward's monumental work, "Fossil Plants" (1898). This works notes that fossil soils are clear evidence for the immensity of geological time and indicators of past worlds. During the late 19th century, loess and till deposits were also recognized to be ancient soils. These 'weathered zones', 'forest zones' and 'soils', as they were variously termed, were found in Russia by Feofilatkov (in the 1870s, as recounted by Polynov 1927), in the mid-continental USA by McGee (1878), and in New Zealand by Hardcastle (1889). By the turn of the century such observations had been used to construct a preliminary stratigraphic subdivision of glacial deposits (Chamberlain 1895).

However, relating paleosols to modern soils is difficult because the term 'soil' has very different meanings for agronomists, engineers, geologists, and soil scientists

(http://accessscience.com/content/Paleosol/484200). Thus no system for relating paleosols (fossil soils) to modern soils exists. Several attempts to classify paleosols have been made. Mack et al. (1993) attempted a descriptive classification of paleosols utilizing pedogenic features. Nettleton et al. (2000) classified paleosols using a property-based classification system linked to soil-forming processes. Krasilnikov and Calderón (2006) proposed a classification for paleosols based on the World Reference Base for Soil Resources. In this work, we propose a preliminary classification scheme that relates modern soil types to their ancient equivalents using ancient climatic models.

The paleoclimatic importance of paleosols stems from studies of Quaternary soil development, which have shown that some pedogenic features can be quantitatively related to soil-forming factors such as climate (Kraus, 1999). Paleosols have been used not only to interpret ancient climatic regimes but, in some cases, to estimate paleo-precipitation and paleo-temperature (Kraus, 1999). Paleosols have also proven to be helpful in understand the composition of the ancient atmosphere and atmospheric changes over geologic time (Kraus, 1999). Hence, paleosols have gained immense importance during the last century because of their potential relationship to ancient climate and climatic change. For example, Hubert (1977),Alley et al. (1986), Retallack (1986), Zhisheng et al. (1987) studied the climatic aspects of paleosols. Miller et al. (1986) studied climatic cyclicity of Early Permian paleosols from US Midcontinent. In 1994, Mack and James developed a theoretical model for the relationship between paleoclimate and paleosols for the time interval following the widespread appearance of vascular land plants. Tabor et al. (2008) presented a detailed study of the environmental and climatic history of paleosols from Pennsylvanian through Early Permian time.

Most paleosol investigations may be categorized as follows:

a) Proxy Data: Different kinds of proxy data have been used by the scientists to describe ancient climate. Lithological indicators of climate, such as calcrete, kaolinite and bauxites have been used to map the past position of the major climatic zones (Scotese et al., 1999; Boucot et al., 2011). Retallack used paleosols as a climate indicator in several of his works (Retallack 2001,

2002, 2009; Retallack and Krull 1999; Sheldon and Retallack 2002; Sheldon and Retallack 2004). In 1969, Birkeland did a classic study of Quaternary paleoclimatic implications of soil clay using kaolinite from the Sierra Nevada. Pal et al. (1989) used smectitie-kaolinite as evidence for paleoclimatic changes in Southern and Central Peninsular India. Girard et al. (2000) studied climatic patterns from kaolinite in laterites from Yaou, French Guiana. Srivastava (2001) attempted to reconstruct the Holocene climatic history of the Indo-Gangetic Plains based on micro-morphological characteristics and stable isotope composition of calcretes. Felix-Henningsen et al. (2003) studied the significance of calcretes and paleosols associated with ancient dunes in the Western Cape, South Africa, as stratigraphic markers and paleoenvironmental indicators. Sinha et al. (2006) also used calcrete to study the types of the interfluvial Gangetic sediments and monsoonal patterns. Similar to calcrete and kaolinite, bauxites have also been used as proxy indicators of climate. Carboniferous to Jurassic bauxite deposits were compiled by Bardossy (1994) as paleoclimatic and paleogeographic indicators. Price et al. (1997) used the modern geographic distribution of bauxites to test the General Circulation Models (GCMs). His results satisfactorily predicted “potential” bauxite formation.

b) Atmospheric gas concentrations CO_2/O_2: Several studies have used paleosols to estimate atmospheric gas concentrations. In 1989, Holland et al. interpreted the composition of the atmosphere from paleosols. Cerling (1991) estimated pCO_2 of the atmosphere using carbon isotopic composition of paleosol carbonates. In 1998, Rye and Holland, did a critical review of paleosols with respect to the evolution of oxygen. It is important to note that paleosols were also used to revise Phanerozoic atmospheric CO_2 concentration curve constructed by Breecker et al. (2009). The pioneering work of Berner and Kothavala (2001) also used estimates of RCO_2 derived from paleosols (Ekart et al., 1999) to determine ancient CO_2 concentrations.

c) Quaternary Research: Paleosols have been used extensively to understand Quaternary climate change. Wang and Zheng (1989) used Pleistocene paleosols as paleoclimatic indicators. Rutter et al. (1990) described a site in north-central China where known loess-paleosol

units and a complete record of Pleistocene magnetic reversals occurred in the same section. Verosub et al. (1993) studied pedogenesis and paleoclimate of Chinese loess-paleosol sequences. Maher (1998) evaluated paleoclimatic implications of Quaternary paleosols. Maher and Thompson, (1995) reconstructed paleorainfall from pedogenic magnetic susceptibility variations in the Chinese loess and paleosols. Oches and Banerjee (1996) demonstrated rock-magnetic proxies of climate change from loess-paleosols. In 1998, Madsen et al. worked on the nature of climate during the Younger Dryas from paleosols found in central China. Chen et al. (1999) used variations in Rb/Sr ratios in the loess-paleosol sequences of central China to better understand the history of monsoons. Another interesting work from Xiao and Zhisheng (1999) predicted three large shifts in East Asian monsoon circulation based on loess–paleosol sequences in China and Late Cenozoic paleosols in Japan. Wang et al. (2000) described the ancient El-Nino-Southern Oscillation cycles, in an innovative way using paleosols.

These works clearly demonstrate that paleosols have been used to understand ancient climates and climatic change, the converse, however, is not true. No one has used climate or more specifically simulations of past climates to predict the occurrence and geographic distribution of paleosols. A possible exception is the work of Moore et al. (2007). In this pioneering study, Moore used a paleoclimate modeling simulation called FOAM (Fast Ocean Atmosphere Model) to predict the occurrence and geographic distribution of Cretaceous and Permian coals and evaporites. To do this, he developed a methodology called “climate envelopes”, which we have adopted in this study and will describe in detail in the next section.

1.2 Methodology

In this section I shall describe the methods and techniques used to construct the maps that predict the ancient geographic distribution of paleo-soils. Figure 1.1 depicts the general workflow of this project and is a visual outline for this section.

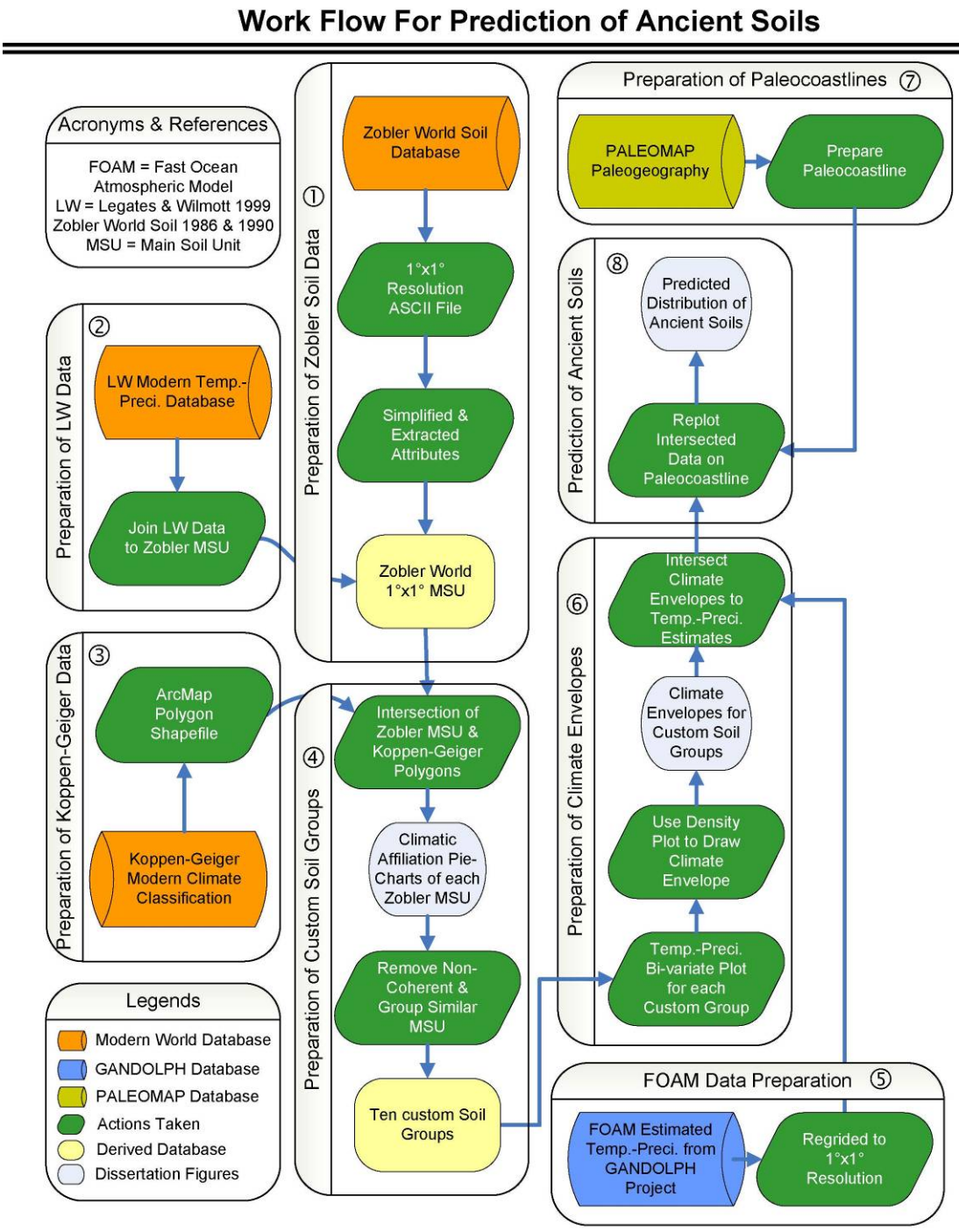

Figure 1.1 Work Flow for Prediction of Ancient Soils.

1.2.1 Overview

The methodology can be summarized as follows:

1. The geographic distribution of modern soil types was identified (Zobler 1986 and 1999). In Figure 1.1 this step is marked with ①.
2. These soil types were associated with specific temperature-precipitation regimes (Legates and Wilmott 1999). In Figure 1.1 these steps are marked with ②,③,④,⑤ and ⑥.
3. The ancient geographic distribution of these soil types were predicted using temperature-precipitation data from paleoclimate simulations (FOAM). In Figure 1.1 these steps are marked with ⑦ and ⑧.

1.2.2 Preparation of Zobler Soil Data (① Figure 1.1)

In order to predict the ancient soils we must first start with the geographic distribution and classification of modern soils. There are several modern soil classification systems: the World Soil Classification developed by the Food and Agriculture Organization of the United Nations (FAO), the Zobler World Soil Classification, the USDA Soil Taxonomy and the World Reference Base for Soil Resources (WRB) developed by the International Union of Soil Sciences (IUSS). Among these I chose to use the Zobler World Soil classification scheme which is similar to the FAO Soil Map of the World (FAO, 1974). The Zobler scheme also takes into account the Matthews Vegetation (1983) criteria. The Zobler World Soil Data is conveniently available in a gridded 1°x1° latitude-longitude dataset (CISL Research Data Archive at http://dss.ucar.edu/datasets/ds770.0/data/zoblerworldsoil) suitable for large-area studies such as climate research with GCMs or small-scale studies in soils, agriculture, forestry and hydrology (Staub and Rosenzweig, 1987).

The Zobler database contains the global distribution of soil types, including data for dominant soil units (classification of soil types), slope classes, soil texture classes and soil phases. Soil types are described at two levels of detail, including 106 types based on Zobler's

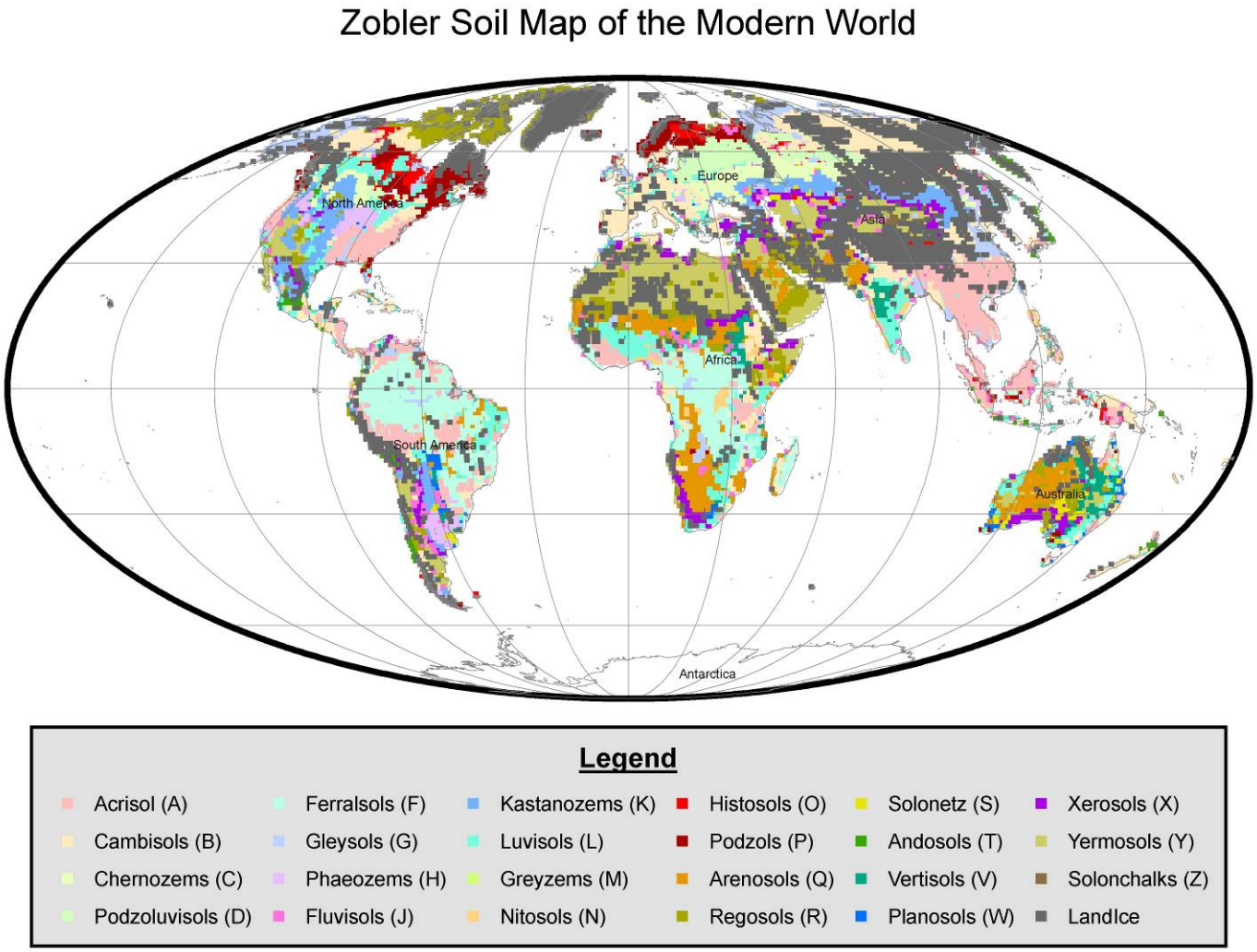

Figure 1.2 Modern World Distributions of Zobler Soil Types

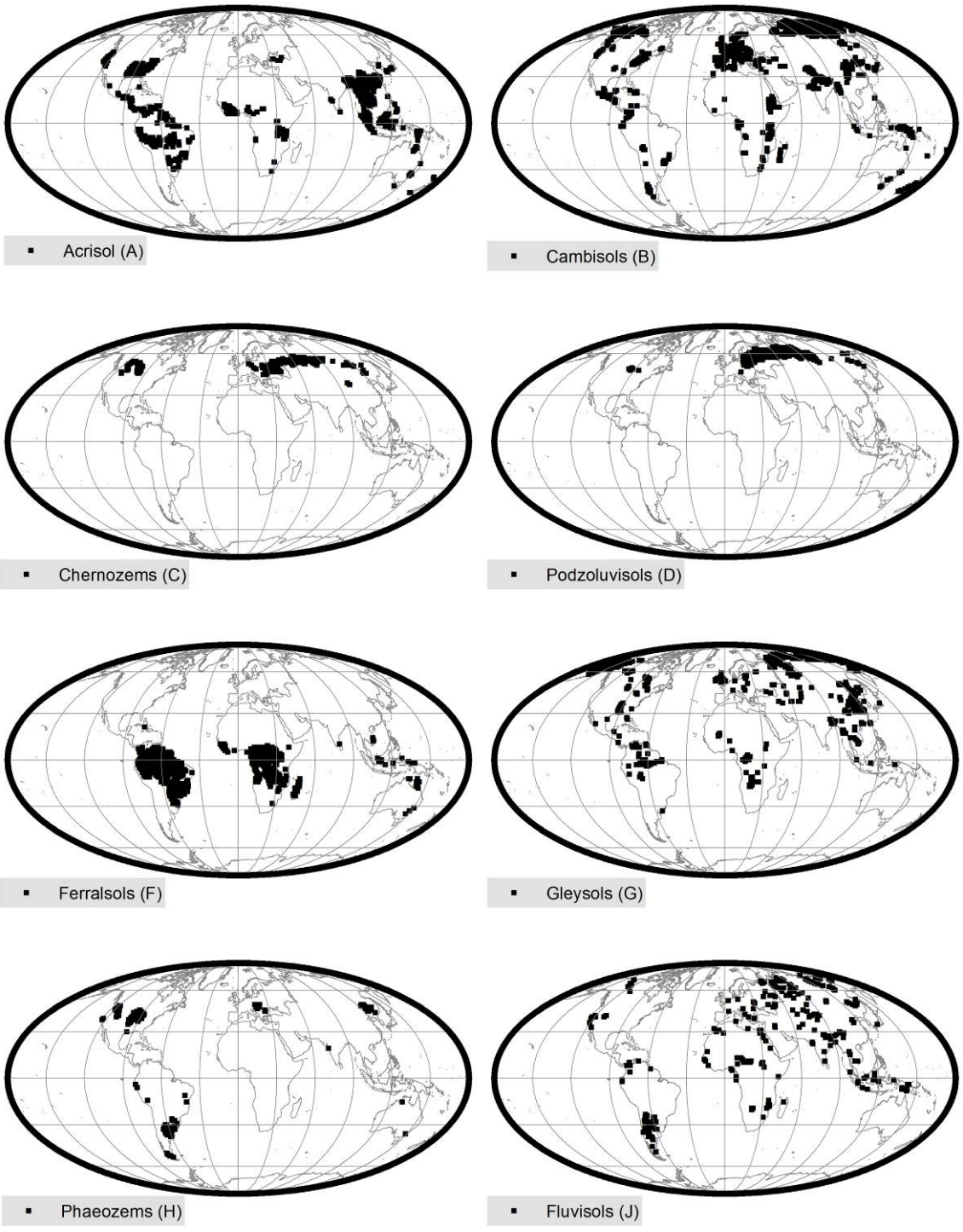

Figure 1.3 Modern Distributions of Zobler Main Soil Units (MSU A, B, C, D, F, G, H and J)

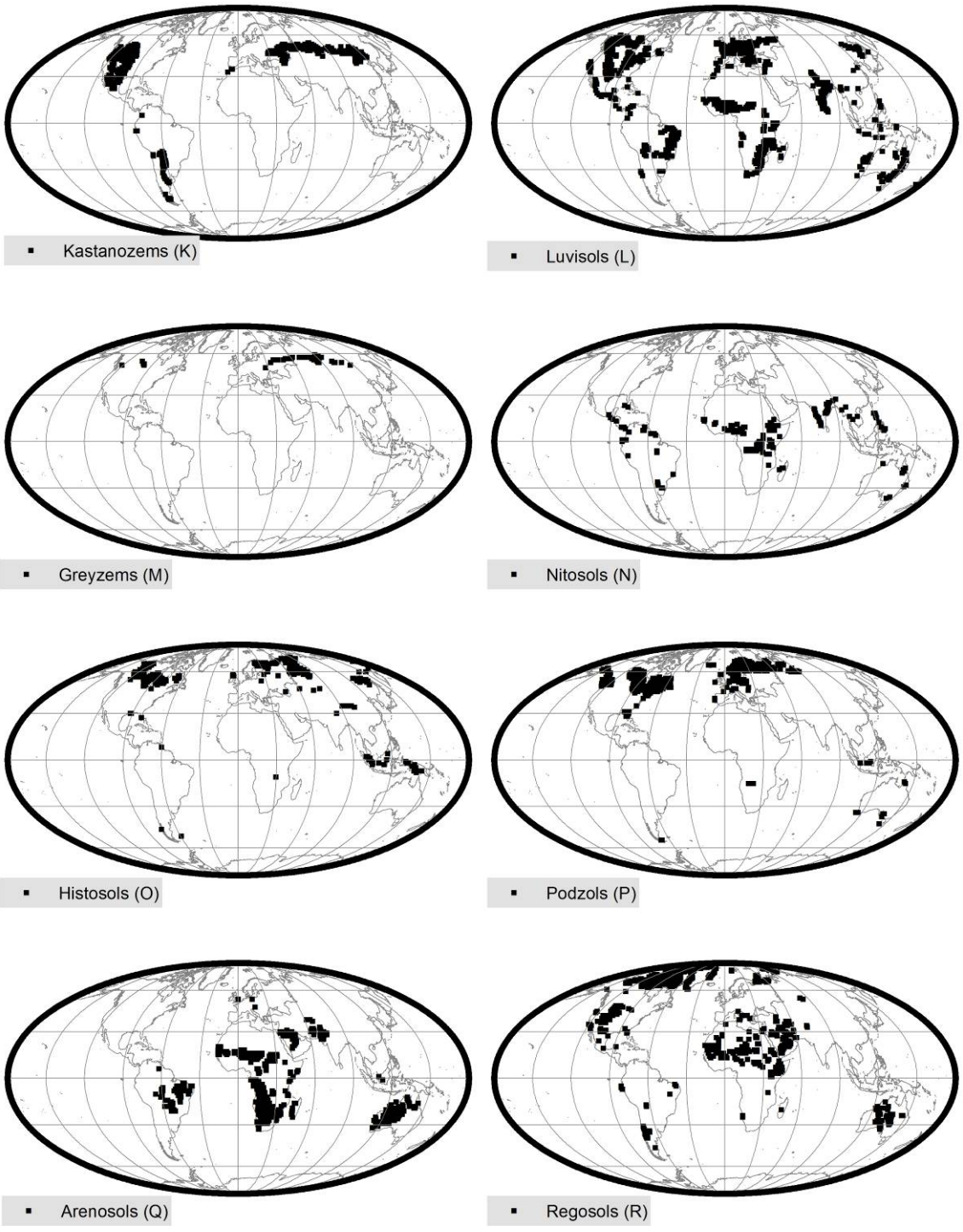

Figure 1.4 Modern Distributions of Zobler Main Soil Units (MSU K, L, M, N, O, P, Q and R)

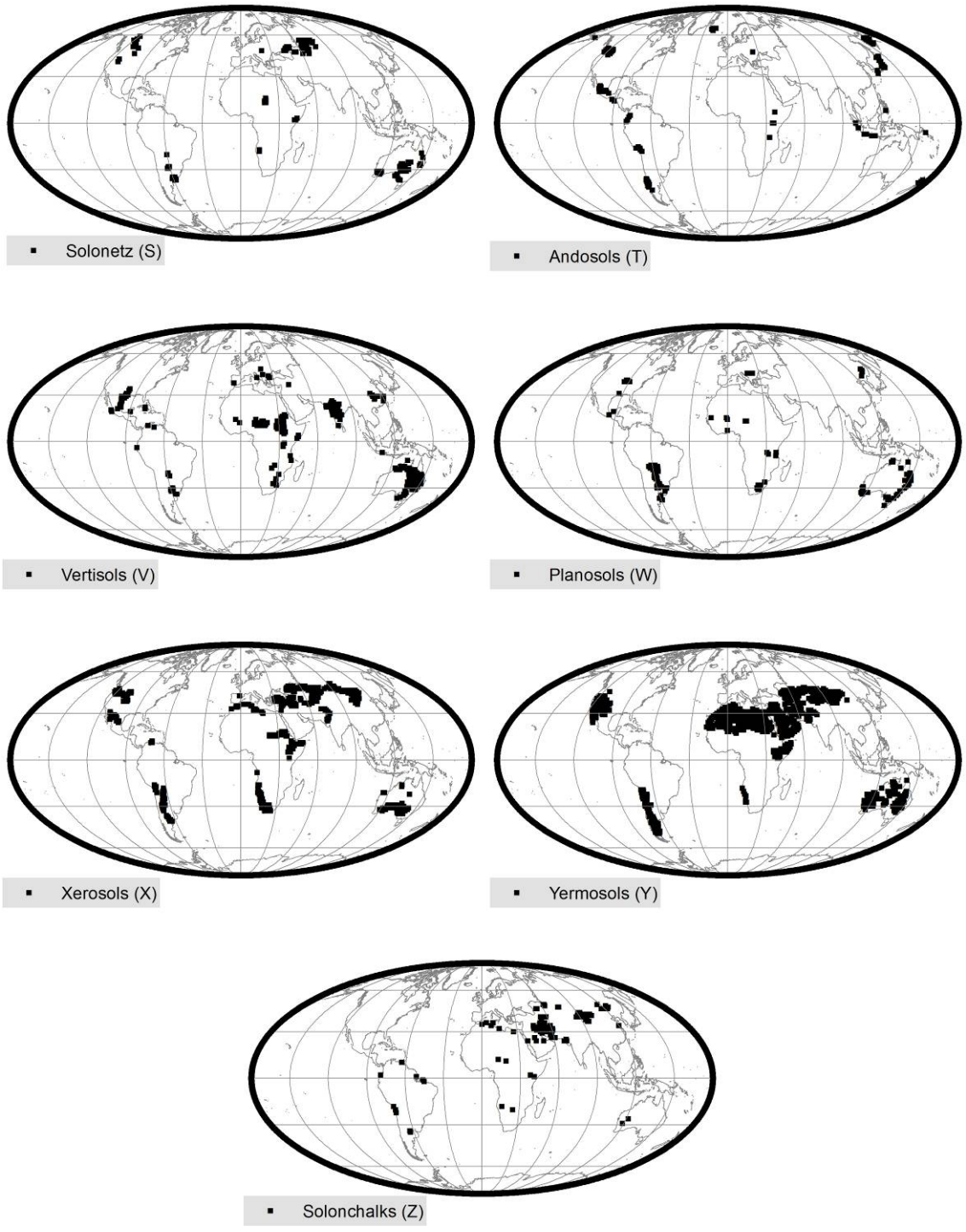

Figure 1.5 Modern Distributions of Zobler Main Soil Units (MSU S, T, V, W, X, Y and Z)

assessment of FAO Soil Units (Zobler, 1986) and an aggregated list of 27 types of Main Soil Units (MSU). Brief descriptions of each soil type (MSU) are given here. These descriptions are mostly taken directly from IRSIC World Soil Information (http://www.isric.org/Isric/Webdocs/ Docs/Major_Soils_of_the_World/start.pdf).

1. Zobler MSU A - (Acrisol): Acrisols are clay-rich, strongly weathered acid soils with low base saturation, usually associated with humid, tropical climates or regions with a wet tropical/monsoonal, subtropical or warm temperate climate, mostly found around old land surfaces with hilly or undulating topography. They are most extensive in Southeast Asia, the southern fringes of the Amazon Basin, the southeastern USA and in both east and West Africa. Figure 1.2 and 1.3 presents an overview of major Acrisol areas.
2. Zobler MSU B - (Cambisol): Cambisol are common in temperate climates and are among the most productive soils on earth. They are also well represented in temperate and boreal regions that were under the influence of glaciation during the Pleistocene, partly because the soil's parent material is still young and also because soil formation is comparatively slow in the cool, northern regions. Cambisol are less common in the tropics and subtropics. But they are common in areas with active erosion where they may occur in association with mature tropical soils. Cambisol are developed in medium and fine-textured materials derived from a wide range of rocks, mostly in alluvial, colluvial and aeolian deposits. Figure 1.2 and 1.3 presents an overview of major Cambisol areas.
3. Zobler MSU C - (Chernozem): Chernozems are dark-colored zonal soils with a deep rich humus horizon found in regions (as the grasslands of central North America) of temperate to cool climate. Parent materials are mostly eolian and re-washed eolian sediments (loess). They are found in regions with a continental climate with cold winters and hot summers; in flat to undulating plains with tall-grass vegetation (forest in the northern transitional zone). Figure 1.2 and 1.3 presents an overview of major Chernozem areas.

4. Zobler MSU D - (Podzoluvisol): Podzoluvisols are widespread in European Russia, where they form from loess-like loams. They have medium fertility because of the leaching processes, but are nevertheless quite favorable for forest growth. Figure 1.2 and 1.3 presents an overview of major Podzoluvisol areas.
5. Zobler MSU E - (Rendzina): Rendzinas are soils developed on calcareous (dolomite, limestone, marl, chalk) or sulphurous (gypsum) materials with the ACca-Cca-R profile, which contains of coarse fragments of hard bedrock in ACca or Cca horizon. Rendzina is one of the most interesting soil names. The name originates from a Polish colloquial word "rzędzić", which means "to chat": the soils of this type contain a significant amount of gravel and stones, which, during plowing, produce various sounds (clicking, screeching, etc.) (https://sites.google .com /site/galeriagleb/).
6. Zobler MSU F - (Ferralsol): Ferralsol are deep, strongly weathered soils with chemically poor, but physically stable subsoil, commonly found at low latitudes and present specific properties related to genesis, geographic location, and management practices. These soils occur mainly under tropical climates, and cover extensive areas on flat, generally well drained land. They are considered as being strongly weathered, and to be associated with old geomorphic surfaces. Ferralsols' red and yellow colors result from an accumulation of metal oxides, particularly iron and aluminum. Figure 1.2 and 1.3 presents an overview of major Ferralsol areas (http://www.fao.org/ag/agl/agll/wrb/ wrbmaps/htm/ferralso.htm).
7. Zobler MSU G - (Gleysol): Gleysols are wetland soils that, unless drained, are saturated with groundwater for long enough periods to develop a characteristic "gleyic color pattern". This pattern is essentially made up of reddish, brownish or yellowish colors in combination with grayish/bluish. Gleysols are technically characterized by both chemical and visual evidence of iron reduction. Subsequent downward translocation (migration) of the reduced iron in the soil profile is associated with gray or blue colors in subsurface

horizons (layers). Typically Gleysols occur in association with Fluvisol and Cambisol. Figure 1.2 and 1.3 presents an overview of major Gleysols areas.

8. Zobler MSU H - (Phaeozem): Phaeozem are soils of wet and warm steppe (prairie) regions, very intensively leached in wet seasons. Consequently, it has a dark, humus surface which provides evidence of removal of carbonates. They are common in flat to undulating land in warm to cool (e.g. tropical highland) regions where weather is humid enough most of the year with a pronounced short, dry season. This results in some percolation of the soil. The natural vegetation is tall grass steppe and/or forest. Figure 1.2 and 1.3 presents an overview of major Phaeozem areas.
9. Zobler MSU I - (Lithosol): Lithosols are a group of shallow azonal soils consisting of imperfectly weathered rock fragments. In other words, Lithosols are very shallow soils developed in situ from various non-carbonate hard rocks with an incomplete solum and/or without clearly expressed morphological features. They are particularly common in mountainous regions.
10. Zobler MSU J - (Fluvisol): Fluvisols are found typically on level topography that is flooded periodically by surface waters or rising groundwater, as in river floodplains/ alluvial plains, deltas, in coastal lowlands, river fans, valleys and (tidal) marshes on all continents and in all climate zones. They are cultivated for dryland crops or rice and are used for grazing in the dry season. They occupy about 2.8% of the continental land area on Earth, mainly in the great river basins and deltas of the world (e.g., the Amazon basin and the Nile delta). Figure 1.2 and 1.3 presents an overview of major Fluvisol areas.
11. Zobler MSU K - (Kastanozem): Kastanozem are the zonal soils of the short grass steppe belt with similar profile as Chernozem but less deep humus-rich surface horizon and less black color. Kastanozem show more prominent accumulation of secondary carbonates and are associated with dry and warm, flat to undulating grasslands with ephemeral short grasses. The chestnut-brown color of the surface soil is reflected in the name

'Kastanozem'. They are typically found in dry and warm climatic conditions. Major distribution of modern Kastanozems are in the Eurasian short grass steppe belt (southern Ukraine, southern Russia, and Mongolia), in the Great Plains of the USA, and in South America (Mexico, southwestern Brazil, and the Pampa regions of Northern Argentina, Uruguay and Paraguay). Figure 1.2 and 1.3 shows the worldwide occurrence of Kastanozems.

12. Zobler MSU L - (Luvisol): Luvisols form on flat or gently sloping landscapes under climatic regimes that range from cool temperate to warm Mediterranean. The mixed mineralogy, high nutrient content, and good drainage of these soils make them suitable for a wide range of agriculture, from grains to orchards to vineyards. Occupying just over 5% of the total continental land area on Earth, they are found typically in west-central Russia, the United States, central Europe, the Mediterranean basin, and southern Australia. Figure 1.2 and 1.4 presents an overview of major Luvisol areas.
13. Zobler MSU M - (Greyzem): Greyzems (Grey Forest Soils) are zonal soils of the forest–steppe, mostly found mostly in Russia. Greyzems are characterized by a dark mollic horizon, i.e., dark soils rich in organic matter, with uncoated (bleached) silt and sand grains on pedfaces, and an argic horizon as diagnostic horizons (Miedemaa et al. 1999). Typically they form under forests in cold temperate climate. Figure 1.2 and 1.4 represents an overview of major Greyzem areas.
14. Zobler MSU N - (Nitosol): By definition, Nitosols are deep, well drained, slightly acidic, well structured reddish clay and with moderate inherent fertility. Nitosols are tropical soils with diffuse horizon boundaries and a subsurface horizon with more than 30 percent clay and moderate to strong angular blocky structural elements that easily fall apart into characteristic shiny, polyhedric ('nutty') elements. Nitosols are strongly weathered soils but far more productive than most other red tropical soils. Nitosols are predominantly

found in level to hilly land under tropical rain forest or savanna vegetation. Figure 1.2 and 1.4 represents an overview of major Nitosol areas.

15. Zobler MSU O - (Histosol): Histosols comprises soils formed under waterlogged conditions in 'organic soil material'. These vary from soils developed in moss peat in boreal, arctic and subarctic regions, via moss peat, reeds/sedge peat and forest peat in temperate regions to mangrove peat and swamp forest peat in the humid tropics. Histosols occur extensively in boreal, arctic and subarctic regions. Elsewhere, they are confined to poorly drained basins and depressions, swamp and marshlands with shallow groundwater, and highland areas with a high precipitation/evapotranspiration ratio. Histosols are found at all altitudes but the vast majority occurs in lowlands. Common international names are 'peat soils', 'muck soils', 'bog soils' and 'organic soils'. The accumulated tissues of dead plants and animals and their decomposition products in Histosols are preserved, resulting in soils of high organic content. They are characterized by at least 12% to 18% organic carbon by mass (depending on the clay content) if occasionally waterlogged or by at least 20% organic carbon by mass if never waterlogged. After drainage for agricultural use (particularly vegetable crops and cranberries), the organic material is prone to oxidation, leading to fire hazards as well as subsidence. Sphagnum and other types of fibrous material are extracted from Histosols for use in horticulture and as fuel. Larger areas of these soils have been managed for flood control, water purification, and wildlife preservation. Histosols occupy less than 2% of the nonpolar continental land area on Earth, mostly in Canada, Russia, and Scandinavia. Figure 1.2 and 1.4 represents an overview of major Histosol areas.
16. Zobler MSU P - (Podzol): Podzols typically occur in humid areas in the Boreal and Temperate Zones and locally also in the tropics. These soils are found in areas that are wet and cold (for example in Northern Ontario or Russia) and also in warm areas such as Florida where sandy soils have fluctuating water tables (humic variant of the northern

Podzol). Podzols form under forested landscapes on coarse parent material that is high in quartz. They have a characteristic subsurface layer known as the spodic horizon made up of accumulated humus and metal oxides, usually iron and aluminum. Above the spodic horizon there is often a bleached-out layer from which clay and iron oxides have been leached, leaving a layer of coarse-textured material containing primary minerals and little organic matter. Podzols usually defy cultivation because of their acidity and climatic environment. Occupying almost 4% of the total continental land area on Earth, they range from Scandinavia to Russia and Canada in the Northern Hemisphere, to The Guianas near the Equator, to Australia and Indonesia in the Southern Hemisphere. Figure 1.2 and 1.4presents an overview of major Podzol areas.

17. Zobler MSU Q - (Arenosol): Arenosols consists of sandy soils, developed in residual sands, in situ after weathering of old, usually quartz-rich soil material or rock, and also soils developed in recently deposited sands as occur in deserts and beach lands, with the A-C profile. Often they are found in shifting sand dunes but also in areas of very coarse-textured parent material subject to millions of years of weathering. Humic horizon thickness is generally 10 cm or more. These soils have no other diagnostic horizons. This latter case is characteristic of the Guiana Highlands of northern South America. Arenosols also have no distinct soil horizons, and must consist entirely of material of loamy sand or coarser in texture. Arenosols are one of the most extensive soil found on the planet, covering about 7-9% of the land surface area. Figure 1.2 and 1.4 represents an overview of major Arenosol areas.
18. Zobler MSU R - (Regosol): Regosols are a taxonomic rest group containing all soils that could not be accommodated in any of the other soil groups. They are very weakly developed mineral soils in unconsolidated materials that have only an ochric surface horizon and that are not very shallow (Leptosols), sandy (Arenosols) or with fluvic properties (Fluvisols). Regosols are extensive in eroding lands, in particular in arid and

semi-arid areas and in mountain regions. They are typically found in all climate zones without permafrost and at all elevations. Regosols are particularly common in arid areas, in the dry tropics and in mountain regions. Figure 1.2 and 1.4 represents an overview of major Regosol areas.

19. Zobler MSU S - (Solonetz): Solonetz are soils with a dense, strongly structured, clayey subsurface horizon that has a high proportion of adsorbed sodium and/or magnesium ions. Solonetz are normally associated with flat lands in a climate with hot, dry summers, or with coastal deposits that contain a high proportion of sodium ions. Major concentrations of Solonetz are in flat or gently sloping grasslands with loess/loam or clay in semi-arid, temperate and subtropical regions. Because of the high sodium content and dense, clay-rich subsoil, irrigated agriculture of these soils requires extensive reclamation—through leaching with fresh water and the construction of engineered drainage systems. Solonetz soils occur in dry climatic zones and on parent materials either naturally enriched in sodium-bearing minerals or influenced by saline waters. They occupy about 1% of the continental land area on Earth (northeastern Argentina, Chile, and the coastal edges of every continent). Figure 1.2 and 1.5 represents an overview of major Solonetz areas.
20. Zobler MSU T - (Andosol): Andosols are highly porous, dark-colored soils developed from parent material of volcanic origin, such as volcanic ash, tuff, and pumice. Their worldwide extent is estimated at less than 1% of the total soil area on Earth. They are found from Iceland to Indonesia, but they typically occur in wooded highland areas of the continental lands bordering the Pacific Ocean. Figure 1.2 and 1.5 represents an overview of major Andosol areas.
21. Zobler MSU U - (Ranker): Rankers are soils having an umbric A horizon which is not more than 25 cm thick; having no other diagnostic horizons. In other words, Rankers are soils poorly diversified morphologically, with the AC-C-R profile, developed on the non-

carbonate hard rocks. These soils have limitation of depth by continuous rock within 50 cm of the soil surface.

22. Zobler MSU V - (Vertisol): Vertisols are with high content of expansive clay known as montmorillonite that forms deep cracks in drier seasons or years. Alternate shrinking and swelling causes self-mulching, where the soil material consistently mixes itself, causing Vertisols to have an extremely deep A horizon and no B horizon. Their very low water permeability when wet and unstable structures make them unsuitable for most other commercial uses. Vertisols typically form from highly basic rocks such as basalt in climates that are seasonally humid or subject to erratic droughts and floods, or to impeded drainage. Depending on the parent material and the climate, they can range from grey or red to the more familiar deep black (known as black earths in Australia, and black cotton soils in East Africa). Although broadly distributed on every nonpolar continent, they occupy just over 2% of the land area on Earth, primarily in subtropical or tropical zones of Australia, India, and Africa and in parts of the western United States (California and Texas) and Europe (Austria and the Balkans). Figure 1.2 and 1.5 represents an overview of major Vertisol areas.
23. Zobler MSU W - (Planosol): A Planosol is a soil with a light-colored, coarse-textured, surface horizon that shows signs of periodic water stagnation and abruptly overlies a dense, slowly permeable subsoil with significantly more clay than the surface horizon. These soils are typically in seasonally waterlogged flat lands, occurring mainly in subtropical and temperate, semi-arid and sub-humid regions. Planosols are formed mostly in clayey alluvial and colluvial deposits. They occupy about 1% of the total continental land area on Earth. Major areas with Planosols occur in subtropical and temperate regions with clear alternation of wet and dry seasons, as in Latin America (southern Brazil, Paraguay and Argentina), Africa (Sahelian zone, East and Southern Africa), the east of the United States of America, Southeast Asia (Bangladesh and

Thailand), and Australia. Figure 1.2 and 1.5 represents an overview of major Planosol areas.

24. Zobler MSU X - (Xerosol): Xerosols are soils in arid and semi-arid regions, with a weakly developed A horizon. They are found in regions with an arid climate where natural vegetation is sparse. Figure 1.2 and 1.5 presents an overview of major Xerosol areas.
25. Zobler MSU Y - (Yermosol): Yermosol are soils with substantial secondary accumulation of gypsum ($CaSO_4.2H_2O$). They are found in the driest parts of the arid climate zones. Hence they are also named as 'Desert soils'. They dominate the deserts and xeric shrub lands which occupy about one third of the Earth's land surface. They also have a very low concentration of organic matter. Water deficiency is the major defining characteristic of Yermosols. Major occurrences are in and around Mesopotamia, in desert areas in the Middle East and adjacent central Asian republics, in the Lybian and Namib deserts, in southeast and central Australia and in the southwestern USA. Figure 1.2 and 1.5 presents an overview of major Yermosol areas.
26. Zobler MSU Z - (Solonchak): Solonchaks are defined by high soluble salt accumulation within 30 cm (1 foot) of the land surface and by the absence of distinct subsurface horizonation (layering), except possibly for accumulations of gypsum, sodium, or calcium carbonate or layers showing the effects of water logging. Solonchaks are formed from saline parent material under conditions of high evaporation—conditions encountered in closed basins under warm to hot climates with a well-defined dry season, as in arid, Mediterranean, or subtropical zones. Solonchaks is pale or grey soil type found in arid to sub-humid, poorly-drained conditions. Solonchaks includes soils that have a high concentration of 'soluble salts' at some time in the year. Solonchaks are largely confined to the arid and semi-arid climatic zones and to coastal regions in all climates. Solonchaks are most extensive in the northern hemisphere, notably in the arid and semi-arid parts of northern Africa, the Middle East, the former USSR and central Asia; they are also

widespread in Australia and the Americas. Figure 1.2 and 1.5 shows the major occurrences of Solonchaks in the world (www.isric.org).

27. Glacier/Ice: The continental glaciers and/or the ice covers are grouped as a separate unit in the Zobler World Soil Classification. The places having no visible soils and ice cover are taken care of in this group.

The downloaded Zobler dataset (Zobler 1999) contained more information than this project required. Using a Python code (Appendix A: Zobler Formating.py) a subset of the dataset was extracted to a comma-separated file containing Latitude, Longitude, MSU(Main Soil Unit Code), MSUName (Main Soil UnitName), SU(Sub Soil Unit Code), SUName (Sub Soil Unit Name), Area (Geographic Location Code) and AreaName (Geographic Location Name) and converted to a ArcGIS point type shapefile with the attributes Latitude, Longitude, Main Soil Unit Code (MSU) and the Main Soil Unit Name using the Python scripts CSV2SHP.py and ExportA2Z.py. These scripts (listed in Appendix A) were used to minimize risk of errors in repetitive jobs, as well as, to speed up the processing.

1.2.3 Preparation of Legates-Wilmott Temperature-Precipitation Data (② Figure 1.1)

Though the factors that control soil formation are complex (Retallack 1990), we have found that a bi-variate approach using only temperature and precipitation satisfactorily describes the climatic conditions under which different types of soil form. For this project we have chosen to use the Legates and Willmott Average Monthly Surface Air Temperature dataset (Legates and Wilmott, 1990a) and the Legates and Willmott Average Monthly Surface Air Precipitation dataset (Legates and Wilmott, 1990b).

Legates and Wilmott (1990a) compiled mean monthly surface air temperature using terrestrial observations of shelter-height air temperature and shipboard measurements. The mean monthly surface air precipitation was compiled by Legates and Wilmott (1990b) using traditional land-based gauge measurements and shipboard estimates. The precipitation data were obtained

from ten existing sources, screened and corrected for gauge-induced biases and interpolated to a 0.5° latitude by 0.5° of longitude grid (Legates and Wilmott, 1990b).

The Legates and Willmott Average Monthly Surface Air Temperature and Precipitation data were downloaded from the NOAA GED site (http://www.ngdc.noaa.gov/ecosys/cdroms/ged_iia/datasets/a04/lw.htm). This 1°x1° NetCDF dataset was then converted to a comma-delimited text file using a Python script (Appendix A: Legates Willmott NetCDF to CSV.py). The temperature and precipitation datasets include: latitude, longitude and monthly values of temperature (°C) and precipitation (cm/month). A Python script was written to calculate the seasonal and annual mean values for both temperature (Figure 1.6) and precipitation (Figure 1.7). The global mean annual temperature (GMAT) and global mean annual precipitation (GMAP) were imported to ArcGIS and joined together to create a single Legates-Wilmott Temperature-Precipitation shapefile. This dataset is a record of the mean global temperature and mean global precipitation for second half of the 20th century (1951-2000).

The final step in this procedure was to join the global mean annual temperature and global mean annual precipitation data with the Zobler World Soil dataset described in the previous section. This new dataset called the 'Zobler-LW dataset', represents the integration of soil information and climatology. In the next procedure, I will describe how I used the climate envelope technique of Moore et al. (2007) and the Köppen-Geiger classification scheme to associate specific temperature and precipitation regimes with each major soil category.

1.2.4 Preparation of Köppen-Geiger Climate Classification (③ Figure 1.1)

The fundamental question — do soils form under coherent climatic regimes? — is yet to be answered satisfactorily. In other words, does the geographic distribution of different soil types reflect ambient temperature and precipitation conditions?

Intuitively, this seems to be the case. Quick reviews of Figures 1.3 to 1.7 clearly show that some soils, e.g., Chernozems, Podzoluvisols, Ferralsols, Podzols and Yermosols are

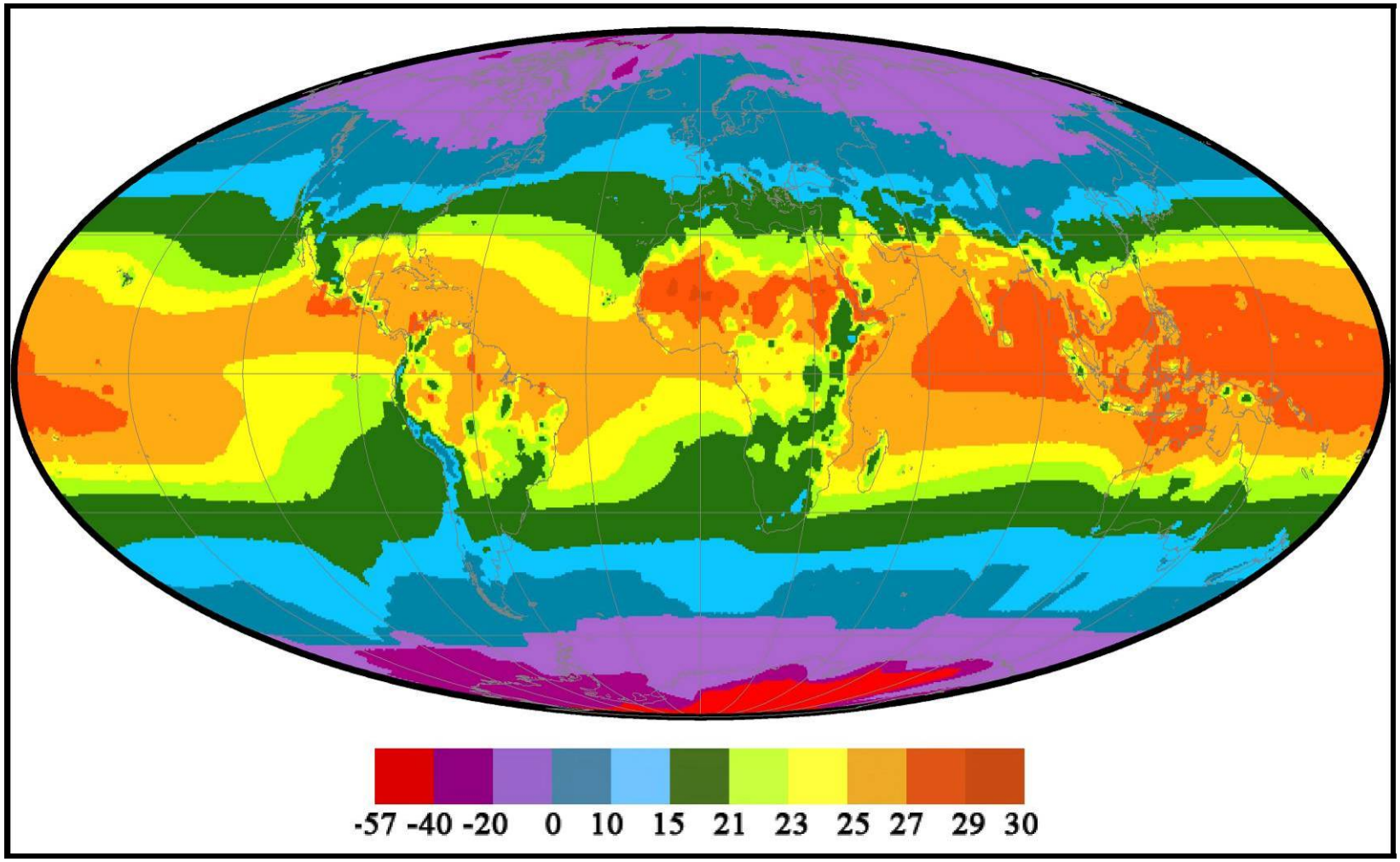

Figure 1.6 Legates-Willmott (1990) Global Mean Annual Temperatures (°C)

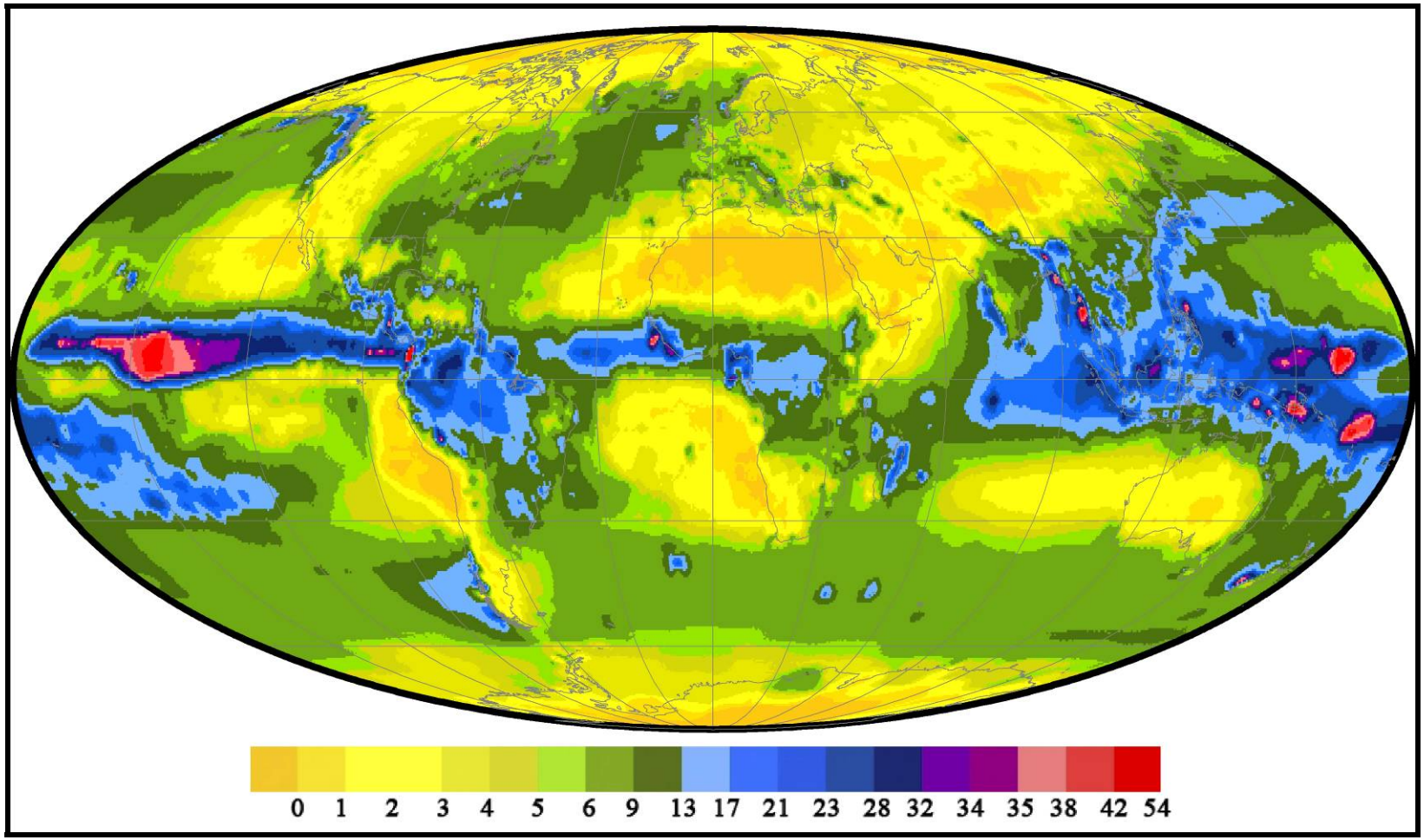

Figure 1.7 Legates-Willmott (1990) Global Mean Annual Precipitations (cm)

Table 1.2 Köppen -Geiger World Climate Classification Scheme

Climate Name	Climate Code	Main Climate Code	Main Climate Name	Precipitation Code	Precipitation Name	Temperature Code	Temperature Name
Equatorial Fully Humid	Af	A	Equatorial	f	Fully Humid	-	-
Equatorial Monsoonal	Am			m	Monsoonal	-	-
Equatorial Summer Dry	As			s	Summer Dry	-	-
Equatorial Winter Dry	Aw			w	Winter Dry	-	-
Cold Arid Desert	BWk	B	Arid	W	Desert	k	Cold Arid
Hot Arid Desert	BWh					h	Hot Arid
Cold Arid Steppe	BSk			S	Steppe	k	Cold Arid
Hot Arid Steppe	BSh					h	Hot Arid
Warm Temperate Fully Humid Hot Summer	Cfa	C	Warm Temperate	f	Fully Humid	a	Hot Summer
Warm Temperate Fully Humid Warm Summer	Cfb					b	Warm Summer
Warm Temperate Fully Humid Cool Summer	Cfc					c	Cool Summer
Warm Temperate Dry Summer Hot Summer	Csa			s	Summer Dry	a	Hot Summer
Warm Temperate Dry Summer Warm Summer	Csb					b	Warm Summer
Warm Temperate Dry Summer Cool Summer	Csc					c	Cool Summer
Warm Temperate Dry Winter Hot Summer	Cwa			w	Winter Dry	a	Hot Summer
Warm Temperate Dry Winter Warm Summer	Cwb					b	Warm Summer
Warm Temperate Dry Winter Cool Summer	Cwc					c	Cool Summer
Snow Fully Humid Hot Summer	Dfa	D	Snow	f	Fully Humid	a	Hot Summer
Snow Fully Humid Warm Summer	Dfb					b	Warm Summer
Snow Fully Humid Cool Summer	Dfc					c	Cool Summer
Snow Fully Humid Extreamly Continental	Dfd					d	Extreamly Continental
Snow Dry Summer Hot Summer	Dsa			s	Summer Dry	a	Hot Summer
Snow Dry Summer Warm Summer	Dsb					b	Warm Summer
Snow Dry Summer Cool Summer	Dsc					c	Cool Summer
Snow Dry Summer Extreamly Continental	Dsd					d	Extreamly Continental
Snow Dry Summer Hot Summer	Dwa			w	Winter Dry	a	Hot Summer
Snow Dry Summer Warm Summer	Dwb					b	Warm Summer
Snow Dry Summer Cool Summer	Dwc					c	Cool Summer
Snow Dry Summer Extreamly Continental	Dwd					d	Extreamly Continental
Polar Frost	EF	E	Polar			F	Polar Frost
Polar Tundra	ET					T	Polar Tundra

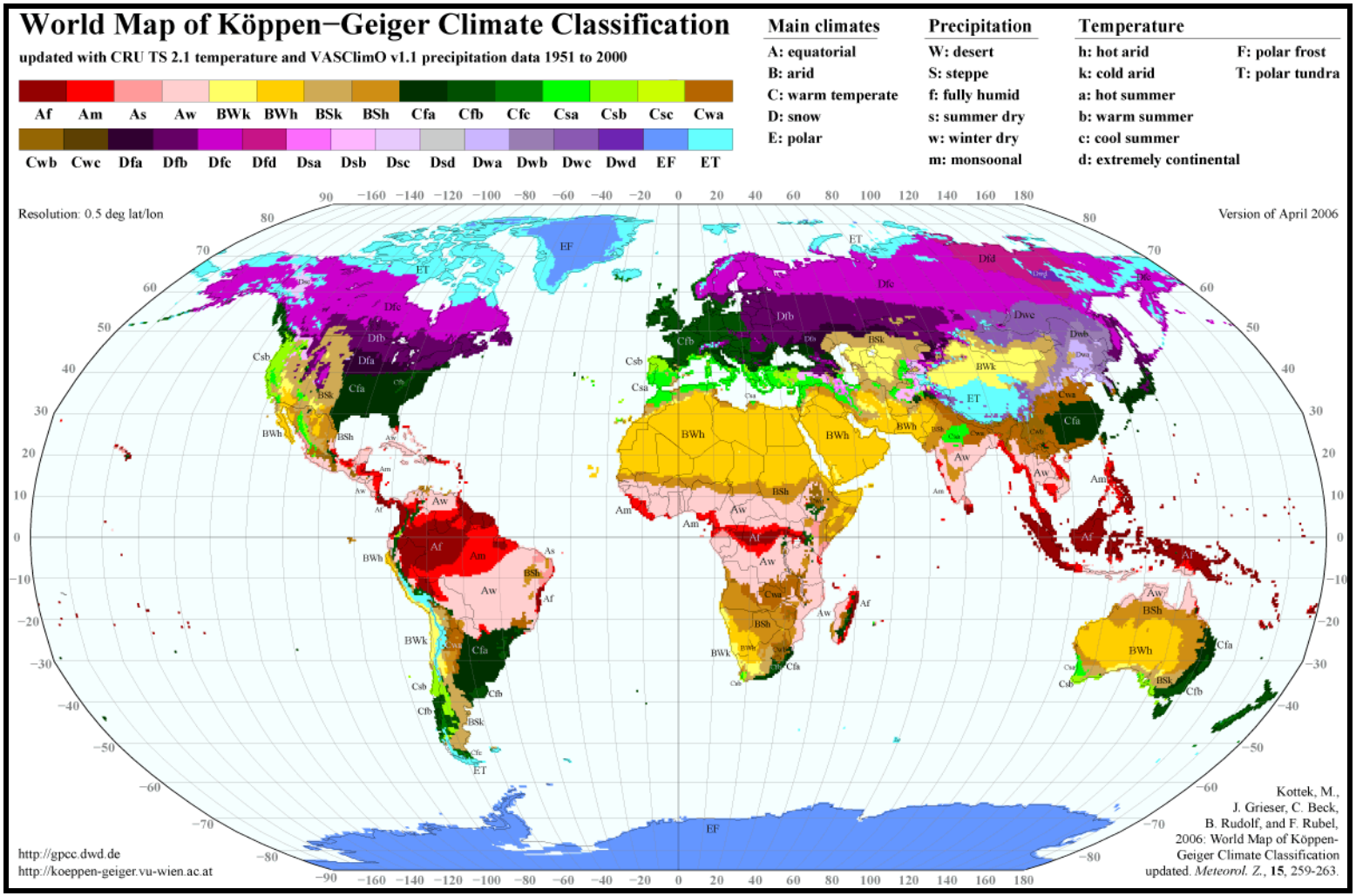

Figure 1.8 World Map of Köppen-Geiger Climate Classification

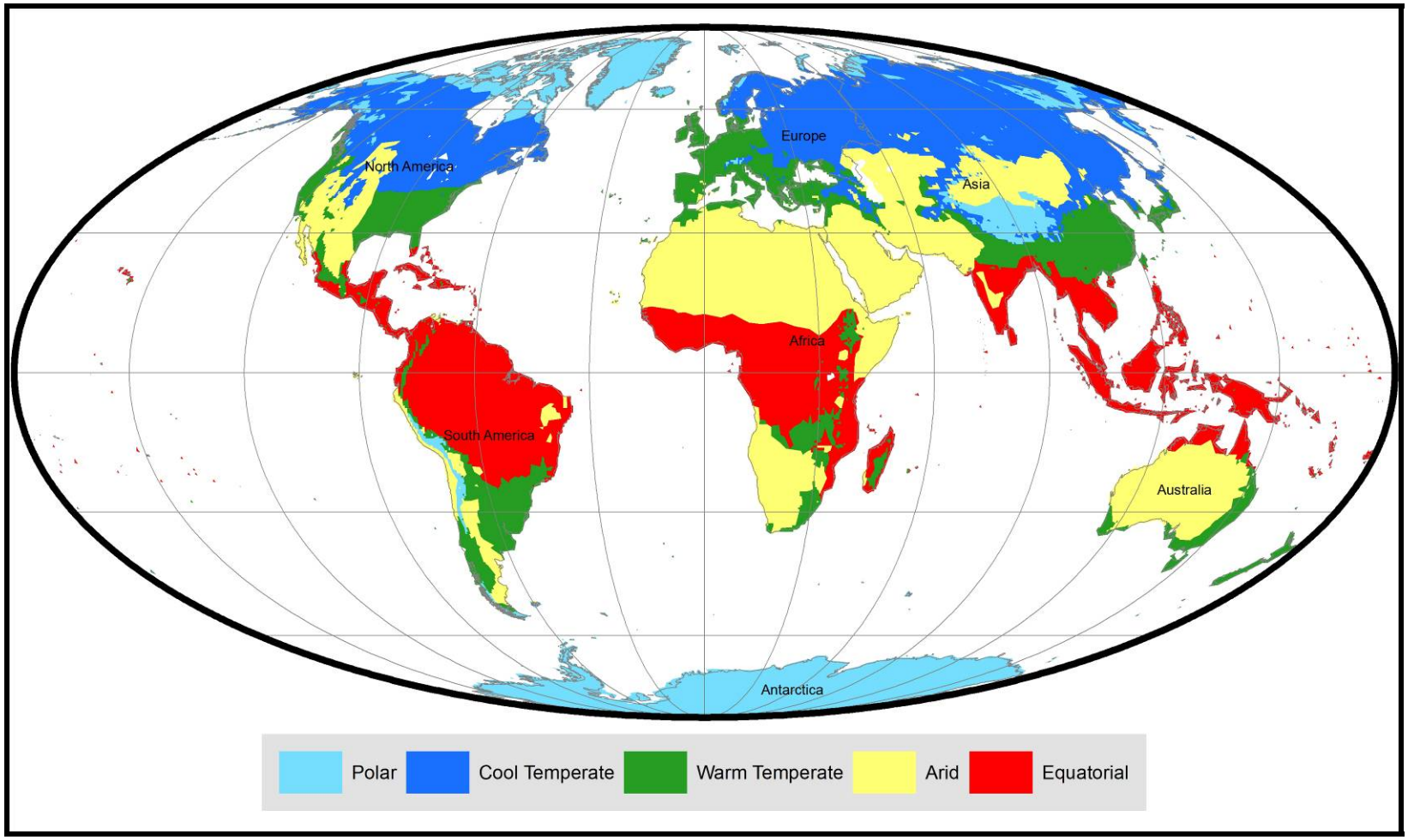

Figure 1.9 Köppen-Geiger Main Climate Zone Classification

geographically coherent (i.e., occur in similar geographic zones). However, other major soil types seem to be geographically dispersed e.g., Fluvisols, Luvisols, Regosols and Andosols.

How can we differentiate between the soil groups that seem to reflect coherent climatic regimes from those that do not? The approach that I have taken is to use the Köppen-Geiger climate classification scheme to identify those soils that are climatically coherent.

The Köppen-Geiger climate classification scheme is one of the most widely used systems for classifying climate because it is easy to understand and data requirements are minimal. It is an empirical system based largely on annual and monthly means of temperature and precipitation. It was first published by German climatologist Wladimir Köppen in 1884, with several later modifications by Köppen himself, notably in 1918 and 1936. Later, German climatologist Rudolf Geiger collaborated with Köppen on changes to the classification system. A large number of climate studies have adopted the Köppen-Geiger climate classification system (Otto-Bliesner and Upchurch, 1997; Mendez and Maier, 2008; Black et. al 2008 etc.).

The Köppen-Geiger classification uses five letters (e.g., A: Equatorial, B: Arid, C: Warm Temperate, D: Cool Temperate and E: Polar) to divide the world into five major climate regions based on the Hadley Cell circulation pattern and the pole-to-equator temperature gradient. Each region is further divided into sub-categories based on seasonal variation in temperature and precipitation. The precipitation subcategories are represented by another six letters (e.g., W: desert, S: steppe, f: Fully humid, s: summer dry, w: winter dry and m: monsoonal), whereas, the temperature subcategories are represented by different set of eight letters (e.g., h: hot arid, k: cold arid, a: hot summer, b: warm summer, c: cool summer, d: extremely continental, F: polar frost and T: polar tundra). Thus, by combining latitude, temperature, and precipitation, the Köppen-Geiger classification scheme describes the Earth's climate using thirty one different climate categories. Table 1.2 lists the name and codes for Köppen-Geiger climate classification scheme.

Kottek et al. (2006) produced a digital version of Köppen-Geiger classification scheme using datasets compiled by the Climatic Research Unit (CRU) of the University of East Anglia and the Global Precipitation Climatology Centre (GPCC) and the German Weather Service. His map is shown in Figure 1.8. A GIS compatible version of this dataset was downloaded from the website of Institute for Veterinary Public Health Vienna (http://koeppen-geiger.vu-wien.ac.at/data/Koeppen-Geiger-GIS.zip). This data consisted of a raster image with numeric gridcode for each of the thirty one climate zones described in the Köppen-Geiger classification scheme. Using Spatial Analysis tools (ArcGIS), the raster was converted to a polygon shapefile. Later, a Python script was used to associate the numeric and alphabetic codes for Köppen-Geiger climate zones with the gridcode attributes in the original raster file (Appendix A: KG Update.py). To simplify the analysis, we have reduced the number of climate zones from thirty one to five (A-E main climate zones of Köppen-Geiger Classification). ArcMap function “dissolve polygons” were used to reduce the thirty one climatic zones to five main climatic zones (Figure 1.9).

In the next step of the procedure, the geographic location for the Zobler soils were intersected with the polygon shapefiles that describe the Köppen-Geiger climatic zones. If soils represent coherent climatic regimes, then they should cluster within specific Köppen-Geiger climatic zones. Conversely, soils that appear in multiple Köppen-Geiger climatic zones are not climatically coherent.

1.2.5 Preparation of Paleo-Soil Groups (④ Figure 1.1)

In order to predict the geographic distribution of paleo-soils, it is necessary to demonstrate that soils form under specific climatic conditions. In this section, I describe how ten paleo-soil groups that were identified with well-defined climatic signatures. These ten paleo-soil groups were used to produce the paleo-soil reconstructions plotted on the paleogeographic maps in section 1.4.10.

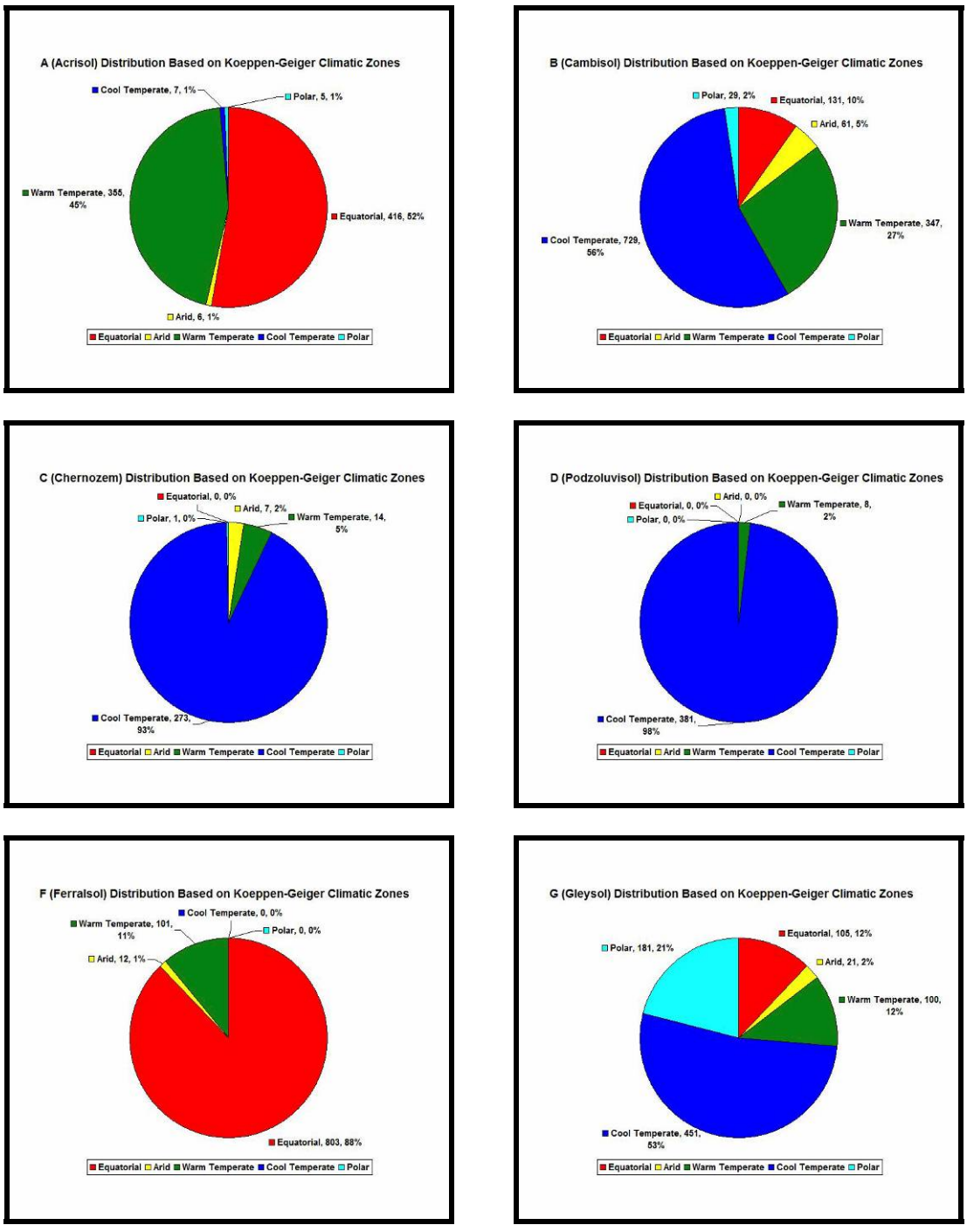

Figure 1.10 Climatic affiliations of different Main Soil Types (MSU) of Zobler Soil Classification (MSU A, B, C, D, F and G).

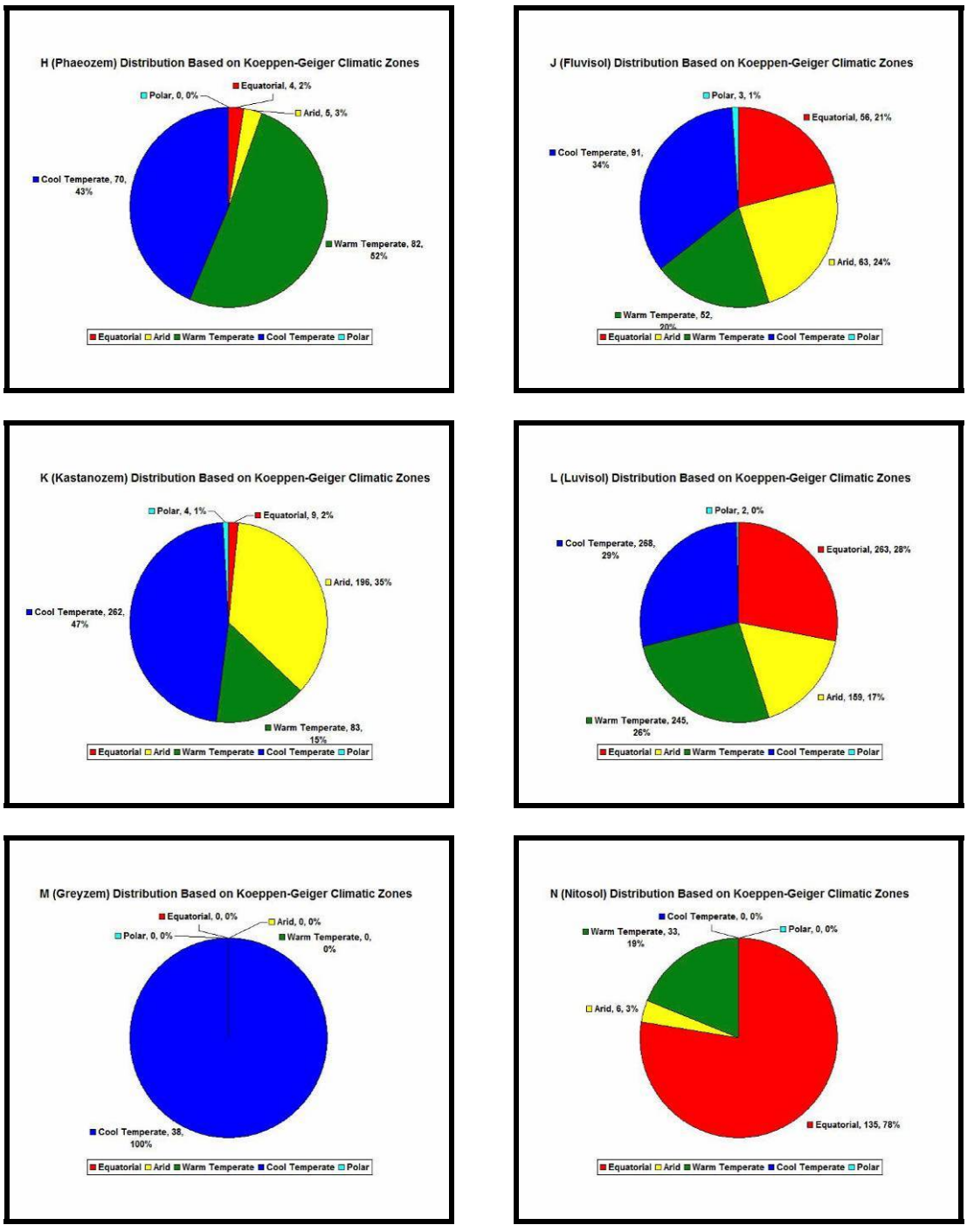

Figure 1.11 Climatic affiliations of different Main Soil Types (MSU) of Zobler Soil Classification (MSU H, J, K, L, M and N).

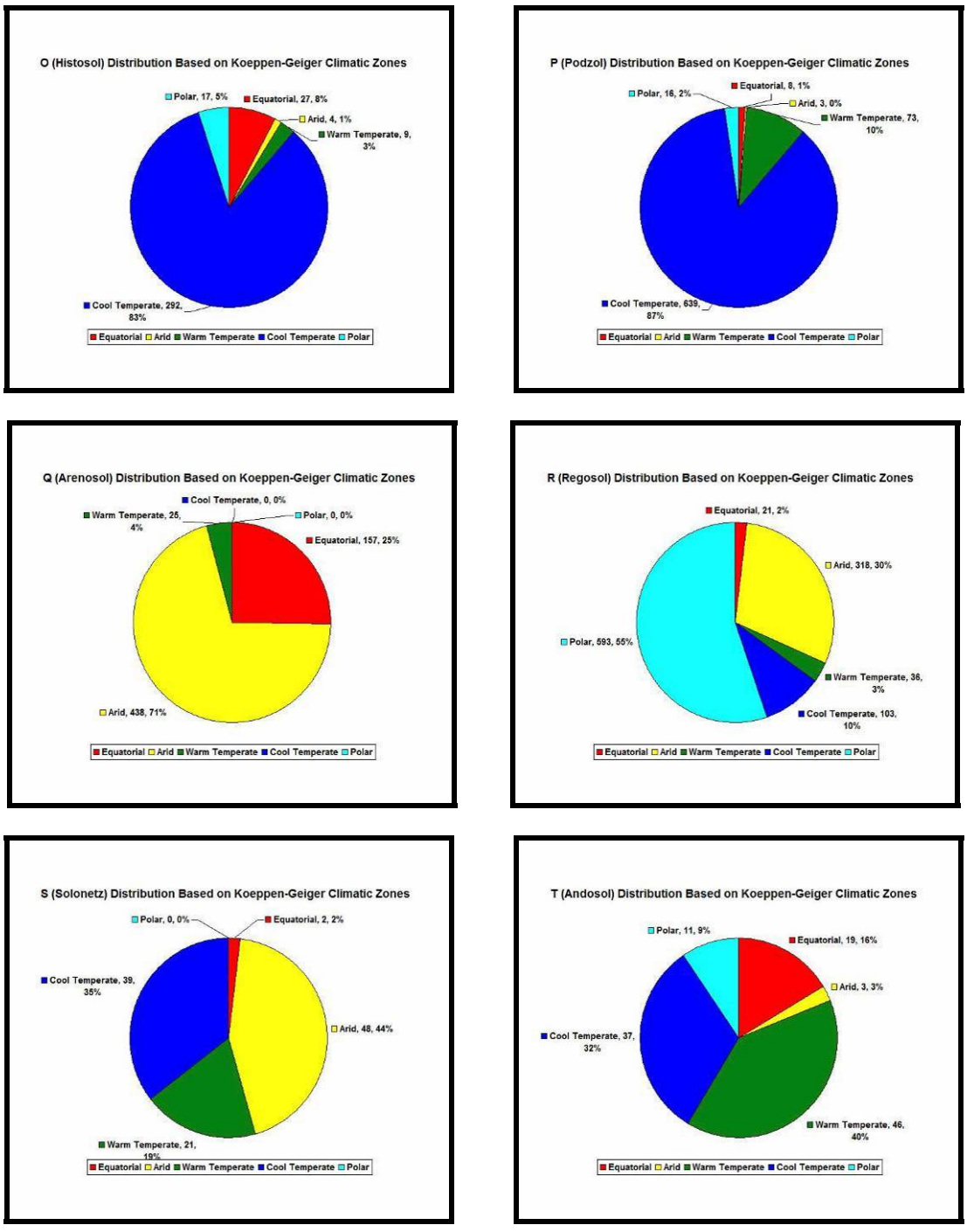

Figure 1.12 Climatic affiliations of different Main Soil Types (MSU) of Zobler Soil Classification (MSU O, P, Q, R, S and T).

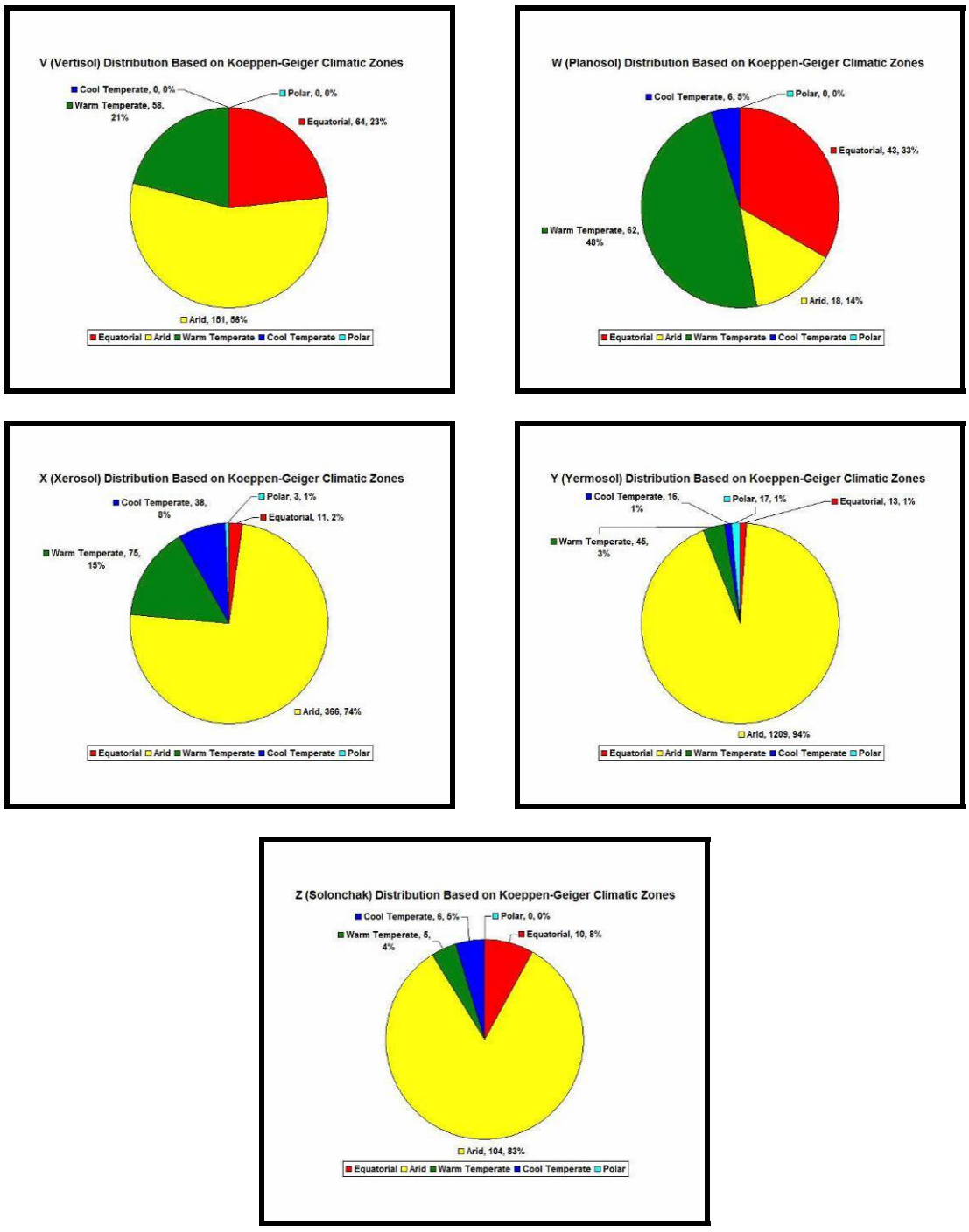

Figure 1.13 Climatic affiliations of different Main Soil Types (MSU) of Zobler Soil Classification (MSU V, W, X, Y and Z).

Table 1.3 Percentage of each Zobler soil types in the five main Köppen-Geiger zones

No.	MSU	Name	Equatorial	Arid	Warm Temperate	Cool Temperate	Polar	Accepted or Rejected
1	A	Acrisol	***52.72***	0.76	***44.99***	0.89	0.63	Accepted
2	B	Cambisol	10.10	4.70	**26.75**	**56.21**	2.24	Accepted
3	C	Chernozem	0.00	2.37	4.75	**92.54**	0.34	Accepted
4	D	Podzoluvisol	0.00	0.00	2.06	**97.94**	0.00	Accepted
5	E	Rendzina	* -					**Rejected**
6	F	Ferralsol	**87.66**	1.31	11.03	0.00	0.00	Accepted
7	G	Gleysol	12.24	2.45	11.66	**52.56**	**21.10**	Accepted
8	H	Phaeozem	2.48	3.11	**50.93**	**43.48**	0.00	Accepted
9	I	Lithosol	* -					**Rejected**
10	J	Fluvisol	21.13	23.77	19.62	34.34	1.13	**Rejected**
11	K	Kastanozem	1.62	***35.38***	14.98	***47.29***	0.72	Accepted
12	L	Luvisol	28.07	16.97	26.15	28.60	0.21	**Rejected**
13	M	Greyzem	0.00	0.00	0.00	**100.00**	0.00	Accepted
14	N	Nitosol	**77.59**	3.45	18.97	0.00	0.00	Accepted
15	O	Histosol	7.74	1.15	2.58	**83.67**	4.87	Accepted
16	P	Podzol	1.08	0.41	9.88	**86.47**	2.17	Accepted
17	Q	Arenosol	**25.32**	**70.65**	**4.03**	0.00	0.00	Accepted
18	R	Regosol	1.96	29.69	3.36	9.62	55.37	**Rejected**
19	S	Solonetz	1.82	***43.64***	19.09	***35.45***	0.00	Accepted
20	T	Andosol	16.38	2.59	39.66	31.90	9.48	**Rejected**
21	U	Ranker	* -					**Rejected**
22	V	Vertisol	**23.44**	**55.31**	**21.25**	0.00	0.00	Accepted
23	W	Planosol	***33.33***	13.95	***48.06***	4.65	0.00	Accepted
24	X	Xerosol	2.23	**74.24**	15.21	7.71	0.61	Accepted
25	Y	Yermosol	1.00	**94.00**	3.00	1.00	1.00	Accepted
26	Z	Solonchak	8.00	**83.00**	4.00	5.00	0.00	Accepted
27	Glacier/Ice	Glacier/Ice	Not included in the study					**Rejected**
* No records in the Zobler World soil dataset								

Table 1.4 Distance scores for Zobler soil types.

MSU	A Affinity Score	B Affinity Score	C Affinity Score	D Affinity Score	F Affinity Score	G Affinity Score	H Affinity Score	K Affinity Score	M Affinity Score	N Affinity Score	O Affinity Score	P Affinity Score	Q Affinity Score	S Affinity Score	V Affinity Score	W Affinity Score	X Affinity Score	Y Affinity Score	Z Affinity Score
A	0.00	72.30	113.15	118.51	***48.74***	76.44	66.18	82.85	120.95	***36.11***	103.41	105.96	85.52	79.35	66.32	***23.96***	94.25	114.60	102.28
B	72.30	0.00	43.77	49.81	97.16	***24.63***	***28.50***	***35.12***	52.56	88.21	36.93	36.06	90.89	45.59	77.03	61.17	85.94	108.03	96.33
C	113.15	43.77	0.00	***6.49***	127.63	47.19	67.43	56.96	***9.16***	121.60	***12.86***	***8.46***	117.76	71.91	110.40	104.15	111.70	129.54	119.29
D	118.51	49.81	***6.49***	0.00	131.76	52.46	73.29	63.15	***2.91***	126.14	***17.00***	***14.10***	123.40	78.12	116.49	110.12	117.61	135.04	124.88
F	48.74	97.16	127.63	131.76	0.00	94.33	103.64	104.00	133.45	***13.01***	116.12	122.39	93.50	102.39	84.53	67.12	112.67	127.16	114.43
G	76.44	***24.63***	47.19	52.46	94.33	0.00	***46.54***	40.63	54.65	86.79	36.54	40.49	89.93	50.97	78.87	68.14	87.74	107.92	96.29
H	66.18	***28.50***	67.43	73.29	103.64	46.54	0.00	48.47	76.19	92.48	63.31	59.56	95.78	52.17	77.05	50.84	87.27	111.21	100.48
K	82.85	35.12	56.96	63.15	104.00	40.63	48.47	0.00	65.25	95.09	51.99	52.79	64.52	***15.03***	56.12	66.16	55.48	75.65	64.95
M	120.95	52.56	***9.16***	***2.91***	133.45	54.65	76.19	65.25	0.00	128.03	***18.93***	***16.93***	125.09	80.24	118.58	112.73	119.44	136.56	126.47
N	***36.11***	88.21	121.60	126.14	***13.01***	86.79	92.48	95.09	128.03	0.00	110.35	115.87	86.43	92.81	75.01	54.19	103.75	119.67	106.86
O	103.41	36.93	***12.86***	***17.00***	116.12	***36.54***	63.31	51.99	***18.93***	110.35	0.00	***10.64***	110.30	66.79	102.73	95.68	106.40	124.56	113.64
P	105.96	36.06	***8.46***	***14.10***	122.39	40.49	59.56	52.79	***16.93***	115.87	***10.64***	0.00	114.18	67.54	105.48	96.85	108.11	126.94	116.39
Q	85.52	90.89	117.76	123.40	93.50	89.93	95.78	64.52	125.09	86.43	110.30	114.18	0.00	52.59	***23.13***	72.38	27.04	33.77	***21.86***
S	79.35	45.59	71.91	78.12	102.39	50.97	52.17	***15.03***	80.24	92.81	66.79	67.54	52.59	0.00	43.19	60.52	41.50	63.12	52.37
V	66.32	77.03	110.40	116.49	84.53	78.87	77.05	56.12	118.58	75.01	102.73	105.48	***23.13***	43.19	0.00	**50.49**	30.07	48.33	36.44
W	***23.96***	61.17	104.15	110.12	67.12	68.14	50.84	66.16	112.73	54.19	95.68	96.85	72.38	60.52	50.49	0.00	75.44	97.46	85.74
X	94.25	85.94	111.70	117.61	112.67	87.74	87.27	55.48	119.44	103.75	106.40	108.11	27.04	***41.50***	***30.07***	75.44	0.00	***24.21***	***15.60***
Y	114.60	108.03	129.54	135.04	127.16	107.92	111.21	75.65	136.56	119.67	124.56	126.94	33.77	63.12	48.33	97.46	***24.21***	0.00	***13.71***
Z	102.28	96.33	119.29	124.88	114.43	96.29	100.48	64.95	126.47	106.86	113.64	116.39	***21.86***	52.37	36.44	85.74	***15.60***	***13.71***	0.00

Table 1.5 Summaries of Zobler Main Soil Units Selection Results.

No.	MSU	Name	Accepted or Rejected	Comment
1	A	Acrisol	Accepted	Selected as an independent Custom Group
2	B	Cambisol	Accepted	Grouped with G to make a Custom Group
3	C	Chernozem	Accepted	Grouped with D and M to make a Custom Group
4	D	Podzoluvisol	Accepted	Grouped with C and M to make a Custom Group
5	E	Rendzina	**Rejected**	No Records in Zobler World Soil Dataset
6	F	Ferralsol	Accepted	Grouped with N to make a Custom Group
7	G	Gleysol	Accepted	Grouped with B to make a Custom Group
8	H	Phaeozem	Accepted	Selected as an independent Custom Group
9	I	Lithosol	**Rejected**	No Records in Zobler World Soil Dataset
10	J	Fluvisol	**Rejected**	Occur in more than two Koppen-Geiger Climate Zones
11	K	Kastanozem	Accepted	Grouped with S to make a Custom Group
12	L	Luvisol	**Rejected**	Occur in more than two Koppen-Geiger Climate Zones
13	M	Greyzem	Accepted	Grouped with C and D to make a Custom Group
14	N	Nitosol	Accepted	Grouped with F to make a Custom Group
15	O	Histosol	Accepted	Grouped with P to make a Custom Group
16	P	Podzol	Accepted	Grouped with O to make a Custom Group
17	Q	Arenosol	Accepted	Grouped with V to make a Custom Group
18	R	Regosol	**Rejected**	Occur in more than two Koppen-Geiger Climate Zones
19	S	Solonetz	Accepted	Grouped with K to make a Custom Group
20	T	Andosol	**Rejected**	Occur in more than two Koppen-Geiger Climate Zones
21	U	Ranker	**Rejected**	No Records in Zobler World Soil Dataset
22	V	Vertisol	Accepted	Grouped with Q to make a Custom Group
23	W	Planosol	Accepted	Selected as an independent Custom Group
24	X	Xerosol	Accepted	Grouped with Y and Z to make a Custom Group
25	Y	Yermosol	Accepted	Grouped with X and Z to make a Custom Group
26	Z	Solonchak	Accepted	Grouped with X and Y to make a Custom Group
27	Glacier/Ice	Glacier/Ice	**Rejected**	Not included in the study

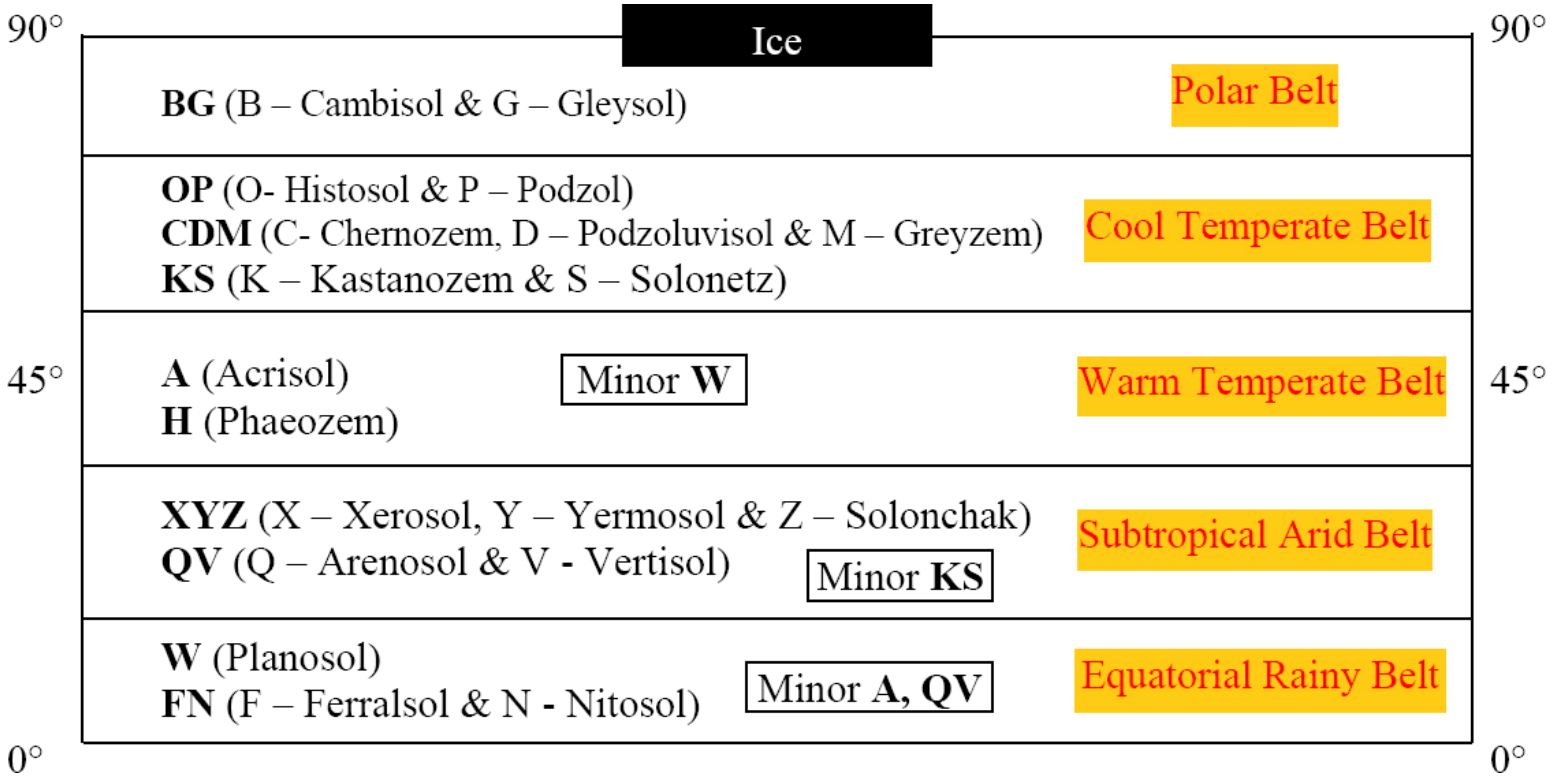

Figure 1.14 Schematic Latitudinal Distributions of Paleo-Soil Groups

In the first step of this procedure, the 'Zobler-LW dataset' was intersected with the Köppen-Geiger shapefiles (using the 'intersect tool of ArcGIS). From this intersection it became clear that some of the Zobler soil groups fell within discrete climatic zones and hence were acceptable for paleo-soil prediction and some of the Zobler soil groups were dispersed across many Köppen-Geiger climatic zones and hence were not suitable for use in this study. Only soils that fell predominantly in 2 adjacent climatic zones were accepted. The soil types that were spread across more than two climatic zones or were found in widely separated climatic zones were not used in this study. Exceptions that were made to this rule are described below.

In this section, we review the criteria used to accept or reject the Zobler soil types based on their climatic signature. The association between the Zobler soil types and the Köppen-Geiger climate zones are summarized in Table 1.3 and shown in the pie charts (Figure 1.10-13). Table 1.3 lists the percentage of each Zobler soil type in the five main Köppen-Geiger climatic zones. For example, 52.72% of all Acrisols occur in the Equatorial Rainy Belt (Zone A); 0.76% occurs in the Subtropical Arid Belt (Zone B); 44.99% occur in the Warm Temperate Belt (Zone C); 0.89% occurs in the Cool Temperate Belt (Zone D) and 0.63% occurs in the Polar Belt (Zone E). It is clear from this distribution that Acrisols develop in warm, wet climates.

There are 27 Zobler soil types. Of these, three have no mapped localities (E - Rendzinas, I - Lithosol and U - Rankers) in the downloaded Zobler World Soil dataset and the fourth (Ice/Glacier) was not considered in this study.

For a Zobler soil type to be accepted, 72% of the soil localities must occur within either a single Köppen-Geiger climatic zone or in two adjacent Köppen-Geiger climatic zones. Of the remaining 23 soil types, the following ten Zobler soil types fell predominantly in one Köppen-Geiger climatic zone: C (Chernozem), D (Podzoluvisol), F (Ferralsol), M (Greyzem), N (Nitosol), O (Histosol), P (Podzol), X (Xerosol), Y (Yermosol) and Z (Solonchak). An additional five Zobler soil types fell within two adjacent Köppen-Geiger climatic zones: B (Cambisol), G (Gleysol), H (Phaeozems), Q (Arenosol) and V (Vertisol). Another four Zobler soil types fell in either arid or

wet belts: A (Acrisol), K (Kastanozem), S (Solonetz) and W (Planosol). Only four of the Zobler soil types were rejected. They are J (Fluvisol), L (Luvisol), R (Regosol) and T (Andosol). These Zobler soil types have very dispersed geographic distributions and do not exhibit any climatic coherence. For a more detailed description of the climatic affinities of Zobler soil types see Table 1.3. The climatic affinities for each Zobler soil type are also shown as pie-charts in Figure 1.10-13.

Once the Zobler soil types that have strong climatic signatures were selected, we grouped soil types that fell in the same Köppen-Geiger climatic zone(s). The similarity was measured in a pair-wise comparison using the following 'distance' equation:

$$d = \sqrt{(A_x - A_y)^2 + (B_x - B_y)^2 + (C_x - C_y)^2 + (D_x - D_y)^2 + (E_x - E_y)^2}$$

Where, A, B, C, D and E are the Köppen-Geiger scores for each soil type (see Table 1.3); x and y are two different Zobler soil types and d is the 'Distance Score'.

The values of the Distance Score ranged from 2.91 to 136.56 (Table 1.4). Soils that occur in the same climatic zone had a low Distance score (for example, the Distance Score for Zobler soil types C and D, both of which occur in the Cool Temperate Belt, is 6.49). Soils from different climatic zones have a higher Distance Score (for example, the Distance Score for Zobler soil type C, occurring in the Cool Temperate Belt, and N, occurring predominantly in the Equatorial Rainy Belt, is 121.60). Soils that occur in the same climatic zones generally had a distance score of 10 or less. Grouping the soil types that occurred in the same Köppen-Geiger climatic zone reduced the number of soil groups from 23 to 10. Table 1.5 summarizes the results of this grouping procedure. The latitudinal distribution of the new paleo-soil groups, according to the Köppen-Geiger scheme, is shown in Figure 1.14. In the following section, we describe these new paleo-soil groups.

1.2.5.1 Paleo-soils found in the Equatorial Rainy Belt

The Equatorial Rainy Belt (Köppen-Geiger zone A) is represented by two soil groups: FN (Ferralsol-Nitosol) and W (Planosols). The modern geographic distribution of these paleo-

soil groups are shown in Figure 1.30A and 1.33A respectively. In the geological record, these groups of paleo-soils are often represented by laterites, bauxites and sometimes kaolinite.

The FN paleo-soil group is composed of Zobler soil types F (Ferralsols) and N (Nitosols). The Distance Score for these two soil types is 13.01 (Table 1.4) and hence, they are considered to have a similar climatic signature. Figure 1.30A illustrates the modern geographic distribution of the FN paleo-soil group. Both soil types are abundant in low latitudes and are characteristic of well-drained lowlands. Ferralsols are more abundant than Nitosols. In the northern hemisphere, the Nitosols develop poleward of the Ferralsols. In the geologic record, Ferralsols and Nitosols are often represented by laterites and bauxites.

The Zobler soil types A (Acrisol) and W (Planosols) do not occur in a single Köppen-Geiger climatic zone, but rather are found in two non-adjacent climatic zones (Equatorial Rainy Belt and the Warm Temperate Belt). The formation of these two soil types are probably controlled by high precipitation and warm temperatures. It is clear from Figure 1.20 (Temperature-Precipitation plot for Acrisols and Planosols) that Acrisols occur across a wide range of temperature and precipitation values. Acrisols and Planosols develop in similar temperature range, but Planosols are restricted to areas with less precipitation. Figure 1.32A and Figure 1.33A display the modern geographic distribution of A and W soil types respectively. It is clear from these figures that Planosols (W) are restricted to southern subtropical regions, while Acrisols (A) are found in both the northern and southern subtropical regions. Though there are similarities between these two paleo-soil groups, they have not been grouped together. In the geologic record, Acrisols (A) are represented by kaolinite while Planosols are represented by laterites (http://www.isric.org/ISRIC/webdocs/docs/major_soils_of_the_world/).

1.2.5.2 Paleo-soils found in the Subtropical Arid Belt

The Subtropical Arid Belt (Köppen-Geiger zone B) is represented by two major soil groups: XYZ (Xerosol-Yermosol-Solonchak) and QV (Arenosol-Vertisol). There are some localities with soil type KS (Kastanozem-Solonetz). The modern geographic distribution of these

paleo-soil groups are shown in Figure 1.34A and 1.31A. In the geological record, these groups of paleo-soils are often represented by evaporites and calcretes.

The XYZ paleo-soil group combines the Zobler soil types X (Xerosol), Y (Yermosol) and Z (Solonchaks). The Distance Score for these soil units indicates that they should be grouped into a single paleo-soil group (Table 1.4: X/Y – 24.21, Y/Z – 13.71 and X/Z – 15.60). These soil groups develop in the Subtropical Arid Belt (Köppen-Geiger zone B) (Figure 1.34) and have evaporitic characteristics. Yermosols (Y) are the most abundant and widespread Zobler soil type in this group. Yermosols occur in all modern desert regions (Sahara, Mojave, Atacama, Arabian, Simpson, Karakum, Taklamakan). Xerosols (X) surround the Yermosols and generally exist in slightly wetter, more poleward environments. Solonchaks (Z) are less numerous than either Yermosols or Xerosols and their geographic distribution overlaps with both the soil types. Yermosol often have substantial secondary accumulation of gypsum ($CaSO_4.2H_2O$). Solonchaks are characterized by accumulations of highly soluble salt within 30 cm (1 foot) of the land surface. In the geologic record the XYZ paleo-soil is represented by evaporites and calcretes.

The QV paleo-soil group is composed of Zobler soil types Q (Arenosol) and V (Vertisols). The Distance Score for these two soils types is 23.13 (Table 1.4). Figure 1.31A represents the modern geographic distribution of QV paleo-soil group. The Q and V soil types occur in climatic zones with significant diurnal and seasonal temperature variations. Compared to paleo-soil FN, the QV paleo-soil group more often occurs in subtropical latitudes, though the geographic distribution does overlap with the FN paleo-soil group near the Equator. This paleo-soil is often represented in the geologic record by laterites.

1.2.5.3 Paleo-soils found in the Warm Temperate Belt

The Warm Temperate Belt (Köppen-Geiger zone C) is represented by two major soil groups: A (Acrisol) and H (Phaeozems). There are also some locations with soil type W (Planosols). The modern geographic distribution of these paleo-soil groups are shown in Figure

1.32A, 1.36A and 1.33A respectively. In the geological record, these groups of paleo-soils are often represented by coal beds, peat deposits, laterites and sometimes by kaolinite. The occurrence of A and W was discussed in section 1.4.5.1.

The paleo-soil group H (Phaeozem) did not group with any other Zobler soil type. This distinctive soil group occurs only in warm temperate zones, characterized by seasonal high rainfall and warm temperature. The rather limited modern geographic distribution of paleo-soil H is shown in Figure 1.36A. Phaeozems are characterized by a humus-rich layer with abundant grass or deciduous forest vegetation (http://www.britannica.com/EBchecked/topic/708005/ Phaeozem). In geologic records Phaeozems are usually represented by temperate coals and peat deposits.

1.2.5.4 Paleo-soils found in the Cool Temperate Belt

The Cool Temperate Belt (Köppen-Geiger zone D) is represented by three major soil groups: CDM (Chernozem-Podzoluvisol-Greyzem) and OP (Histosol-Podzol) and KS (Kastanozem-Solonetz). The modern geographic distributions of these three paleo-soil groups (KS, CDM and OP) are shown in Figure 1.37A, 1.38A and 1.35A. In the geological record, these groups of paleo-soils are often represented by peat, lignite and coal beds.

The CDM paleo-soil combines Zobler soil types C (Chernozem), D (Podzoluvisols) and M (Greyzem). The Distance Score for these soil units are: C/D – 6.9, D/M – 2.91 and C/M – 9.16 (Table 1.4). We can confidently infer that these soil types can be grouped together because Distance Scores between these soil types are low. As illustrated in Figure 1.37A, all of these soil types are restricted to the northern hemisphere Cool Temperate Belt. The absence of CDM paleo-soil group in the southern hemisphere is due to the fact that there are no land areas between 50°-65°S latitude. It is also clear from the figure that, Podzoluvisols (D) are developed in cool climates closer to the pole. Greyzems (M) are less numerous than either Chernozems or Podzoluvisols and their geographic distribution overlaps with both these soil types. These cool temperate soil types represent the temperate rain forests and typically have greater than 10%

organic content. In the geologic record, this paleo-soil group is associated with peat, lignite and coal.

The KS paleo-soil group is composed of Zobler soil types K (Kastanozem) and S (Solonetz). The Distance Score between K and S is 15.03 (Table 1.4). The Kastanozem and Solonetz Zobler soil types do not occur in a single Köppen-Geiger climatic zone, but rather are found in two non-adjacent climatic zones (Subtropical Arid Belt and Cool Temperate Belt). The formation of these two soil types are probably controlled by arid or seasonally arid climatic conditions. As we see in Figure 1.35A, Kastanozems occur primarily in North America and Central Eurasia, whereas Solonetz are found almost exclusively in Australia. Solonetz also tend to occur in cooler climates than Kastanozems. It is not clear how the KS (Kastanozem-Solonetz) paleo-soil group is presented in the geological record.

The OP paleo-soil group, composed of Zobler soil types O (Histosols) and P (Podzol), has a Distance Score of 10.64 (Table 1.4). Figure 1.38A represents the modern geographic distribution of the OP paleo-soil group. Compared to the geographic distribution of CDM, Histosols and Podzols both occur in the cooler regions closer to the pole. Similar to the CDM, OP is organic rich and is represented in the geologic record as coal beds.

1.2.5.5 Paleo-soils found in the Polar Belt

The Polar Belt (Köppen-Geiger zone E) is represented by one soil group: BG (Cambisols- Gleysols). The modern geographic distribution of this paleo-soil group is shown in Figure 1.39A.

The BG paleo-soil group combines Zobler soil types B (Cambisols) and G (Gleysols). They have a Distance Score of 24.63 and were provisionally combined in this study. Gleysol (G) typically occurs in association with the Cambisol (B) but it tends to occur poleward of Cambisol. Geographically they occur near the northern pole and at high altitudes. The Cambisol and Gleysol are ‘tundra’ soils that are not often represented in the geological record. Glacial objects

such as tills and glacial features such as moraines, eskers and drumlins may be associated with BG paleo-soil group.

In summary, ten paleo-soil groups have been defined and I will use these paleo-soil groups to predict the distribution of ancient soils. These ten paleo-soil groups and their equivalent Zobler soil type name(s) are listed below:

1. Paleo-soil BG – Cambisols (B) and Gleysols (G)
2. Paleo-soil CDM – Chernozems (C), Podzoluvisols (D) and Greyzems (M)
3. Paleo-soil OP – Histosols (O) and Podzols (P)
4. Paleo-soil KS – Kastanozems (K) and Solonetz (S)
5. Paleo-soil H – Phaeozems (H)
6. Paleo-soil A – Acrisols (A)
7. Paleo-soil QV – Arenosols (Q) and Vertisols (V)
8. Paleo-soil XYZ – Xerosols (X), Yermosols (Y) and Solonchaks (Z)
9. Paleo-soil FN – Ferralsols (F) and Nitosols (N)
10. Paleo-soil W – Planosols (W)

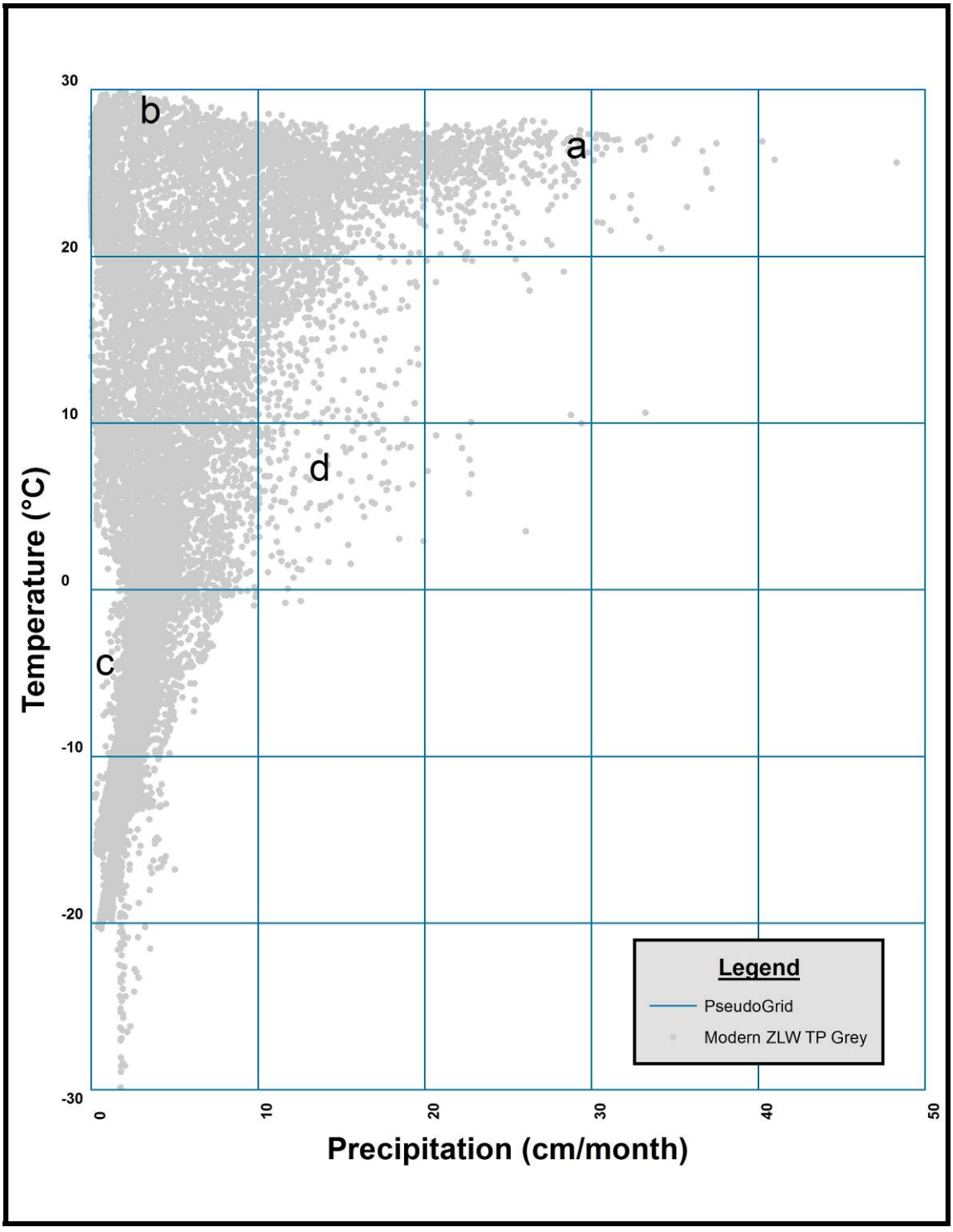

Figure 1.15 Modern Temperature-Precipitation Plot

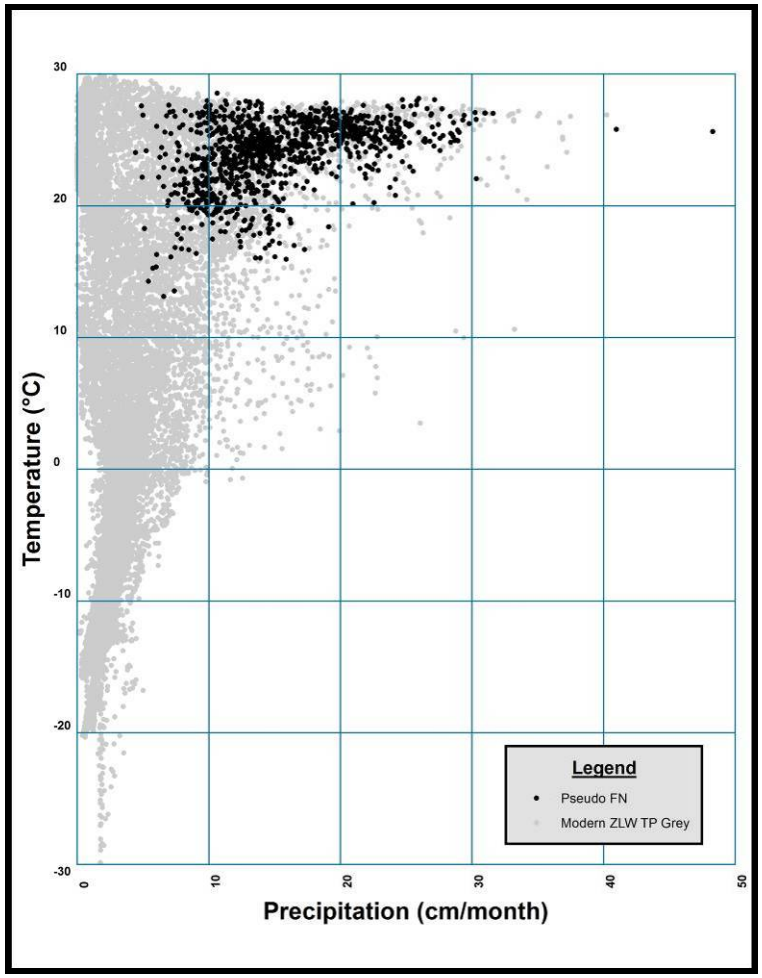

Figure 1.16 Temperature-Precipitation Plot for Paleo-soil FN

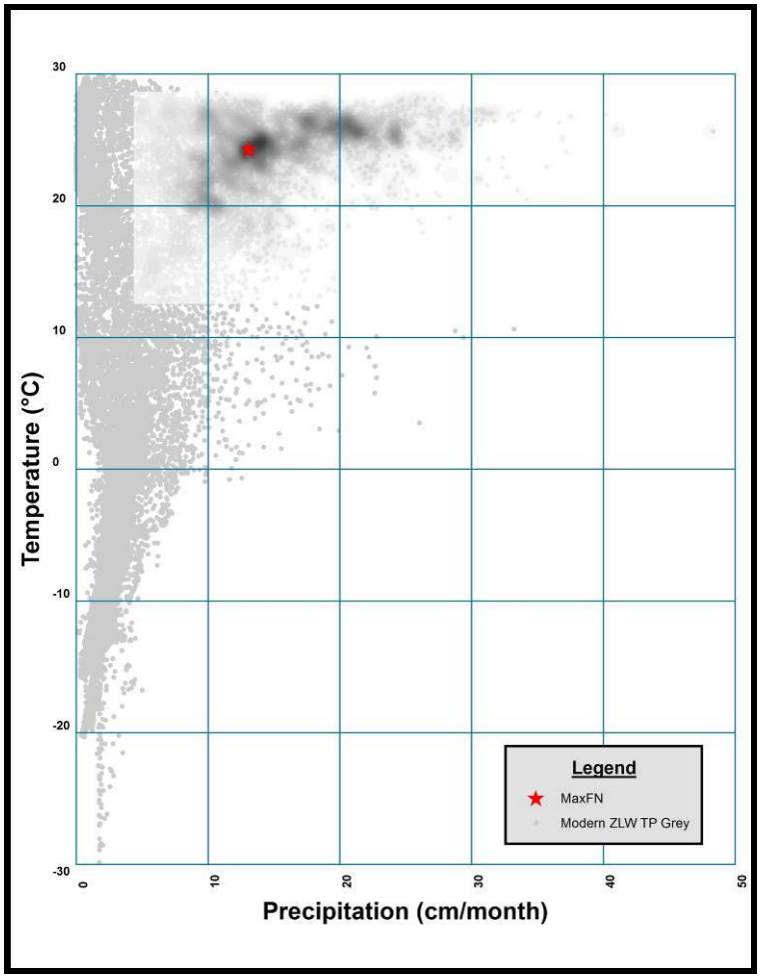

Figure 1.17 Density Raster for Paleo-soil FN

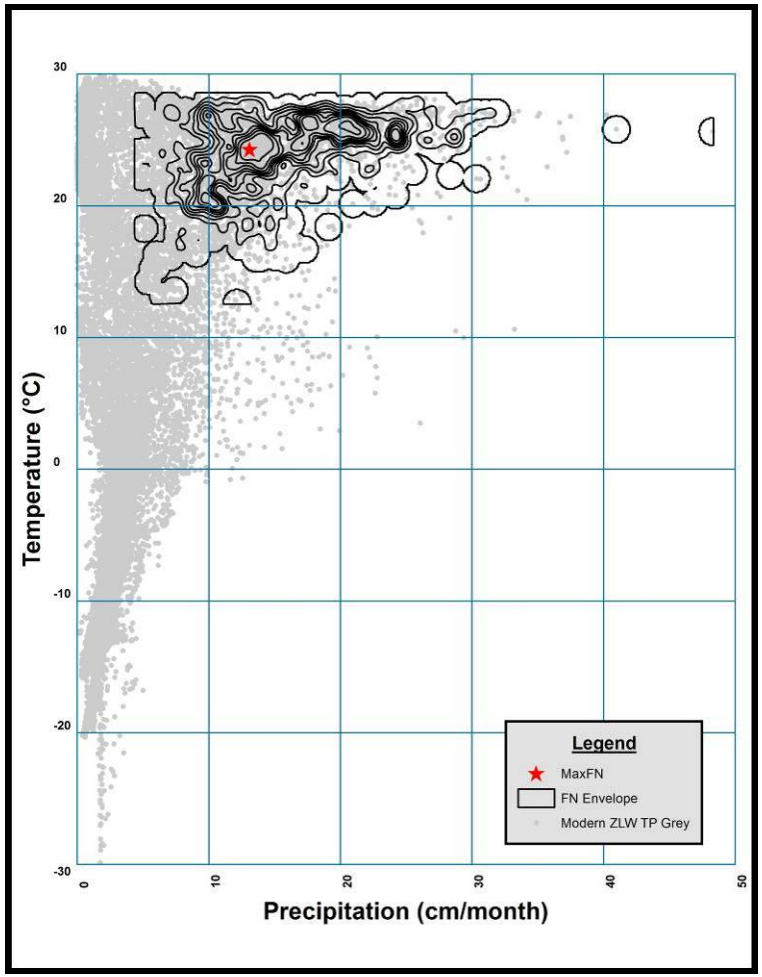

Figure 1.18 Envelope for Paleo-soil FN

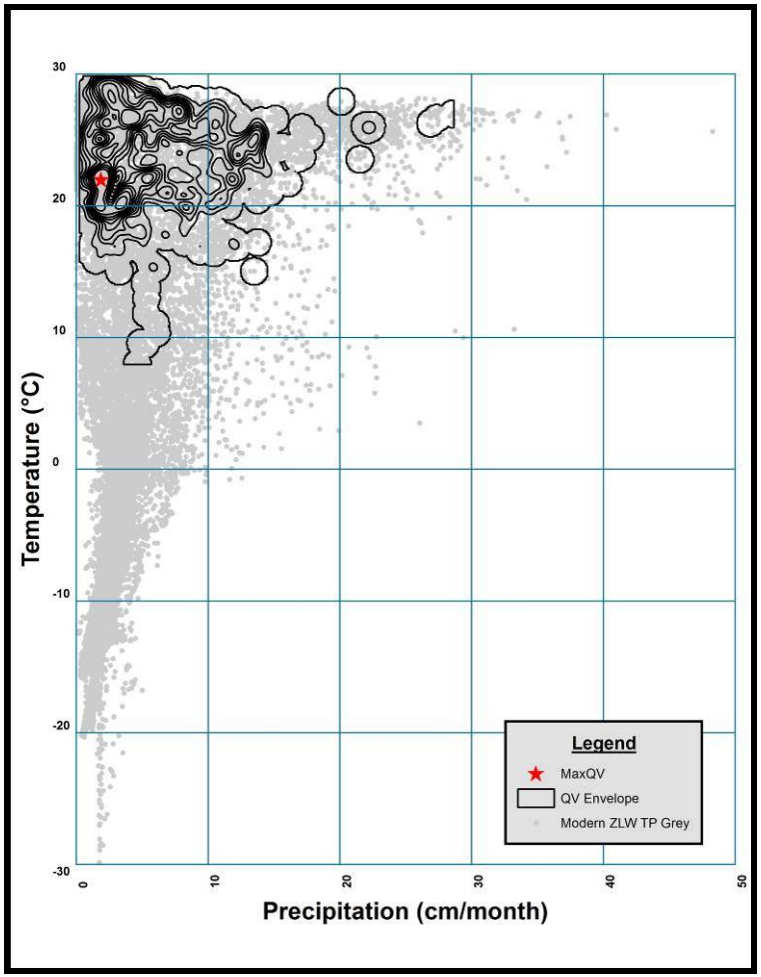

Figure 1.19 Envelope for Paleo-soil QV

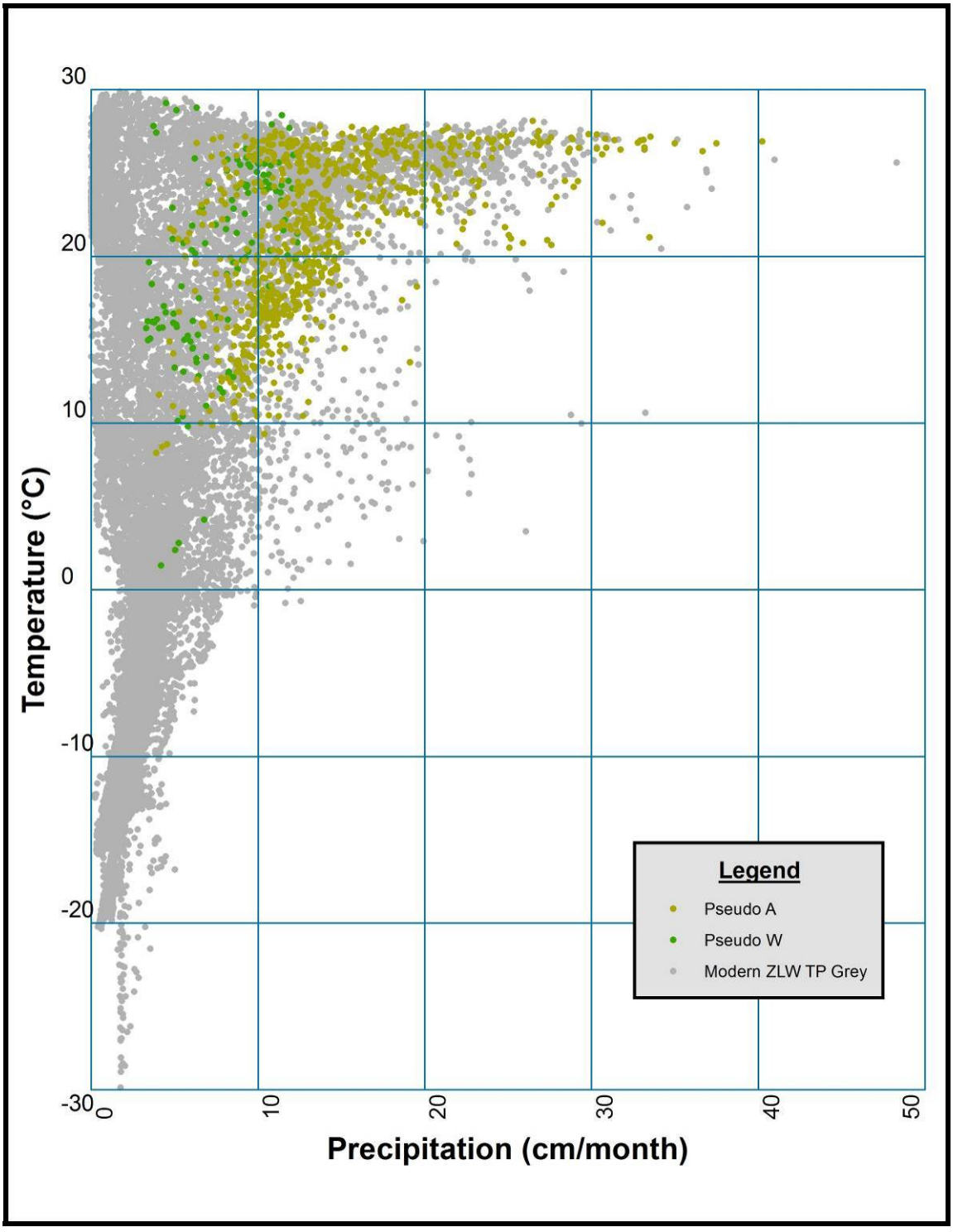

Figure 1.20 Temperature Precipitation Plot for Acrisol (A) and Planosol (W)

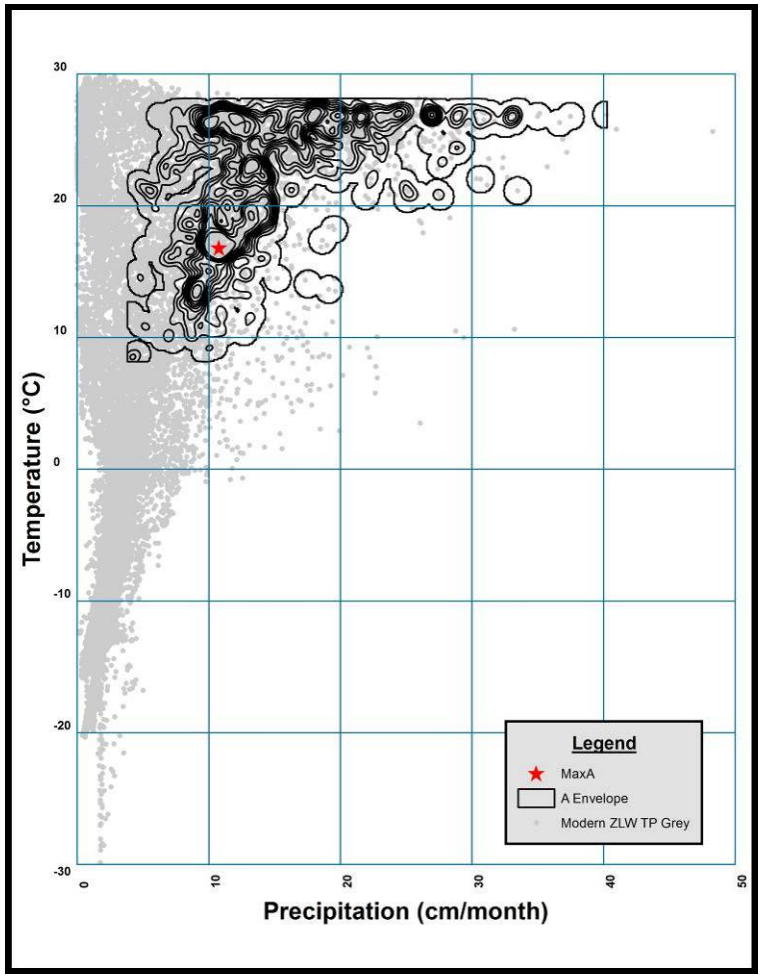

Figure 1.21 Envelope for Paleo-soil A

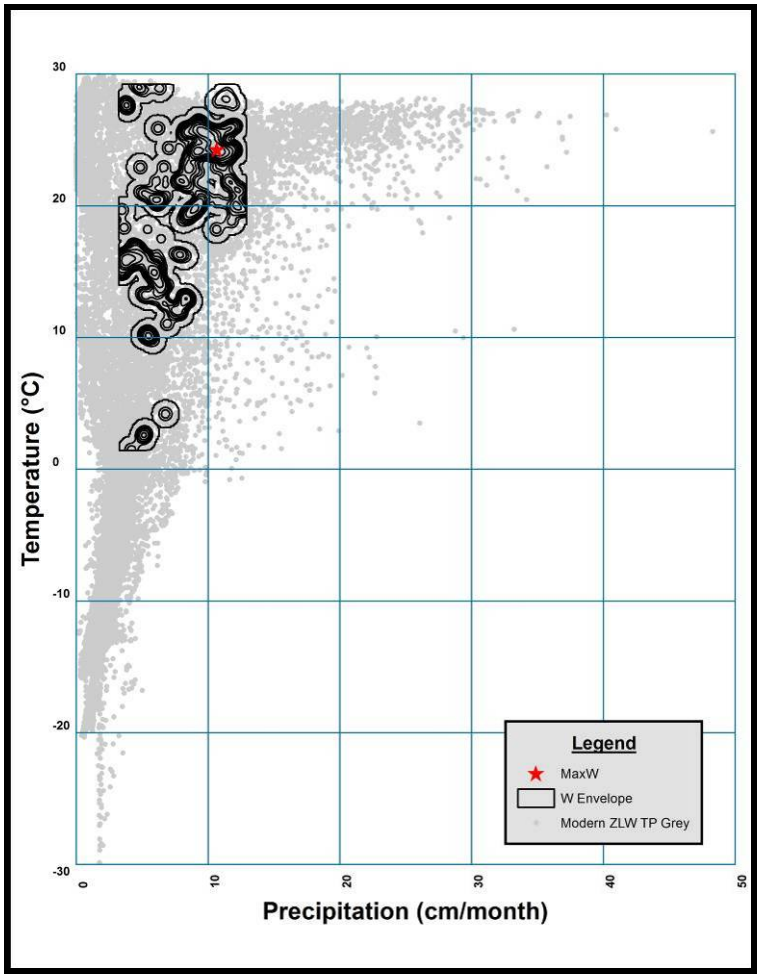

Figure 1.22 Envelope for Paleo-soil W

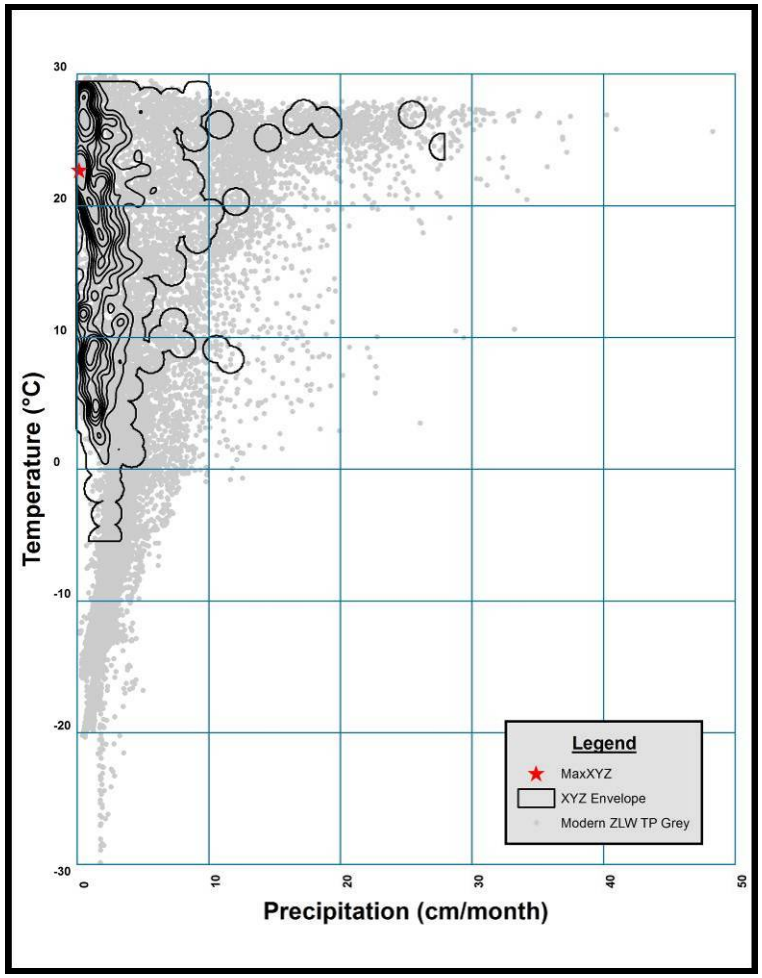

Figure 1.23 Envelope for Paleo-soil XYZ

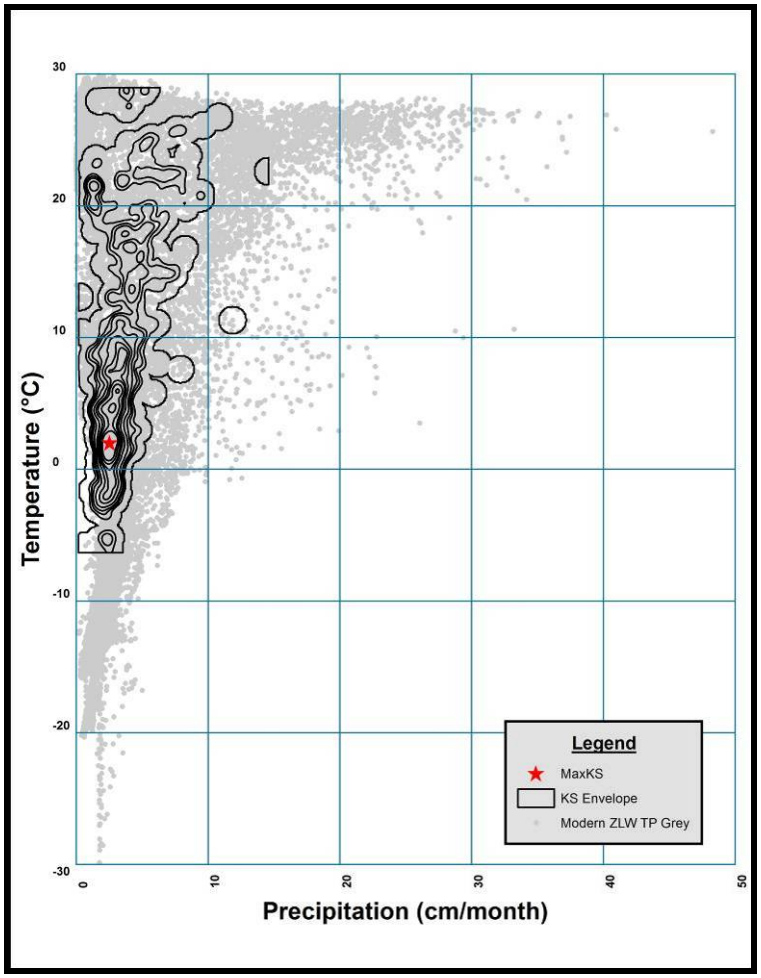

Figure 1.24 Envelope for Paleo-soil KS

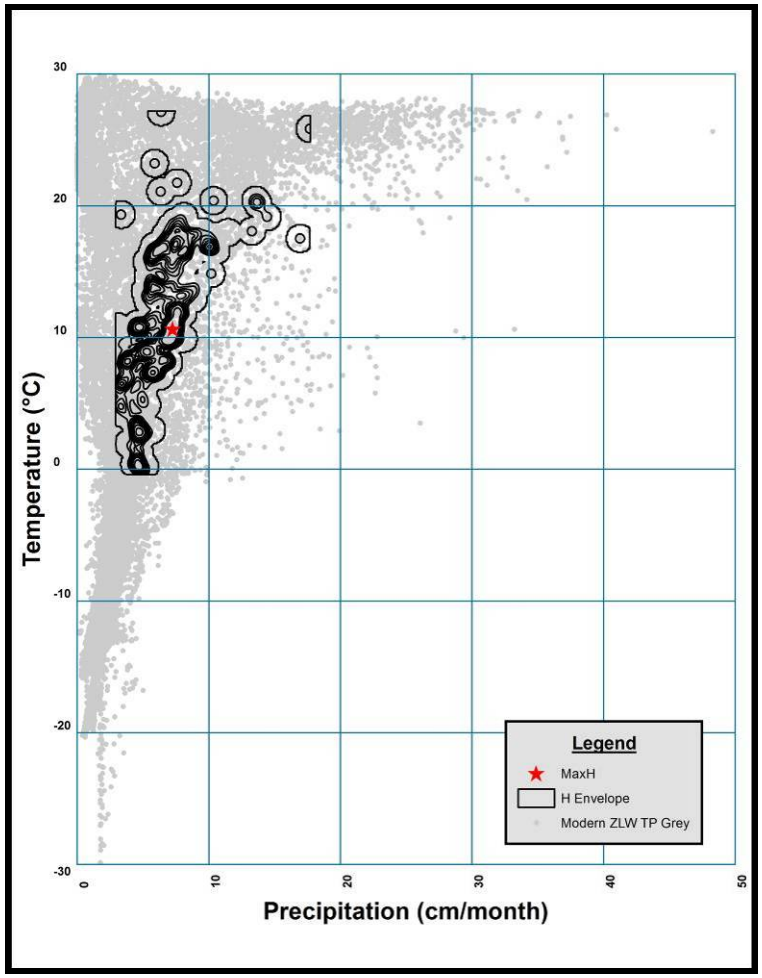

Figure 1.25 Envelope for Paleo-soil H

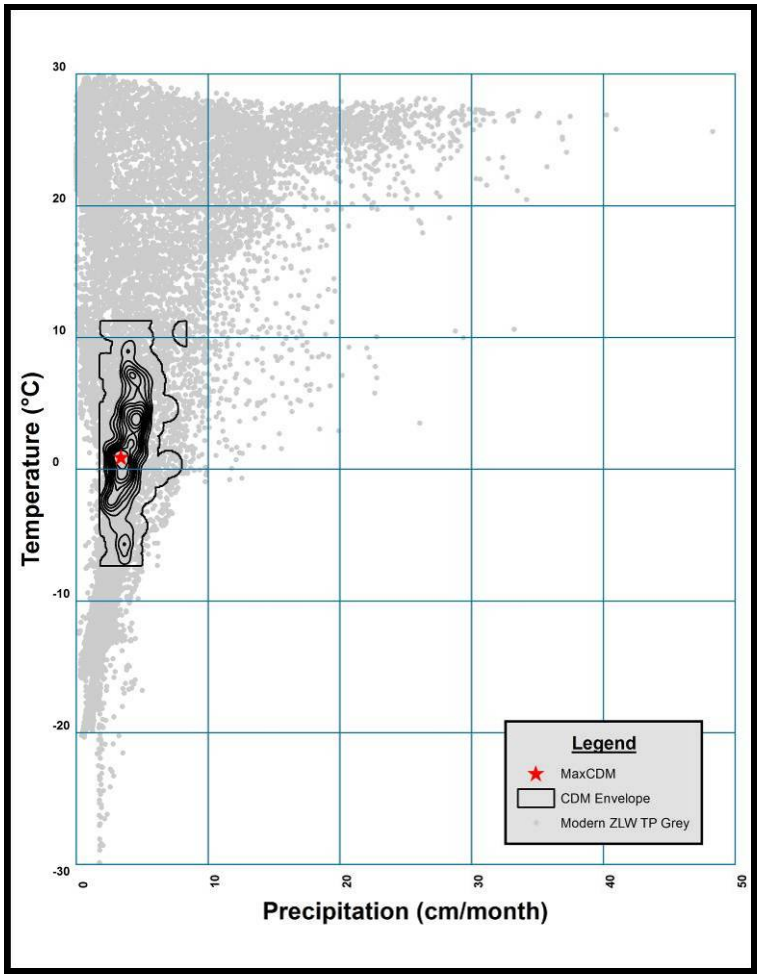

Figure 1.26 Envelope for Paleo-soil CDM

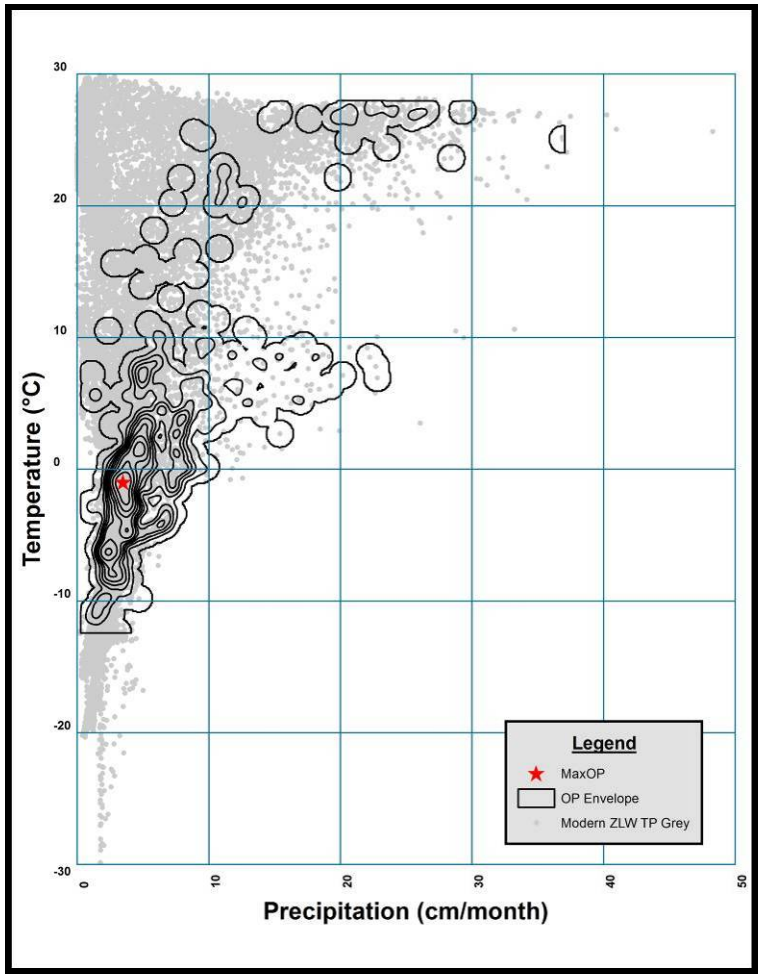

Figure 1.27 Envelope for Paleo-soil OP

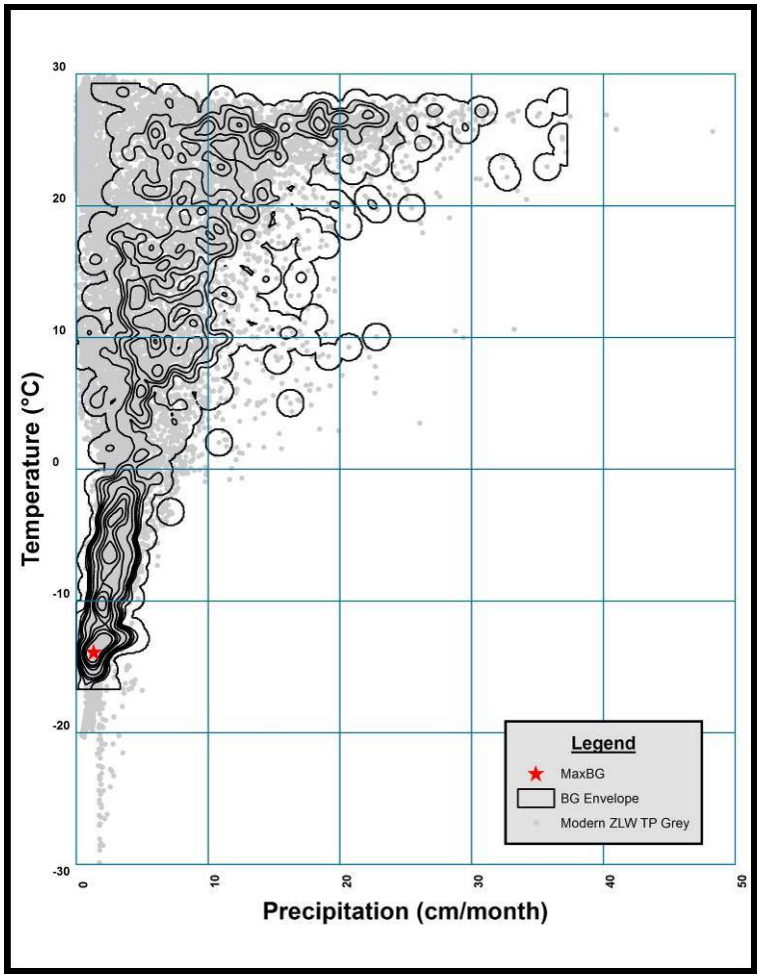

Figure 1.28 Envelope for Paleo-soil BG

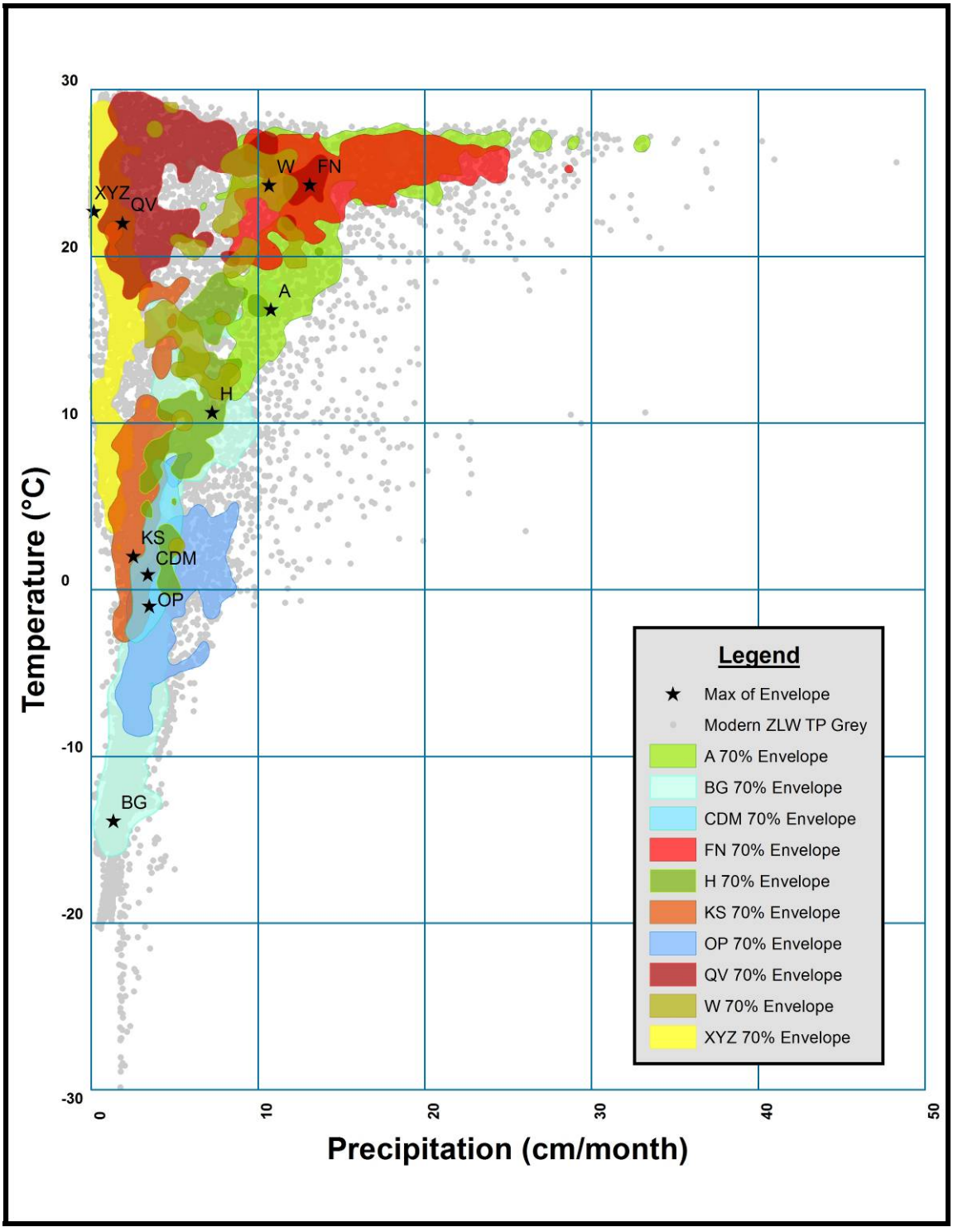

Figure 1.29 Envelopes for All Ten Paleo-Soil Groups

1.2.6 Preparation of Temperature-Precipitation Climate Envelopes (⑤ Figure 1.1)

1.2.6.1 Introduction

Soil formation is primarily governed by climatic conditions (Retallack, 1990). The most important theme of this work is that these climatic conditions can be described by two variables: mean annual temperature (MAT) and mean annual precipitation (MAP). Hence, for the ten paleo-soil groups it is important to characterize their temperature-precipitation ranges.

Figure 1.15 is a bi-variate plot of the mean annual temperature (MAT) and mean annual precipitation (MAP) for all Zobler soil localities (Zobler 1999). The MAT and MAP values are taken from Legates and Willmott (1990a, b) temperature precipitation database. In other words, each point on the plot represents the temperature and precipitation at a 1°x1° latitude-longitude location on the globe for a particular soil type. Temperature is plotted on vertical axis (°C), while precipitation is plotted on horizontal axis (cm/month). The highest temperature in this dataset is 29.90°C while the lowest temperature is -29.86°C. The highest precipitation is 48.29 cm/month (~ 19 inches/month) and the lowest value of precipitation is 0 cm/month.

The plot has a very distinctive triangular shape. It is extremely narrow at low temperatures (-30°C and -20°C), and starts to widen as temperature increases (-20°C ~ -10°C). In these cold climatic conditions precipitation is very reduced (< 5 cm/month). Precipitation gradually increases as temperature increases (~0.28 cm/month/°C). Above 15°C, the precipitation increases rapidly with rising temperatures (~1.33 cm/month/°C).

Though the overall shape of the temperature-precipitation plot is triangular, there are several features worth mentioning. For example, the highest precipitation values (> 25 cm/month) are not necessarily associated with the highest temperatures (> 28°C) (Figure 1.15a). Maximum precipitation tends to occur in the temperature range 23°C to 28°C. The highest temperature occurs in the Subtropical Arid Belt (deserts) where precipitation is absent (Figure 1.15b). Also, between -15°C and 5°C there is a gap in the precipitation dataset (Figure

1.15c). At these temperatures, near the freezing point of water, there is no precipitation less than 2 cm/month. Finally, between 0-20°C temperature and 10-20 cm/month precipitation, there is a widely scattered population of data points (Figure 1.15d). These points do not appear to be connected with any particular soil type or geographic location.

1.2.6.2 Defining Paleo-soil Temperature-Precipitation Climate Envelopes: An Example

Figure 1.16 plots the temperature-precipitation distribution for the FN paleo-soil type (black dots). It is clear from the figure that this paleo-soil group occurs in areas with high temperature and medium to high precipitation. Though the temperature range for the FN paleo-soil is 28.55° - 12.61°C and the precipitation range is 48.29 - 4.43 cm/month, the majority of the FN paleo-soils points occur between 22° - 28°C and 10 – 25 cm/month.

The next step in the analysis was to identify the region with highest density of FN paleo-soil type occurrences. Spatial Analyst (ArcGIS) was used to produce a density raster (Figure 1.17). This raster clearly shows that the greatest density of the FN paleo-soil type (Table 1.17, marked with red ★ in Figure 1.17 and 1.18) occurs near 24.5°C and 13.5 cm/month. A set of contours representing the density raster was created (Figure 1.18) using the 'Hawth's Percent Volume Contour' (PVC, http://www.spatialecology.com/htools/ pctvolcontour.php) technique. The 100% contour outlines all the FN data points; the 90% contour includes 90% of all FN data points; 80% contour includes 80% of all FN data points and so on. As shown in Figure 1.18 the densest part of FN paleo-soil type distribution is represented by thickest cluster of contours near the center of the plot. This cluster represents highest probability for the occurrence of the FN paleo-soil type. Detailed descriptions of how the percent volume contours were produced are described in detail in Appendix B.

Following the work of Moore et al. (2007), we have used the percent volume contours to build the "Temperature-Precipitation Climate Envelopes" that characterize the temperature-precipitation values at which different paleo-soils are most likely to occur. The same technique has been used in ecological studies to describe the range of environmental conditions that

characterize a species' habitat or niche (Walker and Cocks, 1991). In this study we have adopted the same concept to create "Climate Envelopes" that describe the temperature-precipitation conditions that characterize environments where different paleo-soil types form.

1.2.6.3 Climate Envelopes for Different Paleo-soil Types

In this section we describe the climate envelopes for the ten paleo-soil types (Figure 1.19 -1.28). Figure 1.29 is a summary plot that combines the climate envelopes for all ten paleo-soil types.

As described in the previous section, Figure 1.18 plots the temperature-precipitation climate envelope for the FN paleo-soil type. The FN paleo-soil type is well populated with 1090 localities worldwide (Table 1.6). Though the FN temperature-precipitation climate envelope covers a wide range of temperature and precipitation, there is a good cluster near 24°C and 13 cm/month (Table 1.17, marked with red ★ in Figure 1.18).

In Figure 1.29 it is clear that the range of temperature and precipitation for the FN paleo-soil type overlaps with the A and W paleo-soil types. However, the maximum density cluster for paleo-soil type FN is distinct from the peak of A and W paleo-soil types.

Paleo-soil QV (N = 890, Table 1.6 and Figure 1.19) has a broad envelope with a relatively wide distribution along the precipitation axis. Though the temperature range for this group is 8.02 -29.82°C and the precipitation range is 0.31-28.58 cm/month (Table 1.6), most of the points are found within the 0.31-3.30 cm/month precipitation range. The densest cluster for the paleo-soil type QV occurs near the temperature-precipitation values of 22°C and 2 cm/month (Table 1.7, marked with red ★ in Figure 1.19).

As evident from Figure 1.29, the range of temperature and precipitation for the QV paleo-soil type overlaps significantly with XYZ. The maximum density cluster for QV is close to the peak for paleo-soil type XYZ.

Paleo-soil type A (N = 789, Table 1.6 and Figure 1.21) occurs over a wide range of temperatures (8.23° - 28.13°C) and precipitation values (3.90 - 40.23 cm/month, Table 1.6). As

a consequence, the data are more scattered and the density contours are more dispersed. The majority of the points in this group lie within a precipitation range of 7.5 - 27.2 cm/month and temperature range of 12° - 28.2°C. The densest cluster of temperature-precipitation values for the A paleo-soil type occurs near 17°C and11 cm/month (Table 1.17, marked with red ★ in Figure 1.21).

From Figure 1.29 it is clear that the climate envelope for the A paleo-soil type overlaps significantly with the climate envelopes of three other paleo-soil types (around 50% with FN, slightly with W and H). However, the maximum density cluster for paleo-soil type A occurs at cooler temperatures and is distinct from the peaks of FN, W and H paleo-soil types.

Paleo-soil W is the least abundant paleo-soil type (N = 129, Table 1.6, Figure 1.22). Though the actual temperature range is 1.47° - 29.22°C, most of the points are found within a temperature range of 9° - 26°C (Table 1.6). The precipitation range for this group is 3.28 - 12.89 cm/month. The densest cluster for this paleo-soil type W occurs near 24°C and 10.5 cm/month (Table 1.17, marked with red ★ in Figure 1.22).

As evident from Figure 1.29, the range of temperature and precipitation for the W paleo-soil type overlaps the range of temperature and precipitation of the FN and A paleo-soil types. The maximum density cluster of paleo-soil W is close to the peak of FN paleo-soil type.

Paleo-soil XYZ is a very tight group (N = 1918, Table 1.6, Figure 1.23) that occurs at high temperatures and very low precipitation. Though temperatures range between -5° - 30°C and precipitation ranges between 0 - 27.82 cm/month, almost 96% of the points have a precipitation values less than 5 cm/month (Table 1.6). The densest cluster of temperature-precipitation values for the XYZ paleo-soil type occurs near 22.5°C and zero precipitation (Table 1.17, marked with red ★ in figure 1.23).

From Figure 1.29 it is clear that at high temperatures the XYZ climate envelope overlaps with QV paleo-soil climate envelope (around 40%) and at low temperature it slightly

overlaps with KS paleo-soil climate envelope. However, the maximum density cluster for paleo-soil type XYZ is distinct from the peak of these overlapping paleo-soil types.

Paleo-soil KS (N = 664, Table 1.6, Figure 1.24) is another moderately tight group. The temperature range is -6.28° - 28.90°C and precipitation range is 0.25 - 14.56 cm/month. But more than 70% of all KS paleo-soil points have a temperature range of -2.5° – 12°C and 0 - 7cm/month precipitation range. The densest cluster for the KS paleo-soil type occurs near the temperature-precipitation value of 2°C and 2.5 cm/month (Table 1.7, marked with red ★ in figure 1.24).

As evident from Figure 1.29, the climate envelope for the KS paleo-soil type overlaps with four other paleo-soil climate envelopes (moderately with BG, CDM and XYZ, slightly with OP). The maximum density cluster for the KS paleo-soil type is close to the peaks of CDM and OP, but is very distinct from the peaks of the XYZ and BG paleo-soil types.

Paleo-soil group H is the second least abundant paleo-soil type (N = 161, Table 1.6, Figure 1.25). Consequently, this paleo-soil type has a poorly defined climate envelope characterized by a wide range of temperature (-0.35° - 27.12°C) and precipitation values (2.97 - 17.68 cm/month). However, more than 90% of the points fall within a narrow temperature (-0.35° - 20°C) and precipitation (2 - 11 cm/month) range. The densest cluster of temperature-precipitation values for the H paleo-soil type occurs near 10.5°C and 7 cm/month (Table 1.7, marked with red ★in Figure 1.25).

The temperatures that characterize H paleo-soil climate envelope lie (Figure 1.29) between the high temperature paleo-soil types (FN, W, QV and XYZ) and the low temperature paleo-soil types (KS, CDM, OP and BG). Though, the climate envelope of the H paleo-soil type overlaps slightly with the climate envelopes of nearly all the other paleo-soil types, the maximum density cluster is very distinct.

The CDM paleo-soil group (N = 722, Table 1.6, Figure 1.26) has the most distinct and compact climatic envelope of all the ten paleo-soil groups described here. The temperature and

precipitation range for this group is -7.30° – 11.27°C and 1.79 - 8.37 cm/month. The densest cluster for the paleo-soil type CDM occurs near the temperature-precipitation value of 1°C and 3.5 cm/month (Table 1.7, marked with red ★in Figure 1.26).

As evident from Figure 1.29, the range of temperature and precipitation for the CDM paleo-soil type overlaps with the climate envelopes of three other paleo-soil types (about 50% with BG, OP and KS). Though the maximum density cluster for the CDM paleo-soil type is close to the peaks of KS and OP, it occurs at lower temperatures than KS peak and higher temperatures than OP peak. The peak of the CDM paleo-soil type is distinct from that of BG.

The climate envelope of OP paleo-soil group (N = 1088, Table 1.6, Figure 1.27) is similar to the climate envelope of CDM paleo-soil type, but includes higher precipitation values. The actual temperature and precipitation range of this group is -12° – 27.88°C and 0.35 - 36.91 cm/month, but more than 87% of the points are found within a temperature range of -9° – 9°C and a precipitation range of 1 – 10 cm/month. The densest cluster of temperature-precipitation values for the OP paleo-soil type occurs near -1°C and almost 3.5 cm/month (Table 1.7, marked with red ★ in Figure 1.27).

From Figure 1.29 it is clear that the range of temperature and precipitation for the OP paleo-soil type overlaps with three other paleo-soil types (around 40% with both BG and CDM, and around 20% with KS). However, the maximum density cluster for paleo-soil type OP, though close to that of CDM and KS, occurs at a lower temperature. The OP density maximum is widely separated from the peak of BG paleo-soil type.

Of all of the paleo-soil climate envelopes the BG paleo-soil climate envelope (N = 2155, Table 1.6, Figure 1.28) is the most problematic. It has the widest range of temperatures (-16.61° – 29.19°C) and the widest range of precipitation values (0.09-37.21 cm/month). The densest cluster of temperature-precipitation values for the BG paleo-soil type occurs near -14°C and almost 1.5 cm/month (Table 1.7, marked with red ★ in figure 1.28).

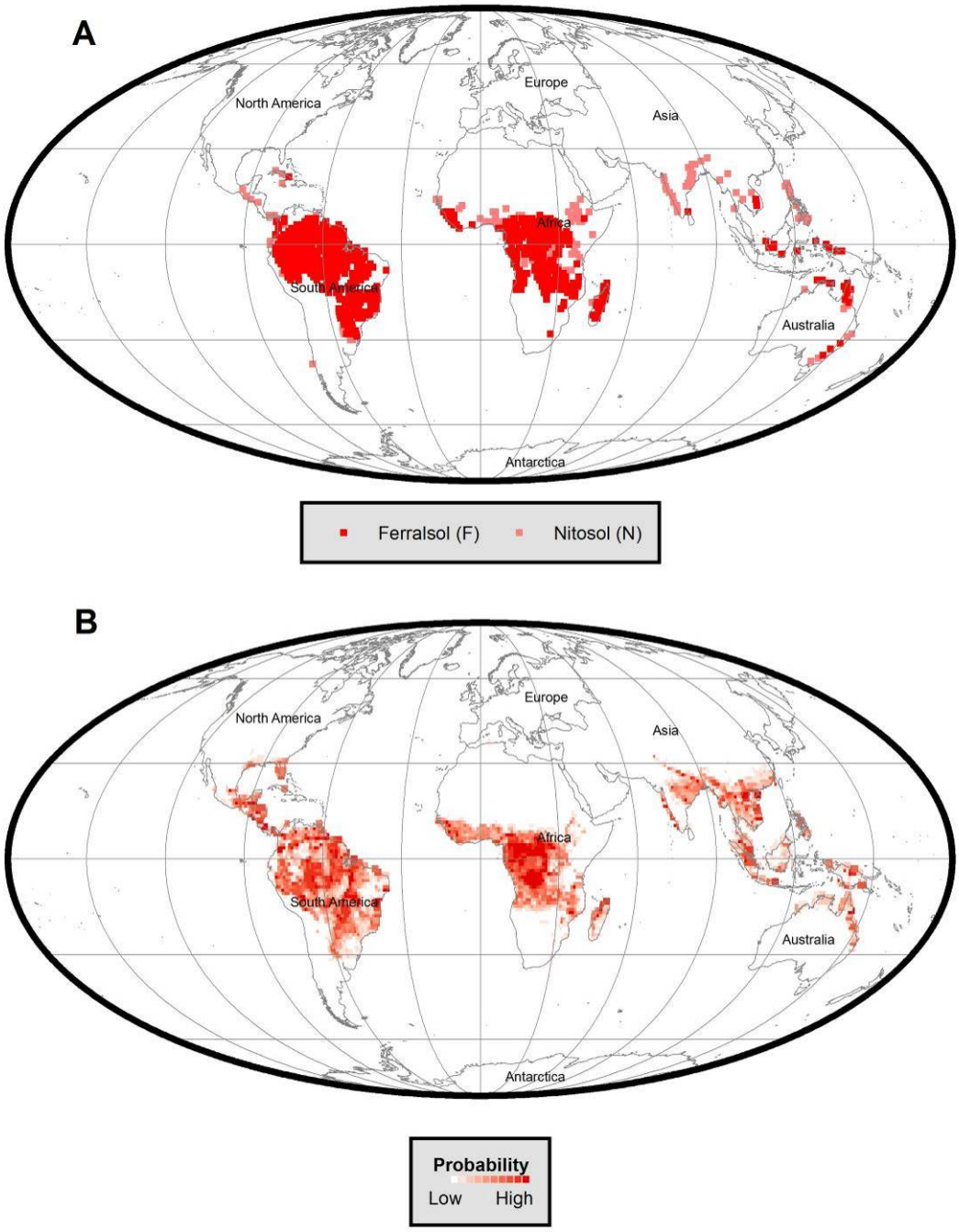

Figure 1.30 A. Actual Modern Geographic Distribution of Paleo-soil FN, B. Predicted Modern Geographic Distribution of Paleo-soil FN Using Paleo-soil Envelope

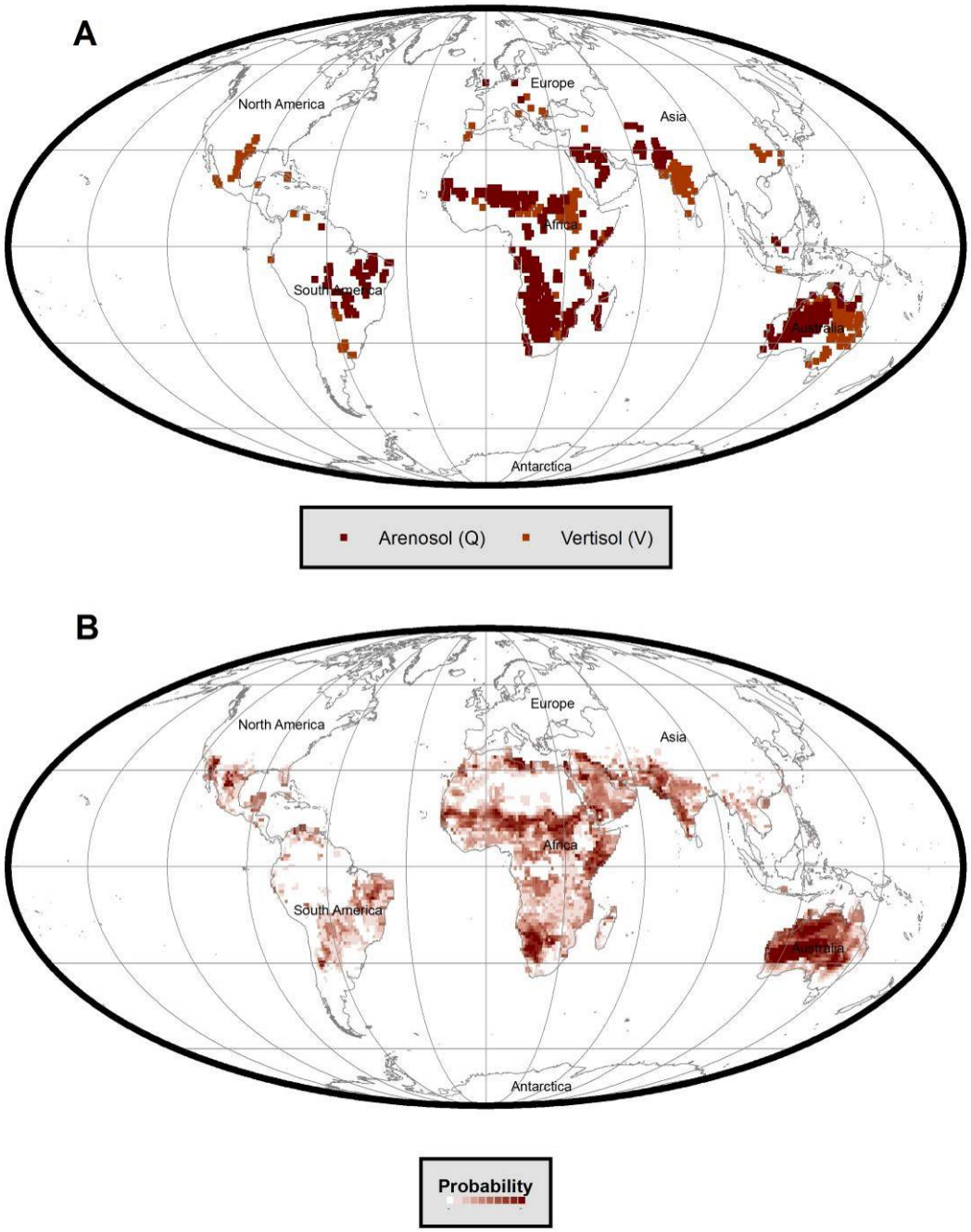

Figure 1.31 A. Actual Modern Geographic Distribution of Paleo-soil QV, B. Predicted Modern Geographic Distribution of Paleo-soil QV Using Paleo-soil Envelope

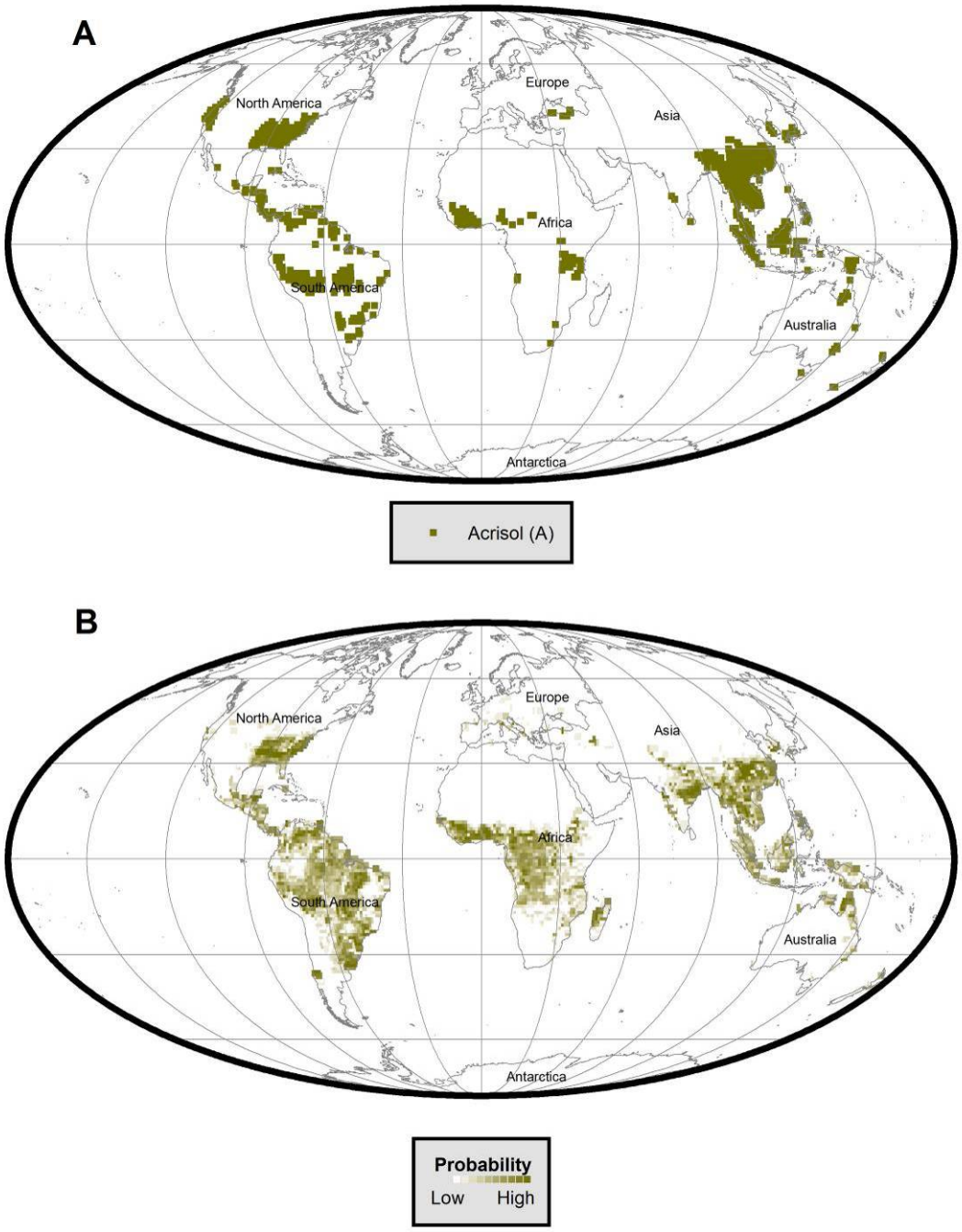

Figure 1.32 A. Actual Modern Geographic Distribution of Paleo-soil A, B. Predicted Modern Geographic Distribution of Paleo-soil A Using Paleo-soil Envelope

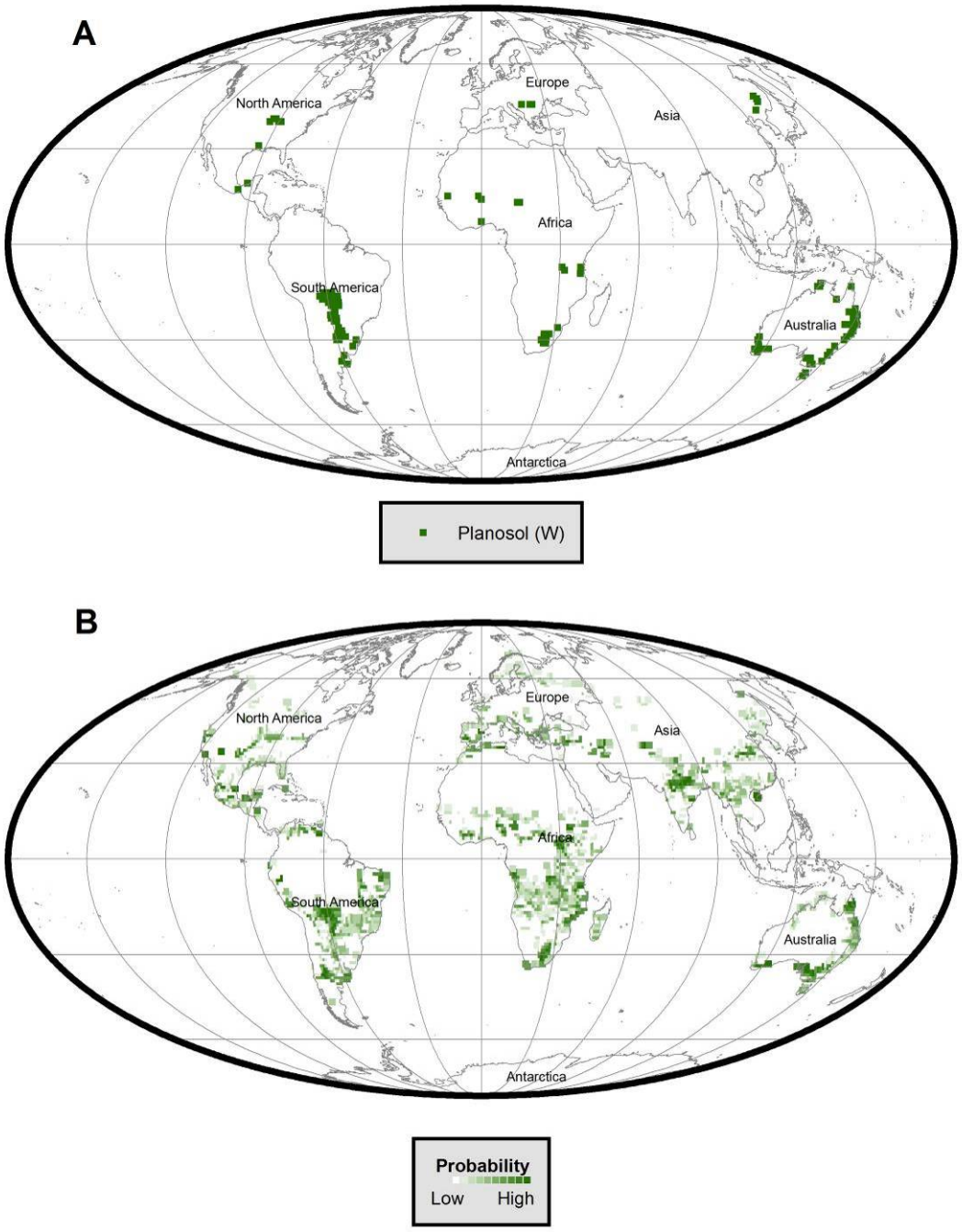

Figure 1.33 A. Actual Modern Geographic Distribution of Paleo-soil W, B. Predicted Modern Geographic Distribution of Paleo-soil W Using Paleo-soil Envelope

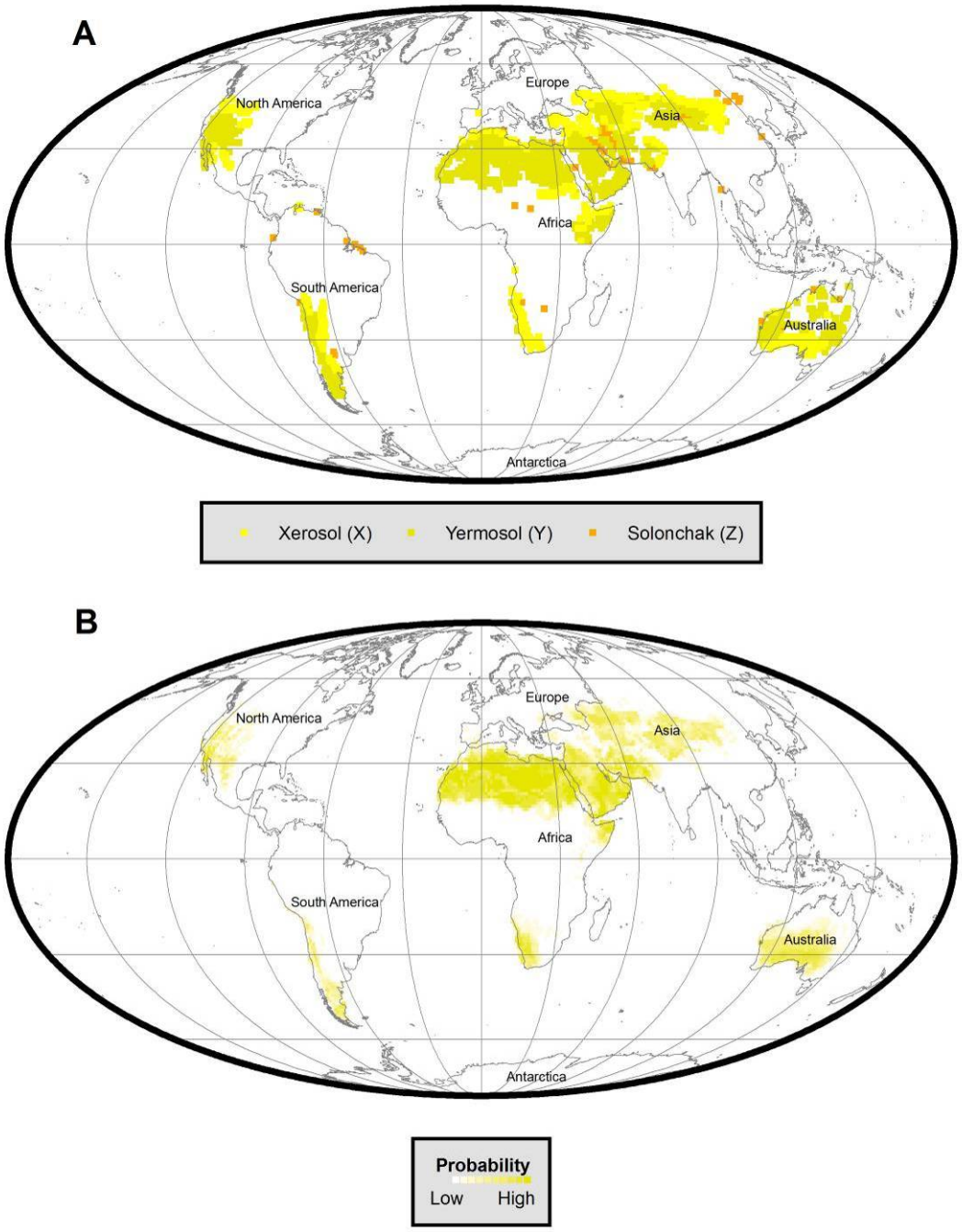

Figure 1.34 A. Actual Modern Geographic Distribution of Paleo-soil XYZ, B. Predicted Modern Geographic Distribution of Paleo-soil XYZ Using Paleo-soil Envelope

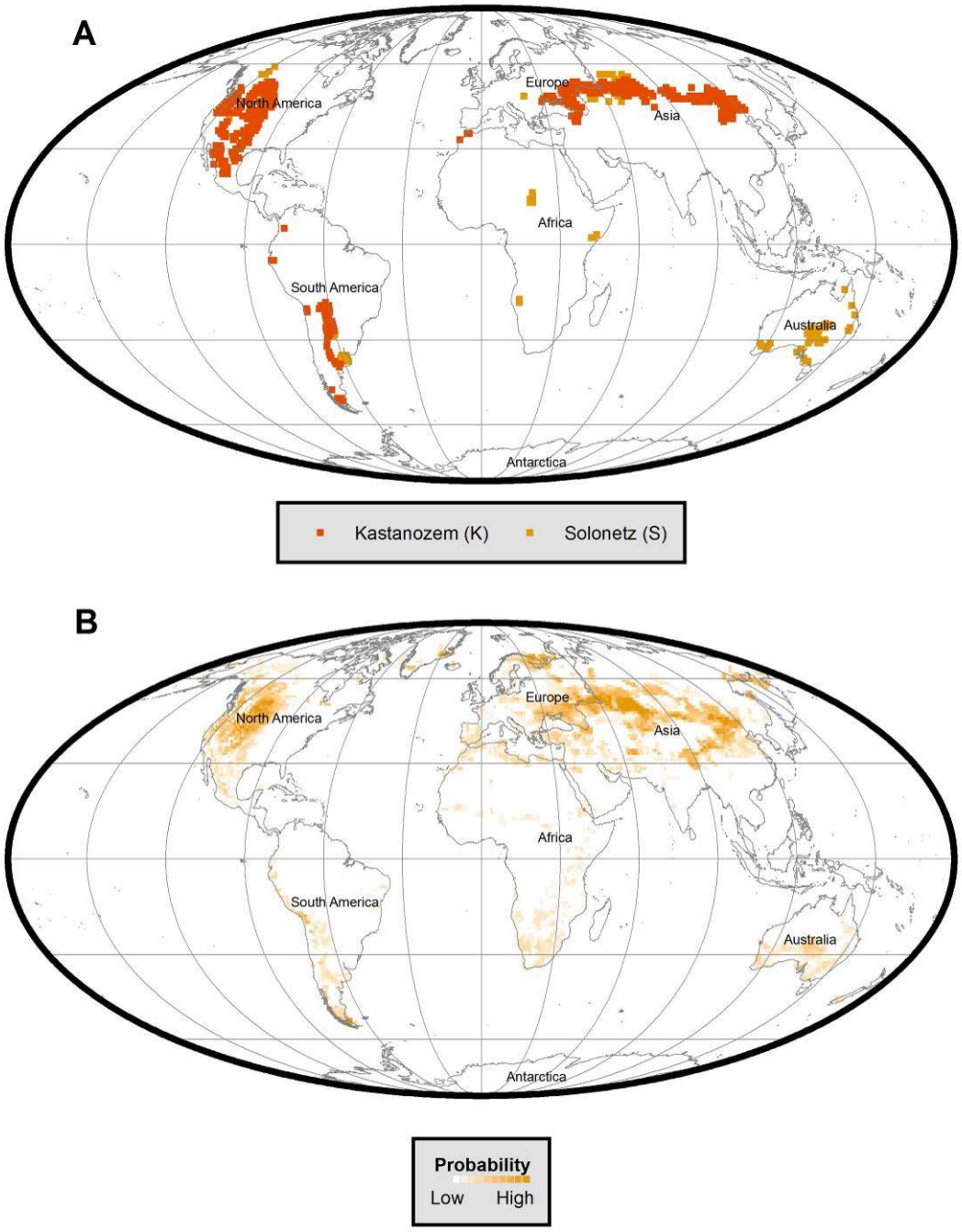

Figure 1.35 A. Actual Modern Geographic Distribution of Paleo-soil KS, B. Predicted Modern Geographic Distribution of Paleo-soil KS Using Paleo-soil Envelope

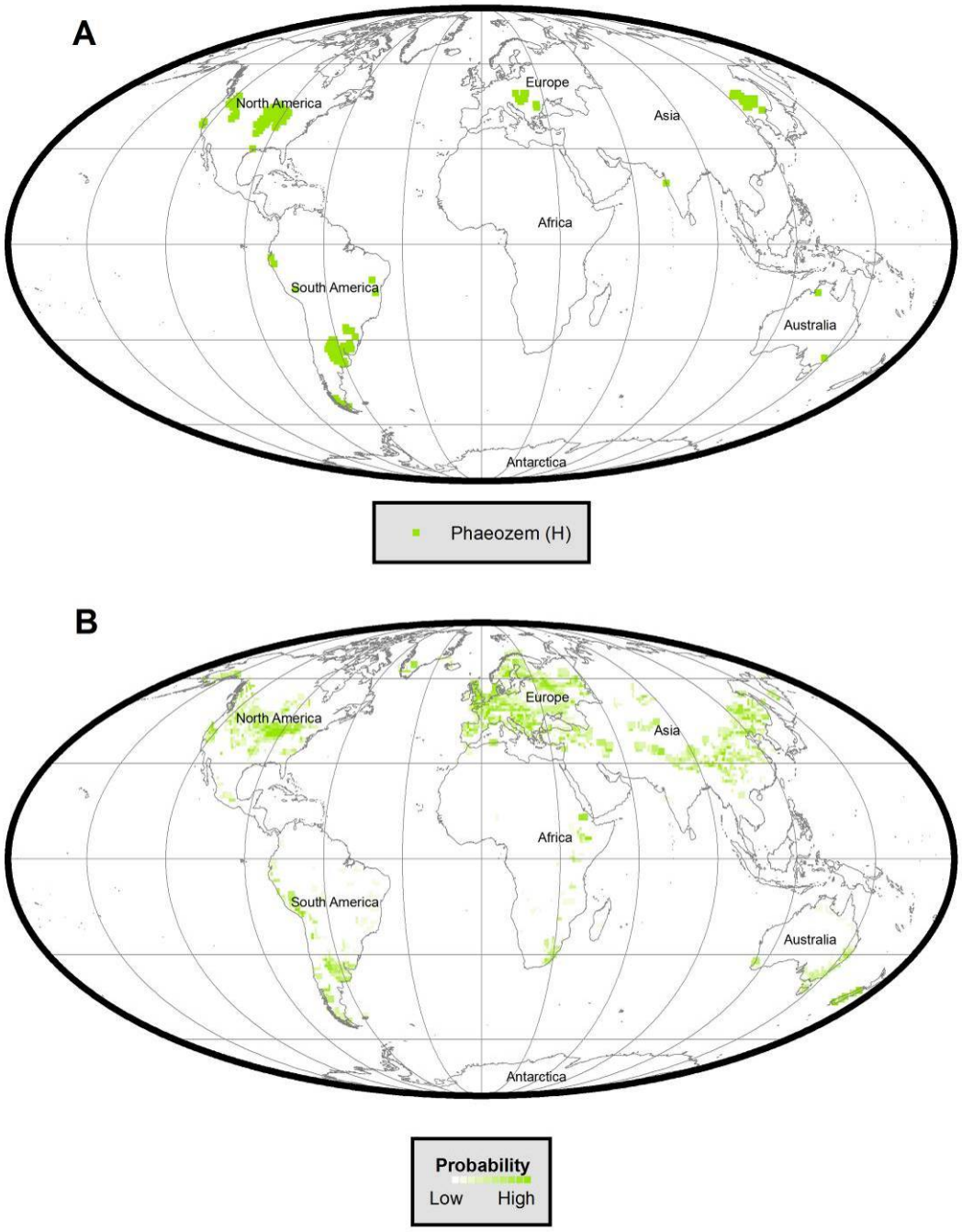

Figure 1.36 A. Actual Modern Geographic Distribution of Paleo-soil H, B. Predicted Modern Geographic Distribution of Paleo-soil H Using Paleo-soil Envelope

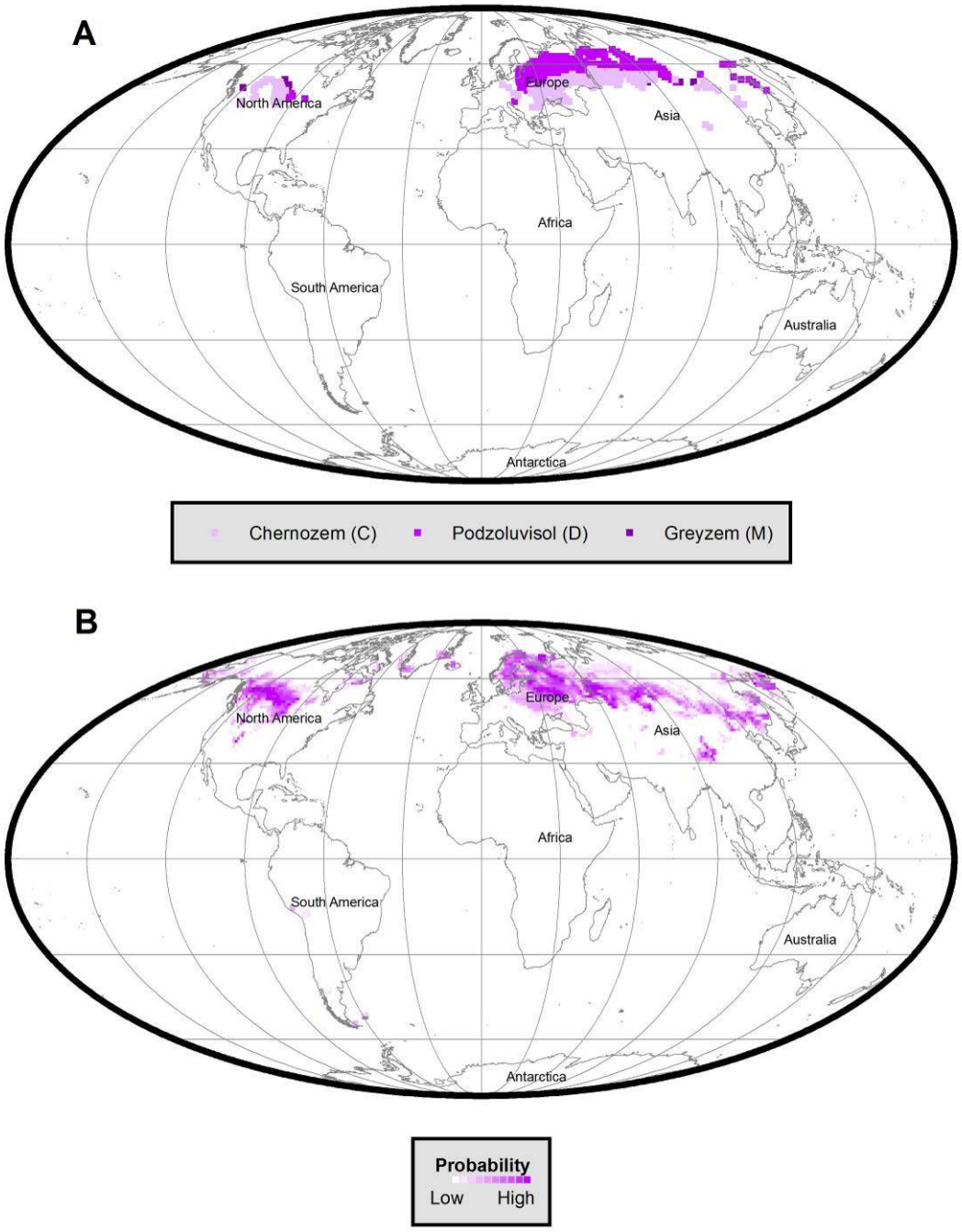

Figure 1.37 A. Actual Modern Geographic Distribution of Paleo-soil CDM, B. Predicted Modern Geographic Distribution of Paleo-soil CDM Using Paleo-soil Envelope

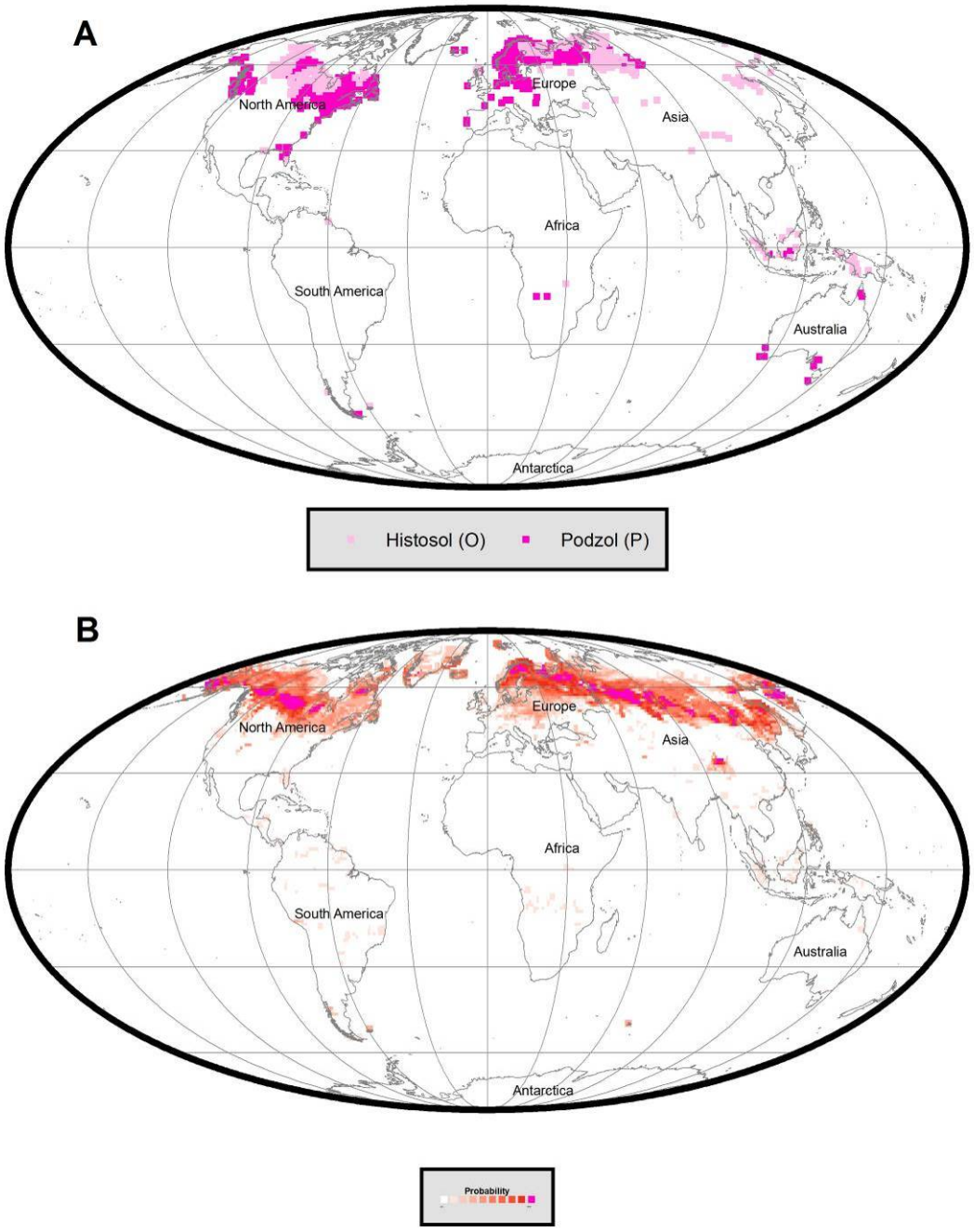

Figure 1.38 A. Actual Modern Geographic Distribution of Paleo-soil OP, B. Predicted Modern Geographic Distribution of Paleo-soil OP Using Paleo-soil Envelope

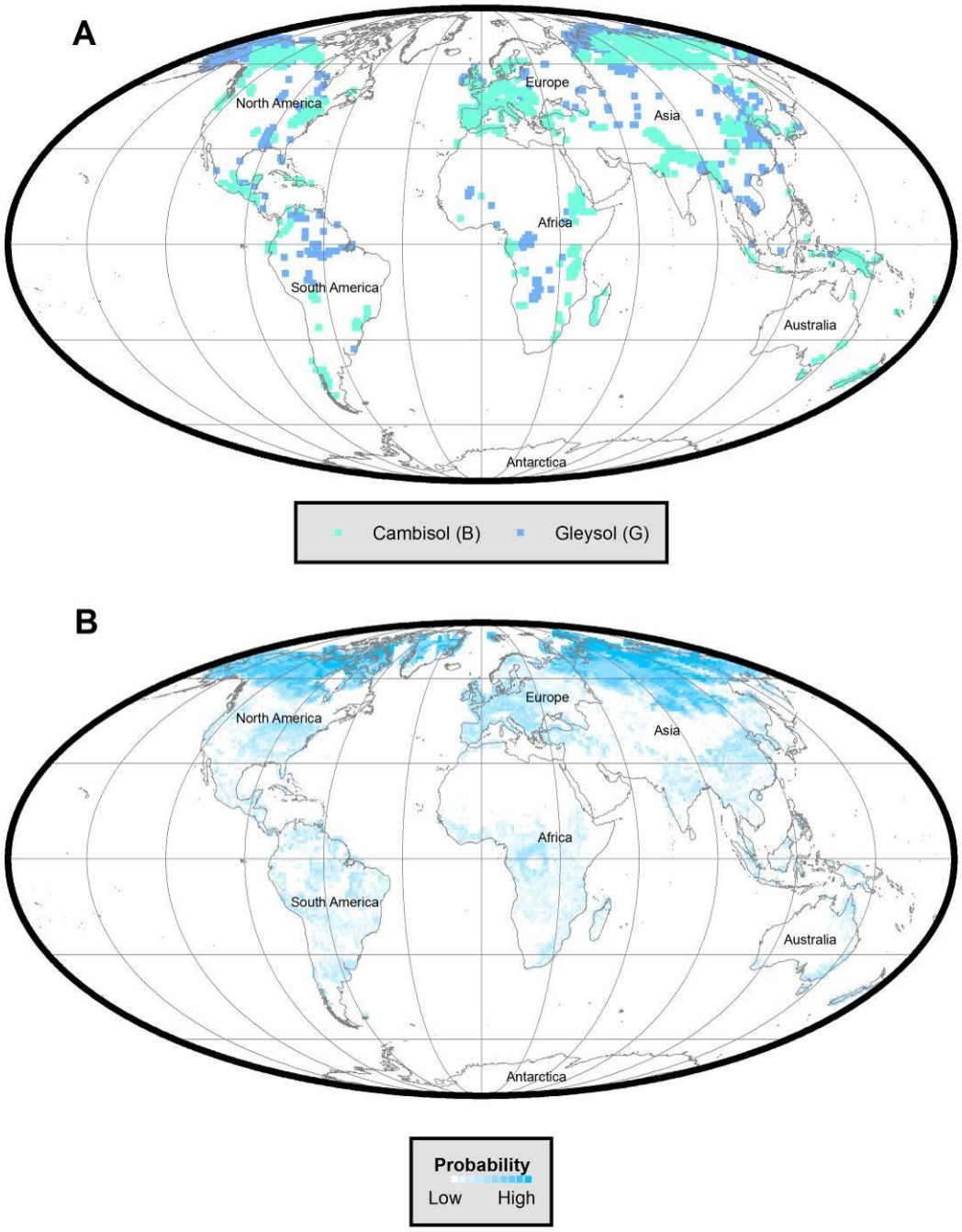

Figure 1.39 A. Actual Modern Geographic Distribution of Paleo-soil BG, B. Predicted Modern Geographic Distribution of Paleo-soil BG Using Paleo-soil Envelope

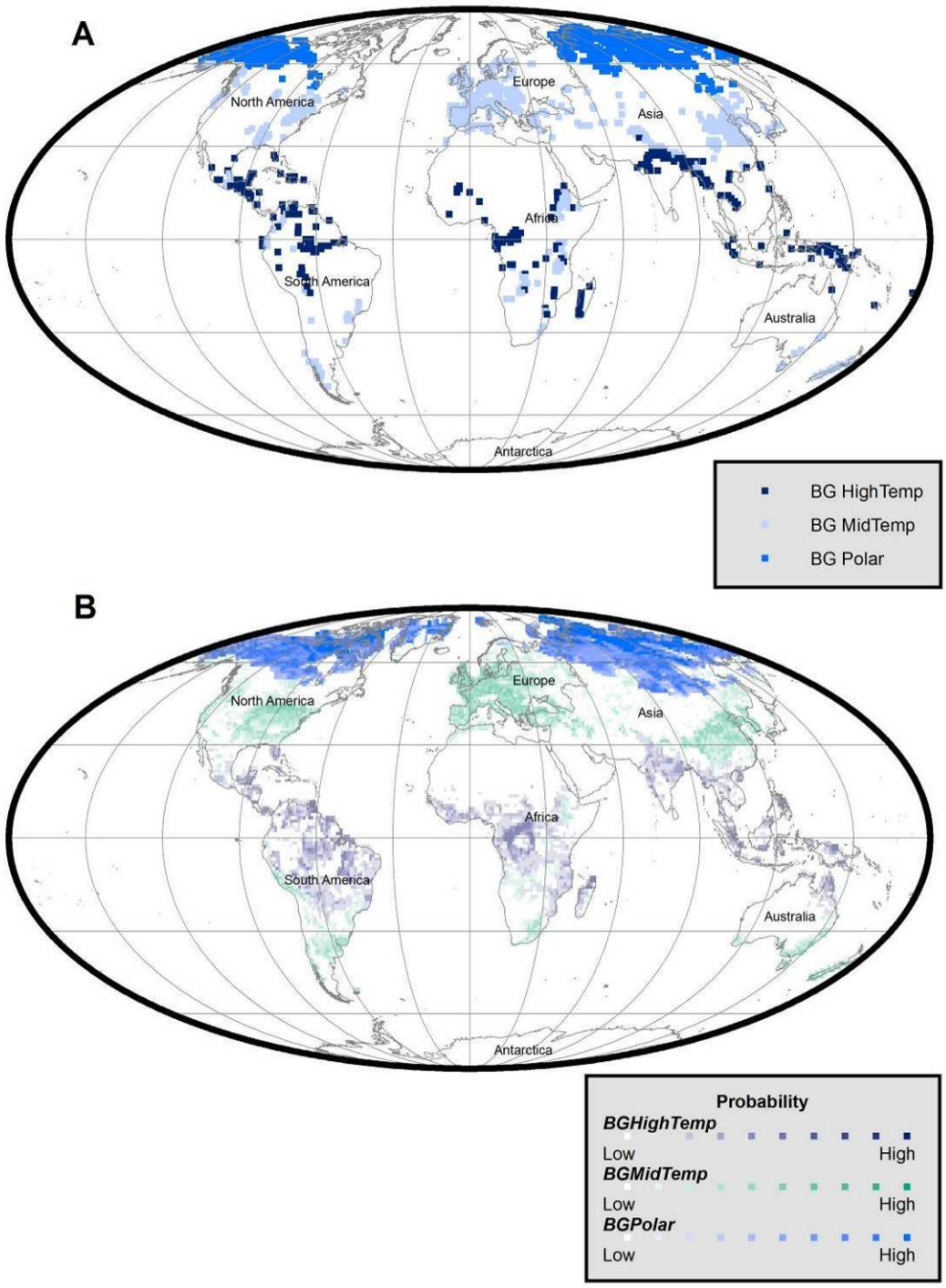

Figure 1.40 A. Actual Modern Geographic Distribution of Paleo-soil BG with Sub-Groups, B. Predicted Modern Geographic Distribution of Paleo-soil BG Sub-Groups Using Paleo-soil Envelope

Careful examination of the BG Climate envelope reveals a coherent low-temperature cluster with a range of temperatures (-30° - 0.5°C) and precipitation values of less than 5 cm/month. All other data points can not be interpreted. We have chosen to divide the remaining BG data points into two sub-groups based on two arbitrary temperature ranges. In addition to the low-temperature BG sub-group, we have constructed a mid-temperature sub-group (0.5° - 22°C) and a high-temperature sub-group (> 22°C). The three sub-groups of BG paleo-soil are shown in Figure 1.40.

Due to wide-ranging values of temperature and precipitation, the climate envelope of the BG paleo-soil type overlaps with all other climate envelopes. This suggests that, with the exception of the low-temperature low-precipitation sub-group, the BG paleo-soil type is a classic example of “garbage can” group and does not represent any single soil type. This assumption is certainly worth future study and consideration.

1.2.6.4 Discussion of Paleo-Soil Climate Envelope Summary Diagram (Figure 1.29)

Figure 1.29 illustrates the temperature-precipitation ranges for all ten paleo-soil climate envelopes. It is remarkable that, for the most part, the ten paleo-soil climate envelopes defined here are distinct, and have their own recognizable domains of temperature and precipitation.

From this diagram (Figure 1.29), we can make the following observations:

1) Upon reviewing the maximum cluster density location points for the ten paleo-soil types (marked with ★), we noticed that there are three major groupings. There is a high temperature group made of XYZ, QV, W and FN that occurs at a nearly constant temperature range of 20°– 25°C and appears to be primarily regulated by the degree of precipitation (0 - 14 cm/month). Conversely, there is a low temperature group consisting of BG, OP, CDM and KS that occurs at a nearly constant precipitation range of 1– 4 cm/month. The paleo-soils in this group appear to be regulated by slight changes in temperature. Finally, it should be noted that paleo-soil type H and A loosely form a third group that lies in a region between the high and low temperature paleo-soil groups.

2) Detailed observation reveals that these three major paleo-soil groups can be further subdivided into five different subgroups that reflect the five principal Köppen-Geiger climate belts.

   i) Equatorial Rainy Belt Paleo-soils (Köppen-Geiger Zone A): The paleo-soil types FN and W characterized by high temperatures (above 20°C) and medium to high precipitation values (above 10 cm/month) are member of this subgroup. These soils are typically found in the Equatorial Rainy Belt (FN: Figure 1..25A and W: Figure 1.33A).

   ii) Subtropical Arid Belt Paleo-soils (Köppen-Geiger Zone B): The paleo-soil types QV and XYZ characterized by high temperatures (above 20°C) and very low precipitation values (less than 5 cm/month) are members of this subgroup. XYZ paleo-soils are found typically in the Subtropical Arid Belts (Figure 1.34A) and QV (Figure 1.31A) paleo-soils appear to be transitional between the Equatorial Rainy Belt and the Subtropical Arid Belts.

   iii) Warm Temperate Belt Paleo-soils (Köppen-Geiger Zone C): The paleo-soil types A and H, are representative of moderate climatic conditions. On the modern map these two paleo-soil types are typically found in the Warm Temperate Belt (A: Figure 1.32A and H: Figure 1.36A).

   iv) Cool Temperate Belt Paleo-soils (Köppen-Geiger Zone D): The fourth subgroup consists of the KS, CDM and OP paleo-soil types. They all form under seasonally cold climatic conditions (7° --7°C). On the modern map these soils are found in the areas between the latitudes of 40 - 70° (KS: Figure 1.35A, CDM: Figure 1.37A and OP: Figure 1.38A). This group of paleo-soils represents the Cool Temperate Belt.

   v) Polar Belt Paleo-soils (Köppen-Geiger Zone E): This final subgroup has only one paleo-soil type — BG. As discussed in section 1.4.6.3, we have only included the low-temperature BG sub-group (Figure 1.40A) in this analysis. The BG paleo-soil

type forms at very low temperatures (< 0 °C). This subgroup is usually found above 60° latitude.

1.2.6.5 Comparison of Paleo-soil Predictions

In the preceding section, we defined ten paleo-soil climate envelopes based on the temperature and precipitation domains for the nineteen Zobler Main Soil Units. In this section we use these climate envelopes to reproduce the modern geographic distribution of these paleo-soil types. Strictly speaking, this is not a true prediction because modern data were used to create these climate envelopes. Rather, it is simply a test of the procedure and has been done in order demonstrate that the climate envelope technique accurately reproduces the original geographic distribution of the soil types.

To test the effectiveness of these ten paleo-soil envelopes, we intersected the modern temperature – precipitation data (Legates and Willmott, 1990) with the climate envelope polygons to predict the modern distribution of the ten paleo-soil types. A comparison of the predicted geographic distribution of each paleo-soil with its modern geographic distribution is shown in Figures 1.30 – 1.40. In the following section we review how well the predicted geographic distributions of the paleo-soils match with the actual geographic distributions of the paleo-soil types. In each of these figures (Figure 1.30 – 1.40) the modern observed geographic distribution of the paleo-soil is shown in Figure A and the predicted geographic distribution is shown in Figure B. The gradation in the shading of the predicted soil localities indicates the confidence level of the paleo-soil predictions (darker shade represents higher density and higher probability). The results are described below.

1) Prediction for Equatorial Rainy Belt Paleo-soils (Köppen-Geiger Zone A)

There is an excellent match between the predicted geographic distribution and the observed modern geographic distribution for the FN paleo-soil type (Figure 1.30). A very good match between the predicted and observed paleo-soil occurrences is found in southern North America, north and central South America, central Africa, and north-eastern regions of

Australia. The only mismatch is in Southeast Asia where a few additional localities are predicted.

For paleo-soil type W, the climate envelope technique predicts a more widespread geographic distribution (Figure 1.33) than is observed in the modern data. In the coastal areas of Australia there is a very good match between the predicted and observed geographic distribution. In Northern America, South America and south-central Africa the climate envelope technique predicts a wider distribution of the W paleo-soil than is observed. This pattern is also seen in Europe and southern Asia.

2) Subtropical Arid Belt Paleo-soils (Köppen-Geiger Zone B)

Comparison of the predicted geographic distribution and the observed modern geographic distribution for the QV paleo-soil type (Figure 1.31) shows a very good match. In North America, South America, southern Asia, and Australia there is an excellent match between the predicted and observed geographic distribution. Around the Mediterranean region, the climate envelope technique predicted additional localities not seen in the modern geographic distribution. Conversely, in Europe and eastern China, the climate envelope technique failed to predict scattered observed occurrences of paleo-soil type QV (Figure 1.31).

There is an excellent match between the predicted occurrences of XYZ paleo-soil type and the modern observed geographic distribution (Figure 1.34). In western North America, southwestern South America, Africa, central Eurasia, Mediterranean Region and south central Australia, we see a very good match between the observed and predicted geographic distribution. The climate envelope technique fails to predict the modern occurrences of the XYZ paleo-soil type in northern Australia.

3) Warm Temperate Belt Paleo-soils (Köppen-Geiger Zone C)

There is a good match between the predicted geographic distribution and observed modern geographic distribution for the paleo-soil type A (Figure 1.32). In eastern North America, central America, northern South America, Southeast Asia, and the eastern coast of Australia

there is an exact match between the predicted and observed geographic distribution. The method failed to predict A paleo-soils in western North America and Turkey. Conversely, the method over predicted the occurrence of A paleo-soil type in central South America and central Africa.

For paleo-soil type H, the comparison between the predicted geographic distribution and the observed modern geographic distribution (Figure 1.36) reveals a fair match. There is an excellent match in South America, but in North America, eastern Asia, Europe and Australia, the climate envelope technique predicts a more widespread distribution of the H paleo-soil type than is observed in the modern geographic distribution. In Africa and central Asia we see scattered predictions of paleo-soil type H that are not observed in the modern distribution.

4) Cool Temperate Belt Paleo-soils (Köppen-Geiger Zone D)

The predicted geographic distribution and the observed modern geographic distribution for the paleo-soil type KS (Figure 1.35) are very similar. In North America, central Eurasia and Australia there is an excellent match between the predicted geographic distribution and the observed geographic distribution. In southern South America and in Africa, there is a slight mismatch between the predicted localities and the observed localities.

For the paleo-soil type CDM (Figure 1.37) there is an excellent match between the predicted geographic distribution and the observed modern geographic distribution. There is a near one-to-one match between the predictions and observations in northern North America and northern Eurasia.

There is a good match between the predicted geographic distribution and the observed modern geographic distribution for the paleo-soil type OP. In northern North America and northern Eurasia the predicted geographic distribution matches very well with the observed modern geographic distribution. In addition, the scattered occurrences of this paleo-soil type at low latitude, and in southernmost South America, south central Africa, Southeast Asia, are also

well predicted by this technique. Conversely, the observed occurrences of paleo-soil type OP in Australia are not predicted by the climate envelope technique.

5) Polar Belt Paleo-soil (Köppen-Geiger Zone E)

There is a very good match between predicted geographic distribution and the observed modern geographic distribution for the three subgroups of the BG paleo-soil type (Figure 1.39 and 1.40). The predicted geographic distribution of the low-temperature BG subgroup matches the observed occurrences (Figure 1.40A). Though there is a reasonable match between the predicted geographic distribution and observed geographic distribution of BG mid-temperature and high-temperature subgroups, they have not been included in the study (see section 1.4.6.3).

1.2.6.6 Global Map: Prediction Vs. Observed

One of the most important figures in this dissertation is Figure 1.41B. This figure compares the predicted geographic distribution of all ten paleo-soil types with the observed modern geographic distribution of the paleo-soil types. Upon visual inspection, it is clear that there is a excellent match between the predicted geographic distribution (Figure 1.41B) and observed geographic distribution (Figure 1.41A).

To estimate the goodness of fit between the predicted localities and the observed localities, we calculated the number of “hits” and “misses”. A prediction was considered to be a “hit” if the predicted soil type (primary or secondary prediction) matched the observed modern soil type. A prediction was considered to be a “miss” if the prediction (primary or secondary prediction) was something other than the observed modern soil type. In this study 85% of the predictions matched the observations. The results are summarized in the pie chart (Figure 1.43) and match-mismatch map (Figure 1.42).The pie chart (Figure 1.43) shows that 63% of the primary predictions and 22% of the secondary predictions matched the observed modern geographic distributions.

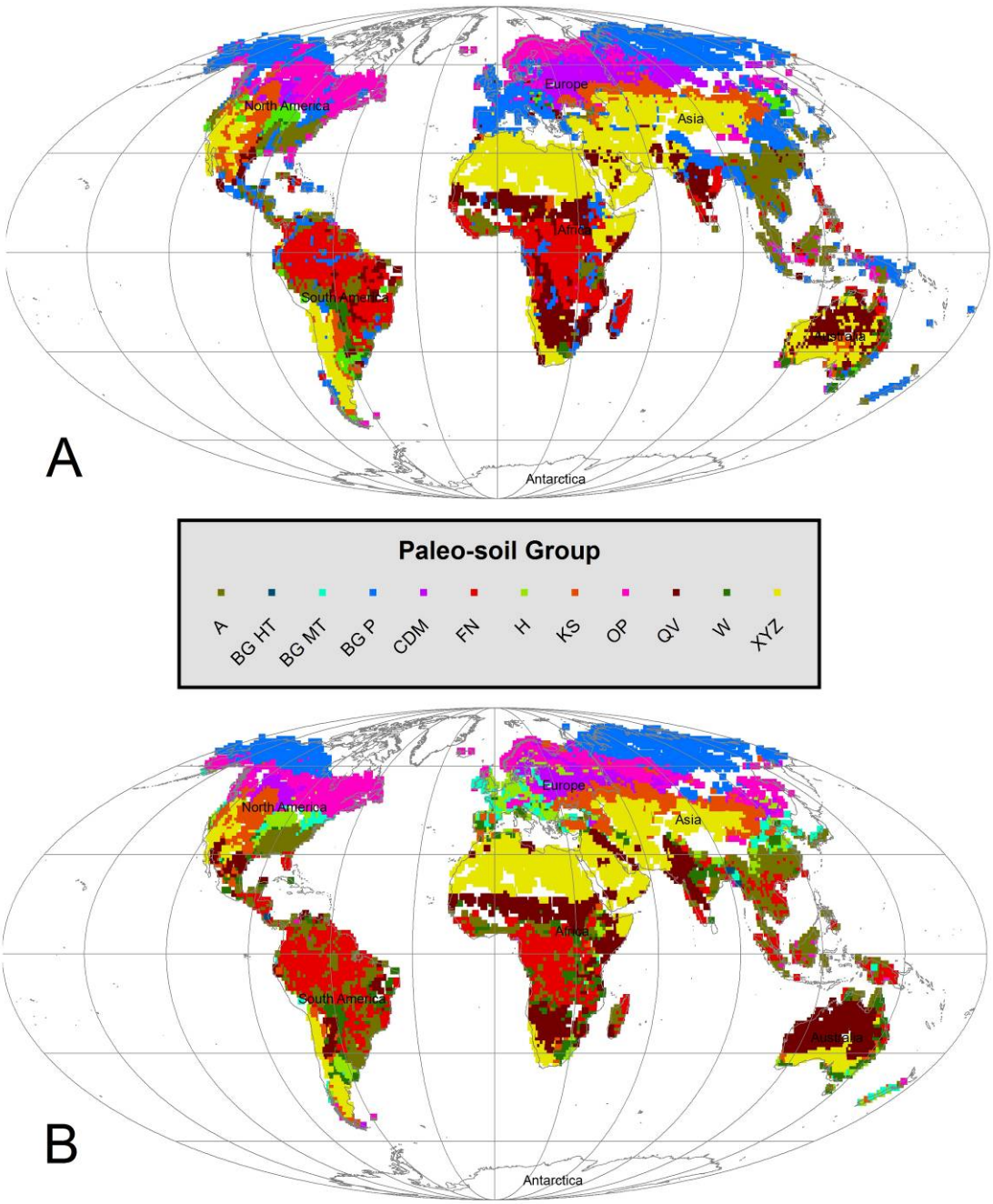

Figure 1.41 A. Actual Modern Geographic Distribution of the Ten Paleo-soils, B. Predicted Primary Paleo-soils for the Modern time

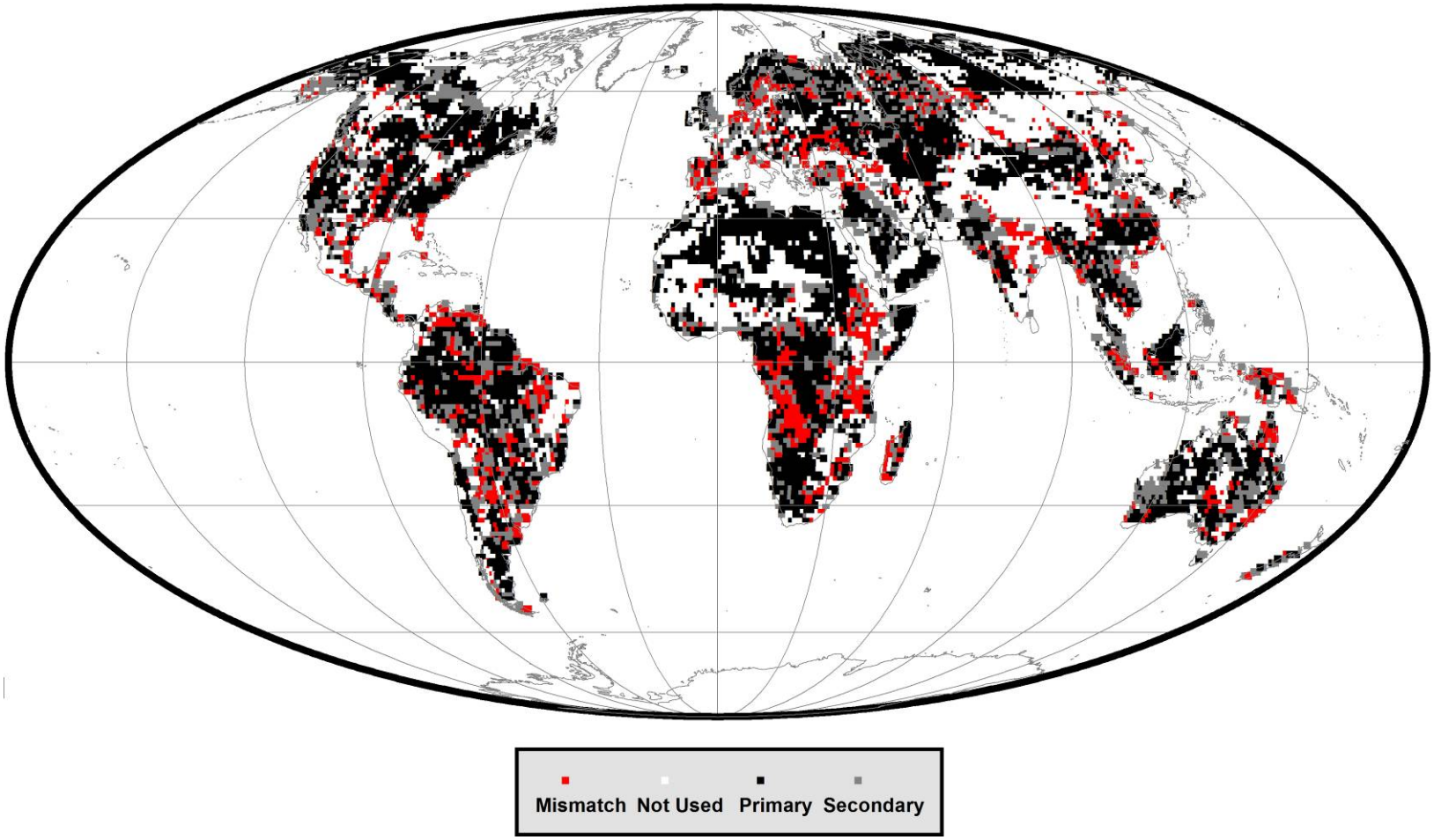

Figure 1.42 Match Mismatch Map

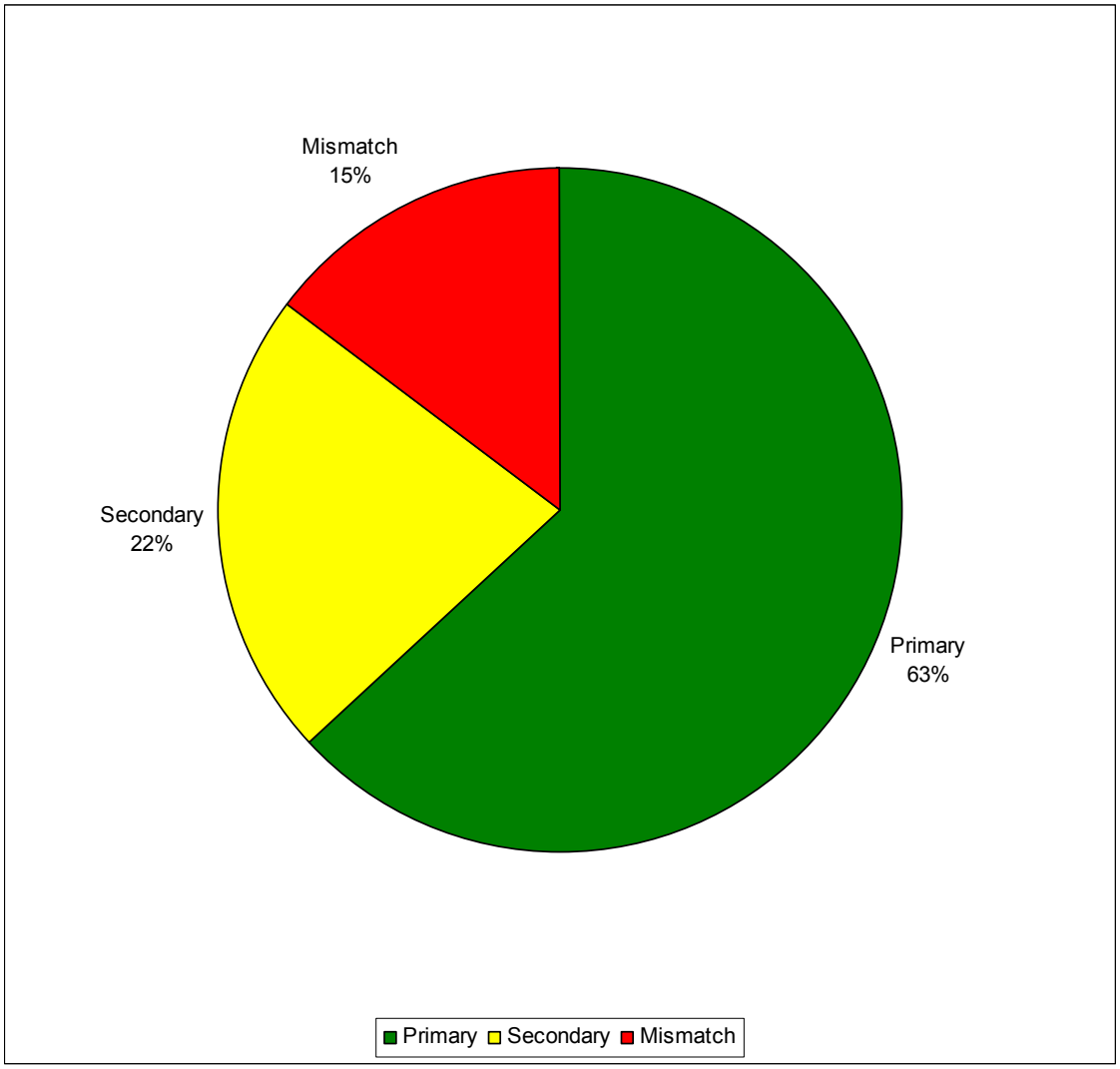

Figure 1.43 Pie-chart showing the percentage of match/mismatch between Actual Modern distributions of ten paleo-soils to the primary/secondary predicted paleo-soil types.

Table 1.6 Summary of the ten Paleo-soil envelopes

No	Paleo-Soil	Frequency	Precipitation		Temperature	
			Max	Min	Max	Min
1	A	789	40.23	3.90	28.13	8.23
2	BG	2155	37.21	0.09	29.19	-16.61
3	CDM	722	8.37	1.79	11.27	-7.30
4	FN	1090	48.29	4.43	28.55	12.61
5	H	161	17.68	2.97	27.13	-0.35
6	KS	664	14.56	0.25	28.90	-6.28
7	OP	1088	36.91	0.35	27.88	-12.33
8	QV	893	28.58	0.31	29.82	8.02
9	W	129	12.89	3.28	29.22	1.47
10	XYZ	1918	27.82	0.00	29.40	-5.38
11	Modern	15413	48.29	0.00	29.90	-29.86

Table 1.7 Maximum Density locations for the different paleo-soil types

PaleoSoil	Precipitation (cm/month)	Temperature (°C)
A	10.78	16.81
BG	1.34	-13.86
CDM	3.41	0.92
FN	13.11	24.29
H	7.26	10.65
KS	2.54	2.01
OP	3.50	-0.98
QV	1.90	22.01
W	10.68	24.27
XYZ	0.17	22.69

Table 1.8 Details percentage for Mismatch of Modern Prediction

Zobler MSU (Paleo-soil)	A	BG	CDM	FN	H	KS	OP	QV	W	XYZ
A (A)	-	6.10		20.73	28.05	3.66	-	13.41	26.83	1.22
B (BG)	17.50	-	4.29	22.14	7.86	9.29	5.00	13.57	18.21	2.14
C (CDM)	-	6.25	-	-	20.31	62.50	10.94	-	-	-
D (CDM)	-	24.55	-	-	13.64	0.91	60.91	-	-	-
F (FN)	43.10	1.72	-	-	6.90	-	1.72	22.41	24.14	-
G (BG)	24.87	-	5.18	34.20	2.07	5.70	12.44	4.66	5.70	5.18
H (H)	18.52	3.70	14.81	7.41	-	18.52	11.11	11.11	14.81	-
M (CDM)	-	16.67	-	-	-	16.67	66.67	-	-	-
N (FN)	44.12	-	-	-	23.53	2.94	-	23.53	5.88	-
O (OP)	24.14	-	10.34	44.83	3.45	13.79	-	-	-	3.45
P (OP)	12.82	7.69	21.79	6.41	34.62	8.97	-	1.28	6.41	-
Q (QV)	36.15	0.77	-	38.46	2.31	2.31	-	-	17.69	2.31
V (QV)	24.24	3.03	-	13.64	9.09	6.06	1.52	-	37.88	4.55
W (W)	21.43	-	7.14	28.57	21.43	7.14	7.14	7.14	-	-
X (XYZ)	3.26	9.78	-	-	6.52	30.43	1.09	28.26	20.65	-
Y (XYZ)	5.26	2.63	-	-	10.53	39.47	-	31.58	10.53	-
Z (XYZ)	7.41	-	7.41	18.52	18.52	11.11	3.70	18.52	14.81	-

The match-mismatch map (Figure 1.43) illustrates the geographic distribution of the primary matches (black), secondary matches (gray) and the regions of mismatch (red). The blank areas represent regions where no predictions were made. It is interesting to note that except for a small region in west-central Africa, the areas of mismatch are scattered around the globe. In the next chapter of this dissertation, the climate envelope technique described here will be applied to seventeen paleo-reconstructions to predict the ancient geographic distribution of the ten paleo-soil types.

CHAPTER 2

MAPPING THE GEOGRAPHIC DISTRIBUTION OF ANCIENT SOILS USING THE CLIMATE ENVELOPE TECHNIQUE

In this chapter we predict the occurrences of the ten paleo-soil types on seventeen paleogeographic maps. These predictions were made using the climate envelope technique and results from paleoclimate simulations (Fast Ocean Atmospheric Model) discussed in the previous chapter. In order to make these paleo-soil reconstructions, two new datasets were used: 1) seventeen paleogeographic maps from the PALEOMAP Project (Scotese 2011) and 2) temperature-precipitation information from seventeen paleoclimate simulations (FOAM, GANDOLPH Project, Scotese et al. 2007, 2008, 2009, and 2011).

2.1 Paleogeographic Maps

Seventeen paleogeographic maps representing the following time intervals were used in this study: Miocene (10 Ma), Oligocene (30 Ma), Eocene (45 Ma), Late Cretaceous / Campanian (70 Ma), Cenomanian (90 Ma), Aptian (120 Ma), Early Cretaceous / Berriasian-Valanginian (140 Ma), Early Jurassic / Oxfordian (160 Ma), Early Jurassic / Toarcian (180 Ma), Late Triassic / Carnian (220 Ma), Early Triassic / Induan (250 Ma), Permian (280 Ma), Carboniferous (340 Ma), Late Devonian (360 Ma), Early Devonian (400 Ma), Silurian (430 Ma) and Ordovician (480 Ma) (Scotese 2011). A sample paleogeographic map for 90 Ma is shown in Figure 2.1. It is important to note that, in order to maximize the extent of soil forming regions, we have used a paleogeography that represents minimum sea levels (i.e., maximum regression). This lowstand shoreline was estimated using the digital elevation model (PaleoDEM) provided by the PALEOMAP Project. The paleoDEM is a 1°x1° grid of topography and bathymetry (meters). The Python script (PaleoDEM2Coastlines.py) used to construct these paleo-coastlines is given in (Appendix A).

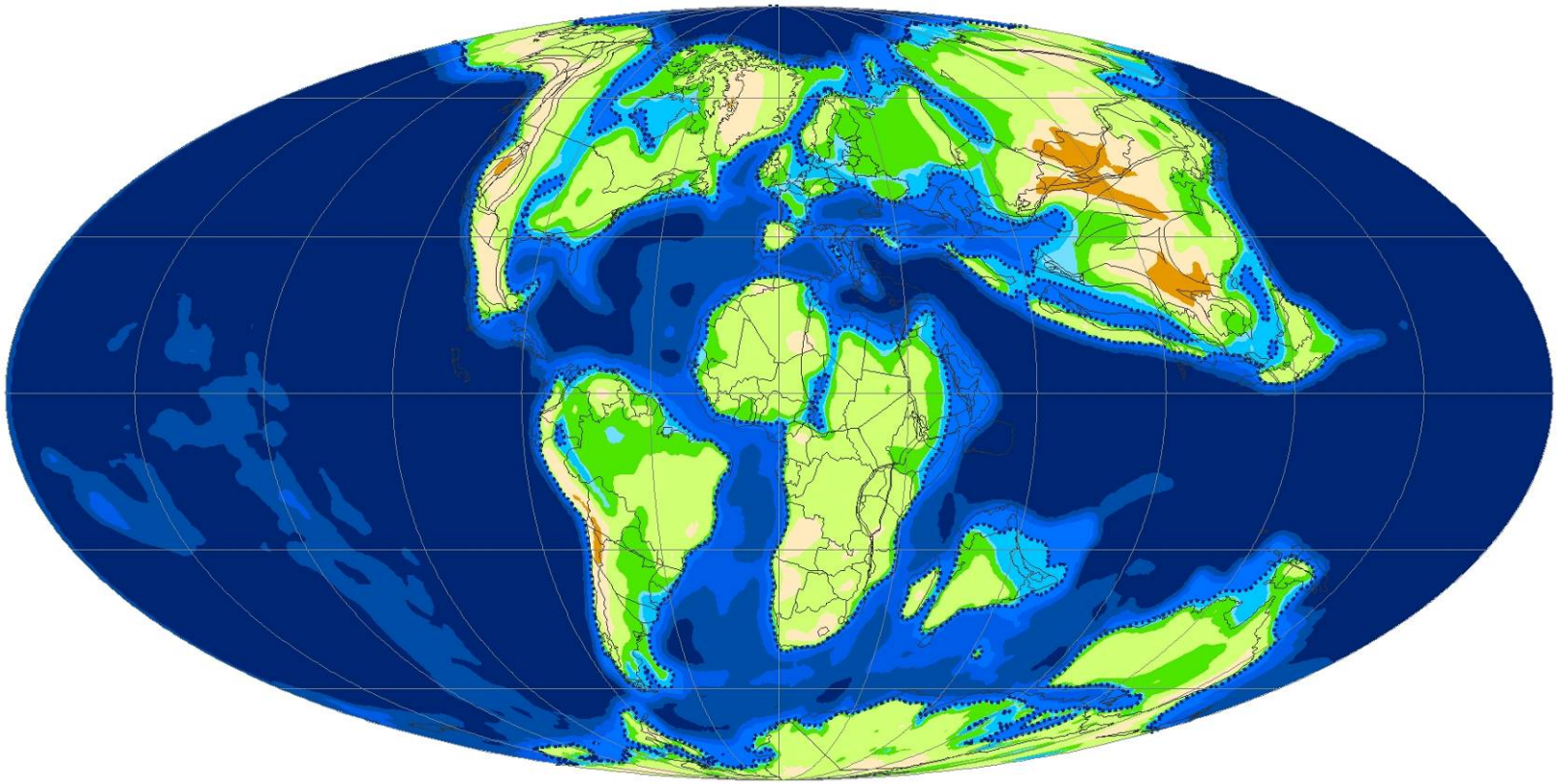

Figure 2.1 Simple Paleogeography (90 Ma)

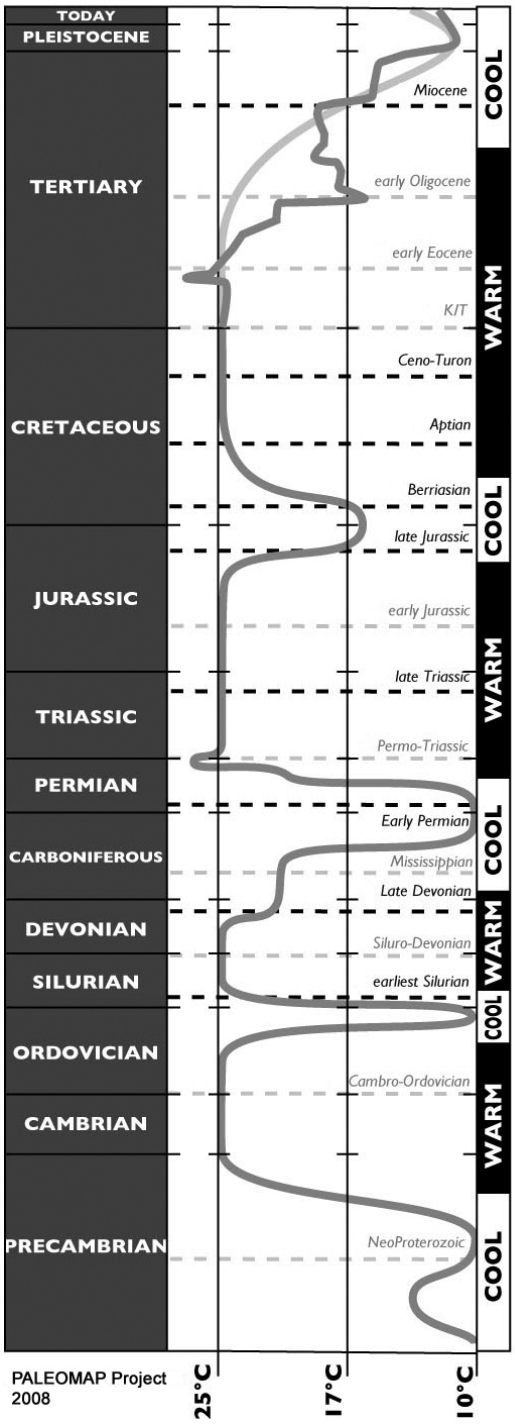

Figure 2.2 Global Temperatures During the Phanerozoic and Late Precambrian (Scotese & Boucot 1999).

2.2 Paleoclimate Simulation Results (FOAM)

The paleotemperature and paleoprecipitation values needed to predict the ancient geographic distribution of the ten paleo-soil types were obtained from paleoclimate simulations using the Fast Ocean Atmospheric Model (FOAM), a Global Climate Model (GCM). This data was provided by the GANDOLPH Project (Scotese et al. 2007, 2008, 2009, 2010, 2011). A brief description of the FOAM global climate model is given in Appendix D.

For this study, we used two FOAM variables: TS1 (Surface Temperature values) and OPREC (Atmospheric precipitation). Mean Annual Temperature (MAT) and Mean Annual Precipitation (MAP) were calculated from the monthly values and were re-gridded to match the Zobler World Soil database spatial resolution (1°x1°). The units of precipitation were converted from m/sec to cm/month to match the precipitation units of Legates-Willmott global climate dataset. Finally, the MAT and MAP variables were joined in a single table for each time interval. This temperature-precipitation information was then used to predict the geographic distribution of ancient soils for each time interval. Table 2.1 lists the maximum-minimum of temperature as well as maximum-minimum of precipitation for all seventeen time intervals.

2.3 Discussion of Predictions

2.3.1 Miocene (10 Ma)

The climate during the Miocene stage was very similar to present day's climate, but warmer (Zachos et al. 2001, Scotese 2008,). The Miocene was an Ice House World (Figure 2.2), with well-defined climatic belts stretched from Pole to Equator. However, there were palm trees and alligators in England and Northern Europe. Australia was less arid than it is today (www.scotese.com). In addition, during the Miocene modern patterns of atmospheric and ocean circulation formed (Wright et al. 1992). The isolation of Antarctica from Australia and South America meant the establishment of the Circum Polar Ocean circulation, which significantly reduced the mixing of warmer tropical waters and cold polar waters, leading to the buildup of the Antarctic ice cap.

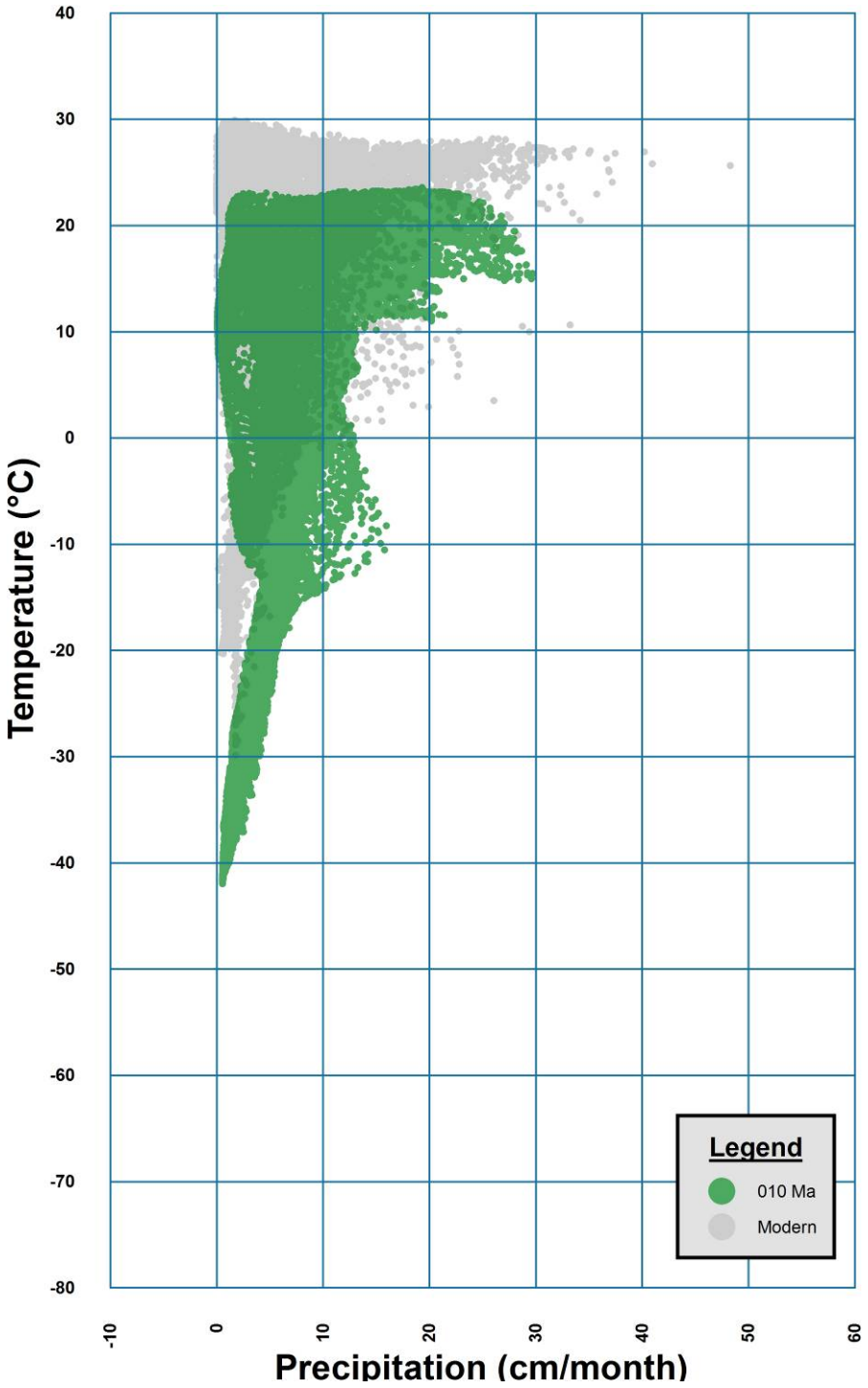

Figure 2.3 Temperature-Precipitation Plot for the Miocene (010 Ma)

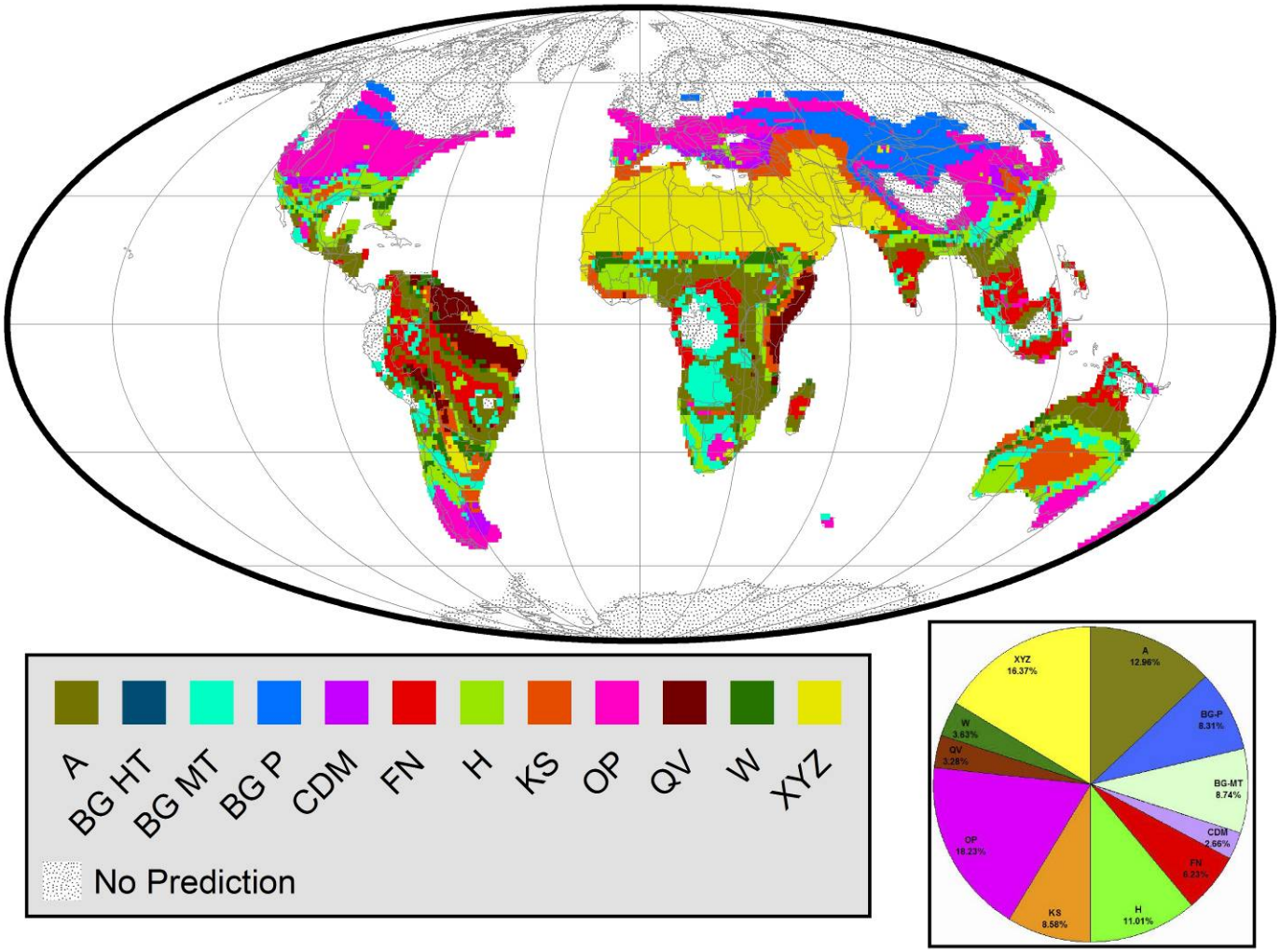

Figure 2.4 Composite Geographic Distribution Map of Primary Predicted Ancient Soils (Paleo-soils) for the Miocene (010 Ma)

Table 2.1 Maximum and Minimum Temperature and Precipitation Values estimated by FOAM

Age	Temperature (°C)		Precipitation (cm/month)	
	Max	Min	Max	Min
Modern	29.90	-29.86	48.29	0.00
10	23.55	-41.97	29.72	0.07
30	28.06	-25.66	32.41	0.08
45	27.50	-26.37	33.08	0.38
70	29.08	-19.74	29.73	0.78
90	31.42	-14.01	52.47	0.04
120	31.97	-9.70	51.62	0.03
140	28.77	-21.54	34.94	0.04
160	29.34	-17.16	41.83	0.00
180	25.40	-42.25	29.74	0.24
220	24.82	-33.96	33.12	0.05
250	27.64	-34.93	31.15	0.10
280	23.40	-70.25	35.28	0.07
340	26.58	-35.47	35.39	0.16
360	24.72	-43.68	33.03	0.77
400	25.83	-39.49	32.52	0.21
430	30.90	-16.23	45.58	0.16
480	26.50	-32.75	33.41	0.39

Table 2.2 Percentage of Predicted Ancient Soil Types for Each Time Interval (Green = Highest Occurrence, Brown = Second Highest Occurrence and Blue = Third Highest Occurrence)

Time (Ma)	A	BG-P	BG-MT	BG-HT	CDM	FN	H	KS	OP	QV	W	XYZ	Total
10	1292	828	871	0	265	621	1097	855	1817	327	362	1632	9967
	12.96%	8.31%	8.74%	0.00%	2.66%	6.23%	11.01%	8.58%	18.23%	3.28%	3.63%	16.37%	100.00%
30	929	1291	730	5	181	1727	940	816	3482	713	710	2042	13566
	6.85%	9.52%	5.38%	0.04%	1.33%	12.73%	6.93%	6.02%	25.67%	5.26%	5.23%	15.05%	100.00%
45	1313	3631	722	16	224	2350	937	804	3949	975	929	761	16611
	7.90%	21.86%	4.35%	0.10%	1.35%	14.15%	5.64%	4.84%	23.77%	5.87%	5.59%	4.58%	100.00%
70	1734	6201	1018	9	93	2326	878	602	5562	1815	1111	406	21755
	7.97%	28.50%	4.68%	0.04%	0.43%	10.69%	4.04%	2.77%	25.57%	8.34%	5.11%	1.87%	100.00%
90	1831	6536	730	27	126	905	557	369	7352	1759	490	2047	22729
	8.06%	28.76%	3.21%	0.12%	0.55%	3.98%	2.45%	1.62%	32.35%	7.74%	2.16%	9.01%	100.00%
120	1997	6448	1097	13	159	954	669	368	10208	2136	554	2025	26628
	7.50%	24.22%	4.12%	0.05%	0.60%	3.58%	2.51%	1.38%	38.34%	8.02%	2.08%	7.60%	100.00%
140	859	3266	562	28	183	1629	619	598	3975	1199	532	2883	16333
	5.26%	20.00%	3.44%	0.17%	1.12%	9.97%	3.79%	3.66%	24.34%	7.34%	3.26%	17.65%	100.00%
160	1277	4786	625	43	122	1463	538	531	4109	1883	393	3704	19474
	6.56%	24.58%	3.21%	0.22%	0.63%	7.51%	2.76%	2.73%	21.10%	9.67%	2.02%	19.02%	100.00%
180	1971	906	267	0	410	1246	805	1532	1816	93	559	2886	12491
	15.78%	7.25%	2.14%	0.00%	3.28%	9.98%	6.44%	12.26%	14.54%	0.74%	4.48%	23.10%	100.00%
220	1463	637	543	2	245	1183	499	1093	2432	627	372	3484	12580
	11.63%	5.06%	4.32%	0.02%	1.95%	9.40%	3.97%	8.69%	19.33%	4.98%	2.96%	27.69%	100.00%
250	825	237	323	4	385	2587	479	1327	1624	923	661	4030	13405
	6.15%	1.77%	2.41%	0.03%	2.87%	19.30%	3.57%	9.90%	12.11%	6.89%	4.93%	30.06%	100.00%
280	1969	1158	900	11	260	449	1349	1403	1327	102	418	2221	11567
	17.02%	10.01%	7.78%	0.10%	2.25%	3.88%	11.66%	12.13%	11.47%	0.88%	3.61%	19.20%	100.00%
340	1222	273	945	3	134	2021	1305	809	2412	715	918	1394	12151
	10.06%	2.25%	7.78%	0.02%	1.10%	16.63%	10.74%	6.66%	19.85%	5.88%	7.55%	11.47%	100.00%
360	1103	107	676	3	263	1585	1436	1475	2057	796	832	471	10804
	10.21%	0.99%	6.26%	0.03%	2.43%	14.67%	13.29%	13.65%	19.04%	7.37%	7.70%	4.36%	100.00%
400	623	95	703	1	57	1563	793	727	1516	871	754	1270	8973
	6.94%	1.06%	7.83%	0.01%	0.64%	17.42%	8.84%	8.10%	16.90%	9.71%	8.40%	14.15%	100.00%
430	1660	5282	806	65	28	1138	321	208	4959	3834	416	957	19674
	8.44%	26.85%	4.10%	0.33%	0.14%	5.78%	1.63%	1.06%	25.21%	19.49%	2.11%	4.86%	100.00%
480	923	62	346	3	202	2959	693	981	1394	1581	1194	786	11124
	8.30%	0.56%	3.11%	0.03%	1.82%	26.60%	6.23%	8.82%	12.53%	14.21%	10.73%	7.07%	100.00%

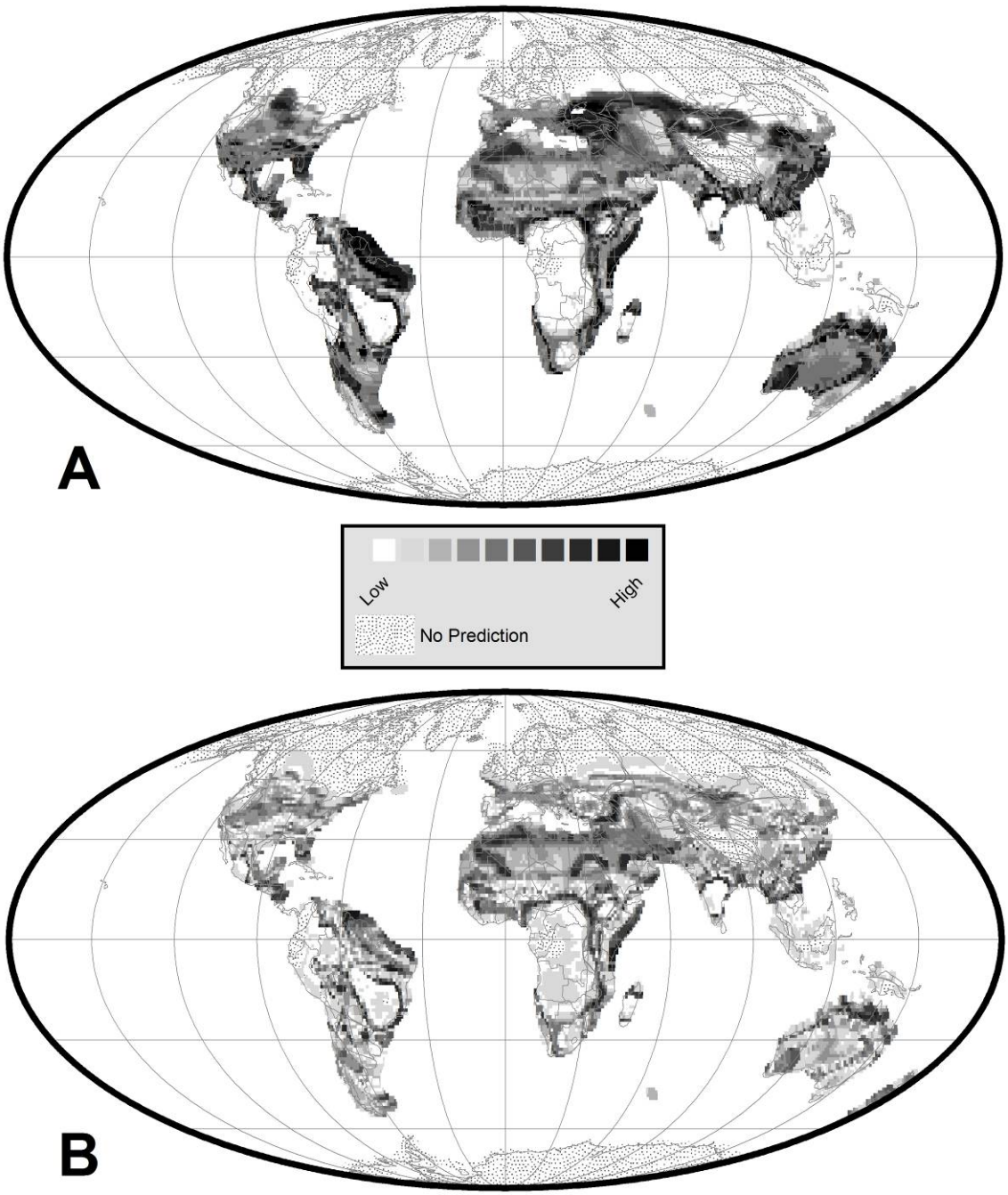

Figure 2.5 A. Levels of Confidence for Predicted Maximum Probable Paleo-soil Type for the Miocene (010 Ma), B. Dominance of Primary Maximum Probable Paleo-soil Type over the Secondary Maximum Probable Paleo-soil Type for the Miocene (010 Ma)

Figure 2.3 plots the distribution of temperature and precipitation values for the Miocene (green) plotted on a background of modern day temperature and precipitation values (gray). For the Miocene, the maximum temperature and precipitation values were 23.55°C and 29.72 cm/month, respectively. The minimum temperature and precipitation values were -41.97°C and 0.07 cm/month, respectively. It is clear from this plot that the FOAM estimated data are quite different than the modern temperature-precipitation data. During the Miocene, the Global Mean Temperature (GMT) appears to be 7 – 8°C cooler than the modern time. It is also important to note that were more low temperature localities (< 5°C) and fewer high temperature localities (>20°C). The highest precipitation values were much less than modern, and there appears to have been a precipitation gap at cooler temperatures (-10°C).

Figure 2.4 is a reconstruction of paleo-soil types for the Miocene (10 Ma). As noted previously, the Miocene was a Global Ice House World (Figure 2.2). Consequently, there are few paleo-soil predictions above 30° latitude (stippled areas on Figure 2.4). A broad prediction of Cool Temperate and Polar type paleo-soils (OP and BG Polar) covers much of the northern hemisphere and the southernmost regions of South America, Australia and New Zeeland. Other dominant paleo-soil types (Table 2.2 and pie chart of Figure 2.4) are the XYZ paleo-soil type, a soil from Subtropical Arid Belts (north Africa, Arabia and northeast Brazil) and the Warm Temperate paleo-soil types (A and H) found in southeast North America, Southeast Asia, central and eastern Africa, northern and southwest Australia.

It is important to note that paleo-soil types characteristic of equatorial rainy belt (FN and W) are poorly formed. This suggests that during the Miocene, tropical rainforests were limited in extent. The stippled area along the equator represents temperature-precipitation conditions that do not exist in the modern world; hence no paleo-soil predictions were made for these regions. The pattern of predicted geographic distribution of paleo-soil types in South America is especially complex and requires additional evaluation.

Figure 2.5A illustrates the confidence levels for the predictions for Miocene period. The prediction confidence level is the probability of the paleo-soil predictions based on the Percent Volume Contours (PVC, see chapter 1). In the prediction confidence level map, the darker shades represent higher levels of confidence while the areas with lighter shading represent regions where multiple soil types are predicted without much difference in their prediction confidence levels. The regions with highest levels of confidence are in northeast Brazil, east Africa, central Eurasia, East Asia, north and southwest Australia. Other areas with high levels of confidence include the Black Sea, northern India, central Africa etc.

The soil dominance map (Figure 2.5B) illustrates where a single paleo-soil type predominates. In other words, in regions with high dominance score there is a large gap between the predicted confidence levels of the primary and the secondary (Appendix C) paleo-soil types. Thus the dominance map is similar in many respects to the prediction confidence level map (Figure 2.5A), but with some significant differences. For the Miocene, though the confidence levels are high in central Eurasia, the dominance is only moderate. In North America there are regions with high levels of confidence, but the overall dominance score is intermediate. In northeast Brazil, areas with high levels confidence do not always have high dominance scores.

We have also prepared a reconstruction showing the secondary paleo-soil type (PPS2) predictions for the Miocene period (10 Ma). The reconstruction along with its levels of confidence is illustrated in Appendix C (Figure C.1).

2.3.2 Oligocene (30 Ma)

Global cooling began in the Early Oligocene with the creation of the vast Antarctic Ice Cap (Barker and Kennett 1990). The increase in ice sheets led to a sea level fall. The tropics diminished, giving way to cooler woodlands and grasslands. Although there was a minor warming phase in the Late Oligocene, by and large cooling trends eventually culminated in the Ice Ages of the Pleistocene (www.paleos.com). The Oligocene climate change was the result of

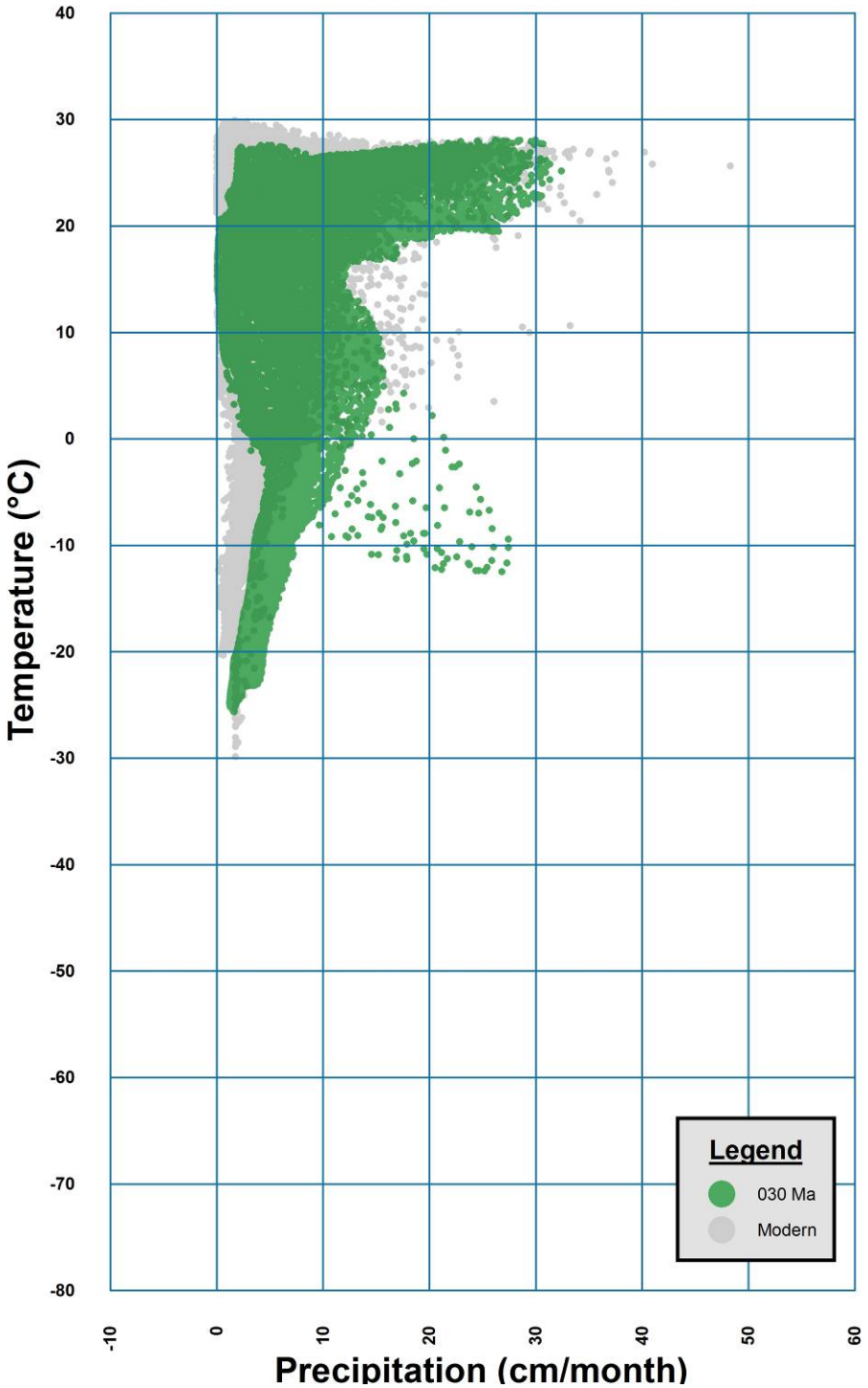

Figure 2.6 Temperature-Precipitation Plot for the Oligocene (030 Ma)

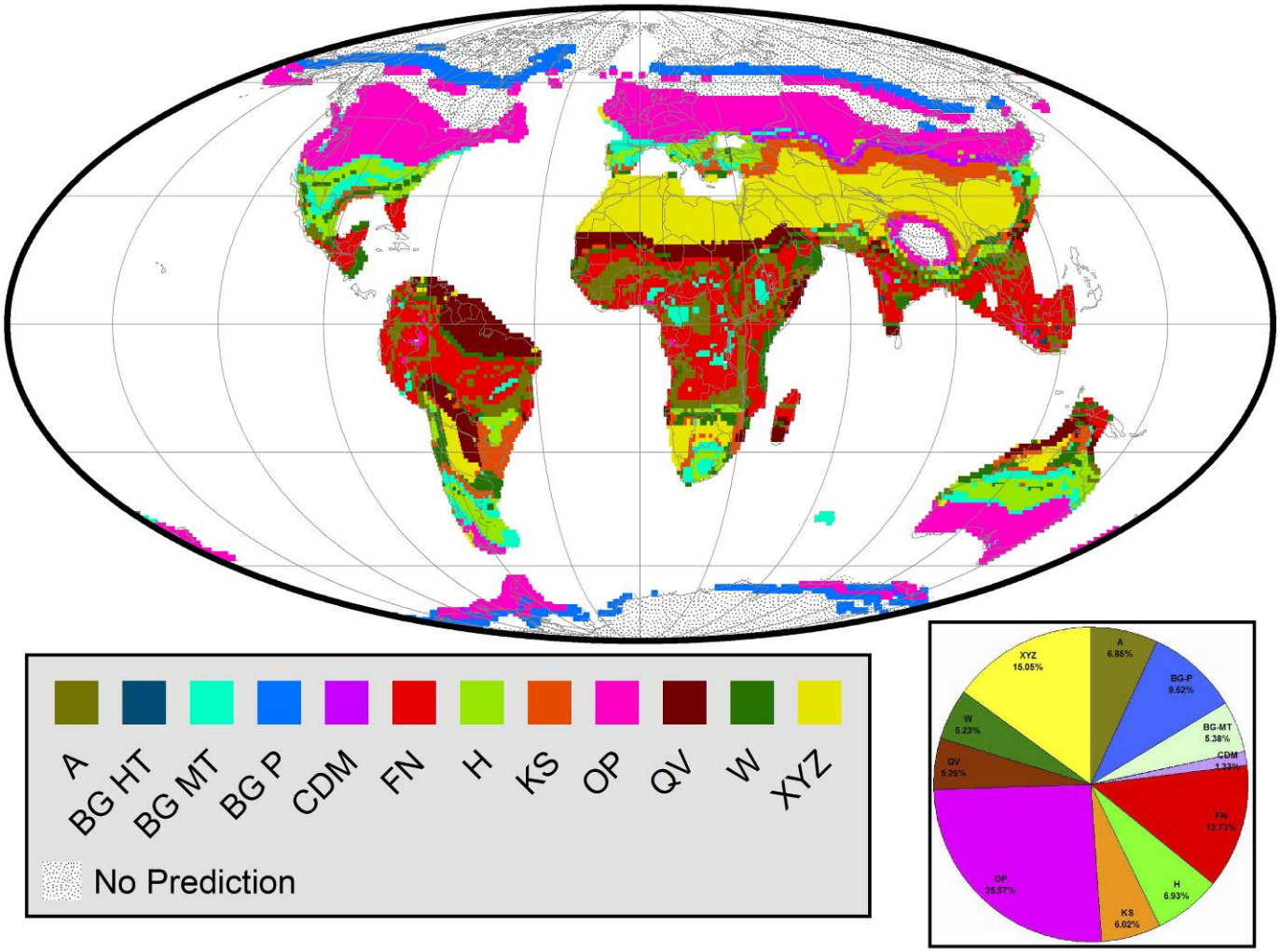

Figure 2.7 Composite Geographic Distribution Map of Primary Predicted Ancient Soils (Paleo-soils) for the Oligocene (030 Ma)

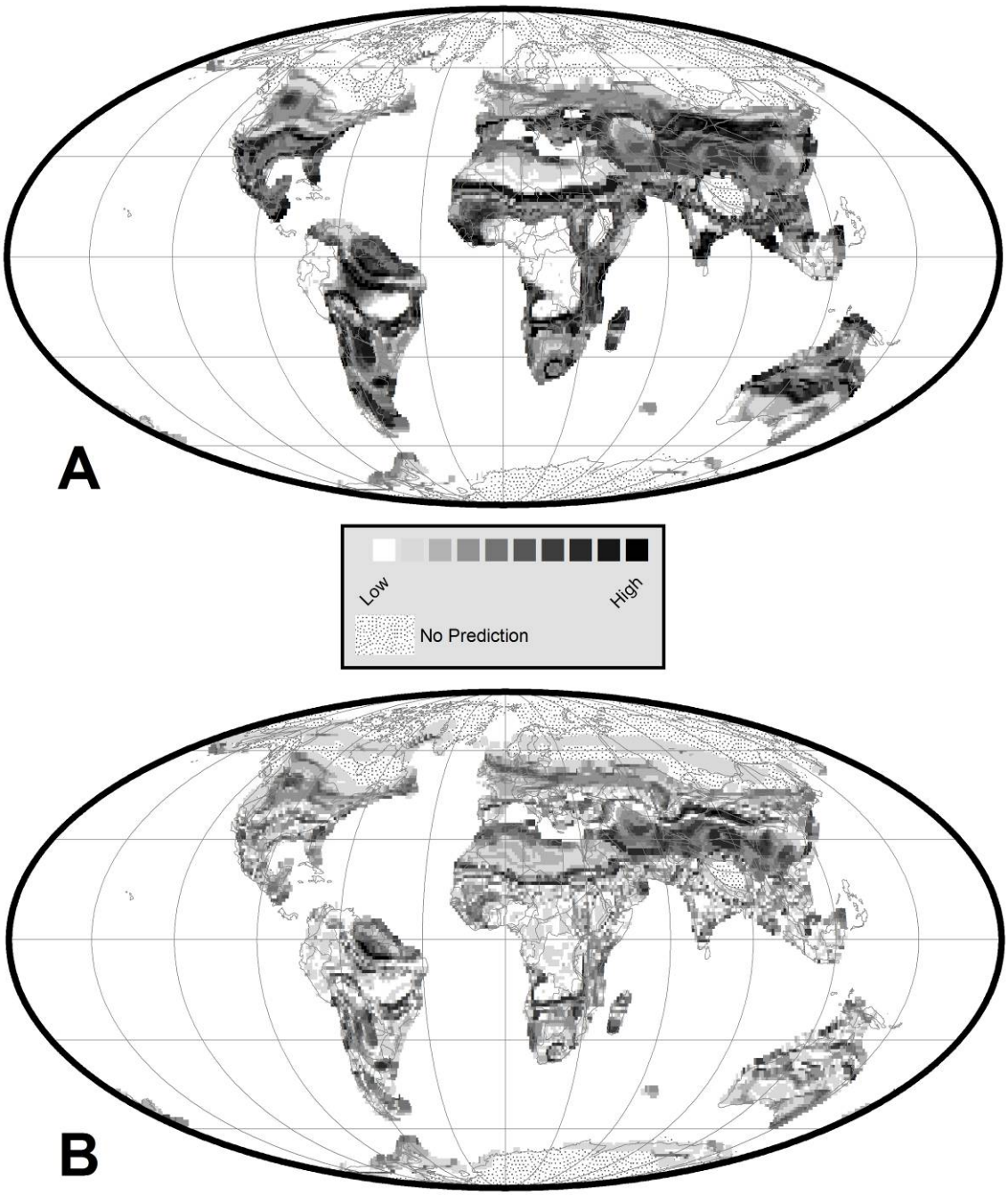

Figure 2.8 A. Prediction Confidence Level for Maximum Probable Paleo-soil Type for Oligocene (030 Ma), B. Dominance of Primary Maximum Probable Paleo-soil Type over the Secondary Maximum Probable Paleo-soil Type for the Oligocene (030 Ma)

a global increase in ice volume (Lisiecki and Raymo 2005) and the associated temperature decrease (Miller et al. 2008).

Figure 2.06 plots the distribution of temperature and precipitation values for the Oligocene (greenish blue) plotted on a background of modern day temperature and precipitation values (gray). For the Oligocene, the maximum temperature and precipitation values were 28.06°C and 32.41 cm/month, respectively. The minimum temperature and precipitation values were -25.66°C and 0.08 cm/month, respectively. It is clear from this plot that the temperature-precipitation values for the Oligocene are quite similar to modern temperature-precipitation data. During the Oligocene, the Global Mean Temperature (GMT) appears to be 2 - 3°C cooler than the modern time. It is also important to note that overall there was more precipitation during the Oligocene. Unlike the modern data, highest precipitation values are associated with highest temperatures. There appears to have been a precipitation gap at cooler temperatures (0 ~ -20°C).

Figure 2.07 is a reconstruction of ancient paleo-soil types for the Oligocene (30 Ma). As noted previously, the Oligocene being a Global Hot House World, there are only few paleo-soil predictions above 60° latitude (stippled areas on Figure 2.07). Polar type paleo-soil (BG Polar), Cool Temperate type paleo-soil (OP) and Subtropical Arid paleo-soil types (XYZ and QV) cover much of the northern hemisphere and the south-central regions of South America, southern Africa, western and southern Australia, and most of New Zealand. Other dominant paleo-soil types (Table 2.2 and pie chart of Figure 2.27) are the FN, A and H paleo-soil types. FN, an Equatorial Rainy belt soil, is found in southern Mexico, southern Florida, central and western South America, Central Africa, peninsular India, Southeast Asia and northern tip of Australia. The warm temperate paleo-soil types (A and H) found in southern North America, southern Europe, central Australia, dispersed throughout eastern and western South America, central Africa, and southeastern Asia.

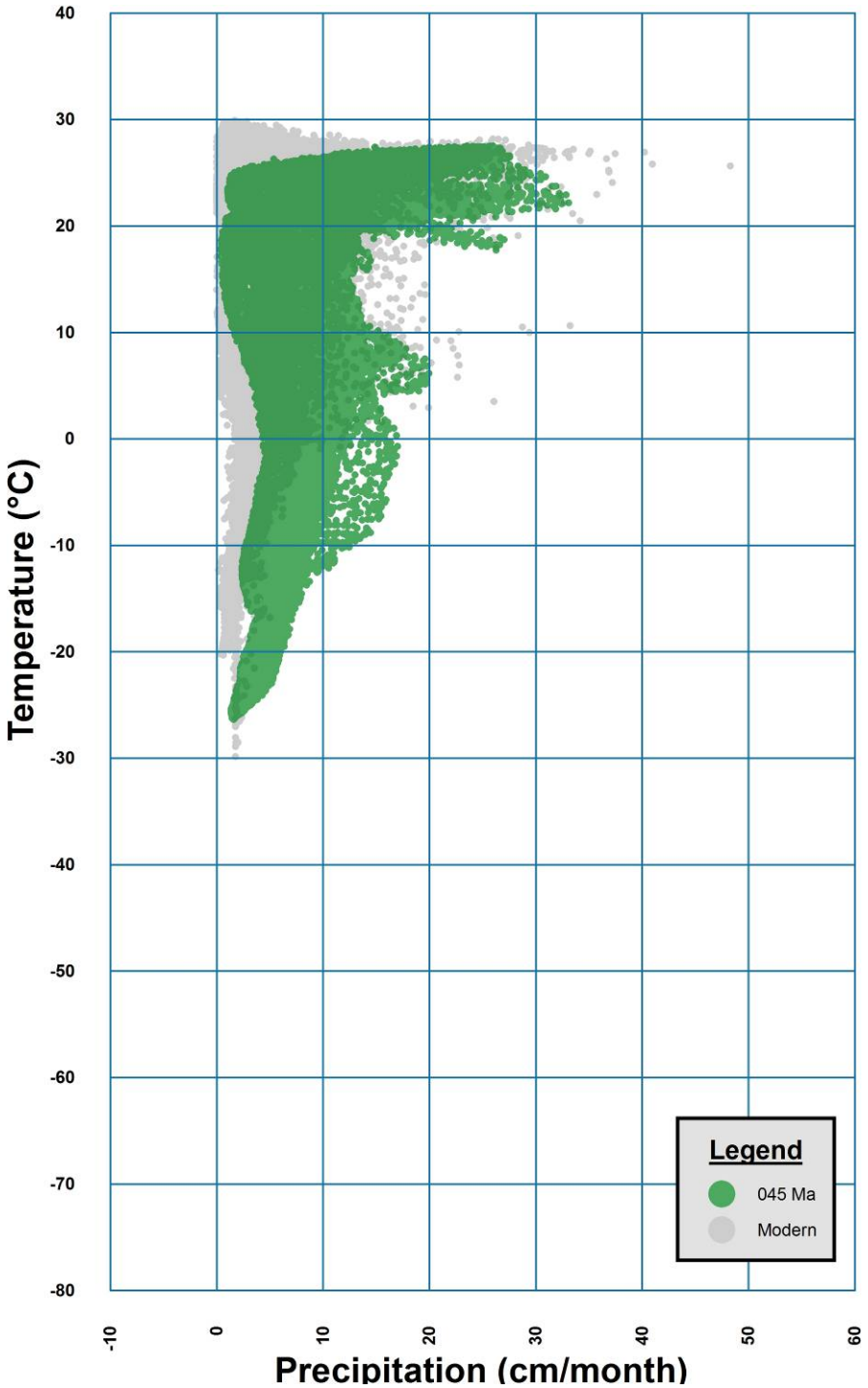

Figure 2.9 Temperature-Precipitation Plot for the Eocene (045 Ma)

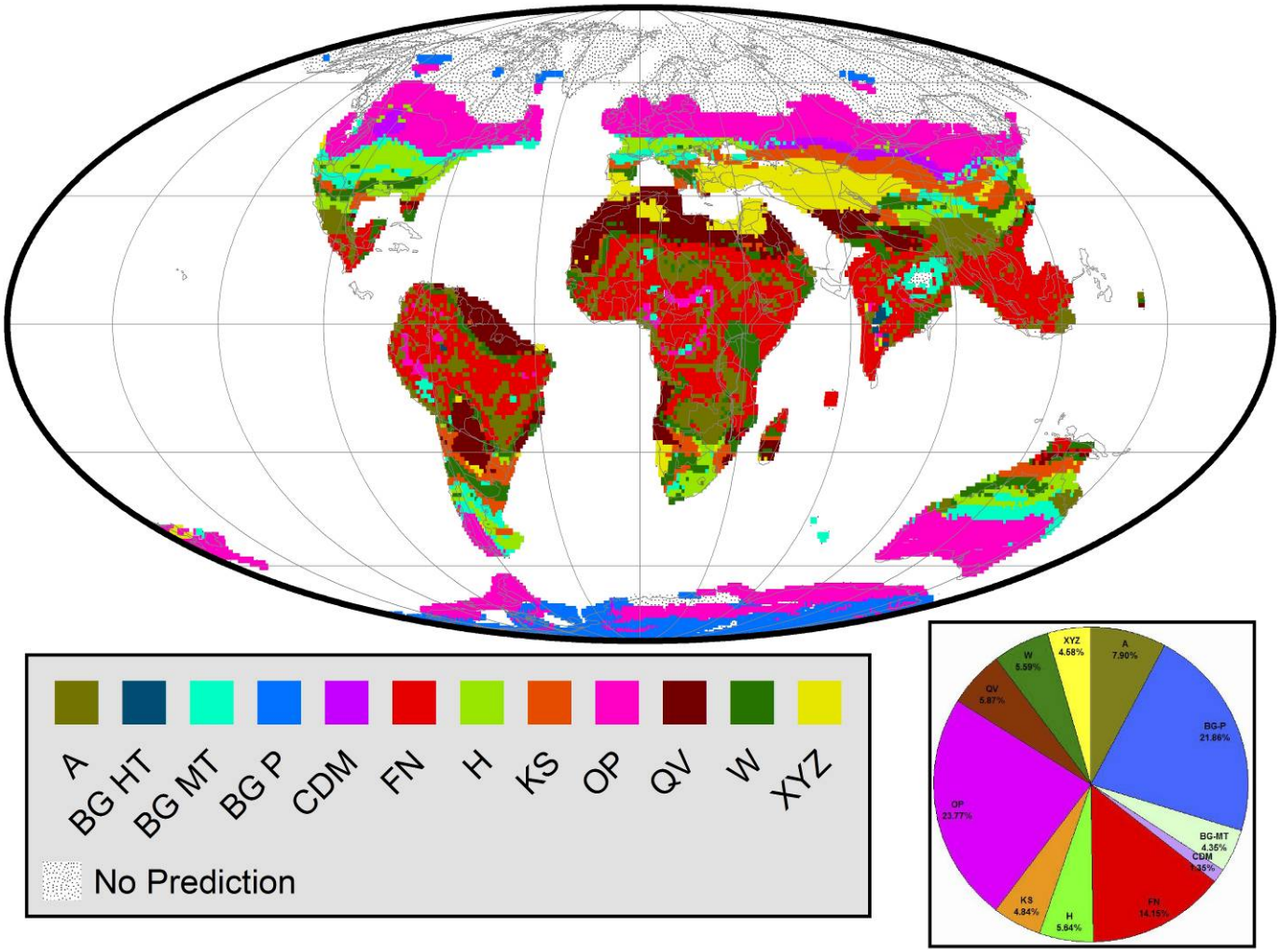

Figure 2.10 Composite Geographic Distribution Map of Primary Predicted Ancient Soils (Paleo-soils) for the Eocene (045 Ma)

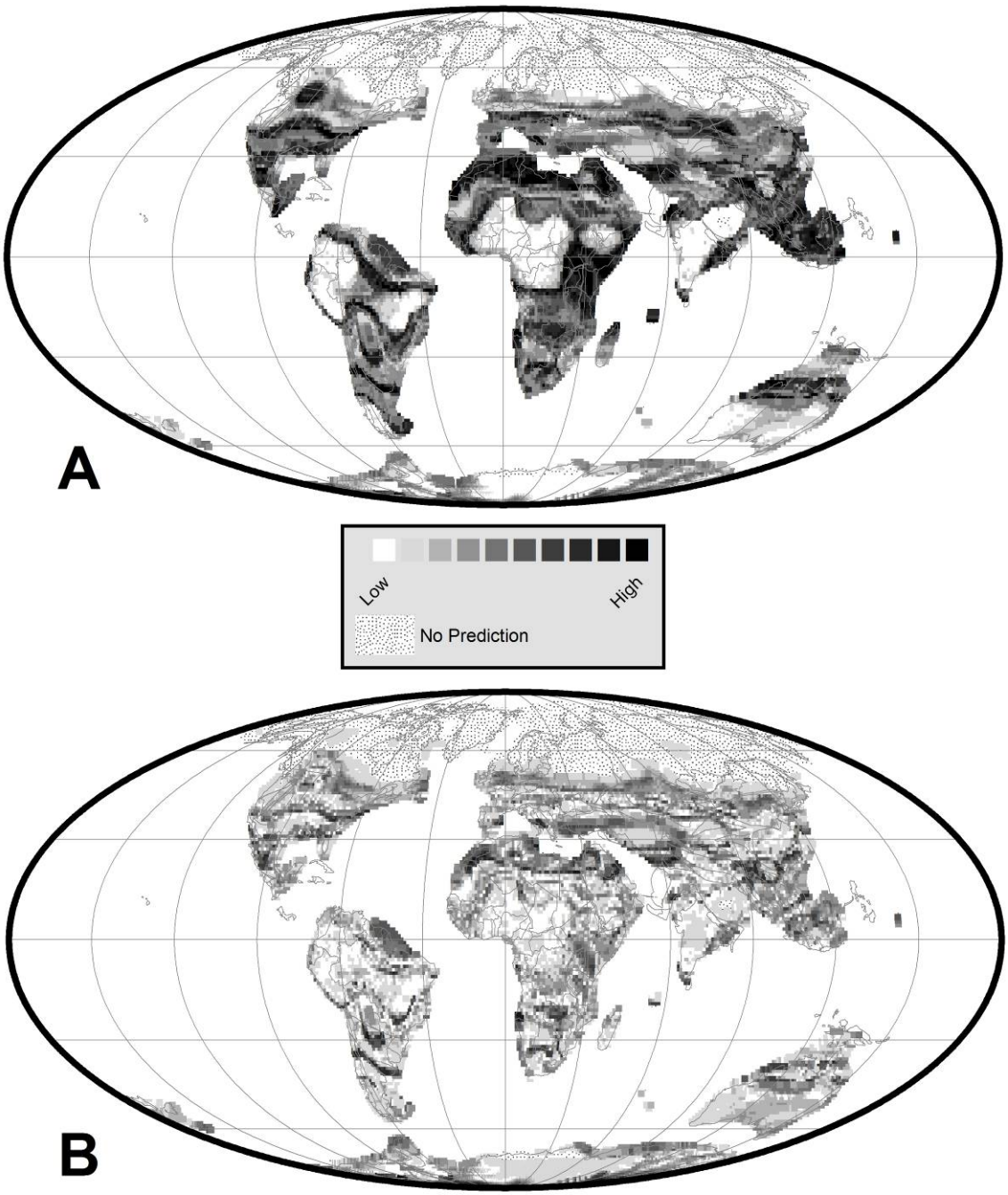

Figure 2.11 A. Prediction Confidence Level for Maximum Probable Paleo-soil Type for the Eocene (045 Ma), B. Dominance of Primary Maximum Probable Paleo-soil Type over the Secondary Maximum Probable Paleo-soil Type for the Eocene (045 Ma)

The vast predicted geographic range of equatorial Rainy Belt soils suggests that during the Oligocene, tropical rainforests were widespread. The stippled area near the 20 °N latitude (Figure 2.07) represents temperature-precipitation conditions that do not exist in the modern world. Hence no paleo-soil predictions were made for these regions. South America and Australia have a relatively complex paleo-soil distribution pattern that requires additional evaluation.

Figure 2.08A illustrates the confidence levels for the predictions of paleo-soils for Oligocene period. The regions with highest levels of confidence occur in the central regions of North America, South America, Eurasia, Australia and are represented in darker shading. Other areas with high levels of confidence include southern margins of the Sahara Desert, peninsular India, Myanmar, etc.

The paleo-soil dominance map (Figure 2.08B) is similar in many respects to the prediction confidence level map (Figure 2.08A) but with some significant differences. For the Oligocene, though the confidence levels are high in several regions around the globe, the dominance levels are mostly moderate to low. Only in regions of central Asia there are high dominance scores.

We have also prepared a reconstruction showing the secondary paleo-soil type (PPS2) predictions for the Oligocene period (30 Ma). The reconstruction along with its levels of confidence is illustrated in Appendix C (Figure C.2).

2.3.3 Eocene (45 Ma)

Global climate during the Eocene was possibly the most equable during Cenozoic. The temperature gradient from equator to pole was only half of today's temperature gradient (Andreasson and Schmitz 2000) and deep ocean currents were exceptionally warm (Norris et al. 2001). The Eocene was a Hot House World (Figure 2.2) and the Polar Regions were much warmer than today, perhaps as mild as the modern-day Pacific Northwest. Temperate forests extended to the poles, while rainy tropical climates extended as far north and south as 45°. The

Tropics were much warmer than today (Huber 2009, Head et al. 2009) — a conclusion that is in accord with numerical simulations of the climate during the Eocene (Huber and Sloan 2001). Overall, global climate during the Late Eocene was warmer than today. Ice had just begun to appear at the South Pole. India was covered by tropical rainforests, and warm temperate forests were found throughout much of Australia. It is notable that during the Early Eocene alligators swam in swamps near the North Pole and palm trees grew in southern Alaska. Much of central Eurasia was also warm and humid (www.scotese.com).

Figure 2.09 plots the distribution of temperature and precipitation values for the Eocene (olive green) plotted on a background of modern day temperature and precipitation values (gray). For the Eocene, the maximum temperature and precipitation values were 27.50°C and 33.08 cm/month, respectively. The minimum temperature and precipitation values were -26.37°C and 0.38 cm/month, respectively. It is clear from this plot that the FOAM estimated data are quite similar to the modern temperature-precipitation data. During the Eocene, the Global Mean Temperature (GMT) appears to be about the same as the modern time. It is also important to note that were more localities with high precipitation below 10°C. The highest precipitation values were less than modern, and were not associated with highest temperatures. There appears to have been a precipitation gap at cooler temperatures (<10°C).

Figure 2.10 is a reconstruction of ancient paleo-soil types for the Eocene (45 Ma). As noted previously, the Eocene was a Global Hot House World, and there are few paleo-soil predictions above 45° latitude (stippled areas on Figure 2.10). In the northern hemisphere there is a broad belt of the Cool Temperate paleo-soil type (OP). Arabia and western Asia are characterized by the Subtropical Arid paleo-soil type (XYZ). In northeastern and central South America, northern Africa, and central west Asia, there are well developed regions with paleo-soil W, which is another Subtropical Arid paleo-soil type. In the equatorial region Equatorial Rainy Belt type paleo-soil (FN) is widely distributed implying that tropical rainforests were extensive during Eocene. In the southern hemisphere, well developed bands of Polar (BG Polar) and Cool

Temperate (OP) paleo-soil types are found in the regions of Antarctic, southern tip of South America and southern Australia and New Zealand. Warm temperate paleo-soil types like A and H are observed in the southern part of North America, south central South America, western Europe, southern Africa, eastern Asia and central Australia. There is some intricate pattern of predicted geographic distribution of paleo-soil types in South America, Africa and northern Australia which are especially complex and requires additional evaluation.

Figure 2.11A illustrates the confidence levels for the predictions of Eocene paleo-soils. The regions with the highest levels of confidence are central North America, northern and eastern central Africa, and Southeast Asia. Other areas with high levels of confidence include northern North America, central Asia, and Western Australia etc.

F1gor the Eocene, the overall dominance score (Figure 2.11B) is moderate. The regions in southeastern North America, northeastern South America, northern Africa and Southeast Asia have relatively high dominance scores.

We have also prepared a reconstruction showing the secondary paleo-soil type (PPS2) predictions for the Eocene period (45 Ma). The reconstruction along with its levels of confidence is illustrated in Appendix C (Figure C.3).

2.3.4 Latest Cretaceous / Maastrichtian (70 Ma)

Global climate during latest Cretaceous was not simple. There were cooler episodes preceding the KT impact as well as some warmer episodes. Two major cool events (71 Ma and 68 Ma) are accompanied by two third-order sea-level regressions (Haq et al., 1987, Dodson et al. 1993). Fossil plants indicate that the climate during Maastrichtian was warm temperate at high and middle latitudes, and subtropical south of 40°N. At high latitudes cold-month mean temperatures were about 3–4°C and probably never dropped below 0°C for extended periods (Golovneva 2000). Precipitation was relatively high (about 70–80 cm) and evenly distributed throughout the year. The annual range of temperatures was similar to that of modern maritime climates, but the latitudinal gradient was lower than at present (Golovneva 2000). The tropics

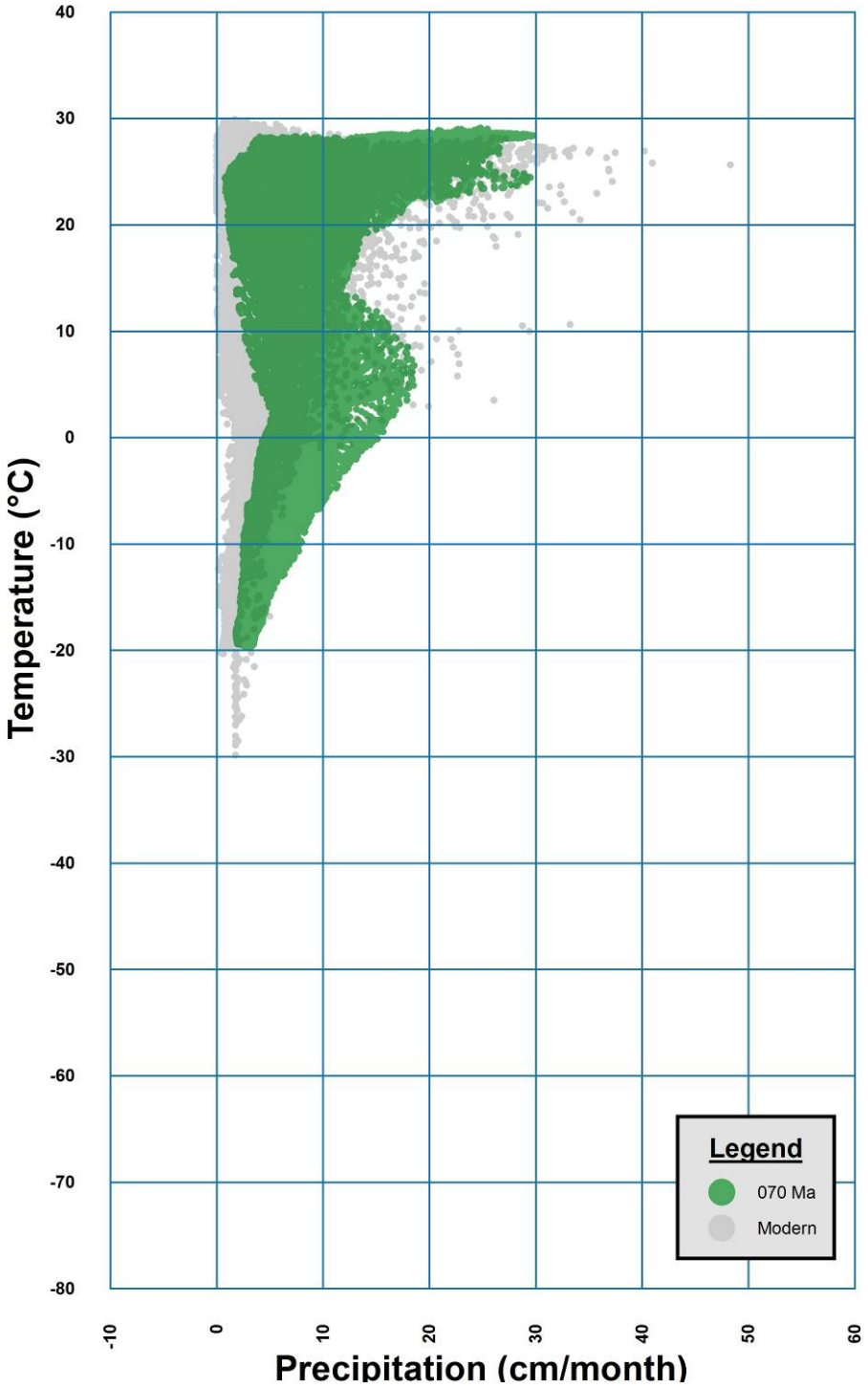

Figure 2.12 Temperature-Precipitation Plot for the Latest Cretaceous / Maastrichtian (70 Ma)

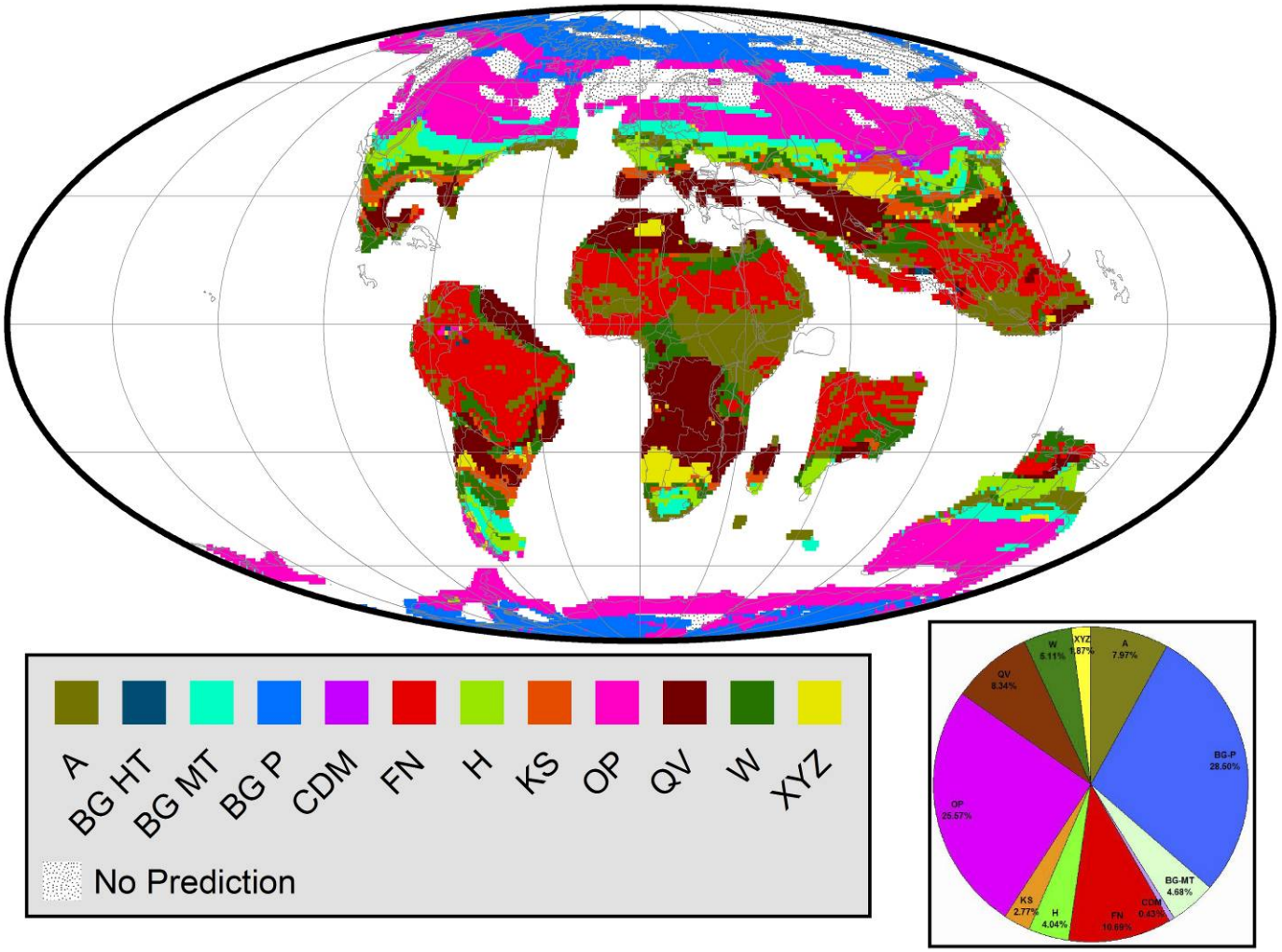

Figure 2.13 Composite Geographic Distribution Map of Primary Predicted Ancient Soils (Paleo-soils) for the Latest Cretaceous / Maastrichtian (70 Ma)

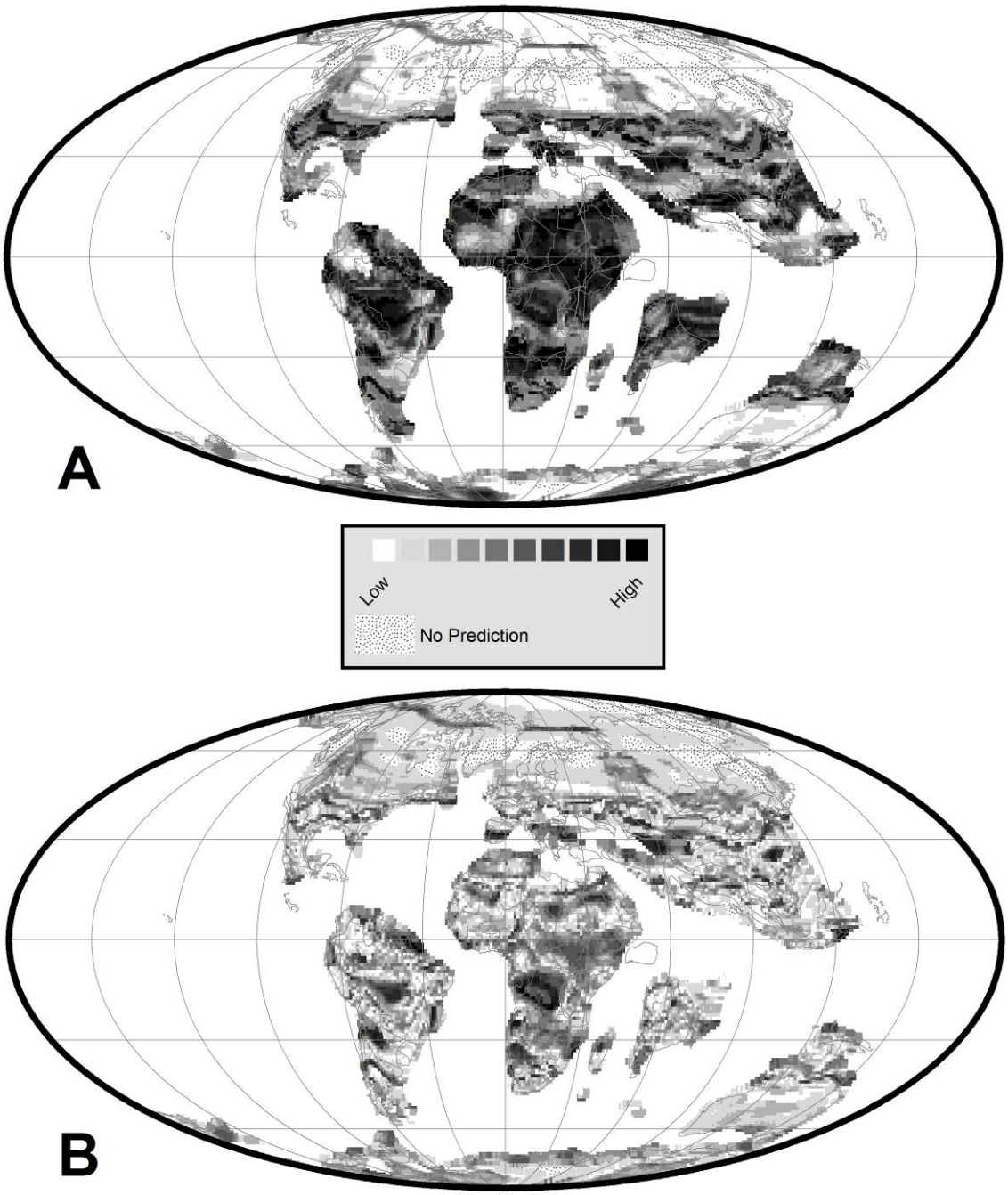

Figure 2.14 A. Prediction Confidence Level for Maximum Probable Paleo-soil Type for the Latest Cretaceous / Maastrichtian (70 Ma), B. Dominance of Primary Maximum Probable Paleo-soil Type over the Secondary Maximum Probable Paleo-soil Type for the Latest Cretaceous / Maastrichtian (70 Ma)

became restricted to equatorial regions and northern latitudes experienced noticeably more seasonal conditions (Dodson et al. 1993). The comparatively mild winter temperatures in polar regions may have been the result of heating by warm oceanic upwelling currents (Golovneva 2000).

Figure 2.12 plots the distribution of temperature and precipitation values for the latest Cretaceous (pink) plotted on a background of modern day temperature and precipitation values (gray). For the latest Cretaceous, the maximum temperature and precipitation values were 29.08°C and 29.73 cm/month, respectively. The minimum temperature and precipitation values were -19.74°C and 0.78 cm/month, respectively. It is clear from this plot that the data from FOAM simulations are quite similar to the modern temperature-precipitation data. During the latest Cretaceous, the Global Mean Temperature (GMT) appears to be 3 – 4°C warmer than modern times. It is also important to note that there were fewer low temperature localities (< 5°C) and more high temperature localities (>20°C). The highest precipitation values were much less than modern, and are associated with the highest temperatures. There appears to have been a precipitation gap at cooler temperatures (10°C ~ -20°C).

Figure 2.13 is a reconstruction of ancient paleo-soil types for the latest Cretaceous (70 Ma). Polar (BG Polar) and Cool Temperate (OP) type paleo-soils cover the northern half of the northern hemisphere and the southern half of the southern hemisphere. In the low latitudes Equatorial Rainy Belt paleo-soils (Mostly FN and W) are widespread across much of northern South America, north central Africa, Southeast Asia, India and northern part of Australia. This implies that rainforests were extensive in these regions during Late Cretaceous. Significant occurrences of Subtropical Arid Belt paleo-soils (mainly QV and a little XYZ) are observed around the Gulf of Mexico, southern Eurasia, northern and south central Africa, and Madagascar. It is important to note that the northeastern part of South America also has a belt of QV paleo-soil type.

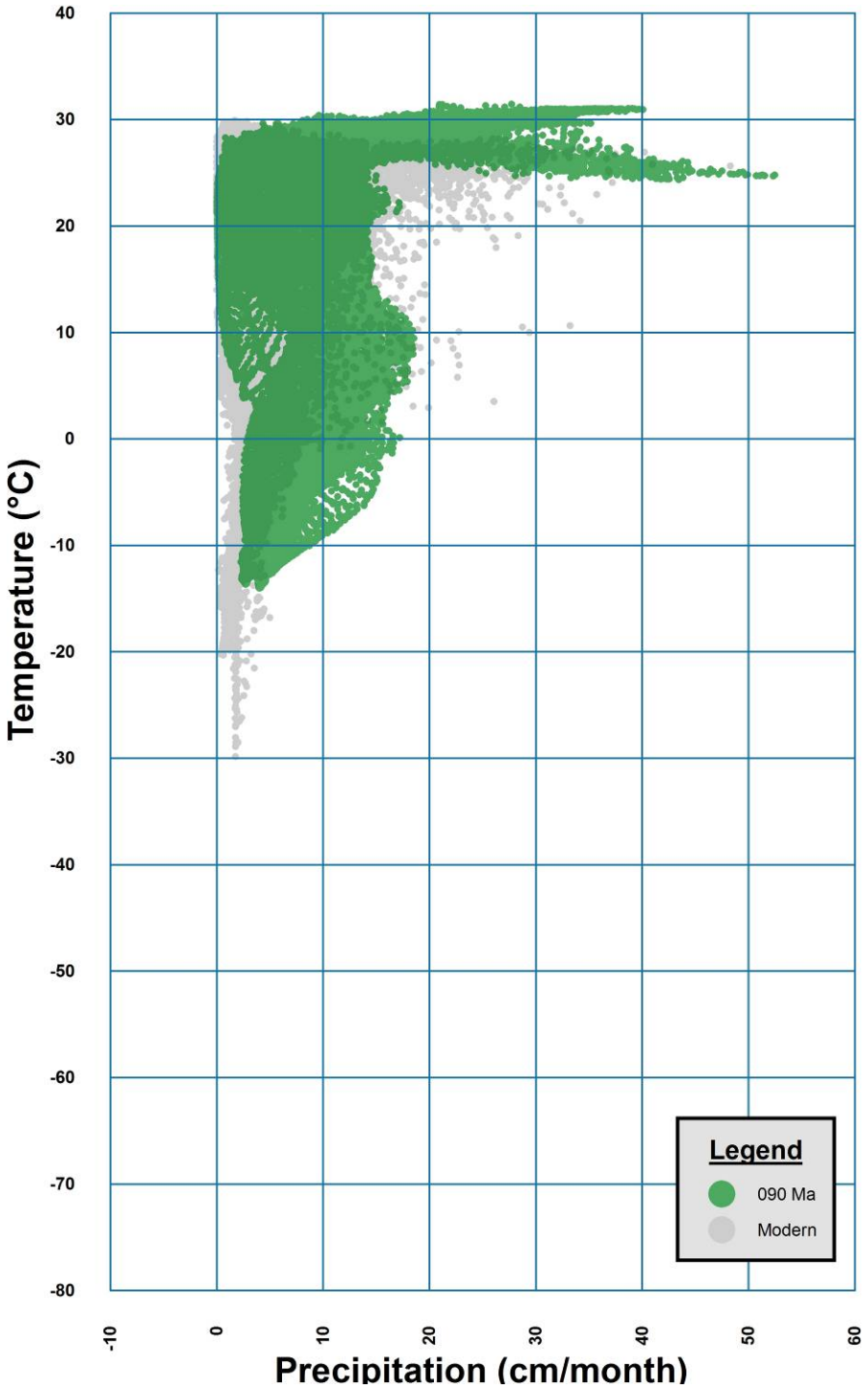

Figure 2.15 Temperature-Precipitation Plot for the Late Cretaceous/ Cenomanian-Turonian (90 Ma)

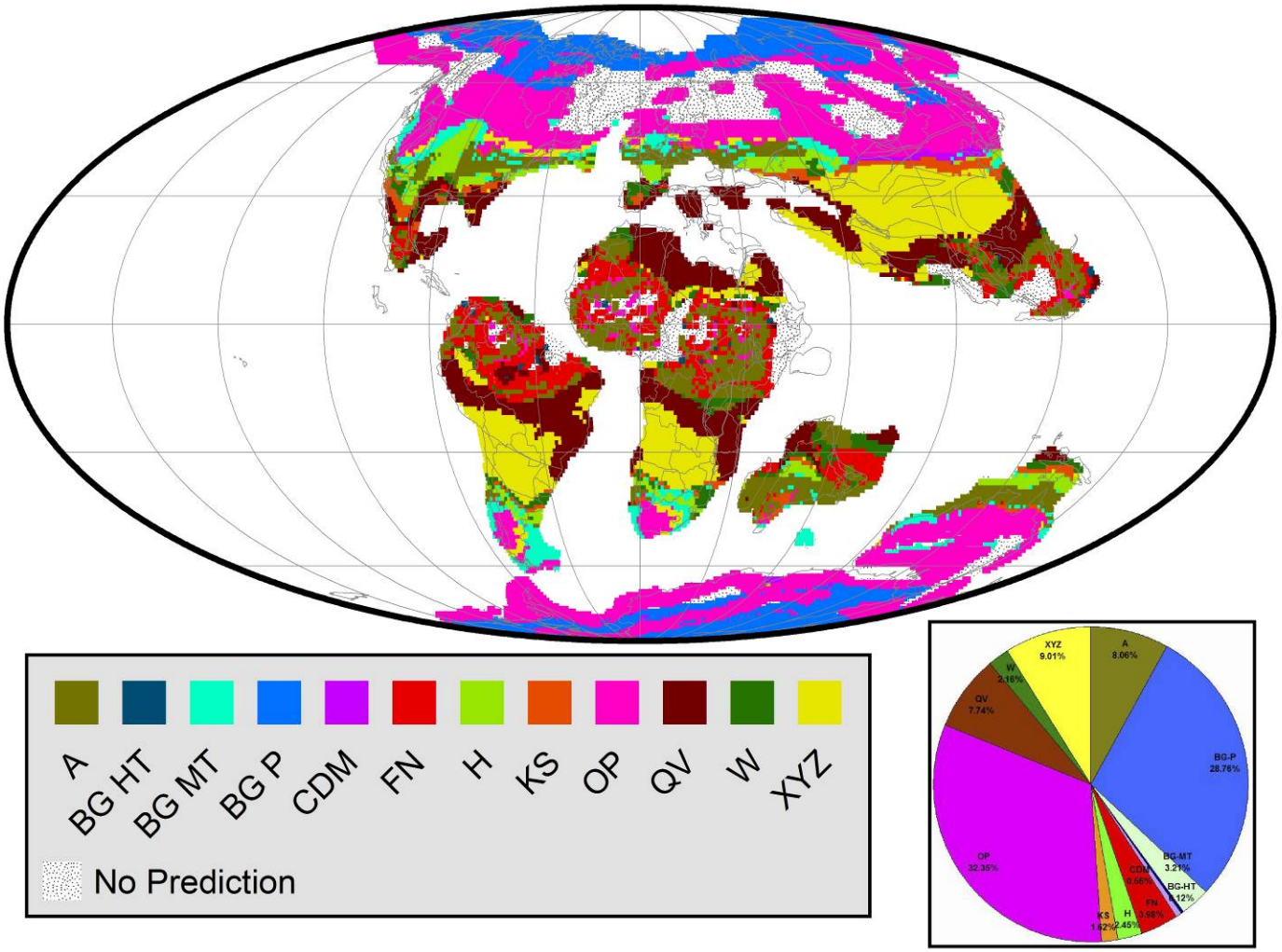

Figure 2.16 Composite Geographic Distribution Map of Primary Predicted Ancient Soils (Paleo-soils) for the Late Cretaceous/ Cenomanian-Turonian (90 Ma)

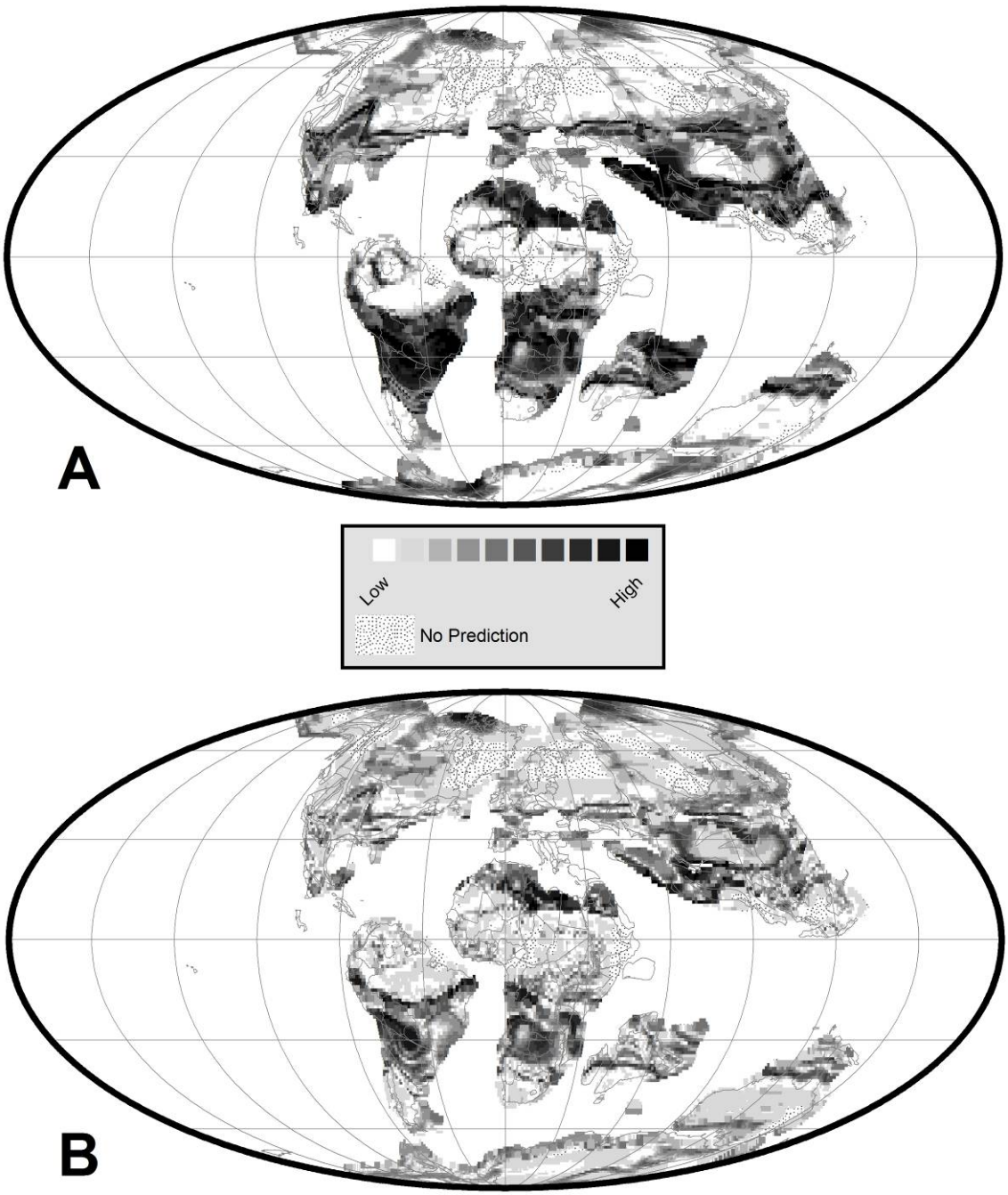

Figure 2.17 A. Prediction Confidence Level for Maximum Probable Paleo-soil Type for the Late Cretaceous/ Cenomanian-Turonian (90 Ma), B. Dominance of Primary Maximum Probable Paleo-soil Type over the Secondary Maximum Probable Paleo-soil Type for the Late Cretaceous/ Cenomanian-Turonian (90 Ma)

The stippled area along the 60°N represents temperature-precipitation conditions that do not exist in the modern world. Therefore, no paleo-soil predictions were made for this region. The patterns of predicted geographic distribution of paleo-soil types in southern South America, India and southeastern Asia are especially complex and requires additional study.

Figure 2.14A illustrates the confidence levels for the predictions for latest Cretaceous period. Overall the levels of confidence for the latest Cretaceous predictions are very high. Northern and southern North America, east central South America and Southeast Asia all have relatively low levels of confidence.

The paleo-soil dominance map (Figure 2.14B) for the latest Cretaceous is very different from the confidence level map (Figure 2.14A). Except central South America, south central Africa and central west Asia, the overall dominance scores are medium to low. This implies that during the Late Cretaceous, more than one type of paleo-soil may have been predominant.

We have also prepared a reconstruction showing the secondary paleo-soil type (PPS2) predictions for the Latest Cretaceous / Maastrichtian period (70 Ma). The reconstruction along with its levels of confidence is illustrated in Appendix C (Figure C.4).

2.3.5 Late Cretaceous/ Cenomanian-Turonian (90 Ma)

The Cenomanian-Turonian (CT) was a period of dramatic palaeoenvironmental change, characterized by a major global positive excursion of δ13C, that occurs in marine carbonate and both marine and terrestrial organic matter (Schlanger et al., 1987; Arthur et al., 1988; Jenkyns et al., 1994). The Cenomanian-Turonian time was the warmest period during the Cretaceous. By mid-Cretaceous times, the Tethys Ocean had begun to close. Deposition of black shales occurred in many basinal and oceanic areas on a global scale, generating one of the world's most important petroleum source rock intervals (Pearce et al. 2009). Enhanced rate of sea-floor spreading and concomitant increase in the volume of mid-ocean ridges resulted in a major eustatic sea-level rise (Schlanger and Jenkyns 1976, Jenkyns 1980, Hays and

Pitman,1973; Schlanger et al., 1981; Larson, 1991). Evidence also points towards an unusually high rate of volcanic activity, especially at mid-oceanic ridges. Rates of sea-floor spreading were about three times as high as they are today. Volcanic outgassing led to increased atmospheric CO_2 concentrations, increased terrestrial weathering and nutrient fluxes, and decreased levels of atmospheric oxygen (Pearce et al. 2009). During the Cenomanian-Turonian time sea levels rose dramatically (200 m higher than present levels) flooding up to 40% of the continents and resulting in the widespread deposition of chalk-dominated facies. The Western Interior Seaway of the USA was at that time, at its maximum. Much of central and western Europe was under water. During Cenomanian–Turonian interval, the atmosphere had high levels of atmospheric CO_2 concentrations, up to four times the present (Berner and Kothavala 2001). Other authors (Barron et al. 1995) have suggested that plate motions may have significantly altered oceanic circulations resulting in global warming.

Figure 2.15 plots the distribution of temperature and precipitation values for the Cenomanian (tan) plotted on a background of modern day temperature and precipitation values (gray). For the Cenomanian, the maximum temperature and precipitation values were 31.42°C and 52.47 cm/month, respectively. The minimum temperature and precipitation values were -14.01°C and 0.04 cm/month, respectively. It is clear from this plot that the data from FOAM simulations are quite different than the modern temperature-precipitation data. During the Cenomanian, the Global Mean Temperature (GMT) appears to be 5 – 6°C warmer than the modern time. It is also important to note that were less low temperature localities (< 5°C) and more high temperature localities (>20°C). The highest precipitation values were greater than modern, and mostly associated with higher temperatures. There appears to have been a precipitation gap at low temperatures (5 ~ -10°C).

Figure 2.16 is a reconstruction of ancient paleo-soil types for the Cenomanian (90 Ma). The Cenomanian was classic example of a Global Hot House World (Figure 2.2). Therefore, it seems unusual that the model predicts broad belts of Polar (BG Polar) and Cool Temperate

(OP) type paleo-soil areas in much of the northern hemisphere and in the southernmost regions of South America, Africa, Australia and Antarctica. Subtropical Arid Belt paleo-soils (XYZ and QV) are extensive and are found in southern North America, central South America, northern and south central Africa and Southeast Asia.

It is important to note that paleo-soil types characteristic of Equatorial Rainy Belt (FN and W) are poorly formed except in northern South America. This suggests that during Cenomanian, tropical rainforests were limited in extent. The stippled area along the equator and at 60° latitude represents temperature-precipitation conditions that do not exist in the modern world, hence no paleo-soil predictions were made for these regions. The patterns of predicted geographic distribution of paleo-soil types in South Africa, India and Southeast Asia are especially complex and requires additional evaluation.

Figure 2.17A illustrates the confidence levels for the predictions for Cenomanian/Turonian period. The regions with highest levels of confidence are in central South America, south central Africa, northern India and southwest Asia. Other areas with high levels of confidence include northern Africa, northern Australia, etc.

The paleo-soil dominance map (Figure 2.17B) is different in many respects to the prediction confidence level map (Figure 2.17A), but there are some significant similarities. For the Cenomanian, though the confidence levels are high in several regions around the globe, the paleo-soil dominance levels are mostly low. Only a few regions like central South America, northern and south central Africa and southwest Asia have high paleo-soil dominance scores.

We have also prepared a reconstruction showing the secondary paleo-soil type (PPS2) predictions for the Late Cretaceous/ Cenomanian-Turonian period (90 Ma). The reconstruction along with its levels of confidence is illustrated in Appendix C (Figure C.5).

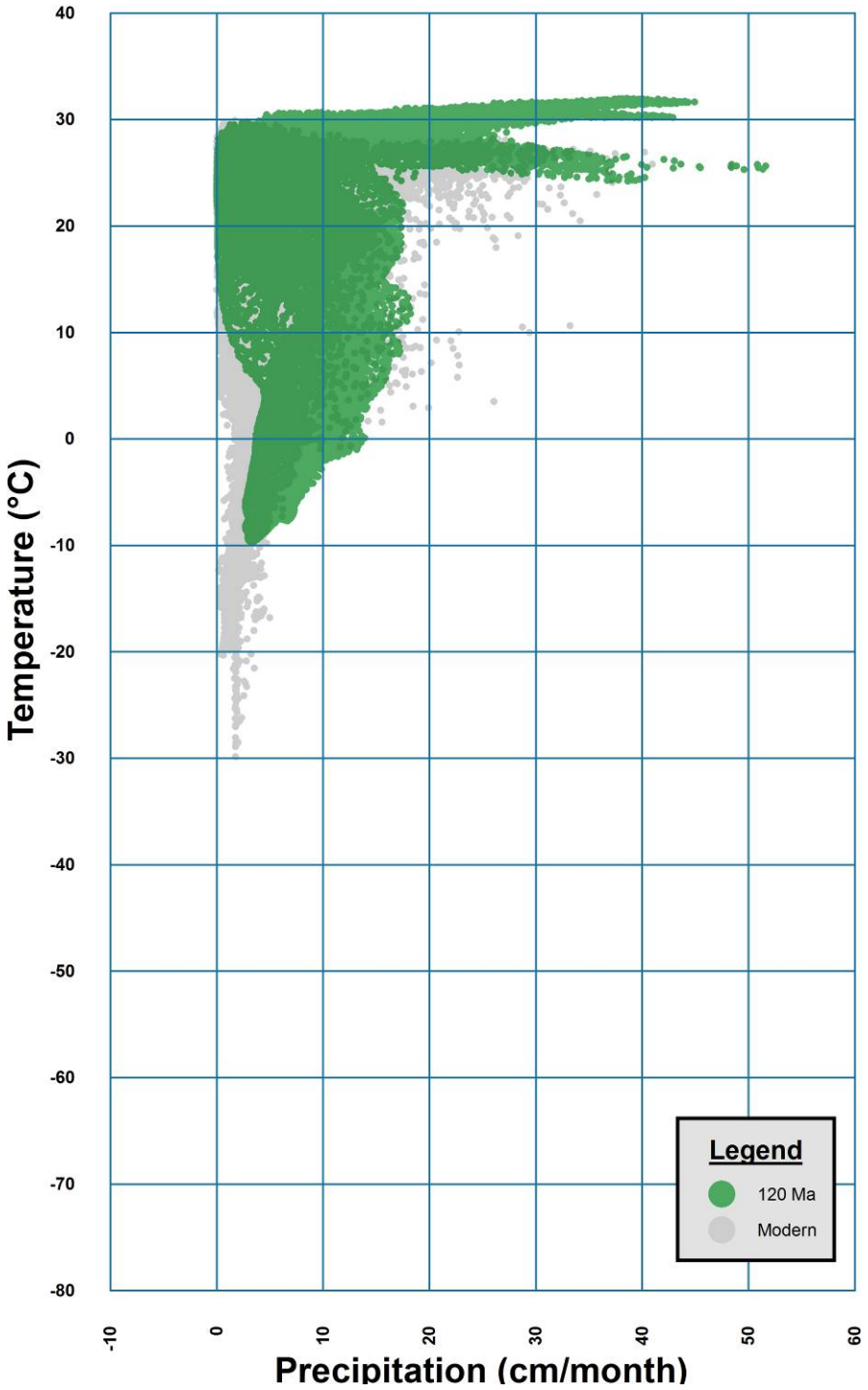

Figure 2.18 Temperature-Precipitation Plot for the Aptian (120 Ma)

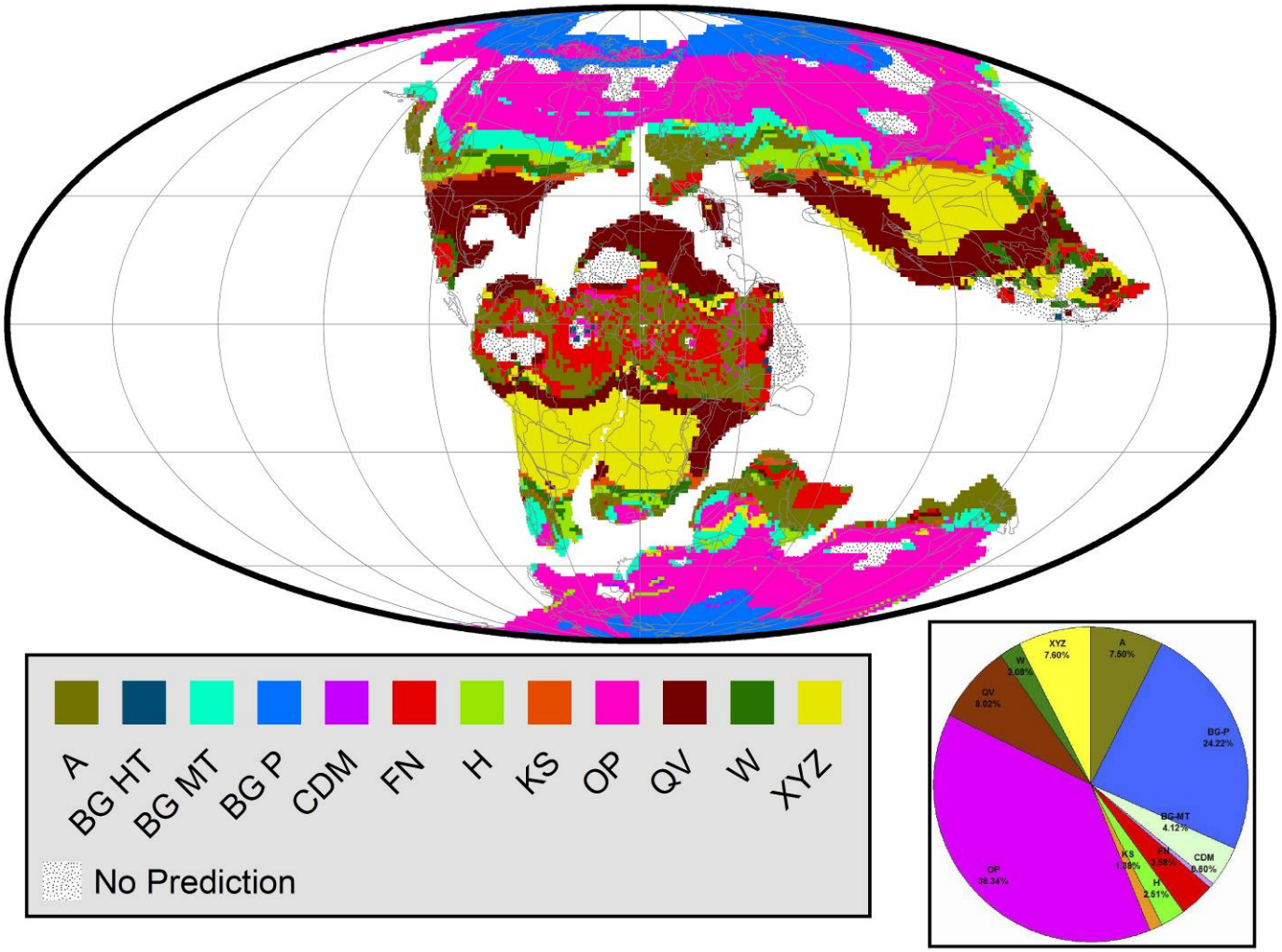

Figure 2.19 Composite Geographic Distribution Map of Primary Predicted Ancient Soils (Paleo-soils) for the Aptian (120 Ma)

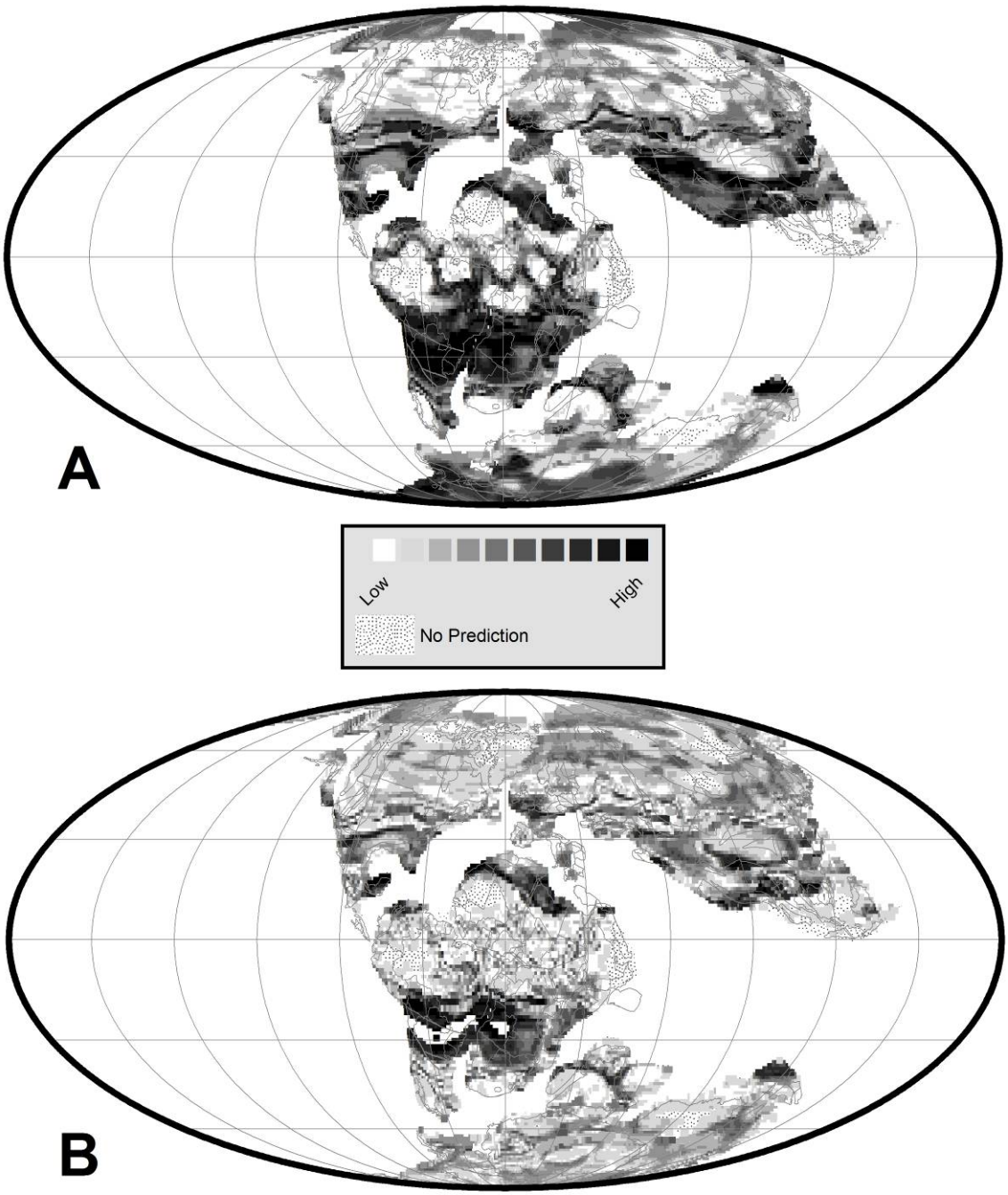

Figure 2.20 A. Prediction Confidence Level for Maximum Probable Paleo-soil Type for the Aptian (120 Ma), B. Dominance of Primary Maximum Probable Paleo-soil Type over the Secondary Maximum Probable Paleo-soil Type for the Aptian (120 Ma)

2.3.6 Aptian (120 Ma)

The Aptian marks the beginning of greenhouse climate conditions in the mid-Cretaceous. During the Early Aptian (120 Ma) there was widespread deposition of organic rich black shales (OAE1a, Arthur et al., 1990). It is not preciously known why these black shales were so widely deposited during this time interval, but the following hypotheses have been proposed: During Aptian large igneous provinces (LIP) and volcanism are reported. Aptian time also had increased rates of sea-floor spreading and hydrothermal activity dominated over continental weathering (Jenkyns 2003). These LIPS and volcanisms helped the global warming and eventually the ocean became very warm. Ultimately methane released from oceanic sediments (Beerling et al. 2002) resulted in a positive feedback and global warming continued. The released of methane was rapidly sequestered by terrestrial and marine components, consequently increased organic carbon and was deposited as black shale.

Figure 2.18 plots the distribution of temperature and precipitation values for the Aptian (red) plotted on a background of modern day temperature and precipitation values (gray). During the Aptian, the maximum temperature and precipitation values were 31.97°C and 51.62 cm/month, respectively. The minimum temperature and precipitation values were -9.70°C and 0.03 cm/month, respectively. It is clear from this plot that the data from FOAM simulations are very different than the modern temperature-precipitation data. During the Aptian, the Global Mean Temperature (GMT) appears to be 6 - 7°C warmer than the modern times. It is also important to note that were fewer low temperature localities (< 5°C) and a greater number of high temperature localities (>20°C). Most of the high precipitation values were more than 50% higher than modern, and occurred in association with high temperatures. There appears to have been a precipitation gap at low temperatures (10 ~ -10°C).

Figure 2.19 is a reconstruction of ancient paleo-soil types for the Aptian (120 Ma). The Aptian marked the start of the Cretaceous Hot House World (Figure 2.2). Broad belts of Polar (BG Polar) and Cool Temperate (OP) cover much of the northern part of hemisphere and southern

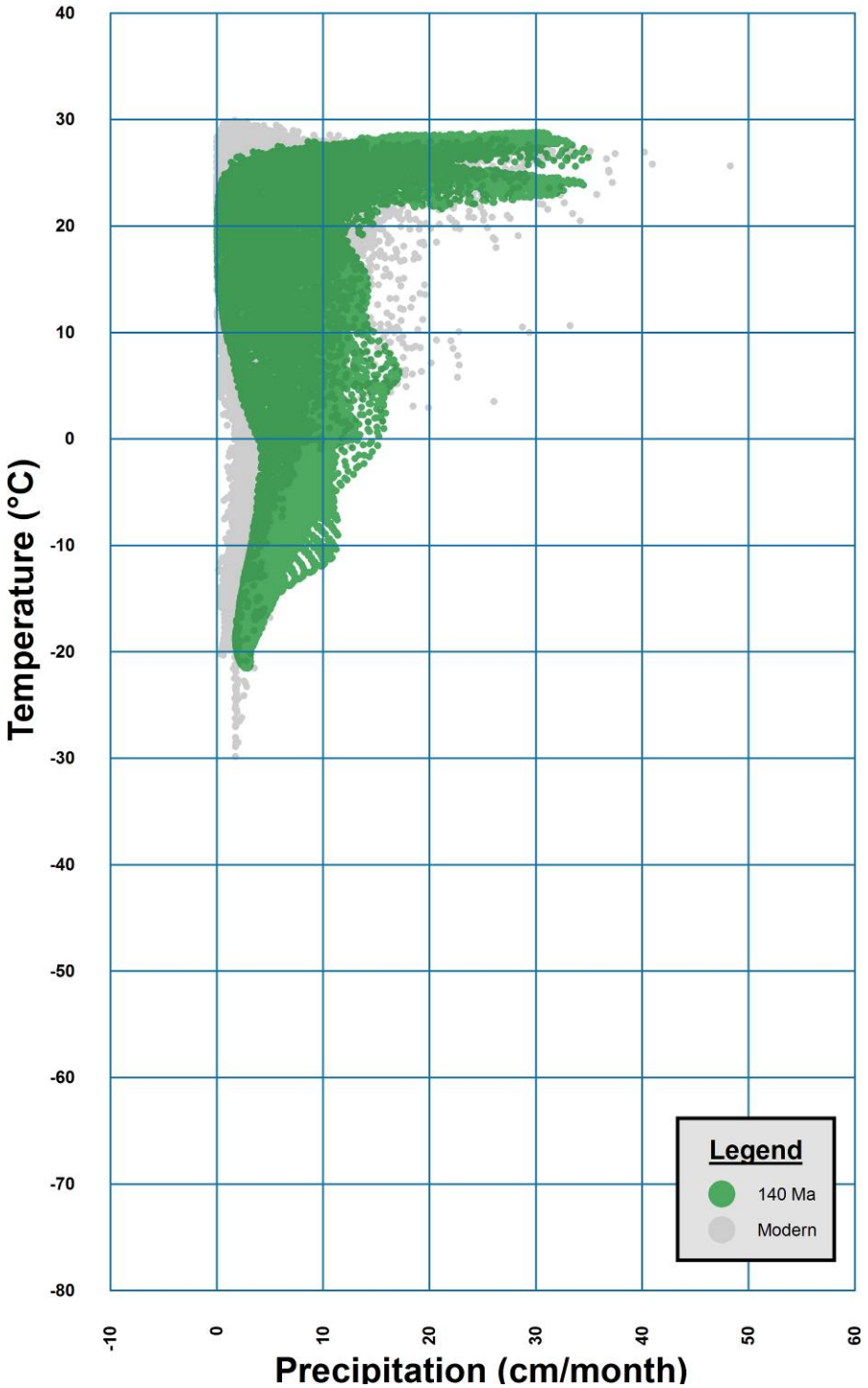

Figure 2.21 Temperature-Precipitation Plot for the Earliest Cretaceous / Berriasian-Valanginian (140 Ma)

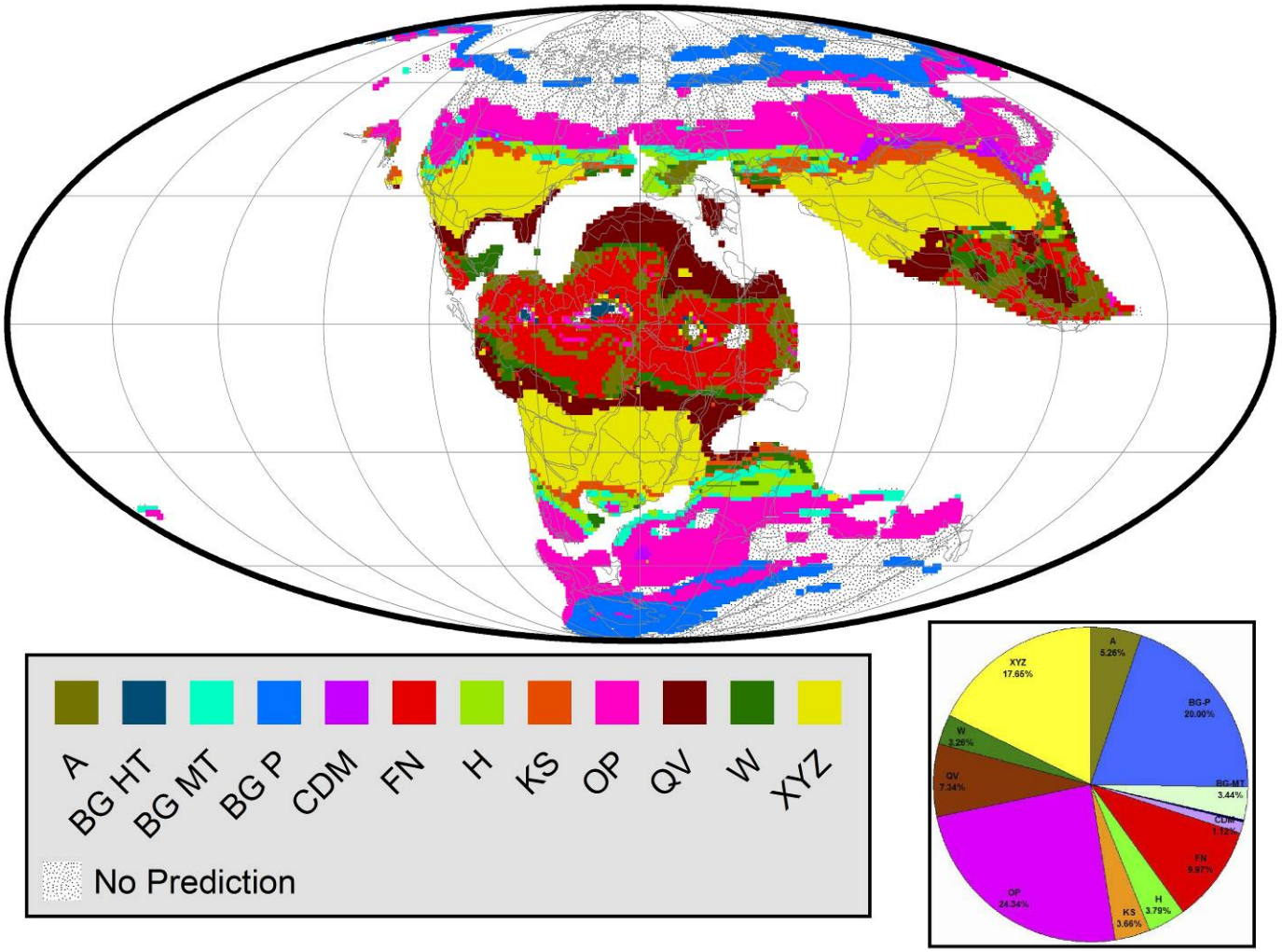

Figure 2.22 Composite Geographic Distribution Map of Primary Predicted Ancient Soils (Paleo-soils) for the Early Cretaceous / Berriasian-Valanginian (140 Ma)

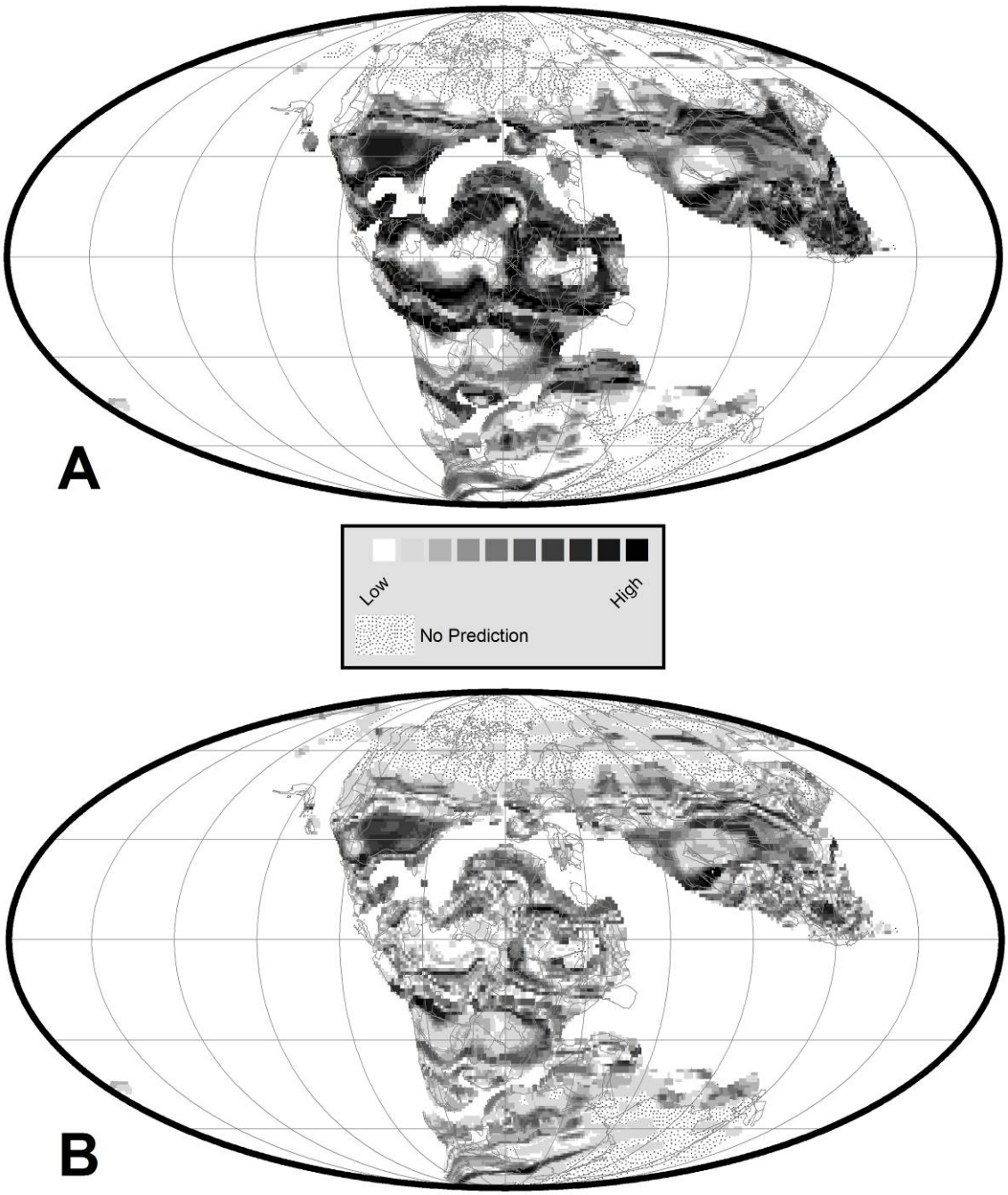

Figure 2.23 A. Prediction Confidence Level for Maximum Probable Paleo-soil Type for the Early Cretaceous / Berriasian-Valanginian (140 Ma), B. Dominance of Primary Maximum Probable Paleo-soil Type over the Secondary Maximum Probable Paleo-soil Type for the Early Cretaceous / Berriasian-Valanginian (140 Ma)

part of southern hemisphere. Other dominant paleo-soil types (Table 2.2 and pie chart of Figure 2.19) are found in the Subtropical Arid Belts (QV and XYZ). The paleo-soil types of Warm Temperate Belts (A and H) are found in central North America, southern South America, Europe, southernmost Africa, India, and northern Australia.

It is important to note that the paleo-soil types found in Equatorial Rainy Belt are a mixture of FN and A which suggests that the climate was a combination of everwet and warm temperate conditions. The stippled area along the equator and at 60° latitude represents temperature-precipitation conditions that do not exist in the modern world. Consequently, no paleo-soil predictions were made for these regions. The patterns of predicted geographic distribution of paleo-soil types in southernmost South America, Africa, south India, Southeast Asia are especially complex and requires additional evaluation.

Figure 2.20A illustrates the confidence levels for the Aptian predictions. The regions with highest levels of confidence are in central South America, south central Africa, and southwest Asia. Other areas with high levels of confidence include the central and southern North America, northern Australia, western Antarctica, etc.

The paleo-soil dominance map (Figure 2.20B) is similar in many respects, to the prediction confidence level map (Figure 2.20A), but with some significant differences. Overall, the dominance score is moderate to low. Areas in central South America, south central Africa, and southwest Asia and northern Australia have high dominance scores.

We have also prepared a reconstruction showing the secondary paleo-soil type (PPS2) predictions for the Aptian period (120 Ma). The reconstruction along with its levels of confidence is illustrated in Appendix C (Figure C.6).

2.3.7 Earliest Cretaceous / Berriasian-Valanginian (140 Ma)

The Early Cretaceous, a mild "Ice House" world. There was snow and ice for the duration of the winter seasons, and cool temperate forests covered the polar regions (Frakes and Francis, 1988 and 1992).

Figure 2.21 plots the distribution of temperature and precipitation values for the Early Cretaceous (violet) plotted on a background of modern day temperature and precipitation values (gray). For the Earliest Cretaceous, the maximum temperature and precipitation values were 28.77°C and 34.94 cm/month, respectively. The minimum temperature and precipitation values were -21.54°C and 0.04 cm/month, respectively. It is clear from this plot that the range of temperature and precipitations during the Berriasian-Valanginian is quite similar to the range of modern temperature-precipitation data. During the Berriasian-Valanginian, the Global Mean Temperature (GMT) appears to be similar to the modern times. There appears to have been a precipitation gap at cool temperatures (<5°C).

Figure 2.22 is a reconstruction of ancient paleo-soil types for the Berriasian-Valanginian (140 Ma). The Earliest Cretaceous was a mild Ice House World (Figure 2.2), consequently, there are few paleo-soil predictions above 45° latitude (stippled areas on Figure 2.22). Overall this map shows a clear distribution of broad belts of paleo-soil types characteristic of different climate belts. It is important to note that not all climate belt soils were equal in extent. The Polar-type (BG Polar), Cool Temperate (OP), and Subtropical Arid (XYZ and QV) paleo-soils are the most extensive. On the other hand, paleo-soil types characteristic of Warm Temperate Belt are almost nonexistent.

Other dominant paleo-soil types (Table 2.2 and pie chart of Figure 2.22) are the FN and W paleo-soil types characteristic of Equatorial Rainy Belt which are found in the northern part of South America-Africa and Southeast Asia. This suggests that during the Early Cretaceous, tropical rainforests were widespread. The stippled areas above 60° latitude represents temperature-precipitation conditions that do not exist in the modern world. Hence, no paleo-soil predictions were made for these regions. The pattern of predicted geographic distribution of paleo-soil types in Southeast Asia is especially complex and requires additional evaluation.

Figure 2.23A illustrates the confidence levels for the predictions for Early Cretaceous period. The regions with highest levels of confidence are in central North America north, and central South

America - Africa block, southwest Eurasia and Southeast Asia. Other areas with high levels of confidence include the central Asia, India, etc.

The paleo-soil dominance map (Figure 2.23B) is very different from the prediction confidence level map (Figure 2.23A). For the Early Cretaceous, though the confidence levels are high in several regions around the globe, the dominance levels are mostly low. Only in regions of central North America, there are high dominance scores. This suggests that in each climatic zone several paleo-soil types were equally dominant.

We have also prepared a reconstruction showing the secondary paleo-soil type (PPS2) predictions for the Earliest Cretaceous / Berriasian-Valanginian period (140 Ma). The reconstruction along with its levels of confidence is illustrated in Appendix C (Figure C.7).

2.3.8 Late Jurassic (160 Ma)

Global climate during Late Jurassic started to change due to the disintegration of Pangea (Weissert and Mohr, 1996). Atmospheric CO_2 levels were high and a monsoonal rainfall pattern prevailed across Pangea (Weissert and Mohr 1996). The interior of Pangea was way dry, and winter snow and ice covered the polar regions (Parrish 1993; Price 1999). On a global scale, evaporites predominated in low latitudes and coals in mid- to high latitudes (Rees et al. 2004). Plant diversity was lowest in equatorial regions, increasing to a maximum in mid-latitudes and then decreasing toward the poles (Rees et al. 2004).

Figure 2.24 plots the distribution of temperature and precipitation values for the Late Jurassic (blue) on a background of modern day temperature and precipitation values (gray). During the Late Jurassic, the maximum temperature and precipitation values were 29.34°C and 41.83 cm/month, respectively. The minimum temperature and precipitation values were -17.16°C and 0.00 cm/month, respectively. It is clear from this plot that the range of temperature and precipitations during the Late Jurassic is different from the range of modern temperature-precipitation values. During the Late Jurassic, the Global Mean Temperature (GMT) appears to be 1 - 2°C warmer than present day. It is also important to note that were fewer low temperature localities (< 5°C). The highest precipitation

values were similar to modern, but generally associated with higher temperatures. There appears to have been a precipitation gap at cooler temperatures (5 ~ -15°C).

Figure 2.25 is a reconstruction of ancient paleo-soil types for the Late Jurassic (160 Ma). The Late Jurassic was a mild Ice House World (Figure 2.2). Several paleo-soil types occupy board geographic belts. Starting at Polar latitudes the following paleo-soil types are arranged from pole to equator pattern: Polar Belt (BG Polar), Cool Temperate Belt (OP), Subtropical Arid Belt (XYZ and QV) and Equatorial Rainy Belt (FN and W). The Warm Temperate Belt paleo-soil type (A and H) are less abundant (Table 2.2 and pie chart of Figure 2.25) and is sandwiched between the Cool Temperate Belt and Arid paleo-soil types.

It is important to note that paleo-soil types characteristic of Equatorial Rainy Belt (FN and W) are widely distributed across north-central Gondwana, suggesting that during Late Jurassic, tropical rainforests were widespread. The stippled areas along the 60° latitude represents temperature-precipitation conditions that do not exist in the modern world. Hence, no paleo-soil predictions were made for these regions.

Figure 2.26A illustrates the confidence levels for the predictions for Late Jurassic period. The regions with highest levels of confidence are the southern margins of western Laurasia, northern boundary of Gondwana and southeastern Asia. Other areas with high levels of confidence occur in western North America, and northern Eurasia, etc.

The paleo-soil dominance map (Figure 2.26B) is similar in many respects to the prediction confidence level map (Figure 2.26A). However, there are some significant differences. For the Late Jurassic, the overall dominance scores are moderate. Regions like western North America, northeastern Gondwana and west central Asia have high dominance scores.

We have also prepared a reconstruction showing the secondary paleo-soil type (PPS2) predictions for the Late Jurassic period (160 Ma). The reconstruction along with its levels of confidence is illustrated in Appendix C (Figure C.8).

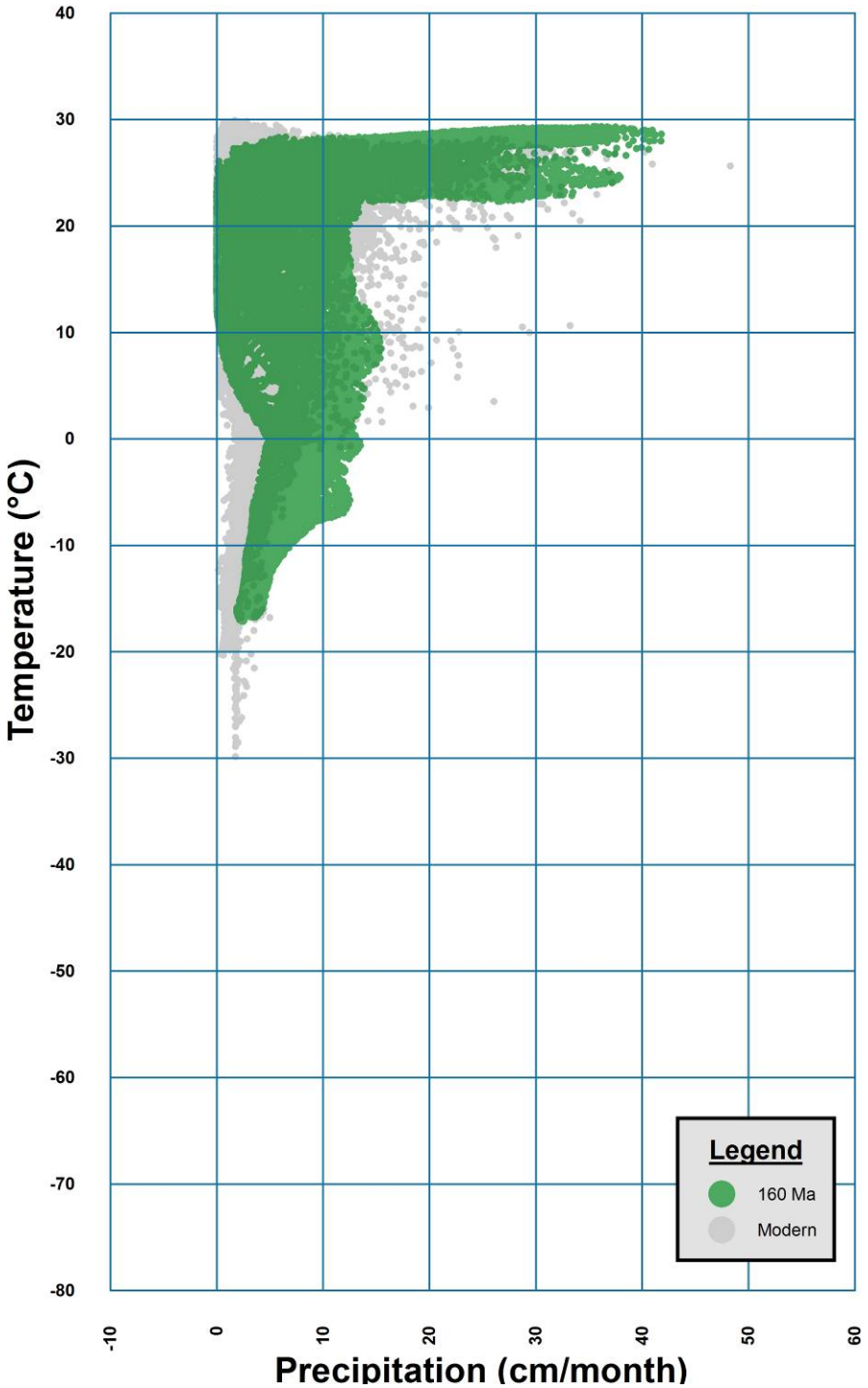

Figure 2.24 Temperature-Precipitation Plot for the Late Jurassic (160 Ma)

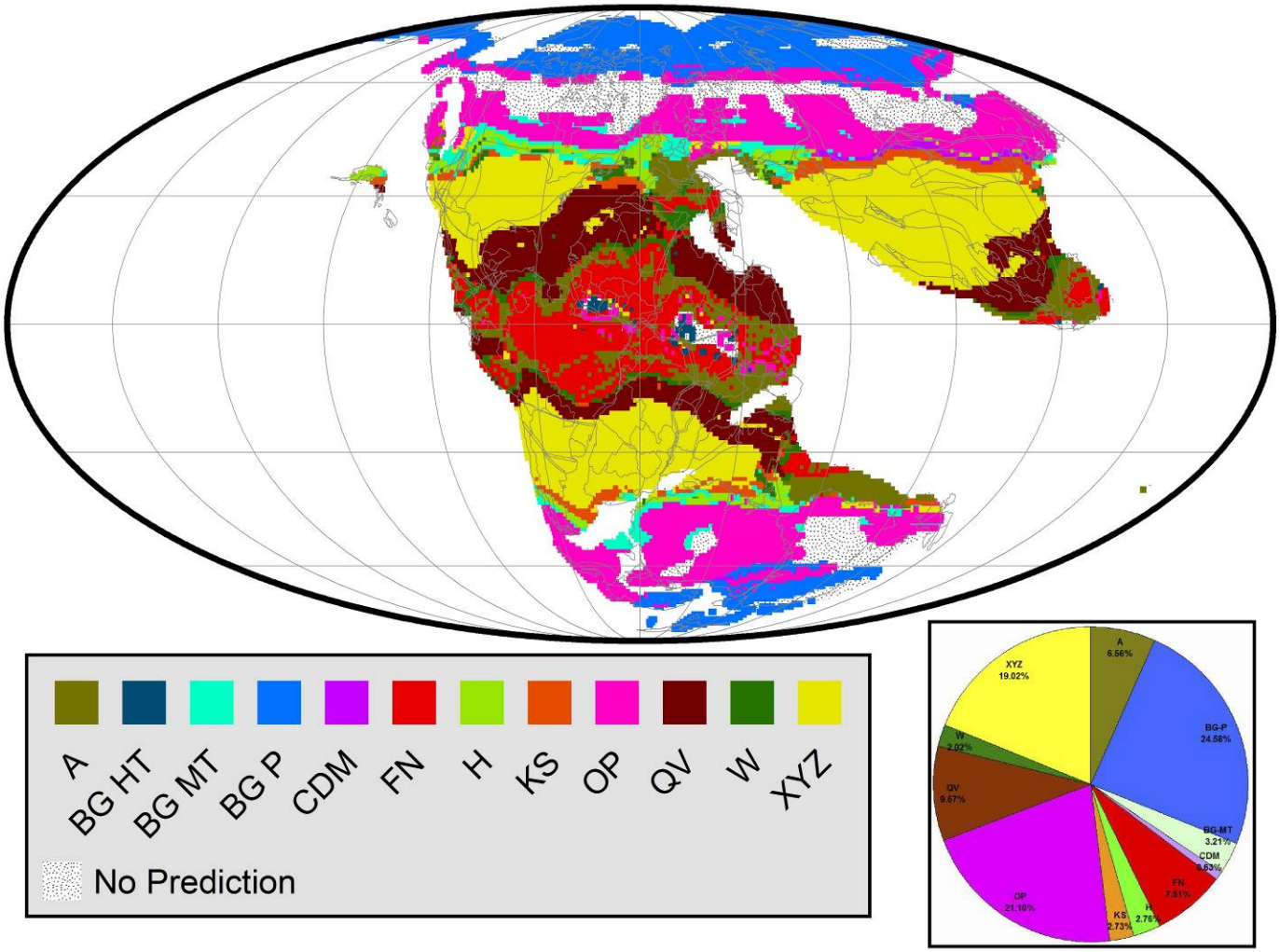

Figure 2.25 Composite Geographic Distribution Map of Primary Predicted Ancient Soils (Paleo-soils) for the Late Jurassic (160 Ma)

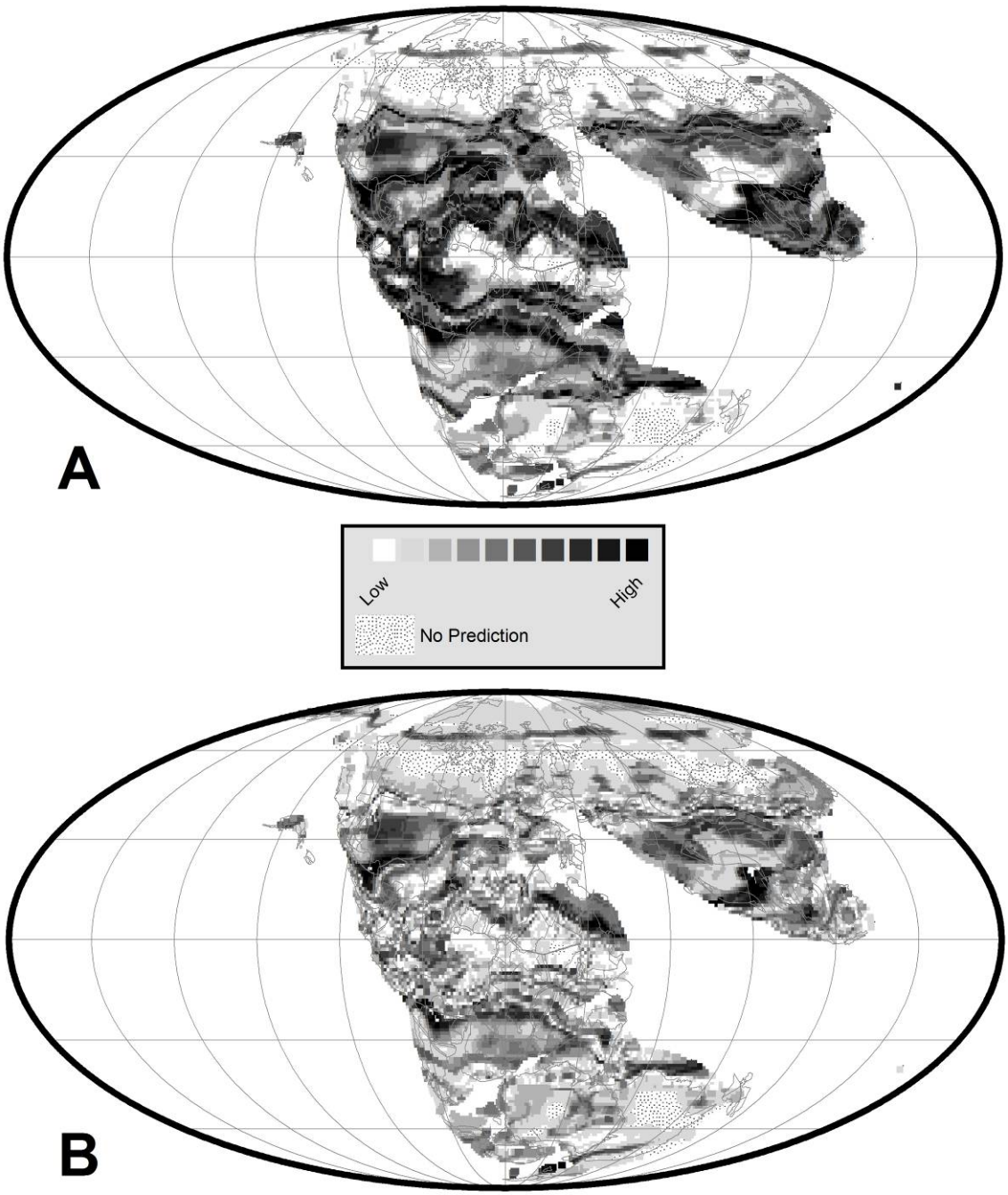

Figure 2.26 A. Prediction Confidence Level for Maximum Probable Paleo-soil Type for the Late Jurassic (160 Ma), B. Dominance of Primary Maximum Probable Paleo-soil Type over the Secondary Maximum Probable Paleo-soil Type for the Late Jurassic (160 Ma)

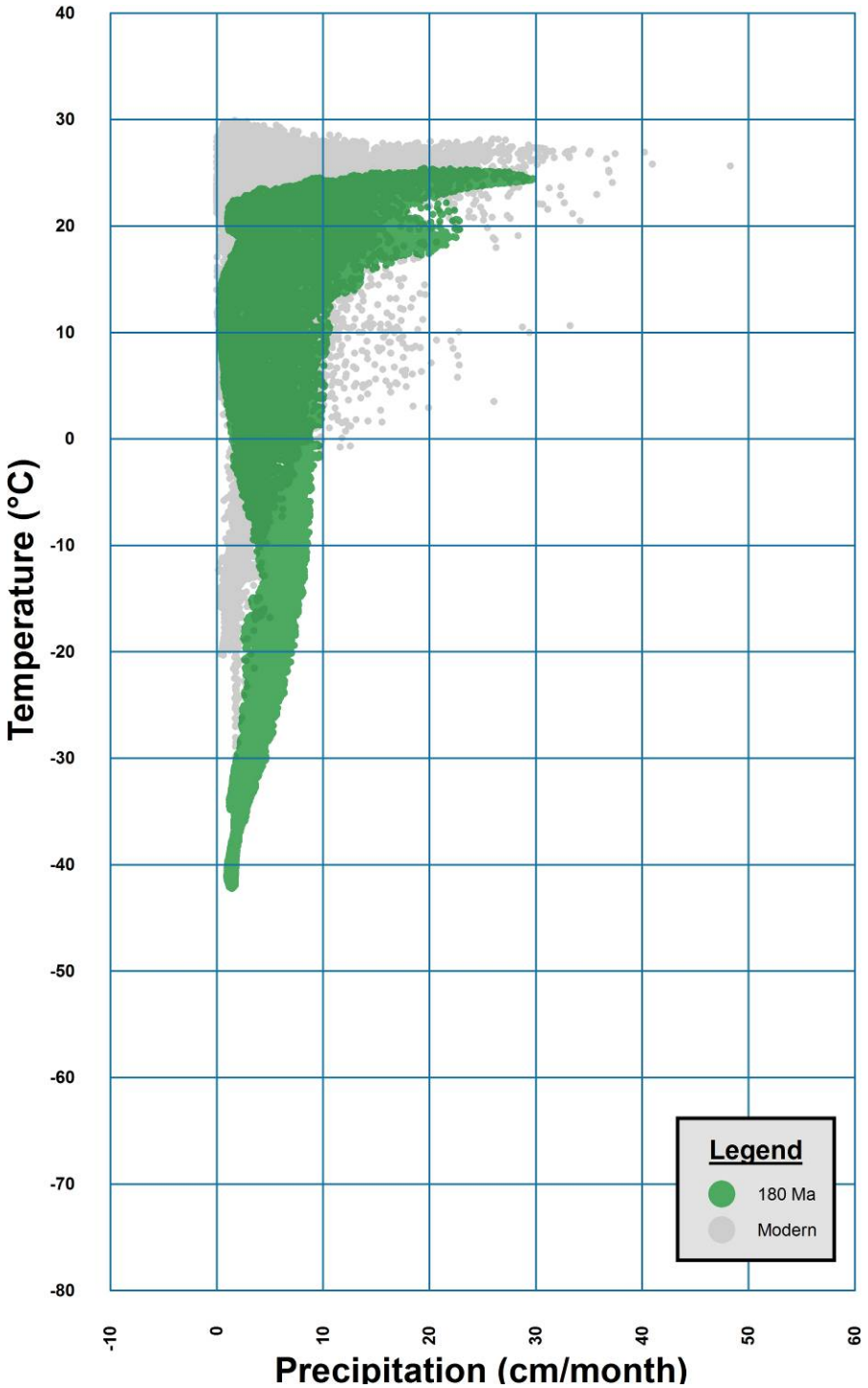

Figure 2.27 Temperature-Precipitation Plot for the Early Jurassic (180 Ma)

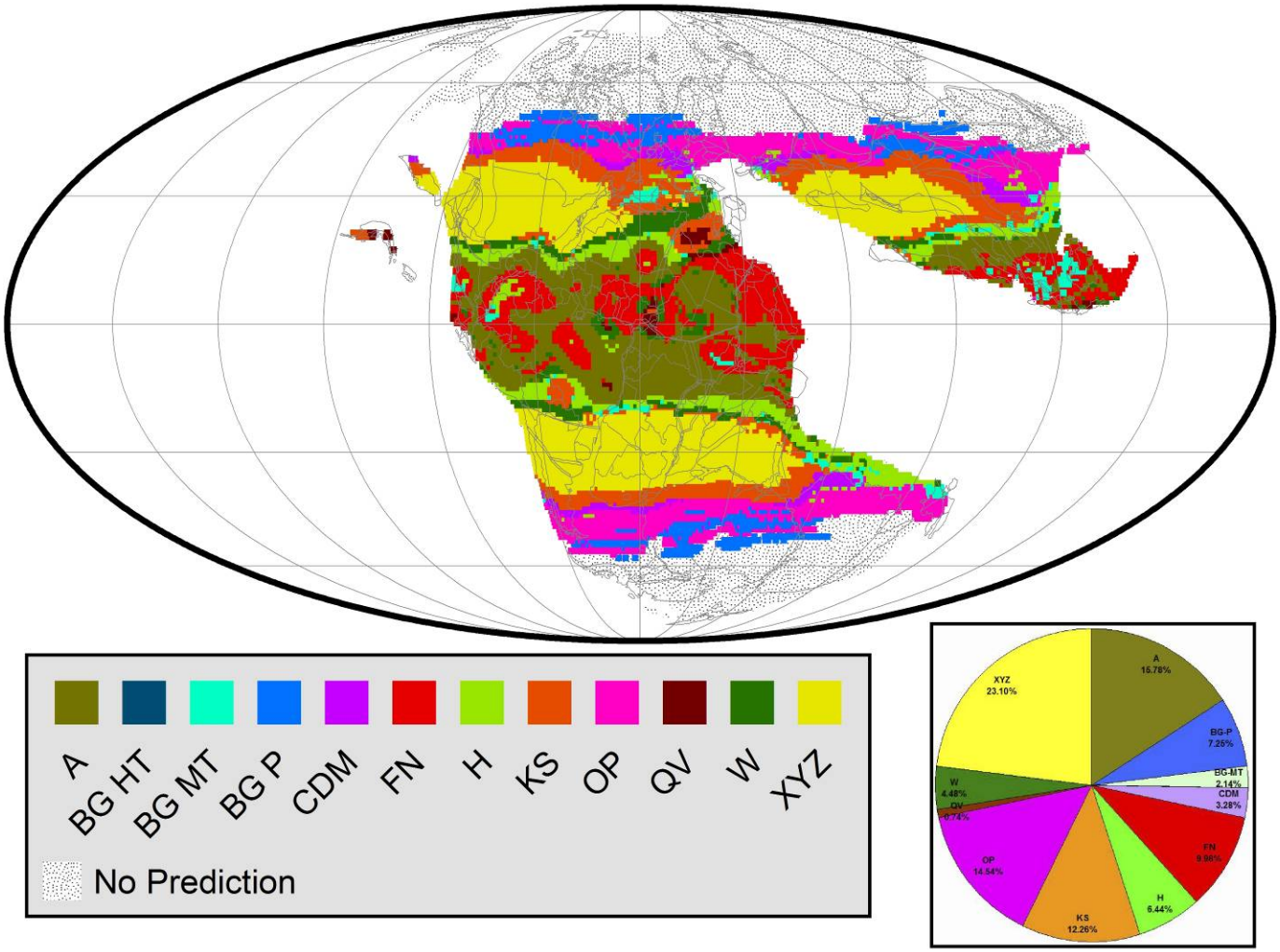

Figure 2.28 Composite Geographic Distribution Map of Primary Predicted Ancient Soils (Paleo-soils) for the Early Jurassic (180 Ma)

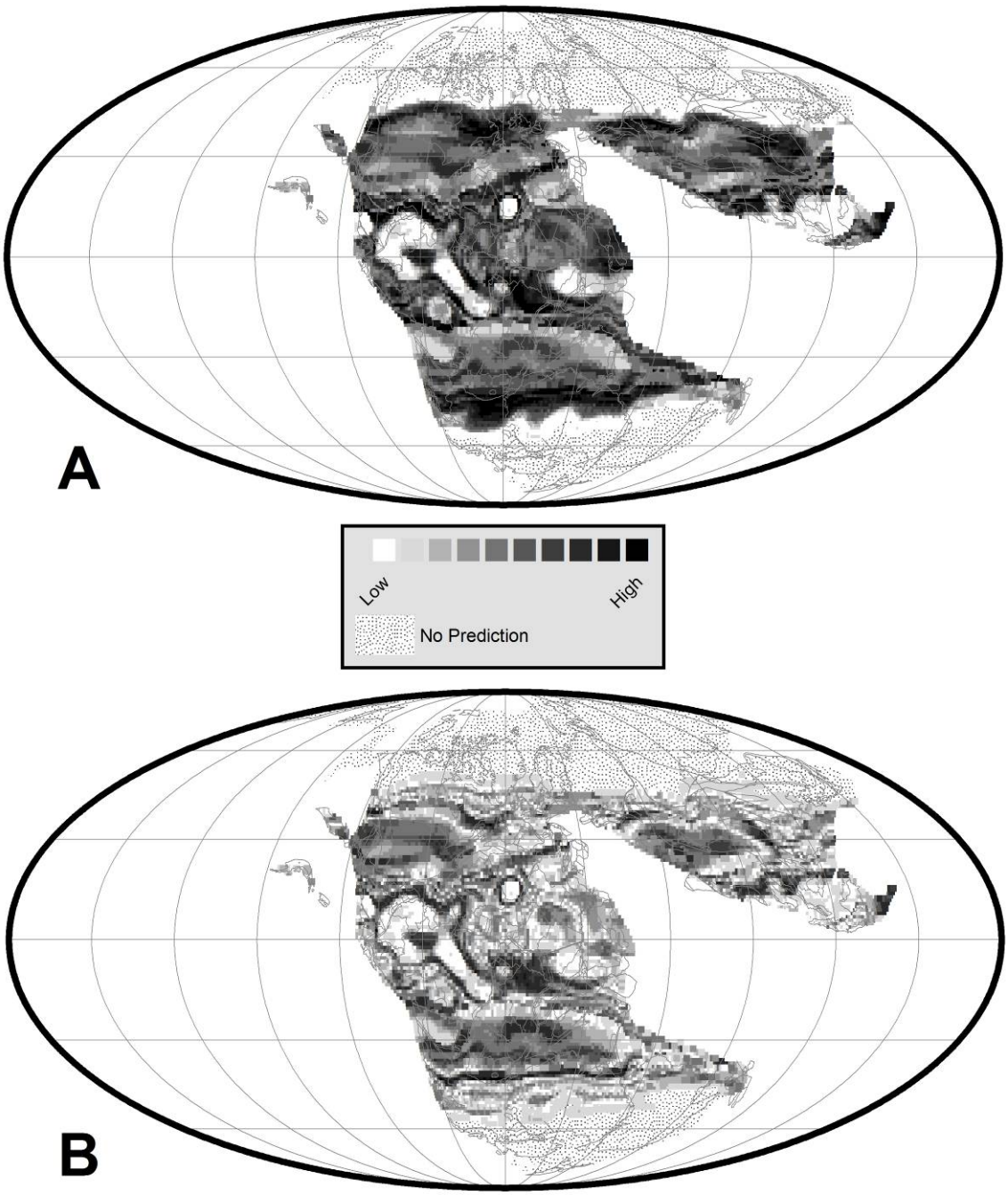

Figure 2.29 A. Prediction Confidence Level for Maximum Probable Paleo-soil Type for the Early Jurassic (180 Ma), B. Dominance of Primary Maximum Probable Paleo-soil Type over the Secondary Maximum Probable Paleo-soil Type for the Early Jurassic (180 Ma)

2.3.9 Early Jurassic (180 Ma)

During the Early Jurassic period the Pangean mega-monsoon was in full swing. Much of the supercontinent Pangea was very arid and hot. Modern day Amazon and Congo rainforests were covered by deserts. China was surrounded by moisture bearing winds (Chandler et al. 1992) and had abundant coal deposits.

Figure 2.27 plots the distribution of temperature and precipitation values for the Early Jurassic (green) on a background of modern day temperature and precipitation values (gray). For the Early Jurassic, the maximum temperature and precipitation values were 25.40°C and 29.74 cm/month, respectively. The minimum temperature and precipitation values were -42.25°C and 0.24 cm/month, respectively. It is clear from this plot that the range of temperature and precipitations during the Early Jurassic was quite different than the range of modern temperature-precipitation data. During the Early Jurassic, the Global Mean Temperature (GMT) appears to be 8 - 9°C cooler than the modern times. It is also important to note that were more low temperature localities (< 5°C) and fewer high temperature localities (>20°C). The highest precipitation values were less than modern precipitation values. There appears to have been a precipitation gap at cooler temperatures (< 0°C).

Figure 2.28 is a reconstruction of ancient paleo-soil types for the Early Jurassic (180 Ma). The Early Jurassic is usually considered to be a Global Hot House World (Figure 2.2). However, these results indicate a much cooler global climate. There is a relatively narrow belt of Polar paleo-soil (BG Polar) and Cool Temperate paleo-soils (OP and KS). The Subtropical Arid Belt paleo-soil (XYZ) is well developed (Table 2.2 and pie chart of Figure 2.28) and occurs in the central North America, southwest Asia, India and south-central Africa and South America. As illustrated in Figure 2.28, all of the paleo-soil belts are compressed towards the Equator. No paleo-soil predictions have been made above 50° north and south latitude (stippled areas near the poles). It is interesting to note that the Equatorial Rainy Belt is dominated by Warm Temperate

Belt paleo-soil types (A). Thin belts of Phaeozems (H), characteristic of Warm Temperate Belt, are found in the regions which are transitional between wet and dry conditions.

It is important to note that paleo-soil types that are typically characteristic of Equatorial Rainy Belt (FN and W) are patchily distributed in the central Pangea and southeastern Asia. This suggests that during the Early Jurassic, tropical rainforests were scattered and limited in extent. In Southeastern Asia, there is complex pattern of paleo-soils that require further study.

Figure 2.29A illustrates the confidence levels for the predictions for Early Jurassic period. During the Early Jurassic the overall levels of confidence for the paleo-soil predictions are relatively high. Notable exceptions are regions in west central Pangea and central-southeast Asia.

The paleo-soil dominance map (Figure 2.29B) is also very similar in many respects to the prediction confidence level map (Figure 2.29A), but with some significant differences. For the Early Jurassic, the overall dominance scores are moderate. Regions like western North America, central Gondwana and west central Asia have high dominance scores.

We have also prepared a reconstruction showing the secondary paleo-soil type (PPS2) predictions for the Early Jurassic period (180 Ma). The reconstruction along with its levels of confidence is illustrated in Appendix C (Figure C.9).

2.3.10 Late Triassic (220 Ma)

The Late Triassic was a Hot House World (Figure 2.2). There was no ice at both poles and warm temperate conditions extended into the polar latitudes (www.scotese.com). The Late Triassic was also marked by a monsoonal climate (Robinson, 1973; Wang, 2009). The western margin of Tethys and the central part of Pangea, between 35° and 15° latitudes (N and S), had dry climate throughout the entire year (Preto et al. 2010). The coasts of eastern Laurasia and Gondwana and the western coasts of Pangaea would have experienced alternate wet and dry seasons (Parrish and Peterson, 1988; Dubiel et al., 1991; Mutti and Weissert, 1995). Paleo-soils and floras indicating wet and warm conditions (Robinson, 1973) occur up to latitudes of 85° (Wesley, 1973; Taylor, 1989; Retallack, 1999; Kidder and Worsley, 2004).

Figure 2.30 plots the distribution of temperature and precipitation values for the Late Triassic (green) on a background of modern day temperature and precipitation values (gray). For the Late Triassic, the maximum temperature and precipitation values were 24.82°C and 33.12 cm/month, respectively. The minimum temperature and precipitation values were -33.96°C and 0.05 cm/month, respectively. It is clear from this plot that the range of temperature and precipitations during the Late Triassic were quite different from the range of modern temperature-precipitation data. During the Late Triassic, the Global Mean Temperature (GMT) appears to be 6 – 8°C cooler than the modern times. It is also important to note that were more low temperature localities (< 5°C) and fewer high temperature localities (>20°C). The highest precipitation values were much less than modern precipitation values and were associated with high temperatures. There appears to have been a precipitation gap at cooler temperatures (0 ~ -15°C).

Figure 2.31 is a reconstruction of ancient paleo-soil types for the Late Triassic (220 Ma). The Late Triassic is usually considered to be a Global Hot House World (Figure 2.2). However, the paleoclimate simulation indicates a much cooler global climate. There is a relatively narrow belt of Polar paleo-soil (BG Polar) and Cool Temperate paleo-soils (OP and KS). The Subtropical Arid Belt paleo-soils (XYZ and QV) are well developed (Table 2.2 and pie chart of Figure 2.31) and are found in central North America, Asia, India and south-central Africa and South America. As illustrated in Figure 2.31, all of the paleo-soil belts are compressed towards the Equator. No paleo-soil predictions have been made above 50° north and 45° south latitude (stippled areas near the poles). It is interesting to note that the Warm Temperate paleo-soil types (A and H) are found mixed with the Equatorial Rainy Belt (FN and W) paleo-soil types. This suggests that during Late Triassic, tropical rainforest were alternating, sporadic and limited in extent. The pattern of paleo-soil types in central Pangea is especially complex and requires additional evaluation.

Figure 2.32A illustrates the confidence levels for the predictions for Late Triassic period. The regions with highest levels of confidence are in central Gondwana and southeastern Asia. Other areas with high levels of confidence include central North America.

The paleo-soil dominance map (Figure 2.32B) is similar in many respects to the prediction confidence level map (Figure 2.32A). For the Late Triassic, the dominance levels are mostly high. However, regions of central Asia and central Pangea have low dominance scores.

We have also prepared a reconstruction showing the secondary paleo-soil type (PPS2) predictions for the Late Triassic period (220 Ma). The reconstruction along with its levels of confidence is illustrated in Appendix C (Figure C.10).

2.3.11 Early Triassic (250 Ma)

Early Triassic climate was quite similar to that at the end of the Permian. Much of Pangea was warm and dry, and the interior of this supercontinent was particularly arid. Lithologic indicators of climate suggest that warm temperate climates extended to the Poles (www.scotese.com). These environments were often dominated by conifers and other gymnosperms. However, the Triassic saw an increase in seasonality, with prominent monsoon weather cycles. Rapid Global Warming after Permian may have created a super - "Hot House" world that caused the end Permian extinction event (www.scotese.com).

Figure 2.33 plots the distribution of temperature and precipitation values for the Early Triassic (green) plotted on a background of modern day temperature and precipitation values (gray). During the Early Triassic, maximum temperature and precipitation values were 27.64°C and 31.15 cm/month, respectively. The minimum temperature and precipitation values were -34.93°C and 0.10 cm/month, respectively. It is clear from this plot that the range of temperature and precipitations during the Early Triassic were similar to the range of modern temperature-precipitation data. During the Early Triassic, the Global Mean Temperature (GMT) appears to be close to present day (1 -2°C cooler). The highest precipitation values were similar to modern

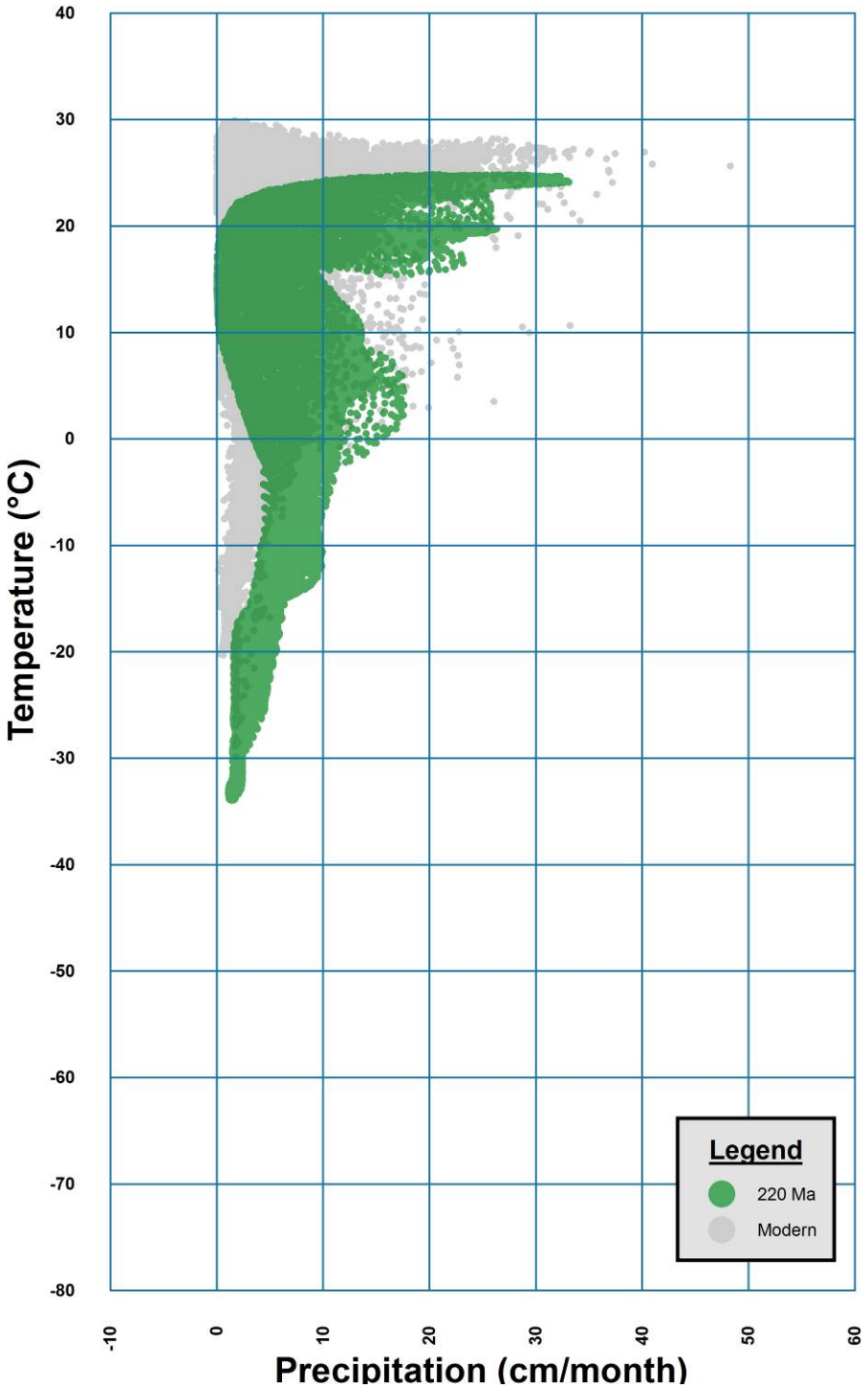

Figure 2.30 Temperature-Precipitation Plot for the Late Triassic (220 Ma)

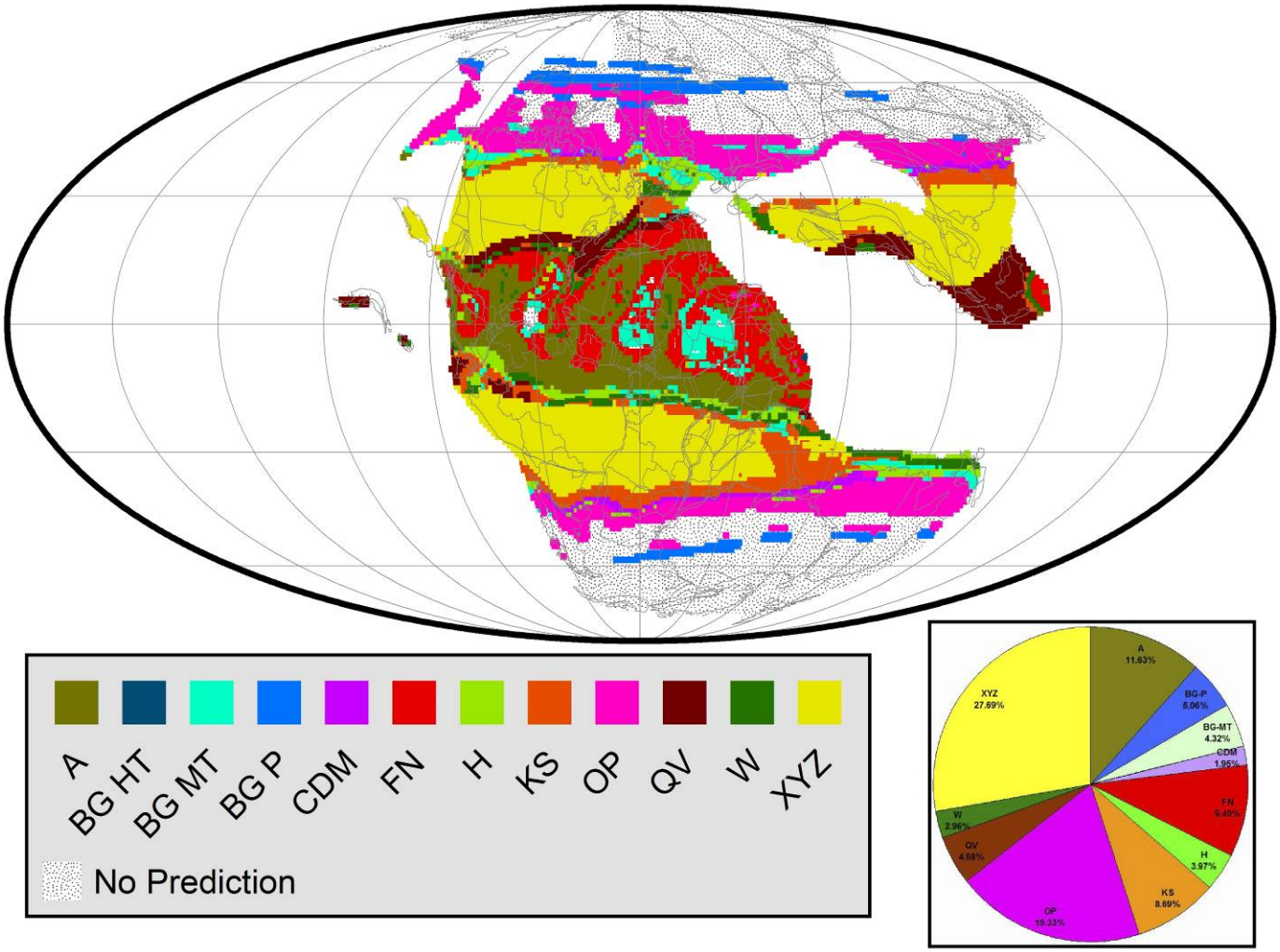

Figure 2.31 Composite Geographic Distribution Map of Primary Predicted Ancient Soils (Paleo-soils) for the Late Triassic (220 Ma)

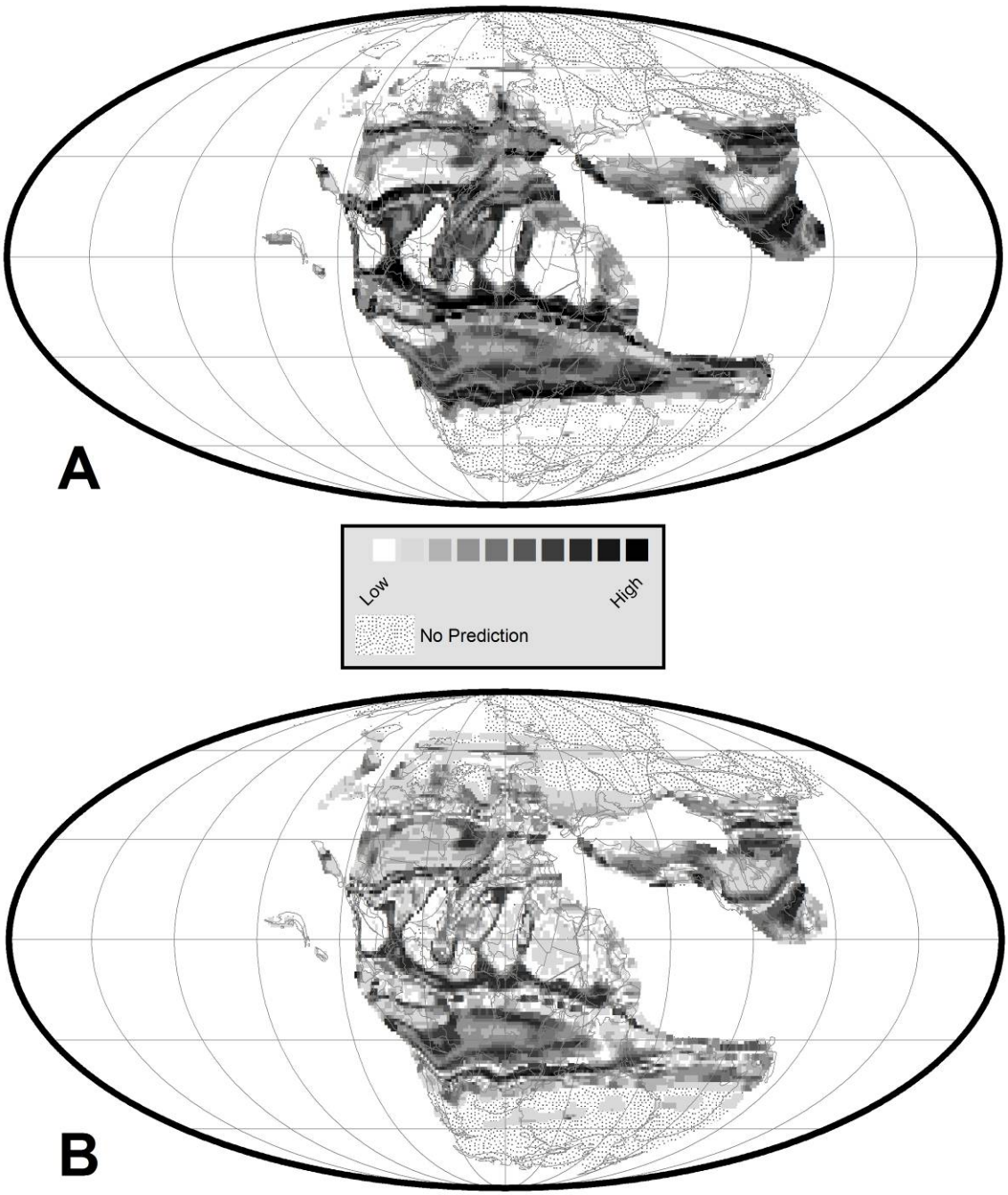

Figure 2.32 A. Prediction Confidence Level for Maximum Probable Paleo-soil Type for the Late Triassic (220 Ma), B. Dominance of Primary Maximum Probable Paleo-soil Type over the Secondary Maximum Probable Paleo-soil Type for the Late Triassic (220 Ma)

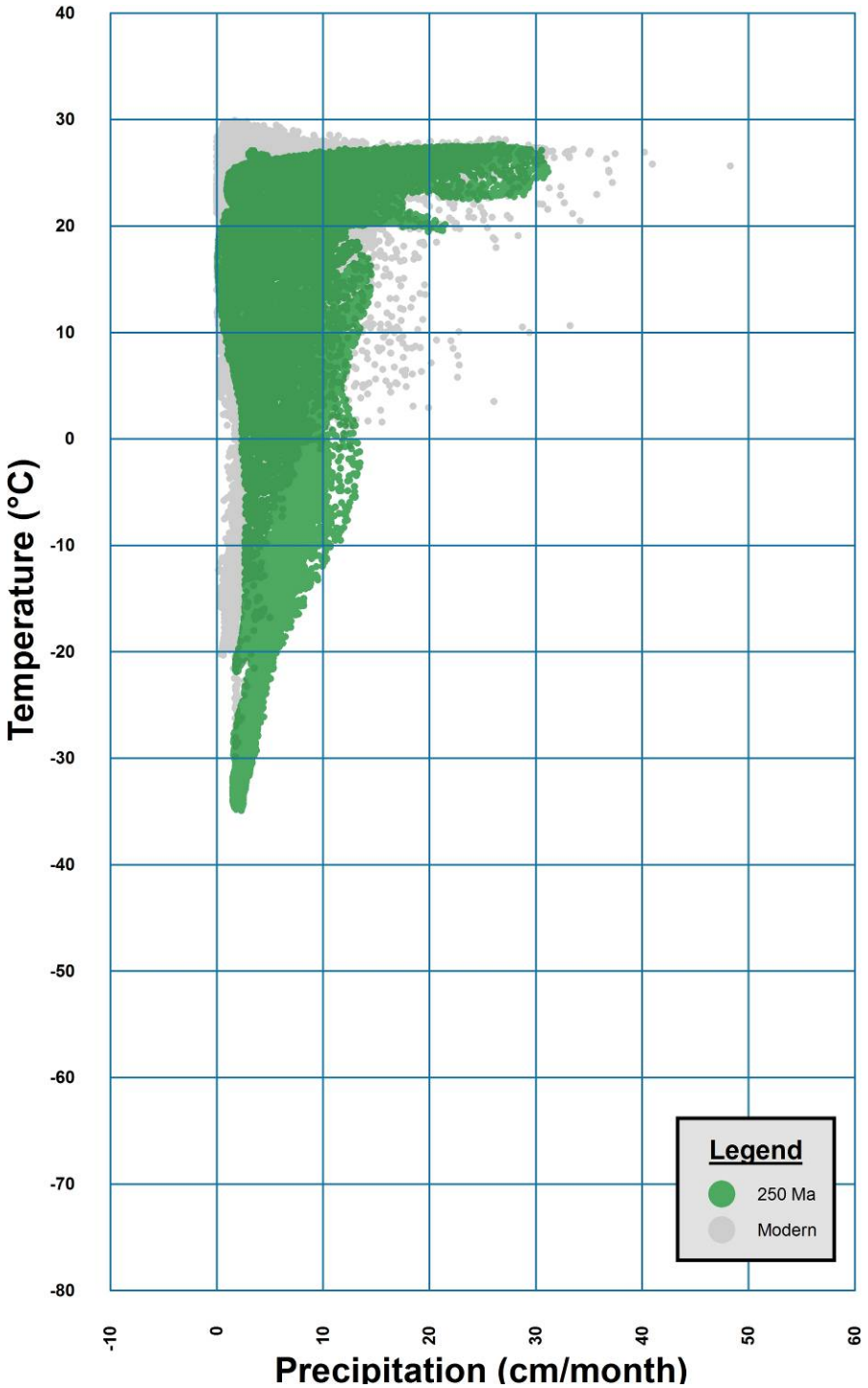

Figure 2.33 Temperature-Precipitation Plot for the Early Triassic (250 Ma)

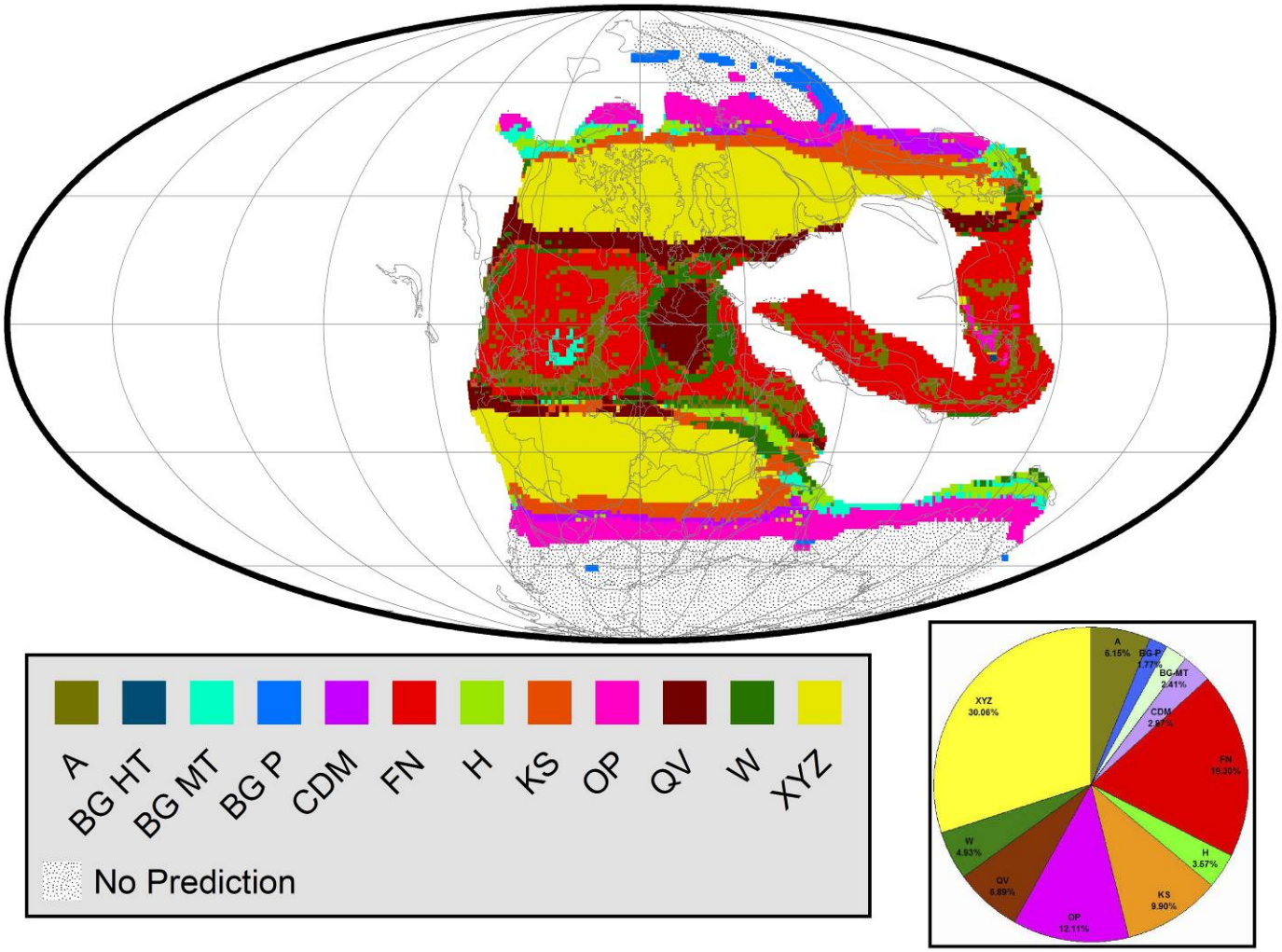

Figure 2.34 Composite Geographic Distribution Map of Primary Predicted Ancient Soils (Paleo-soils) for the Early Triassic (250 Ma)

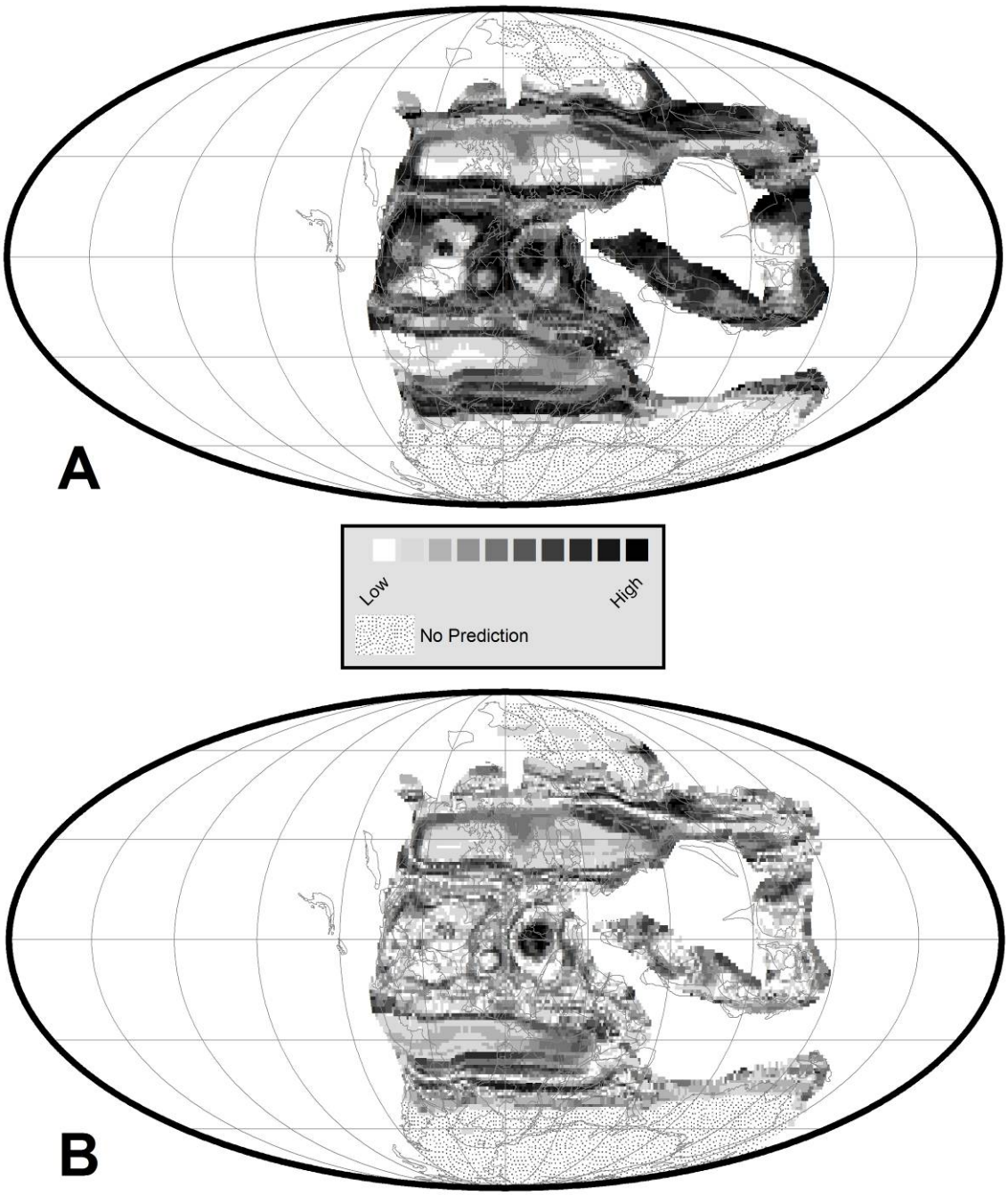

Figure 2.35 A. Prediction Confidence Level for Maximum Probable Paleo-soil Type for the Early Triassic / Induan (250 Ma), B. Dominance of Primary Maximum Probable Paleo-soil Type over the Secondary Maximum Probable Paleo-soil Type for the Early Triassic (250 Ma)

precipitation values and are associated with high temperatures. There appears to have been a precipitation gap at cooler temperatures (5 ~ -20°C).

Figure 2.34 is a reconstruction of ancient paleo-soil types for the Early Triassic (250 Ma). As evident from Figure 2.34, Early Triassic had two dominant belts of paleo-soil types — a broad Subtropical Arid paleo-soil types (XYZ and QV) extending from 20° to 45° (N and S) and a vast Equatorial Rainy Belt paleo-soil type (mainly FN) extending from 20°N to 20°S including the regions around Tethys (Ciommenia and Cathysia). This suggests that during Early Triassic, tropical rainforests were extensive.

In central equatorial Pangea there is an anomalous dry area characterized by QV arid paleo-soil type and surrounded by W. It is not clear what this arid paleo-soil implies and requires further study.

Warm Temperate Belt paleo-soils are not well-developed except in northern Australia, northern North America and northeastern Asia. Cool Temperate Belt paleo-soil types (OP and KS) are found in a narrow belt around 45° latitude. Traces of Polar paleo-soil (BG Polar) are observed above 45°N. The stippled area above the 50° latitude represents temperature-precipitation conditions indicating the occurrence of polar ice caps; hence no paleo-soil predictions were made for these regions. It is extremely unlikely that the Early Triassic would have polar ice caps. This suggests that, the paleoclimate simulation is in error.

Figure 2.35A illustrates the levels of confidence for the predictions for Early Triassic. The regions with highest levels of confidence are located at 15° and 45° on either side of the equator. Other areas with high levels of confidence include regions around Tethys (Cimmenia and Cathysia).

The patterns observed on paleo-soil dominance map (Figure 2.35B) are similar in many respects to the patterns seen on the confidence level map (Figure 2.35A). Overall, the paleo-soil dominance levels are moderate to low. The anomalously arid regions in central equatorial Pangea have a high dominance score.

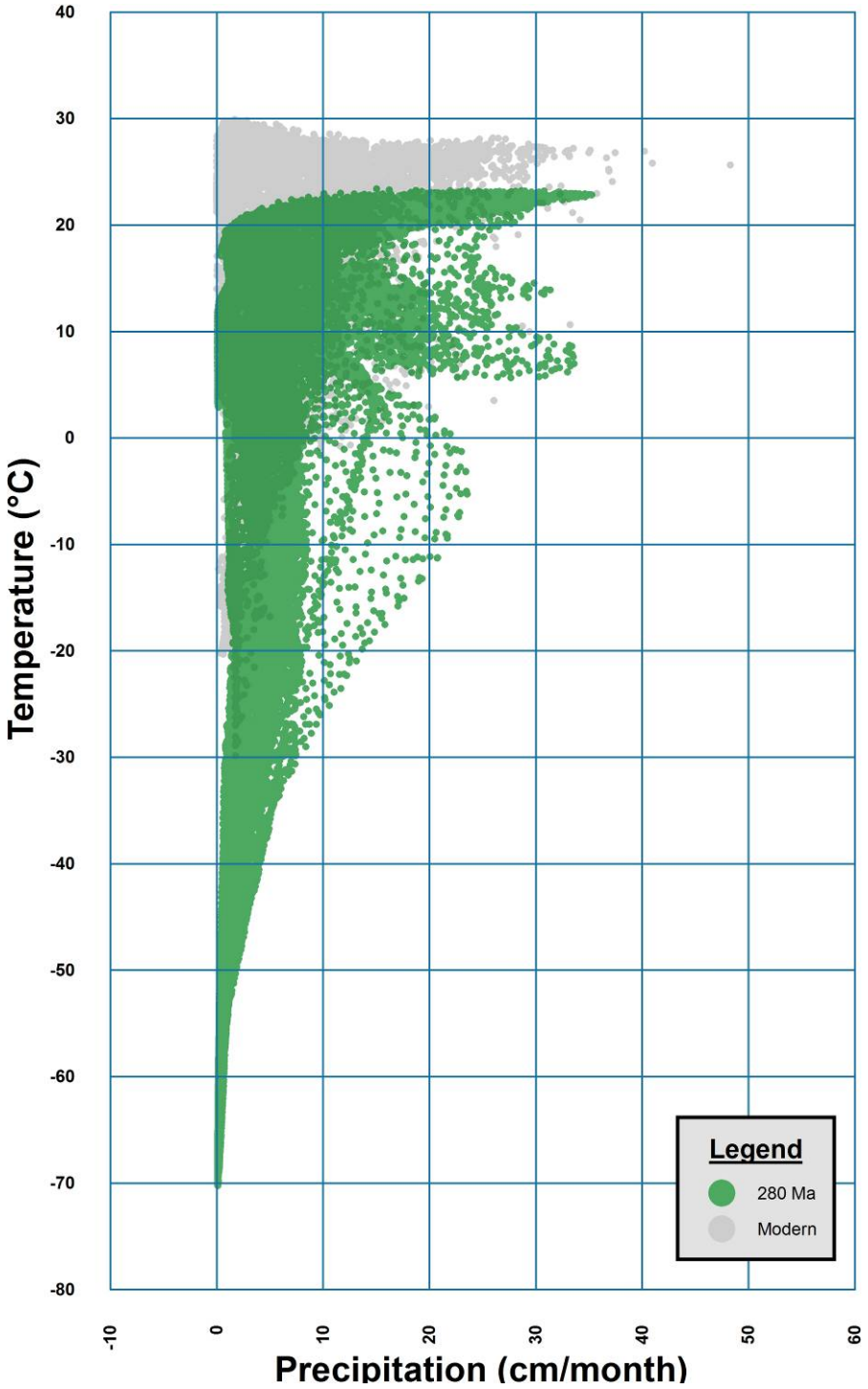

Figure 2.36 Temperature-Precipitation Plot for the Early Permian (280 Ma)

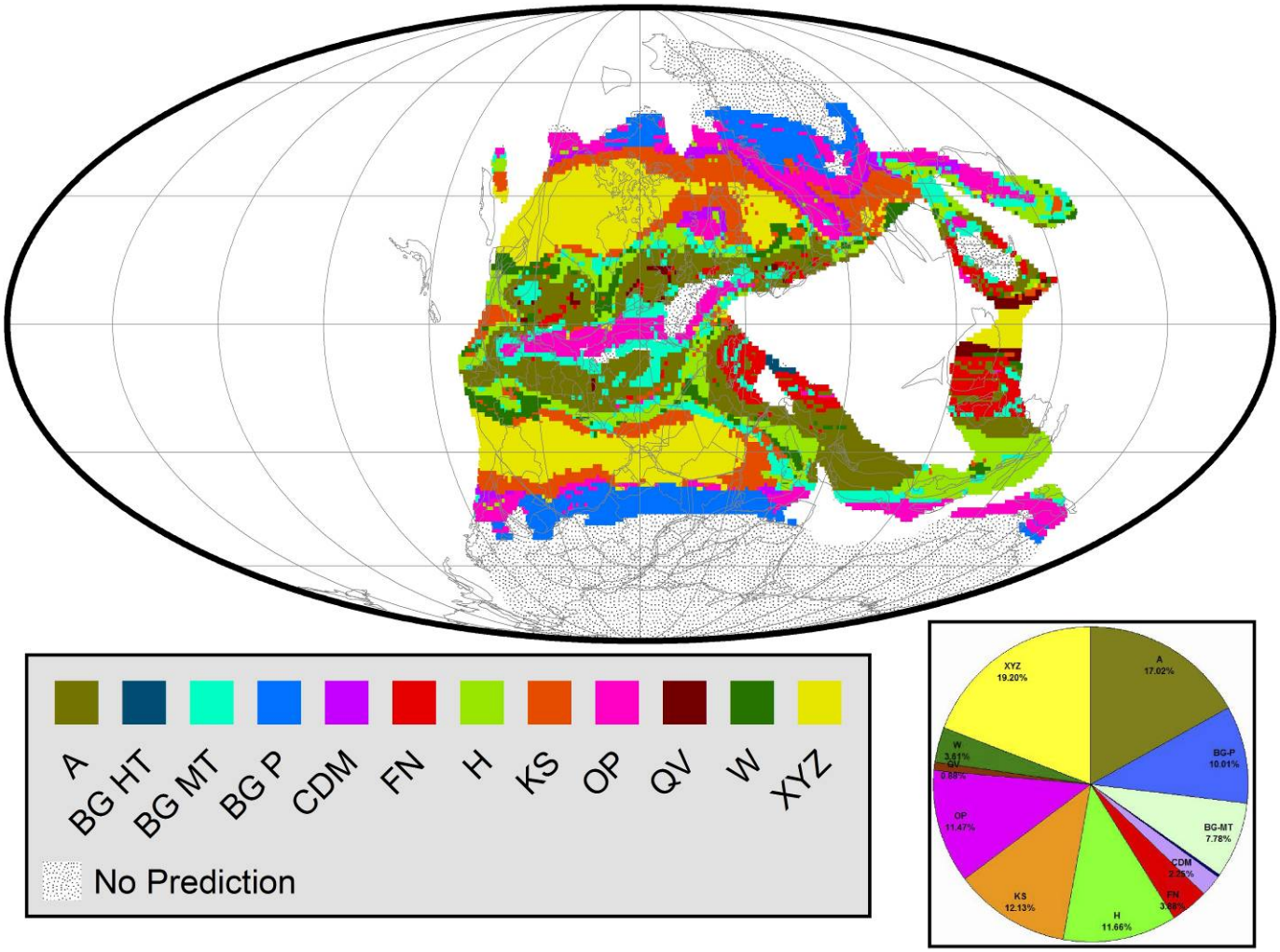

Figure 2.37 Composite Geographic Distribution Map of Primary Predicted Ancient Soils (Paleo-soils) for the Early Permian (280 Ma)

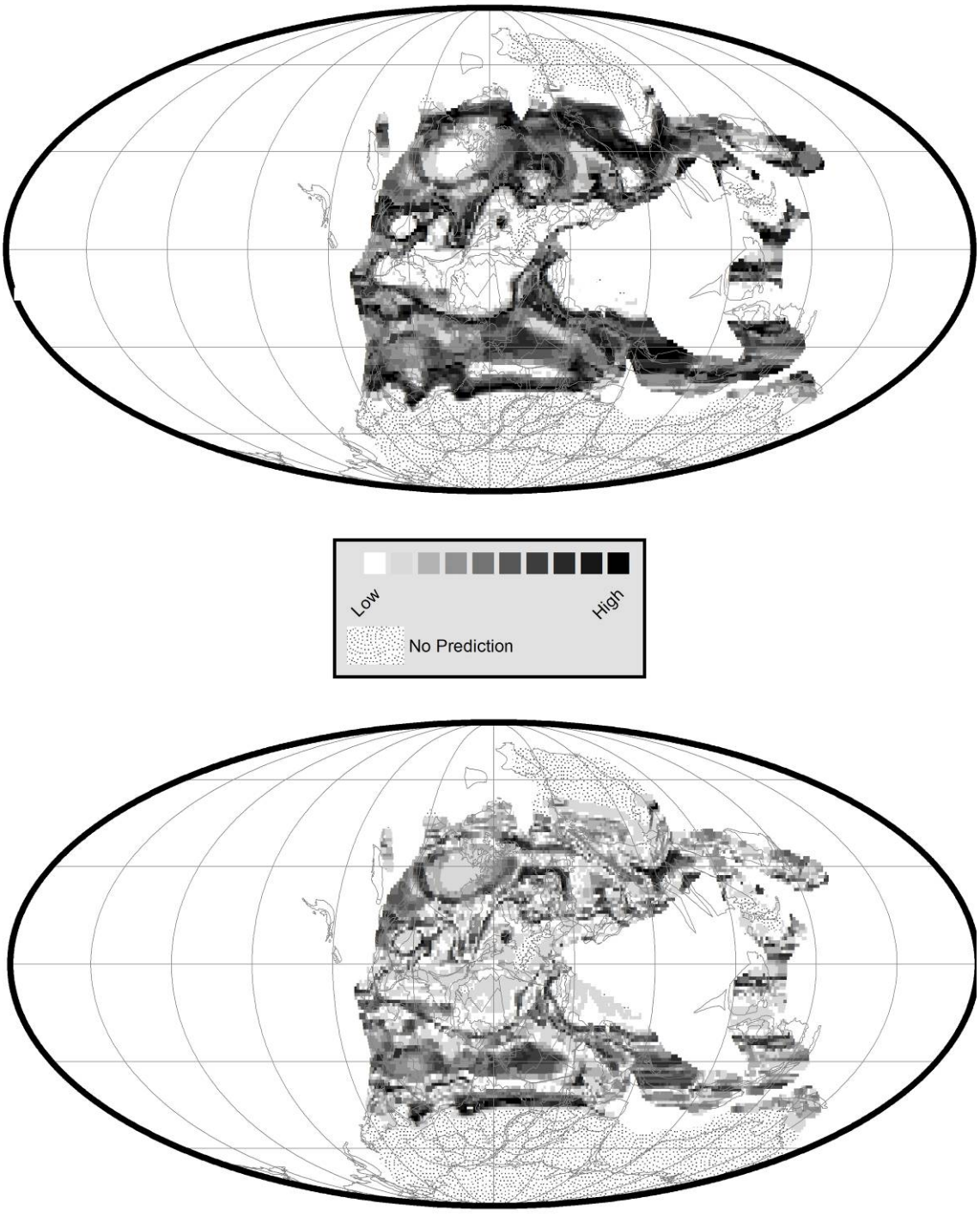

Figure 2.38 A. Prediction Confidence Level for Maximum Probable Paleo-soil Type for the Early Permian (280 Ma), B. Dominance of Primary Maximum Probable Paleo-soil Type over the Secondary Maximum Probable Paleo-soil Type for the Early Permian (280 Ma)

We have also prepared a reconstruction showing the secondary paleo-soil type (PPS2) predictions for the Early Triassic period (250 Ma). The reconstruction along with its levels of confidence is illustrated in Appendix C (Figure C.11).

2.3.12 Early Permian (280 Ma)

During the Permian, all the Earth's major land masses clubbed together to form a single supercontinent known as Pangea. Pangea straddled the equator and extended to the poles. Two large ocean basins, Panthalassa and the Paleo-Tethys Ocean surrounded the Pangea. The Late Carboniferous and Early Permian was an Ice House World. Glaciers receded during the mid-Permian period as global climate gradually warmed. During the Early Permian the tropics were covered by rainforests as was the small region in northeast Pangea (Mongolia). However, the interior of the continents was arid. The seasonal heating and cooling of the large Pangean landmass produced a climate characterized by extreme variations in temperature and monsoonal conditions with highly seasonal rainfall patterns. Deserts seem to have covered wide areas of Pangaea. Such dry conditions favored gymnosperms, plants with seeds enclosed in a protective cover, over plants such as ferns that reproduce by spores. The first modern trees (conifers, ginkgos and cycads) appeared in the Permian.

Figure 2.36 plots the distribution of temperature and precipitation values for the Early Permian (green) on a background of modern day temperature and precipitation values (gray). During the Early Permian the maximum temperature and precipitation values were 23.40°C and 35.28 cm/month, respectively. The minimum temperature and precipitation values were –70.25°C and 0.07 cm/month, respectively. It is clear from this plot that the range of temperature and precipitation values during the Early Permian was very different from the modern values. During the Permian, the Global Mean Temperature (GMT) appears to be at least 10 - 12°C cooler than the modern time. It is also important to note that were more low temperature localities (< 5°C) and fewer high temperature localities (>20°C) than the modern world. The highest precipitation values were similar to present-day values and were associated with the higher temperatures.

Figure 2.37 is a reconstruction of ancient paleo-soil types for the Early Permian (280 Ma). As noted previously, the Permian was a Global Ice House World (Figure 2.2). Subtropical Arid Belt paleo-soil type XYZ is the predominant paleo-soil type (Table 2.2 and pie chart of Figure 2.37) and occurs in a broad belt extending from 15° to 40° latitudes (N and S). It is interesting to note that equatorial region (15°N to 20°S) is dominated by Warm Temperate paleo-soil types (A and H) with occasional occurrences of W, an Equatorial Rainy Belt paleo-soil.

It is also important to mention that in central Pangea, there is a narrow belt of OP (Histosol-Podzol). The OP paleo-soil type is usually associated with Cool Temperate conditions. In the modern world there are some Histosol occurrences in the warm and humid equatorial regions. These equatorial occurrences of histosols may be the equivalent of modern tropical Histosol. The other Equatorial Rainy Belt paleo-soil (FN) is found only in the southern regions of Tethys.

The Cool Temperate paleo-soil types (OP and KS) occur in relatively narrow belts above 30° latitudes. Above 40° latitude relatively narrow belts of polar type paleo-soils (BG Polar) are found. The stippled areas above 45° represent glacial temperature-precipitation conditions; hence no paleo-soil predictions were made for these regions.

Figure 2.38A illustrates the confidence levels for paleo-soil predictions for Early Permian. The regions with highest levels of confidence are in the tropics. Other areas with high levels of confidence include the western and eastern Pangea. A broad region low confidence areas covers the central equatorial Pangea.

The paleo-soil dominance map (Figure 2.38B) is quite similar to the paleo-soil confidence map (Figure 2.38A). Dominance levels are high in the subtropics. Central Pangea similarly exhibits low dominance scores.

We have also prepared a reconstruction showing the secondary paleo-soil type (PPS2) predictions for the Early Permian period (280 Ma). The reconstruction along with its levels of confidence is illustrated in Appendix C (Figure C.12).

2.3.13 Early Carboniferous (340 Ma)

The supercontinent Pangea moved northward during the Early Carboniferous and the climatic belts moved southward across Pangea. Tropical rainforests crossed from Arctic Canada into Newfoundland and Western Europe. The desert region in mid-North America began to shrink. The Southern Hemisphere cooled off. During the late Early Carboniferous, extensive rainforests covered the tropical regions of Pangea which was bounded to the north and south by deserts. An ice cap covered the South Pole (www.scotese.com).

Figure 2.39 plots the distribution of temperature and precipitation values for the Early Carboniferous (green) plotted on a background of modern day temperature and precipitation values (gray). During the Carboniferous, the maximum temperature and precipitation values were 26.58°C and 35.39 cm/month, respectively. The minimum temperature and precipitation values were -35.47°C and 0.16 cm/month, respectively. It is clear from this plot that the range of temperature and precipitation values during the Early Carboniferous was similar in some respect to the range of modern temperature and precipitation values. During the Early Carboniferous, the Global Mean Temperature (GMT) appears to be 3 – 5°C cooler than the modern times. It is also important to note that were more low temperature localities (< 5°C) and fewer high temperature localities (>20°C). The highest precipitation values were less than the modern highest precipitation and precipitation values were associated with lower temperatures (10°C). There appears to have been a precipitation gap at cooler temperatures (10 ~ -20°C).

The paleo-soil pattern (Figure 2.40) for the Early Carboniferous (340 Ma) is very complex. Figure 2.40 is a reconstruction of paleo-soil types for the Early Carboniferous. FN paleo-soil type, characteristic of Equatorial Rainy Belt, covers a wide swath of tropical Pangea (25°N to almost 30°S). It is important to note that A, a Warm Temperate Belt paleo-soil also occurs throughout the tropical region. This suggests that during the Early Carboniferous, tropical rainforests were very extensive, but the climate was a blend of equatorial everwet and warm temperate conditions., The arid paleo-soil type, QV, occurs in three small belts along the western coast of central Pangea.

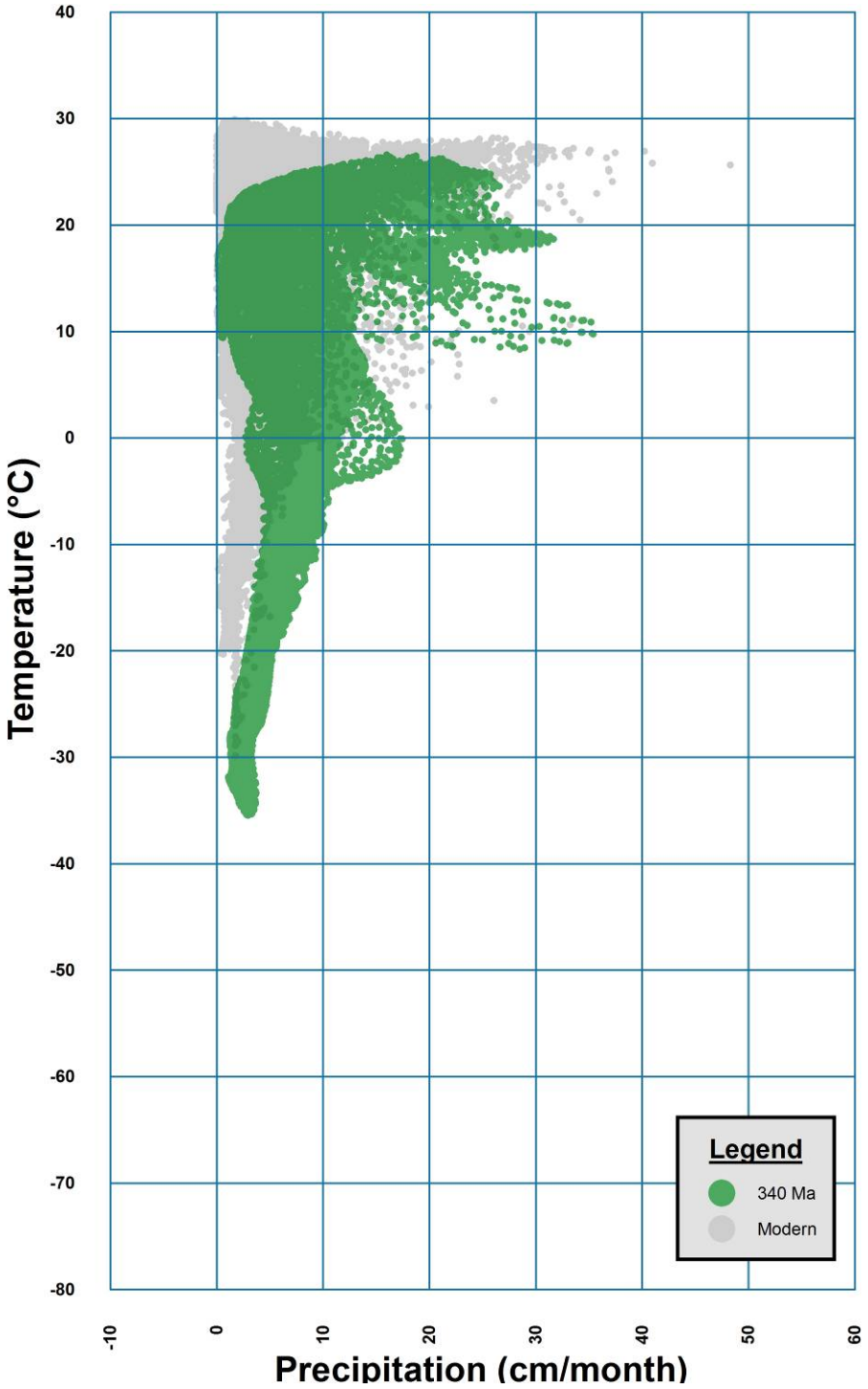

Figure 2.39 Temperature-Precipitation Plot for the Early Carboniferous (340 Ma)

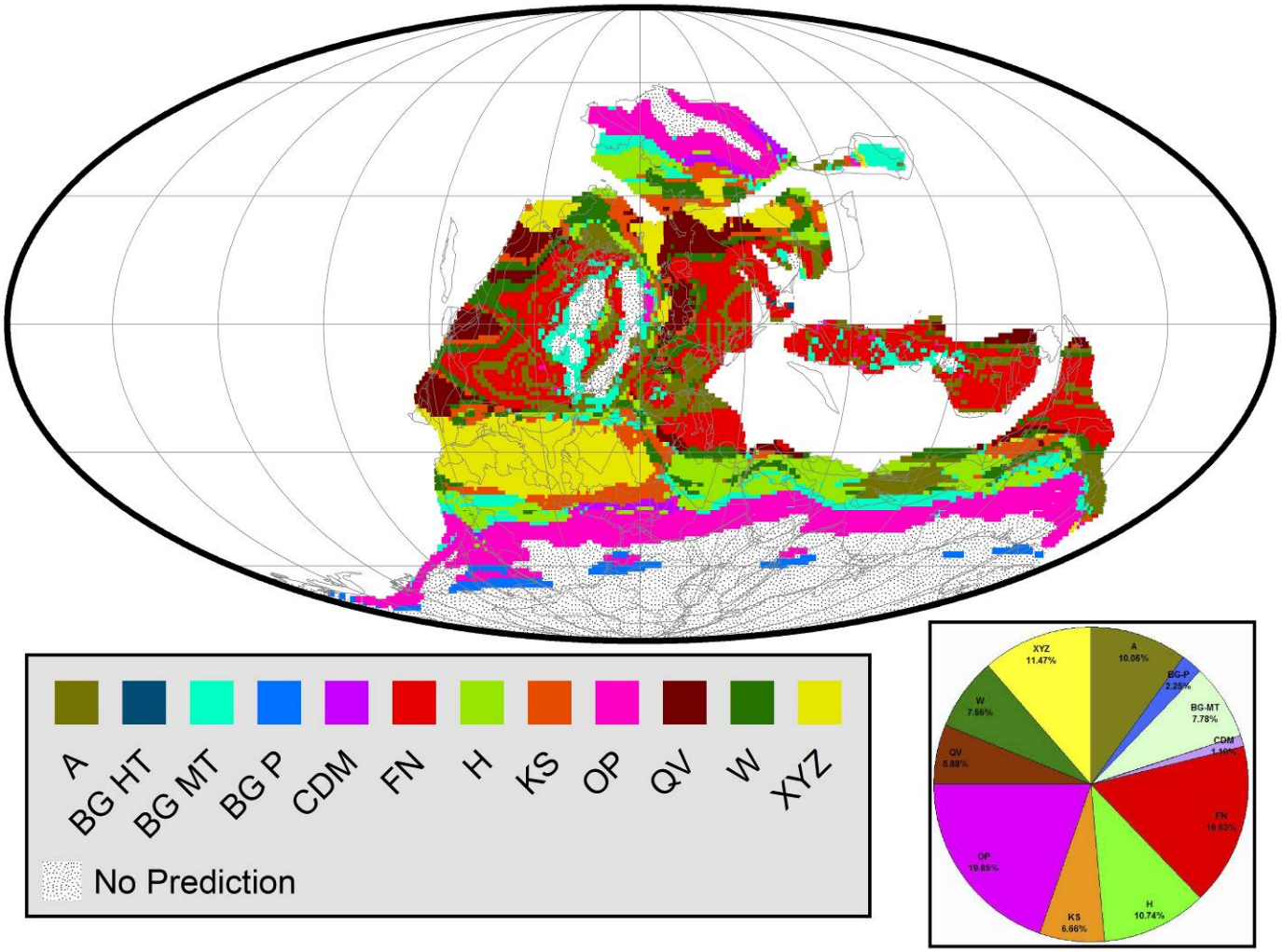

Figure 2.40 Composite Geographic Distribution Map of Primary Predicted Ancient Soils (Paleo-soils) for the Early Carboniferous (340 Ma)

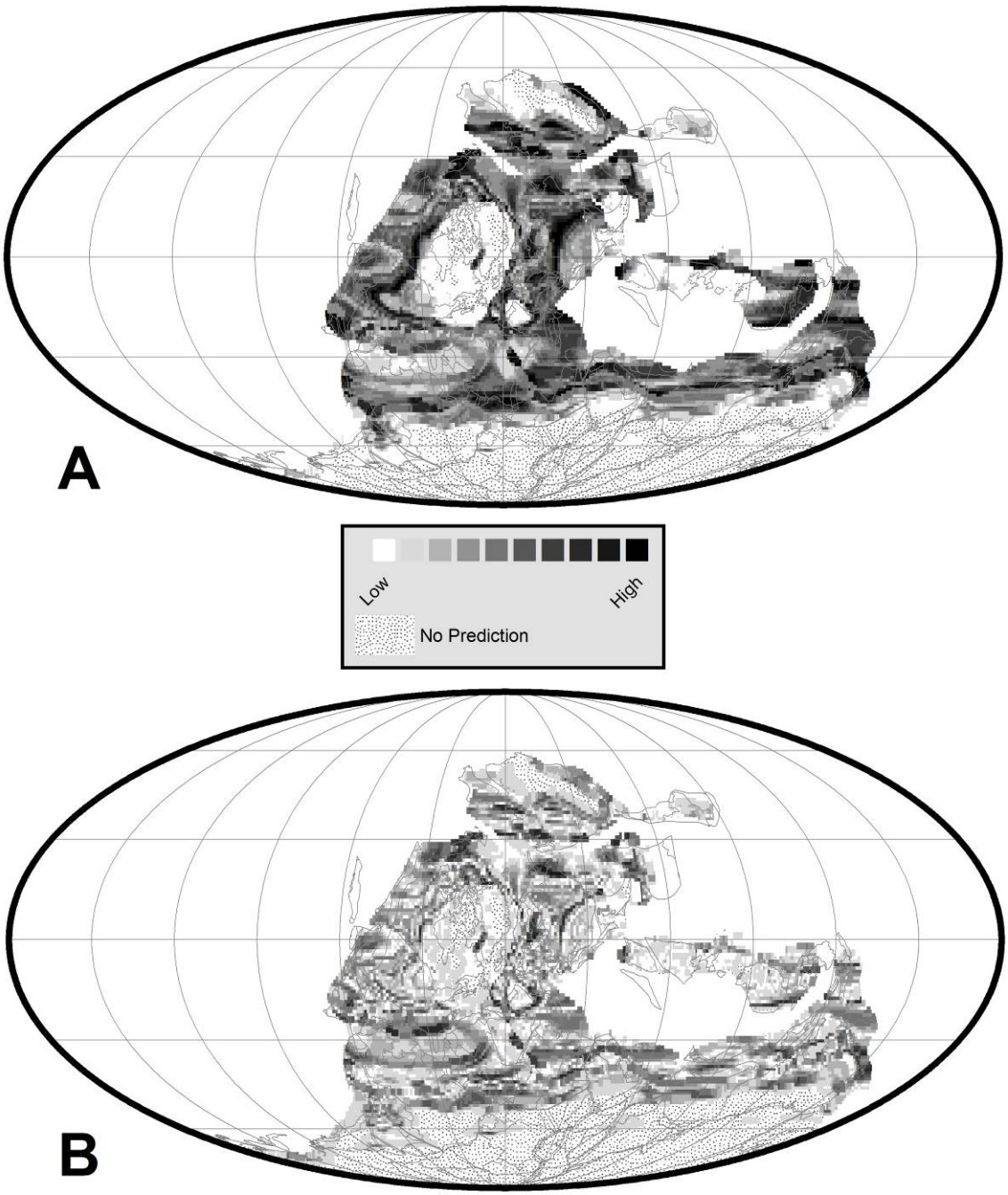

Figure 2.41 A. Prediction Confidence Level for Maximum Probable Paleo-soil Type for the Early Carboniferous (340 Ma), B. Dominance of Primary Maximum Probable Paleo-soil Type over the Secondary Maximum Probable Paleo-soil Type for the Early Carboniferous (340 Ma)

The XYZ arid paleo-soil type forms a broad belt in northern South America and northwestern Africa.

The paleo-soils characteristic of Warm Temperate Belt occurs in a narrow, discontinuous belt along 30°N latitude. In the southern hemisphere, paleo-soils characteristic of Warm Temperate Belts, are relatively well developed and mainly occur along the costal regions of Gondwana to the south of the Tethys. In both hemispheres, the Cool Temperate Belt paleo-soil types (OP and KS) are well developed in the regions above the warm temperate paleo-soils. A few occurrences of the polar paleo-soil type (BG Polar) are found on the southern hemisphere. The stippled areas above 45° latitude represent temperature-precipitation conditions that do not exist in the modern world. Hence, no paleo-soil predictions were made for these regions.

Figure 2.41A illustrates the confidence levels for the predictions of paleo-soil types for Early Carboniferous period. Overall the paleo-soil types of the Early Carboniferous have relatively high levels of confidence. The regions with highest confidence levels are east and west central Pangea.

The paleo-soil dominance map (Figure 2.41B) is very different from the paleo-soil prediction map (Figure 2.41A). For the Early Carboniferous, though the confidence levels are high in several regions around the globe, the dominance levels are mostly moderate to low.

We have also prepared a reconstruction showing the secondary paleo-soil type (PPS2) predictions for the Early Carboniferous period (340 Ma). The reconstruction along with its levels of confidence is illustrated in Appendix C (Figure C.13).

2.3.14 Late Devonian (360 Ma)

The Late Devonian marked the transition from the Middle Paleozoic Hot House World to the Late Paleozoic Ice House World. As Pangea began to assemble, thick coals formed for the first time in the equatorial rainforests in the Canadian Arctic and in southern China. Glaciers began to grow in the Amazon Basin, which was located close to the South Pole (Caputo 1985). By

the Late Devonian, the land had been colonized by plants, insects, and amphibians, in the oceans there were massive coral reefs.

Figure 2.42 plots the distribution of temperature and precipitation values for the Late Devonian (green) on a background of modern day temperature and precipitation values (gray). During the Late Devonian, the maximum temperature and precipitation values were 24.72°C and 33.03 cm/month, respectively. The minimum temperature and precipitation values were -43.68°C and 0.77 cm/month, respectively. It is clear from this plot that the range of temperature and precipitation values during the Late Devonian was quite different than the range of modern temperature-precipitation data. During the Late Devonian, the Global Mean Temperature (GMT) appears to be 6 – 7°C cooler than the modern times. It is also important to note that were more low temperature localities (< 5°C) and fewer high temperature localities (>20°C). The highest precipitation values were much less than modern and associated with relatively low temperatures. There appears to have been a precipitation gap at cooler temperatures (10 ~ -30°C).

Figure 2.43 is a reconstruction of ancient paleo-soil types for the Late Devonian (360 Ma). As illustrated in Figure 2.43, because of the extremely cold temperature at high southern latitudes, all the climatic belts are compressed towards the Equator. The Late Devonian is considered to be the transition from Global Hot House World of the Middle Paleozoic to Global Ice House World of the Late Paleozoic (Figure 2.2). On the Late Devonian paleo-soil map there is a relatively broad Equatorial Rainy Belt characterized by FN paleo-soil type which is mixed with some occurrences of A (a Warm Temperate Belt paleo-soil). This suggests that during Late Devonian, tropical rainforests were developing in areas of central Pangea. It is important to note that within this broad tropical rainy belt, there are three regions characterized by arid conditions. These ‘desert’ found in western North America, in northern Europe and in northern Australia.

Overall, the paleo-soil types of Subtropical Arid Belt are poorly developed during the Late Devonian. Small patches of XYZ and a few patches of QV occur along the 30° north and south latitudes. The Warm Temperate Belt is very narrow in the northern hemisphere and in the

southern hemisphere and appears as a broad belt in the central and eastern part of Gondwana. Along 45° north and south there is a well developed belt of Cool Temperate paleo-soil types (OP and KS). The BG paleo-soil characteristic of Polar Belt is nearly nonexistent during Late Devonian period. The stippled area along the equator and above 45° latitude represents temperature-precipitation conditions that do not exist in the modern world. Hence, no paleo-soil predictions were made for these regions. In general, the pattern of predicted geographic distribution of paleo-soil types for Late Devonian is especially complex and requires additional evaluation.

Figure 2.44A illustrates the confidence levels for the predictions of paleo-soil types for the Late Devonian period. During the Late Devonian most of the regions have high levels of confidence, except the central and eastern equatorial regions. Other areas with low levels of confidence include the northern margins of the Siberia.

The paleo-soil dominance map (Figure 2.44B) is similar in many respects, to the paleo-soil confidence map (Figure 2.44A), but with some significant differences. For the Late Devonian, though the confidence levels are high in several regions around the globe, the dominance levels are mostly moderate. Only southern tropical areas have high dominance scores.

We have also prepared a reconstruction showing the secondary paleo-soil type (PPS2) predictions for the Late Devonian period (360 Ma). The reconstruction, along with its levels of confidence, is illustrated in Appendix C (Figure C.14).

2.3.15 Early Devonian (400 Ma)

During the Early Devonian, arid conditions prevailed across much of North America, Siberia, China and Australia. South America and Africa were covered by cool, temperate seas (Wilson 1980; Boucot 1985). The Devonian period was a time of great tectonic activity, as Euro-America and Gondwana drew closer together. Global climate was relatively warm, and glaciers were absent (Joachimski et al. 2009).

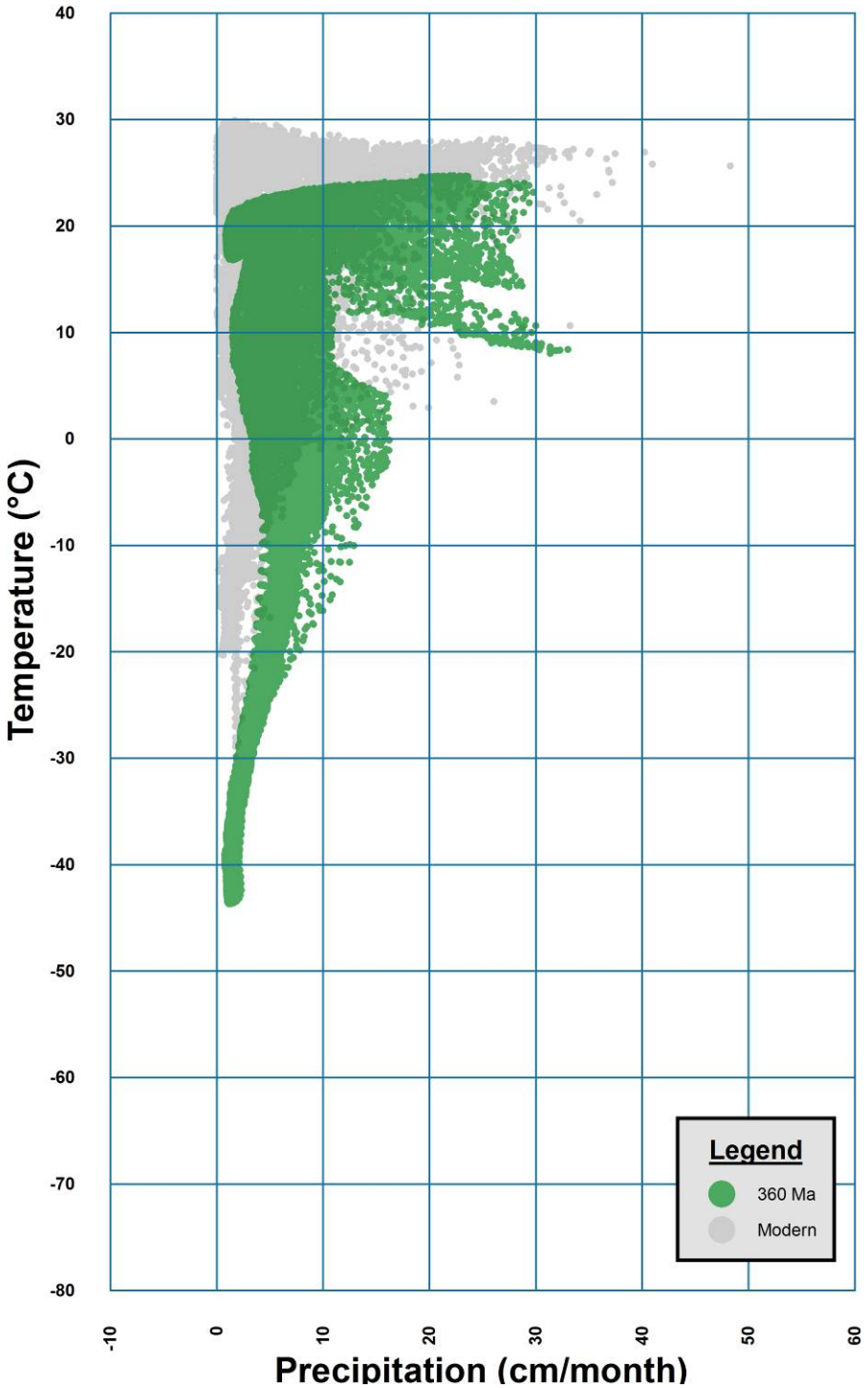

Figure 2.42 Temperature-Precipitation Plot for the Late Devonian (360 Ma)

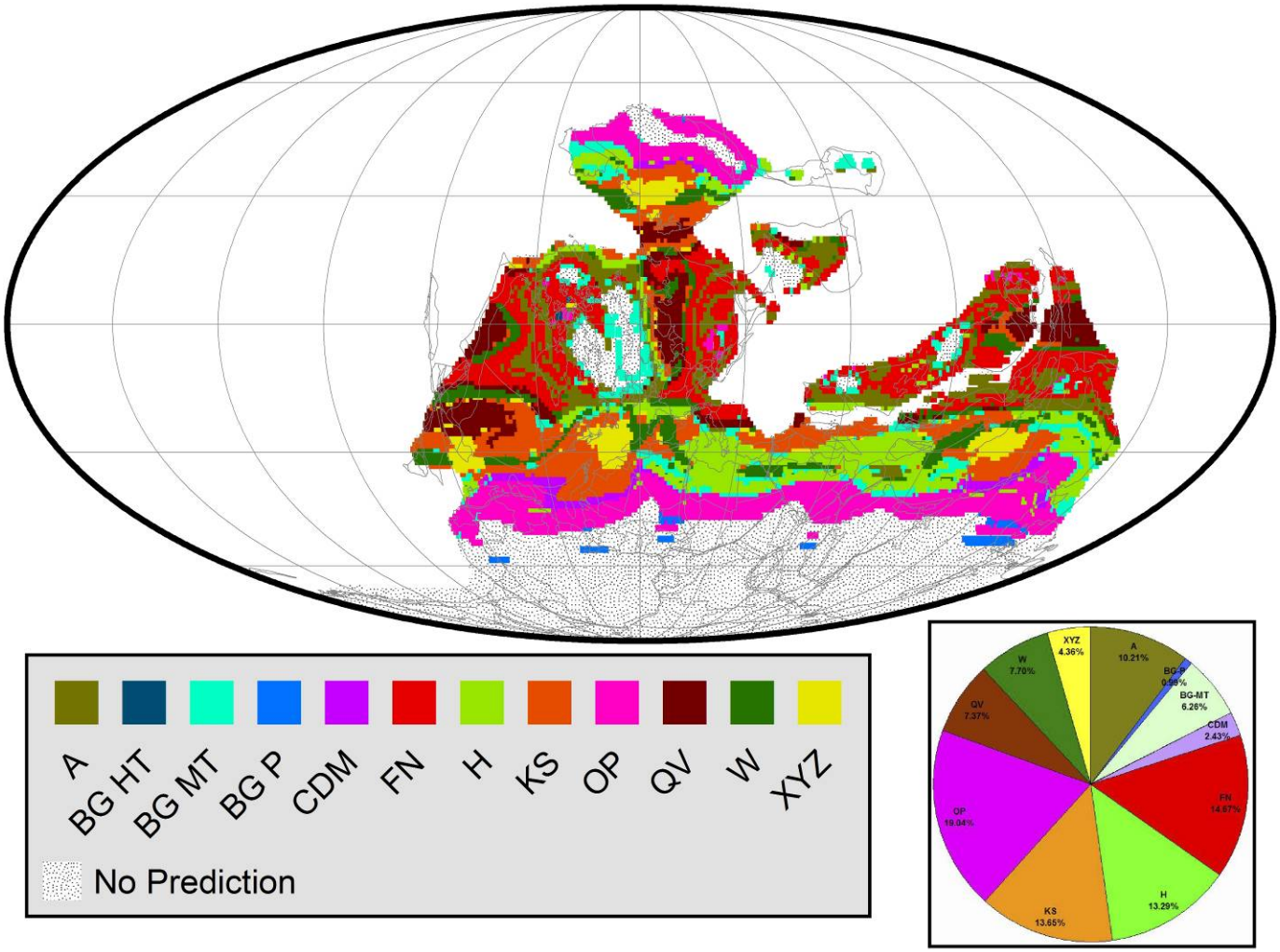

Figure 2.43 Composite Geographic Distribution Map of Primary Predicted Ancient Soils (Paleo-soils) for the Late Devonian (360 Ma)

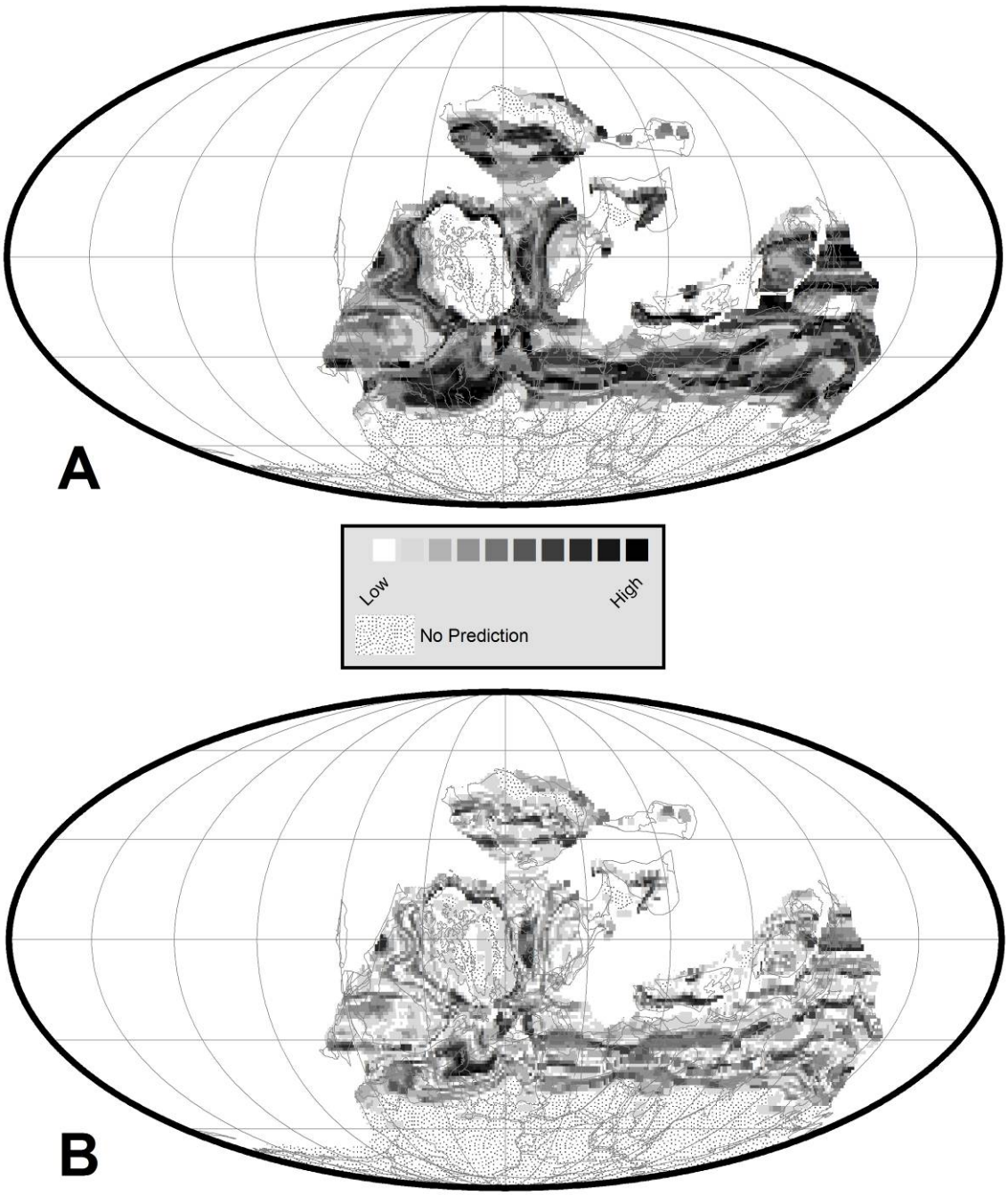

Figure 2.44 A. Prediction Confidence Level for Maximum Probable Paleo-soil Type for the Late Devonian (360 Ma), B. Dominance of Primary Maximum Probable Paleo-soil Type over the Secondary Maximum Probable Paleo-soil Type for the Late Devonian (360 Ma)

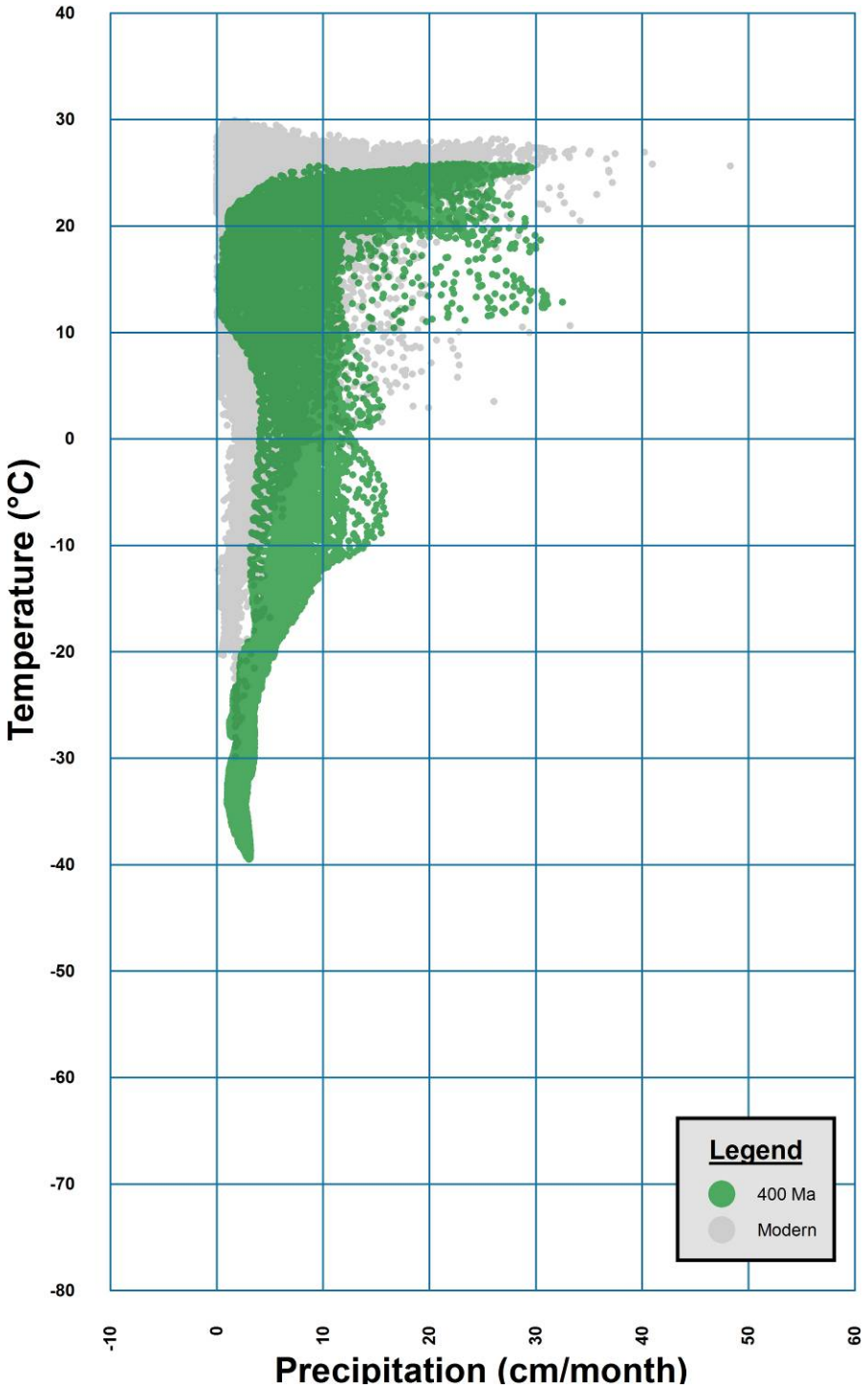

Figure 2.45 Temperature-Precipitation Plot for the Early Devonian (400 Ma)

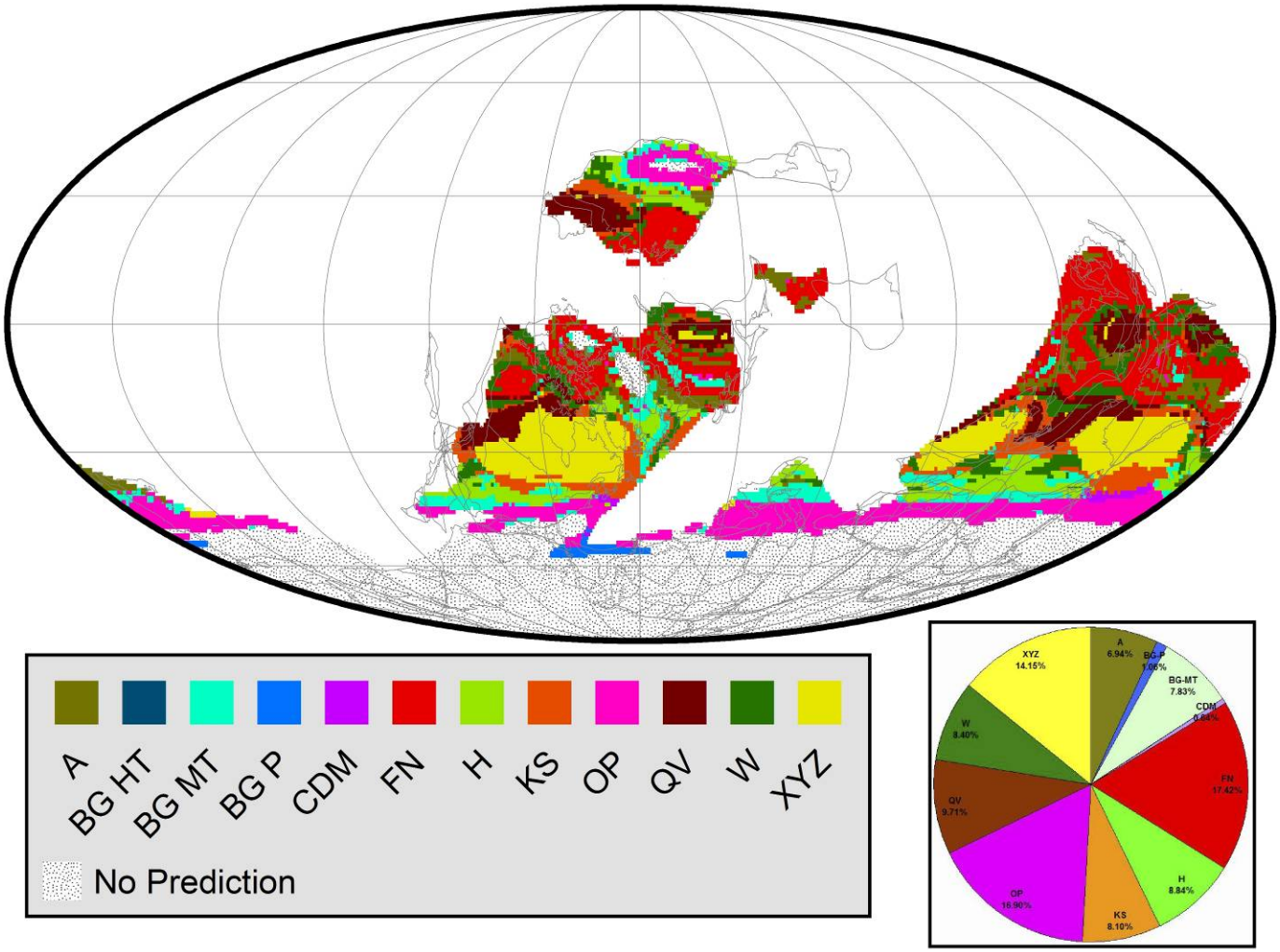

Figure 2.46 Composite Geographic Distribution Map of Primary Predicted Ancient Soils (Paleo-soils) for the Early Devonian (400 Ma)

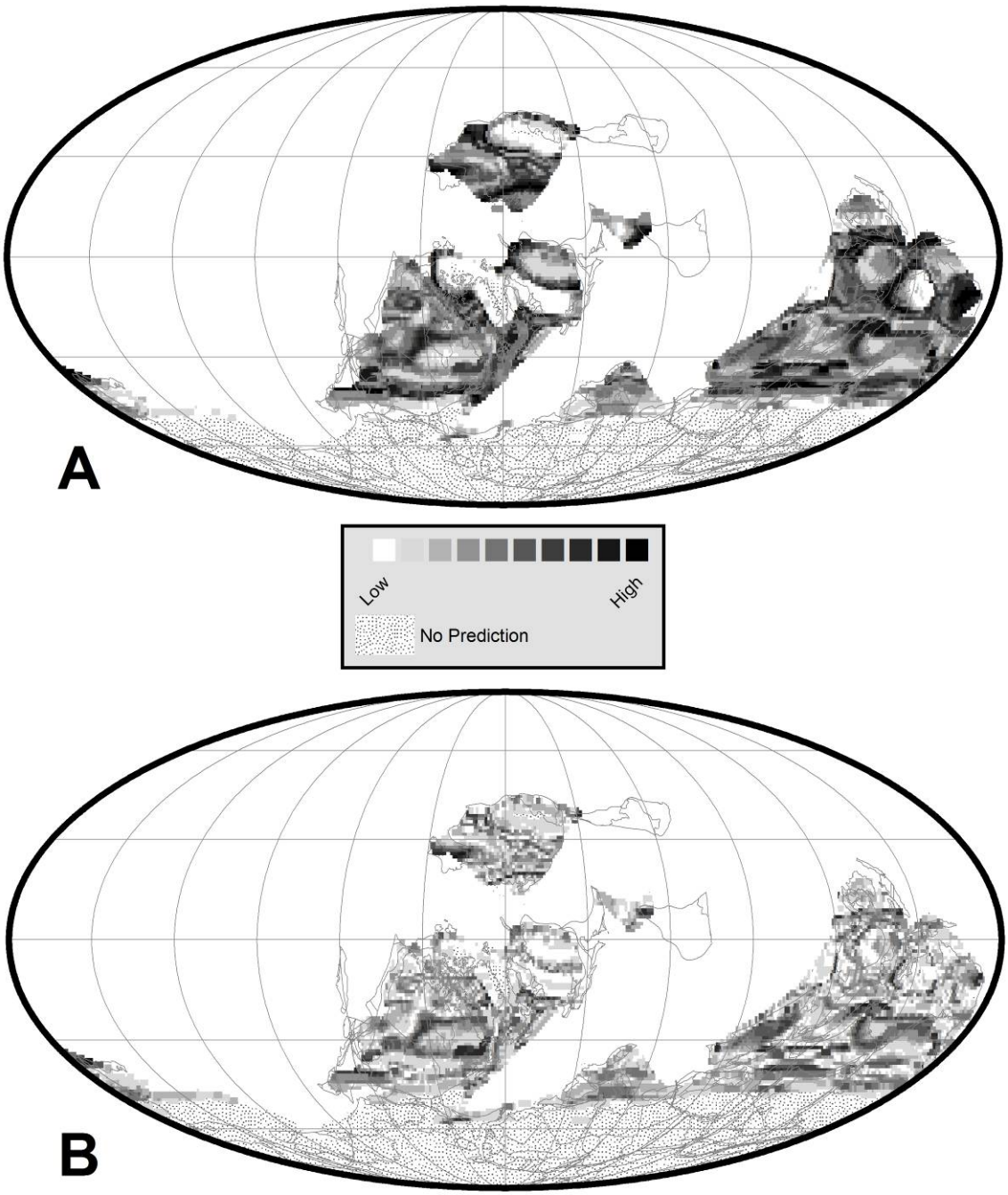

Figure 2.47 A. Prediction Confidence Level for Maximum Probable Paleo-soil Type for the Early Devonian (400 Ma), B. Dominance of Primary Maximum Probable Paleo-soil Type over the Secondary Maximum Probable Paleo-soil Type for the Early Devonian (400 Ma)

Figure 2.45 plots the distribution of temperature and precipitation values for the Early Devonian (green) on a background of modern day temperature and precipitation values (gray). During the Early Devonian, the maximum temperature and precipitation values were 25.83°C and 32.52 cm/month, respectively. The minimum temperature and precipitation values were -39.49°C and 0.21 cm/month, respectively. It is clear from this plot that the range of temperature and precipitation during the Early Devonian was quite different from the modern range of temperature and precipitation. During the Early Devonian, the Global Mean Temperature (GMT) appears to be 4 – 5°C cooler than the modern times. It is also important to note that were more low temperature localities (< 5°C) and fewer high temperature localities (>20°C). The highest precipitation values were similar to present day and there appears to have been a precipitation gap at cooler temperatures (10° ~ -20°C).

The Early Devonian has a very complex paleo-soil distribution pattern. Figure 2.46 is a reconstruction of ancient paleo-soil types for the Early Devonian (400 Ma). The Early Devonian is believed to be a Global Hot House World (Figure 2.2). There are two major paleo-soil belts. A broad belt of Equatorial Rainy Belt paleo-soil types (FN and W), extends from almost 30°N to 25°S. This suggests that during Early Devonian the conditions that would have favored the colonization of primitive land plants were widespread. It is important to note that along the Equator there are three circular regions with arid paleo-soil types (mainly QV with some XYZ). The significance of these arid paleo-soil types in the equatorial regions is not well understood.

There is a broad belt of the Subtropical Arid Belt paleo-soil type (XYZ) at 30°S. The Warm Temperate Belt paleo-soil type (A and H) are moderately developed and are sandwiched between Cool Temperate Belt and Arid Belt or Arid Belt and Equatorial Belt. There is a narrow belt of Cool Temperate Belt paleo-soils (OP and KS) above 30°N and 45°S. The stippled areas below 45°S represent temperature-precipitation conditions that do not exist in the modern world, and so no paleo-soil predictions were made for these regions.

Figure 2.47A illustrates the levels of confidence for the paleo-soil types for the Early Devonian period. During the Early Devonian, most of the regions have high levels of confidence except for the central continental areas.

The paleo-soil dominance map (Figure 2.47B) is very different to the paleo-soil confidence map (Figure 2.47A). During the Early Devonian, though the confidence levels are high in several regions around the globe the dominance levels are mostly low. Only the regions along 30°S have high dominance scores.

We have also prepared a reconstruction showing the secondary paleo-soil type (PPS2) predictions for the Early Devonian period (400 Ma). The reconstruction along with its levels of confidence is illustrated in Appendix C (Figure C.15).

2.3.16 Silurian (430 Ma)

The Silurian was a relatively warm period even though levels of atmospheric CO_2 may have been less than modern levels. The Silurian is noted for the first appearance of land plants and the radiation of the fish (Holland and Bassett, 1989; Bassett et al., 1991; Landing and Johnson, 1998, 2003). Similar to the Ordovician, several continents occupied low latitudes (Laurentia, Baltica, Siberia, Kazakhstania), a vast ocean covered the northern hemisphere, and the supercontinent Gondwana extended from equatorial latitudes to the South Pole. The sea level was high. Large shallow epicontinental seas were widely distributed, and the continents had a low relief.

Figure 2.48 plots the distribution of temperature and precipitation values for the Silurian (green) plotted on a background of modern day temperature and precipitation values (gray). During the Silurian, the maximum temperature and precipitation values were 30.90°C and 45.58 cm/month, respectively. The minimum temperature and precipitation values were -16.23°C and 0.16 cm/month, respectively. It is clear from this plot that the ranges of temperature and precipitation values during the Silurian were quite similar to the modern range. During the Silurian, the Global Mean Temperature (GMT) appears to be 3 – 4°C warmer than modern times.

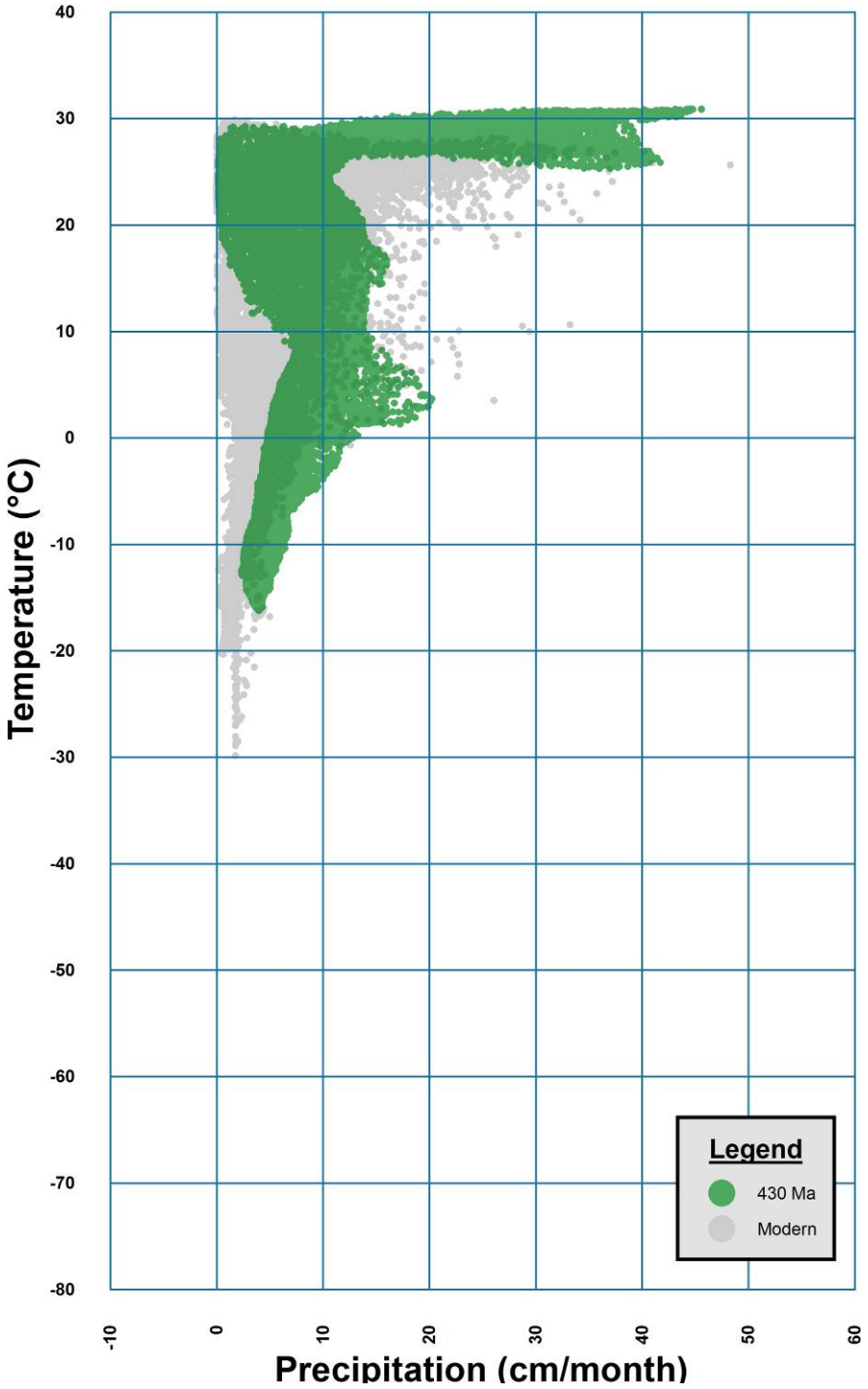

Figure 2.48 Temperature-Precipitation Plot for the Silurian (430 Ma)

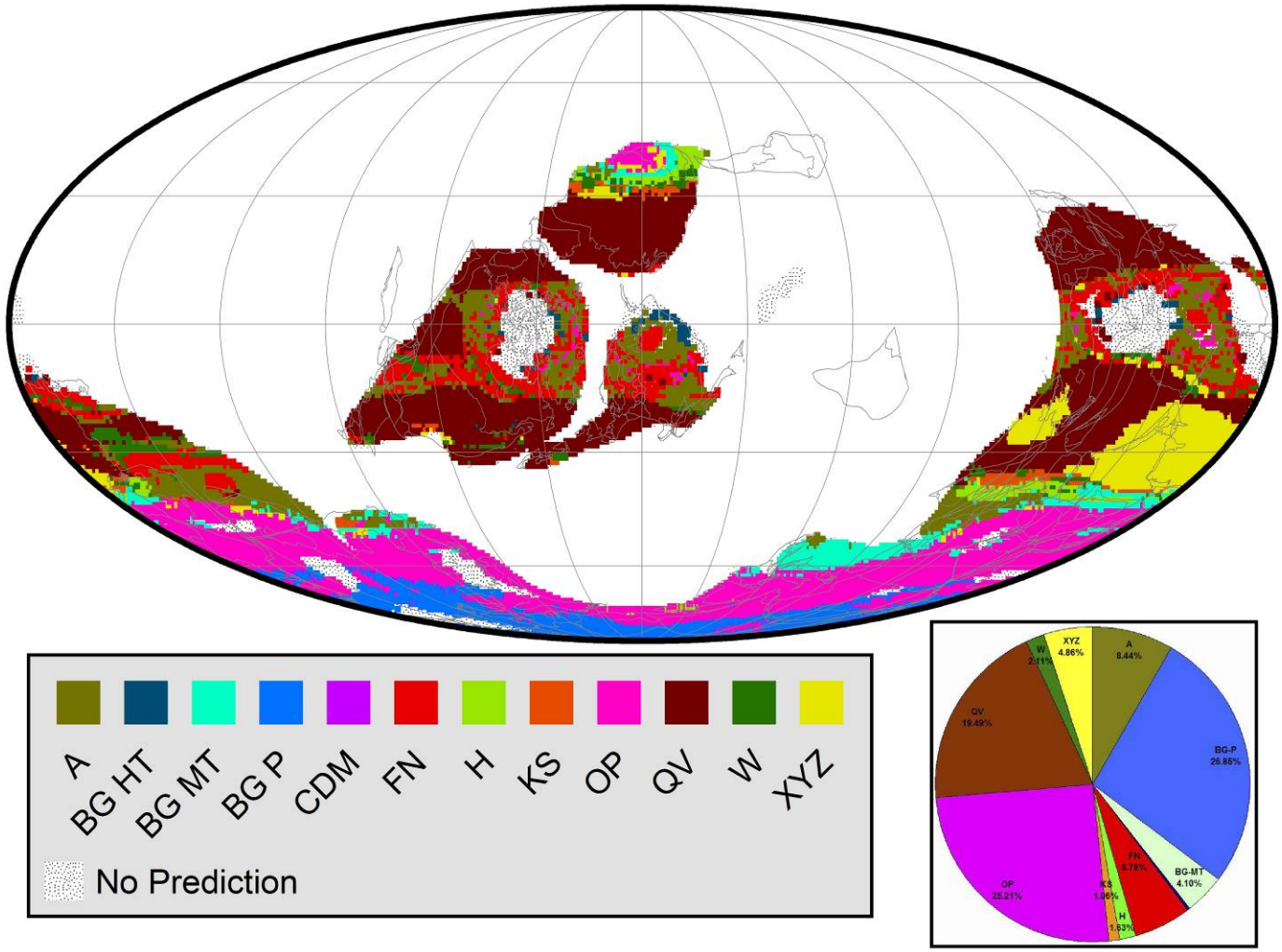

Figure 2.49 Composite Geographic Distribution Map of Primary Predicted Ancient Soils (Paleo-soils) for the Silurian (430 Ma)

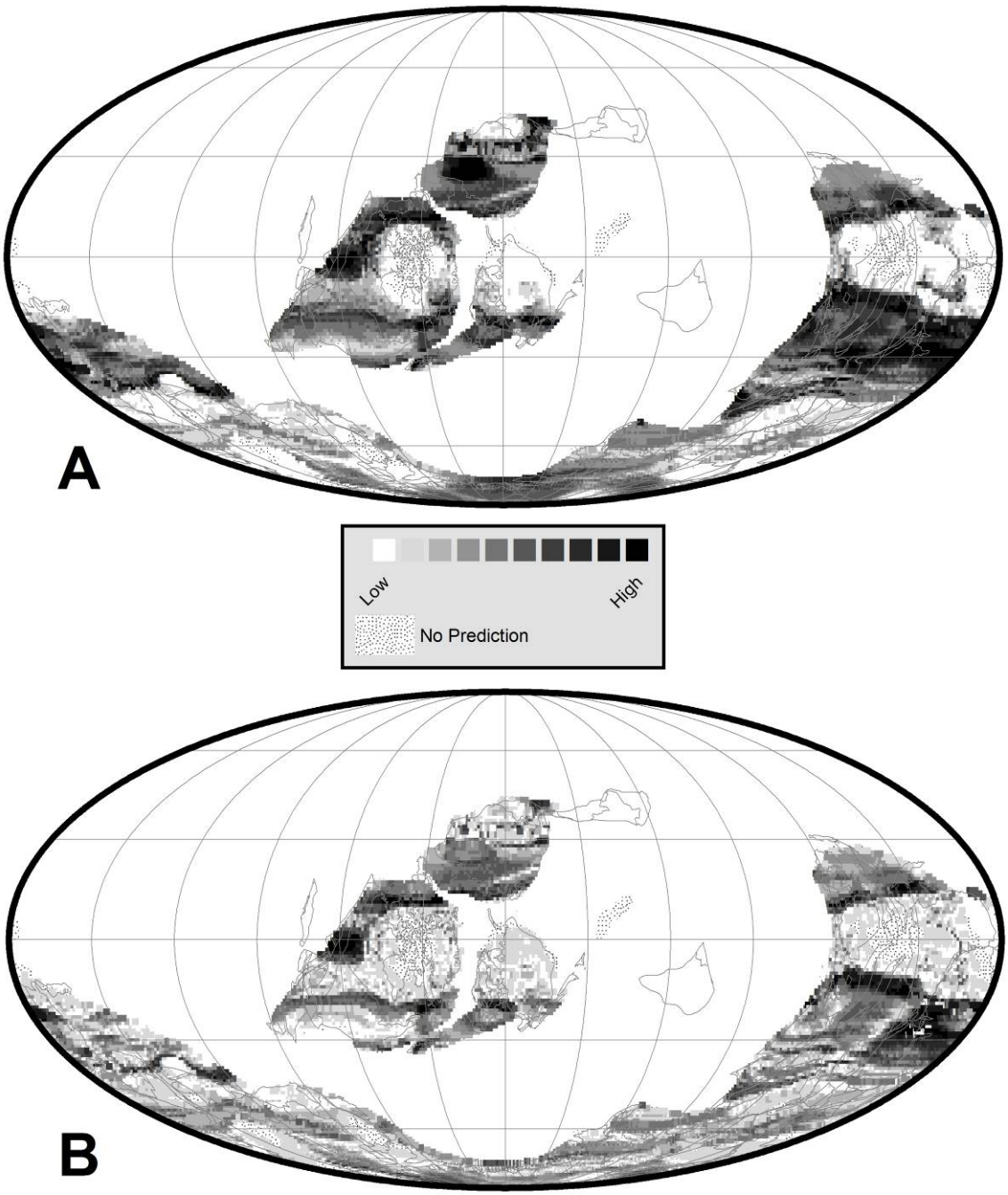

Figure 2.50 A. Prediction Confidence Level for Maximum Probable Paleo-soil Type for the Silurian (430 Ma), B. Dominance of Primary Maximum Probable Paleo-soil Type over the Secondary Maximum Probable Paleo-soil Type for the Silurian (430 Ma)

It is also important to note that were more high temperature localities (>20°C) and fewer low temperature localities (< 5°C). The highest precipitation values were similar to the present day, and there appears to have been a precipitation gap at low temperatures (<15°C).

Figure 2.49 is a reconstruction of paleo-soil types for the Silurian (430 Ma). Though the Silurian is considered to be Global Hot House World (Figure 2.2), the model predicts fairly cold temperature-precipitation conditions near the South Pole. There is a narrow belt of the Polar paleo-soil type (BG Polar) near the pole. Next to the BG Polar paleo-soil is a broad belt of the Cool Temperate Belt paleo-soil (OP) extending from 45°S to almost 80°S. Except for the areas between 15° north and south, the rest of the continental regions are dominated by Subtropical Arid Belt type paleo-soil types (QV and few XYZ). Along the Equator, the equatorial paleo-soil FN occurs in association with A, a Warm Temperate paleo-soil. This suggests that during the Silurian, distributions of the primitive land plants were discontinuous and patchy and that temperature-precipitation conditions in the equatorial region were a combination of everwet and warm temperate climate. Paleo-soils characteristic of the Warm Temperate Belt (A and H) are sandwiched between arid and cool temperate soils. The stippled area along the equator represents temperature-precipitation conditions that do not exist in the modern world. Therefore, no paleo-soil predictions were made for these regions. The pattern of paleo-soil types during the Silurian is especially complex and requires additional study.

Figure 2.50A illustrates the levels of confidence for the paleo-soil predictions for Silurian period. Overall, the Silurian levels of confidence are high and the regions with highest levels of confidence occur in the tropical regions.

The paleo-soil dominance map (Figure 2.50B) is similar in many respects to the paleo-soil confidence map (Figure 2.50A), but there are some significant differences. During the Silurian, the dominance scores are also mostly high except for the western part of Gondwana along the 30°S.

We have also prepared a reconstruction showing the secondary paleo-soil type (PPS2) predictions for the Silurian period (430 Ma). The reconstructions along with its levels of confidence are illustrated in Appendix C (Figure C.16).

2.3.17 Early Ordovician (480 Ma)

The Early Ordovician was characterized by a mild global climate. During this time, period the continents were flooded by the oceans creating warm, broad tropical seaways. The Late Ordovician, in contrast, was an Ice House World. The South Polar Ice Cap covered much of Africa and South America. The climate in North America, Europe, Siberia and the eastern part of Gondwana was tropical (Retallack and Feakes, 1987). The density of marine organisms increased dramatically during the Ordovician. There were wide-ranging reef complexes in the Tropics. That is why the Early Ordovician was thought to be quite warm, at least in the Tropics. Despite the tremendous expansion of life during the Ordovician Period, there was major mass extinction at the end of the Ordovician.

Figure 2.51 plots the distribution of temperature and precipitation values for the Early Ordovician (green) on a background of modern day temperature and precipitation values (gray). During the Ordovician, the maximum temperature and precipitation values were 26.50°C and 33.41 cm/month, respectively. The minimum temperature and precipitation values were -2.75°C and 0.39 cm/month, respectively. It is clear from this plot that the ranges of temperature and precipitation values during the Ordovician were quite similar to the range of modern temperature-precipitation data. During the Ordovician, the Global Mean Temperature (GMT) appears to be 3 – 5°C cooler than the modern times. It is also important to note that were more low temperature localities (< 5°C) and fewer high temperature localities (>20°C). The highest precipitation values were similar to present day, and there appears to have been a precipitation gap at cooler temperatures (<10°C).

During the Ordovician land plants had not yet evolved. Therefore the soils of the Ordovician were realistically much different than today's soils. Still we have chosen to make

paleo-soil prediction because these predictions none-the-less represent possible Ordovician climatic conditions (for example, tropical, wet, arid, temperate, polar).

Figure 2.52 is a reconstruction of paleo-soil types for the Early Ordovician (480 Ma). During the Early Ordovician, the climate near the South Pole was extremely cold. Hence, there are few paleo-soil predictions above 50° latitude. This region was characterized by temperature-precipitation conditions that do not exist in the modern world (stippled areas on Figure 2.52). A very broad belt of Equatorial Rainy Belt paleo-soils (mainly FN and a few W) and relatively wide belt of Subtropical Arid paleo-soils (QV and XYZ) paleo-soil types covered much of the continental regions. This suggests that during the Early Ordovician, in the equatorial regions, hot and wet conditions prevailed. Along the Equator there is also a broad region of arid paleo-soil QV, whose significance is not well understood. Towards 45°S there is a narrow belt of Cool Temperate paleo-soil (OP). It is also notable that at places along the tropics, Warm Temperate Belt paleo-soils (A and H) are developed. Overall, the geographic pattern of paleo-soil types during Early Ordovician is especially complex and requires additional study.

Figure 2.53A illustrates the levels of confidence for the Ordovician paleo-soils. During the Early Ordovician, most of the predicted paleo-soil occurrences have high levels of confidence. The paleo-soil dominance map (Figure 2.53B) is very different from the paleo-soil confidence map (Figure 2.53A). Though the confidence levels are high for all the regions around the globe, the dominance levels are mostly moderate to low.

We have also prepared a reconstruction showing the secondary paleo-soil type (PPS2) predictions for the Early Ordovician period (480 Ma). The reconstruction along with its levels of confidence is illustrated in Appendix C (Figure C.17).

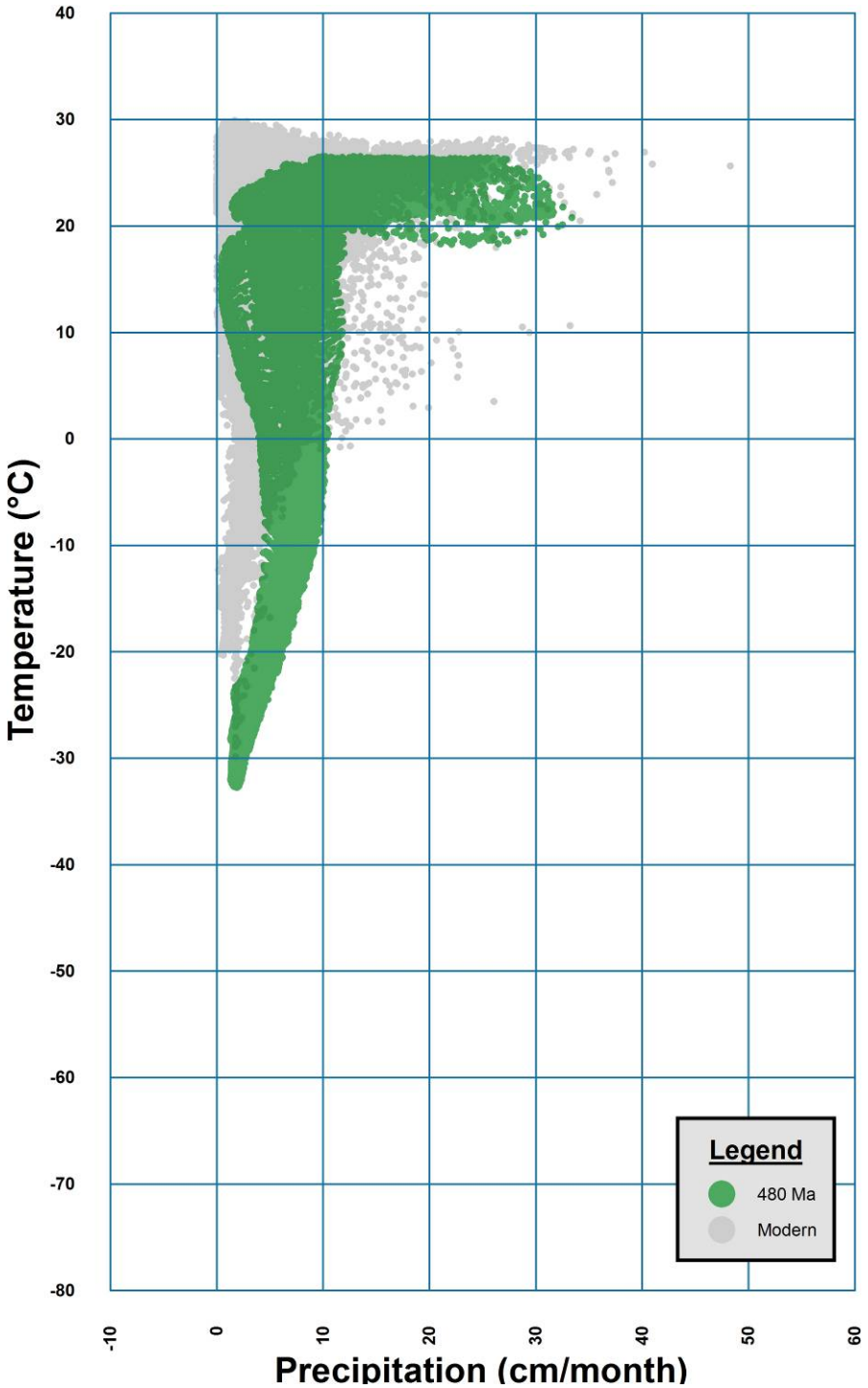

Figure 2.51 Temperature-Precipitation Plot for the Ordovician (480 Ma)

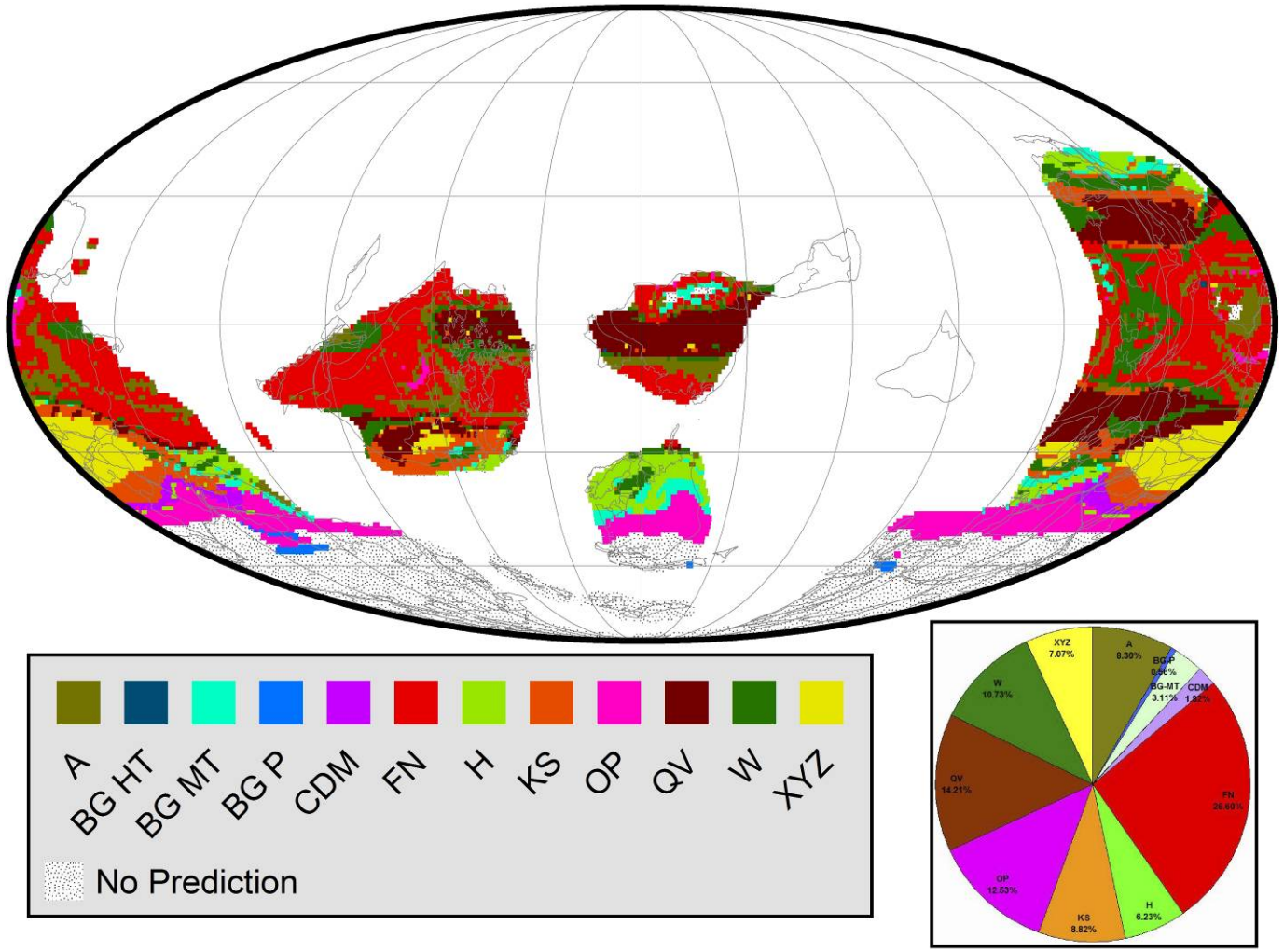

Figure 2.52 Composite Geographic Distribution Map of Primary Predicted Ancient Soils (Paleo-soils) for the Ordovician (480 Ma)

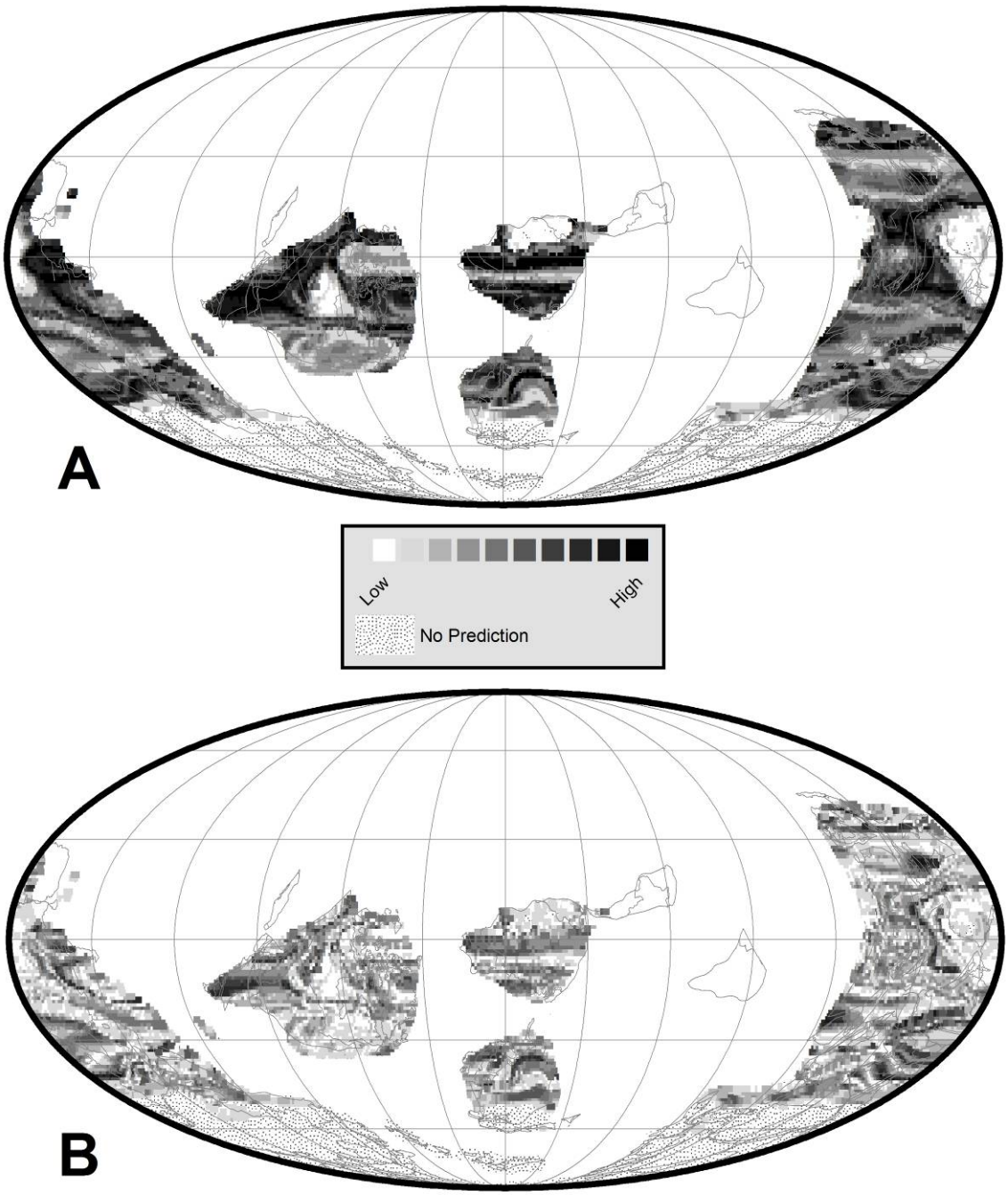

Figure 2.53 A. Prediction Confidence Level for Maximum Probable Paleo-soil Type for the Ordovician (480 Ma), B. Dominance of Primary Maximum Probable Paleo-soil Type over the Secondary Maximum Probable Paleo-soil Type for the Ordovician (480 Ma)

2.4 Conclusion

The predictions of ten types of ancient soils (paleo-soils) for the seventeen time intervals are entirely based on temperature (TS1) and precipitation values (OPREC) obtained from the Fast Ocean Atmospheric Model (FOAM). Assuming that these temperature and precipitation data are correct, then the predictions should resemble known geologic climatic conditions. However, for most of the time, the estimated temperature and precipitation values estimated by the FOAM simulations are quite different from the known geologic climatic conditions. In every case, where there is a significant mismatch between the FOAM prediction and the geologic climatic conditions, the FOAM datasets are much cooler. The FOAM climatic model predicts Ice House conditions for the Eocene, Aptian, Early Jurassic, Late Triassic, Early Devonian, Silurian. But, all of these times are thought to be Hot House Worlds based on geologic evidence.

Figure 2.56 (A – D) illustrates the temperature-precipitation setting for these seventeen time intervals compared to modern Legates and Willmott (1999) temperature-precipitation conditions. Figure 2.56A shows the temperature-precipitation boundaries for the Cenozoic simulations. It is clear from this figure that the Miocene was the coldest of all the three paleo-simulations during the Cenozoic. The Oligocene (30Ma) and the Eocene (45 Ma) had comparable temperature-precipitation condition as present day. For the Cretaceous (Figure 2.54B), the plots illustrates that during all the four Cretaceous paleo-simulations, the temperature was higher than present. The Aptian and Cenomanian-Turonian time was the warmest of all. Also during the Cenomanian-Turonian, the precipitation was much higher than present day. Figure 2.56C illustrates the temperature-precipitation conditions for Jurassic-Triassic paleo-simulations. The Late Jurassic climate was similar to modern, where as the Early Jurassic and Triassic climates were colder than present day. Figure 2.57B, illustrates the six paleo-simulations for the Paleozoic. Among these, the Early Permian simulation produces the coldest climatic condition with minimum temperature being in -70°C range. The Silurian climate is either comparable or little warm than present day while all other are cooler than present day.

Figure 2.56 illustrates the maximum precipitation for these seventeen time periods as projected by the FOAM. It is important to note that only during the Cretaceous the precipitation values exceed the modern maximum. During the Silurian, estimated maximum precipitation is equal to that of modern maximum precipitation values. During the other times, the maximum precipitation values are less than the modern maximum precipitation values.

Figure 2.57 illustrates four different temperature parameters. The red line demarcates the maximum temperature for the seventeen time intervals while the blue line demarcates the minimum temperature. The green line signifies the Global Average Temperature (GAT) as estimated from FOAM simulated data. The smooth line in brown demarcates the known geological average temperature curve after Scotese & Boucot 1999. It is clear from this graph that there exists a huge difference between the FOAM estimated global average temperatures and the best known estimates of average temperatures. Moreover, the difference is more pronounced for the Jurassic-Middle/Early Paleozoic. Obviously, the Fast Ocean Atmospheric Model is consistent in estimating much cooler temperature conditions for each of these seventeen time intervals and that is why we have seen broad belt of Polar (BG Polar) and/or Cool Temperate Belt (OP, CDM and KS) paleo-soils predicted in each of the ancient geographic distributions. During the geologic past, we also noticed that (hot house or cold house) the latitudinal climatic belts also shift with climatic changes and the predicted soil distributions should reflect these phenomena. But in the predictions made this latitudinal shifting of the climatic belts as well as the paleo-soil predictions are not observed. It is worth to remembering that all climate models, coupled or not, fail to estimate higher temperatures towards the pole and also underestimate the equator to pole heat transport. It is clear that the FOAM results are displaying similar limitation and this need to be addressed to get appropriate paleo-soil prediction maps.

Hence, in the next chapter, FOAM predicted temperature estimates are adjusted to conform the observed/known trend based on the pole-to-equator temperature gradient and temperatures from published lithological indicators, fossils and isotope measurements. It is expected to produce a better prediction of the geographic distribution of various ancient soils.

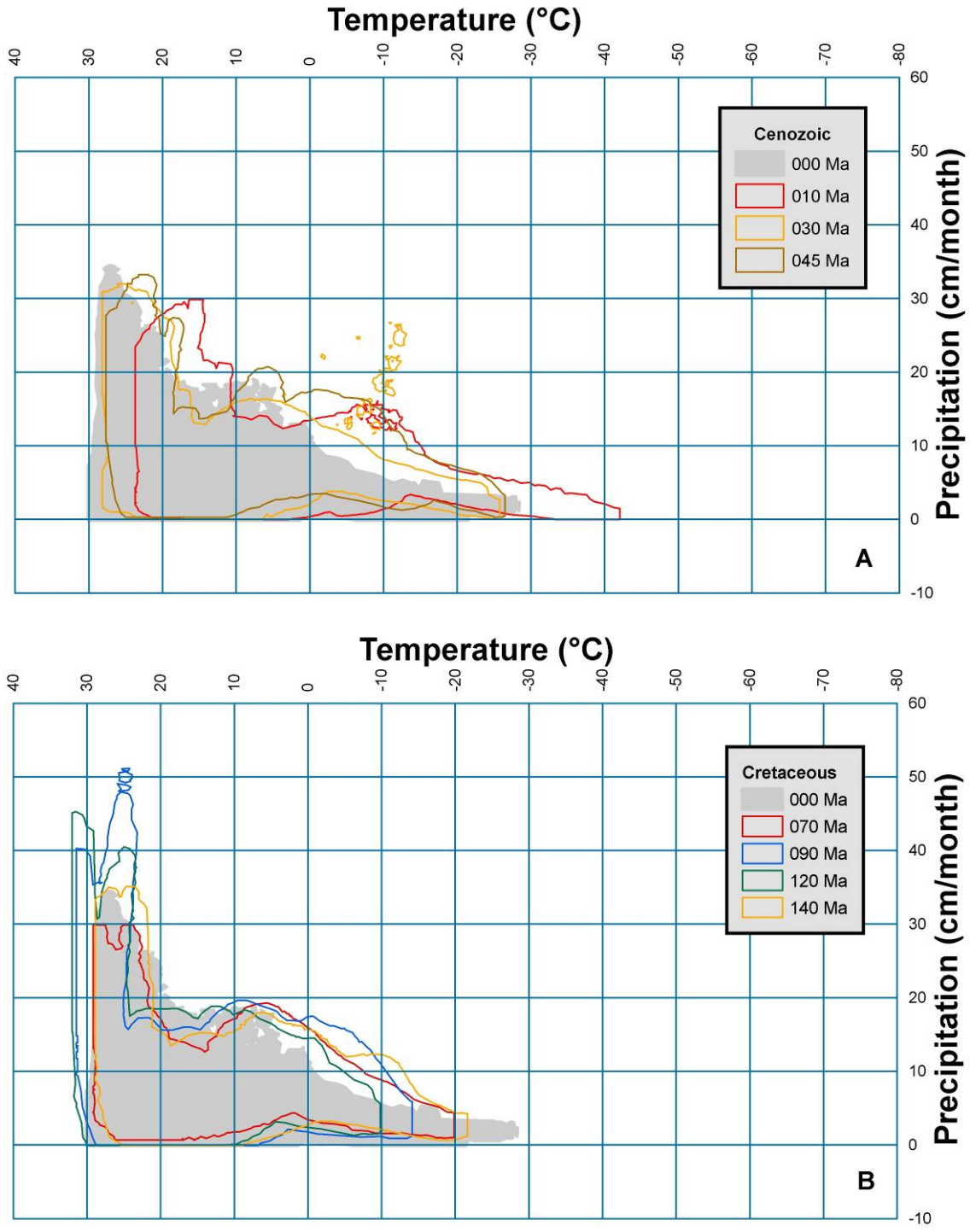

Figure 2.54 Composite Temperature-Precipitation Plot for the Cenozoic (A) and Cretaceous (B)

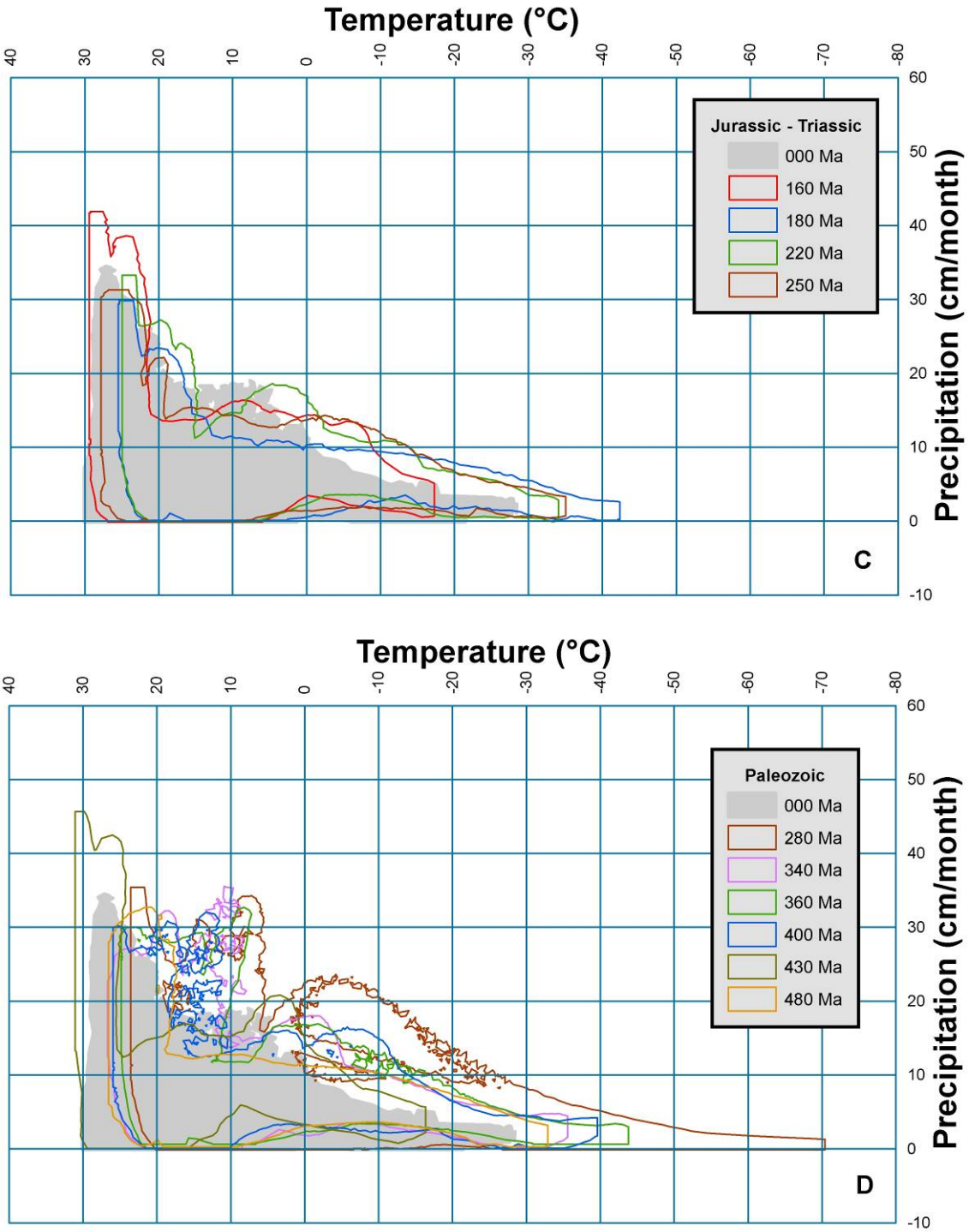

Figure 2.55 Composite Temperature-Precipitation Plot for the Jurassic-Triassic and Paleozoic

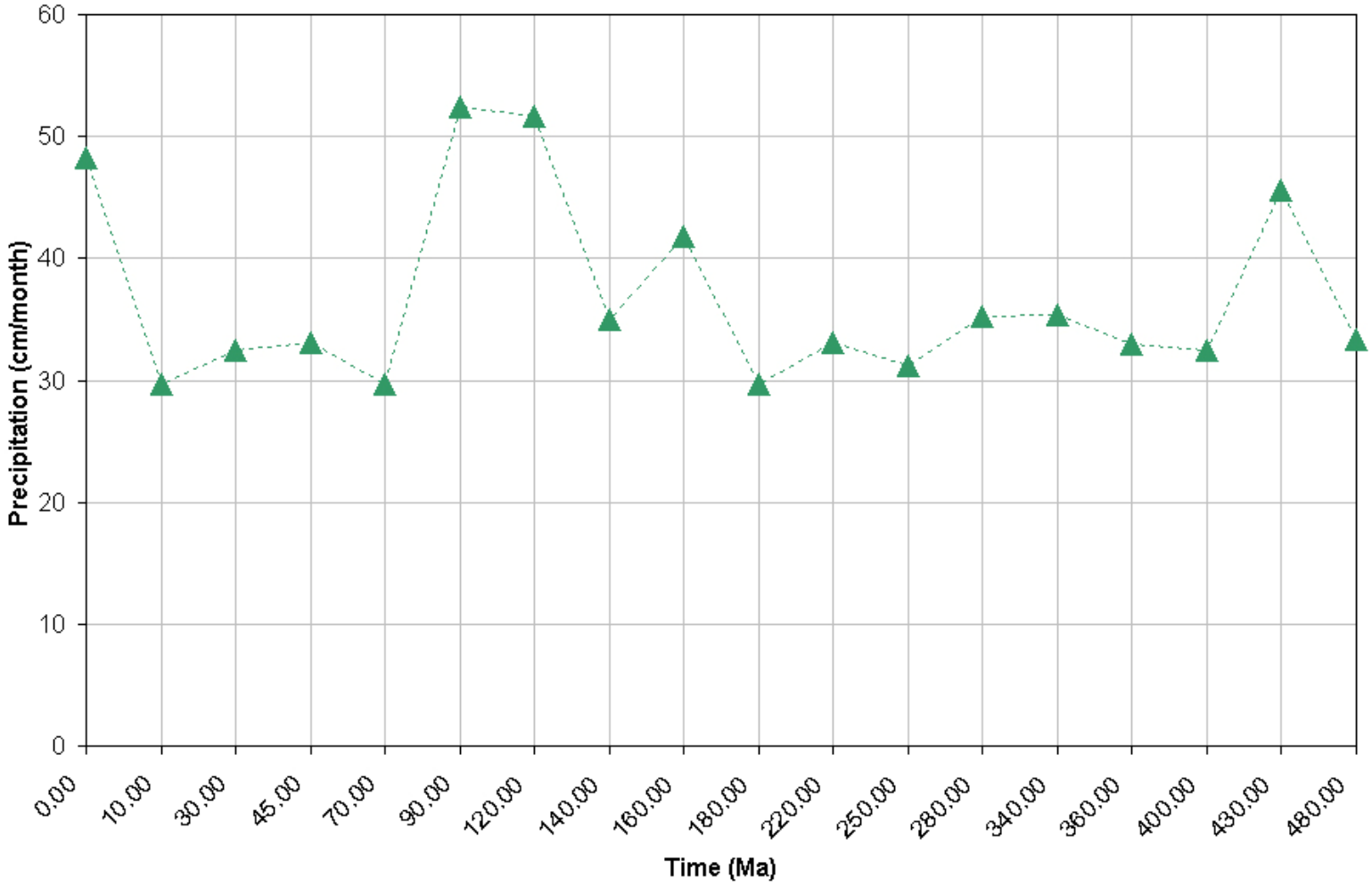

Figure 2.56 Summary of Global Maximum Precipitation from Seventeen FOAM Simulations

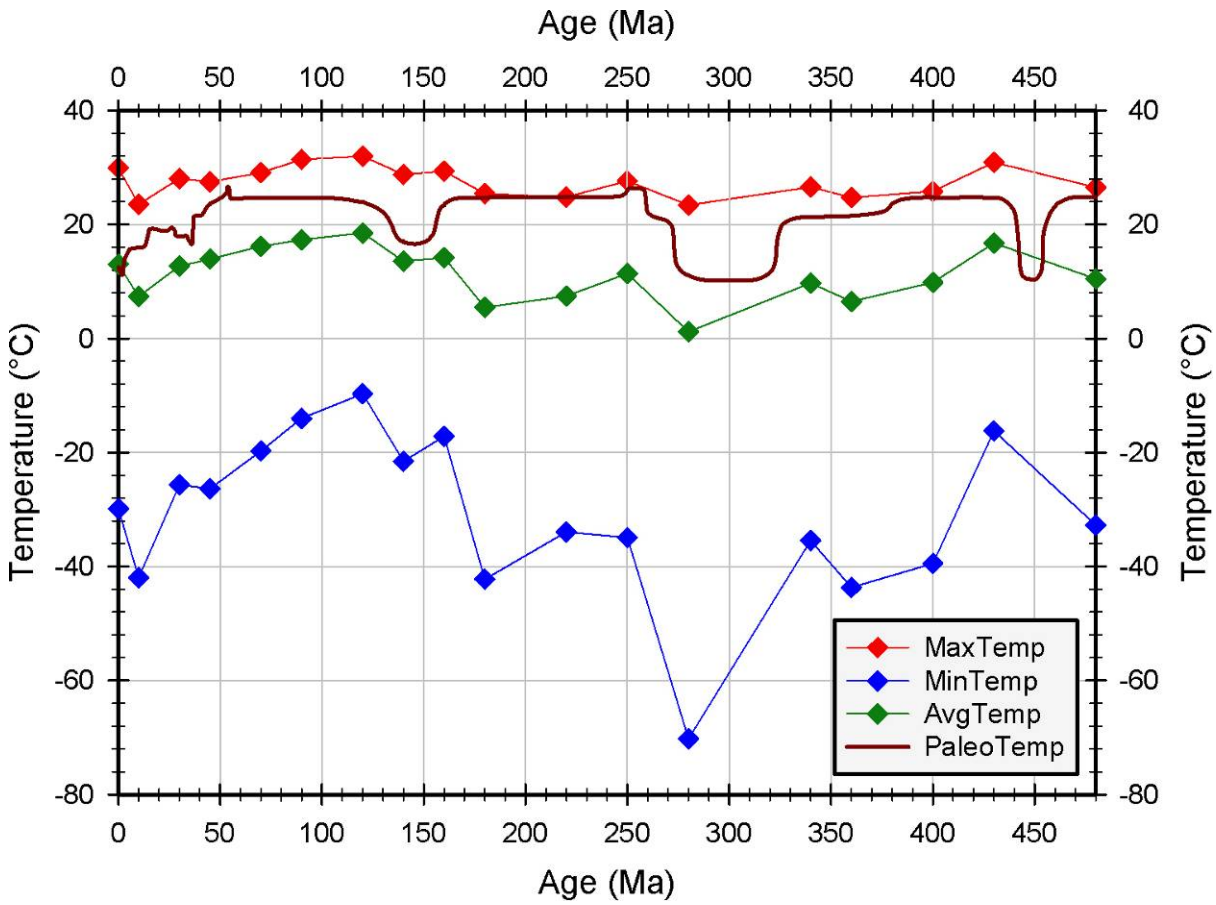

Figure 2.57 Comparison of Estimated Global Temperatures (Scotese & Boucot 1999) with Global Maximum (MaxTemp), Minimum (MinTemp) and Average Temperatures (AvgTemp) from Seventeen FOAM Simulations

CHAPTER 3

POLE-TO-EQUATOR TEMPERATURE GRADIENTS FOR THE CRETACEOUS

One of the major challenges of paleoclimate research is that climate models (both coupled and uncoupled ocean-atmosphere models, for example FOAM) often underestimate the warm polar temperatures that are indicated by fossil and geochemical data (e.g., DeConto et al., 2000). This is especially true for the Late Cretaceous when the latitudinal thermal gradient may have been at its lowest. In this chapter the pattern of global temperatures calculated by FOAM for the Cretaceous time intervals are adjusted to conform to the temperature data obtained from fossil plants and animals, and with various kinds of isotopic temperature estimates. Four Cretaceous paleoclimate simulations: Early Maastrichtian (70 Ma), Cenomanian-Turonian (90 Ma), Early Aptian (120 Ma) and Valanginian – Berriasian (140 Ma), are compared to temperature estimates from published geologic records. A statement of strong argument can be made that the initial pole-to-equator temperature gradient calculated by FOAM is too steep, and that a more equable pole-to-equator temperature gradient is required to explain the available geological records.

The Earth's pole-to-equator temperature gradient represents a fundamental climatological property related to equator-to-pole heat transport efficiency, hydrological cycling and atmospheric chemistry (Cronin, 2009). Of the all past warm climate periods, the Cretaceous has the richest terrestrial fossil and marine chemical record. This evidence, therefore, presents a special opportunity to test the Cretaceous paleoclimate simulations. Knowledge of latitudinal thermal gradients is critical to define the Earth's climatic modes because they reflect the presence or absence of polar ice caps and the dynamics of heat transfer from low to high latitudes (Amiot et al. 2004). Additionally, Cretaceous climatic variations provide an opportunity to examine climate change within a hot house world on several time scales. Cretaceous climate data can therefore help us understand both near-term

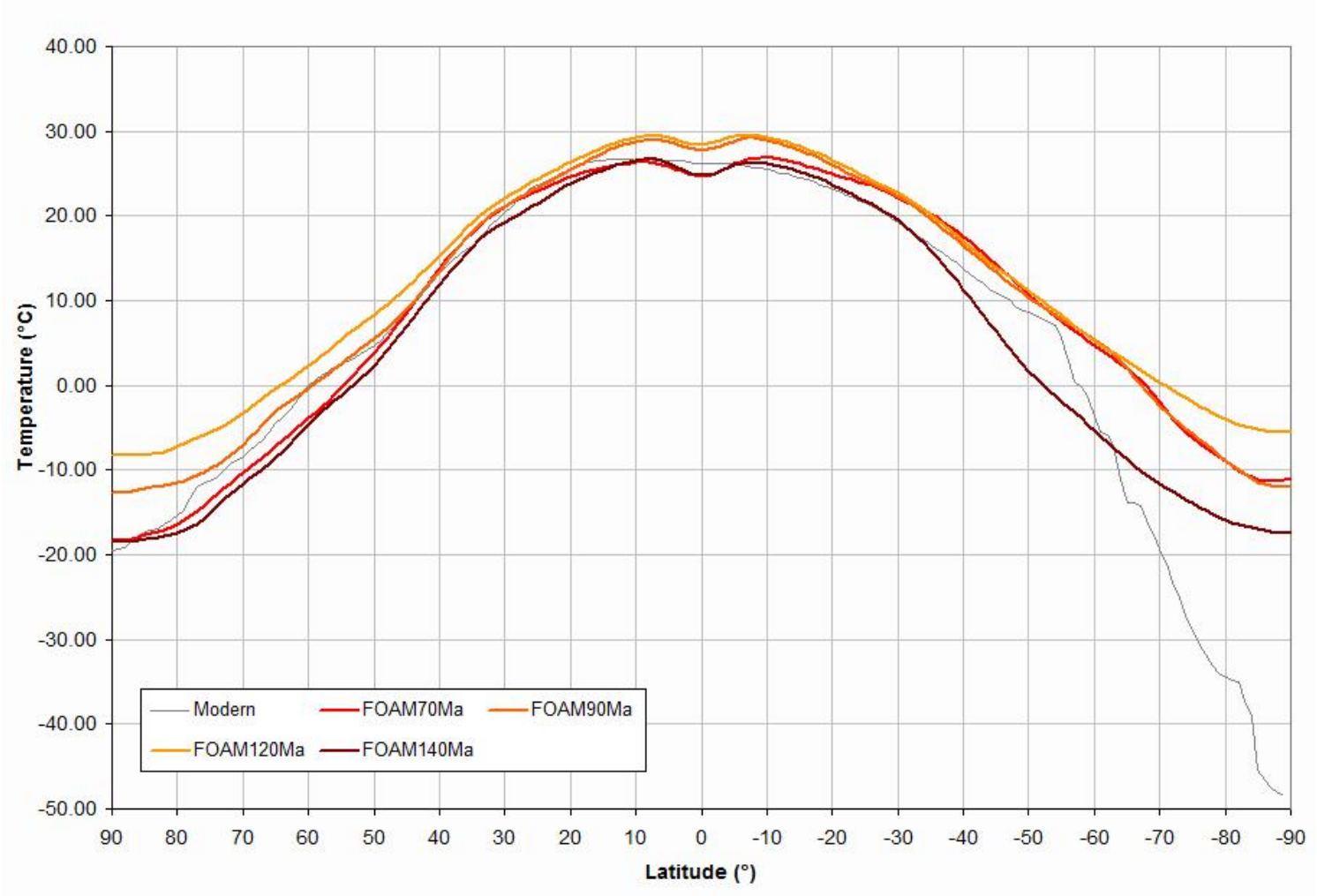

Figure 3.1 Pole-to-Equator Temperature Gradients Estimated by FOAM Simulations. The Gray Curve Represents Modern Actual Pole-to-Equator Temperature Gradient.

Table 3.1 Sample Database for the Cenomanian-Turonian (88.6 – 99.6 Ma)

UID	Age/Stage	Ma	PLatitude	Temperature	pRef	Data Type	Comment
1	Turonian	93.00	41.00	13.50	Bowen 1961	Belemnoidea oxygen isotope paleotemperature	Chilcombe, Belemnite Marls, England
2	Cenomanian	95.00	44.66	16.10	Bowen 1961a	Belemnites sp.	Pagorki, Poland
6	Cenomanian	96.00	39.04	16.10	Lowenstam & Epstein 1954	Belemnitella mucronata s.l.	Table 4, Location: Bois Poteries, Belgium
7	Cenomanian	96.00	44.21	15.40	Lowenstam & Epstein 1954	Actinocamax plenus	Table 4, Location: Bornholm, Denmark
10	Turonian	92.50	39.45	16.70	Lowenstam & Epstein 1954	Actinocamax quadratus ?	Table 4, Location: Rouen, France
11	Cenomanian	95.84	2.42	17.72	Douglas & Savin 1971, 1973	benthonic forams	DSDP 44,47,48,49,50,167,171,305,306 & PointTracker estimate: 100Ma
12	Cenomanian	97.44	2.42	17.64	Douglas & Savin 1975	Shatsky Benthonic Forams	DSDP 49, 50, 305, 306 & PointTracker estimate: 100Ma
13	Turonian	90.27	7.34	21.24	Douglas & Savin 1975	Hess benthonic Forams	DSDP 49, 50, 305, 306 & PointTracker estimate: 90Ma
14	Cenomanian	96.00	-39.96	21.50	Dorman 1968	Baculites sp.	South coast of Bathurst Island near Pipiyanyamili Creek, Northern Australia
15	Turonian	90.30	39.45	25.50	Lowenstam & Epstein 1954	Bourgueticrinus sp. Columner	Table 4, Location: Rouen, France
17	Turonian	90.50	38.38	25.84	Puceat et al 2007	Fish Tooth	
21	Cenomanian	96.00	11.94	29.25	Puceat et al 2007	Fish Tooth	
34	Cenomanian	96.00	64.30	17.80	Miller et al 2006	Floral Assemblage	
35	Cenomanian	96.00	43.30	19.90	Miller et al 2006	Floral Assemblage	
45	Turonian	93.00	5.00	26.00	Frakes 1999	Marine	Ages in million years (Ma) are taken from Gradstein et al. 1994.
58	Cenomanian	99.00	64.00	10.00	Frakes 1999	Marine	Determination on belemnites. Ages in million years (Ma) are taken from Gradstein et al. 1994.
59	Cenomanian	98.00	25.00	21.90	Sellwood et al 1999	Mixed Plantonics	ODP 627B
60	Cenomanian	96.92	2.42	25.04	Douglas & Savin 1971, 1973	Nanofossils	DSDP 44,47,48,49,50,167,171,305,306 & PointTracker estimate: 100Ma
62	Cenomanian	95.83	5.57	27.03	Douglas & Savin 1971, 1973	Nanofossils	DSDP 44,47,48,49,50,167,171,305,306 & PointTracker estimate: 90Ma
63	Cenomanian	97.20	2.42	27.27	Douglas & Savin 1975	Shatsky Nanofossils	DSDP 49, 50, 305, 306 & PointTracker estimate: 100Ma

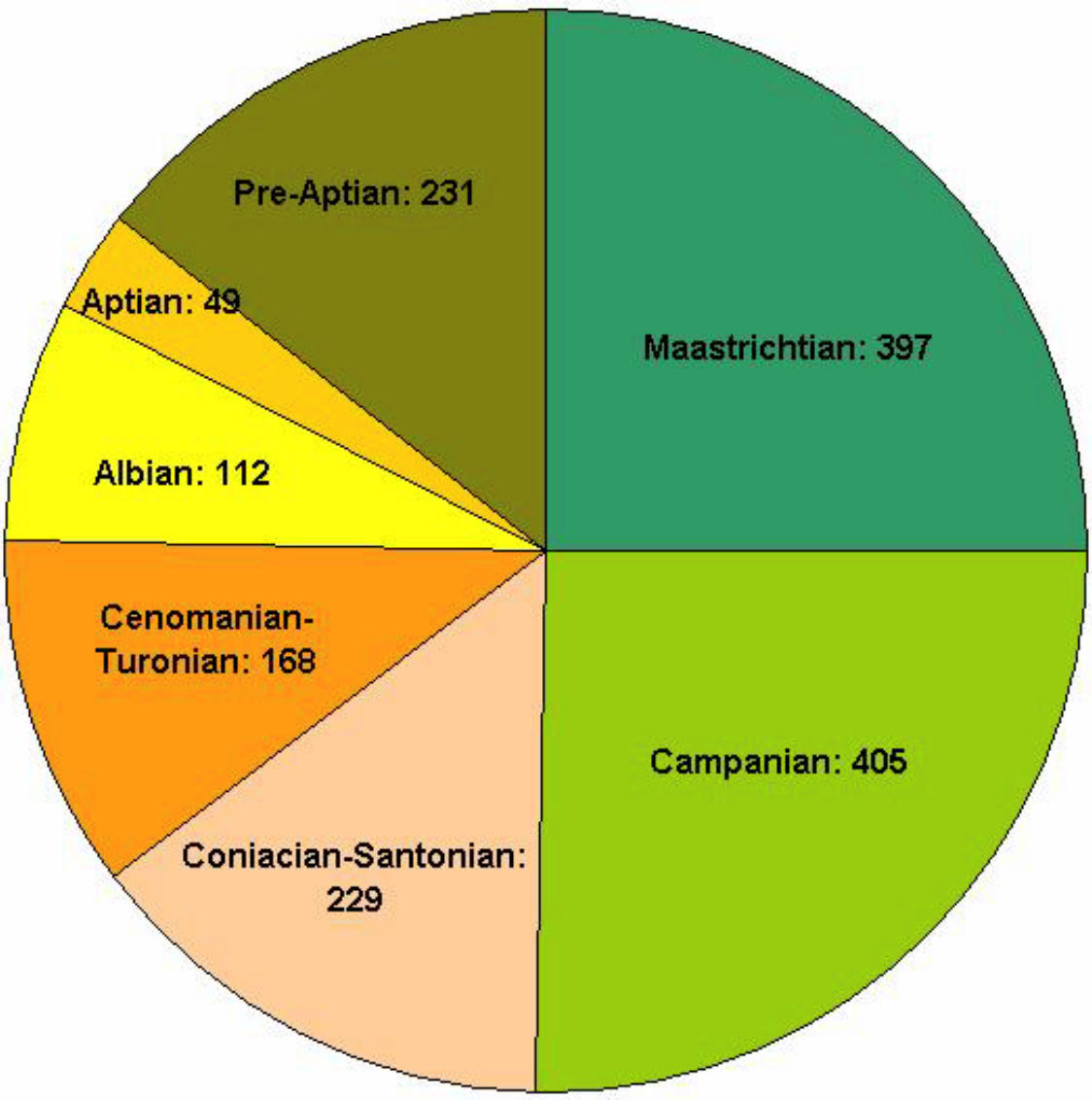

Figure 3.2 Number of data points in the compiled database.

Table 3.2 Key 22 Publications

Year	Author(s)	No of Points	Title
1954	Lowenstam & Epstein	402	Paleotemperatures of the post-Aptian Cretaceous as determined by the oxygen isotope method
1961	Bowen	47	Oxygen isotope paleotemperature measurements on Cretaceous Belemnoidea from Europe, India and Japan
1961	Bowen	28	Paleotemperature analyses of Mesozoic Belemnoidea from Germany and Poland
1973	Douglas & Savin	44	Oxygen and carbon isotope analyses of Cretaceous and Tertiary foraminifera from the central North Pacific
1975	Douglas & Savin	47	Oxygen and carbon isotope analyses of Tertiary and Cretaceous microfossils from Shatsky Rise and other sites in the North Pacific Ocean
1990	Prirrie & Marshall	77	High latitude Late Cretaceous palaeotemperatures: New data from JamesRoss Island, Antarctica
1994	Sellwood et al	7	Cooler estimates of Cretaceous temperatures
1995	Pirrie et al	19	Cool Cretaceous climates: new data from the Albian of Western Australia
1996	D'Hondt & Arthur	60	Late Cretaceous oceans and the cool tropic paradox
1997	Ditchfield	31	High northern palaeolatitude Jurassic-Cretaceous palaeotemperature variation: new data from Kong Karls Land, Svalbard
1998	Huber	165	Tropical paradise at the cretaceous poles?
1999	Clark & Jenkyns	11	New oxygen isotope evidence for long-term Cretaceous climatic change in the Southern Hemisphere
1999	Frakes	98	Estimating the global thermal state from Cretaceous sea surface and continental temperature data
2000	Goloneva	6	The Maastrichtian (Late Cretaceous) climate in the Northern Hemisphere
2004	Pirrie et al	9	Cool early Albian climates; new data from Argentina
2004	Amiot et al.	28	Latitudinal temperature gradient during the Cretaceous upper Campanian-middle Maastrichtian: $\delta^{18}O$ record of continental vertebrates
2005	Steuber et. al.	48	Low-latitude seasonality of Cretaceous temperatures in warm and cold episodes
2005	Zakharov et al	92	Seasonal temperature fluctuations in the high northern latitudes during the Cretaceous Period: isotopic evidence from Albian and Coniacian shallow-water invertebrates of the Talovka River Basin, Koryak Upland, Russian Far East
2006	Miller et al	12	Using leaf margin analysis to estimate the mid-Cretaceous (Albian) paleolatitude of the Baja BC block
2007	Puceat et al	134	Fish tooth $\delta^{18}O$ revising Late Cretaceous meridional upper ocean water temperature gradients
2010	Mutterlose et al	186	TEX86 and stable $\delta^{18}O$ paleothermometry of early Cretaceous sediments: Implications for belemnite ecology and paleotemperature proxy application
2011	Upchurch et al.	13	Latitudinal temperature gradients and high latitude temperatures during the latest Cretaceous: Congruence of geologic data and climate models

and long-term effects of global climatic change.

3.1 Evidence for Cretaceous Hot House World

The Cretaceous is known to have a climate which was one of the most unusual in geologic history. The Early Cretaceous is characterized by cool poles and moderate global temperatures (~16º C) (De Lurio and Frakes 1999, Price et al. 2000 and Steuber et al. 2005). During the mid and Late Cretaceous, long-term global warming (~20º - 22º C) was driven by increasing levels of atmospheric CO_2, rising sea level (lowering the albedo) and the continuing breakup of Pangea. This gentle, long-term warming trend was interrupted by several "spikes" in global temperature that were caused by the rapid injection of greenhouses gases (CO_2 and CH_4) into the atmosphere due to the eruption of large igneous provinces and superplumes (e.g., Pacific Superplume, Aptian, 120 Ma (Larson, 1991 and Larson and Erba 1999)), and the release of methane clathrates from the deep oceans due to the warming of oceanic bottom waters (Jahren et al. 2001).

The impact of a 10 km meteorite at the end of the Cretaceous caused a brief period of global cooling (nuclear winter scenario), followed by a period of global warming that lasted for several million years. The more equable Cretaceous pole-to-equator gradients can be used to correct all cooler polar temperatures and rectify the steep pole-to-equator temperature gradients produced by climate models such as, FOAM (Figure 3.1).

The tectonic forcing of climate and oceanic productivity had a profound impact on terrestrial and marine ecosystems and on the evolution of life during the Cretaceous (Bice et al., 2004). Though as we know, the Cretaceous was overall a hothouse world, Early Cretaceous period was much cooler (Price et al., 2000). In fact, the Cretaceous climate was very variable, consisting of cooler and warmer periods. Warm periods (post Aptian) are known to be among the warmest episodes known in earth history (Frakes, 1979 and 1986). From floral provincial boundaries and interpretation of thermal tolerance of plants, during Early Cretaceous, in Europe, North America and Asia, a decrease in global temperature and a corresponding increase in humidity is also needed before the Aptian warming started (Vakhrameev, 1978).

A similar temperature trend is detectable in the oxygen isotope curves for Russia and Australia (Stevens, 1971). The Early Cretaceous cool interval is also documented by the occurrences of cold water glendonites in high-latitude marine deposits (Kemper, 1987) and by the common occurrence of ice-rafted rocks in mudrocks of high-latitude basins (Australia, Arctic Canada, Siberia, Alaska) (Frakes and Francsis, 1988).

Glassy Turonian foraminifera from Demerara Rise in the western tropical South Atlantic yields the warmest (up to 36°C) sea-surface temperatures (SSTs) yet reported for the entire Cretaceous-Cenozoic time interval (Wilson et al., 2002). CO_2 concentration in the atmosphere has been estimated to have been 4-12 times today's atmosphere (Barron and Washington, 1985, Bice and Norris, 2002). Continents were flooded. There is evidence of increased volcanic and plate tectonic activity, i.e., Gondwana breakup, opening of Atlantic, and subduction of Tethyan Ocean floor. There were no permanent polar ice caps at any time during the Cretaceous. Polar Regions were often characterized by tropical climate (Boucot et al., 2001).

Paleoclimatologists have hypothesized that the pole-to-equator surface-temperature gradient is the dominant control on the paleocirculation of the oceans and atmosphere. Barron and Washington (1982) used a simplified Cretaceous (100 Ma ago) geography to examine quantitatively the relationships between paleogeography, surface-temperature gradients, and the nature of the atmospheric circulation. Sellwood et al. (1994) concluded Cretaceous Equator-to-Pole temperature gradient was much flatter than today's. Huber et al. (1995) suggested that low equator-to-pole temperature differences during the mid-Late Cretaceous indicated much higher poleward heat transport than at present. Huber (1998) described the Cretaceous polar regions as tropical paradise and inferred low equator-to-pole temperature differences. Brady et al. (1998) challenged the reduced pole-to-equator temperature gradient based on results from their GENESIS model.

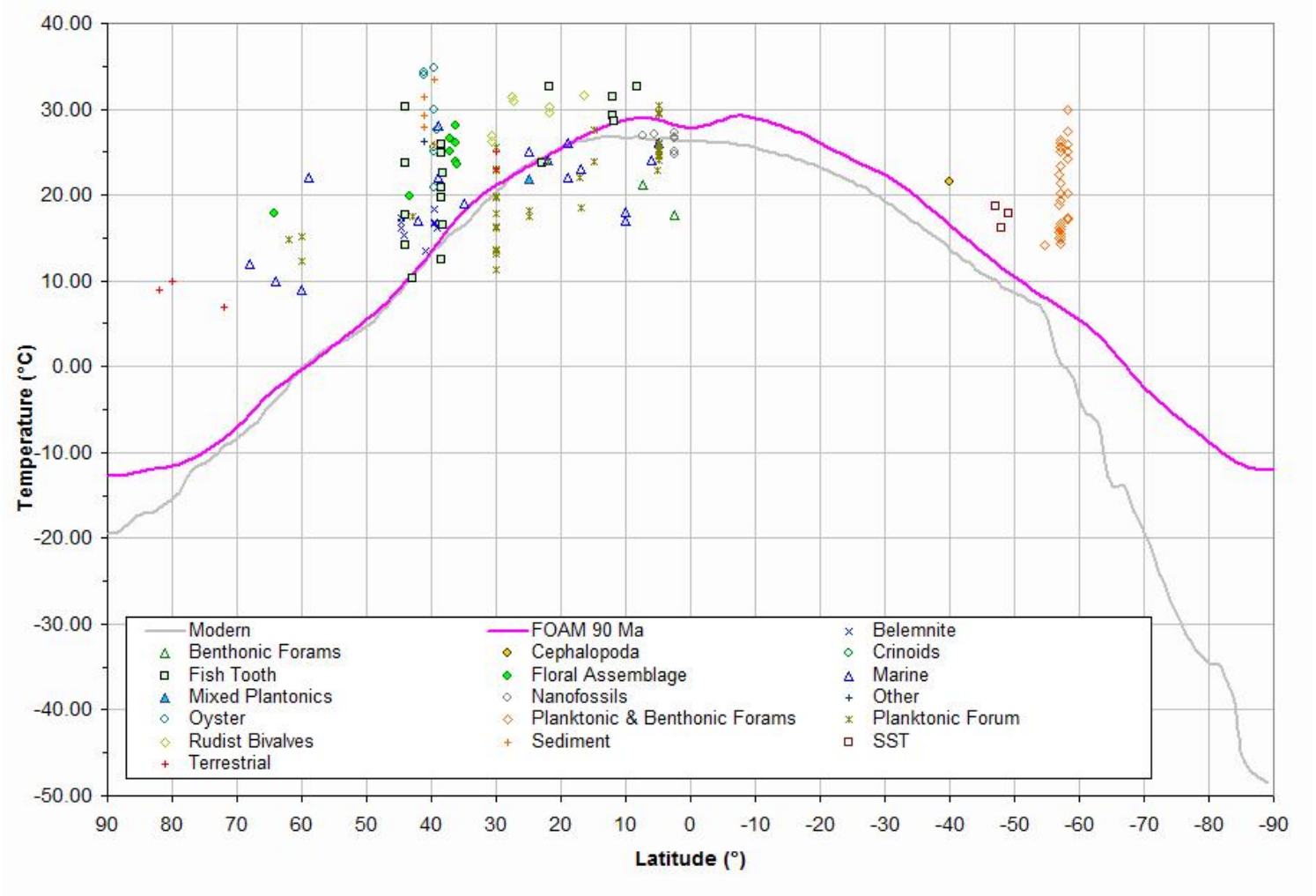

Figure 3.3 Pole-to-Equator Temperature Data Points for the Cenomanian-Turonian (88.6 – 99.6 Ma)

Table 3.3 The FOAM Predicted Pole-To-Equator Temperature Gradient and Revised Pole-To-Equator Temperature Gradient Values at Major Latitudes

	No of Data Points	FOAM Low Latitude Data Used?	Additional FOAM Points	Polynomial Degree	RMS	90°N (°C)	60°N (°C)	30°N (°C)	0° (°C)	-30°S (°C)	-60°S (°C)	-90°S (°C)
Modern	**NA**	**NA**	**NA**	**NA**	**NA**	**-19.41**	**-0.09**	**20.43**	**26.16**	**19.21**	**-3.71**	**-48.41**
Maastrichtian 70 Ma (FOAM)	**NA**	**NA**	**NA**	**NA**	**NA**	**-18.22**	**-3.87**	**21.10**	**24.67**	**22.18**	**4.76**	**-11.15**
Maastrichtian 65.5 – 70.6 Ma (This Study)	397	Yes	41	4	0.4249	2.26	14.75	21.02	22.91	20.71	13.16	-2.57
Campanian 70.6 – 83.5 Ma (This Study)	405	No	0	2	0.5040	9.06	17.83	22.64	23.50	20.39	13.32	2.29
Cenomanian 90Ma (FOAM)	**NA**	**NA**	**NA**	**NA**	**NA**	**-12.69**	**-0.31**	**21.13**	**27.79**	**22.33**	**5.38**	**-12.03**
Coniacian-Santonian 83.5 – 88.6 Ma (This Study)	229	No	0	2	0.4088	13.00	21.51	26.25	27.20	24.38	17.77	7.38
Cenomanian-Turonian 88.6 – 99.6 Ma (This Study)	168	No	0	2	0.2750	5.23	16.32	23.28	26.09	24.76	19.30	9.69
Aptian 120 Ma (FOAM)	**NA**	**NA**	**NA**	**NA**	**NA**	**-8.16**	**2.35**	**22.08**	**28.42**	**22.71**	**5.27**	**-5.52**
Albian 99.6-112 Ma (This Study)	112	Yes	41	2	0.6949	3.05	16.95	24.74	26.40	21.95	11.37	-5.32
Aptian 112-125 Ma (This Study)	49	Yes	41	2	0.2690	10.11	21.35	26.82	26.54	20.50	8.70	-8.87
Pre-Aptian 140 Ma (FOAM)	**NA**	**NA**	**NA**	**NA**	**NA**	**-18.50**	**-4.59**	**19.26**	**24.79**	**19.46**	**-5.28**	**-17.38**
Pre-Aptian 125-145 Ma (This Study)	231	No	0	2	0.2464	-2.65	13.52	23.03	25.88	22.06	11.59	-5.54
Cretaceous 65.5-145 Ma (This Study)	**1591**	**Yes**	**164**	**3**	**0.3817**	**8.95**	**16.37**	**22.36**	**25.28**	**23.53**	**15.47**	**-0.50**

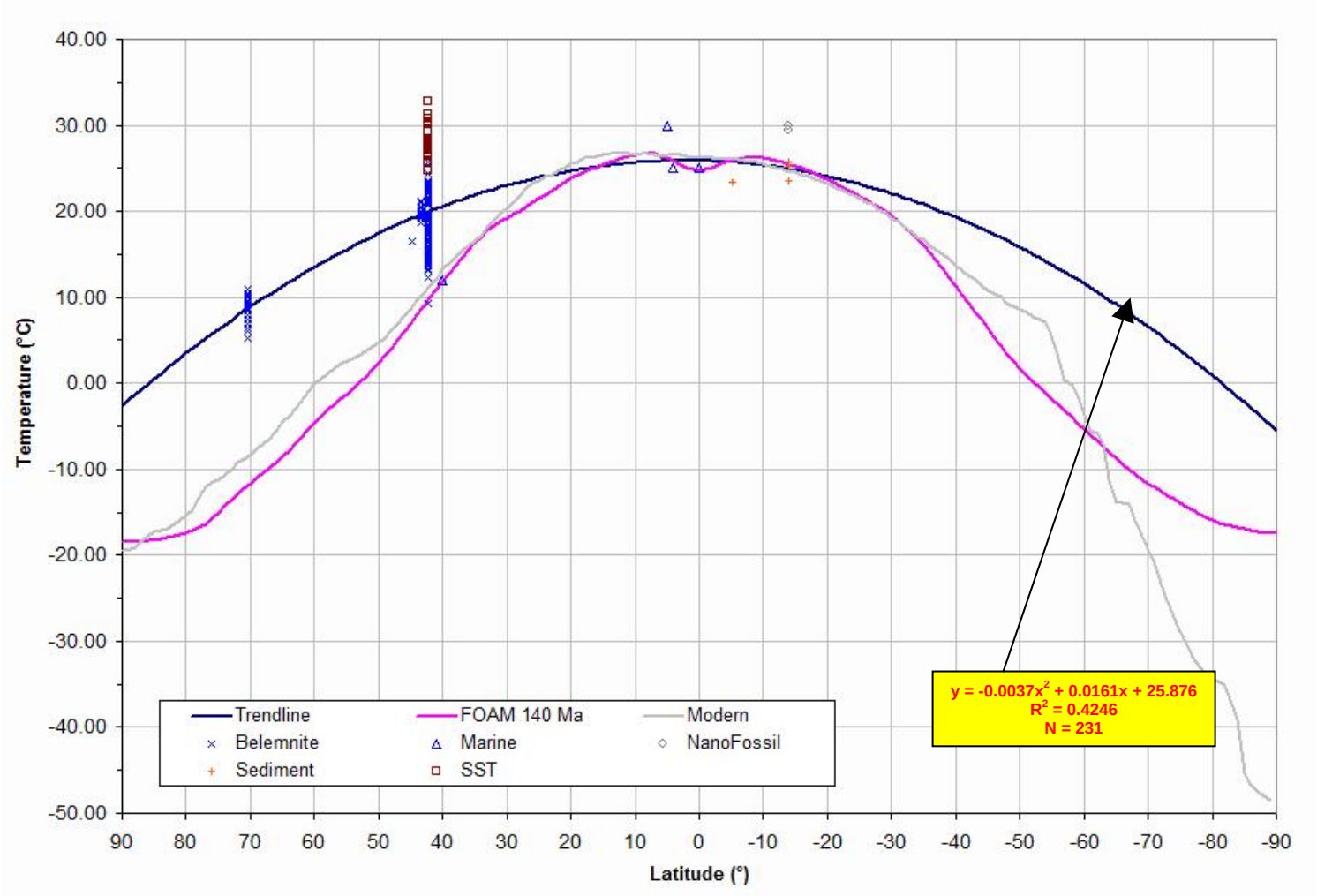

Figure 3.4 Pole-to-Equator Temperature Gradient for the Pre-Aptian (125 – 145.5 Ma)

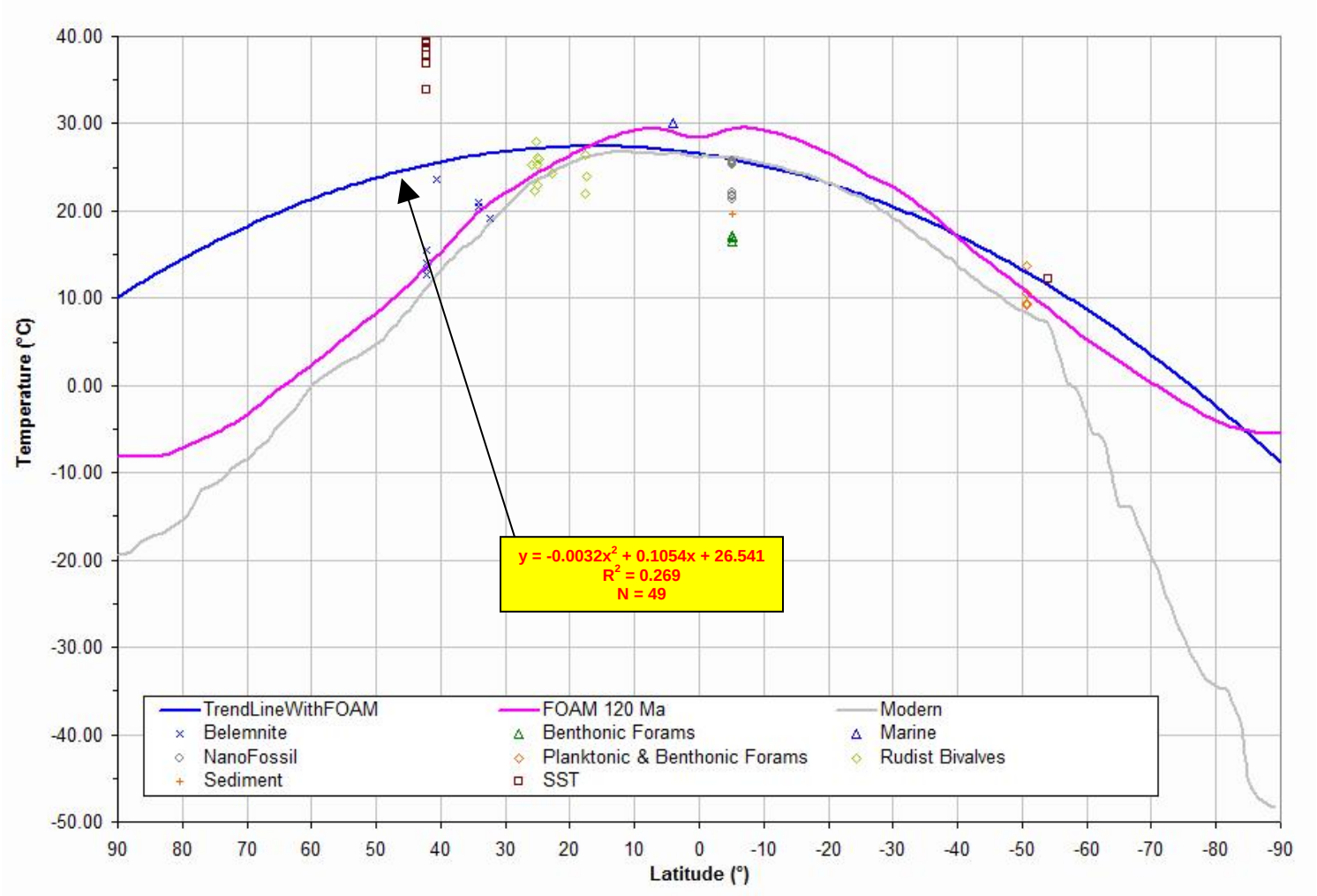

Figure 3.5 Pole-to-Equator Temperature Gradient for the Aptian (112 - 125 Ma)

Bice et al. (2003) constructed a latitudinal temperature gradient for the Turonian stage based on various proxy records. In 2004 Amiot et al. published a latitudinal temperature gradient for Upper Campanian–Middle Maastrichtian based on $\delta^{18}O$ record of continental vertebrates. Donnadieu et al. (2006) investigated the impact of paleogeography on global climate with the climate model FOAM. Using early, mid and Late Cretaceous continental configurations they were able to simulate a reduced pole-to-equator temperature gradient.

Upchurch et al. (2011) have obtained a good match between temperature indicators and climate model output for the latest Cretaceous (Maastrichtian) with the use of a comprehensive database of terrestrial and marine indicators and fully coupled simulations with the Community Climate System Model. They successfully replicated warm polar temperatures and a shallow latitudinal temperature gradient without overheating the tropics, using geologically realistic levels of atmospheric CO_2 and vegetative cover.

3.2 Methodology

The first step in this analysis was to compile a dataset of paleo-temperature estimates derived from fossils and isotopic measurements for seven Cretaceous time intervals: 1) Maastrichtian (65.5 – 70.6 Ma), 2) Campanian (70.6 – 83.5 Ma), 3) Coniacian – Santonian (83.5 – 88.6 Ma), 4) Cenomanian - Turonian (88.6 – 99.6 Ma), 5) Albian (88.6 - 112 Ma), 6) Aptian (112 - 125 Ma) and 7) Pre-Aptian (125 – 145.5 Ma). A sample dataset is given in Table 1 and the complete dataset is listed in Appendix E.

For each data point the following information was recorded: 1) Age/Stage (Name), 2) Ma (Numerical Age), 3) PLatitude (Paleo-Latitude), 4) Temperature (in °C), 5) pRef (Primary Reference), 6) Data Type and 7) Comment. The dataset was created from literature studies and is not meant to be a complete record of all studies that have been done for the Cretaceous. This database has around 1600 records from about 200 different sources. Majority of the data comes from 22 papers published from the 1950s – 2010 (Table 2 lists the key 22 publications). Additional literature study would certainly enrich this database and provide more complete information in both time and space.

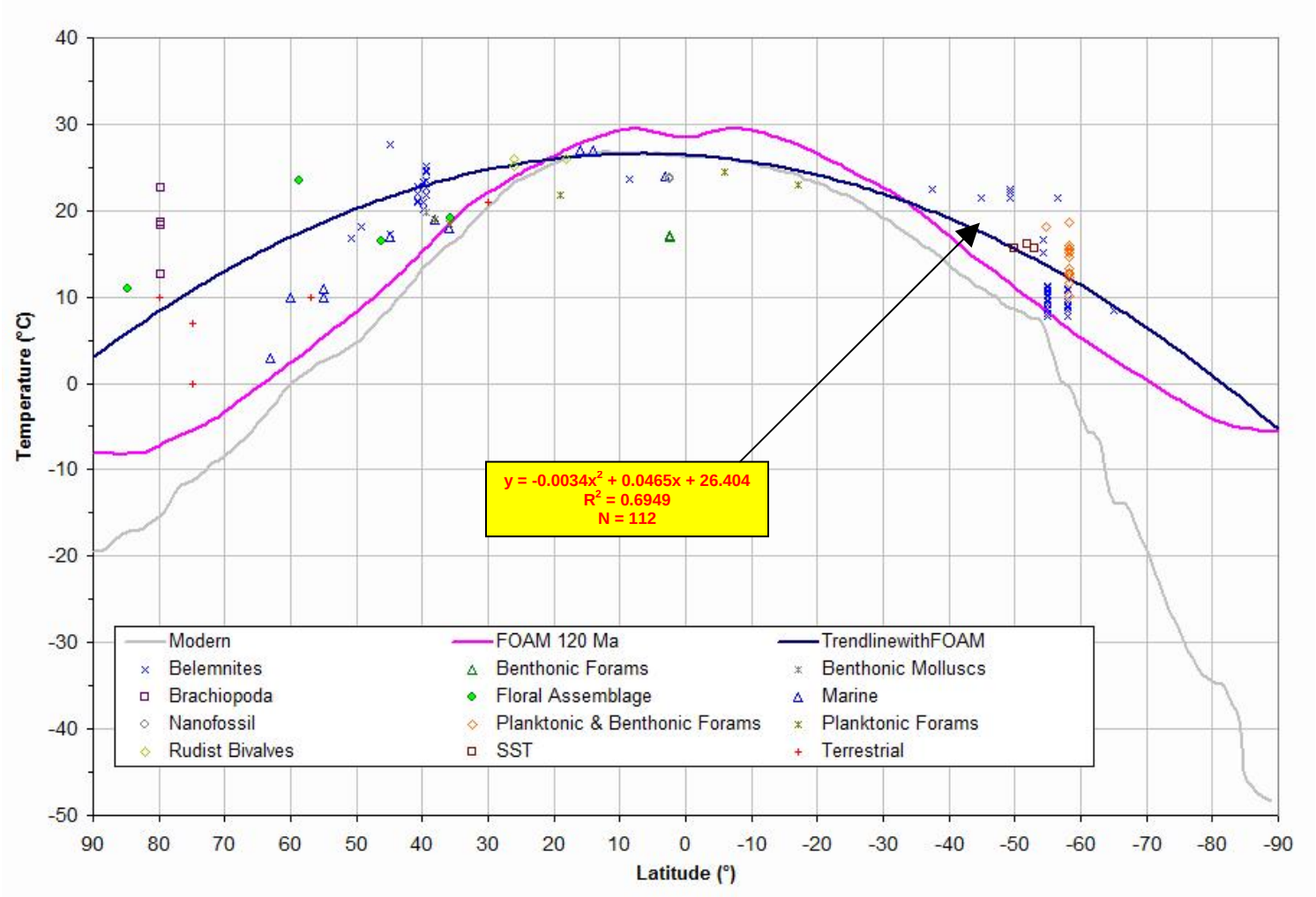

Figure 3.6 Pole-to-Equator Temperature Gradient for the Albian (88.6 - 112 Ma)

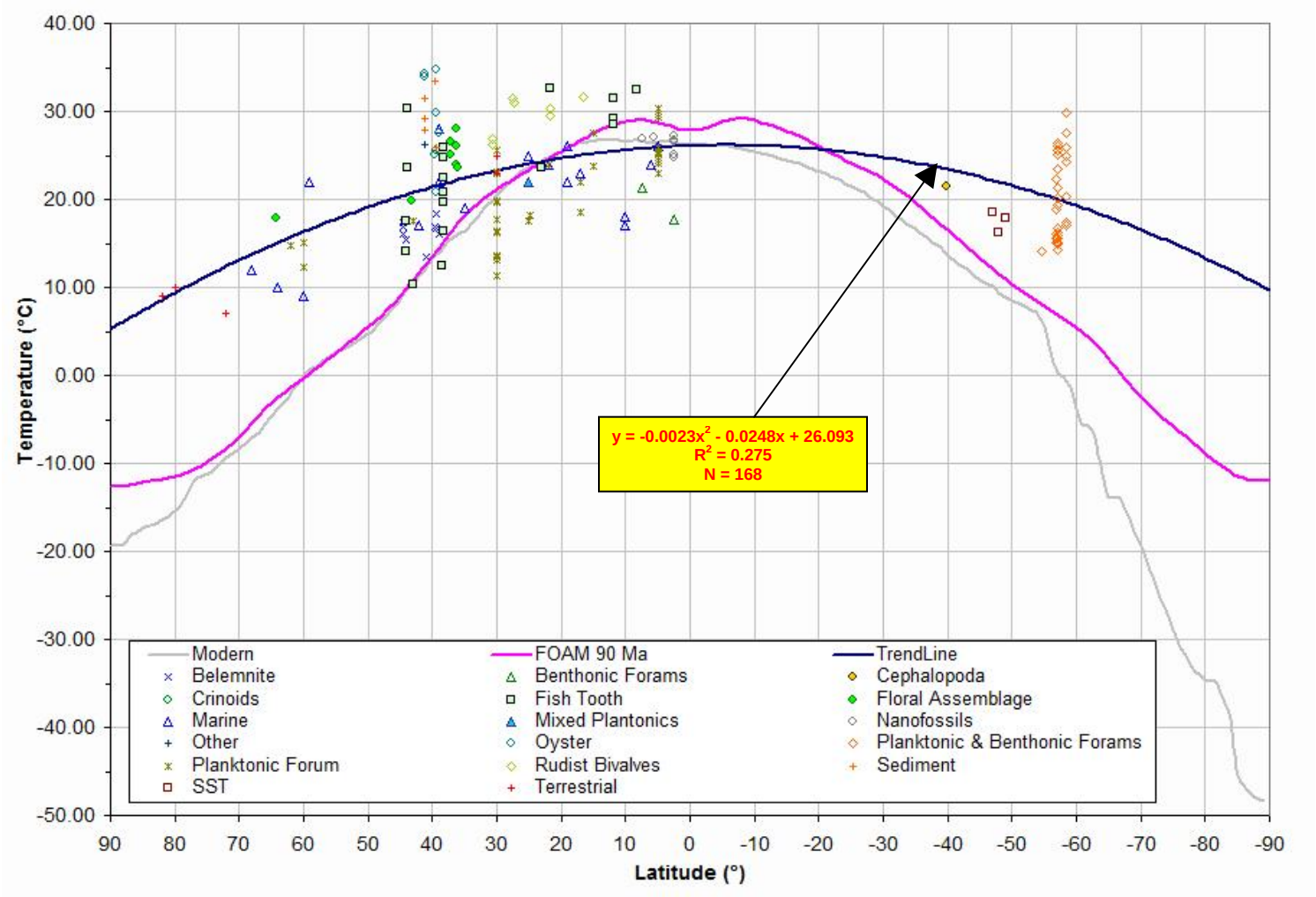

Figure 3.7 Pole-to-Equator Temperature Gradient for the Cenomanian - Turonian (88.6 – 99.6 Ma)

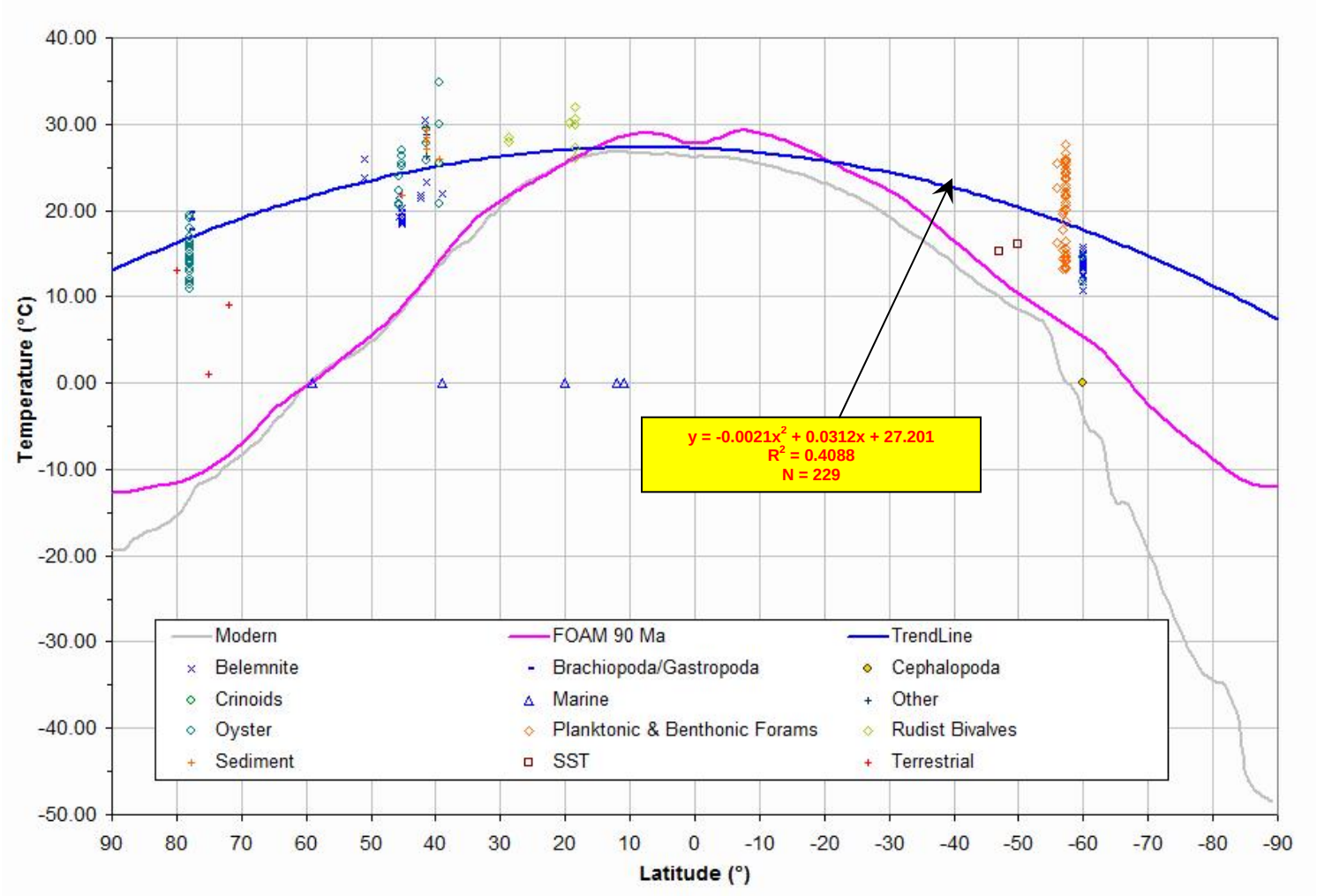

Figure 3.8 Pole-to-Equator Temperature Gradient for the Coniacian – Santonian (83.5 – 88.6 Ma)

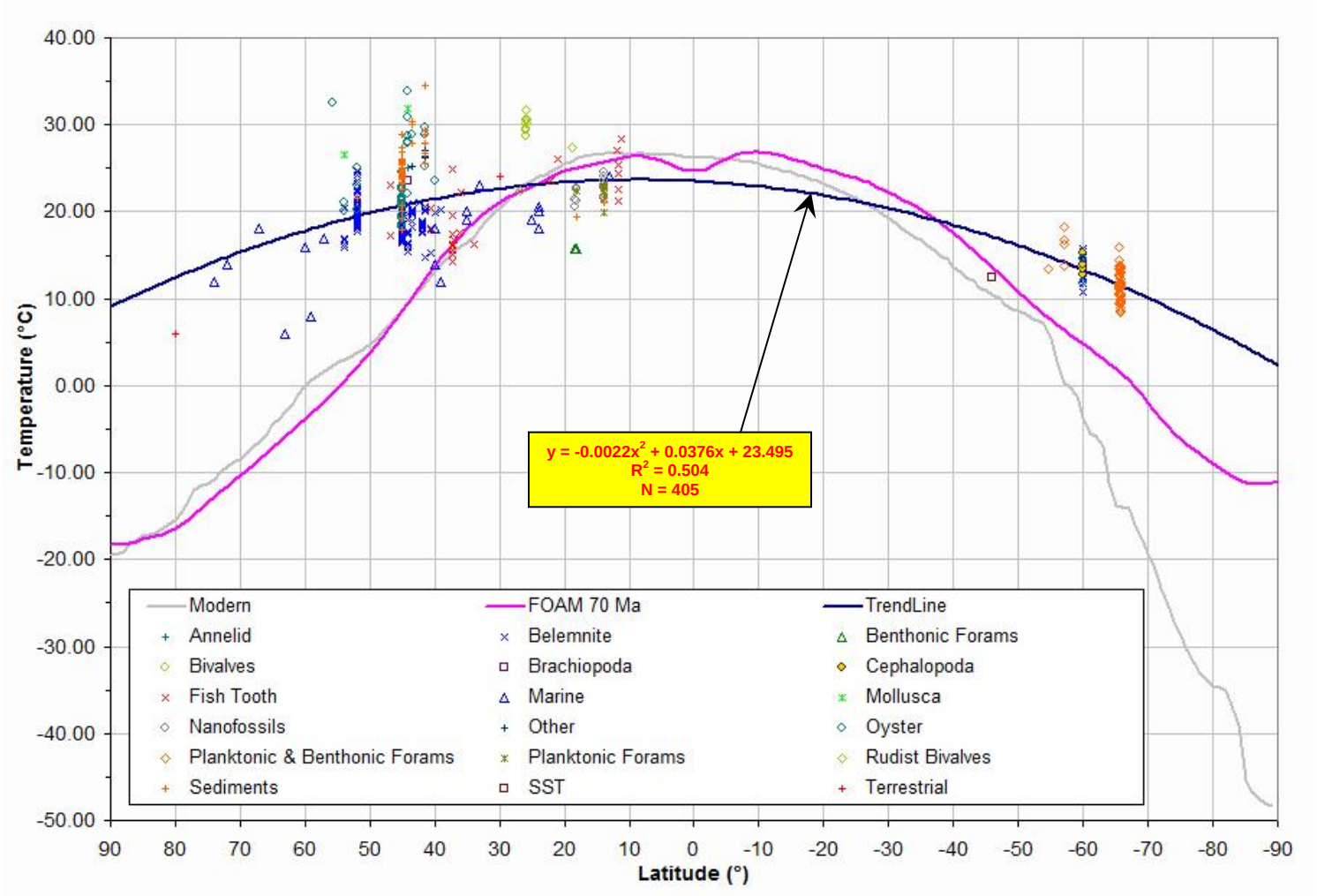

Figure 3.9 Pole-to-Equator Temperature Gradient for the Campanian (70.6 – 83.5 Ma)

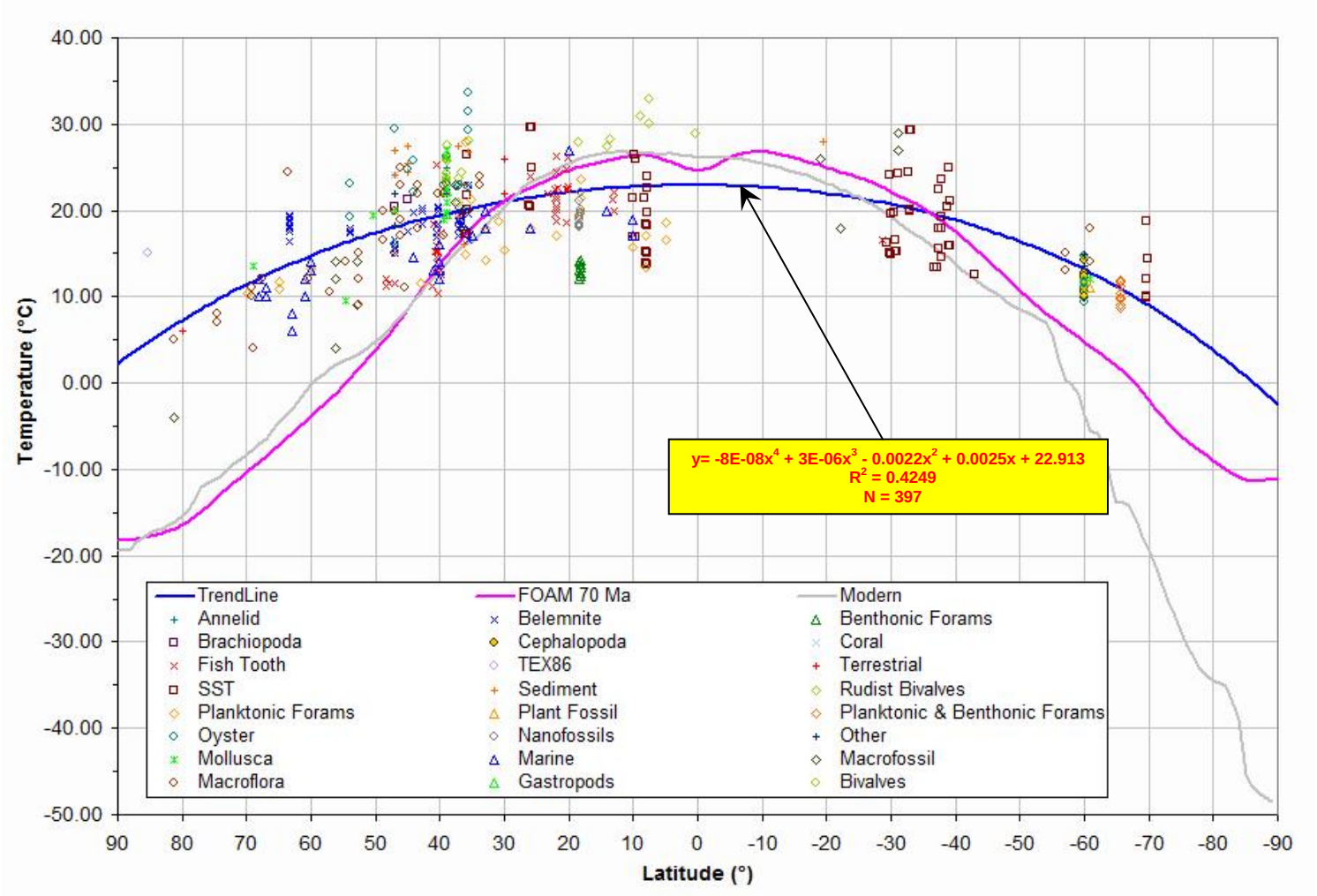

Figure 3.10 Pole-to-Equator Temperature Gradient for the Maastrichtian (65.5 – 70.6 Ma)

Most of these temperature records give the location of the sample and the estimated paleo-temperature at the sample locality. The modern coordinates of the sample localities were reconstructed in Point Tracker Program provided by the PALEOMAP Project (C. R. Scotese). The program calculates the paleo-latitudes of sample localities every 10 million years back to 100Ma and every 20 years before that. For the Cretaceous, the rotated paleo-latitudes used here are 70 Ma, 80 Ma, 90 Ma, 100 Ma, 120Ma and 140 Ma.

The compiled dataset for each of these time periods were widely scattered on temperature-latitude plots and included various data types (e.g., belemnites, foraminifera, mollusk, crinoids, fish tooth, floral assemblages, and sea surface temperatures). The number of data points collected for the seven time intervals also varied (Figure 3.2). Out of the total number of data points collected in the database (1591), we see a great number of data points for the Maastrichtian (n = 397) and the Campanian (n = 405). The number of data points for the Coniacian-Santonian (n = 229) and the pre-Aptian (n = 231) are high while number of data points for the Cenomanian-Turonian (n = 168) and the Albian (n = 112) are moderate. The Aptian has fewest data points (n = 49) in the database. It is also important to note that some of these data points are collected at the same paleo-locality, and overall they are not distributed evenly between all latitudinal belts.

In the second stage of the analysis, the dataset was arranged by time and plotted as pole-to-equator temperature gradient plots as shown in Figure 3.3 – 3.10. In each of these plots, paleolatitude is plotted along X-axis and the paleotemperature is plotted along Y-axis. The dataset also shows the type of temperature proxy data used in these plots (see legends). In each plot the grey colored line represents modern pole-to-equator temperature gradient. This plot was constructed using Legates and Willmott (1990) temperature and precipitation data set (see Chapter 1). Figure 3.3 is an example for the Cenomanian-Turonian.

The final step in this analysis was to draw a best-fit curve for each of the seven time intervals based on the observed data points. In most cases, these best-fit curves give more equable pole-to-equator temperature gradient compared to FOAM generated pole-to-equator

temperature gradient especially poleward of 35° latitudes. The temperature estimates generated by the FOAM climate simulation poleward of 35° latitude are much too cool compared with temperature estimates from latitude data mostly in agreement with the fossils, geochemical as well as geological information. On the other hand, temperature estimates within 0°~20° latitudes are mostly in agreement with the climate proxy data. Hence, for some time periods (for example, Maastrichtian, Albian and Aptian), which lack data points in the equatorial region, we have also included the FOAM estimated temperatures between 20°N and 20°S for comparison. Based on the distribution of the observed paleolatitude vs. paleotemperature points in each dataset, a best-fit curve (trend line) was calculated for each time interval (blue curve). This best-fit curve represents our best estimate of the pole-to-equator temperature gradient for each time interval. For each best-fit curve we have calculated the root mean square (RMS) values and the polynomial equation that describes the shape of the curve. For the Cenomanian-Turonian time period, for example, the best-fit curve (Figure 3.7) was described by the equation "$\mathbf{y = -0.0023x^2 - 0.0248x + 26.093}$", with an RMS = 0.275. The low RMS values for these curves are due to the fact that there are often multiple temperature estimates for a single latitudinal location. To compare the difference between this revised pole-to-equator temperature gradient curve and the FOAM generated pole-to-equator temperature gradient curve, we have also plotted the pole-to-equator temperature gradient determined by FOAM in pink. This revised pole-to-equator temperature gradient clearly helps in visualizing the difference between the climate models (FOAM) predicted pole-to-equator temperature gradient and that is suggested by geologic information.

3.3 Discussion

3.3.1 Pre-Aptian (125-145 Ma)

During Pre-Aptian, as a result of the breakup of Pangea, faunal provincialism increased. During the Berriasian, East Gondwana (India, Australia and Antarctica) separated from West Gondwana (Africa and South America) and India had begun to break away from East Gondwana. The Tethys was wide and the Pacific Plate was growing larger, but still was quite

small, and the entire western margin of North and South America was fringed with volcanic island arcs (Zharkov et al. 1998).

The cooling trend of the Late Jurassic continued at least into the middle of the Berriasian, and there were seasonal ice caps at the poles. The Valanginian world was quite seasonal and climate was regional with distinct climate zones reflected in distinct "boreal" faunas in both the Northern Tethys (future North Atlantic) and Northwest Pacific provinces. During the Valanginian, there were two episodes of sea level rise at the very base of the Valanginian, and during the later Valanginian.

For Pre-Aptian stage during the Cretaceous, 231 data points were collected from literature studies. These temperatures are obtained from isotopic temperatures, from belemnites, nanofossils, some marine sediment, and sea surface temperatures. A full table with the details of the Pre-Aptian dataset is given in Appendix E. Though are some gaps in the collected data points along the equatorial region and southern hemisphere, the best-fit trend line remains same with or without the inclusion of 41 FOAM generated temperature estimates for 20°N to 20°S. Hence, we have not included the 41 FOAM data points while plotting the Pre-Aptian pole-to-equator temperature gradient (Figure 3.4). This pole-to-equator temperature gradient is defined by the equation:

$$\mathbf{y = 0 - 0.0037x^2 + 0.0161x + 25.876}$$

It is a 2nd degree polynomial with a root mean square value of 0.2464. The results of the Pre-Aptian can be summarized as follows. At polar latitudes (60° - 90°) the mean annual temperature was 0°C - 7°C. The minimum mean annual temperature is estimated to be -5.54°C. At high temperate latitudes (40° – 60°) the mean annual temperature was 12°C - 17°C. At subtropical latitudes (20° - 40°) the mean annual temperature ranges from 20°C - 23°C and at the Equatorial region (0° - 20°) the mean annual temperature was above 25°C.

For the Pre-Aptian, pole-to-equator temperature gradient is compared to the latitudinal temperature estimates predicted by 140 Ma FOAM simulation. Table 3.3 records the difference in latitudinal average temperatures between these two at major latitudes. Towards the poles the

mean difference in latitudinal temperature is 15° -18°C while near mid and low latitudes, the differences are around 8° - 15°C and 0° - 4°C respectively. Compared to the FOAM generated pole-to-equator temperature gradient (values in Table 3.3 and pink colored line in Figure 3.4) this revised pole-to-equator temperature gradient is much more equable. Thus, the overall pole-to-equator temperature gradient for Pre-Aptian, was also much shallower than that of the present.

3.3.2 Aptian (112-125 Ma)

As the breaking up of the Pangea was continuing and Atlantic was about to open up, the Aptian climate was gradually warming up. The beginning of greenhouse climate conditions in the mid-Cretaceous was associated with widespread deposition of organic-carbon C_{org}-rich sediments, informally known as black shales, in the oceans. C_{org}-rich sedimentary rocks are well documented as evidence for OAE1a during the Early Aptian (120 Ma) by Arthur et al. (1990). Large igneous province (LIP) and volcanism are also reported during this time, helping global warming. Eventually methane released from oceanic sediments, rapidly sequestered by terrestrial and marine components in the global carbon cycle, and this effect strongly increased the potential for ancient methane gas-hydrate dissociation events to act as major amplifiers in global warming (Beerling et al. 2002).

The database for the Aptian had least number of data points (n = 49). These data represents temperature records based on mollusk, nanofossils, belemnite, planktonic and benthonic forams, marine sediments and sea surface temperatures. A full table with the details of the Aptian dataset is given in Appendix E. Having least data points, we included 41 FOAM generated temperature estimates for 20°N to 20°S in this dataset. The pole-to-equator temperature gradient for the Aptian stage (Figure 3.5) is drawn based on these observed temperature records as well as the 41 FOAM generated low latitude temperatures and is defined by the equation:

$$\mathbf{y= -0.0032x^2 + 0.1054x + 26.541}$$

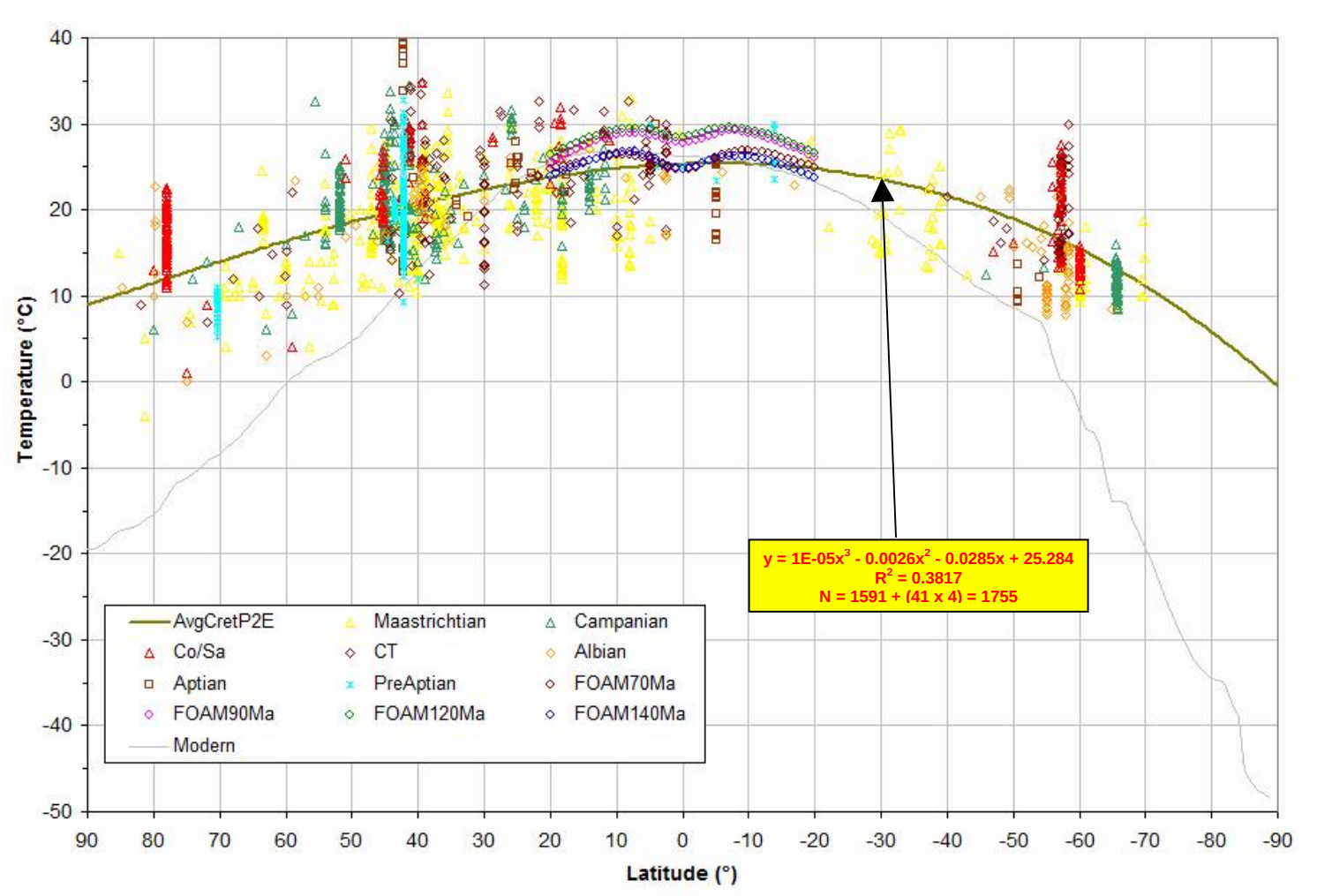

Figure 3.11 Average Pole-to-Equator Temperature Gradient for the Cretaceous (65.5 – 145.5 Ma)

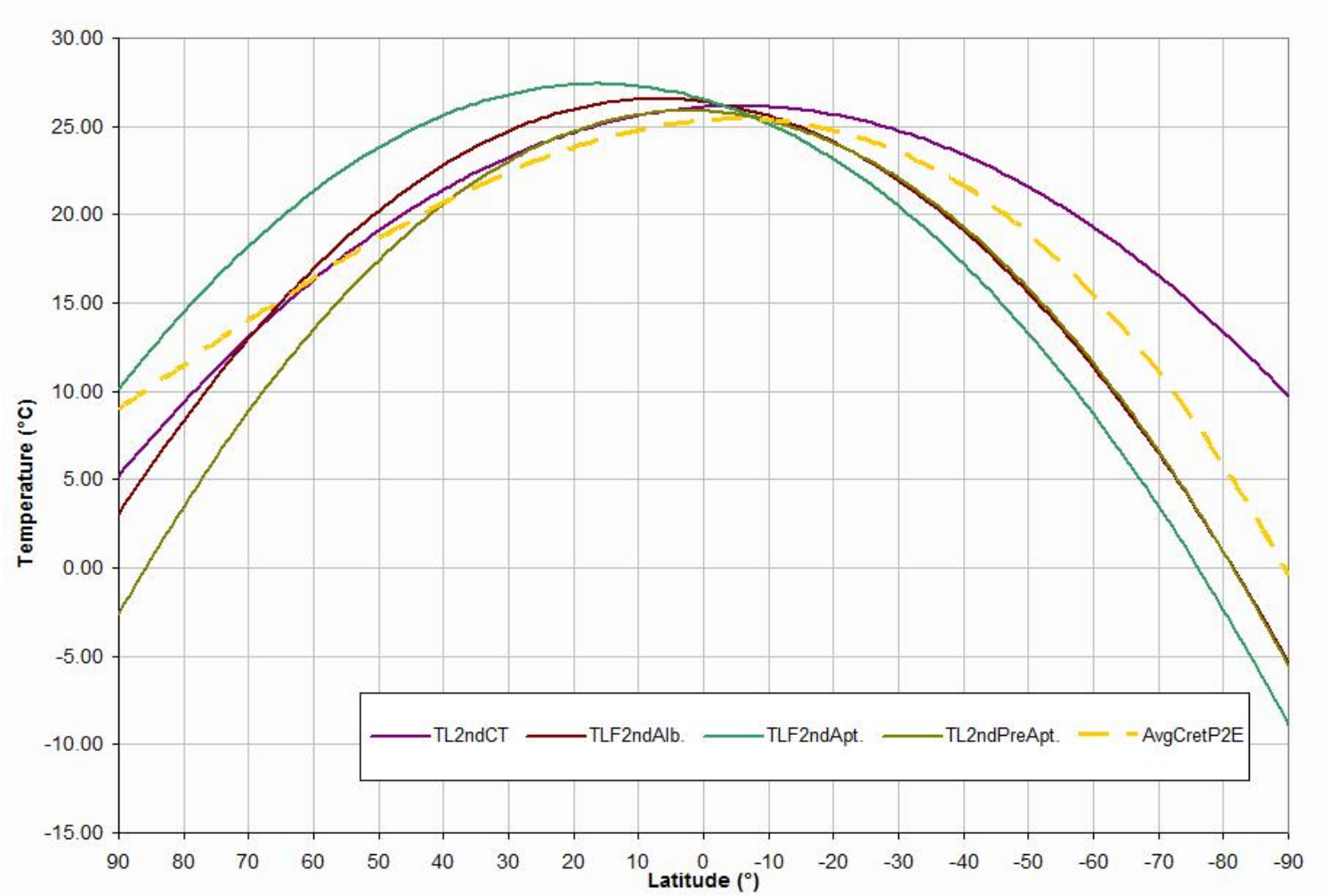

Figure 3.12 Early Cretaceous Pole-to-Equator Temperature Gradients (TL = Trend Line, CT = Cenomanian-Turonian, Alb. = Albian, Apt. = Aptian, PreApt. = Pre- Aptian, AvgCretP2E = Average Cretaceous Pole-to-Equator Temperature Gradient; the no represents the order of the polynomial curve)

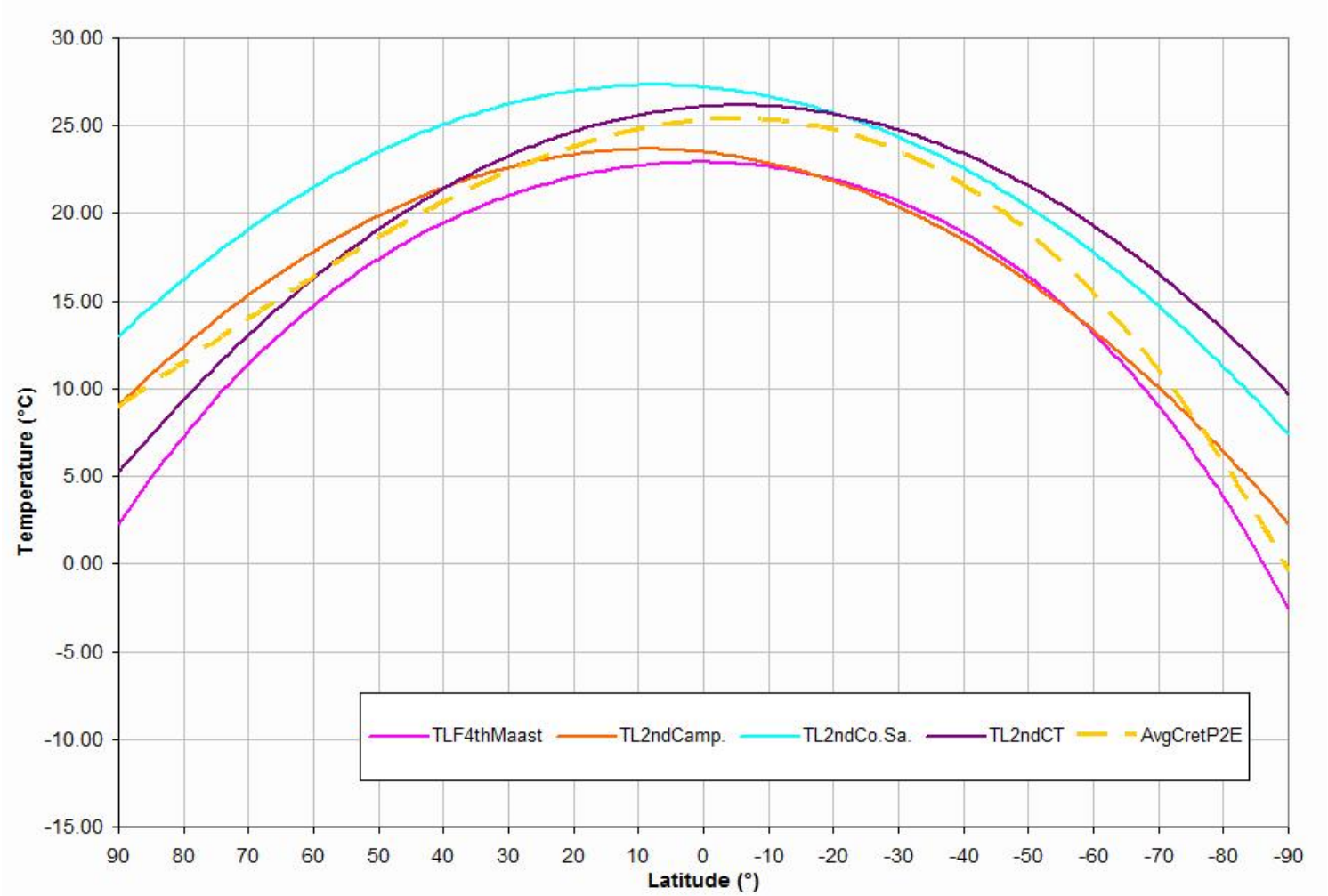

Figure 3.13 Late Cretaceous Pole-to-Equator Temperature Gradients (TL = Trend Line, Maast = Masstrichtian, Camp. = Campanian, Co.Sa. = Coniacian-Santonian, CT = Cenomanian-Turonian, AvgCretP2E = Average Cretaceous Pole-to-Equator Temperature Gradient; the no represents the order of the polynomial curve)

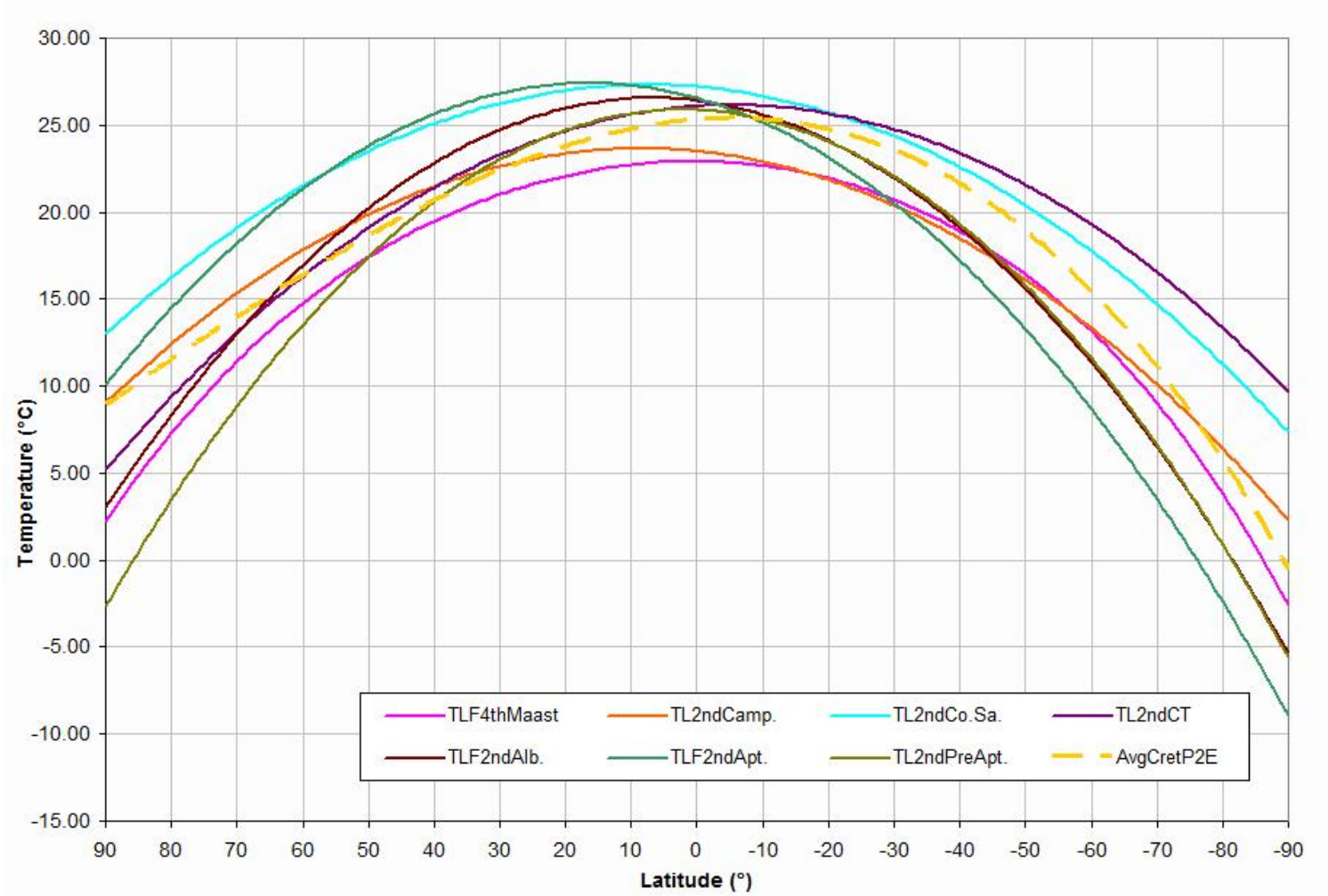

Figure 3.14 All Pole-to-Equator Temperature Gradients during the Cretaceous (TL = Trend Line, Maast = Masstrichtian, Camp. = Campanian, Co.Sa. = Coniacian-Santonian, CT = Cenomanian-Turonian, Alb. = Albian, Apt. = Aptian, PreApt. = Pre- Aptian, AvgCretP2E = Average Cretaceous Pole-to-Equator Temperature Gradient; the no represents the order of the polynomial curve)

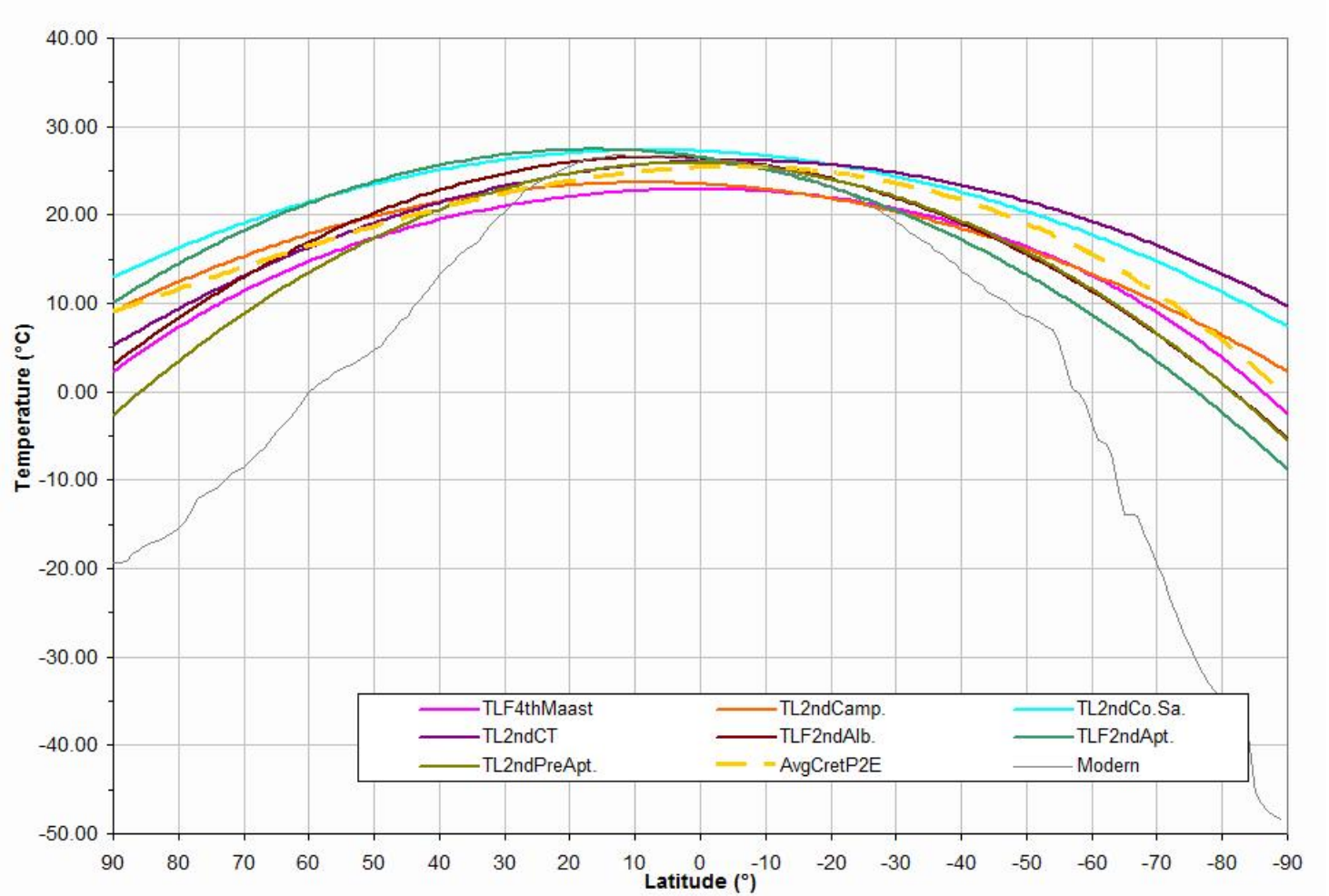

Figure 3.15 All Pole-to-Equator Temperature Gradients during the Cretaceous with Modern Pole-to-Equator Temperature Gradient (TL = Trend Line, Maast = Masstrichtian, Camp. = Campanian, Co.Sa. = Coniacian-Santonian, CT = Cenomanian-Turonian, Alb. = Albian, Apt. = Aptian, PreApt. = Pre- Aptian, AvgCretP2E = Average Cretaceous Pole-to-Equator Temperature Gradient; the no represents the order of the polynomial curve)

It is a 2nd degree polynomial with a root mean square value of 0.269. The results of the Aptian can be summarized as follows. At polar latitudes (60° - 90°) the mean annual temperature was 5°C - 9°C. The minimum mean annual temperature is estimated to be -8.87°C. At high temperate latitudes (40° – 60°) the mean annual temperature was 15°C - 20°C. At subtropical latitudes (20° - 40°) the mean annual temperature ranges from 20°C - 24°C and in the Equatorial regions (0° - 20°) the mean annual temperature was above 25°C.

The Aptian pole-to-equator temperature gradient is compared to the latitudinal temperature estimates predicted by 120 Ma FOAM simulation. Table 3.3 records the difference in latitudinal temperatures between these two. A major limitation for the comparison is the lack of data points. Despite the lack of continued data points it is interesting to note that the predicted pole-to-equator temperature gradient closely match the results from the FOAM simulation.

3.3.3 Albian (99.6-112 Ma)

During the Albian the South Atlantic was not yet connected to Central Atlantic (Nurnberg and Muller 1991). A shallow marine seaway opened in the northern South Atlantic during the Late Albian connecting western Tethys and the South Atlantic (Kennedy and Cooper, 1975; Widemann and Neugebaur, 1978; and Foerster 1978). During this intensive crustal production period, there was also evidence of intraplate volcanism in Pacific regions, Crimea and Caucasus (Menard, 1964; Larson and Pitman, 1972; Hinz, 1981; Schlanger et al., 1981; Vakhrameev, 1987; Larson, 1991; and Larson and Kincaid, 1996). Albian was a time of major change in the configuration of the Atlantic and a time of major magmatic activity, which can be expected to have had an influence on global climate by increasing atmospheric CO_2 (Fenner 2001). For the Middle and Late Albian though, there is no indication of permanent polar ice caps or even persistent shore ice in the northern polar regions though widespread humid conditions at mid-latitudes are established by the coal and bauxite occurrences in this belt (Fenner 2001).

For Albian stage 112 data points were collected from literature studies. The dataset includes various types of data, most commonly isotopic temperatures from belemnite, planktonic and benthonic forams, mollusks, brachiopods, floral assemblage, nanofossils, marine and terrestrial data, and some sea surface temperatures. A full table with the details of the Albian dataset is given in Appendix E. There are some gaps in the collected data points along the equatorial region and hence we included 41 FOAM generated temperature estimates for 20°N to 20°S. The pole-to-equator temperature gradient for the Albian stage (Figure 3.6) is drawn based on these observed temperature records as well as the 41 FOAM generated low latitude temperatures and is defined by the equation:

$$\mathbf{y = -0.0034x^2 + 0.0465x + 26.404}$$

It is a 2nd degree polynomial with a root mean square value of 0.6949. The results of the Albian can be summarized as follows. At polar latitudes (60° - 90°) the mean annual temperature was 0°C - 7°C. The minimum mean annual temperature is estimated to be -5.32°C. At high temperate latitudes (40° – 60°) the mean annual temperature was 15°C - 19°C. At subtropical latitudes (20° - 40°) the mean annual temperature ranges from 20°C - 24°C and in the Equatorial regions (0° - 20°) the mean annual temperature was above 25°C.

There is no FOAM simulation for the Albian. Hence, the Albian pole-to-equator temperature gradient is compared to the latitudinal temperature estimates predicted by 120 Ma FOAM simulation. Table 3.3 records the difference in latitudinal average temperatures between these two models. Towards the poles the mean difference in latitudinal temperature is 8°C - 10°C while near mid and low latitudes the differences are around 4°C – 6°C and 0°C - 3°C respectively. Compared to the FOAM generated pole-to-equator temperature gradient (values in Table 3.3 and pink colored line in Figure 3.6) this pole-to-equator temperature gradient is much more equable. Thus the overall pole-to-equator temperature gradient for Albian was much shallower than that of the present.

3.3.4 Cenomanian-Turonian (88.6 – 99.6 Ma)

Most authors consider Cenomanian-Turonian to be the warmest time during the Cretaceous (Huber et al. 2002, Bice and Norris 2002, Clarke and Jenkyns 1999). By mid-Cretaceous times, the Tethys Ocean has begun to close. Evidence points towards an unusually high level of volcanic activity, especially at mid-oceanic ridges. Magma erupted at oceanic ridges and formed new oceanic crust, thereby forcing the continental landmasses away from each other. Rates of sea-floor spreading were about three times as great as they are now. During the Cenomanian-Turonian time sea levels rose dramatically, possibly up to 200m higher than present levels, flooding up to 40% of the continents and resulting in the widespread deposition of chalk-dominated facies. The Western Interior Seaway of the USA was at this time at its maximum. Much of central and western Europe was under water. During Cenomanian–Turonian interval, the atmosphere had high levels of atmospheric CO_2 concentrations, up to four times the present (Berner and Kothavala 2001) and there were important changes in oceanic circulation patterns (Barron et al. 1995).

For Cenomanian-Turonian stage 168 data points were collected from literature studies. These includes several data types, for example, isotopic temperatures from Planktonic & Benthonic Forams and Plantonics, Fish Tooth, Belemnite, Mollusks, Nanofossils, some terrestrial as well as marine sediments and sea surface temperatures. A full table with the details of the Cenomanian-Turonian dataset is given in Appendix E. Though are some gaps in the collected data points along the equatorial region and southern hemisphere, the best-fit trend line remains same with or without the inclusion of 41 FOAM generated temperature estimates for 20°N to 20°S. Hence, we have not included the 41 FOAM data points while plotting the Cenomanian-Turonian pole-to-equator temperature gradient (Figure 3.7). This pole-to-equator temperature gradient is defined by the equation:

$$\mathbf{y = -0.0023x^2 - 0.0248x + 26.093}$$

It is 2nd degree polynomial with a root mean square value of 0.275. The results of the Cenomanian-Turonian can be summarized as follows. At polar latitudes (60° - 90°) the mean annual temperature was 8°C - 12°C. The minimum mean annual temperature is estimated to be 5.23°C. At high temperate latitudes (40° – 60°) the mean annual temperature was 18°C - 20°C. At subtropical latitudes (20° - 40°) the mean annual temperature ranges from 20°C - 24°C and in the Equatorial regions (0° - 20°) the mean annual temperature was above 25°C.

The Cenomanian-Turonian pole-to-equator temperature gradient is compared to the latitudinal temperature estimates predicted by 90 Ma FOAM simulation. Table 3.3 records the difference in latitudinal temperatures between these two. It is clear that the climate model predicted temperatures are much cooler towards the poles (18 -20°C) and gradually the difference minimizes as we approach the equator (1-2 °C). This pole-to-equator temperature gradient has a shallow slope and higher temperatures as compared to modern pole-to-equator temperature gradient. The observed temperatures and the constructed pole-to-equator gradient for the Cenomanian-Turonian demonstrate extreme hot climatic conditions that are clearly valid with the general consensus about the mid-Cretaceous climatic condition.

3.3.5 Coniacian-Santonian (83.5 – 88.6 Ma)

Some consider that the Coniacian-Santonian stage was the maximum period of warming during the Late Cretaceous (Savin 1977). A colder climatic maximum occurred later in the Coniacian-Santonian (Lower Senonian) (Bowen 1961). Middle Coniacian is also characterized by an anoxic event (OAE-3) in the Atlantic Ocean, causing large scale deposition of black shales in the Atlantic domain. The anoxic event lasted till the Middle Santonian (from 87.3 to 84.6 Ma). This is the longest anoxic event during the Cretaceous (Meyers et al. 2006).

For Coniacian-Santonian stage we have 229 data points collected from literature studies. These include several data types, for example, isotopic temperatures from planktonic and benthonic forams, mollusks, belemnites, brachiopods, some terrestrial as well as marine sediments and sea surface temperatures. A full table with the details of the Coniacian-

Santonian dataset is given in Appendix E. Though are a lot of gaps in the collected data points along various latitudinal regions, the best-fit trend line remains the same with or without the inclusion of 41 FOAM generated temperature estimates for 20°N to 20°S. Hence, we have not included the 41 FOAM data points while plotting the Campanian pole-to-equator temperature gradient (Figure 3.8). This pole-to-equator temperature gradient is defined by the equation:

$$y = -0.0021x^2 + 0.0312x + 27.201$$

It is a 2nd degree polynomial with a root mean square value of 0.4088. The results of the Coniacian-Santonian can be summarized as follows. At polar latitudes (60° - 90°) the mean annual temperature was 10°C - 16°C. The minimum mean annual temperature is estimated to be 7.38°C. At high temperate latitudes (40° – 60°) the mean annual temperature was 18°C - 22°C. At subtropical latitudes (20° - 40°) the mean annual temperature ranges from 22°C - 26°C and in the Equatorial regions (0° - 20°) the mean annual temperature was above 26°C. The average global temperature for Coniacian-Santonian time as estimated from this trend is a few degree centigrade higher than the Campanian stage. This pole-to-equator temperature gradient matches well with the Late Santonian Cretaceous maxima event suggested by Savin 1977 and Bowen 1961. The pole-to-equator temperature gradient during the Coniacian-Santonian was also shallower and overall higher in temperature as compared to modern pole-to-equator temperature gradient.

There is no FOAM simulation for the Coniacian-Santonian stage. Hence, the Coniacian-Santonian pole-to-equator temperature gradient has been compared to the latitudinal temperature estimates predicted by FOAM simulation for the 90 Ma. Table 3.3 shows the difference in latitudinal average temperatures between these two estimates. Towards the poles the mean difference in latitudinal temperature is 19 -23°C, while near mid and low latitudes, the difference is around 1-4°C maximum. Compared to the FOAM generated pole-to-equator temperature gradient (values in Table 3.3 and pink colored line in Figure 3.8) this revised pole-

to-equator temperature gradient is much more equable. Thus the overall pole-to-equator temperature gradient for Coniacian-Santonian was much shallower than that of the present.

3.3.6 Campanian (70.6 – 83.5 Ma)

After the Cenomanian-Turonian extreme hot house world, a gradual fall of temperature took place during the Campanian and was succeeded by cooler stable conditions in the Maastrichtian (Bowen 1961a). Ambient climatic conditions (generally warm climates) along with large continental areas covered by shallow seas during the Campanian probably favored the radiation of dinosaur species (Weishampel et al. 2004). During the Campanian stage, evidence suggests mean annual temperatures were 7-14°C warmer than today (DeConto, 1996). There is no evidence of significant ice at high latitudes (Frakes et al., 1992) and meridional thermal gradients were very low in the oceans (Barrera et al., 1987, Huber et al., 1995) and on land (Parrish and Spicer, 1988).

For Campanian stage 405 data points were collected from literature studies. These include several data types, for example, isotopic temperatures from belemnites, planktonic and benthonic forams, mollusks, fish tooth, nanofossils, brachiopods, some terrestrial as well as marine sediments and sea surface temperatures. A table with the details of the Campanian dataset is given in Appendix E. Though are some gaps in the collected data points along the equatorial region and southern hemisphere, the best-fit trend line remains almost the same with or without the inclusion of 41 FOAM generated temperature estimates for 20°N to 20°S. Hence, we have not included the 41 FOAM data points while plotting the Campanian pole-to-equator temperature gradient (Figure 3.9). This pole-to-equator temperature gradient is defined by the equation:

$$\mathbf{y = 0.0022x^2 + 0.0376x + 23.495}$$

It is a 2nd degree polynomial with a root mean square value of 0.504. The results of the Campanian can be summarized as follows. At polar latitudes (60° - 90°) the mean annual temperature was 8°C - 12°C. The minimum mean annual temperature is estimated to be

2.29°C. At high temperate latitudes (40° – 60°) the mean annual temperature was 15°C - 18°C. At subtropical latitudes (20° - 40°) the mean annual temperature ranges from 20°C - 22°C and in the Equatorial regions (0° - 20°) the mean annual temperature was near 23°C. These observations are in agreement with the Campanian ocean simulation prediction by Levitus (1982). He predicted a global mean annual sea surface temperature (SST) of 25.8ºC which is about 8º C warmer than present day. Needless to mention, like the Maastrichtian pole-to-equator temperature gradient, Campanian pole-to-equator temperature gradient was also shallower and warmer than the modern pole-to-equator temperature gradient.

There is no FOAM simulation for the Campanian stage. Hence, the Campanian pole-to-equator temperature gradient has been compared to the latitudinal temperature estimates predicted by FOAM simulation for the 70 Ma. Table 3.3 shows the difference in latitudinal average temperatures between these two estimates. Towards the poles the mean difference in latitudinal temperature is 18 -21°C, while near mid and low latitudes the difference is around 1-3°C maximum. Compared to the FOAM generated pole-to-equator temperature gradient (values in Table 3.3 and pink colored line in Figure 3.9) this pole-to-equator temperature gradient is much more equable. Thus the overall pole-to-equator temperature gradient for Campanian was much shallower than that of the present.

3.3.7 Maastrichtian (65.5 – 70.6 Ma)

The Maastrichtian was the last stage of the Cretaceous epoch and the Mesozoic Era. It spanned from 65.5 Ma to 70.6 Ma. Maastrichtian climate was not as warm or as equable as the average climate of the Cretaceous (Barron and Washington, 1984). Geologic evidence indicates that temperate and polar regions were warm during the Maastrichtian. Precipitation was relatively high (about 700–800 mm) and evenly distributed over the year (Golovneva, 2000). The end of the Maastrichtian is marked by Cretaceous–Tertiary Extinction Event (K-T Mass Extinction) (Macleod et al. 1997). About 17% of all families, 50% of all genera and 75% of all species became extinct (Raup and Sepkoski 1982).

For the Maastrichtian stage 397 data points were collected from literature studies. Though the dataset includes various types of data, most commonly they are sea surface temperatures, isotopic temperature estimates of belemnite, fish tooth, mollusca, brachiopoda, annelid, planktonic & benthonic forams, coral, TEX86, plant fossil, some macrofossil and macroflora, and marine as well as terrestrial plant fossils. A table with the details of the Maastrichtian dataset is given in Appendix E. There are some gaps in the collected data points along the equatorial region and hence we included 41 FOAM generated temperature estimates for 20°N to 20°S. The pole-to-equator temperature gradient for the Maastrichtian stage (Figure 3.10) is drawn based on these observed temperature records as well as the 41 FOAM generated low latitude temperatures and is defined by the equation:

$$y = -8E\text{-}08x^4 + 3E\text{-}06x^3 - 0.0022x^2 + 0.0025x + 22.913$$

It is a 4th degree polynomial with a root mean square value of 0.4249. The results of the Maastrichtian can be summarized as follows. At polar latitudes (60° - 90°) the mean annual temperature was 3°C - 8°C. The minimum mean annual temperature is estimated to be -2.57°C. At high temperate latitudes (40° – 60°) the mean annual temperature was 15°C - 18°C. At subtropical latitudes (20° - 40°) the mean annual temperature ranges from 20°C - 22°C and in the Equatorial regions (0° - 20°) the mean annual temperature was near 23°C.

The Maastrichtian pole-to-equator temperature gradient can be compared to the latitudinal temperature estimates predicted by 70 Ma FOAM simulation. Table 3.3 shows the difference in latitudinal temperatures between FOAM and the best-fit pole-to-equator curve. It is clear that FOAM predicted temperatures were much cooler near the poles (15 -18 °C) and difference between FOAM and the best fit pole-to-equator curve is minimal near the equator (1-2 °C). Compared to the FOAM generated pole-to-equator temperature gradient (values in Table 3.3 and pink colored line in Figure 3.10) this pole-to-equator temperature gradient is much more equable. Thus the overall pole-to-equator temperature gradient for Maastrichtian was much shallower than that of the present.

3.4 Summary and Conclusion

We have also drawn a best-fit line for the entire Cretaceous period using the entire proxy dataset. The entire database of 1591 data points as well as the 41 low latitude data (20°N to 20°S) from each of the four (70 Ma, 90 Ma, 120 Ma and 140 Ma) FOAM simulations are used here. Figure 3.11 shows the distribution of all these data points and the best fit line in green color. This is defined by the equation:

$$y = 1E\text{-}05x^3 - 0.0026x^2 - 0.0285x + 25.284$$

It is a 3rd degree polynomial with a root mean square value of 0.3817. The results of the entire Cretaceous can be summarized as follows. At polar latitudes (60° - 90°) the mean annual temperature was 5°C - 11°C. The minimum mean annual temperature is estimated to be -0.50°C. At high temperate latitudes (40° – 60°) the mean annual temperature was 14°C - 19°C. At subtropical latitudes (20° - 40°) the mean annual temperature ranges from 20°C - 23°C and in the Equatorial regions (0° - 20°) the mean annual temperature was near 25°C. Compared to modern pole-to-equator temperature gradient this average Cretaceous pole-to-equator temperature gradient is much more equable and realistic.

The pole-to-equator temperature gradients constructed for seven time intervals of the Cretaceous are summarized in Figures 3.12 - 15. The Early Cretaceous (Pre-Aptian to Cenomanian-Turonian) is documented by fluctuations in global temperature. It is important to note that all of these pole-to-equator gradients had similar trends that are very different than the modern pole-to-equator temperature gradient. It is also noted from Figure 3.12 that these fluctuations in overall global temperatures were documented differently in the northern and southern hemispheres. In the southern hemisphere, starting from Pre-Aptian, we see an initial cooling during Aptian followed by gradual warming through Albian and Cenomanian-Turonian. In the northern hemisphere, on the other hand, the pole-to-equator latitudinal average temperatures show a warming during Pre-Aptian to Aptian, followed by cooling until the Cenomanian-Turonian. These variations may simply be due to the limitations of the database

used for this study as it has relatively less temperature data points for Albian and Aptian as opposed to other Cretaceous times. The average Cretaceous pole-to-equator temperature gradient lies in the middle of these four Early Cretaceous pole-to-equator temperature gradients.

Figure 3.13 summarizes the Late Cretaceous pole-to-equator temperature gradients. Surprisingly, though an overall cooling trend from Cenomanian-Turonian/Coniacian-Santonian to Maastrichtian is noted, the detailed look unfolds that this cooling trend was not straightforward. In the southern hemisphere, there is a gradual cooling from Cenomanian-Turonian to Maastrichtian, but in the northern hemisphere, Coniacian-Santonian stage had the highest temperatures. Similar to the Early Cretaceous, the average Cretaceous pole-to-equator temperature gradient lies in the middle of these four Late Cretaceous pole-to-equator temperature gradients.

Figure 3.14 plots all of the Cretaceous pole-to-equator temperature gradients, including the average for the Cretaceous. Figure 3.15 plots the same Cretaceous pole-to-equator temperature gradients with modern pole-to-equator temperature gradient. Except the low latitudes of the northern hemisphere, without any question Coniacian-Santonian and Cenomanian-Turonian latitudinal temperature gradients are the highest of all other time intervals compared to both Early and Late Cretaceous. In the northern hemisphere the polar regions were warmest during the Coniacian-Santonian and coolest during the Pre-Aptian. The middle and low latitudes experienced high temperatures during the Aptian (?) and Coniacian-Santonian and cooler climates during Pre-Aptian and Maastrichtian. In the southern hemisphere, the polar region was coldest during Aptian and warmest during Cenomanian-Turonian stage.

On an average during the whole Cretaceous period the polar regions were near ice free (based on average pole-to-equator temperature gradient) and overall climatic conditions were much warmer than present. The low latitudes had average annual temperatures of above 20°C;

whereas the mid latitudes were characterized by 12-20°C. It is also important to note that the climate in the northern hemisphere were relatively warmer than the southern hemisphere.

CHAPTER 4

REINTERPRETATION OF CRETACEOUS SOILS USING REVISED POLE-TO-EQUATOR TEMPERATURE GRADIENTS

In Chapter Three, detailed pole-to-equator temperature gradients for four Cretaceous time intervals were constructed based on a compiled dataset of published paleo-temperature estimates from plant and animal fossils, as well as isotopic proxy records. These estimates of paleo-temperatures were compared to paleoclimate model (FOAM) results for the Cretaceous. The observed pole-to-equator temperature gradients produced by these two techniques were very different. It is also noteworthy that the temperature differences, in each of these estimates of pole-to-equator gradients, were greater in high and mid-latitudes and gradually decreased towards the equator. In general, as evident from the pole-to-equator temperature gradient plots (see Figure 3.3 – 3.9), the climate models (like FOAM) do not adequately simulate warm polar temperatures and fail to predict shallower pole-to-equator temperature gradients that characterize hot house worlds. In this chapter, an attempt is made to fix these temperature dissimilarities. The predictions made in Chapter Two regarding the geographic distribution of ancient soil types, based on “Climate Envelope Technique”, have been adjusted using the revised temperature estimates. The new paleo-soil maps for the Cretaceous are more consistent with the geological evidence.

4.1 Methodology

To rectify the temperatures (TS1) estimated by FOAM for four Cretaceous time intervals (70 Ma, 90 Ma, 120 Ma and 120 Ma), a straightforward approach was taken. The average latitudinal temperature difference between the pole-to-equator temperature gradient estimated by the FOAM paleoclimate simulation and the pole-to-equator temperature gradient estimated by fossils and geologic data was recorded. The FOAM estimated and observed pole-

to-equator latitudinal temperature gradients and the difference between them for Maastrichtian (70 Ma), Cenomanian – Turonian (90 Ma), Aptian (120 Ma) and Pre-Aptian (140 Ma) are shown in Figure 4.1 – 4.4 respectively. FOAM estimated temperatures being normally lower than observed temperatures, for each degree of latitude change, the measured temperature difference is then added to the FOAM estimated temperatures. Thus for each of the four Cretaceous simulations for which a temperature – precipitation (variables TS1 vs. OPREC) plot was prepared in Chapter One, a new set of values are generated with the adjusted temperatures (based on the difference of the FOAM pole-to-equator temperature gradient and observed pole-to-equator temperature gradient) and separately plotted as shown in Figure 4.5 – 4.8.

In Figure 4.5 – 4.8, the dark red outline represents the temperature-precipitation conditions estimated by FOAM and the green colored area represents the adjusted temperature-precipitation conditions. The gray area shows the modern temperature-precipitation (Legates and Willmott 1990) plot as reference. It is also important to note here that except for the Maastrichtian (Figure 4.5), there are some areas in these temperature–precipitation couplets that are beyond the known range of modern temperature-precipitation values. These zones have been marked as 'unknown zones' because we cannot predict what kind of soils formed in this temperature-precipitation regime because these temperatures – precipitation conditions are non-existent in the modern world.

The revised temperature – precipitation values for each of the four time intervals were then used to predict paleo-soil types using the same soil envelope technique described in Chapter Two. Each of the ten soil group "climate envelopes" were intersected with the adjusted temperature-precipitation and the intersected points are plotted and symbolized accordingly on paleo-coastline maps to display the revised geographic distribution of respective ancient soils.

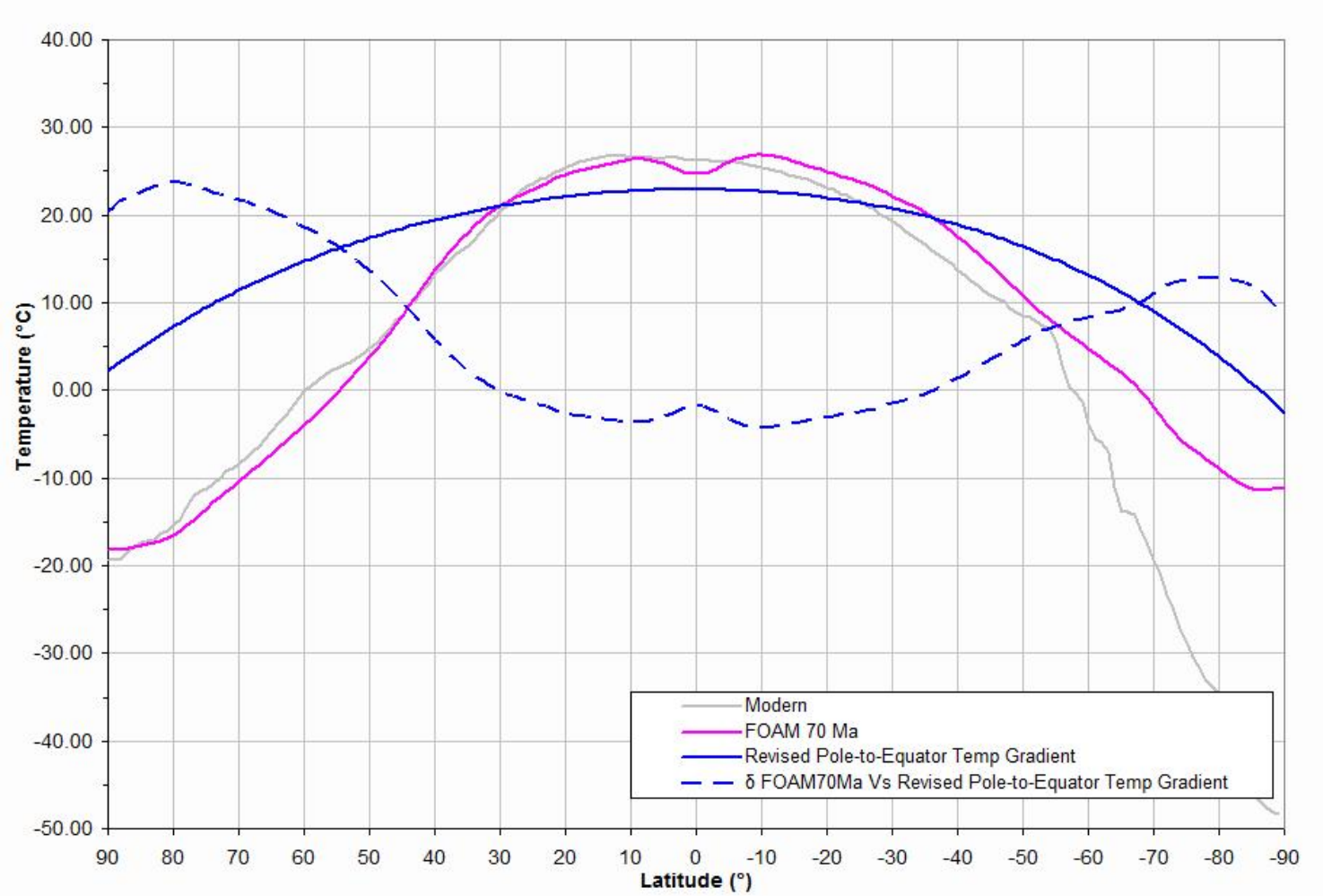

Figure 4.1 Pole-to-Equator temperature gradients for the Maastrichtian (70 Ma) and the difference between the FOAM estimated and observed pole-to-equator temperature gradients.

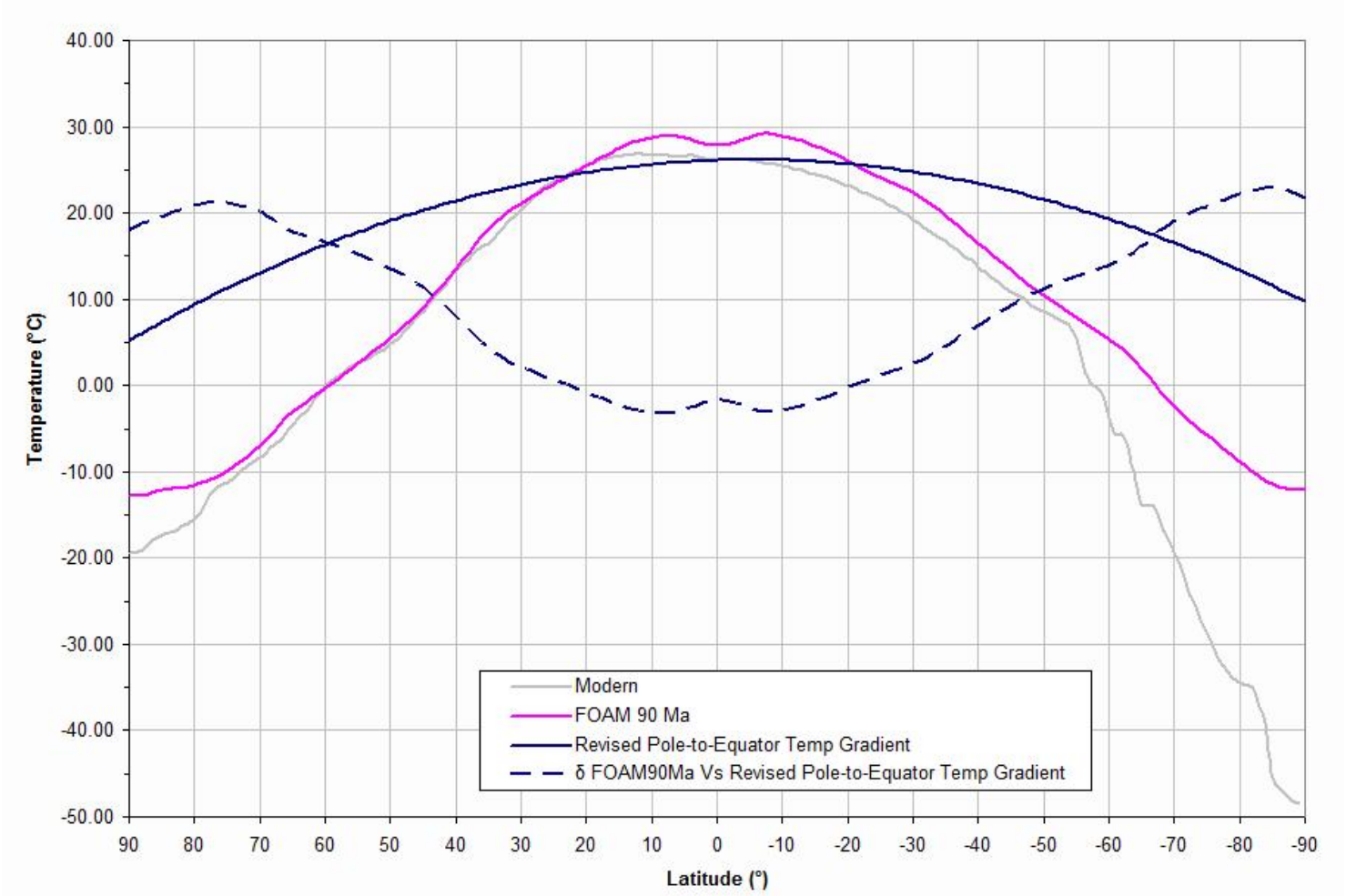

Figure 4.2 Pole-to-Equator temperature gradients for the Cenomanian - Turonian (90 Ma) and the difference between the FOAM estimated and observed pole-to-equator temperature gradients.

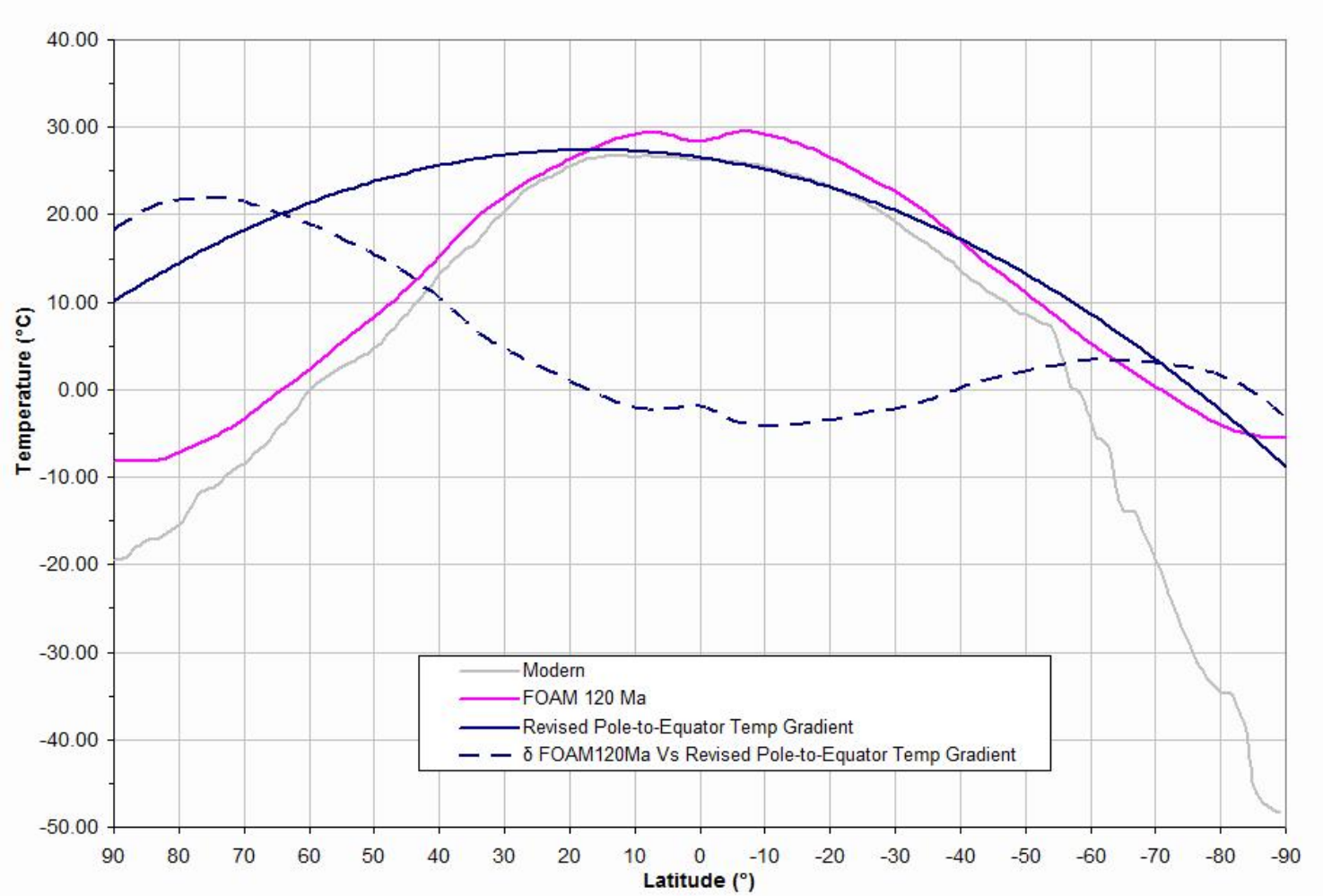

Figure 4.3 Pole-to-Equator temperature gradients for the Aptian (120 Ma) and the difference between the FOAM estimated and observed pole-to-equator temperature gradients.

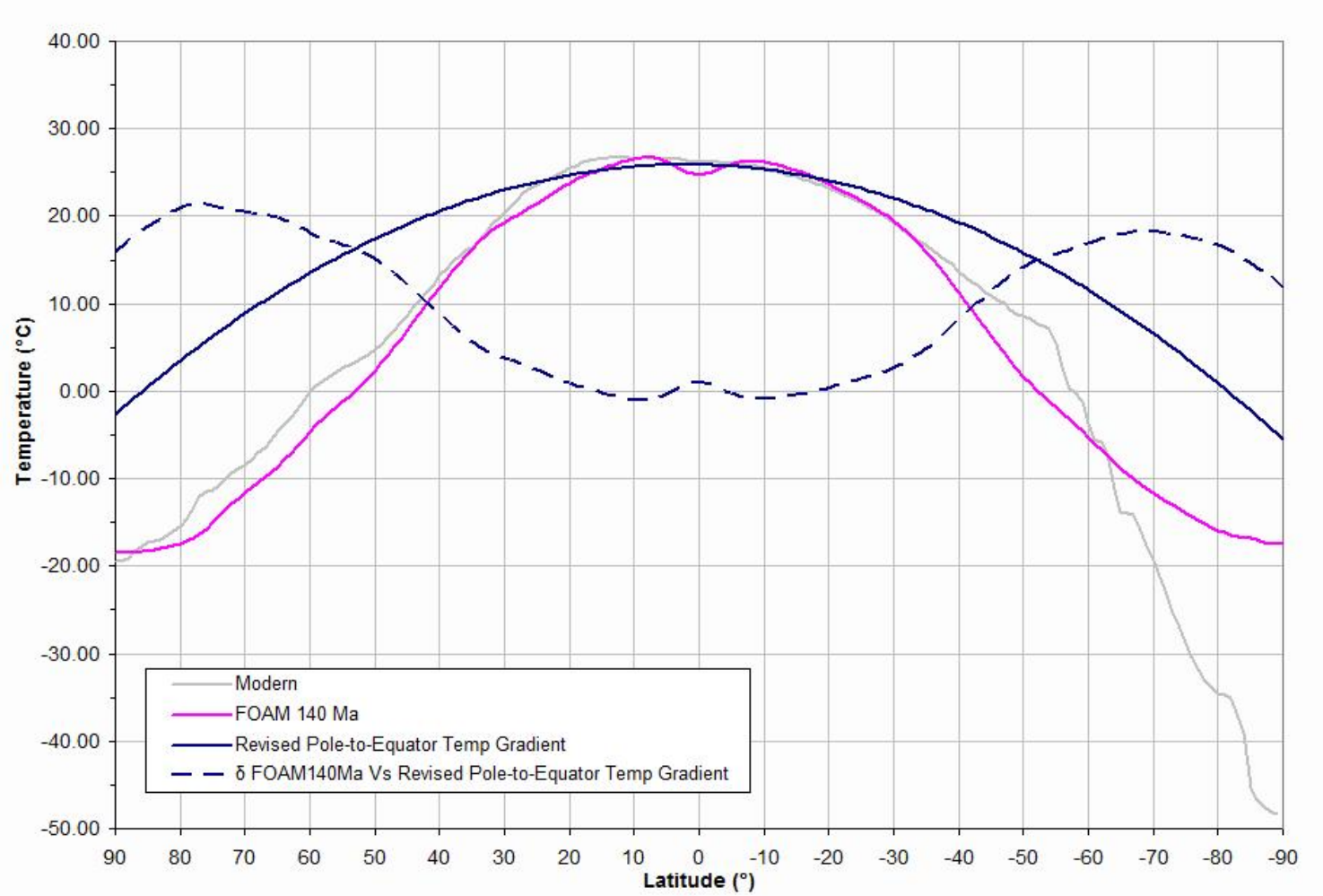

Figure 4.4 Pole-to-Equator temperature gradients for the Pre-Aptian (140 Ma) and the difference between the FOAM estimated and observed pole-to-equator temperature gradients.

Table 4.1 Average Temperature and the Difference Between Observed Temperature and Temperatures Estimated By FOAM

Age	Name	90° - 60° Avg	60° - 40° Avg	40° - 20° Avg	20° - 0° Avg	Max	Min
Maastrichtian	*Tendline*	7.61	16.79	20.77	22.60	22.91	-2.57
	δT70Ma	16.41	9.20	-0.35	-3.20	23.74	-4.19
Campanian	*Tendline*	10.94	17.91	21.43	23.19	23.66	2.29
	δT70Ma	19.74	10.33	0.32	-2.61	28.92	-3.98
Coniacian-Santonian	*Tendline*	15.22	21.87	25.23	26.91	27.32	7.38
	δT90Ma	21.86	13.60	4.05	-1.09	27.88	-2.40
Cenomanian-Turonian	*Tendline*	12.97	20.26	23.94	25.77	26.16	5.23
	δT90Ma	19.61	11.99	2.75	-2.23	22.99	-3.20
Albian	*Tendline*	7.01	17.78	23.22	25.93	26.56	-5.32
	δT120Ma	9.96	7.97	1.25	-2.59	16.45	-3.68
Aptian	*Tendline*	8.29	18.42	23.54	26.09	27.41	-8.87
	δT120Ma	11.24	8.62	1.57	-2.42	21.94	-4.11
Pre-Aptian	*Tendline*	4.77	16.49	22.41	25.36	25.89	-5.54
	δT140Ma	18.16	13.86	3.71	-0.15	21.53	-0.99
CretAvg	*Tendline*	10.45	18.69	22.85	24.92	25.36	-0.50

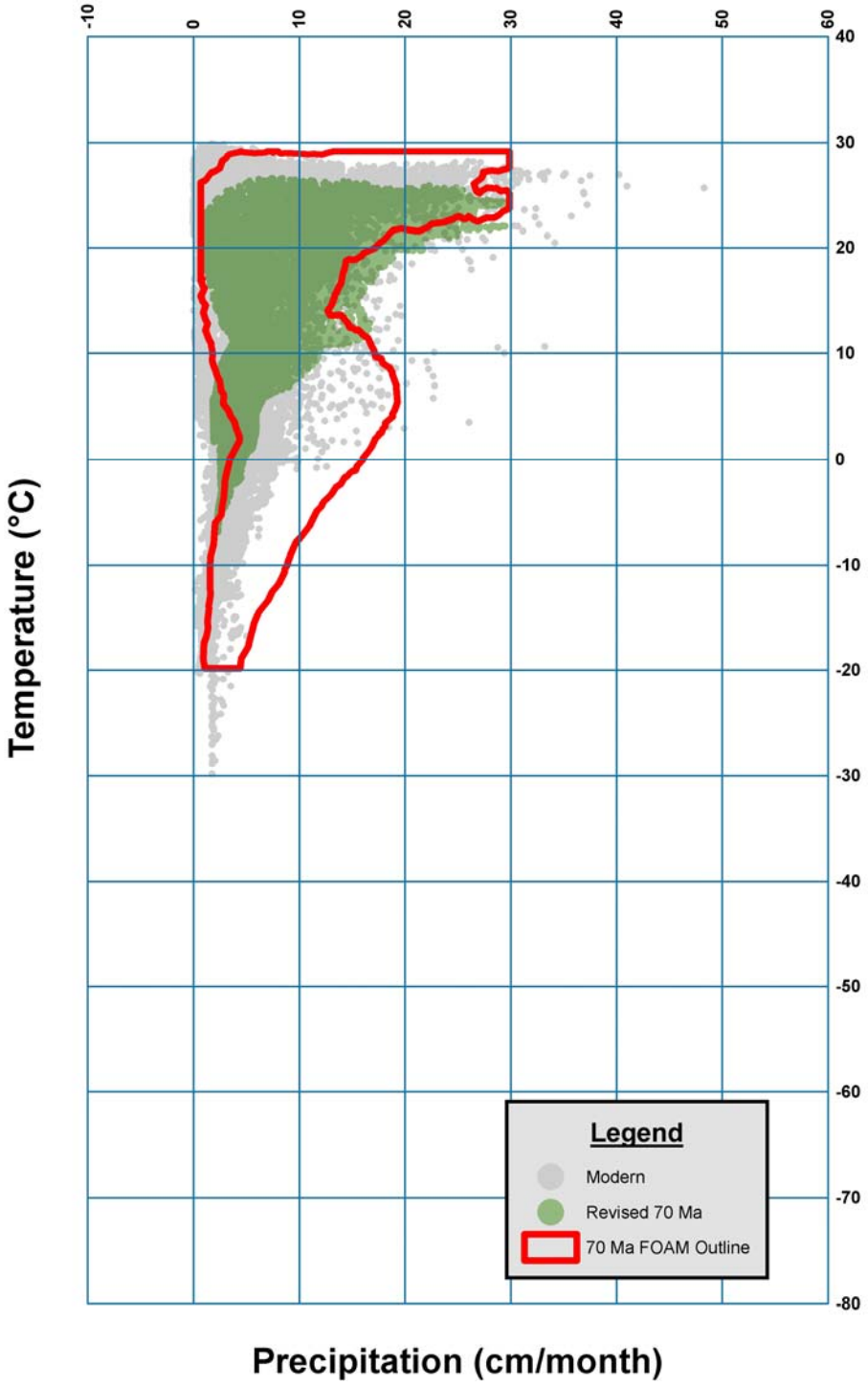

Figure 4.5 Revised Temperature – Precipitation Plots for the Maastrichtian (70Ma)

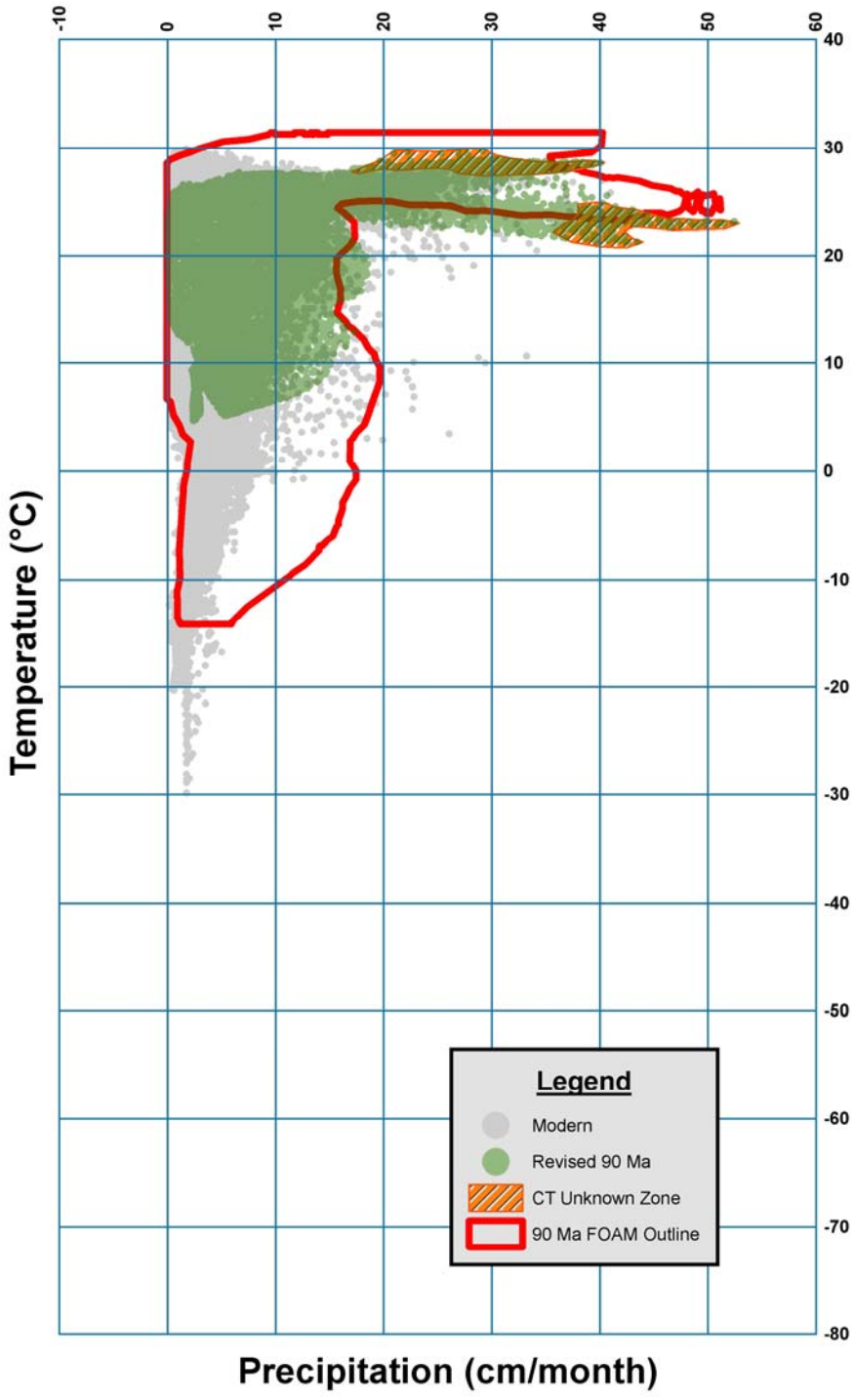

Figure 4.6 Revised Temperature – Precipitation Plots for the Cenomanian – Turonian (90 Ma)

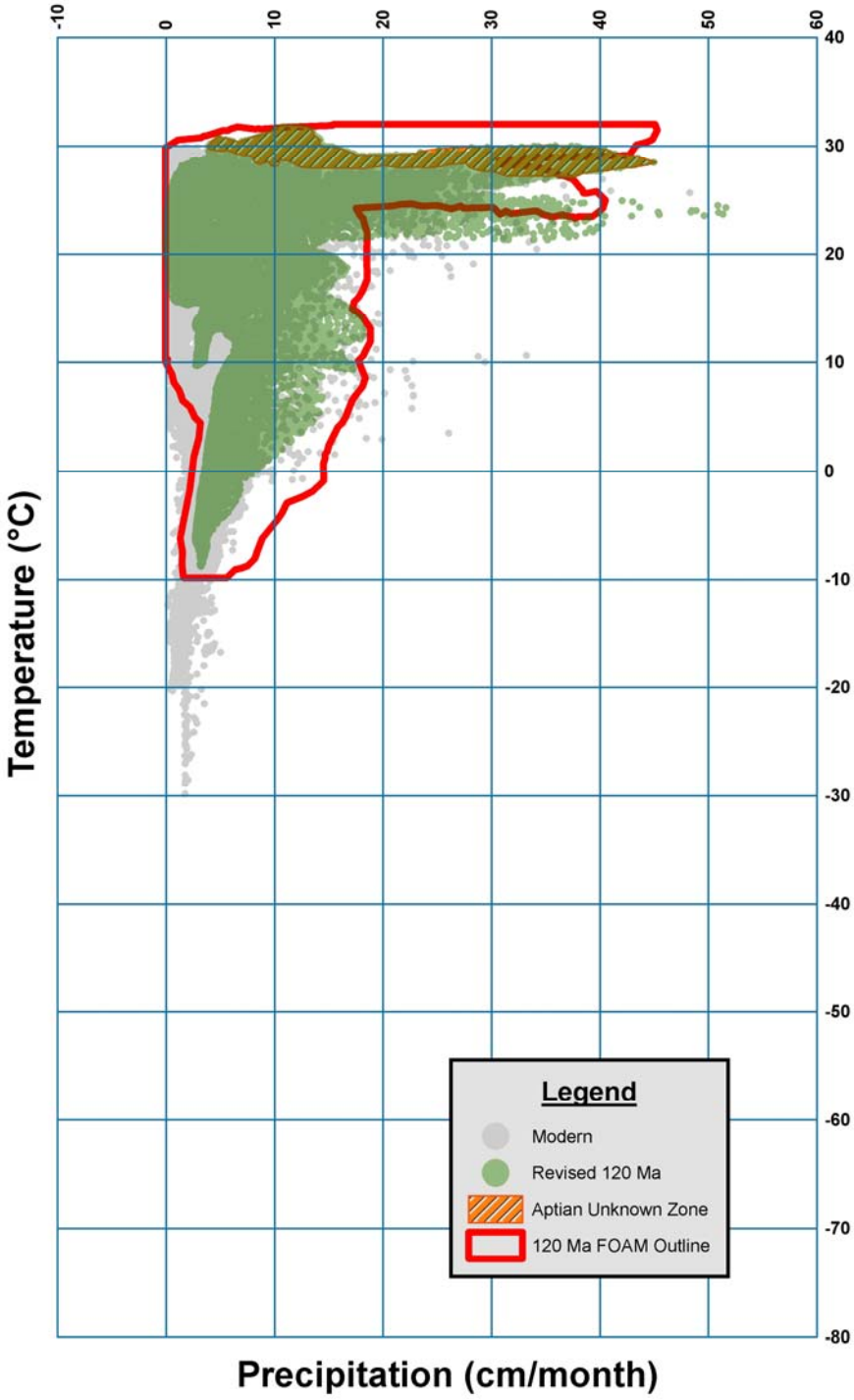

Figure 4.7 Revised Temperature – Precipitation Plots for the Aptian (120 Ma)

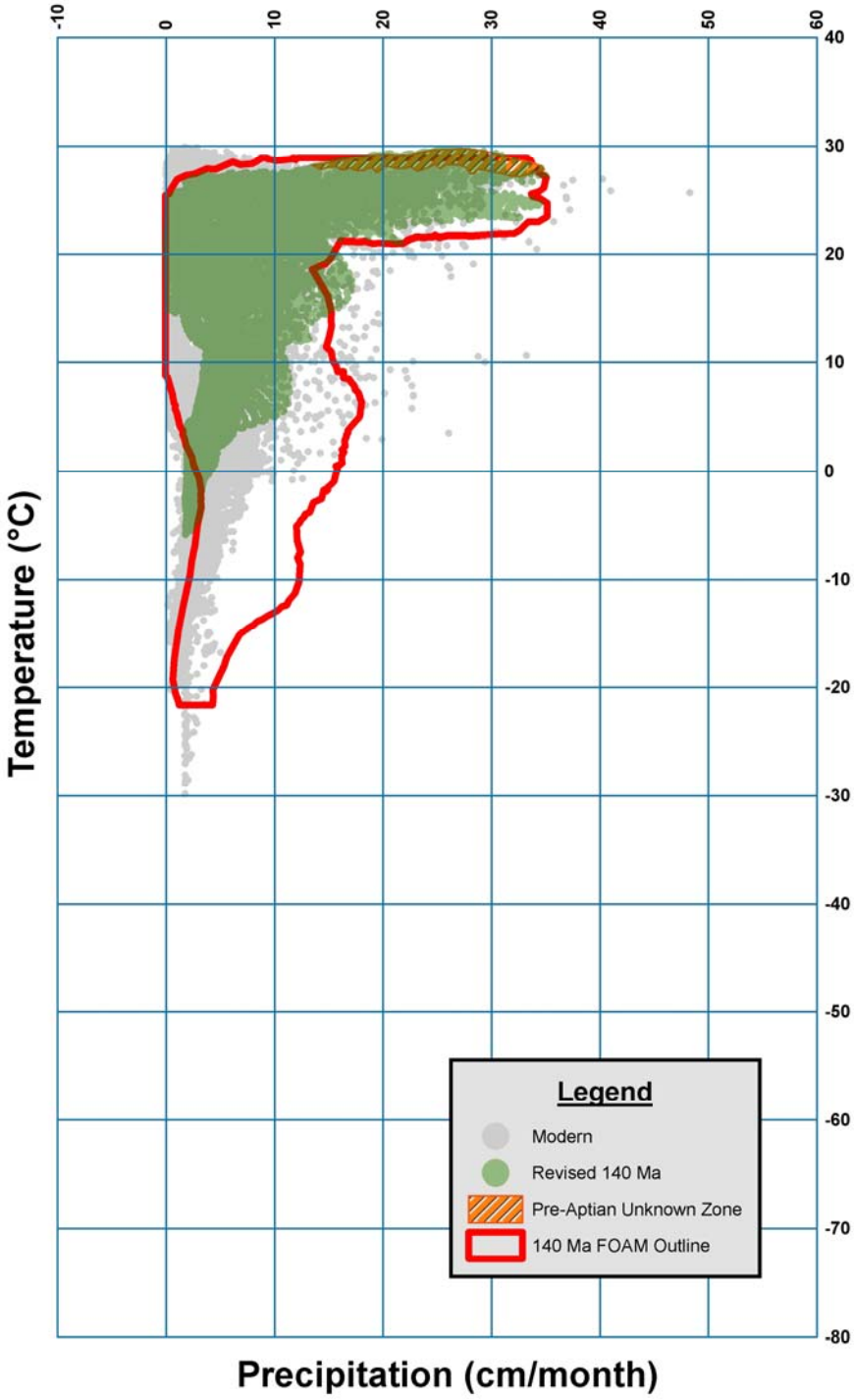

Figure 4.8 Revised Temperature – Precipitation Plots for the Pre-Aptian (140 Ma)

4.2 Discussion

4.2.1 Maastrichtian (70 Ma)

Figure 4.1 plots the Maastrichtian temperature difference between the pole-to-equator average latitudinal temperature gradient estimated by FOAM and the revised pole-to-equator temperature gradient based on geologic, geochemical and fossil data as described in Chapter Three. The gray line represents the modern pole-to-equator temperature gradient based on Legates-Willmott dataset (Legates and Willmott 1990 a and b). The pink line is the FOAM estimated pole-to-equator temperature gradient. The blue solid line represents the pole-to-equator temperature gradient estimated from geologic, geochemical and fossil data. The dashed blue line is the difference between temperature estimated by FOAM and the temperature estimated from geologic, geochemical and fossil data.

Figure 4.5 plots the revised temperature and precipitation values for the latest Cretaceous plotted on a background of modern day temperature and precipitation values (gray). The red outline delineates the previous temperature – precipitation values estimated by FOAM for the Maastrichtian (see Figure 2.12). The green area represents the revised temperature and precipitation values for the Maastrichtian. For the latest Cretaceous, the maximum and minimum revised temperatures are 26.53°C and -6.93°C respectively. The precipitation values have not been adjusted (maximum 29.73cm/month and 0. 78 cm/month, respectively). The temperatures are now much lower than the previous estimates. As a result, the revised temperature-precipitation plot retains its shape but is reduced in extent. Though the overall shape of this temperature - precipitation plot is very different from the modern temperature-precipitation plot, all of the temperature–precipitation values are within the modern domain.

Figure 4.9 shows the reconstruction of different paleo-soils for the Maastrichtian stage. Compared to initial prediction of the geographic prediction of different paleo-soil types for the Maastrichtian (see Figure 2.13) this revised map of paleo-soils is drastically different. First of all, using the revised temperature-precipitation conditions, we get a continuous prediction for the

whole land area starting from the north to south polar regions. There are no ‘stippled areas’ in the new reconstruction like the initial paleo-soil map (see Figure 2.13), where we had no idea about the kind of paleo-soil that might have existed.

Overall the different soil belts are very well developed. As expected from the geologic, geochemical and fossil data, there are no predictions for Polar paleo-soil types in either the northern or southern hemisphere of the Maastrichtian world. The polar regions are covered with Cool Temperate paleo-soils (KS, CDM and OP). There is a very well developed belt of Warm Temperate paleo-soils (A, H and W) in the northern hemisphere. In the southern hemisphere Warm Temperate paleo-soils are predicted, but the geographic distribution is much less extensive than in the northern hemisphere. In the southern hemisphere Warm Temperate paleo-soils are shown in southern and western South America, southern tip of Africa, southern part of India and most of Australia. Paleo-soils representing the Equatorial Rainy Belt (FN and QV with few narrow regions of A and W) cover the equatorial region and extend 30° north and south of the Equator. The paleo-soil types representing the Subtropical Arid belts (mainly XYZ and KS) are less abundant. In the northern hemisphere arid soil types are present in central Eurasia. In southern hemisphere arid soils are shown in southern Africa and traces are found in southwestern South America. The XYZ paleo-soil type is also mapped in the northwestern part of Africa (25°N).

Figure 4.10A illustrates the confidence levels for the primary paleo-soil type (PPS) predictions for latest Cretaceous period. Overall the levels of confidence for the latest Cretaceous predictions are high. However, southern and west-central North America, northern South America, central, eastern and south-central Africa, southeast Asia, and southern Australia have relatively low levels of confidence.

The paleo-soil dominance map (Figure 4.10B) for the latest Cretaceous is very similar to the confidence level map (Figure 4.10A). The overall dominance scores are medium to high. except for parts of southern and west-central North America, northern South America, central,

eastern and south-central Africa, Southeast Asia, and southern Australia. This implies that during the Late Cretaceous, in these regions more than one type paleo-soils may have been predominant.

We have also prepared a reconstruction showing the secondary paleo-soil type (PPS2) predictions for the latest Cretaceous period. The reconstruction along with its levels of confidence is illustrated in Appendix C (Figure C.18).

4.2.2 Cenomanian-Turonian (90 Ma)

Figure 4.2 plots the Cenomanian-Turonian temperature difference between the pole-to-equator average latitudinal temperature gradient estimated by FOAM and the revised pole-to-equator temperature gradient based on geologic, geochemical and fossil data as described in Chapter Three. The gray line represents the modern pole-to-equator temperature gradient based on Legates-Willmott dataset (Legates and Willmott 1990 a and b). The pink line is the FOAM estimated pole-to-equator temperature gradient. The blue solid line represents the pole-to-equator temperature gradient estimated from geologic, geochemical and fossil data. The dashed blue line is the difference between temperature estimated by FOAM and the temperature estimated from geologic, geochemical and fossil data.

Figure 4.6 plots the revised temperature and precipitation values for the Cenomanian-Turonian stage plotted on a background of modern day temperature and precipitation values (gray). The red outline delineates the previous temperature – precipitation values estimated by FOAM for the Cenomanian-Turonian (see Figure 2.15). The green area represents the revised temperature and precipitation values for the Cenomanian-Turonian. For the Cenomanian-Turonian, the maximum and minimum revised temperatures are 29.69°C and 4.73°C respectively. The precipitation values have not been adjusted (maximum 52.47cm/month and 0.04 cm/month, respectively). The temperatures are now almost one half of previous estimate. As a result, the revised plot retains its shape but is reduced in extent. It is important to note that on this revised temperature-precipitation plot, there are certain ranges of high temperatures-

high precipitation values which are non-existent in the modern world. This region is marked as Cenomanian-Turonian 'unknown zone' on the plot.

Figure 4.11 shows the reconstruction of different paleo-soils for the Cenomanian-Turonian stage. Compared to initial prediction of the geographic prediction of different paleo-soil types for the Cenomanian-Turonian (Figure 2.16), this revised map of paleo-soils is very different. First of all, similar to Maastrichtian, using the revised temperature-precipitation conditions, we get a continuous prediction for the whole land area starting from the north to south polar regions. There are only three small 'stippled areas' in the equatorial regions as opposed to the high percentage of 'stippled areas' in the initial prediction, where we had no idea about the kind of paleo-soil that might have existed. These areas can be explained by the "Cenomanian-Turonian Unknown Zone" marked in Figure 4.6. In the modern world, we have no experience of the kind of soil that might form/dominate at those high temperature high precipitation conditions. These 'stippled areas', located in the equatorial regions represent the similar conditions.

Overall we see a mixed development of different latitudinal-soil belts. As expected from the geologic, geochemical and fossil data, there are no predictions of Polar paleo-soil types in either the northern or southern hemispheres of the Cenomanian-Turonian world. The polar regions are covered with Cool Temperate paleo-soils (mainly KS, a localized area with OP and very less CDM). There is a very well developed belt of Warm Temperate paleo-soils (A, H and W) in the northern hemisphere. In the southern hemisphere Warm Temperate paleo-soil belt is present but the geographic distribution is much less extensive than in the northern hemisphere. Paleo-soils representing the Equatorial Rainy Belt (FN and QV with few narrow regions of A and W) cover the equatorial regions and extend 30° north and south of the Equator. The paleo-soil types representing the Subtropical Arid belts (mainly XYZ and KS) cover extensive regions in southwest Asia, western South America and south western Africa. In this regard, it is also

important to note that there is another rather unexpected occurrence of the XYZ paleo-soil type in the northeastern part of Africa (5°N).

Figure 4.12A illustrates the confidence levels for the primary paleo-soil type (PPS) predictions for Cenomanian-Turonian stage. Overall the levels of confidence for the Cenomanian-Turonian predictions are high. Eastern and western North America, equatorial South America and Africa, central Europe and Asia and central Australia have relatively low levels of confidence.

The paleo-soil dominance map (Figure 4.12B) for the latest Cretaceous is very similar to the confidence level map (Figure 4.12A). The overall dominance scores are medium to high, except for the regions in central Africa and central Australia. This implies that during the Late Cretaceous, in these regions more than one type of paleo-soil may have existed.

We have also prepared a reconstruction showing the secondary paleo-soil type (PPS2) predictions for the Cenomanian-Turonian stage. The reconstruction along with its levels of confidence is illustrated in Appendix C (Figure C.19).

4.2.3 Aptian (120 Ma)

Figure 4.3 plots the Aptian temperature difference between the pole-to-equator average latitudinal temperature gradient estimated by FOAM and the revised pole-to-equator temperature gradient based on geologic, geochemical and fossil data as described in Chapter Three. The gray line represents the modern pole-to-equator temperature gradient based on Legates-Willmott dataset (Legates and Willmott 1990 a and b). The pink line is the FOAM estimated pole-to-equator temperature gradient. The blue solid line represents the pole-to-equator temperature gradient estimated from geologic, geochemical and fossil data. The dashed blue line is the difference between temperature estimated by FOAM and the temperature estimated from geologic, geochemical and fossil data.

Figure 4.7 plots the revised temperature and precipitation values for the Aptian stage plotted on a background of modern day temperature and precipitation values (gray). The red

outline delineates the previous temperature – precipitation values estimated by FOAM for the Aptian (see Figure 2.18). The green area represents the revised temperature and precipitation values for the Aptian. For the Aptian, the maximum and minimum revised temperatures are 31.79°C and -8.76°C respectively. The precipitation values have not been adjusted (maximum 51.62cm/month and 0.03 cm/month, respectively). The revised range of temperatures for Aptian is almost similar to initial FOAM estimate. As a result the revised plot does not retain its shape. It is important to note that on this revised temperature-precipitation plot, there are certain range of high temperatures and low to high precipitation values which are non-existent on the modern world. This region is marked as Aptian 'unknown zone' on the plot.

Figure 4.13 shows the reconstruction of different paleo-soils for the Aptian stage. Compared to the initial geographic prediction of different paleo-soil types for the Maastrichtian (Figure 2.19), this revised map of paleo-soils is not very different. First of all, we get a continuous prediction for the whole land areas starting from the north to south polar regions. There are only five very small 'stippled areas' in the equatorial regions, where we had no idea of the kind of paleo-soil that might have existed. These areas can be explained by the "Aptian Unknown Zone" marked in Figure 4.7. In the modern world, we have no experience of what kind of soil might form/dominate at those high temperature-high precipitation conditions. The 'stippled areas' located in the equatorial region represent the similar conditions.

Overall we see well developed but different paleo-soil belts. As expected from the geologic, geochemical and fossil data, there are no predictions of Polar paleo-soil types in the northern hemisphere and in the southern hemisphere there is a small area around the south pole where Polar paleo-soils (BG Polar) are predicted. The sub polar regions are covered with Cool Temperate paleo-soils (mainly KS in northern hemisphere, and OP and very less CDM in southern hemisphere). There is a very well developed belt of Warm Temperate paleo-soils (A, H and W) in the northern hemisphere. In the southern hemisphere Warm Temperate paleo-soil belt is very thin and found at the southern tips of South America, Africa and India. Paleo-soils

representing the Equatorial Rainy Belt (FN and QV with few narrow regions of A and W) cover the equatorial region and extend 25° north and south of the Equator. The paleo-soil types representing the Subtropical Arid belts (mainly XYZ and KS) cover extensive regions in southwest Asia, central South America and south-central Africa.

Figure 4.14A illustrates the confidence levels for the primary paleo-soil type (PPS) predictions for Aptian stage. Overall the levels of confidence for the Aptian predictions are very high. Equatorial Gondwana regions have relatively low levels of confidence.

The paleo-soil dominance map (Figure 4.14B) for the Aptian is very different to the confidence level map (Figure 4.14A). The overall dominance scores are low, except for the tropical North America, Eurasia and Gondwana regions,. This implies that during the Aptian, these regions had more than one type of paleo-soils.

We have also prepared a reconstruction showing the secondary paleo-soil type (PPS2) predictions for the Aptian stage. The reconstruction along with its levels of confidence is illustrated in Appendix C (Figure C.20).

4.2.4 Berriasian-Valanginian (140 Ma)

Figure 4.4 plots the Early Cretaceous temperature difference between the pole-to-equator average latitudinal temperature gradient estimated by FOAM and the revised pole-to-equator temperature gradient based on geologic, geochemical and fossil data as described in Chapter Three. The gray line represents the modern pole-to-equator temperature gradient based on Legates-Willmott dataset (Legates and Willmott 1990 a and b). The pink line is the FOAM estimated pole-to-equator temperature gradient. The blue solid line represents the pole-to-equator temperature gradient estimated from geologic, geochemical, and fossil data. The dashed blue line is the difference between temperature estimated by FOAM and the temperature estimated from geologic, geochemical and fossil data.

Figure 4.8 plots the revised temperature and precipitation values for the Berriasian-Valanginian stage plotted on a background of modern day temperature and precipitation values

(gray). The red outline delineates the previous temperature - precipitation values estimated by FOAM for the Pre-Aptian (see Figure 2.21). The green area represents the revised temperature and precipitation values for the Early Cretaceous. For the Berriasian-Valanginian, the maximum and minimum revised temperatures are 31.79°C and -8.76°C respectively. The precipitation values have not been adjusted (maximum 34.94 cm/month and 0.04 cm/month, respectively). The range of temperatures for Berriasian-Valanginian is less than that of the initial FOAM estimate. As a result the revised plot retains its shape but is reduced in extent. It is important to note that on this revised temperature-precipitation plot, there are certain range of high temperatures and medium to high precipitation values which are non-existent in the modern world. This region is marked as Pre-Aptian 'unknown zone' on the plot.

Figure 4.15 shows the reconstruction of different paleo-soils for the Pre-Aptian stage. Compared to initial geographic prediction of different paleo-soil types for the Pre-Aptian (Figure 2.22), this new distribution is very similar. First of all, using the revised temperature-precipitation conditions, we get a continuous prediction for the whole land area starting from the north to south polar regions. There are very few small 'stippled areas' in the equatorial regions as opposed to the high percentage of stippled areas in the initial prediction, where we had no idea of what kind of paleo-soil might have existed. These areas can be explained by the "Pre-Aptian Unknown Zone" marked on Figure 4.8. In the modern world, we have no experience of the kind of soil that might form/dominate at those high temperature-high precipitation conditions. The 'stippled areas' located in the equatorial regions represent similar conditions.

Overall we see very well developed bands of different paleo-soil belts. As expected from the geologic, geochemical, and fossil data, there are no predictions of Polar paleo-soil in the northern hemisphere of the Pre-Aptian world. In the southern hemisphere, there is a narrow belt of Polar (BG Polar) paleo-soil. The polar regions are covered with Cool Temperate paleo-soils (mainly KS, OP and CDM). There is a very well developed belt of Warm Temperate paleo-soils (A, H and W) in both hemispheres. Paleo-soils representing the Equatorial Rainy Belt (FN

and QV with few narrow regions of A and W) cover the equatorial regions and extend 30° north and south of the Equator. The paleo-soil types representing the Subtropical Arid belts (mainly XYZ and KS) are extensive regions in southern North America, southwest Asia, and southern Gondwana. In this regard, it is also important to note that there is another rather unexpected occurrence of the XYZ arid paleo-soil in the north-central part of Africa (5°N).

Figure 4.16A illustrates the confidence levels for the primary paleo-soil type (PPS) predictions for Pre-Aptian stage. Overall the levels of confidence for the Pre-Aptian predictions are very high. Equatorial Gondwana regions and central Asia have relatively low levels of confidence.

The paleo-soil dominance map (Figure 4.16B) for the Aptian is very different to the confidence level map (Figure 4.16A). The overall dominance scores are medium to low, except for the northern regions. This implies that during the Aptian, these regions might have had more than one type of paleo-soils.

We have also prepared a reconstruction showing the secondary paleo-soil type (PPS2) predictions for earliest Cretaceous period. The reconstruction along with its levels of confidence is illustrated in Appendix C (Figure C.21).

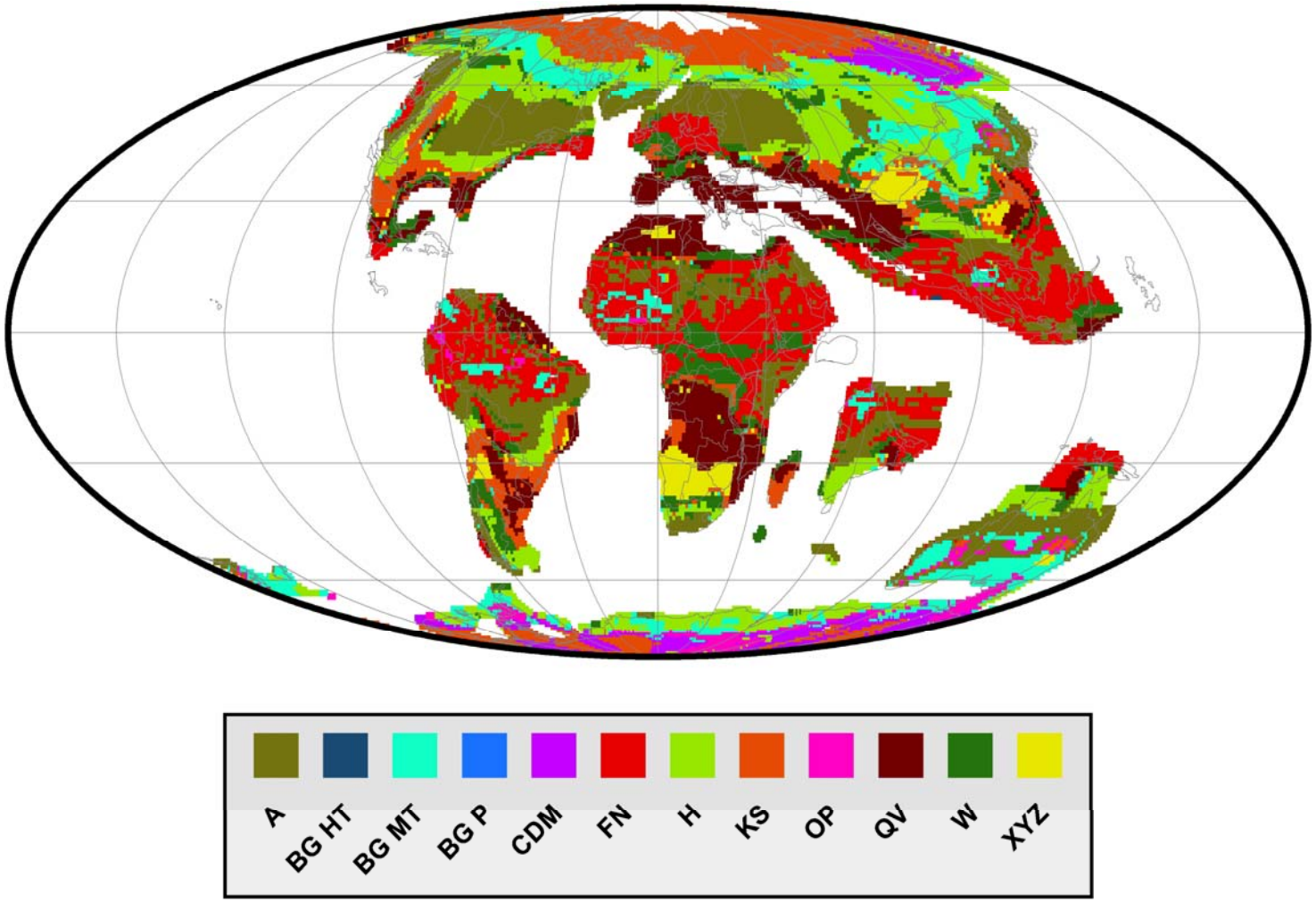

Figure 4.9 Revised geographic distribution of different soil groups for the Maastrichtian (70 Ma)

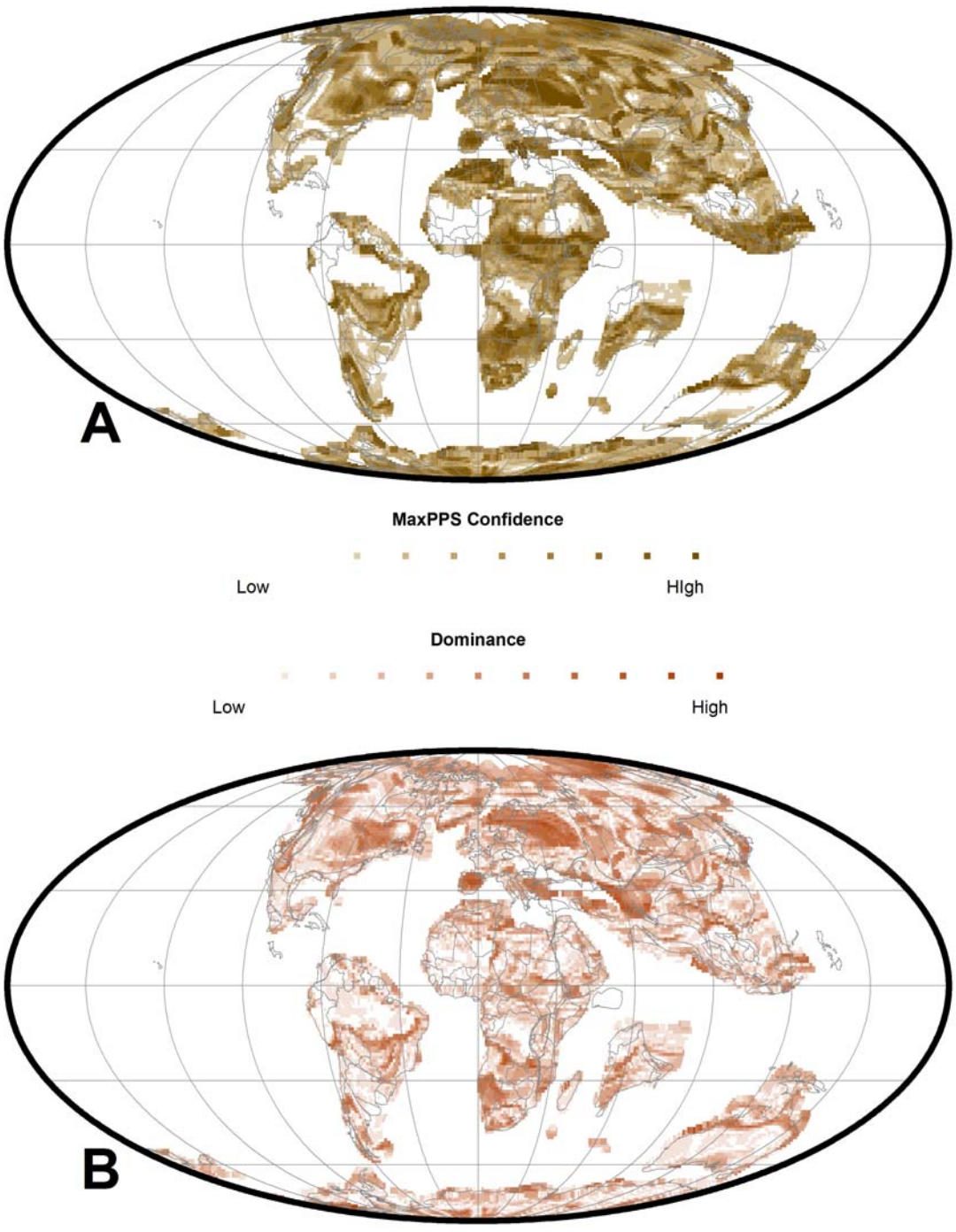

Figure 4.10 A. Prediction Confidence Level for Maximum Probable Paleo-soil Type for the Maastrichtian (70 Ma), B. Dominance of Primary Maximum Probable Paleo-soil Type over the Secondary Maximum Probable Paleo-soil Type for the Late Cretaceous / Maastrichtian (70 Ma)

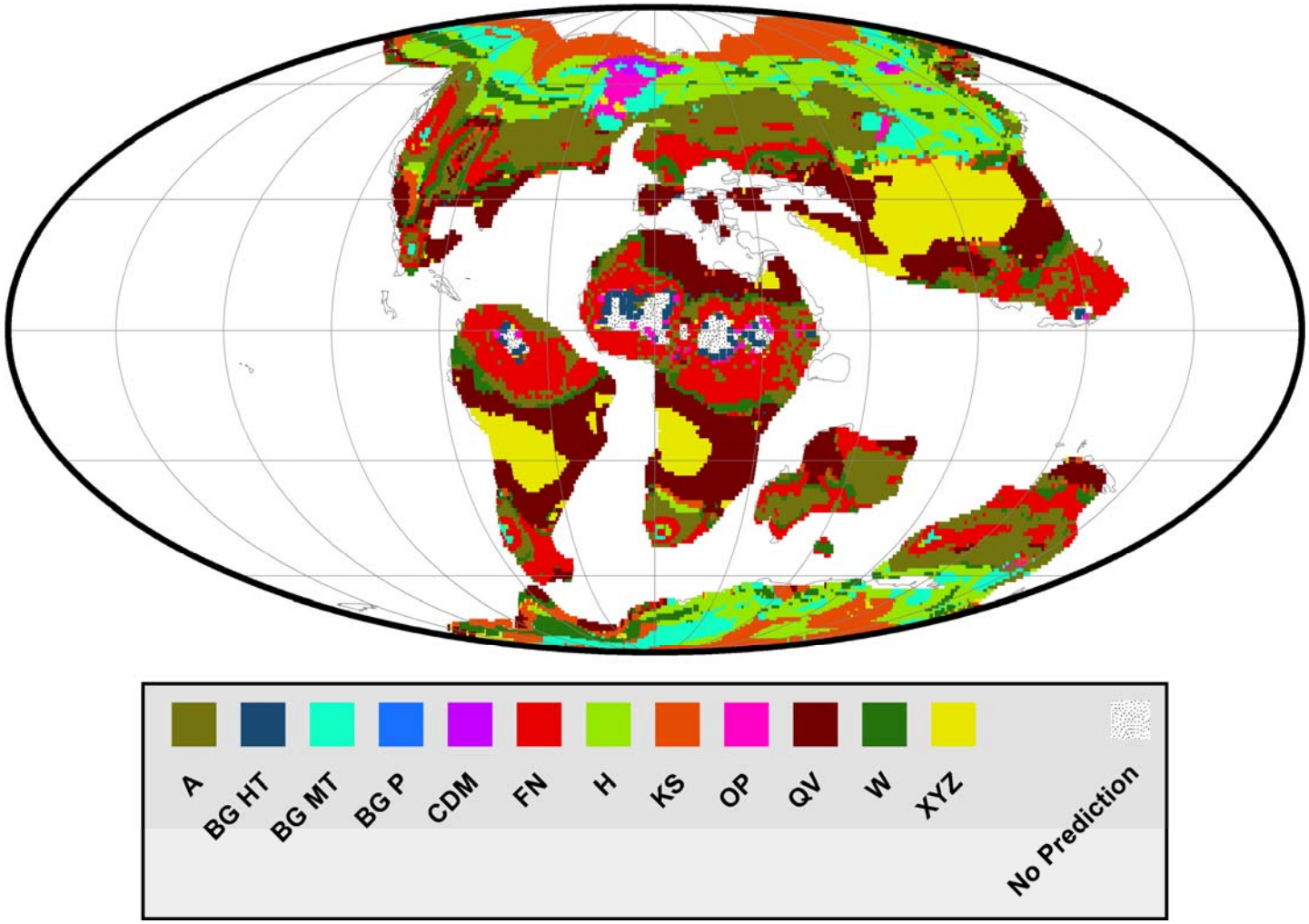

Figure 4.11 Revised geographic distribution of different soil groups for the Cenomanian - Turonian (90 Ma)

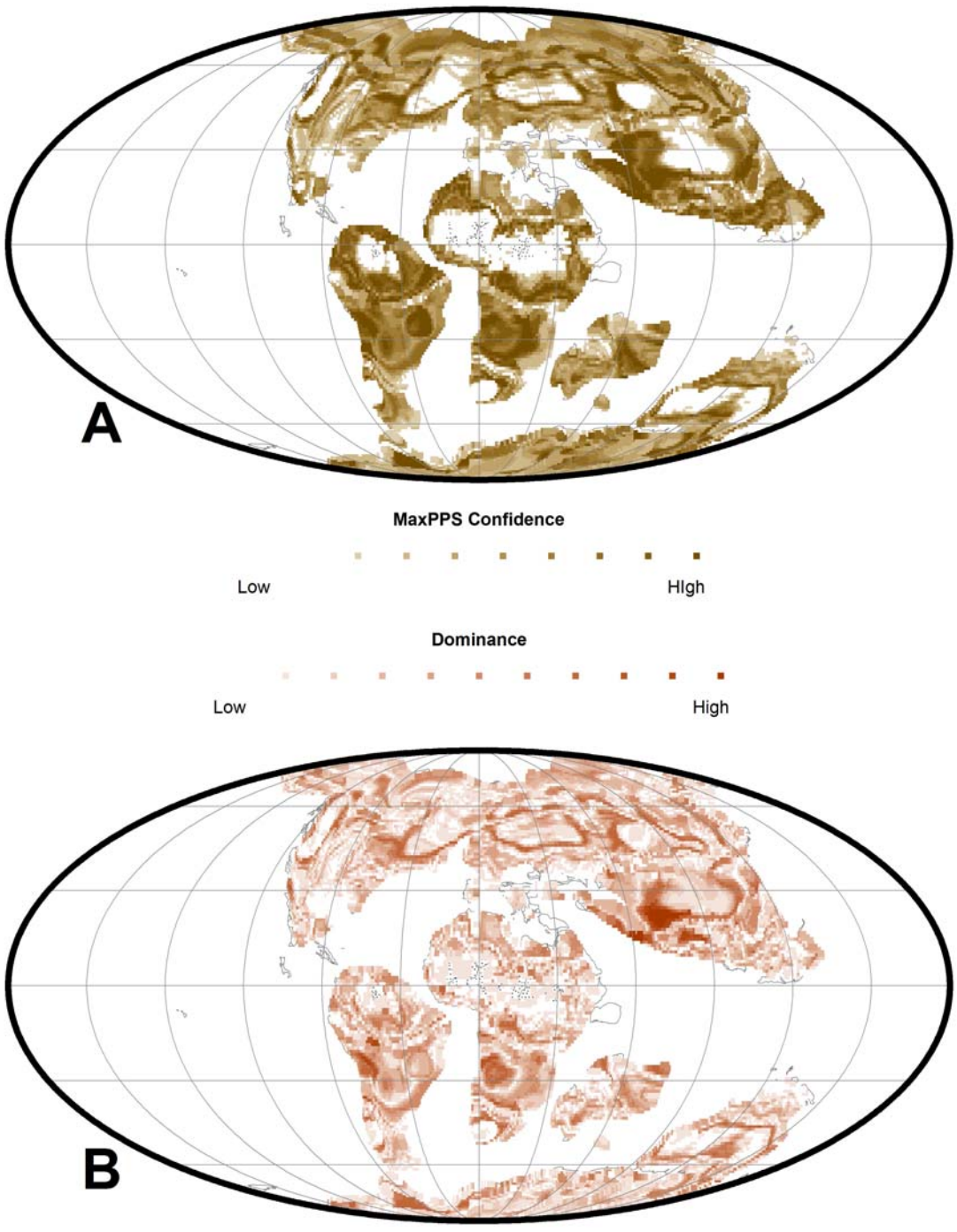

Figure 4.12 A. Prediction Confidence Level for Maximum Probable Paleo-soil Type for the Cenomanian-Turonian (90 Ma), B. Dominance of Primary Maximum Probable Paleo-soil Type over the Secondary Maximum Probable Paleo-soil Type for the Cenomanian-Turonian (90 Ma)

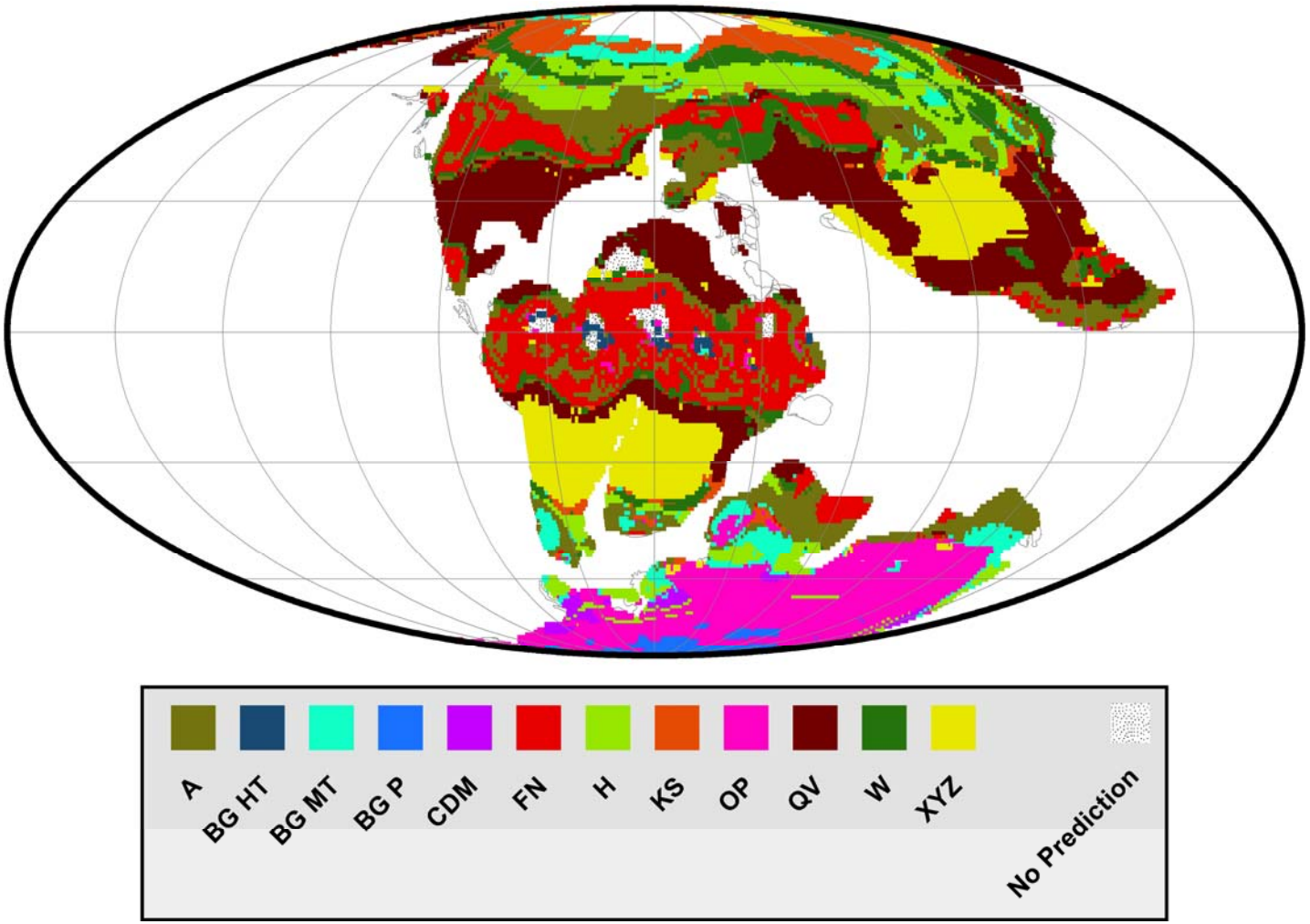

Figure 4.13 Revised geographic distribution of different soil groups for the Aptian (120 Ma)

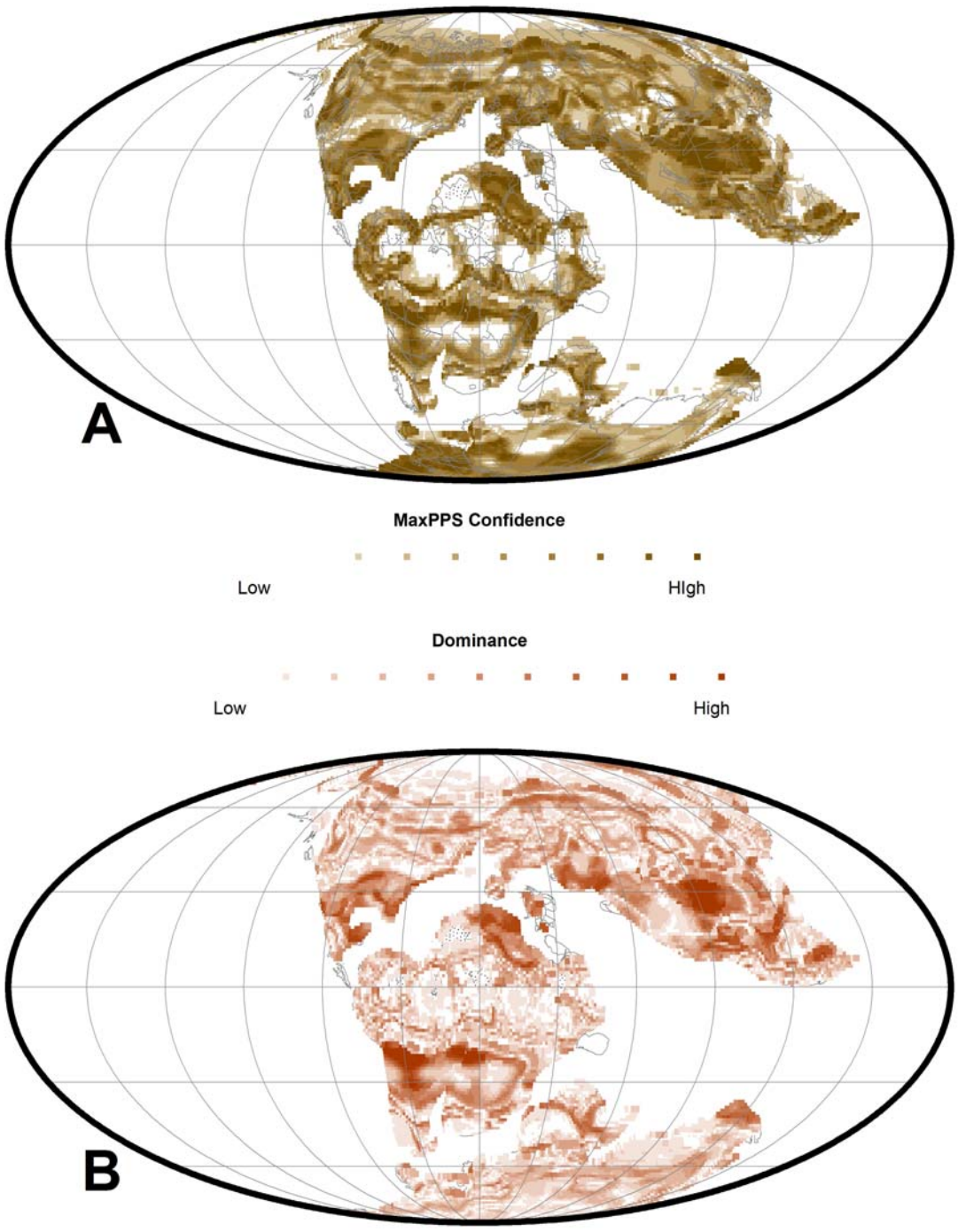

Figure 4.14 A. Prediction Confidence Level for Maximum Probable Paleo-soil Type for the Aptian (120 Ma), B. Dominance of Primary Maximum Probable Paleo-soil Type over the Secondary Maximum Probable Paleo-soil Type for the Aptian (120 Ma)

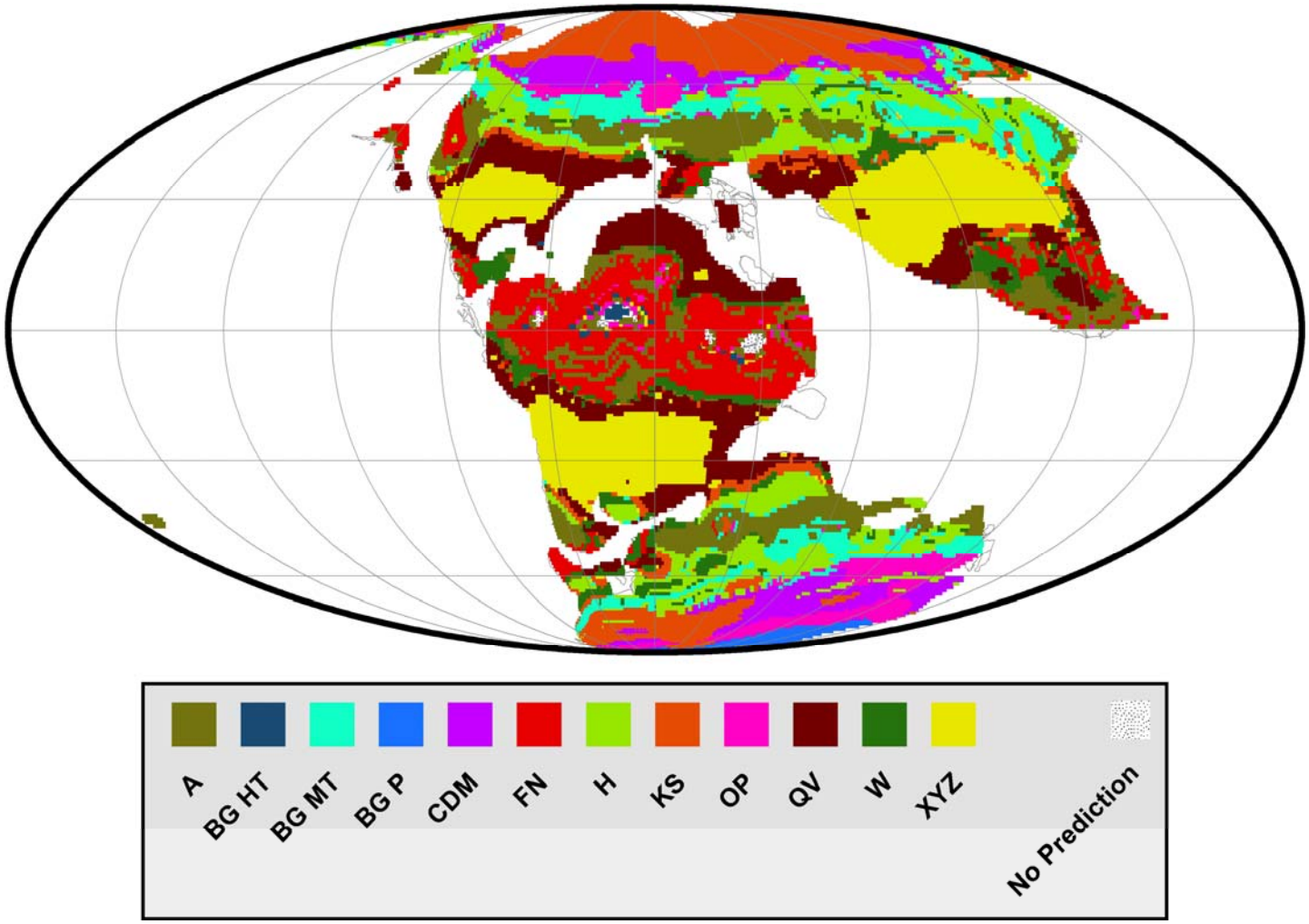

Figure 4.15 Revised geographic distribution of different soil groups for the Berriasian-Valanginian (140 Ma)

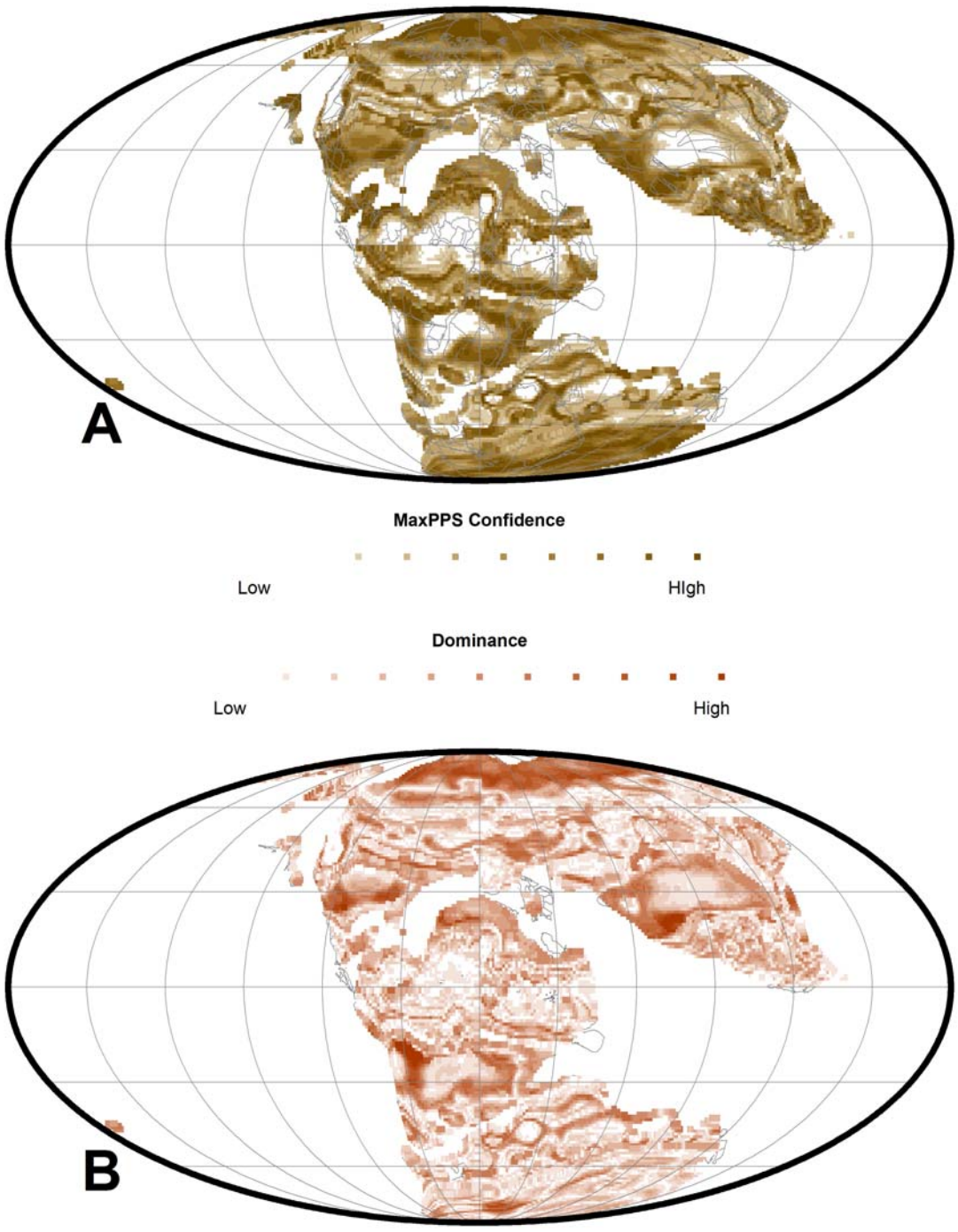

Figure 4.16 A. Prediction Confidence Level for Maximum Probable Paleo-soil Type for the Pre-Aptian (140 Ma), B. Dominance of Primary Maximum Probable Paleo-soil Type over the Secondary Maximum Probable Paleo-soil Type for the Early Cretaceous / Pre-Aptian (140 Ma)

4.3 Conclusion

The Cretaceous period was a hot house world. The poles were ice-free during the mid and Late Cretaceous and warm ocean currents spread from the Equator to the poles. Unlike the modern world polar regions had warm tropical climates, with extended forest cover to the poles. Starting with the geographic distribution of modern soils based on temperature and precipitation records, no analogues for mid-Cretaceous like high temperatures was possible to take in account for the prediction of geographic distribution of ancient soils. Using the temperature adjustment based on the difference between the pole-to-equator temperature gradients (FOAM predicted and observed), revised prediction overall does a impressive job to estimate the probable geographic distributions of ancient soils. The prediction results do not have big gaps ('stippled areas'), rather all the Cretaceous predictions give very good global coverage of the predicted soils. The 'stippled areas' in the Cenomanian – Turonian results can be attributed to our lack of detailed knowledge of possible soil types existing in this extreme climatic conditions that are not present in the modern climatic conditions. Furthermore, the prediction results are expected to be more enhanced with incorporation of higher number of observed temperature estimates and better observed pole-to-equator temperature gradients.

APPENDIX A

PYTHON SCRIPTS

Zobler Formating.py

```
#Variables Used
Lat=Long=MSU=MSUName=SU=SUName=SubSID=Area=AreaName=""
a=[]
b=c=z=0
newline =""
#Open input file
fin = open("H:\\000. Thesis Final Work\\Zobler Soil Work\\Downloaded original Data\\zoblerworldsoil.txt","r")
#open outputfile
fout =open("H:\\000. Thesis Final Work\\Zobler Soil Work\\Downloaded original Data\\zoblerworldsoilv2.txt","w")
fout.write("Lat,Long,MSU,MSUName,SU,SUName,SubSID,Area,AreaName\n")
#read the input file line by line and remove all null entries
ftext = fin.readlines()
for line in ftext:
    a=line.split(" ")
    b=len(a)
    c=0
    while c<b:
        if a[c]=="":
            del a[c]
            b= len(a)
        else:
            c = c+1
            b=len(a)
#now assigning the values to individual variables
    Lat=Long=MSU=MSUName=SU=SUName=SubSID=Area=AreaName =""
    z=0
    while z<b:
        if z==0:
            Lat = a[z]
        elif z==1:
            Long = a[z]
        elif z==2 and a[z].isalpha() and len(a[z])==2:
            SU = a[z]
            if SU.startswith("A"):
                MSU ="A"
                MSUName ="Acrisols"
                if SU=="AF":
                    SUName ="Ferric Acrisols"
                elif SU=="AH":
                    SUName ="Humic Acrisols"
                elif SU=="AG":
                    SUName ="Gleyic Acrisols"
                elif SU=="AO":
                    SUName ="Orthic Acrisols"
                else:
                    SUName ="Plinthic Acrisols"
            if SU.startswith("B"):
             MSU ="B"
```

```
 MSUName ="Cambisols"
 if SU=="BC":
            SUName ="Chromic Cambisols"
 elif SU=="BD":
            SUName ="Dystric Cambisols"
 elif SU=="BE":
            SUName ="Eutric Cambisols"
 elif SU=="BF":
    SUName ="Ferralic Cambisols"
 elif SU=="BG":
            SUName ="Gleyic Cambisols"
 elif SU=="BH":
            SUName ="Humic Cambisols"
 elif SU=="BK":
            SUName ="Calcic Cambisols"
 elif SU=="BV":
            SUName ="Vertic Cambisols"
 else:
            SUName ="Gelic Cambisols"
if SU.startswith("C"):
 MSU ="C"
 MSUName ="Chernozems"
 if SU=="CG":
            SUName ="Glossic Chernozems"
 elif SU=="CH":
            SUName ="Haplic Chernozems"
 elif SU=="CK":
            SUName ="Calcic Chernozems"
 else:
            SUName ="Luvic Chernozems"
if SU.startswith("D"):
 MSU ="D"
 MSUName ="Podzoluvisols"
 if SU=="DD":
            SUName ="Dystric Podzoluvisols"
 elif SU=="DE":
            SUName ="Eutric Podzoluvisols"
 else:
            SUName ="Gleyic Podzoluvisols"
if SU.startswith("E"):
 MSU ="E"
 MSUName ="Rendzinas"
    SUName = "Not Applicable"
if SU.startswith("F"):
 MSU ="F"
 MSUName ="Ferralsols"
 if SU=="FA":
            SUName ="Aerie Ferralsols"
 elif SU=="FH":
            SUName ="Humic Ferralsols"
 elif SU=="FO":
            SUName ="Orthic Ferralsols"
```

```
 elif SU=="FP":
            SUName ="Plinthic Ferralsols"
 elif SU=="FR":
            SUName ="Rhodic Ferralsols"
 else:
            SUName ="Xanthic Ferralsols"
if SU.startswith("G"):
 MSU ="G"
 MSUName ="Gleysols"
 if SU=="GC":
            SUName ="Calcaric Gleysols"
 elif SU=="GD":
            SUName ="Dystric Gleysols"
 elif SU=="GE":
            SUName ="Eutric Gleysols"
 elif SU=="GH":
            SUName ="Humic Gleysols"
 elif SU=="GM":
            SUName ="Mollic Gleysols"
 elif SU=="GP":
            SUName ="Plinthic Gleysols"
 else:
            SUName ="Gelic Gleysols"
if SU.startswith("H"):
 MSU ="H"
 MSUName ="Phaeozems"
 if SU=="HC":
            SUName ="Calcic Phaeozems"
 elif SU=="HG":
            SUName ="Gleyic Phaeozems"
 elif SU=="HH":
            SUName ="Haplic Phaeozems"
 else:
            SUName ="Luvic Phaeozems"
if SU.startswith("I"):
 MSU ="I"
 MSUName ="Lithosols"
    SUName = "Not Applicable"
if SU.startswith("J"):
 MSU ="J"
 MSUName ="Fluvisols"
 if SU=="JC":
            SUName ="Calcaric Fluvisols"
 elif SU=="JD":
            SUName ="Dystric Fluvisols"
 elif SU=="JE":
            SUName ="Eutric Fluvisols"
 else:
            SUName ="Thionic Fluvisols"
if SU.startswith("K"):
 MSU ="K"
 MSUName ="Kastanozems"
```

```
 if SU=="KH":
            SUName ="Haplic Kastanozems"
 elif SU=="KK":
            SUName ="Calcic Kastanozems"
 else:
            SUName ="Luvic Kastanozems"
if SU.startswith("L"):
 MSU ="L"
 MSUName ="Luvisols"
 if SU=="LA":
            SUName ="Albic Luvisols"
 elif SU=="LC":
            SUName ="Chromic Luvisols"
 elif SU=="LF":
            SUName ="Ferric Luvisols"
 elif SU=="LK":
            SUName ="Calcic Luvisols"
 elif SU=="LG":
            SUName ="Gleyic Luvisols"
 elif SU=="LO":
            SUName ="Orthic Luvisols"
 elif SU=="LP":
            SUName ="Plinthic Luvisols"
 else:
            SUName ="Vertic Luvisols"
if SU.startswith("M"):
 MSU ="M"
 MSUName ="Greyzems"
 if SU=="MG":
            SUName ="Gleyic Greyzems"
 else:
            SUName ="Orthic Greyzems"
if SU.startswith("N"):
 MSU ="N"
 MSUName ="Nitosols"
 if SU=="NE":
            SUName ="Eutric Nitosols"
 elif SU=="NH":
            SUName ="Humic Nitosols"
 else:
            SUName ="Dystric Nitosols"
if SU.startswith("O"):
 MSU ="O"
 MSUName ="Histosols"
 if SU=="OD":
            SUName ="Dystric Histosols"
 elif SU=="OE":
            SUName ="Eutric Histosols"
 else:
            SUName ="Gelic Histosols"
if SU.startswith("P"):
 MSU ="P"
```

```
 MSUName ="Podzols"
 if SU=="PF":
            SUName ="Ferric Podzols"
 elif SU=="PH":
            SUName ="Humic Podzols"
 elif SU=="PL":
            SUName ="Leptiv Podzols"
 elif SU=="PG":
            SUName ="Gleyic Podzols"
 elif SU=="PO":
            SUName ="Orthic Podzols"
 else:
            SUName ="Placic Podzols"
if SU.startswith("Q"):
 MSU ="Q"
 MSUName ="Arenosols"
 if SU=="QA":
            SUName ="Albic Arenosols"
 elif SU=="QC":
            SUName ="Cambic Arenosols"
 elif SU=="QF":
            SUName ="Ferra1ic Arenosols"
 else:
            SUName ="Luvic Arenosols"
if SU.startswith("R"):
 MSU ="R"
 MSUName ="Regosols"
 if SU=="RC":
            SUName ="Calcaric Regosols"
 elif SU=="RD":
            SUName ="Dystic Regosols"
 elif SU=="RE":
            SUName ="Eutric Regosols"
 else:
            SUName ="Gelic Regosols"
if SU.startswith("S"):
 MSU ="S"
 MSUName ="Solonetz"
 if SU=="SG":
            SUName ="Gleyic Solonetz"
 elif SU=="SM":
            SUName ="Mollic Solonetz"
 else:
            SUName ="Orthic Solonetz"
if SU.startswith("T"):
 MSU ="T"
 MSUName ="Andosols"
 if SU=="TH":
            SUName ="Humic Andosols"
 elif SU=="TM":
            SUName ="Mollic Andosols"
 elif SU=="TO":
```

```
            SUName ="Ochric Andosols"
 else:
            SUName ="Vitric Andosols"
if SU.startswith("U"):
 MSU ="U"
 MSUName ="Rankers"
   SUName = "Not Applicable"
if SU.startswith("V"):
 MSU ="V"
 MSUName ="Vertisols"
 if SU=="VC":
            SUName ="Chromic Vertisols"
 else:
            SUName ="Pellic Vertisols"
if SU.startswith("W"):
 MSU ="W"
 MSUName ="Planosols"
 if SU=="WD":
            SUName ="Dystric Planosols"
 elif SU=="WE":
            SUName ="Eutric Planosols"
 elif SU=="WH":
            SUName ="Humic Planosols"
 elif SU=="WM":
            SUName ="Mollie Planosols"
 elif SU=="WS":
            SUName ="Solodic Planosols"
 else:
            SUName ="Oe1ic Planosols"
if SU.startswith("X"):
 MSU ="X"
 MSUName ="Xerosols"
 if SU=="XH":
            SUName ="Haplic Xerosols"
 elif SU=="XK":
            SUName ="Calcic Xerosols"
 elif SU=="XL":
            SUName ="Luvic Xerosols"
 else:
            SUName ="Gypsic Xerosols"
if SU.startswith("Y"):
 MSU ="Y"
 MSUName ="Yermosols"
 if SU=="YH":
            SUName ="Haplic Yermosols"
 elif SU=="YK":
            SUName ="Calcic Yermosols"
 elif SU=="YL":
            SUName ="Luvic Yermosols"
 elif SU=="YT":
            SUName ="Takyric Yermosols"
 else:
```

```
                SUName ="Gypsic Yermosols"
         if SU.startswith("Z"):
          MSU ="Z"
          MSUName ="Solonchaks"
          if SU=="ZG":
                SUName ="Gleyic Solonchaks"
          elif SU=="ZM":
                SUName ="Mollic Solonchaks"
          elif SU=="ZO":
                SUName ="Orthic Solonchaks"
          else:
                SUName ="Takyric Solonchaks"

      elif SU=="":
         SU = "Land Ice"
         SUName = "Land Ice"
         MSU = "Land Ice"
         MSUName = "Land Ice"
      elif a[z].isalpha() and z==3 and len(a[z])!=3:
         SubSID = a[z]
         if SubSID == "":
            SubSID = "None"
      elif a[z].isalpha() and len(a[z])==3:
         Area=a[z]
         if Area=="AUS":
            AreaName = "Australia & South pacific"
         if Area=="SAM":
          AreaName = "South America"
         if Area=="AFR":
          AreaName = "Africa"
         if Area=="EUR":
          AreaName = "Europe"
         if Area=="NAM":
          AreaName = "North America"
         if Area=="NCA":
          AreaName = "North Central Asia"
         if Area=="SAS":
          AreaName = "Southern Asia"
         if Area=="SEA":
          AreaName = "South East Asia"
      else:
         pass
      z=z+1
   newline                                                                                  =
Lat+","+Long+","+MSU+","+MSUName+","+SU+","+SUName+","+SubSID+","+Area+","+AreaNa
me+"\n"
   fout.write(newline)
fin.close()
fout.close()
```

Export A2Z.py

```
#-------------------------------------------------------------------------------
# Name:        ExportA2Z.py
# Purpose:
#
# Author:      Arghya Goswami
# Cotact:      arghya.goswami@gmail.com
# History:
#
# Reference:
#
# Credits:
#
# Created:     5/28/2011 2:46:12 PM (Month/Day/Year)
#
# Modified:
#
# Copyright:   (c) Arghya Goswami 05/2011
#
# Licence:     This program is free software; you can redistribute it and/or
#              modify it under the terms of the GNU General Public License,
#              version 2, as published by the Free Software Foundation.
#
#              This program is distributed in the hope that it will be useful,
#              but WITHOUT ANY WARRANTY; without even the implied warranty of
#              MERCHANTABILITY or FITNESS FOR A PARTICULAR PURPOSE.  See the
#              GNU General Public License for more details.
#
#              You should have received a copy of the GNU General Public License
#              along with this program; if not, write to:
#
#              Free Software Foundation, Inc.,
#              51 Franklin St, Fifth Floor,
#              Boston, MA, 02110-1301  USA
#
#-------------------------------------------------------------------------------
#!/usr/bin/env python

#-------------------------------------------------------------------------------
# Create the Geoprocessor object
#-------------------------------------------------------------------------------

try:
   # Version ArcGIS 9.2
   import arcgisscripting, sets, sys, os, glob, time, fileinput, string, Tkinter, tkFileDialog
   from Tkinter import *
   gp = arcgisscripting.create()

except:
   # Version ArcGIS 9.1
   import win32com.client, sets, sys, os, glob, time, fileinput, string, Tkinter, tkFileDialog
   from Tkinter import *
```

```
    from win32com.client import Dispatch
    gp = win32com.client.Dispatch("esriGeoprocessing.GPDispatch.1")

StartTime = time.asctime(time.localtime(time.time()))
print "Start Time: ", StartTime

#---------------------------------------------------------------------------
# Definitions used in this Script
#---------------------------------------------------------------------------
def BrowseFile(msg1,indir):
    #Creating Main Window
    root = Tk()
    # Creating Secondary Window for File Browsing
    filename = tkFileDialog.askopenfilename(filetypes = [('Shapefiles','*.shp'),('All files','*')], title =
msg1, initialdir = indir)
    # Close the Main Window
    root.withdraw()
    # Return Filename
    return filename

def BrowseDir(msg2,indir):
    #Creating Main Window
    root = Tk()
    # Creating Secondary Window for Folder Browsing
    dirname = tkFileDialog.askdirectory(title = msg2, initialdir=indir)
    # Close the Main Window
    root.withdraw()
    # Return Dirname
    return dirname

#---------------------------------------------------------------------------
# Main Script
#---------------------------------------------------------------------------

msg1 = "Please browse to select the Input Shapefile"
inFC = BrowseFile(msg1, "D:\\Thesis\\")

print "Selected Shapeile is ", inFC, "\n"

inFCFile = os.path.basename(inFC)
inFCFolder = inFC.replace(inFCFile,"")
##inFCFolder = inFCFolder.replace(".shp","")

# Make a Feature Layer
try:
    t = t + 1
except:
    t = 0

FL = "FL" + str(t)
gp.MakeFeatureLayer(inFC,FL)
```

```
# Do the Work Here.....in loop
MSU = ["A","B","C","D","F","G","H","J","K","L","M","N","O","P","Q","R","S","T","V","W","X","Y","Z"]
for items in MSU:
    # Create Output File Name
    if "Pseudo" in inFCFolder:
        OutF = inFCFolder + "Pseudo " + items + ".shp"
    else:
        OutF = inFCFolder + items + ".shp"

    # Select By Attribute
    exp = "\"MSU\"='" + items + "'"
    gp.SelectLayerByAttribute_management (FL, "NEW_SELECTION", exp)

    # Copy the selected features to the output file
    gp.CopyFeatures_management (FL, OutF)

    print OutF, " created.....\n"

PS = [["B","G"],["C","D","M"],["F","N"],["K","S"],["O","P"],["Q","V"],["X","Y","Z"]]
for items in PS:
    x = ""
    for item in items:
        if x == "":
            x = item
        else:
            x = x + item

    # Create Output File Name
    if "Pseudo" in inFCFolder:
        OutF = inFCFolder + "Pseudo " + x + ".shp"
    else:
        OutF = inFCFolder + x + ".shp"

    # Select By Attribute
    exp = ""
    for item in items:
        if exp == "":
            exp = "\"MSU\"='" + item + "'"
        else:
            exp = exp + " OR " + "\"MSU\"='" + item + "'"

    gp.SelectLayerByAttribute_management (FL, "NEW_SELECTION", exp)

    # Copy the selected features to the output file
    gp.CopyFeatures_management (FL, OutF)

    print OutF, " created.....\n"

EndTime = time.asctime(time.localtime(time.time()))
print "End Time: ", EndTime
```

LEAGATES WILLMOTT NETCDF TO CSV.PY

```
# Import Statement
import sys, os, glob, time, fileinput, string, array

# Define Binary to ASCII Function
def BIN2ASCII(BINfile):
    columns = rows = count = 0
    f = open(BINfile, "rb")                    # Open in binary mode for portability

    # Output File to save (it will be saved in the same folder where the input file is)
    BINflist = BINfile.split(".")
    BINf = BINflist[0].split("\\")
    lenBINf = len(BINf)
    BINfolder = ""
    c = 0
    while c < (lenBINf-2):
        BINfolder = BINfolder + BINf[c] + "/"
        c = c+1

    #Check if required "ASCII" folders exixts
    a=BINfolder+"ASCII"
    if os.path.exists(a):
        pass
    else:
        os.mkdir(a)
        print a, "created"

    # Creating ASCII File Names from the input filename
    temp1 = BINf[lenBINf-1].replace("_","")
    outfile = a+ "/" + temp1+ ".txt"

    # Open Output File for Writing
    o = open(outfile,"w")
    a = array.array('h')
    columns = 720                              #raw_input("Please enter column numbers: ")
    rows = 360                                 #raw_input("Please enter row numbers: ")
    count = int(columns)*int(rows)
    a.fromfile(f,count)

    x = 0
    latitude = 90
    longitude = -180
    header = "lat,long,"+ temp1 + "\n"
    o.write(header)
    while x < count:
        while latitude > -90:
            while longitude < 180:
                if int(latitude)==latitude:
                    if int(longitude)==longitude:
                        o.write(str(latitude)+ ","+ str(longitude)+ "," + str(a[x])+"\n")
                longitude = longitude + 0.5
```

```
            x = x+1
        longitude = -180
        latitude = latitude - 0.5

    # Success Message
    print outfile, "Created"

    # Close input and output files
    o.close
    f.close

# Create a list of files for batch operation
root = raw_input("Please enter the folder location with ASCII Files:") # one specific folder
filelist = []

# select the type of file, for instance *.jpg or all files *.*
for folder in glob.glob(root):
    pass
    print "Files in", folder, "is being populated to a list.\n"

for file in glob.glob(folder + '/*.*'):

    filelist.append(file)

print "\nFile List Prepared, starting \"Binary to ASCII\" file engine....."

for items in filelist:
        BIN2ASCII(items)

print "\nASCII Files Prepared, closing \"Binary to ASCII\" file engine....."
```

LW Binary IMG 2 ASCII Text 0.5x0.5 GRID.py

```
#---------------------------------------------------------------------------
# Create the Geoprocessor object
#---------------------------------------------------------------------------

try:
   # Version ArcGIS 9.2
   import arcgisscripting, sets, sys, os, glob, time, fileinput, string, Tkinter, tkFileDialog, array
   from Tkinter import *
   gp = arcgisscripting.create()

except:
   # Version ArcGIS 9.1
   import win32com.client, sets, sys, os, glob, time, fileinput, string, Tkinter, tkFileDialog, array
   from Tkinter import *
   from win32com.client import Dispatch
   gp = win32com.client.Dispatch("esriGeoprocessing.GPDispatch.1")

StartTime = time.asctime(time.localtime(time.time()))
print "Start Time: ", StartTime

#---------------------------------------------------------------------------
# Definitions used in this Script
#---------------------------------------------------------------------------
def BrowseDir(msg2,indir):
   #Creating Main Window
   root = Tk()
   # Creating Secondary Window for Folder Browsing
   dirname = tkFileDialog.askdirectory(title = msg2, initialdir=indir)
   # Close the Main Window
   root.withdraw()
   # Return Dirname
   return dirname

def BIN2ASCII(BINfile):
##BINfile ="H:\\Dump\\1TB\\LW\\LWData\\lwmpr00.img"
   columns =0
   rows =0
   count = 0
   f = open(BINfile, "rb")  # Open in binary mode for portability
   # Output File to save (it will be saved in the same folder where the input file is)
   BINflist = BINfile.split(".")
   BINf = BINflist[0].split("/")
   lenBINf = len(BINf)
   BINfolder = ""
   c = 0
   while c < (lenBINf-2):
      BINfolder = BINfolder + BINf[c] + "/"
      c = c+1

   #Check if required "ASCII" folders exixts
   a=BINfolder+"ASCII"
```

```
    if os.path.exists(a):
        pass
    ##      print "ASCII Folder exits"
    else:
        os.mkdir(a)
        print a, "created"

    # Creating ASCII File Names from the input filename
    temp1 = BINf[lenBINf-1].replace("_","")
    outfile = a+ "/" + temp1+ ".txt"

    o = open(outfile,"w")
    a = array.array('h')
    columns = 720 #raw_input("Please enter column numbers: ")
    rows = 360 #raw_input("Please enter row numbers: ")
    count = int(columns)*int(rows)
    a.fromfile(f,count)
    x = 0
    latitude = 90.0
    longitude = -180.0
    line = "Latitude,Longitude," + (BINf[lenBINf-1].replace(".img","")).upper() + "\n"
##    print line
    o.write(line)
    while x < count:
        while latitude > -90.0:
            while longitude < 180.0:
##                print str(latitude),",",str(longitude),",",str(a[x]),"\n"
                o.write(str(latitude)+ ","+ str(longitude)+ "," + str(a[x])+"\n")
                longitude = longitude + 0.5
                x = x+1
            longitude = -180
            latitude = latitude - 0.5
    print outfile, "Created"
    o.close
    f.close

root = BrowseDir("Please enter the folder location with ASCII Files:","D:\\") # one specific folder
filelist = []

# select the type of file, for instance *.jpg or all files *.*
for folder in glob.glob(root):
    pass
    print "Files in", folder, "is being populated to a list.\n"

for file in glob.glob(folder + '/*.*'):

    # retrieves the stats for the current file as a tuple
    # (mode, ino, dev, nlink, uid, gid, size, atime, mtime, ctime)
    # the tuple element mtime at index 8 is the last-modified-date
    filelist.append(file)

print "\nFile List Prepared, starting \"Binary to ASCII\" file engine....."
```

```
for items in filelist:
    items = items.replace("\\","/")
    BIN2ASCII(items)

print "\nASCII Files Prepared, closing \"Binary to ASCII\" file engine....."
```

LW All ASCII Join.py

```
#---------------------------------------------------------------------------
# Create the Geoprocessor object
#---------------------------------------------------------------------------

try:
   # Version ArcGIS 9.2
   import arcgisscripting, sets, sys, os, glob, time, fileinput, string, Tkinter, tkFileDialog
   from Tkinter import *
   gp = arcgisscripting.create()

except:
   # Version ArcGIS 9.1
   import win32com.client, sets, sys, os, glob, time, fileinput, string, Tkinter, tkFileDialog
   from Tkinter import *
   from win32com.client import Dispatch
   gp = win32com.client.Dispatch("esriGeoprocessing.GPDispatch.1")

StartTime = time.asctime(time.localtime(time.time()))
print "Start Time: ", StartTime

#---------------------------------------------------------------------------
# Definitions used in this Script
#---------------------------------------------------------------------------
def BrowseFile(msg1,indir):
   #Creating Main Window
   root = Tk()
   # Creating Secondary Window for File Browsing
   filename = tkFileDialog.askopenfilename(filetypes = [('CSV Files','*.csv'),('All files','*')], title =
msg1, initialdir = indir)
   # Close the Main Window
   root.withdraw()
   # Return Filename
   return filename

def BrowseDir(msg2,indir):
   #Creating Main Window
   root = Tk()
   # Creating Secondary Window for Folder Browsing
   dirname = tkFileDialog.askdirectory(title = msg2, initialdir=indir)
   # Close the Main Window
   root.withdraw()
   # Return Dirname
   return dirname

#---------------------------------------------------------------------------
# Main Script
#---------------------------------------------------------------------------

root = BrowseDir("Please enter the folder location with ASCII Text Files:","D:\\Thesis\\") # one
specific folder
root = root + "/"
```

```
filelist = []

# select the type of file, for instance *.jpg or all files *.*
for folder in glob.glob(root):
    pass
    print "Files in", folder, "is being populated to a list.\n"

for file in glob.glob(folder + '/*.txt'):

    # retrieves the stats for the current file as a tuple
    # (mode, ino, dev, nlink, uid, gid, size, atime, mtime, ctime)
    # the tuple element mtime at index 8 is the last-modified-date
    filelist.append(file)

print "File List Prepared, working now to merge the data in these files.....\n"

l = len(filelist)
h = 259201    # 0.5x0.5 GRID has 259200 points + header
w = l + 2     # Lat,Long,and no of files

lw = []

for i in range(h):
    row = []
    for j in range(w):
        row.append("N")
    lw.append(row)

fno = 1
j = 0
for items in filelist:
    ftxt = ""
    items = items.replace("\\","/")
    print "Processing ", items, ".....\n"
    f = open(items,'r')
    ftxt = f.readlines()
    f.close()
    i = 0
    for lines in ftxt:
        line = lines.replace("\n","")
        values = line.split(",")
        if fno == 1:
            lw[i][0] = values[1]
            lw[i][1] = values[0]
            lw[i][2] = values[2]
            j = 2
        else:
            lw[i][j] = values[2]
        i = i + 1
    j = j + 1
    fno = fno + 1
```

```
print "Writing Output File.....\n"
outF = root + "LW.csv"
fw = open(outF,'w')
for i in range(h):
    line = ""
    for j in range(w):
        if line == "":
            line = lw[i][j]
        else:
            line = line + "," + lw[i][j]
    line = line + "\n"
    fw.write(line)

fw.close()

EndTime = time.asctime(time.localtime(time.time()))
print "End Time: ", EndTime
```

LW InfoSummary.py

```
#---------------------------------------------------------------------------
# Create the Geoprocessor object
#---------------------------------------------------------------------------

try:
   # Version ArcGIS 9.2
   import arcgisscripting, sets, sys, os, glob, time, fileinput, string, Tkinter, tkFileDialog
   from Tkinter import *
   gp = arcgisscripting.create()

except:
   # Version ArcGIS 9.1
   import win32com.client, sets, sys, os, glob, time, fileinput, string, Tkinter, tkFileDialog
   from Tkinter import *
   from win32com.client import Dispatch
   gp = win32com.client.Dispatch("esriGeoprocessing.GPDispatch.1")

StartTime = time.asctime(time.localtime(time.time()))
print "Start Time: ", StartTime

#---------------------------------------------------------------------------
# Definitions used in this Script
#---------------------------------------------------------------------------
def BrowseFile(msg1,indir):
   #Creating Main Window
   root = Tk()
   # Creating Secondary Window for File Browsing
   filename = tkFileDialog.askopenfilename(filetypes = [('MSWord Files','*.doc'),('All files','*')],
title = msg1, initialdir = indir)
   # Close the Main Window
   root.withdraw()
   # Return Filename
   return filename

def BrowseDir(msg2,indir):
   #Creating Main Window
   root = Tk()
   # Creating Secondary Window for Folder Browsing
   dirname = tkFileDialog.askdirectory(title = msg2, initialdir=indir)
   # Close the Main Window
   root.withdraw()
   # Return Dirname
   return dirname

#---------------------------------------------------------------------------
# Main Script
#---------------------------------------------------------------------------
msg1 = "Please select the Input Folder"
root = BrowseDir(msg1,"D:\\Thesis\\")
if root.endswith("/"):
   pass
```

```
else:
    root = root + "/"

filelist = []

# select the type of file, for instance *.jpg or all files *.*
for folder in glob.glob(root):
    pass
    print "Files in", folder, "is being populated to a list.\n"

for file in glob.glob(folder + '/*.doc'):

    # retrieves the stats for the current file as a tuple
    # (mode, ino, dev, nlink, uid, gid, size, atime, mtime, ctime)
    # the tuple element mtime at index 8 is the last-modified-date
    filelist.append(file)

print "File List Prepared, working now to merge the data in these files.....\n"

info = []
l = len(filelist)
h = l+1
w = 4
for i in range(h):
    row = []
    for j in range(w):
        if i == 0:
            if j == 0:
                row.append("Name")
            elif j == 1:
                row.append("Min")
            elif j == 2:
                row.append("Max")
            else:
                row.append("ValueUnit")
        else:
            row.append("x")
    info.append(row)

##print info

i = 1
for items in filelist:
    items = items.replace("\\","/")
    j = 0
    info[i][j] = (os.path.basename(items)).split(".")[0]
    f = open(items,'r')
    ftxt = f.readlines()
    lno = 1
    for lines in ftxt:
        if lno == 15:
            j = j + 1
```

```
            info[i][j] = ((lines.split(":")[1]).lstrip()).replace("\n","")
        if lno == 16:
            j = j + 1
            info[i][j] = ((lines.split(":")[1]).lstrip()).replace("\n","")
        if lno == 17:
            j = j + 1
            info[i][j] = ((lines.split(":")[1]).lstrip()).replace("\n","")
        lno = lno + 1
##    print info
    i = i + 1

print "Writing Output File.....\n"
outF = root + "Info.csv"
fw = open(outF,'w')
for i in range(h):
    line = ""
    for j in range(w):
        if line == "":
            line = info[i][j]
        else:
            line = line + "," + info[i][j]
    line = line + "\n"
    fw.write(line)

fw.close()

EndTime = time.asctime(time.localtime(time.time()))
print "End Time: ", EndTime
```

LW Calculate Seasons.py

```
#---------------------------------------------------------------------------
# Create the Geoprocessor object
#---------------------------------------------------------------------------

try:
   # Version ArcGIS 9.2
   import arcgisscripting, sets, sys, os, glob, time, fileinput, string, Tkinter, tkFileDialog
   from Tkinter import *
   gp = arcgisscripting.create()

except:
   # Version ArcGIS 9.1
   import win32com.client, sets, sys, os, glob, time, fileinput, string, Tkinter, tkFileDialog
   from Tkinter import *
   from win32com.client import Dispatch
   gp = win32com.client.Dispatch("esriGeoprocessing.GPDispatch.1")

StartTime = time.asctime(time.localtime(time.time()))
print "Start Time: ", StartTime

#---------------------------------------------------------------------------
# Definitions used in this Script
#---------------------------------------------------------------------------
def BrowseFile(msg1,indir):
   #Creating Main Window
   root = Tk()
   # Creating Secondary Window for File Browsing
   filename = tkFileDialog.askopenfilename(filetypes = [('All files','*')], title = msg1, initialdir =
indir)
   # Close the Main Window
   root.withdraw()
   # Return Filename
   return filename

def BrowseDir(msg2,indir):
   #Creating Main Window
   root = Tk()
   # Creating Secondary Window for Folder Browsing
   dirname = tkFileDialog.askdirectory(title = msg2, initialdir=indir)
   # Close the Main Window
   root.withdraw()
   # Return Dirname
   return dirname

#---------------------------------------------------------------------------
# Main Script
#---------------------------------------------------------------------------

msg1 = "Please select the Input CSV File"
InFc = BrowseFile(msg1,"D:\\Thesis\\")
OutFc = InFc.replace(".csv"," V2.csv")
```

```
# read source file
fr = open(InFc,'r')
frtxt  = fr.readlines()
fr.close()

# Open output file
fw = open(OutFc,'w')

# Scroll though source text line by line
lno = 1
for lines in frtxt:
    if lno == 1:

        # Header
        line                                                                                           =
"Longitude,Latitude,LWMPR01,LWMPR02,LWMPR03,LWMPR04,LWMPR05,LWMPR06,LWM
PR07,LWMPR08,LWMPR09,LWMPR10,LWMPR11,LWMPR12,AvgMPRWin,AveMPRSpr,Avg
MPRSum,AvgMPRFal,AvgMPRAnn,LWMPR00,LWTMP01,LWTMP02,LWTMP03,LWTMP04,L
WTMP05,LWTMP06,LWTMP07,LWTMP08,LWTMP09,LWTMP10,LWTMP11,LWTMP12,AvgT
MPWin,AvgTMPSpr,AvgTMPSum,AvgTMPFal,AvgTMPAnn,LWTMP00\n"

    else:

        # Define Seasons and Annual Variables
        AvgMPRWin = 0.0
        AveMPRSpr = 0.0
        AvgMPRSum = 0.0
        AvgMPRFal = 0.0
        AvgMPRAnn = 0.0
        AvgTMPWin = 0.0
        AvgTMPSpr = 0.0
        AvgTMPSum = 0.0
        AvgTMPFal = 0.0
        AvgTMPAnn = 0.0


        # Get the individual monthly values
        vals = lines.split(",")

        # calculate seasonal and annual values
        AvgMPRWin = (int(vals[14])+int(vals[3])+int(vals[4]))/3
        AveMPRSpr = (int(vals[5])+int(vals[6])+int(vals[7]))/3
        AvgMPRSum = (int(vals[8])+int(vals[9])+int(vals[10]))/3
        AvgMPRFal = (int(vals[11])+int(vals[12])+int(vals[13]))/3
        AvgMPRAnn                                                                                      =
(int(vals[3])+int(vals[4])+int(vals[5])+int(vals[6])+int(vals[7])+int(vals[8])+int(vals[9])+int(vals[10])+
int(vals[11])+int(vals[12])+int(vals[13])+int(vals[14]))/12
        AvgTMPWin = (int(vals[27])+int(vals[16])+int(vals[17]))/3
        AvgTMPSpr = (int(vals[18])+int(vals[19])+int(vals[20]))/3
        AvgTMPSum = (int(vals[21])+int(vals[22])+int(vals[23]))/3
        AvgTMPFal = (int(vals[24])+int(vals[25])+int(vals[26]))/3
```

```
        AvgTMPAnn                                                                                    =
(int(vals[16])+int(vals[17])+int(vals[18])+int(vals[19])+int(vals[20])+int(vals[21])+int(vals[22])+int(
vals[23])+int(vals[24])+int(vals[25])+int(vals[26])+int(vals[27]))/12
        # create new line
        line = str(float(vals[0])) + "," + str(float(vals[1])) + "," + str(int(vals[3])) + "," + str(int(vals[4]))
+ "," + str(int(vals[5])) + "," + str(int(vals[6])) + "," + str(int(vals[7])) + "," + str(int(vals[8])) + "," +
str(int(vals[9])) + "," + str(int(vals[10])) + "," + str(int(vals[11])) + "," + str(int(vals[12])) + "," +
str(int(vals[13])) + "," + str(int(vals[14])) + "," + str(AvgMPRWin) + "," + str(AveMPRSpr) + "," +
str(AvgMPRSum) + "," + str(AvgMPRFal) + "," + str(AvgMPRAnn) + "," + str(int(vals[2])) + "," +
str(int(vals[16])) + "," + str(int(vals[17])) + "," + str(int(vals[18])) + "," + str(int(vals[19])) + "," +
str(int(vals[20])) + "," + str(int(vals[21])) + "," + str(int(vals[22])) + "," + str(int(vals[23])) + "," +
str(int(vals[24])) + "," + str(int(vals[25])) + "," + str(int(vals[26])) + "," + str(int(vals[27])) + "," +
str(AvgTMPWin) + "," + str(AvgTMPSpr) + "," + str(AvgTMPSum) + "," + str(AvgTMPFal) + "," +
str(AvgTMPAnn) + "," + str(int(vals[15])) + "\n"
    fw.write(line)
    lno = lno + 1

fw.close()

EndTime = time.asctime(time.localtime(time.time()))
print "End Time: ", EndTime
```

LW 1x1 GRID.py

```
#---------------------------------------------------------------------------
# Create the Geoprocessor object
#---------------------------------------------------------------------------

try:
   # Version ArcGIS 9.2
   import arcgisscripting, sets, sys, os, glob, time, fileinput, string, Tkinter, tkFileDialog
   from Tkinter import *
   gp = arcgisscripting.create()

except:
   # Version ArcGIS 9.1
   import win32com.client, sets, sys, os, glob, time, fileinput, string, Tkinter, tkFileDialog
   from Tkinter import *
   from win32com.client import Dispatch
   gp = win32com.client.Dispatch("esriGeoprocessing.GPDispatch.1")

StartTime = time.asctime(time.localtime(time.time()))
print "Start Time: ", StartTime

#---------------------------------------------------------------------------
# Definitions used in this Script
#---------------------------------------------------------------------------
def BrowseFile(msg1,indir):
   #Creating Main Window
   root = Tk()
   # Creating Secondary Window for File Browsing
   filename = tkFileDialog.askopenfilename(filetypes = [('All files','*')], title = msg1, initialdir =
indir)
   # Close the Main Window
   root.withdraw()
   # Return Filename
   return filename

def BrowseDir(msg2,indir):
   #Creating Main Window
   root = Tk()
   # Creating Secondary Window for Folder Browsing
   dirname = tkFileDialog.askdirectory(title = msg2, initialdir=indir)
   # Close the Main Window
   root.withdraw()
   # Return Dirname
   return dirname

#---------------------------------------------------------------------------
# Main Script
#---------------------------------------------------------------------------

msg1 = "Please select the Input CSV File"
InFc = BrowseFile(msg1,"D:\\Thesis\\")
OutFc = InFc.replace(".csv"," 1x1 GRID.csv")
```

```
# read source file
fr = open(InFc,'r')
frtxt  = fr.readlines()
fr.close()

# Open output file
fw = open(OutFc,'w')

# Scroll though source text line by line
lno = 1
for lines in frtxt:
    if lno == 1:
        fw.write(lines)
    else:
        vals = []
        # Get the individual monthly values
        vals = lines.split(",")
        Long = float(vals[0])
        Lat = float(vals[1])
        if (Long % 1) == 0 and (Lat % 1) == 0:
            fw.write(lines)
    lno = lno + 1

fw.close()

EndTime = time.asctime(time.localtime(time.time()))
print "End Time: ", EndTime
```

KG Update.py

```
try:
    # Version ArcGIS 9.2
    import arcgisscripting, sys, os, glob, time, fileinput, string
    gp = arcgisscripting.create()

except:
    # Version ArcGIS 9.1
    import win32com.client, sys, os, glob, time, fileinput, string
    from win32com.client import Dispatch
    gp = win32com.client.Dispatch("esriGeoprocessing.GPDispatch.1")

inFC = "C:\\Documents and Settings\\Goswami\\Desktop\\Koeppen-Geiger-GIS\\koeppen-geiger.shp"
# Create update cursor for feature class
rows = gp.UpdateCursor(inFC)
row = rows.Next()
# Update the field used in buffer so the distance is based on the road
# type. Road type is either 1, 2, 3 or 4. Distance is in meters.
while row:
    if row.GRIDCODE == 11:
        row.KG_Codes = "Af"
    elif row.GRIDCODE == 12 :
        row.KG_Codes = "Am"
    elif row.GRIDCODE == 13 :
        row.KG_Codes = "As"
    elif row.GRIDCODE == 14 :
        row.KG_Codes = "Aw"
    elif row.GRIDCODE == 21 :
        row.KG_Codes = "BWk"
    elif row.GRIDCODE == 22 :
        row.KG_Codes = "BWh"
    elif row.GRIDCODE == 26 :
        row.KG_Codes = "BSk"
    elif row.GRIDCODE == 27 :
        row.KG_Codes = "BSh"
    elif row.GRIDCODE == 31 :
        row.KG_Codes = "Cfa"
    elif row.GRIDCODE == 32 :
        row.KG_Codes = "Cfb"
    elif row.GRIDCODE == 33 :
        row.KG_Codes = "Cfc"
    elif row.GRIDCODE == 34 :
        row.KG_Codes = "Csa"
    elif row.GRIDCODE == 35 :
        row.KG_Codes = "Csb"
    elif row.GRIDCODE == 36 :
        row.KG_Codes = "Csc"
    elif row.GRIDCODE == 37 :
        row.KG_Codes = "Cwa"
    elif row.GRIDCODE == 38 :
        row.KG_Codes = "Cwb"
```

```
    elif row.GRIDCODE == 39 :
        row.KG_Codes = "Cwc"
    elif row.GRIDCODE == 41 :
        row.KG_Codes = "Dfa"
    elif row.GRIDCODE == 42 :
        row.KG_Codes = "Dfb"
    elif row.GRIDCODE == 43 :
        row.KG_Codes = "Dfc"
    elif row.GRIDCODE == 44 :
        row.KG_Codes = "Dfd"
    elif row.GRIDCODE == 45 :
        row.KG_Codes = "Dsa"
    elif row.GRIDCODE == 46 :
        row.KG_Codes = "Dsb"
    elif row.GRIDCODE == 47 :
        row.KG_Codes = "Dsc"
    elif row.GRIDCODE == 48 :
        row.KG_Codes = "Dsd"
    elif row.GRIDCODE == 49 :
        row.KG_Codes = "Dwa"
    elif row.GRIDCODE == 50 :
        row.KG_Codes = "Dwb"
    elif row.GRIDCODE == 51 :
        row.KG_Codes = "Dwc"
    elif row.GRIDCODE == 52 :
        row.KG_Codes = "Dwd"
    elif row.GRIDCODE == 61 :
        row.KG_Codes = "EF"
    elif row.GRIDCODE == 62 :
        row.KG_Codes = "ET"
    rows.UpdateRow(row)
    row = rows.next()

del row, rows

rows = gp.UpdateCursor(inFC)
row = rows.Next()
while row:
    if "W" in row.KG_Codes:
        row.Precipitat = "Desert"
        row.Preci_Code = "W"
    if "S" in row.KG_Codes:
        row.Precipitat = "Steppe"
        row.Preci_Code = "S"
    if "f" in row.KG_Codes:
        row.Precipitat = "Fully Humid"
        row.Preci_Code = "f"
    if "s" in row.KG_Codes:
        row.Precipitat = "Summer Dry"
        row.Preci_Code = "s"
    if "w" in row.KG_Codes:
        row.Precipitat = "Winter Dry"
```

```
            row.Preci_Code = "w"
        if "m" in row.KG_Codes:
            row.Precipitat = "Monsoonal"
            row.Preci_Code = "m"
        if "h" in row.KG_Codes:
            row.Temperatur = "Hot Arid"
            row.Temp_Code = "h"
        if "k" in row.KG_Codes:
            row.Temperatur = "Cold Arid"
            row.Temp_Code = "k"
        if "a" in row.KG_Codes:
            row.Temperatur = "Hot Summer"
            row.Temp_Code = "a"
        if "b" in row.KG_Codes:
            row.Temperatur = "Warm Summer"
            row.Temp_Code = "b"
        if "c" in row.KG_Codes:
            row.Temperatur = "Cool Summer"
            row.Temp_Code = "c"
        if "d" in row.KG_Codes:
            row.Temperatur = "Extremely Continental"
            row.Temp_Code = "d"
        if "F" in row.KG_Codes:
            row.Temperatur = "Polar Frost"
            row.Temp_Code = "F"
        if "T" in row.KG_Codes:
            row.Temperatur = "Polar Tundra"
            row.Temp_Code = "T"
        rows.UpdateRow(row)
        row = rows.next()

    del row, rows

    rows = gp.UpdateCursor(inFC)
    row = rows.Next()
    while row:
        if row.Precipitat != " " and row.Temperatur != " ":
            expression = row.MainClimat+" "+row.Precipitat+" "+row.Temperatur
        else:
            if row.Precipitat == " ":
                expression = row.MainClimat+" X "+row.Temperatur
            else:
                expression = row.MainClimat+" "+row.Precipitat+" X"
        row.KG_Class = expression
        rows.UpdateRow(row)
        row = rows.next()

    del row, rows
```

Shapefile to CSV.py

```
#---------------------------------------------------------------------------
# Create the Geoprocessor object
#---------------------------------------------------------------------------

try:
   # Version ArcGIS 9.2
   import arcgisscripting, sets, sys, os, glob, time, fileinput, string, Tkinter, tkFileDialog
   from Tkinter import *
   gp = arcgisscripting.create()

except:
   # Version ArcGIS 9.1
   import win32com.client, sets, sys, os, glob, time, fileinput, string, Tkinter, tkFileDialog
   from Tkinter import *
   from win32com.client import Dispatch
   gp = win32com.client.Dispatch("esriGeoprocessing.GPDispatch.1")

StartTime = time.asctime(time.localtime(time.time()))
print "Start Time: ", StartTime

#---------------------------------------------------------------------------
# Definitions used in this Script
#---------------------------------------------------------------------------
def BrowseFile(msg1,indir):
   #Creating Main Window
   root = Tk()
   # Creating Secondary Window for File Browsing
   filename = tkFileDialog.askopenfilename(filetypes = [('Shapefiles','*.shp'),('All files','*')], title =
msg1, initialdir = indir)
   # Close the Main Window
   root.withdraw()
   # Return Filename
   return filename

def BrowseDir(msg2,indir):
   #Creating Main Window
   root = Tk()
   # Creating Secondary Window for Folder Browsing
   dirname = tkFileDialog.askdirectory(title = msg2, initialdir=indir)
   # Close the Main Window
   root.withdraw()
   # Return Dirname
   return dirname

def shp2csv(item):
   inFC = item
   global aa
   if aa == "txt" or aa == ".txt":
      outFC = inFC.replace(".shp",".txt")
   elif aa == "csv" or aa == ".csv":
      outFC = inFC.replace(".shp",".csv")
```

```
    f=open(outFC,'w')
    fieldlist = []
    header = ""
    line = ""
    fc = 0
    l=0
    desc = gp.describe(inFC)
    fields = desc.fields
    field = fields.next()
    while field:
        if field.name == "FID" or field.name == "Shape": # or field.name == "Distance"
            pass
        else:
            fieldlist.append(field.name)
            fc = fc + 1
            if fc==1:
                header = field.name
            else:
                header = header + "," + field.name
        field = fields.next()
    header = header + "\n"

    f.write(header)
    l=len(fieldlist)
    rows = gp.SearchCursor(inFC)
    row = rows.Next()
    while row:
        c=0
        #value = getattr(obj, "attribute")
        while c<l:
            if c==0:
                xx = str(getattr(row, fieldlist[c]))+","
            elif c==(l-1):
                xx = xx + str(getattr(row, fieldlist[c]))+"\n"
            else:
                xx = xx + str(getattr(row, fieldlist[c]))+","
            c = c + 1

        line =xx
        f.write(line)
        line = ""
        row = rows.Next()

    del fields, field, rows, row
    print inFC, " converted to ", aa, "Comma Seperated File.\n"

root = BrowseDir("Please enter the folder location with ShapeFiles:","D:\\Thesis\\") # one
specific folder
filelist = []
# select the type of file, for instance *.jpg or all files *.*

for folder in glob.glob(root):
```

```
    print "Files in", folder, "is being populated to a list.\n"
    #raw_input()

for file in glob.glob(folder + '/*.shp'):

    # retrieves the stats for the current file as a tuple
    # (mode, ino, dev, nlink, uid, gid, size, atime, mtime, ctime)
    # the tuple element mtime at index 8 is the last-modified-date
    filelist.append(file)

print "\nFile List Prepared, starting conversion....."
aa = raw_input("What kind (.txt or .csv) of comma seperated file you want to create?")
for items in filelist:
    shp2csv(items)


EndTime = time.asctime(time.localtime(time.time()))
print "End Time: ", EndTime
```

CSV to Shapefile.py

```
# Create the Geoprocessor object
try:
   # Version ArcGIS 9.2
   import arcgisscripting, sys, os, glob, time, fileinput, string
   gp = arcgisscripting.create()

except:
   # Version ArcGIS 9.1
   import win32com.client, sys, os, glob, time, fileinput, string
   from win32com.client import Dispatch
   gp = win32com.client.Dispatch("esriGeoprocessing.GPDispatch.1")

# Load required toolboxes...
##gp.AddToolbox("C:\\Program Files\\ArcGIS\\ArcToolBox\\Toolboxes\\Data Management Tools.tbx")
##gp.AddToolbox("C:\\Program Files\\ArcGIS\\ArcToolBox\\Toolboxes\\Conversion Tools.tbx")

inX  = "Longitude"
inY = "Latitude"

batch = raw_input("Do you want to process multiple files: (Y/y or N/n)")
if batch == "Y" or batch == "y":
   inX = ""
   inY = ""
   r = 0
   def XY2Shp(item):
      global inX
      global inY
      csvname = item
      shpfilefullpath1 = csvname.replace(".txt",".shp")
      shpfilefullpath2 = csvname.replace("Misc","Shapefile")
      print "Processing ", csvname,"....\n"

      f = open(csvname,'r')
      fline=f.readline()
      f.close()

      try:
         t = t + 1
      except:
         t = 0

      out_Layer = "XYEventLayer" + str(t)
      if inX =="":
         xmsg = "Select X Field, also commonly known as Longitude. The present input file has following fields: "+fline.replace(",","," , ")
         in_x = raw_input(xmsg)#"Longitude"#"PLngmprAnn"
         aa = raw_input("Do you want this to be X input field for all rest files?(Y/y or N/n)")
         if aa=="Y" or aa=="y":
            inX = in_x
      else:
```

```
            in_x = inX

        if inY=="":
            ymsg = "Select Y Field, also commonly known as Latitude. The present input file has
following fields: "+fline.replace(","," , ")
            in_y = raw_input(ymsg)#"Latitude"#"PLattmpAnn"
            bb = raw_input("Do you want this to be Y input field for all rest files?(Y/y or N/n)")
            if bb=="Y" or bb=="y":
                inY = in_y
        else:
            in_y = inY


        spref = "Coordinate Systems\\Geographic Coordinate Systems\\World\\WGS 1984.prj"

        gp.MakeXYEventLayer(csvname, in_x, in_y, out_Layer, spref)
        shpfolder = ""
        a = shpfilefullpath2.split("\\")
        b = len(a)
        c = 0
        while c < (b-1):
            if c==0:
                shpfolder = a[c] + "\\"
            else:
                shpfolder = shpfolder + a[c] + "\\"
            c = c + 1
##      if "PLng" in in_x and "PLat" in in_y:
##          pshpfile = a[b-1].replace(".txt",".shp")
##      else:
##          pshpfile = a[b-1].replace(".txt",".shp")
        gp.FeatureclassToFeatureclass_conversion (out_Layer, pfolder, pshpfile)

        print pfolder,pshpfile, " processed.\n"

    root = raw_input("Please enter the folder location with csvfiles:") # one specific folder
    filelist = []
    # select the type of file, for instance *.jpg or all files *.*

    for folder in glob.glob(root):

        print "Files in", folder, "is being populated to a list.\n"
        #raw_input()
    ext = raw_input("Enter extension of your comma seperated value file (txt or csv):")
    if ext=="txt":
        for file in glob.glob(folder + '/*.txt'):
            filelist.append(file)
    else:
        for file in glob.glob(folder + '/*.csv'):
            filelist.append(file)

    print "\nFile List Prepared, starting  to create files.....\n"
```

```
    for items in filelist:
        XY2Shp(items,r)
        r = r+1

else:
    csvname = raw_input("Enter full path of the csv file")
    pshpfilefullpath = csvname.replace(".txt","_pseudo.shp")
    print "Processing ", csvname,"....\n"

    f = open(csvname,'r')
    fline=f.readline()
    f.close()
    try:
        t = t + 1
    except:
        t = 0
    out_Layer = "XYEventLayer" + str(t)
    xmsg = "Select X Field, also commonly known as Longitude. The present input file has
following fields: "+fline.replace(","," , ")
    in_x = raw_input(xmsg)
    ymsg = "Select Y Field, also commonly known as Latitude. The present input file has
following fields: "+fline.replace(","," , ")
    in_y = raw_input(ymsg)

    spref = "Coordinate Systems\\Geographic Coordinate Systems\\World\\WGS 1984.prj"

    gp.MakeXYEventLayer(csvname, in_x, in_y, out_Layer, spref)
    pfolder = ""
    a = pshpfilefullpath.split("\\")
    b = len(a)
    c = 0
    while c < (b-1):
        if c==0:
            pfolder = a[c] + "\\"
        else:
            pfolder = pfolder + a[c] + "\\"
        c = c + 1
    pshpfile = a[b-1].replace(".txt","_pseudo.shp")
    gp.FeatureclassToFeatureclass_conversion (out_Layer, pfolder, pshpfile)
    print pshpfilefullpath, "processed.\n"
```

PaleoDEM2Coastlines.py

```
# Create the Geoprocessor object
try:
   # Version ArcGIS 9.2
   import arcgisscripting, sys, os, glob, time, fileinput, string, Tkinter, tkFileDialog, Tkconstants
   from Tkinter import *
   gp = arcgisscripting.create()

except:
   # Version ArcGIS 9.1
   import win32com.client, sys, os, glob, time, fileinput, string, Tkinter, tkFileDialog, Tkconstants
   from win32com.client import Dispatch
   from Tkinter import *
   gp = win32com.client.Dispatch("esriGeoprocessing.GPDispatch.1")


# Check out any necessary licenses
print "Checking out any necessary licenses....."
gp.CheckOutExtension("spatial")

# Load required toolboxes...
print "Loading required toolboxes..."
##gp.AddToolbox("C:/Program Files/ArcGIS/ArcToolbox/Toolboxes/Spatial Analyst Tools.tbx")

# Declare Variables
inRaster = ""
MSL = []
where_clause=""
InExpression = ""
OutRaster = ""
outPolygon = ""
Coastline = ""
FL = ""

# Define input raster
# Find the file to work on

# Creating main Window
root = Tk()
root.title('Browse and select the PaleoDEM to work on')

# Creating secondary window for folder browsing
inRaster = tkFileDialog.askopenfilename()
inRaster = inRaster.replace(".aux","")
print "Processing ", inRaster, "\n"

# Close the main window
root.withdraw()

MSL  = [0, -500, -1000]
# ""GRIDCODE" = 1"
```

```
where_clause = "\"GRIDCODE\"=1"
where_clauseArea = "\"F_AREA\">= 1.0"
try:
   t = t+1
except:
   t = 0
for items in MSL:

   # Do a raster calculation based on sea level height (0m, -500m or -1000m)
   InExpression=inRaster+">"+str(items)
   OutRaster=inRaster.replace("paleodem","Calc")+"_"+str(items).replace("-","")+ "m"
   gp.SingleOutputMapAlgebra_sa(InExpression, OutRaster)
   print OutRaster, "created...\n"

   # Export the newly created raster calculation grid to a shapefile
   outPolygon = OutRaster + ".shp"
   gp.RasterToPolygon_conversion (OutRaster, outPolygon, "SIMPLIFY")
   print outPolygon, "Created...\n"

   # In the shapefile do a selection by attributes to get features with GRIDCODE 1
   t = t+1
   FL = "FeatureLayer" + str(t)
   gp.MakeFeatureLayer(outPolygon,FL)
   print "Featurelayer created...\n"
   gp.SelectLayerByAttribute_management (FL, "NEW_SELECTION", where_clause)
   print "Select by Attribute Complete...\n"

   # Export selected features to a new shapefile
   Coastline = outPolygon.replace("Calc","CoastLine")
   gp.CopyFeatures_management (FL, Coastline)
   print Coastline, "created....\n"

   # Calculate the area of each polygon in a new shapefile
   CoastlineV2 =Coastline.replace(".shp","V2.shp")
   gp.CalculateAreas_stats (Coastline, CoastlineV2)
   print "Area Calculated in", CoastlineV2, "\n"

   # Select the features with area at least = 1.0 (discarding very small tiny ones)
   # and export then to a new shapefile
   t= t+1
   FLArea ="FeatureLayer" + str(t)
   gp.MakeFeatureLayer(CoastlineV2,FLArea)
   print "Featurelayer created for area manipulation...\n"
   gp.SelectLayerByAttribute_management (FLArea, "NEW_SELECTION", where_clauseArea)
   print "Select by Attribute Complete...\n"
   CoastlineV3 =Coastline.replace(".shp","V3.shp")
   gp.CopyFeatures_management (FLArea, CoastlineV3)
   print Coastline, "created....\n"

   # Finally the multipart features are being exploded, this is the final output
   CoastlineV4 =Coastline.replace(".shp","Final.shp")
   gp.MultipartToSinglepart_management (CoastlineV3, CoastlineV4)
```

```
    print CoastlineV4, " created.\n"

    fieldlist = ""
    desc = gp.describe(CoastlineV4)
    fields = desc.fields
    field = fields.next()
    while field:
        if field.name == "FID" or field.name == "Shape" or field.name == "F_AREA":
            pass
        else:
            if fieldlist ==="":
                fieldlist= field.name
            else:
                fieldlist= fieldlist + ";" + field.name
        field = fields.next()
    print fieldlist
    gp.DeleteField(CoastlineV4, fieldlist)
    print CoastlineV4," cleaned.\n"

    # Delete the shapefiles created in between
    gp.Delete_management (CoastlineV2)
    gp.Delete_management (CoastlineV3)

print "All Coastlines are ready!"
```

APPENDIX B

PERCENT VOLUME CONTOUR

Introduction

Percent Volume contour (PVC) is the name of a free ArcGIS add-in that is available for free (http://www.spatialecology.com/htools/overview.php) called “Hawths Analysis Tool”. Using this tool instead of traditional density contour one can produce contour that represents contour lines representing the x% by volume contour (e.g. the 95% by volume contour).

This tool accepts an input raster layer representing a probability density distribution (e.g. a kernel density raster) and generates a set of percent volume contours as per user defined intervals as output. This tool requires an ESRI Spatial Analyst or 3D Analyst extension license and works with ArcGIS version 9x. Also, this tool can not handle large rasters (e.g. > 7000x7000 pixels) and outputs shapefiles only (no other vector formats are currently supported) as of when this document was created.

A ‘percent volume contour’ (PVC) is not the same as the simple contours that are typically produced in tools like Spatial Analyst. A percent volume contour represents the boundary of the area that contains x% of the volume of a probability density distribution. A simple contour (like the ones that are produced in Spatial Analyst) represent only the boundary of a specific value of the raster data, and does not in any way relate to probability. For applications like animal home range delineation it is the percent volume contour that is required. The 95% volume contour would therefore on average contain 95% of the points that were used to generate the kernel density estimate” (http://www.spatialecology.com/htools/pctvolcontour.php).

This tool is capable of generating many different output layers at once and hence requires a user defined output folder. The tool needs a raster and an out put folder as input. There can be three types of output created using this tool. One is the polygon type output used in this study. The second type of output is of polyline type and the third is the donut polygon type. In the output folder automatically generated output shapefiles are stored. An empty folder ensures that the program is not in conflict with pre-existing shapefile names. The names of the

shapefiles produces (one for each % value supplied) will be: “PVC” + <the name of the raster> + <the percentage value> (http://www.spatialecology.com/htools/pctvolcontour.php). An example of the user requested ‘Percent contour values’ would be a comma delimited list, like: 10, 20, 30, 90, 40, 75.68 (http://www.spatialecology.com/htools/pctvolcontour.php). The numbers in this list do not have to be ordered, and decimals are allowed.

Methodology

First of all in ArcMap, ‘Spatial Analyst’ or ‘3D Analyst’ should be available before the start of this tool (in ArcMap, Tools > Extensions). A compatible raster layer must be loaded into ArcMap in order to use this tool. The raster layer should represent a probability density surface, like a kernel density estimate.

For this study we created the PVC for every 10% of the contour volumes for each of the ten paleo-soil types. More specifically, we created PVC for 10, 20, 30, 40, 50, 60, 70, 80, 90 and 100 percentages for each of the ten raster representing the ten paleo-soil types. Figure 1.13 – 1.22 shows these PVC for the ten paleo-soil types. A three-dimensional view of the PVC contours gives a better idea about them. Figure B.1 illustrates the 3D view of these ten paleo-soil types. It is important to note that in all of these figures a same zoom level was used and the image is taken from the same view point to make easy comparison.

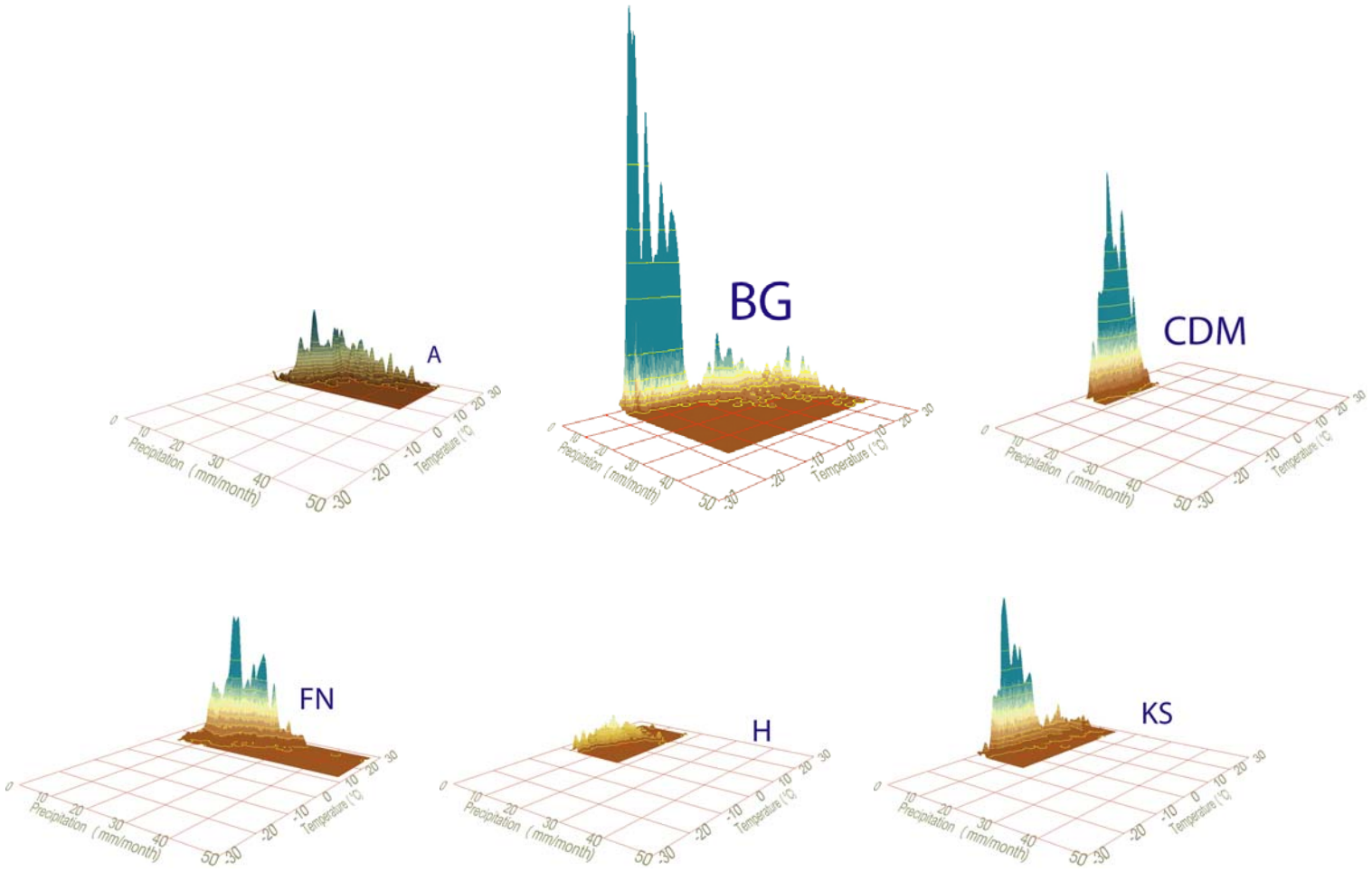

Figure B.1 3D View of Ten Paleo-soil Types (A, BG, CDM, FN, H and KS)

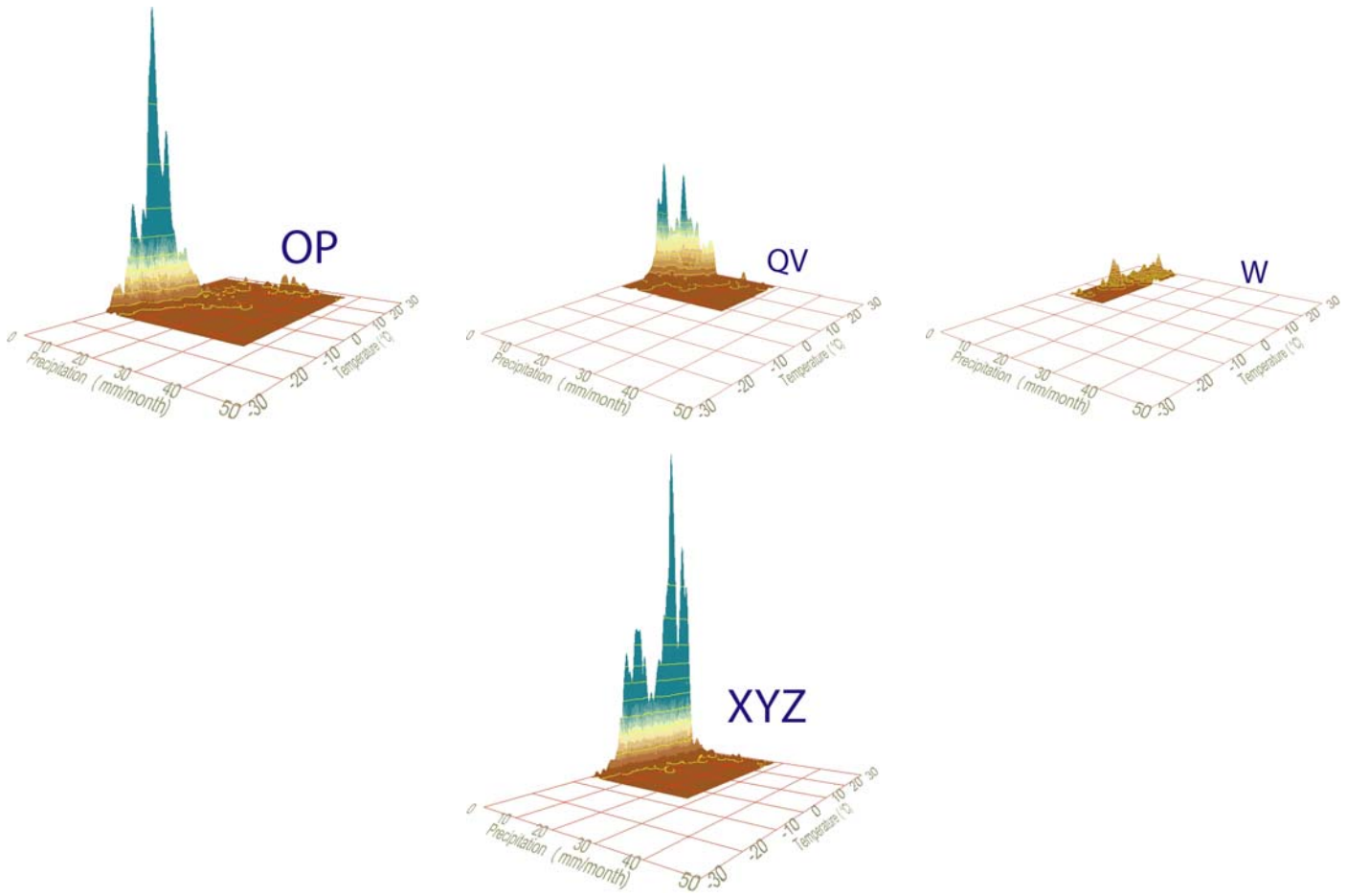

Figure B.2 3D View of Ten Paleo-soil Types (OP, QV, W and XYZ)

APPENDIX C

ADDITIONAL FIGURES

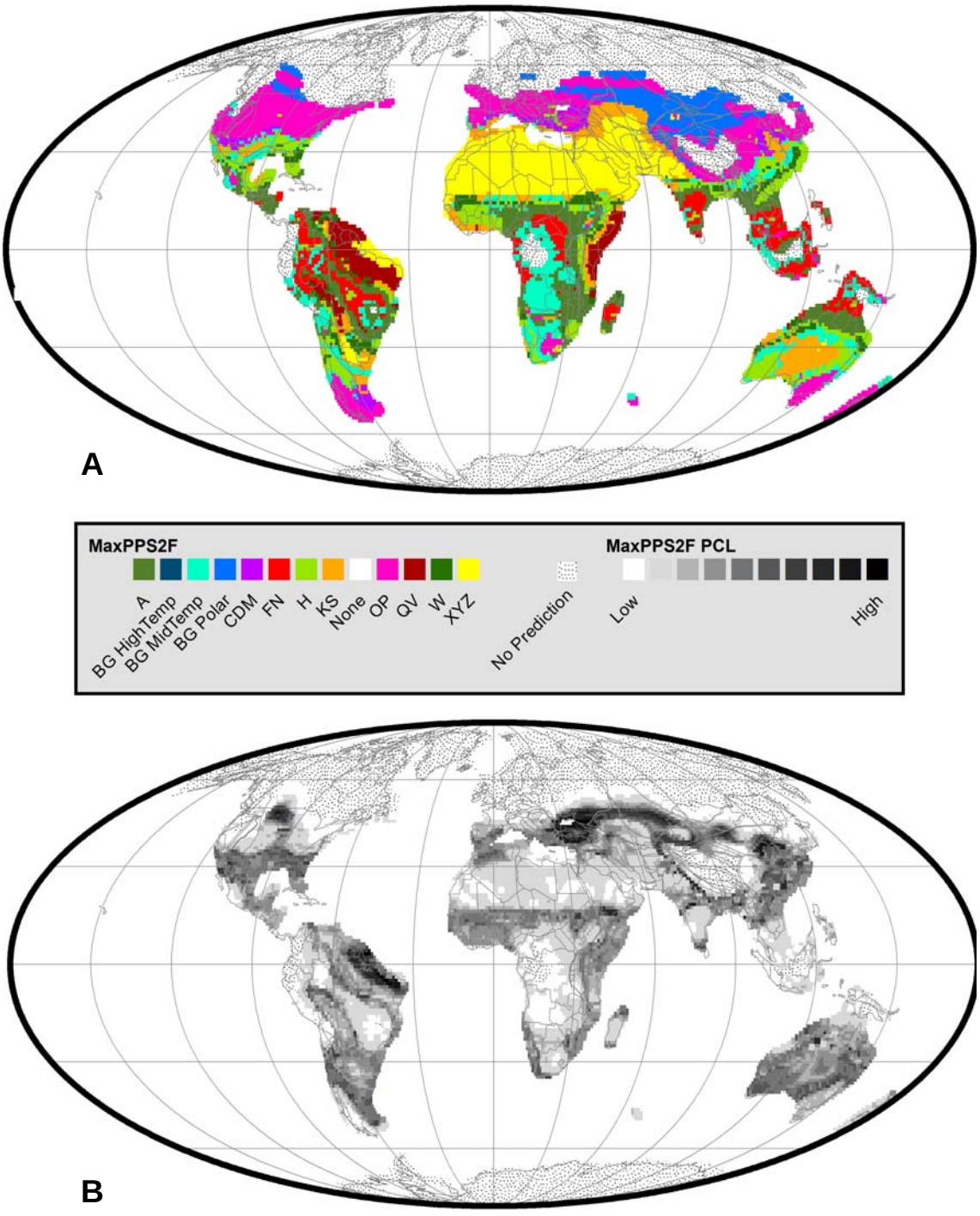

Figure C.1 A. Composite Geographic Distribution Map of Secondary Predicted Ancient Soils (Paleo-soils) for the Miocene (010 Ma), B. Levels of Confidence for Predicted Secondary Probable Paleo-soil Type for the Miocene (010 Ma).

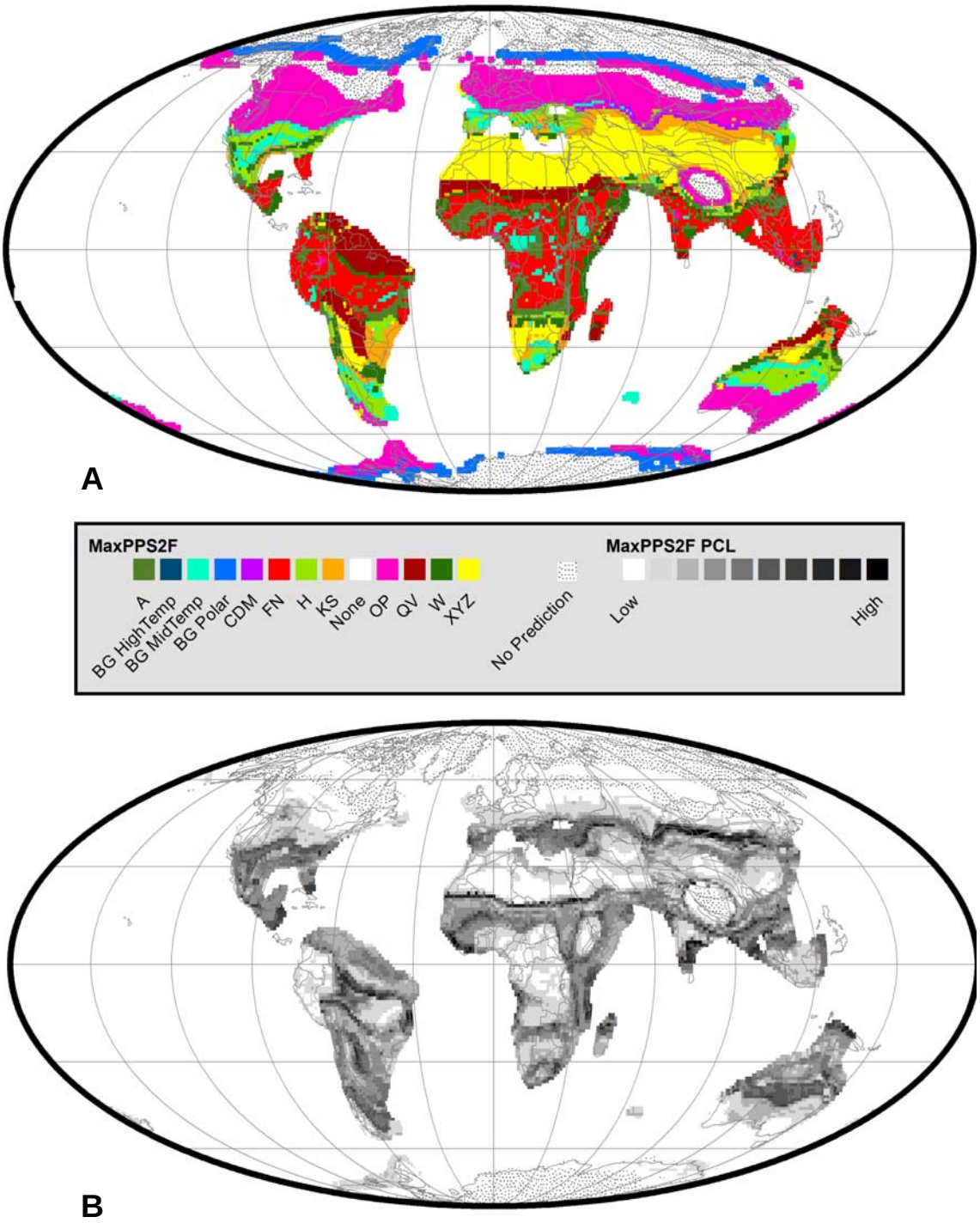

Figure C.2 A. Composite Geographic Distribution Map of Secondary Predicted Ancient Soils (Paleo-soils) for the Oligocene (030 Ma), B. Levels of Confidence for Predicted Secondary Probable Paleo-soil Type for the Oligocene (030 Ma).

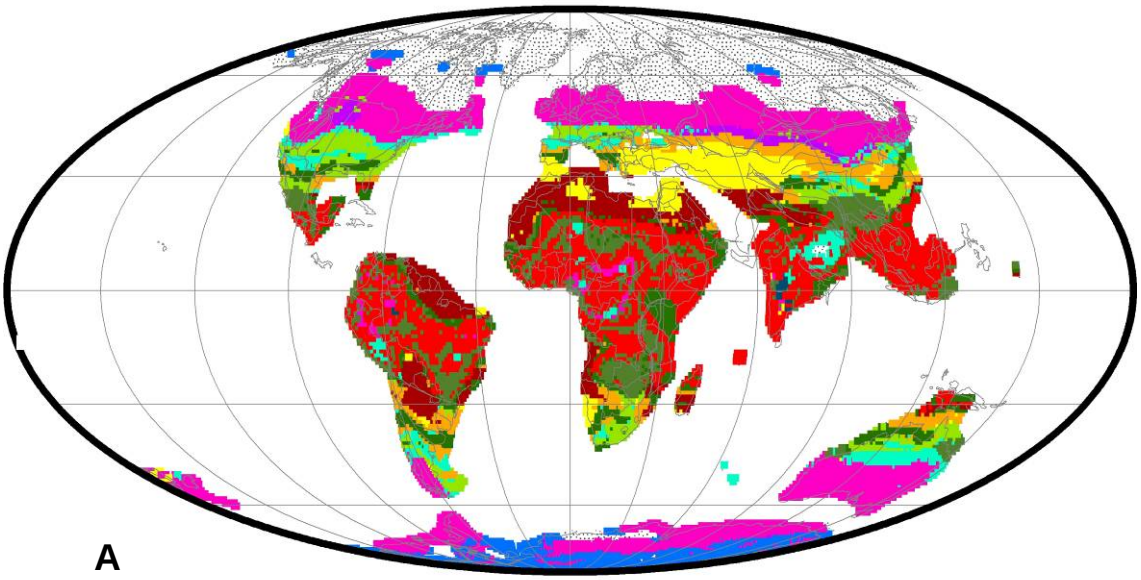

A

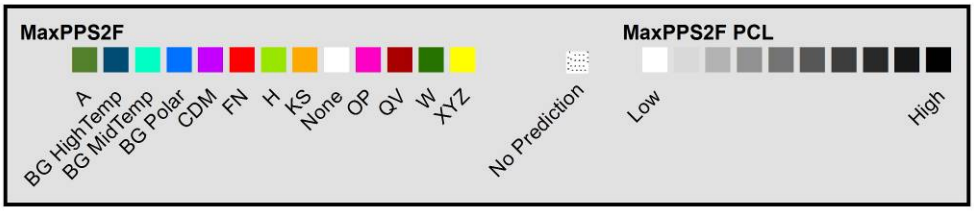

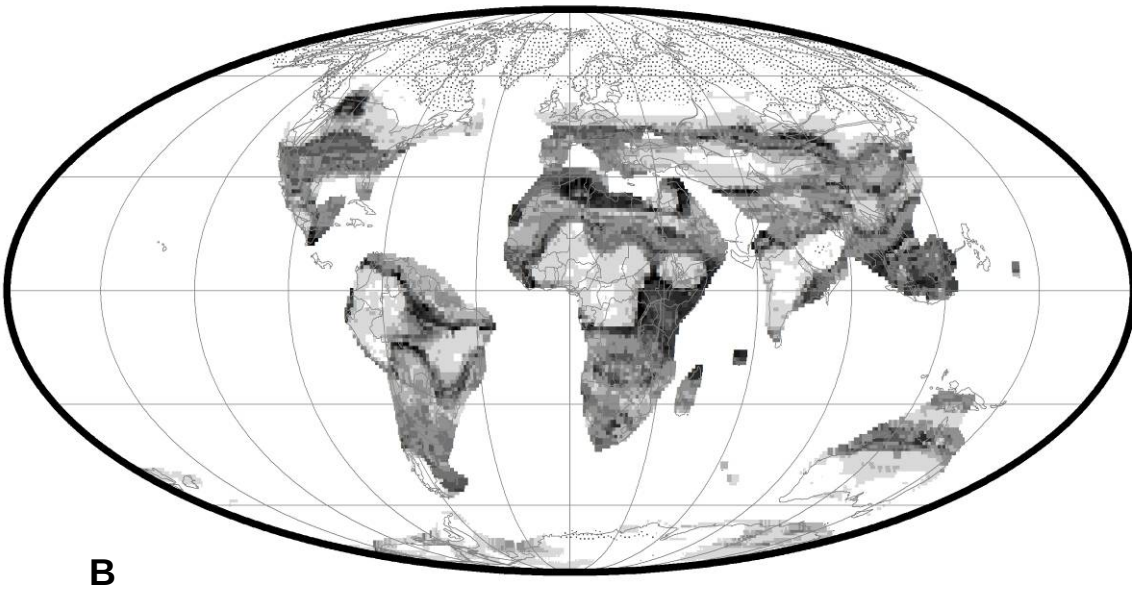

B

Figure C.3 A. Composite Geographic Distribution Map of Secondary Predicted Ancient Soils (Paleo-soils) for the Eocene (045 Ma), B. Levels of Confidence for Predicted Secondary Probable Paleo-soil Type for the Eocene (045 Ma).

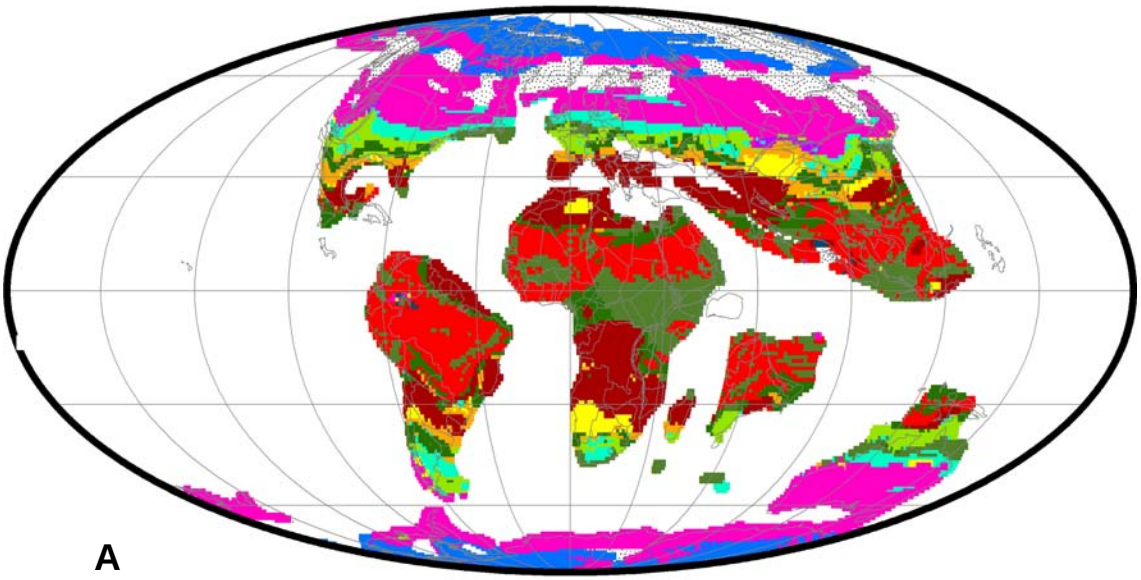

A

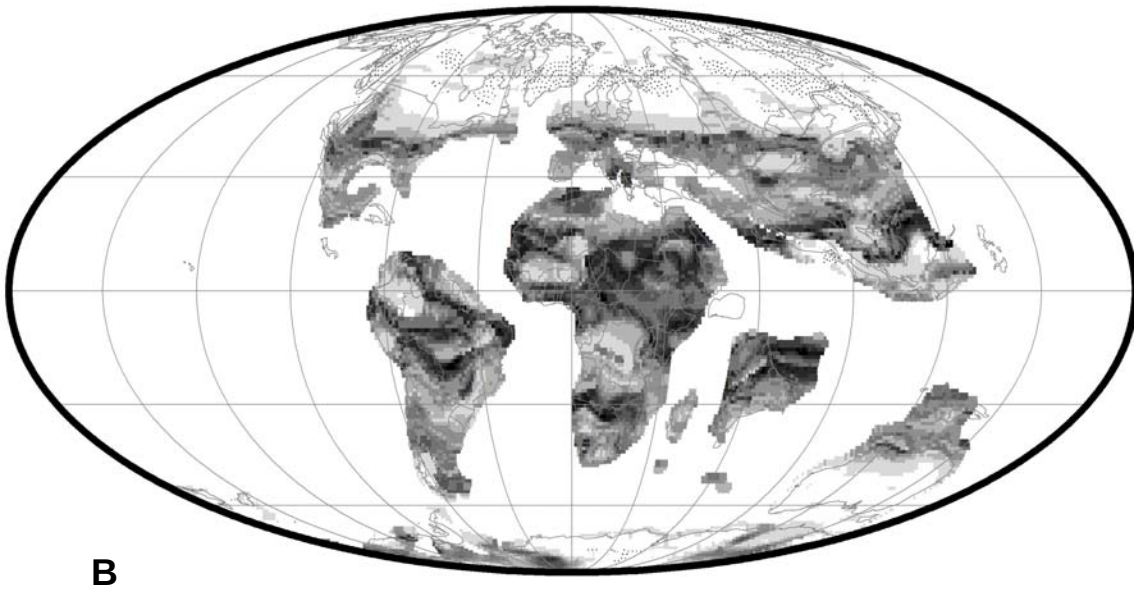

B

Figure C.4 A. Composite Geographic Distribution Map of Secondary Predicted Ancient Soils (Paleo-soils) for the Latest Cretaceous / Maastrichtian (70 Ma), B. Levels of Confidence for Predicted Secondary Probable Paleo-soil Type for the Latest Cretaceous / Maastrichtian (70 Ma).

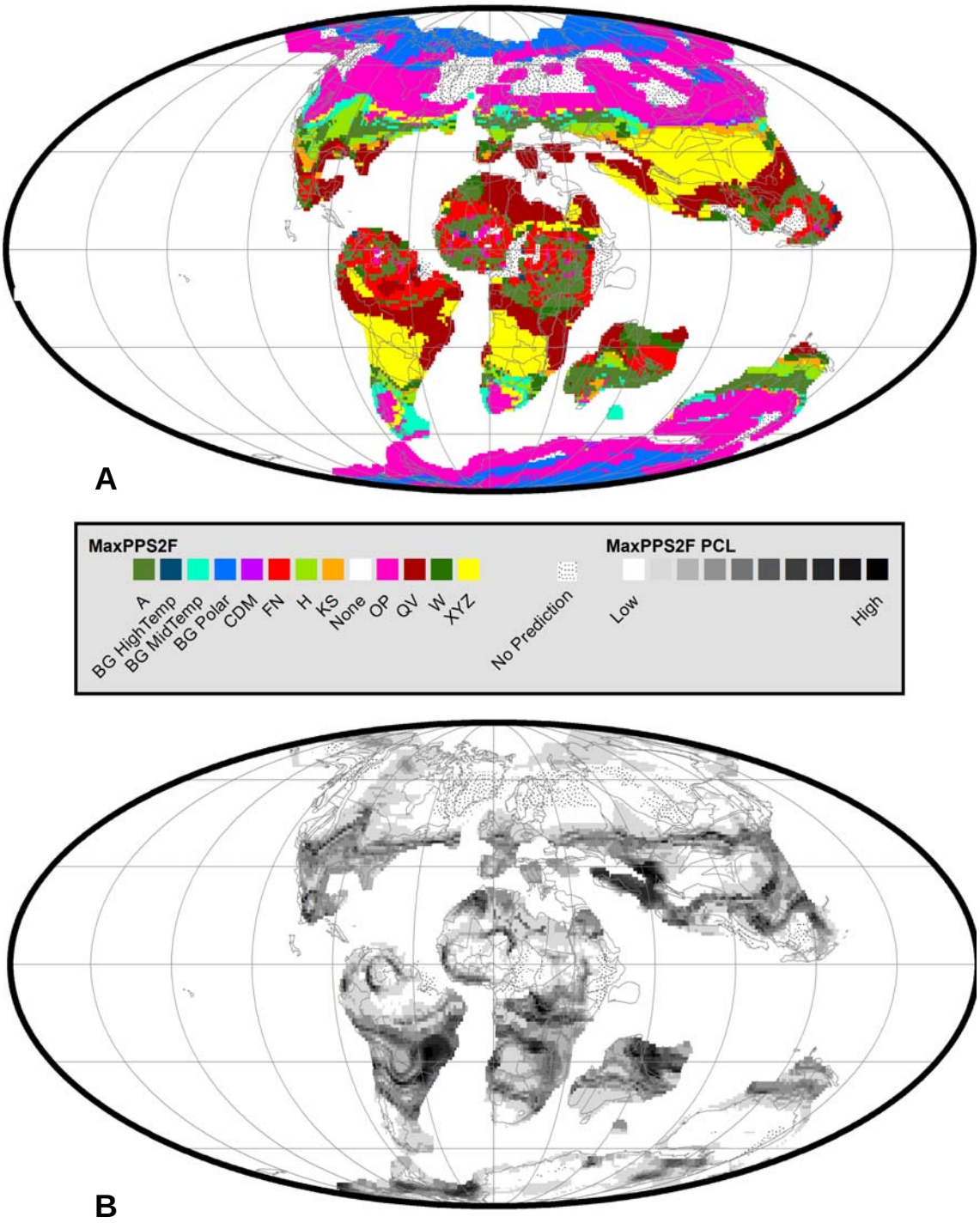

Figure C.5 A. Composite Geographic Distribution Map of Secondary Predicted Ancient Soils (Paleo-soils) for the Late Cretaceous/ Cenomanian-Turonian (90 Ma), B. Levels of Confidence for Predicted Secondary Probable Paleo-soil Type for the Late Cretaceous/ Cenomanian-Turonian (90 Ma).

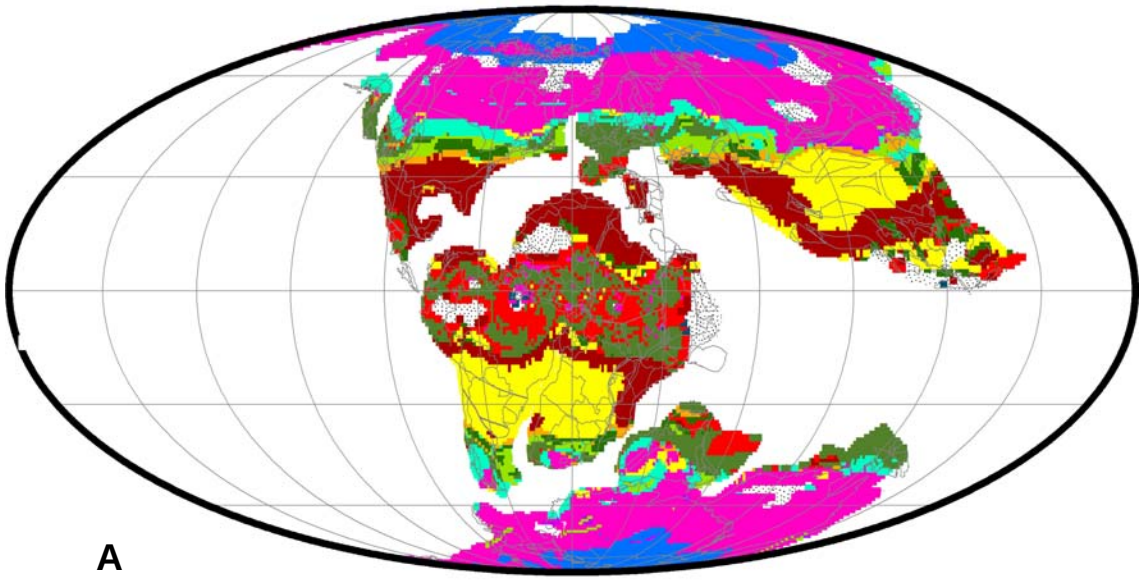

A

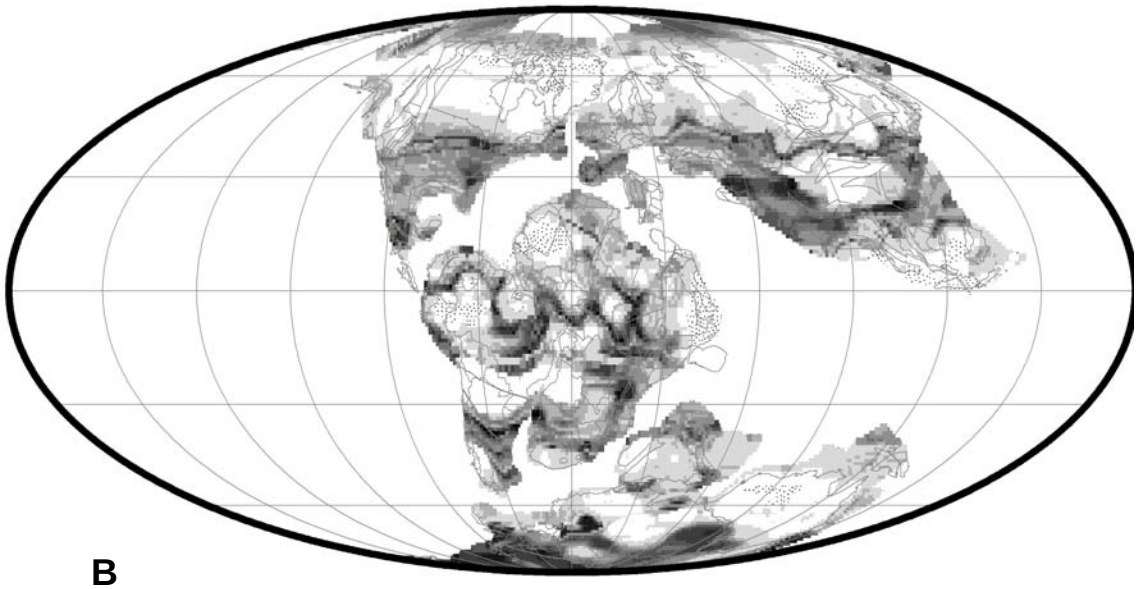

B

Figure C.6 A. Composite Geographic Distribution Map of Secondary Predicted Ancient Soils (Paleo-soils) for the Aptian (120 Ma), B. Levels of Confidence for Predicted Secondary Probable Paleo-soil Type for the Aptian (120 Ma).

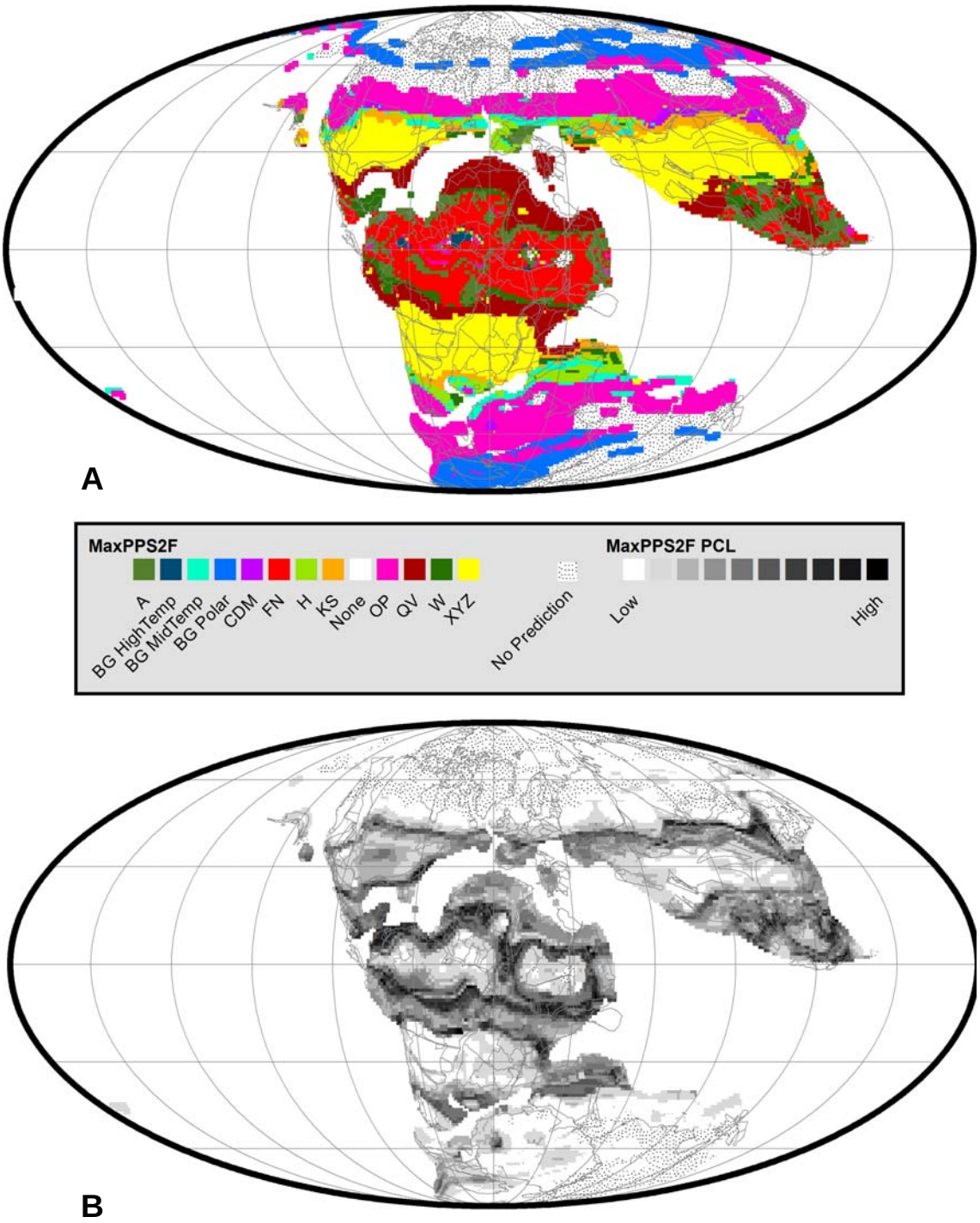

Figure C.7 A. Composite Geographic Distribution Map of Secondary Predicted Ancient Soils (Paleo-soils) for the Earliest Cretaceous / Berriasian-Valanginian (140 Ma), B. Levels of Confidence for Predicted Secondary Probable Paleo-soil Type for the Earliest Cretaceous / Berriasian-Valanginian (140 Ma).

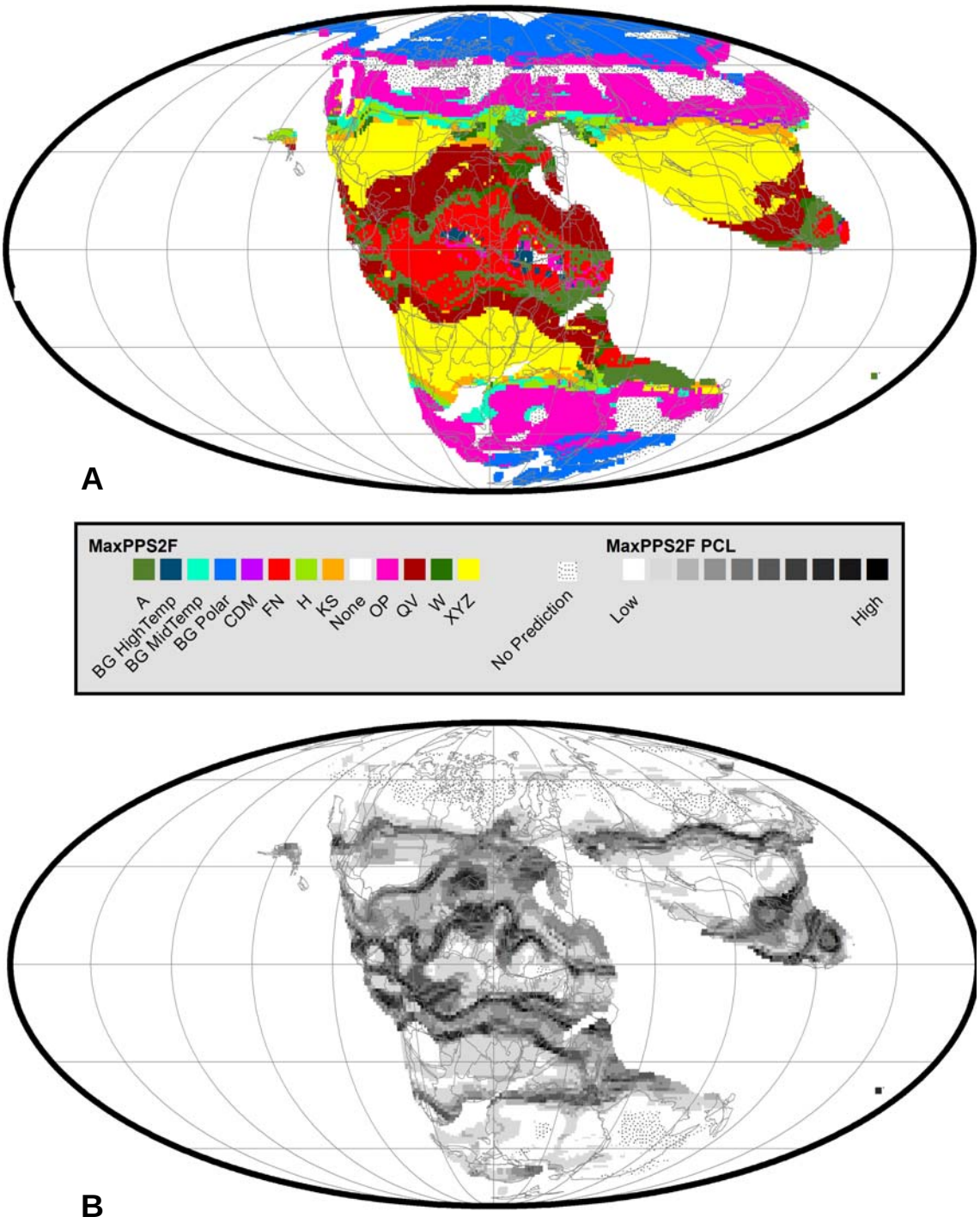

Figure C.8 A. Composite Geographic Distribution Map of Secondary Predicted Ancient Soils (Paleo-soils) for the Late Jurassic (160 Ma), B. Levels of Confidence for Predicted Secondary Probable Paleo-soil Type for the Late Jurassic (160 Ma).

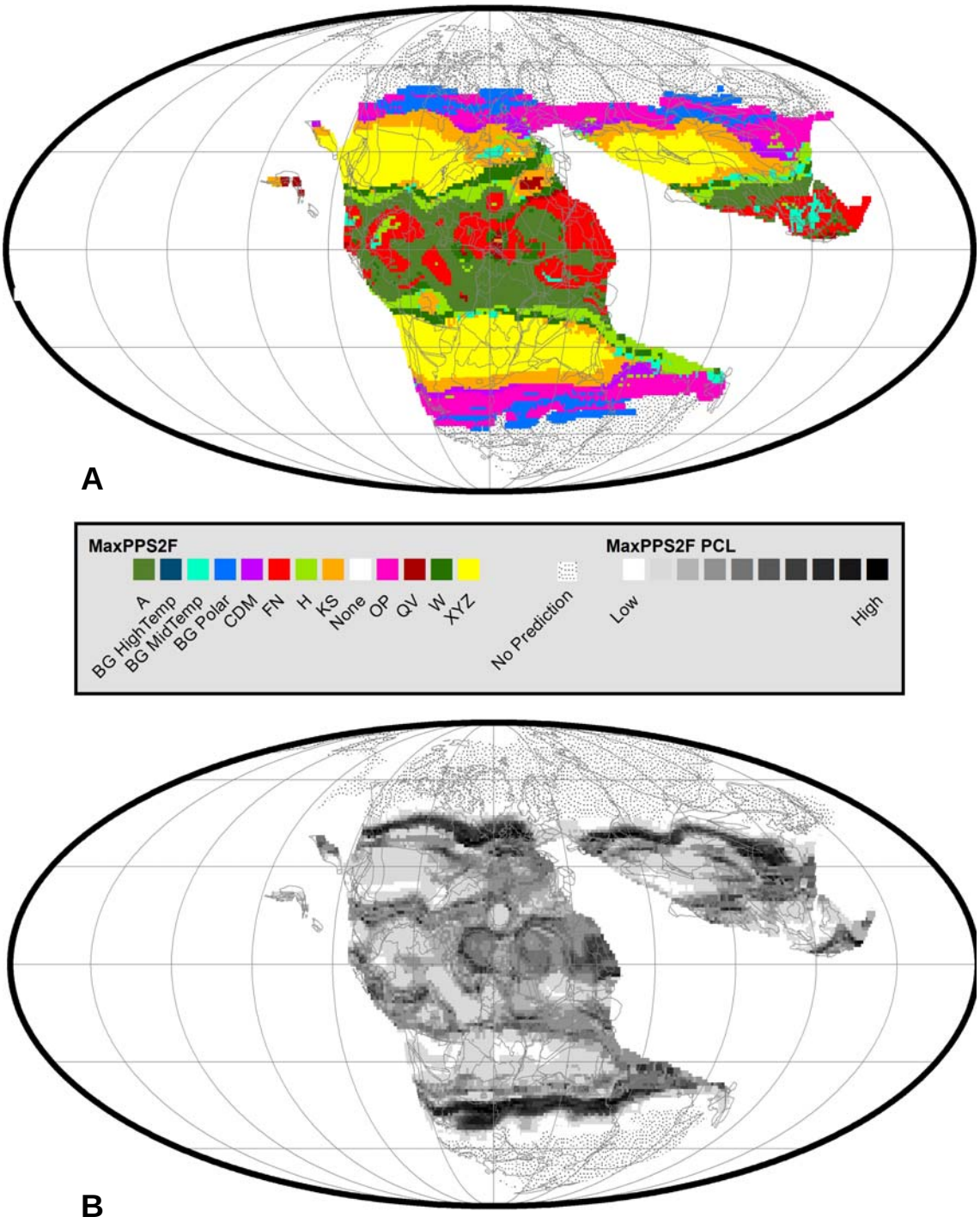

Figure C.9 A. Composite Geographic Distribution Map of Secondary Predicted Ancient Soils (Paleo-soils) for the Early Jurassic (180 Ma), B. Levels of Confidence for Predicted Secondary Probable Paleo-soil Type for the Early Jurassic (180 Ma).

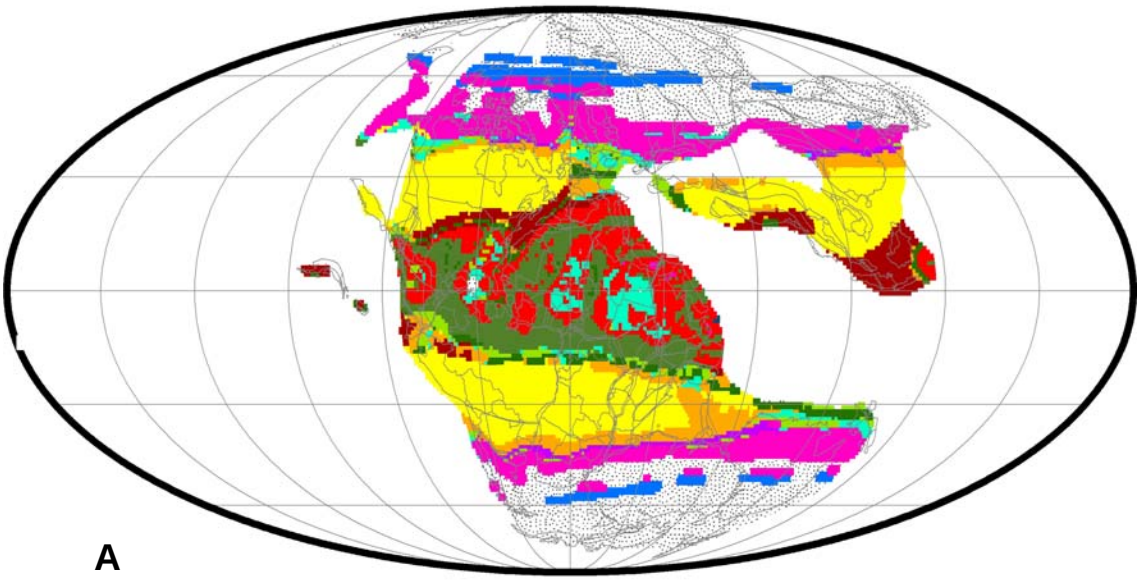

A

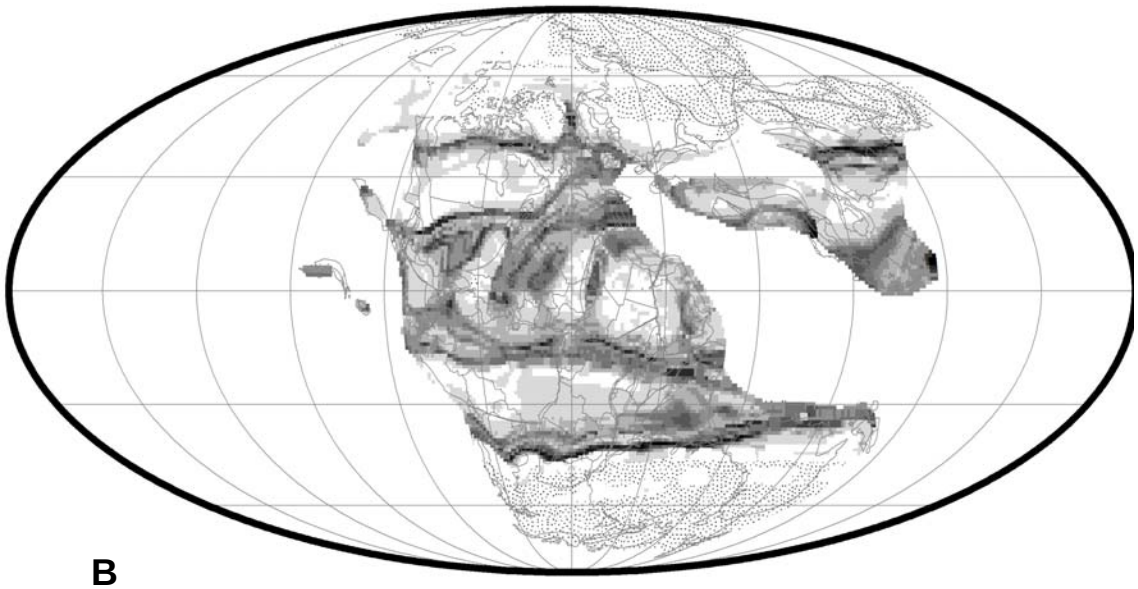

B

Figure C.10 A. Composite Geographic Distribution Map of Secondary Predicted Ancient Soils (Paleo-soils) for the Late Triassic (220 Ma), B. Levels of Confidence for Predicted Secondary Probable Paleo-soil Type for the Late Triassic (220 Ma).

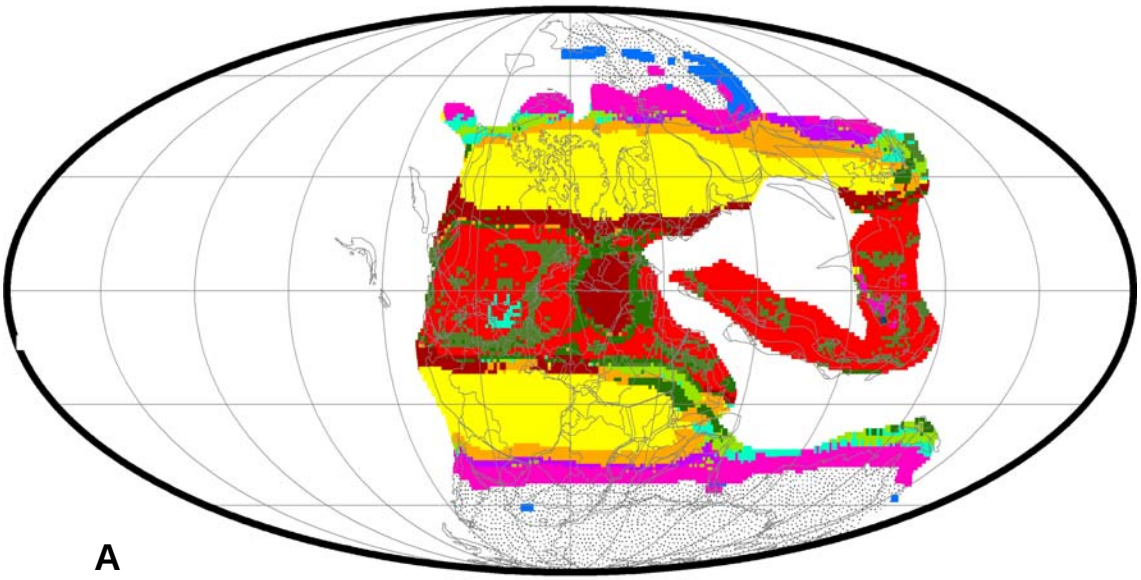

A

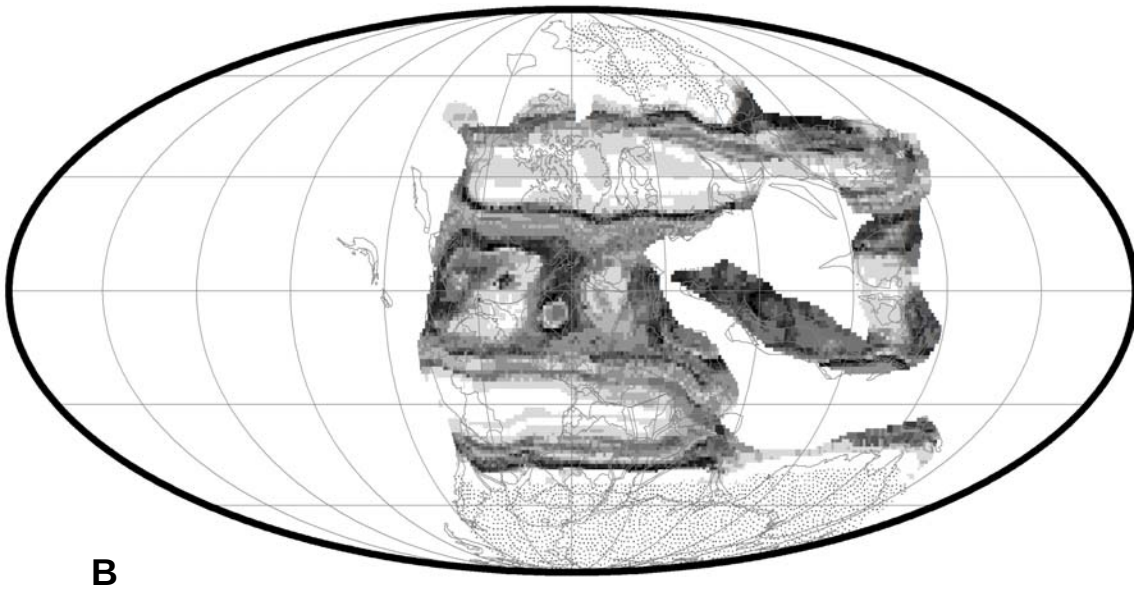

B

Figure C.11 A. Composite Geographic Distribution Map of Secondary Predicted Ancient Soils (Paleo-soils) for the Early Triassic (250 Ma), B. Levels of Confidence for Predicted Secondary Probable Paleo-soil Type for the Early Triassic (250 Ma).

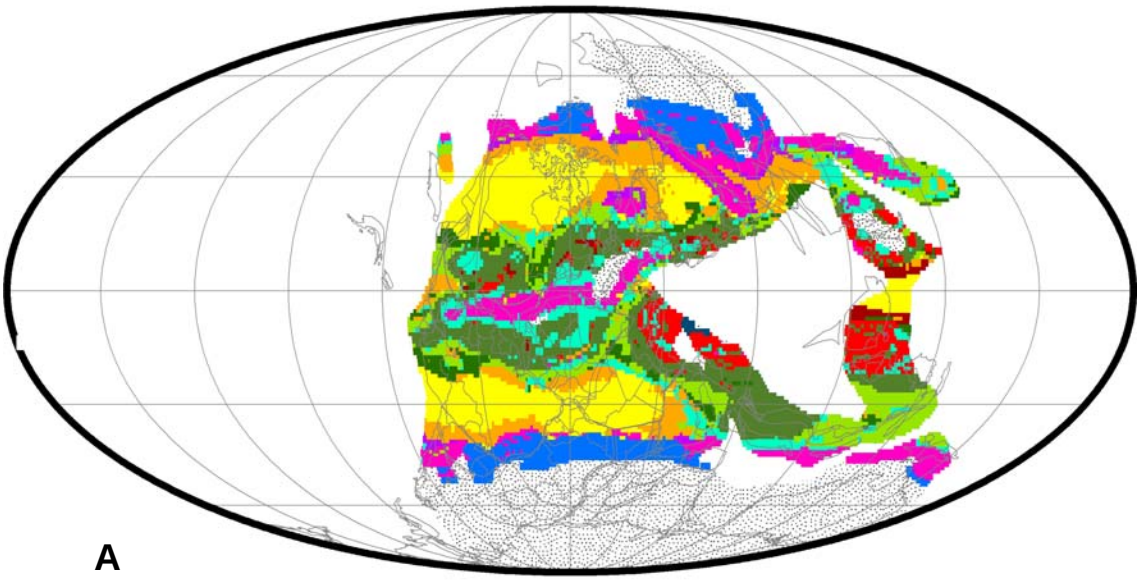

A

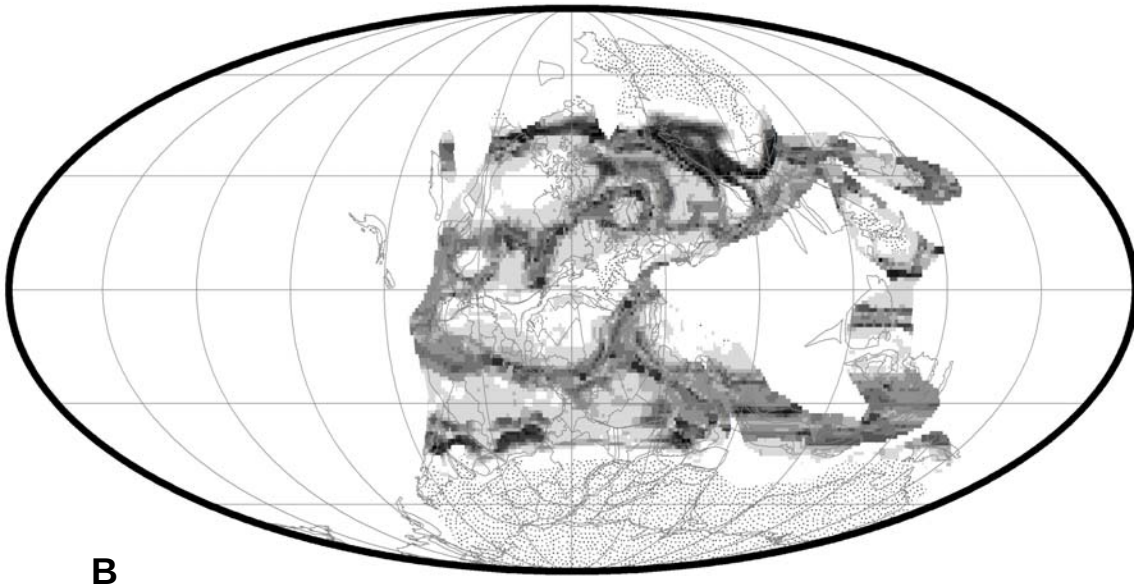

B

Figure C.12 A. Composite Geographic Distribution Map of Secondary Predicted Ancient Soils (Paleo-soils) for the Early Permian (280 Ma), B. Levels of Confidence for Predicted Secondary Probable Paleo-soil Type for the Early Permian (280 Ma).

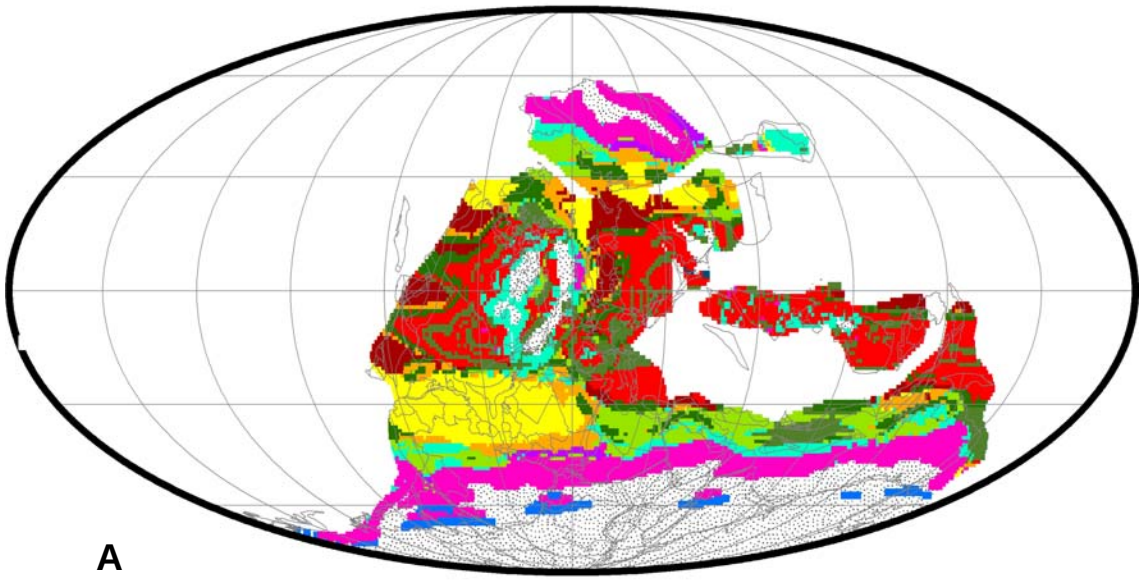

A

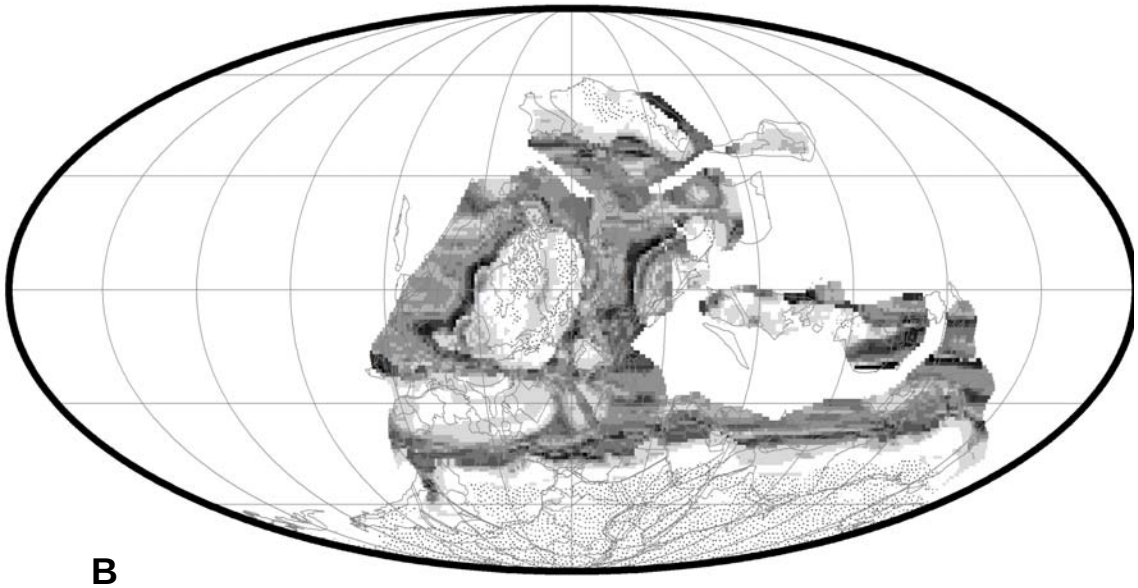

B

Figure C.13 A. Composite Geographic Distribution Map of Secondary Predicted Ancient Soils (Paleo-soils) for the Early Carboniferous (340 Ma), B. Levels of Confidence for Predicted Secondary Probable Paleo-soil Type for the Early Carboniferous (340 Ma).

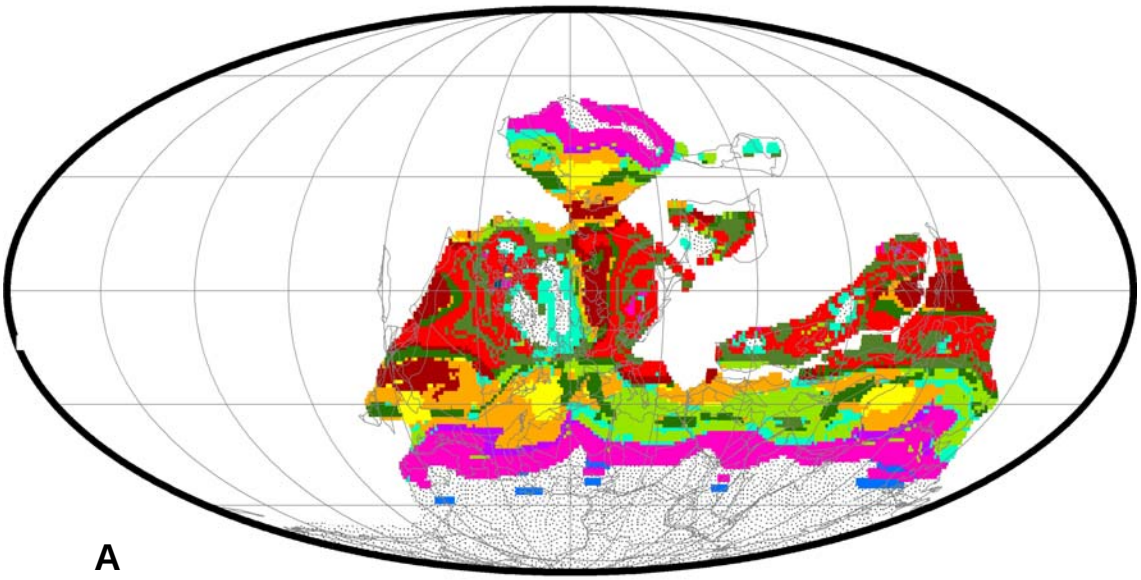

A

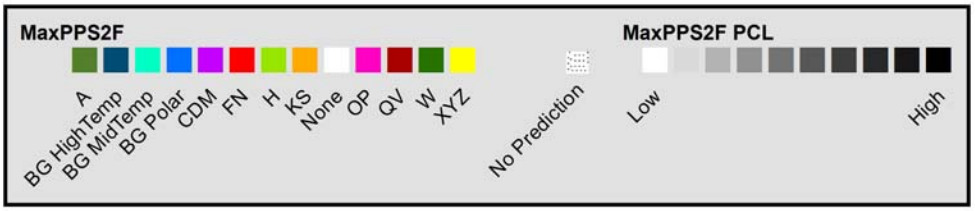

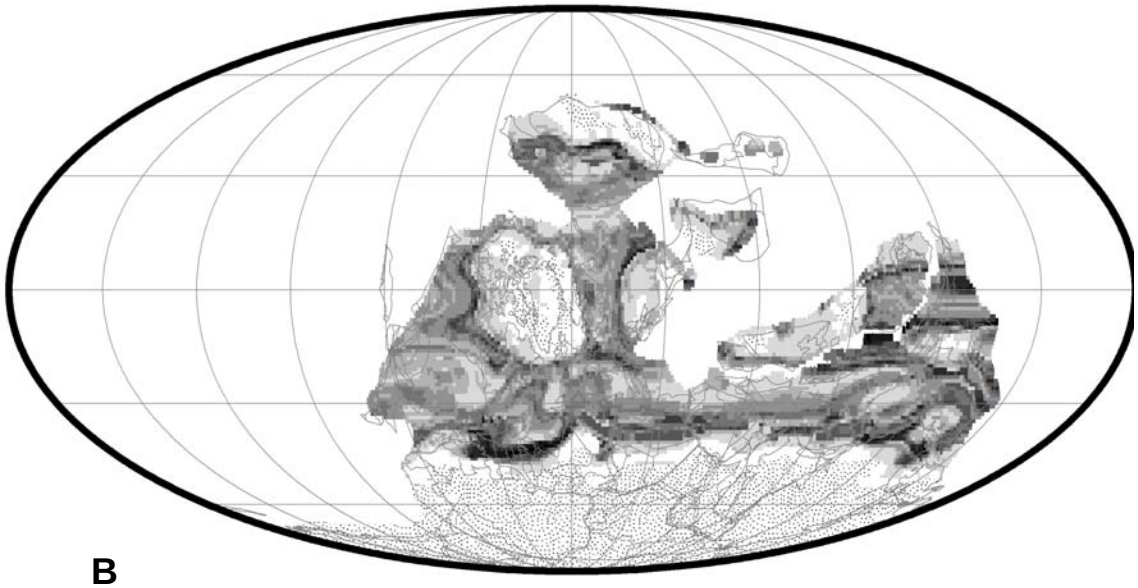

B

Figure C.14 A. Composite Geographic Distribution Map of Secondary Predicted Ancient Soils (Paleo-soils) for the Late Devonian (360 Ma), B. Levels of Confidence for Predicted Secondary Probable Paleo-soil Type for the Late Devonian (360 Ma).

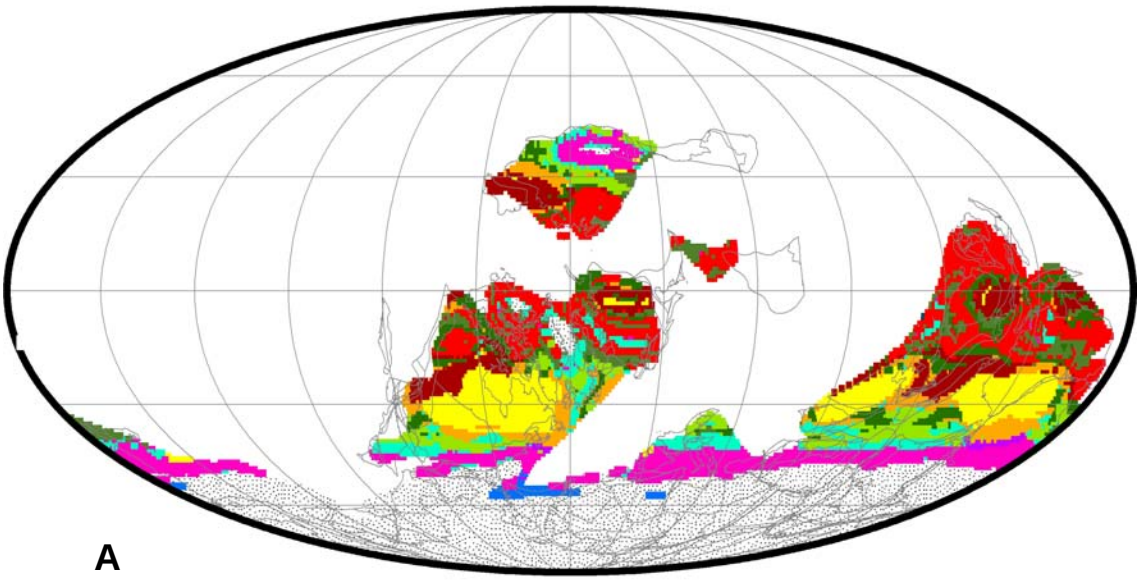

A

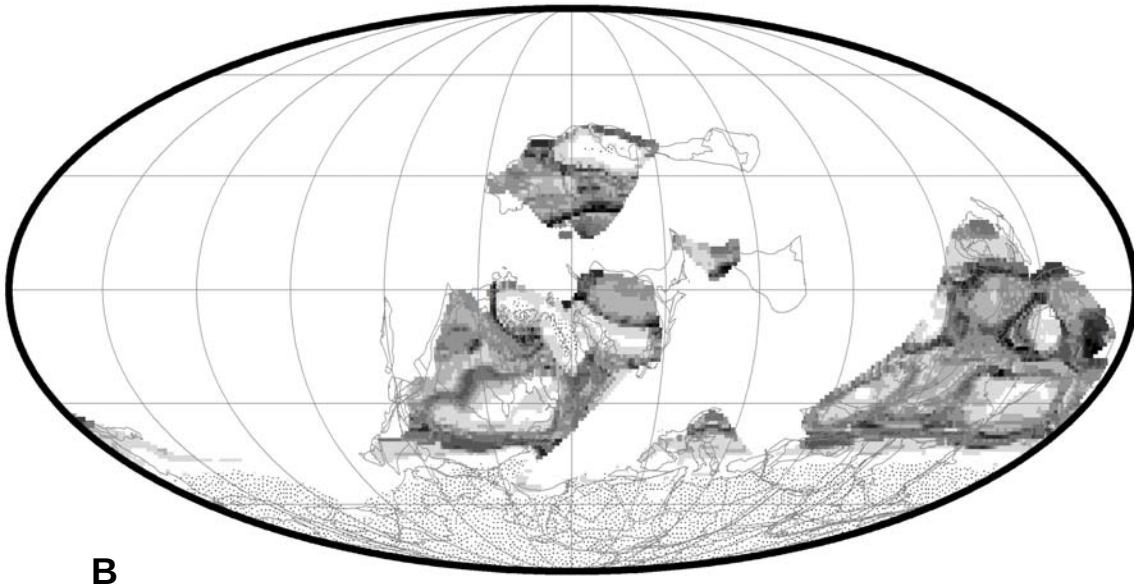

B

Figure C.15 A. Composite Geographic Distribution Map of Secondary Predicted Ancient Soils (Paleo-soils) for the Early Devonian (400 Ma), B. Levels of Confidence for Predicted Secondary Probable Paleo-soil Type for the Early Devonian (400 Ma).

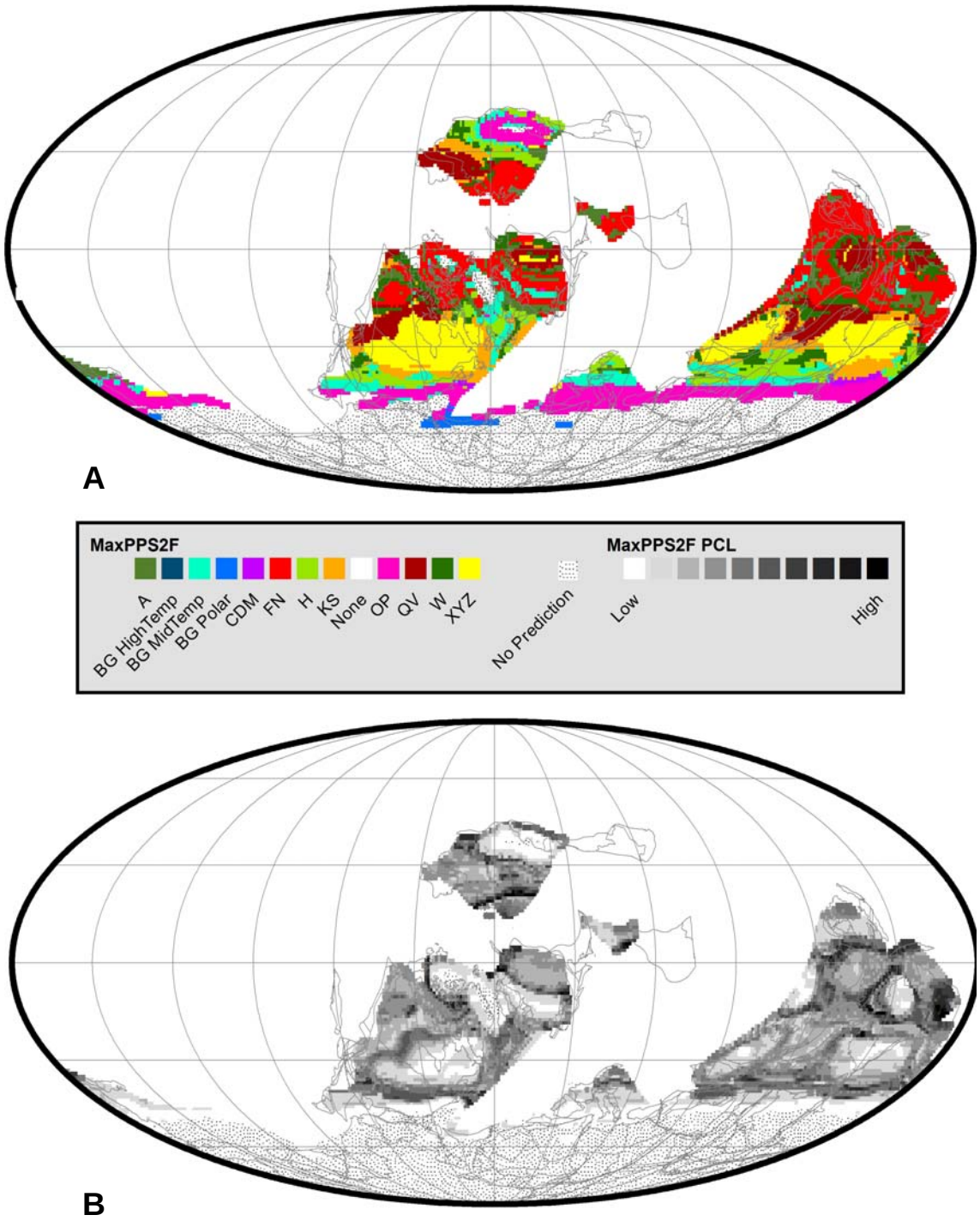

Figure C.16 A. Composite Geographic Distribution Map of Secondary Predicted Ancient Soils (Paleo-soils) for the Silurian (430 Ma), B. Levels of Confidence for Predicted Secondary Probable Paleo-soil Type for the Silurian (430 Ma).

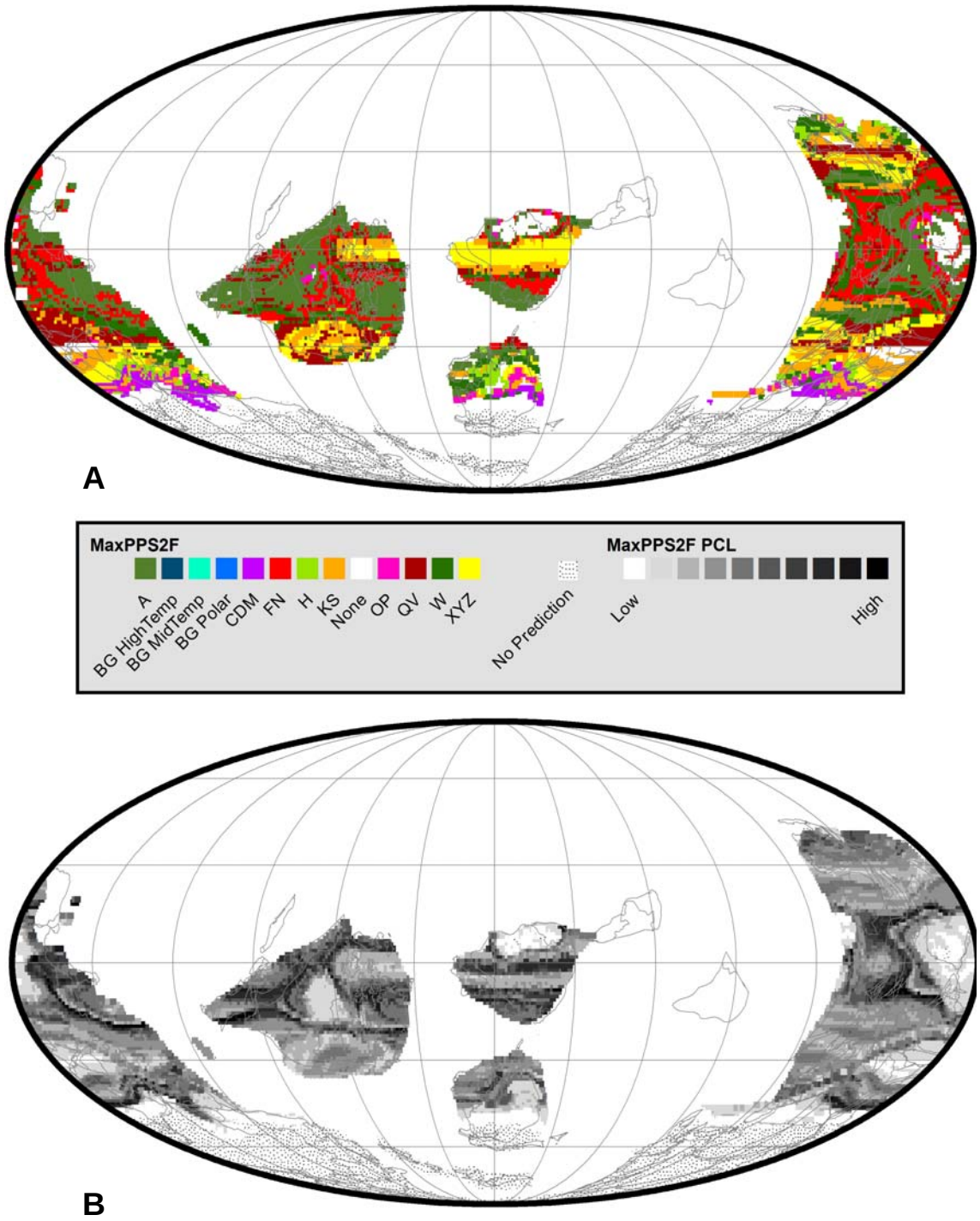

Figure C.17 A. Composite Geographic Distribution Map of Secondary Predicted Ancient Soils (Paleo-soils) for the Ordovician (480 Ma), B. Levels of Confidence for Predicted Secondary Probable Paleo-soil Type for the Ordovician (480 Ma).

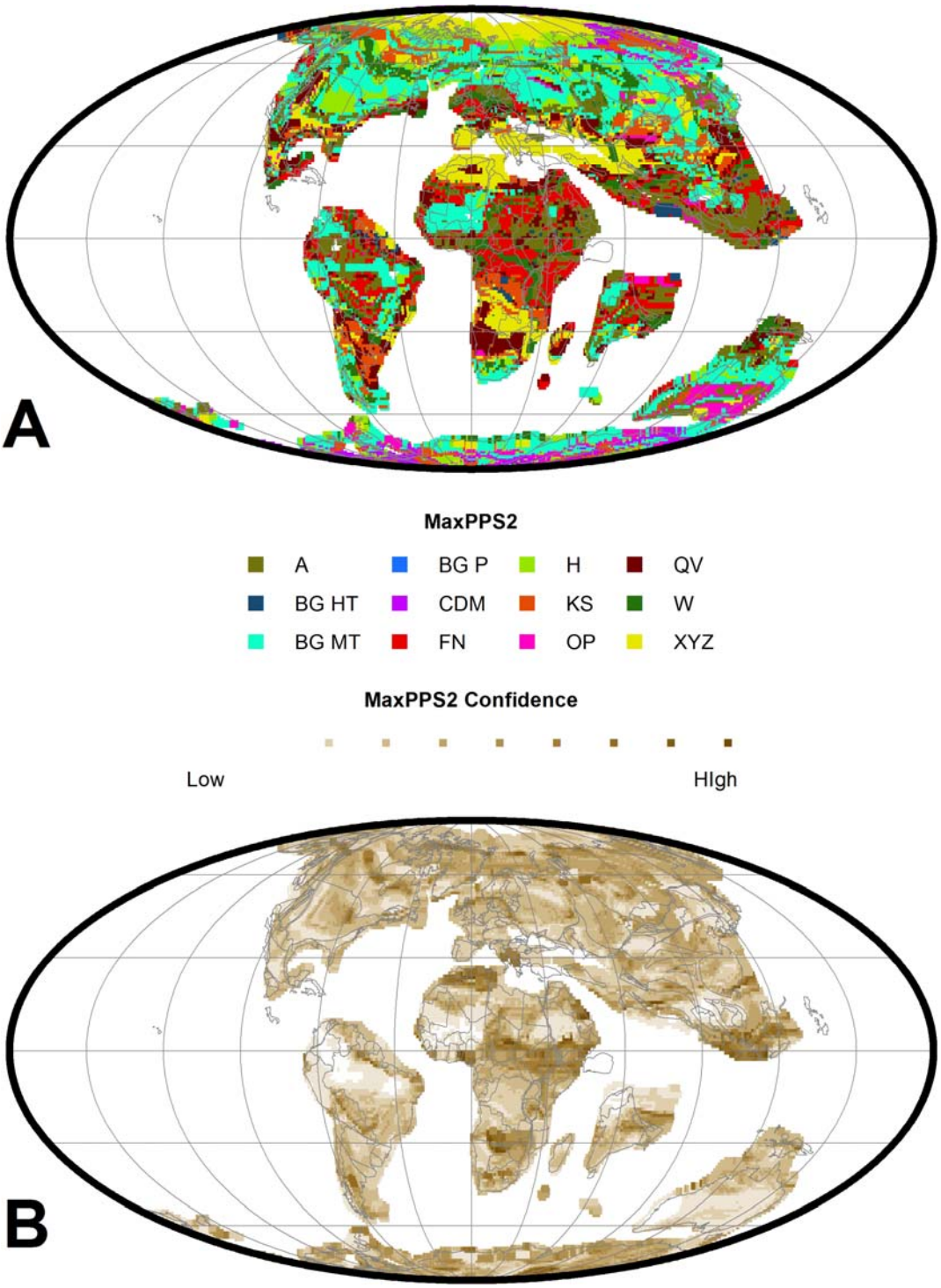

Figure C.18 A. Composite Revised Geographic Distribution Map of Secondary Predicted Ancient Soils (Paleo-soils) for the Latest Cretaceous / Maastrichtian (70 Ma), B. Levels of Confidence for Revised Secondary Probable Paleo-soil Type for the Latest Cretaceous / Maastrichtian (70 Ma).

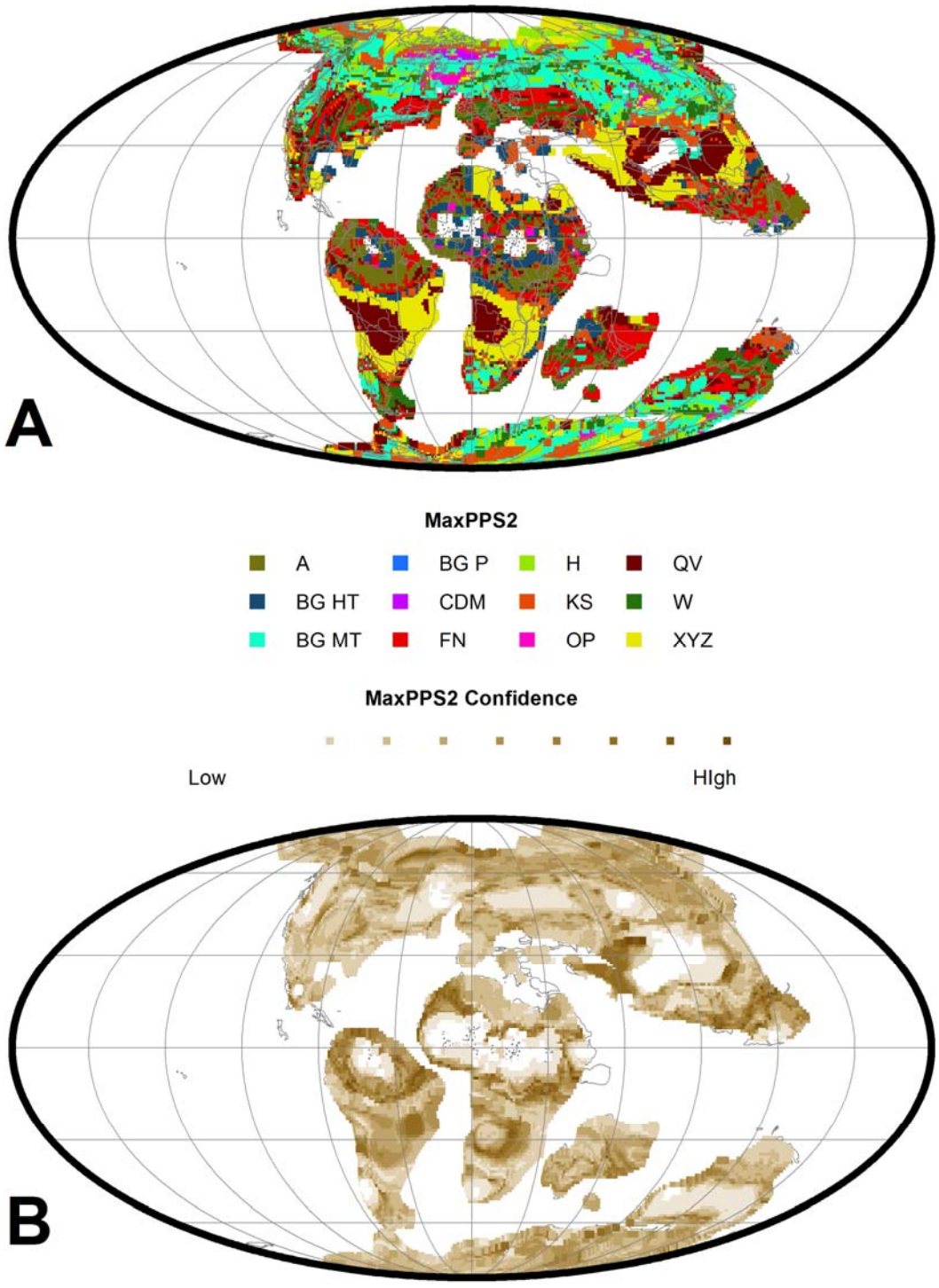

Figure C.19 A. Composite Revised Geographic Distribution Map of Secondary Predicted Ancient Soils (Paleo-soils) for the Late Cretaceous/ Cenomanian-Turonian (90 Ma), B. Levels of Confidence for Revised Secondary Probable Paleo-soil Type for the Late Cretaceous/ Cenomanian-Turonian (90 Ma).

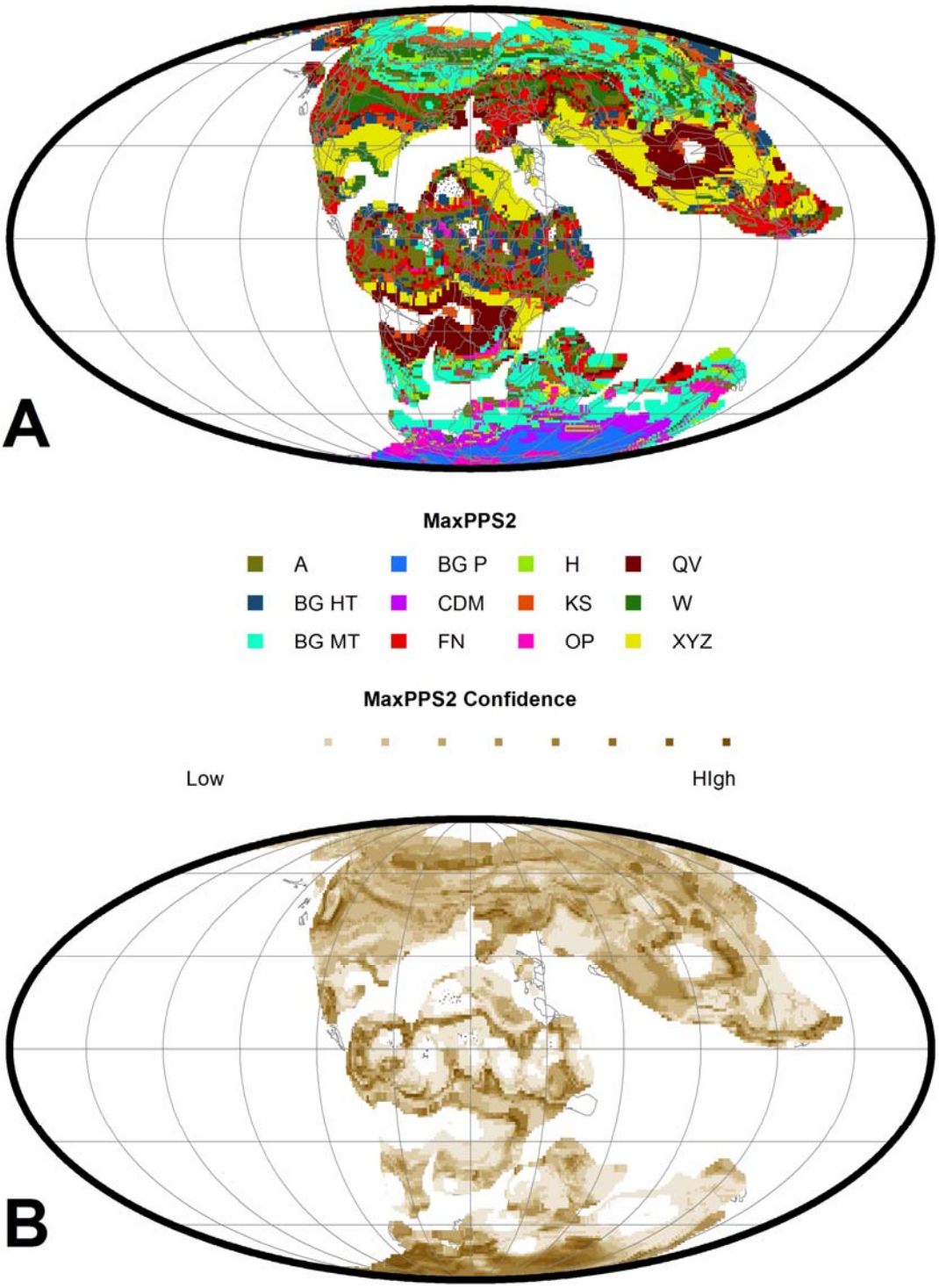

Figure C.20 A. Composite Revised Geographic Distribution Map of Secondary Predicted Ancient Soils (Paleo-soils) for the Aptian (120 Ma), B. Levels of Confidence for Revised Secondary Probable Paleo-soil Type for the Aptian (120 Ma).

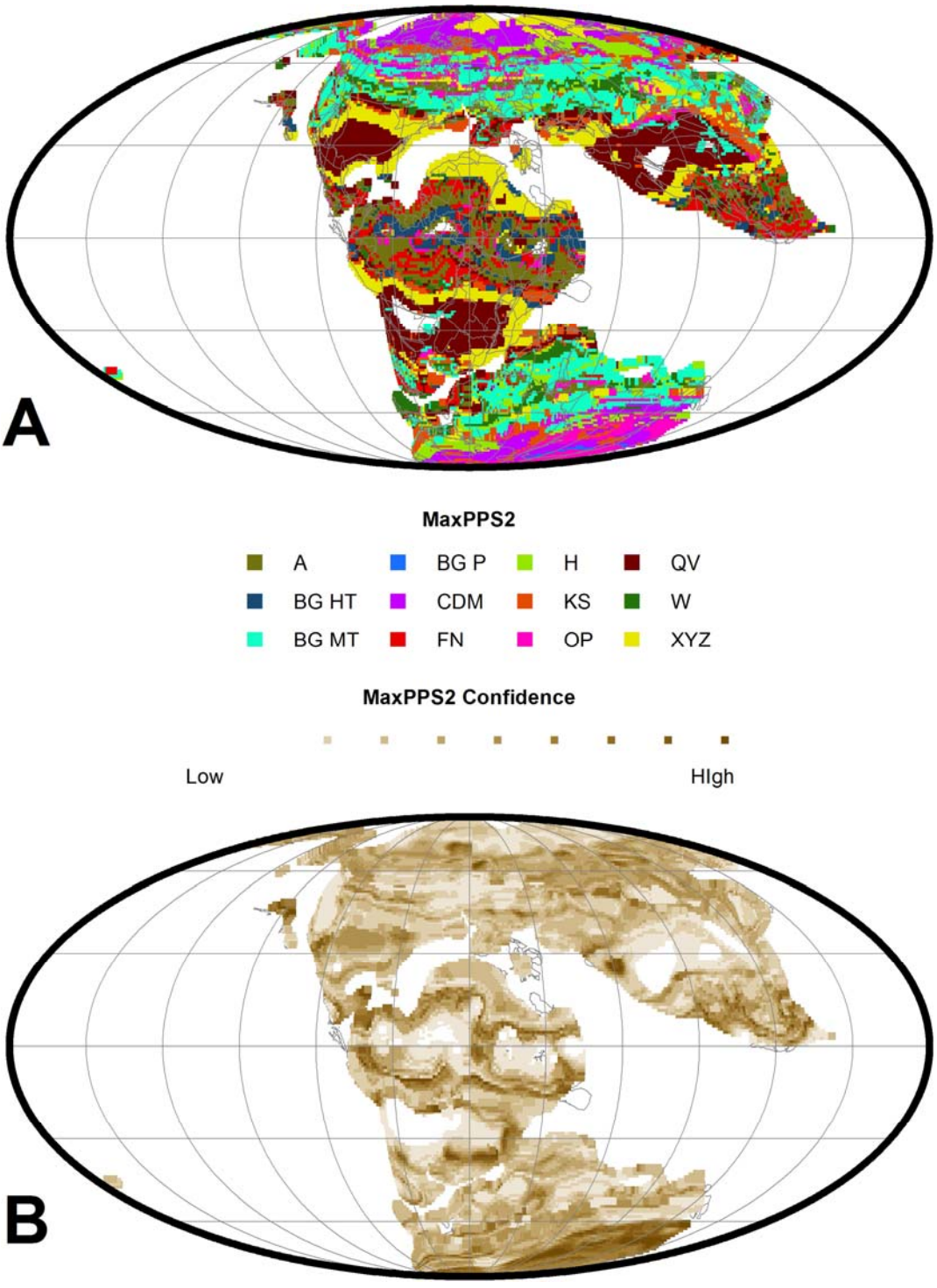

Figure C.21 A. Composite Revised Geographic Distribution Map of Secondary Predicted Ancient Soils (Paleo-soils) for the Earliest Cretaceous / Berriasian-Valanginian (140 Ma), B. Levels of Confidence for Revised Secondary Probable Paleo-soil Type for the Earliest Cretaceous / Berriasian-Valanginian (140 Ma).

APPENDIX D

BRIEF DESCRIPTION OF FAST OCEAN CLIMATE MODEL (FOAM)

FOAM is a fully coupled, mixed-resolution, general circulation mode (Ref. FOAM Website). General Circulation Models (also known as Global Climate Model, GCMs) are a class of computer-driven models for weather forecasting, understanding climate and projecting climate change, and are commonly called Global Climate Models. Coupled Atmosphere-Ocean GCMs have the advantage of sophisticated model predictions of climate. Mixed Resolution means the rage varies from Low Resolution (R15: 4.5º lat x 7.5º lon) atmosphere model to Medium-High Resolution (T42; 1.4º lat x 2.8125º lon) ocean model. (Nefedova et. al., 2006). FOAM uses the combination of a low resolution (R15) atmosphere model, a highly efficient medium-resolution ocean model, and distributed memory parallel processing to achieve high output on a relatively modest numbers of processors (16-64). The quality of the simulated climate compares well with higher resolution models. FOAM's intended purpose is to study long-term natural variability in the climate system. FOAM is also well suited for paleoclimate applications. FOAM runs on Linux clusters and on parallel supercomputers such as the IBM SP and SGI Origin.

Components

There are five components of FOAM. They are as follows:

1. Atmosphere Model: The Atmosphere Model used in FOAM is named PCCM3-UW. It is a combination of two model codes, PCCM2 (major source) and parallel version of CCM2 developed at NCAR, Oak Ridge National Lab and Argonne. The resolution of the model is R15 (40 latitudes x 48 longitudes) with 18 Levels (Figure D.1).
2. Ocean Model: The Ocean Model is called OM3. OM3 was also developed under the CHAMMP program by John Anderson at the University of Wisconsin-Madison. The resolution of OM3 is 128 latitudes x 128 longitudes on a regular polar grid with 24 levels with first 12 in upper 1000 meters (Figure D.1).
3. Land, Hydrology, and River Runoff: The basic land model in FOAM is taken from the default land model of CCM2: the land surface is broken into 5 main vegetation types.

Hydrology is a simple bucket model with a 15cm deep bucket. Evaporation is a smooth function of the depth of water in the bucket. Snow cover is also a simple analytical design. Top "soil" layer thermal and albedo properties are modified by the presence of snow. The overflow from the bucket model is routed to the ocean using a parallel river transport model. The resolution is same as ocean model, i.e., 128x128.

4. Sea Ice: The Sea Ice component uses the thermodynamics of NCAR's CSIM version 2.2.6. Its resolution is same as ocean model, i.e., 128x128.
5. Coupler Model: The coupler component joins the atmosphere, ocean and land based components. The coupler is the bulk of the original code written for FOAM. To accommodate the different resolutions of the oceanic and atmospheric models, the coupler uses an "overlap grid" obtained by laying the atmosphere grid on top of the ocean grid.

FOAM Variables

FOAM calculates values of over 150 variables for each grid cell that describes the atmosphere, ocean and land surface. Out of these about 30 variables are very important with respect to environmental conditions. Some of the important ones are as follows: upwelling (W), temperature (T), salinity (S), surface winds (U & V), Surface ocean currents (U & V), mixed layer depth (Szz, Tzz), precipitation (PCL), surface runoff (WS), soil moisture (ZZ) and river runoff (RNF). The data tables are written in NetCDF format (composite, binary format and in paleoclimate community it is the standard one).

FOAM Inputs

In order to run FOAM simulations, several input files must be created which define important boundary conditions for the simulations.

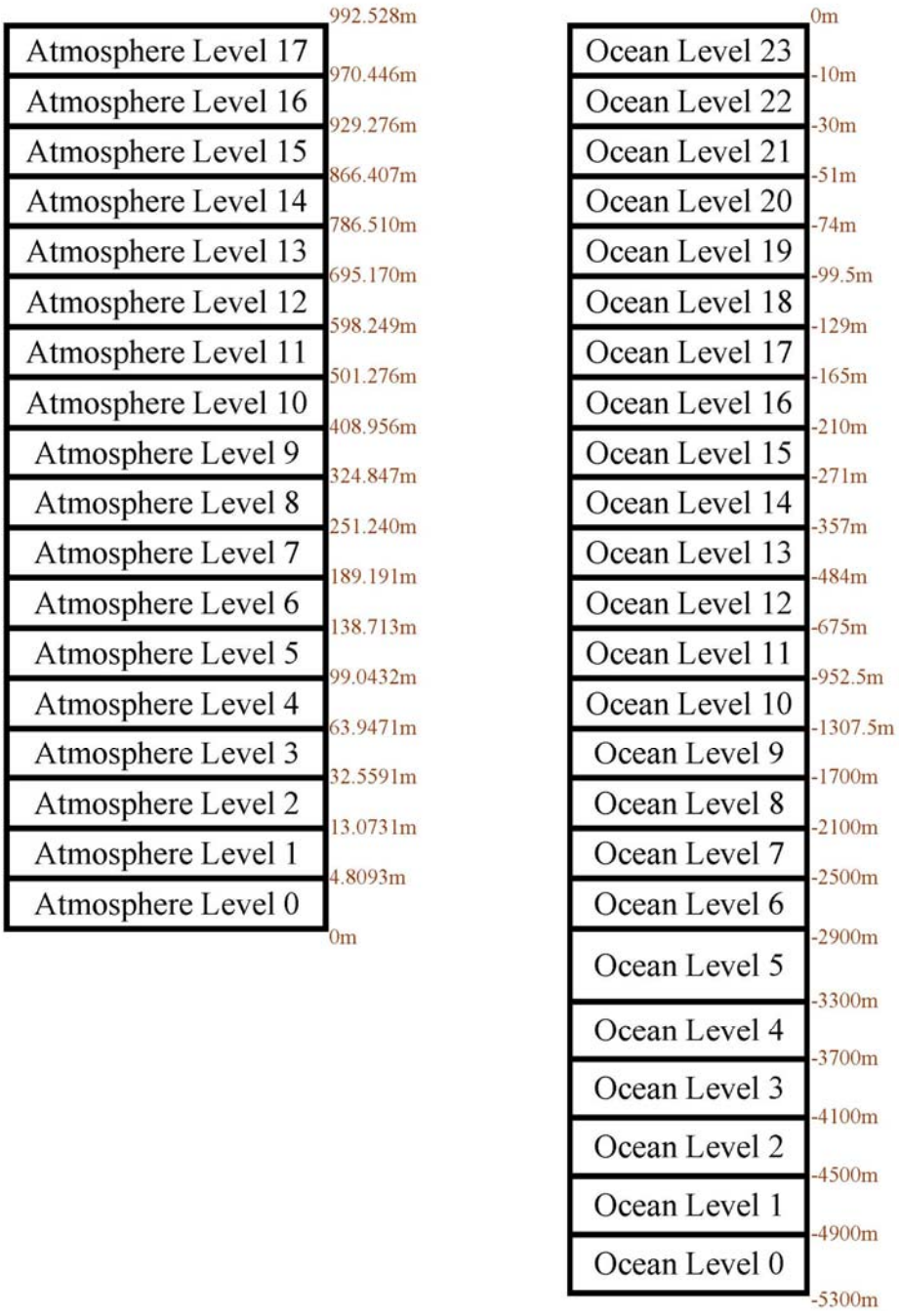

Figure D.1 Atmospheric and Oceanic Levels for FOAM

Name of Directory/File	Brief Description
atmos_params	File, having all atmospheric information.
cleanscript.sh	A shell script to remove junk files created during a model run.
f1.5T42data/	A directory with initial data and boundary conditions generated by Slarti.

<CaseName>.case
albnis.128x128
albniw.128x128
albvss.128x128
albvsw.128x128
area.128
bath.ascii. <CaseName>
ccm2lnd.nc
ddist.128x128
effvel.128x128
frctst.128x128
initial.T42.
<CaseName>.nc
mask.128x128
mask.t42
om3.geometry16
om3.geometry24
om3.salt16
om3.salt24
om3.stress
om3.temp16
om3.temp24
priver.nc
rdirc.128x128
rdirc.128x128.new copy
rdirc.128x128.old
rghnss.128x128
sstinit.ascii
T42.sp.ozn.nc
T42.sp.SEP1.nc
T42.sp.tibds.nc
T42.sp.tvbds.nc
t42area
tibds.T42. <CaseName>.nc
topo.ascii.<CaseName>
veg.Raj110Ma
vegtyp.128x128
weights.128x128_t42
weights.t42_128x128

foam1.5.50Fixsrc_32P	this is the compiled executable for FOAM.
history/	A folder that stores the results and history files.

atmos/
coupler/
ocean/

pbs.foam1.5.script	the shell script used to submit the job in the cluster.
restart/	A folder that stores the restart files.

atmos/
coupler/
ocean/

run_params	A file having the run related information like history frequency, run length, finished run etc.

Figure D.2 Typical Structure of a FOAM Run Directory

1. Paleotopography & Paleobathymetry

PaleoDEMs are used from the PALEOMAP Project (C. R. Scotese). These PaleoDEMs are 0.1ºx0.1º. It is resampled to 128x128 grid spacing required by FOAM. 'Slarti', a program to generate FOAM boundary conditions, is used to prepare the FOAM input from these resampled PaleoDEMs.

2. Atmospheric gases

These are the key variables in the Paleoclimatic simulation. In the 'atmos_params' file, the gas concentrations are provided. The gases that play the major role are CO_2, N_2O and CH_4. The gas concentration is expressed as a multiple of present day's value. For the Cretaceous run the gas concentrations are taken from the GeoCARB Model III (Berner, 2001). Table 1 shows an abridged part of RCO_2 values from GeoCARB III model for Cretaceous time intervals.

Table D.1: RCO_2 values from GeoCARB III Model for the Cretaceous Time Periods

Time (Ma)	R_{CO2} Values	Time (Ma)	R_{CO2} Values
60	2.802144	110	5.88872
70	3.200051	120	6.096954
80	4.185097	130	6.605868
90	4.317839	140	8.198544
100	5.30103	150	7.599305

3. Orbital parameters

The earth's orbital parameters play an important role in modifying climate. Milankovitch cycles describe these orbital parameters (Milankovitch, 1941). There are four types of orbital parameters. Orbital shape (Eccentricity) controls the amount of solar insolation received at any given time. If eccentricity was zero, this insolation is constant as the orbit is circular. But as it is not zero always, Earth receives highest insolation during perihelion (close to sun) and vice versa. Major cycles are 95, 125 and 400 kyr. The axial tilt (obliquity) is the angle of the rotational

axis with respect to the plane of the Earth's orbit. It varies between a tilt of 22.1° and 24.5°. The obliquity has a cycle of 41 kyr. The precession (wobble) is the change in the direction of the Earth's axis of rotation relative to the fixed stars, with a period of roughly 26,000 years. The obliquity and precision control the distribution of solar insolation on Earth. The last type of orbital parameter is orbital inclination (Muller et. al., 1995), which is the inclination of Earth's orbit drifts up and down relative to its present orbit with a cycle having a period of about 70,000 years. Milankovitch did not study this three-dimensional movement. More recent researchers noted this drift and that the orbit also moves relative to the orbits of the other planets.

4. Solar luminosity

The sun is getting brighter day by day as it matures (Sackmann, 2003). During the course of Earth's history the solar illumination has increased 33%. Hence, during the Cretaceous time solar luminosity was approximately 98% of present day's value.

FOAM Output - Example of a Typical FOAM Run

The following is an example of the procedures involved in submitting a FOAM run. After the initial boundary condition is set, the input 'case' is created with Slarti. In Slarti we make sure the land mask is comparable to that of the time of run. As FOAM can not handle any lakes or pits, we remove that from the mask manually. Same check is done at each oceanic levels. Vegetation is edited as required if used. River direction file is fixed with 'RepairRiverDirection Program' (© Dr. Tom Moore). After all these are done the Slarti 'case' is saved for coupled run environment.

To proceed with the run, next, a run directory is created in the cluster. The run directory had a typical structure and content, summary of which is shown in Figure D.2. Once the run folder is ready, the saved case is imported to FOAM's run directory. All parameter files are edited for initial/restart run. Finally the job is submitted using a script (Dr. Moore).

After the model is finished, the binary NetCDF files are processed using a series of scripts (provided by Dr. Moore) first to generate yearly esembles and then 10 year ensembles of the all variables. Lastly the last 30 years for a 100 model year run (this is in case of 100 year runs) is

averaged to make final annual average ensemble. These averaged files are used to create reports and analysis. Using tools like NCView and NCL, the reports are created. These include general plots of different variable for different seasons, both for northern hemisphere and for southern hemisphere and also for the equatorial view of the globe. Sometimes animations are also used to display the results for different variables. Moreover, using some conversion processes (shaplib, Python Data Language) or by traditional 'text file' extraction (time-consuming), the data for individual variables are extracted from the binary NetCDF files and imported to ArcGIS as shapefiles and used to create maps for analysis.

Description of results-Animation/Reports

Once the post processing is done and the reports are ready to look, the variables like upwelling (W), temperature (T), salinity (S), surface winds (UW & VW), Surface ocean currents (UO & VO), mixed layer depth (Szz, Tzz), precipitation (PRECL), land runoff (RNF), soil moisture (WET); which are important for environmental aspects, are plotted as vector images as well as animations. The data for each variable is imported to AcrGIS in text file format (CSV) .

Problems/Debugging with FOAM

FOAM is a difficult program to run because it often crashes due to unexpected/unforeseen reasons. For example, a known problem of FOAM is that the simulated winds at the Poles are often faster than present. Due to grid resolution FOAM has limited capability to handle this problem. This problem is addressed by Dr. Moore and Dr. Jacob, by editing the 'bandij' file (GANDOLPH Report, 2007). Moreover, the ocean component is very sensitive to geography. Minor incompatibilities in between the geography and the ocean model lead to salt sources that cause problem in model stability. There is no dynamic vegetation model in FOAM. Hence, there is limited vegetative response and feedback. Some of the problem(s) usually faced are as follows:

1. The model crashes for different reasons, like salt buildup and etc.
2. The exact reason for model crash is a bit hard to identify.

APPENDIX E

POLE-TO-EQUATOR TEMPERATURE GRADIENT DATABASE

The database attached here as a Microsoft Excel File named “Pole-to-Equator Temperature Gradient Database.xls”. The file has two worksheets in it. The first one named as ‘AllData’ contains all the 1591 paleo-temperature records that have been collected from published literatures. The other worksheet named ‘AllDataWFOAM’ contains all the data that is in the first worksheet along with additional equatorial temperature data (from 20°N to 20°S*) form the four FOAM simulations (70 Ma, 90 Ma, 120 Ma and 140 Ma). So this second worksheet has 1591 + (4 x *41) = 1755 paleo-temperature reords.

REFERENCES

Alley, N. F., Valentine, K. W. G., and Fulton, R.J., 1986. Paleoclimatic implications of middle Wisconsinan pollen and a paleosol from the Purcell Trench, south central British Columbia, Canadian Journal of Earth Sciences, Volume 23, Page: 1156-1168.

Amiot, R., Lécuyer, C., Buffetaut, E., Fluteau, F., Legendre, S., and Martineau, F., 2004. Latitudinal temperature gradient during the Cretaceous upper Campanian-middle Maastrichtian: $\delta^{18}O$ record of continental vertebrates: Earth and Planetary Science Letters, Volume 226, Page 255–272, doi: 10.1016/j.epsl.2004.07.015.

Andreasson, F. P., and Schmitz, B., 2000. Temperature seasonality in the early middle Eocene North Atlantic region: Evidence from stable isotope profiles of marine gastropod shells, Geological Society of America Bulletin, Volume 112, Page: 628.

Arthur, M.A., Brumsack, H. J., Jenkyns, H. C., Schlanger, S.O., 1990. Stratigraphy, geochemistry, and paleoceanography of organic carbon-rich Cretaceous sequences. In: Ginsburg, R., Beaudoin, B. (Eds.), Cretaceous Resources, Events, and Rhythms. Kluwer Academic, pp. 75^119.

Arthur, M.A., Dean,W.E., Pratt, L.M., 1988. Geochemical and climatic effects of increased marine organic carbon burial at the Cenomanian/Turonian boundary. Nature, Volume 335, Page: 714–716.

Bardossy, G., 1994. Carboniferous to Jurassic bauxite deposits as paleoclimatic and paleogeographic indicators. In: Embry, A.F., Beauchamp, B., Glass, D.J. Eds.., Pangea. Mem. Can. Soc. Petrol. Geol. 18, Calgary, Page: 283–293.

Barker, P. E, Kennett, J. P., et al., 1990. Proceeding of Oean Drilling Program, Scientific Results, Pagr :113, College Station, TX (Ocean Drilling Program).

Barrera, E., Huber, B.T., Savin, S.M., and Webb, P.N., 1987. Antarctic marine temperatures: late Campanian through early Paleocene: Paleoceanography, Volume 2, Page: 21-47.

Barrera, E., Keller, G., 1994. Productivity across the Cretaceous/Tertiary boundary in high latitudes. Geol. Sot. Am. Bull. Volume 106, Page: 1254-1266.

Barron, E. J., and W. M. Washington, 1985. Warm Cretaceous climates: High atmospheric CO_2 as a plausible mechanism, in The Carbon Cycle and Atmospheric CO_2: Natural Variations Archean to Present, Geophys. Monogr. Ser., E. T. Sundquist and W. S. Broecker (editors), Volume 32 Page: 546 – 553.

Barron, E. J., and Washington, W. M., 1984. The role of geographic variables in explaining paleoclimates: Results from Cretaceous climate model sensitivity studies: Journal of Geophysical Research, Volume. 89, Page: 1267-1279.

Barron, E. J., Fawcett, P. J., Peterson, W. H., Pollard, D. and Thompson, S. L., 1995. A ‘‘simulation’’ of mid-Cretaceous climate, Paleoceanography, Volume 10 Page : 953–962.

Barron, E., and Washington, W., 1982. Atmospheric circulation during warm geologic periods: Is the equator-to-pole surface-temperature gradient the controlling factor? Geology, Volume 10, Page: 633.

Barron, E.J., 1983. A warm, equable Cretaceous: The nature of the problem. Earth Science Review, Volume 19, Page: 305-338.

Barron, E.J., Fawsett, P.I., Peterson, W.H., Pollard, D., Thompson, S.L., 1995. A simulation of mid-Cretaceous climate. Paleoceanography Volume 10 (no.5), Page: 953-962.

Bassett, M.G., Lane, P.D., Edwards, D. (Eds.), 1991. The Murchison Symposium. Proceedings of an International Conference on the Silurian System: Special Papers in Palaeontology, Volume 44 Page: 397

Beerling, D.J., Lomas, M.R., Gröcke, D., 2002. On the nature of methane gas-hydrate dissociation during the Toarcian and Aptian oceanic anoxic events. American Journal of Sciences Volume 302, Page: 28–49.

Berner, R. A., and Kothavala, Z., 2001. GEOCARB III: A revised model of atmospheric CO_2 over Phanerozoic time: American Journal of Science, Volume 301, Page: 182–204.

Bice, K. L., and Norris, R. D., 2002. Possible atmospheric CO_2 extremes of the Middle Cretaceous (late Albian–Turonian). PALEOCEANOGRAPHY, Volume 17, Page: 1070.

Bice, K. L., Bralower, T. J., Duncan, R. A., Huber, B. T., Leckie, R. M., and Sageman, B. B., 2004. Cretaceous Climate-Ocean Dynamics: Future Directions for Integrated Ocean Drilling Program, Report of a JOI-USSSP/NSF sponsored workshop, Florissant, Colorado.

Bice, K. L., Huber, B. T., and Norris, R. D., 2003. Extreme polar warmth during the Cretaceous greenhouse? Paradox of the late Turonian d18O record at Deep Sea Drilling Project Site 511, Paleoceanography, Volume 18, No 2, Page: 1031.

Birkeland, P. W., 1969. Quaternary paleoclimatic implications of soil clay mineral distribution in a Sierra Nevada Great Basin transect, Journal of Geology, Volume 77, Page: 289 – 302.

Black, R. Et al 2008. "Demographics and Climate Change: future trends and their policy implication for migration". Working Paper No T-27, Development Research Centre on Globalization and Poverty, University of Sussex.

Boucot, A. J., 1985. Late Silurian-Early Devonian Biogeography, Provincialism, Evolution and Extinction [and Discussion], Philosophical Transactions of Royal Society of London (B), Volume 309, No. 1138, Pages: 323-339.

Boucot, A. J., Xu., C., and Scotese, C. R., 2011. Atlas of Lithlogical Indicators of Climate, SEPM, (in press).

Boucot, A.J., and Gray, J., 2001. A critique of Phanerozoic climatic models involving changes in the CO_2 content of the atmosphere. Earth-Sci. Rev., Volume 56, Page: 1–159.

Bowen, R., 1961. Oxygen isotope paleotemperature measurements on Cretaceous Belemnoidea from Europe, India and Japan: Journal of Paleontology, Volume 35, Page: 1077-1084.

Bowen, R., 1961. Paleotemperature analyses of Mesozoic Belemnoidea from Germany and Poland: The Journal of Geology, Volume 69, Page: 75-83.

Brady, E. C., DeConto, R. M., and Thompson, S. L., 1998. Deep water formation and poleward ocean heat transport in the warm climate extreme of the Cretaceous (80 Ma): Geophysical Research Letters, Volume 25, Page: 4205-4208.

Breecker, D., Sharp, Z., McFadden, L., and Quade, J., 2009. Revised Phanerozoic atmospheric CO_2 concentrations from paleosol carbonate: Geochimica Et Cosmochimica Acta Supplement, Volume 73, Page: 158.

Buckland. W., 1837. Geology and Mineralogy Considered with Reference to Natural Theology, Volumes 1 and 2. W. Pickering, London.

Caputo, M. V., 1985. Late Devonian glaciation in South America, Palaeogeography, Palaeoclimatology, Palaeoecology, Volume 51, PageL 291-317.

Cerling, T. E., 1991. Carbon dioxide in the atmosphere: evidence from Cenozoic and Mesozoic paleosols: American Journal of Science, Volume 291, Page: 377.

Chamberlain, T. C., 1895. Theclassificationof American glacial deposits, Journal of Geology, Volume 3, Page: 270 – 277.

Chandler, M. A., Rind, D., Ruedy, R., 1992. Pangaean climate during the Early lurassic: GGCM simulations and the sedimentary record of paleoclimate, Geological Society of American Bulletin, Volume 194, Page: 543-559.

Chen, J., An, Z., and Head, J., 1999. Variation of Rb/Sr Ratios in the Loess-Paleosol Sequences of Central China during the Last 130,000 Years and Their Implications for Monsoon Paleoclimatology, Quaternary Research, Volume 51, Page: 215-219.

Clarke, L. J., and Jenkyns, H. C., 1999. New oxygen isotope evidence for long-term Cretaceous climatic change in the Southern Hemisphere: Geology, Volume 27, Page 699.

Cronin, T. M., 2009. Paleoclimates: Understanding Climate Change Past and Present: Columbia University Press.

De Lurio, J., L., and, Frakes, L., A., 1999. Glendonites as a paleoenvironmental tool: implications for early Cretaceous high latitude climates in Australia. Geochimica et Cosmochimica Acta, Volume 63, Issues 7-8, Page: 1039-1048

DeConto R. M., 1996. Late Cretaceous Climate, Vegetation and Ocean Interactions: An Earth System Approach To Modeling An Extreme Climate, Doctoral Dissertation.

DeConto, R. M., Brady, E. C., Bergengren, J., and Hay, W. W., 2000. Late Cretaceous climate, vegetation, and ocean interactions, in Huber, B. T., MacLeod, K. G., and Wing, S. L., eds., Warm Climates in Earth History, Cambridge, Page: 275-296.

D'Hondt, S., and Arthur, M. A., 1996. Late Cretaceous oceans and the cool tropic paradox: Science, Volume 271, Page: 1838.

Ditchfield, P. W., 1997. High northern palaeolatitude Jurassic-Cretaceous palaeotemperature variation: new data from Kong Karls Land, Svalbard: Palaeogeography, Palaeoclimatology, Palaeoecology, Volume 130, Page: 163-175.

Ditchfield, P., Marshall, J., and Pirrie, D., 1994. High latitude palaeotemperature variation: New data from the Thithonian to Eocene of James Ross Island, Antarctica: Palaeogeography, Palaeoclimatology, Palaeoecology, Volume 107, Page: 79-101.

Dodson, P., Britt, B., Carpenter, K., Forster, C., Gillette, D., Norell, M., Olshevsky, G., Parrish, J., and Weishampel, D., 1993. The age of dinosaurs: Publications International, Ltd., .

Donnadieu, Y., Pierrehumbert, R.T., Fluteau, F., Jacob, R., 2006. Modelling the primary control of paleogeography on Cretaceous climate, Earth and Planetary Science Letters, Volume 248, Page:426–437.

Dorman, F., 1968. Some Australian oxygen isotope temperatures and a theory for a 30-million-year world-temperature cycle: The Journal of Geology, Volume 76, Page: 297-313.

Douglas, R. G., and Savin, S. M., 1973. Oxygen and carbon isotope analyses of Cretaceous and Tertiary Foraminifera from the Central North Pacific. In: E.L. Winterer, W.R. Riedel et al., Intial Reports of the Deep Sea Drilling Project, Volume 17. U.S. Government Printing Office, Washington, D.C., Page: 591-605.

Douglas, R. G., and Savin, S. M., 1978. Oxygen isotopic evidence for the depth stratification of Tertiary and Cretaceous planktic foraminifera: Marine Micropaleontology, Volume 3, Page: 175-196.

Douglas, R., and Savin, S., 1971. Isotopic analyses of planktonic foraminifera from the Cenozoic of the Northwest Pacific, Leg 6: Fischer, A. G., Heezen, BC, Et Al., Init.Repts.DSDP, Volume 6, Page: 1123–1127.

Douglas, R., and Savin, S., 1975. Oxygen and carbon isotope analyses of Tertiary and Cretaceous microfossils from Shatsky Rise and other sites in the North Pacific Ocean: Initial Reports of the Deep Sea Drilling Project, Volume 32, Page: 509–520.

Dubiel, R. F., Parrish, J. T., Parrish, J. M., Good, S. C., 1991. The Pangean megamonsoon — evidence from the Upper Triassic Chinle Formation, Colorado Plateau. Palaios Volume 6, Page: 347–370.

Ekart, D., Cerling, T. E., Montanez, I. P., and Tabor, N. J., 1999. A 400 million year carbon isotope record of pedogenic carbonate: implications for paleoatmospheric carbon dioxide: American Journal of Science, Volume 299, Page: 805–827.

FAO-UNESCO, 1974. Soil Map of the World. Volume I: Legend. UNESCO, Paris, France.

Fassell, M. L., and Bralower, T. J., 1999. Warm, equable mid-Cretaceous: Stable isotope evidence, in Evolution of the Cretaceous Ocean-Climate System, edited by E. Barrera and C.C. Johnson, Geological Society of America, Special Paper 332, Page: 121-142.

Felix-Henningsen, P., Kandel, A. W., Conard, N. J., 2003. The signi?cance of calcretes and paleosols on ancient dunes of the Western Cape, South Africa, as stratigraphic markers and paleoenvironmental indicators. BAR Int. Ser. 1163, Page: 45-52.

Fenner, J., 2001. Middle and Late Albian geography, oceanography, and climate and the setting of the Kirchrode I and II borehole sites, Palaeogeography, Palaeoclimatology, Palaeoecology Volume 174 (2001), Page: 5-32

Foerster, R., 1978. Evidence for an open seaway between northern and southern proto-Atlantic in Albian times. Nahue Volume 272, Page: 158-159.

Frakes, L. A., & Francis, J.E. 1988. A guide to Phanerozoic cold polar climates from high-latitude ice-rafting in the Cretaceous. Nature, Volume 333, Page: 547–549.

Frakes, L. A., 1979. Climate through geological time. New York: Elsevier.

Frakes, L. A., 1986. Mesozoic and Cenozoic oceans; American Geophysical Union, Geodynamics Series, Volume 15, Page: 33-48.

Frakes, L. A., 1999. Estimating the global thermal state from Cretaceous sea surface and continental temperature data: Geological Society of America Special Papers, Volume 332, Page: 49-57, doi: 10.1130/0-8137-2332-9.49.

Frakes, L. A., Francis, J. E. and Syktus, J. I., 1992. Climate Modes of the Phanerozoic, Cambridge Univ. Press, Cambridge.

Girard, J. P., Fryssinet, P., Gilles, C., 2000. Unraveling climatic changes from intraprofile variation in oxygen and hydrogen isotopic composition of goethite and kaolinite in laterites; an integrated study from Yaou, French Guiana. Geochimica et Cosmochimica Acta, Volume 64, Page: 409–426.

Golovneva, L. B., 2000. The Maastrichtian (Late Cretaceous) climate in the Northern Hemisphere, Geological Society, London, Special Publications, Volume 181, Pages 43-54.

Haq, B. U., Hardenbol, J., Vail, P. R., 1987. Chronology of fluctuating sea levels since the Triassic. Science Volume 235, Page: 1156-l167.

Hardcastle, J., 1889. Origin of loessdeposit of theTimaru Plateau. New Zealand Institute Transactions, Wellington, Volume 22, Pages: 406 416.

Hays, J. D., Pitman, W. C., 1973. Lithospheric plate motion, sea-level changes and climatic and ecological consequences. Nature Volume 246, Page: 18–22.

Head, J. J., Bloch, J. I., Hastings, A. K., Bourque, J. R., Cadena, E. A., Herrera, F. A., Polly, P. D., and Jaramillo, C. A., 2009. Giant boid snake from the Palaeocene neotropics reveals hotter past equatorial temperatures: Nature, Volume 457, Page: 715-717.

Hinz, K., 1981. A hypothesis on terrestrial catastrophies. Geol. Ib. E22,3-28.

Holland, C. H., Bassett, M. G. (Eds.), 1989. A Global Standard for the Silurian System: National Museum of Wales Geological Series, Volume 9, Page: 325

Holland, H., Feakes, C., and Zbinden, E., 1989. The Flin Flon paleosol and the composition of the atmosphere 1.8 BYBP: American Journal of Science, Volume 289, Page: 362.

Huber, B. T., 1998. Tropical paradise at the cretaceous poles? Science(Washington), Volume 282, Page: 2199-2200.

Huber, B. T., Hodell, D. A., and C. P. Hamilton, 1995. Middle-Late Cretaceous climate of the southern high latitudes: Stable isotopic evidence for minimal equator-to-pole thermal gradients, Geological Society. America. Bulletin. Volume 107, Page: 1164-1191.

Huber, B. T., Hodell, D. A., and Hamilton, C. P., 1995. Middle–Late Cretaceous climate of the southern high latitudes: stable isotopic evidence for minimal equator-to-pole thermal gradients: Geological Society of America Bulletin, Volume 107, Page: 1164.

Huber, B. T., Norris, R. D., and MacLeod, K. G., 2002. Deep-sea paleotemperature record of extreme warmth during the Cretaceous, Geology, Volume 30, Number 2, Page: 123-126.

Huber, M., 2009. Climate change: Snakes tell a torrid tale: Nature, Volume 457, Page: 669-671.

Huber, M., and Sloan, L. C., 2001. Heat transport, deep waters, and thermal gradients: Coupled simulation of an Eocene greenhouse climate: Geophysical Research Letters, Volume 28, Page: 3481-3484.

Hubert, J. F., 1977. Paleosol caliche in the New Haven Arkose, Connecticut: record of semiaridity in Late Triassic-Early Jurassic time, Geology, Volume 5, Page: 302-304.

Hutton, J.,1795. Theory of the Earth, with proofs and Illustrations, Volumes 1 and 2. J.W. Creech, Edinburgh.

Jacob, R., Schafer, C., Foster, I., Tobis, M., and Anderson, J., 2001. "Computational Design and Performance of the Fast Ocean Atmosphere Model, Version One," Proc. 2001. International Conference on Computational Science, eds. Alexandrov, V. N., Dongarra,

J. J., Tan, C. J. K., Springer-Verlag, Page: 175-184. Also ANL/CGC-005-0401, April 2001.

Jahren, A. H., Arens, N. C., Sarmiento, G., Guerrero, J., Amundson, R., 2001. Terrestrial record of methane hydrate dissociation in the Early Cretaceous. Geology Volume 29, Page: 159–162.

Jenkyns, H. C., 2003. Evidence for rapid climate change in the Mesozoic–Palaeogene greenhouse world. Philosophical Transactions of the Royal Society A Volume 361, Page: 1885–1916.

Jenkyns, H. C., Gale, A. S., Corfield, R. M., 1994. Carbon- and oxygen-isotope stratigraphy of the English Chalk and Italian Scalia and its palaeoclimatic significance. Geol.Mag. Volume 131, Page: 1–34.

Jenkyns, H.C., 1980. Cretaceous anoxic events: from continents to oceans. Journal of Geological Society London, Volume 137, Page: 171–188.

Joachimski, M. M., Breisig, S., Buggisch, W., Talent, J. A., Mawson, R., Gereke, M., Morrow, J. R., Day, J. et al. 2009. "Devonian climate and reef evolution: Insights from oxygen isotopes in apatite". Earth and Planetary Science Letters Volume 284 Page: 599–596. doi:10.1016/j.epsl.2009.05.028.

Judith Totman Parrish, J. T., 1993. Climate of the Supercontinent Pangea, The Journal of Geology, Volume 101, No. 2, Page: 215-233 .

Kellllledy, W. l., Cooper, M., 1975. Cretaceous ammonite distributions and the opening of the South Atlantic. l. Geol. Soc. London. Volume 131, Page: 283-288.

Kemper, E., 1987. Das kalmia der Kreide-Zeit, Geologisches Jahrbuch, A Volume 96 Page: 5-185.

Kennedy, W.J., Cooper, M., 1975. Cretaceous ammonite distributions and the opening of the South Atlantic, Journal of the Geological Society of London, Volume 131, Page 283 - 288.

Kidder, D. L., and Worsley, T. R. 2004. Causes and consequences of extreme Permo-Triassic warming to globally equable climate and relation to Permo-Triassic extinction and recovery. Palaeogeography, Palaeoclimatology, Palaeoecology, Volume 203 Page: 207-237.

Kominz, M. A., 1984. Oceanic ridge volume and sea-level change—An error analysis, in Schlee, J.S., ed., Interregional unconformities and hydrocarbon accumulation: Tulsa, Oklahoma, American Association of Petroleum Geologists Memoir, Volume 36 Page: 109–127.

Köppen, W. 1918. “Klassifikation der Klimate nach Temperatur, Niederschlag und Jahreslauf.” Petermanns Mitt., Volume 64, Page: 193-203.

Köppen, W. 1936. Das geographische System der Klimate (Handbuch der Klimatologie, Bd. 1, Teil C).

Kottek, M., Grieser, J., Beck, C., Rudolf, B., and Rubel, F., 2006. World Map of the Köppen-Geiger climate classification updated. Meteorol. Z., Volume 15, Page: 259-263. DOI: 10.1127/0941-2948/2006/0130.

Krasilnikov, P., and Calderón, N. E. G., 2006. A WRB-based buried paleosol classification: Quaternary International, Volume 156, Page: 176-188.

Kraus, M. J., 1999. Paleosols in clastic sedimentary rocks: their geologic applications, Earth Science Review Volume 47 Page: 41-70.

Landing, E., Johnson, M. E. (Eds.), 2003. Silurian Land and Seas—Paleogeography Outside of Laurentia. New York State Museum, New York. Page: 327

Landing, E., Johnson, M. E., (Eds.), 1998. Silurian Cycles: Linkages of Dynamic Stratigraphy with Atmospheric, Oceanic, and Tectonic Changes: New York State Museum Bulletin, Volume 491 Page: 327

Larson, R L., Pitman 1Il, W. C., 1972. World-wide correlation of Mesozoic magnetic anomalies and its implications. GSA Bulletin Volume 83, Page: 3645-3662.

Larson, R. L., 1991. Geological consequences of superplumes. Geology Volume 19, Page: 963–966.

Larson, R. L., Erba, E., 1999. Onset of the Mid-Cretaceous greenhouse in the Barremian–Aptian: igneous events and the biological, sedimentary and geochemical response. Paleoceanography, Volume 14, Page: 663–678.

Larson, R. L., Kincaid, C., 1996. Onset of mid-Cretaceous volcanism by elevation of the 670 km thermal boundary layer. Geology, Volume 24, Page: 551-554.

Legates, D. R., and Willmott, C. J., 1990b. Mean seasonal and spatial variability in gauge-corrected, global precipitation: International Journal of Climatology, Volume 10, Page: 111-127.

Legates, D. R., and Willmott, C. J., 1990a. Mean seasonal and spatial variability in global surface air temperature: Theoretical and Applied Climatology, Volume 41, Page: 11-21.

Lisiecki, L. E., and Raymo, M. E., 2005. A Plio-Pleistocene stack of 57 globally distributed benthic ? 18 O records: Paleoceanography, Volume 20, Page: 522–533.

Lisiecki, L.E., and Raymo, M.E., 2005. A Plio-Pleistocene stack of 57 globally distributed benthic δ18O records, Paleoceanography, Volume 20, Page: 522–533.

Lowenstam, H., and Epstein, S., 1954. Paleotemperatures of the post-Aptian Cretaceous as determined by the oxygen isotope method: The Journal of Geology, Volume 62, Page: 207-248.

Mack, G. H., and James, W., 1994. Paleoclimate and the global distribution of paleosols: The Journal of Geology, v. 102, p. 360-366.

Mack, G.H., James, W.C., and Monger, H.C., 1993. Classification of paleosols: Bulletin of the Geological Society of America, Volume 105, Page: 129.

MacLeod, N., 2004. Identifying Phanerozoic extinction controls: statistical considerations and preliminary results. In: Beaudoin, A. B., Head, M. J. (Eds.), The palynology and micropaleontology of boundaries. Geological Society of London, Special Publications, Page: 11–33.

MacLeod, N., and 21 others. 1997. The Cretaceous-Tertiary biotic transition, Journal of the Geological Society of London, Volume 154, Page: 265–292.

Madsen, D. B., Jingzen, L., Elston, R. G., Cheng, X., Bettinger, R. L., Kan, G., Brantingham, P. J., and Kan, Z., 1998. The loess/paleosol record and the nature of the Younger Dryas climate in Central China: Geoarchaeology, Volume 13, Page: 847-869.

Maher, B. A., 1998. Magnetic properties of modern soils and Quaternary loessic paleosols: paleoclimatic implications: Palaeogeography, Palaeoclimatology, Palaeoecology, Volume 137, Page: 25-54.

Maher, B. A., and Thompson, R., 1995. Paleorainfall reconstructions from pedogenic magnetic susceptibility variations in the Chinese loess and paleosols: Quaternary Research, Volume 44, Page: 383-391.

Matthews, E, 1983. Global vegetation and land use: New high-resolution data bases for climate studies. Journal of Climate and Applied Meteorology, Volume 22, Page: 474-487.

McGee, W. J., 1878. On the relative positions of the forest bed and associated driit formations in northeastern Iowa, American Journal of Science, Volume 27,Pages; 189 -213.

Menard, H. W., 1964. The Marine Geology of the Pacific. McGrawHill, New York, Page: 269

Mendez, M. O., and Maier, R. M., 2008a. Phytoremediation of mine tailings in temperate and arid environments. Rev. Environ. Sci. Bio/Technol. Volume7, Page: 47–59.

Meyers, P. A., Bernasconi, S. M., Forster, A., 2006. Origins and accumulation of organic matter in Albian to Santonian black shale sequences on the Demerara Rise, South American margin. Organic Geochemistry Volume 37, Page: 1816–1830.

Miedema, R., Koulechova, I. N. and Gerasimova, M. I., 1999. Soil formation in Greyzems in Moscow district: micromorphology, chemistry, clay mineralogy and particle size distribution, Catena, Volume 34, Issue 3-4, Page: 315-347.

Milankovitch, M., 1941. Kanon der Erdbestrahlung und seine Andwendung auf das Eiszeiten-problem. Royal Serbian Academy, Belgrade.

Miller, I. M., Brandon, M. T., and Hickey, L. J., 2006. Using leaf margin analysis to estimate the mid-Cretaceous (Albian) paleolatitude of the Baja BC block: Earth and Planetary Science Letters, Volume 245, Page: 95-114.

Miller, K. B., McCahon, T. J., and West, R.R., 1996. Lower Permian (Wolfcampian) Paleosol-bearing cycles of the US Midcontinent; evidence of climatic cyclicity, Journal of Sedimentary Research, Volume 66, Page: 71.

Miller, K. G., Barrera, E., Olsson, R. K., Sugarman, P. J., and Savin, S. M., 1999. Does ice drive early Maastrichtian eustasy?, Geology, Volume 27, Page: 783-786.

Miller, K. G., Browning, J. V., Aubry, M. P., Wade, B. S., Katz, M. E., Kulpecz, A. A., and Wright, J. D., 2008. Eocene-Oligocene global climate and sea-level changes: St. Stephens Quarry, Alabama: Bulletin of the Geological Society of America, Volume 120, Page 34.

Moore, T. L., Plotnick, R. E., Perlmutter, M., Parrish, J. T., 2007. Evaluating Paleoclimate Indicators Using Climate Envelopes, AAPG Annual Meeting, April 1-4, 2007, Long Beach, California.

Muller, R. A, & MacDonald, G. J., 1995. Glacial cycles and orbital inclination, Nature, 377: 107 - 108.

Mutterlose, J., Malkoc, M., Schouten, S., Sinninghe Damsté, J. S., and Forster, A., 2010. TEX86 and stable ?18O paleothermometry of early Cretaceous sediments: Implications for belemnite ecology and paleotemperature proxy application: Earth and Planetary Science Letters, Volume 298, Page: 286-298, doi: DOI: 10.1016/j.epsl.2010.07.043.

Mutti, M., Weissert, H., 1995. Triassic Monsoonal Climate and its signature in Ladinian–Carnian carbonate platforms (Southern Alps, Italy). Journal of Sedimentary Research Volume B65, Page: 357–367.

Nefedova, V., Jacob, R., Foster, I., Liu, Z., Liu, Y., Deelman, E., Mehta, G., Su, M., Vahi, K., 2006. Automating Climate Science: Large Ensemble Simulations on the TeraGrid with the GriPhyN Virtual Data System, e-science, Second IEEE International Conference on e-Science and Grid Computing, Page:32 at http://csdl2.computer.org/persagen

/DLAbsToc.jsp?resourcePath=/dl/proceedings/andtoc=comp/proceedings/escience/2006/2734/00/2734toc. xmlandDOI=10.1109/ESCIENCE. 2006.30.

Nefedova, V., Jacob, R., Foster, I., Liu, Z., Liu, Y., Deelman, E., Mehta, G., Su, M., Vahi, K., 2006. Automating Climate Science: Large Ensemble Simulations on the TeraGrid with the GriPhyN Virtual Data System, e-science, Second IEEE International Conference on e-Science and Grid Computing, p. 32 at http://csdl2.computer.org/persagen/DLAbsToc.jsp?resourcePath=/dl/proceedings/&toc=comp/proceedings/escience/2006/12734/00/12734toc .xml&D01=10.11 09/ESCIENCE.2006.30.

Nettleton, W., Olson, C., and Wysocki, D., 2000. Paleosol classification: Problems and solutions: Catena, Volume 41, Page: 61-92.

Norris, R. D., and P. A. Wilson, 1998. Low-latitude sea-surface temperatures for the mid-Cretaceous and the evolution of planktonic foraminifera, Geol., Volume 26, Page:823-826.

Norris, R., Klaus, A., and Kroon, D., 2001. Mid-Eocene deep water, the Late Palaeocene Thermal Maximum and continental slope mass wasting during the Cretaceous-Palaeogene impact: Geological Society London Special Publications, Volume 183, Page: 23.

Nurnberg, D., Muller, R. D., 1991. The tectonic evolution of the South Atlantic from Late Jurassic to present. Tectonophysics Volume191, Page: 27–53.

Oches, E. A., and Banerjee, S. K., 1996. Rock-magnetic proxies of climate change from loess-paleosol sediments of the Czech Republic: Studia Geophysica Et Geodaetica, Volume 40, Page: 287-300.

Otto-Bliesner, B. L. and Upchurch, G. R. Jr., 1997. Vegetation-induced warming of high-latitude regions during the Late Cretaceous period. Nature Volume 385, Page: 804–807.

Pal, D. K., Deshpande, S. B., Venugopal, K. R., and Kalbande, A. R., 1989. Formation of di- and trioctahedral smectite as evidence for paleoclimatic changes in southern and central Peninsular India. Geoderma Volume 45, Page: 175–184.

Parrish, J. M., 1993. Phylogeny of the Crocodylotarsi, with reference to archosaurian and crurotarsan monophyly, Journal of Vertebrate Paleontology, Volume 13, Page:287–308.

Parrish, J. T., and Peterson, F., 1988. Wind directions predicted from global circulation models and wind directions determined from aeolian sandstones of the western United States. Sedimentary Geology, Volume 56, Page: 261–282.

Parrish, J. T., and Spicer, R. A., 1988. Late Cretaceous terrestrial vegetation: a near-polar temperature curve: Geology, Volume 16, Page: 22.

Pearce, M. A., Jarvis, I. and Tocher, B. A. 2009. The Cenomanian–Turonian boundary event, OAE2 and palaeoenvironmental change in epicontinental seas: new insights from the dinocyst and geochemical records. Palaeogeogr. Palaeoclimatol. Palaeoecol., Volume 280, Page: 207–234.

Pirrie, D., and Marshall, J. D., 1990. High latitude Late Cretaceous palaeotemperatures: New data from JamesRoss Island, Antarctica: Geology, Volume 18, Page: 31–34.

Pirrie, D., Doyle, P., Marshall, J., and Ellis, G., 1995. Cool Cretaceous climates: new data from the Albian of Western Australia: Journal of the Geological Society, Volume 152, Page: 739.

Pirrie, D., Marshall, J.D., Doyle, P., and Riccardi, A.C., 2004. Cool early Albian climates; new data from Argentina. Cret. Res., Volume 25, Page: 27–33.

Playfair, J. (1802) Illustrations of the Huttonian Theory of the Earth. CadeU&Davies, London: William Creech,

Polynov, B. B., 1927. Contributionsof RussianScientists topaleopedology. USSR Academy of Sciences, Leningrad.

Preto, N., Kustatscher, E., Wignall, P. B., 2010. Triassic climates - state of the art and perspectives. Palaeogeogr Palaeoclimatol Palaeoecol Volume 290 Page: 1–10

Price, G. D., Ruffell, A. H., Jones, C. E., Kalin, R. M. and Mutterlose, J., 2000. Isotopic evidence for temperature variation during the early Cretaceous (late Ryazanian–mid-Hauterivian); Journal of the Geological Society; March 2000; Volume 157, (no. 2), Page: 335-343.

Price, G. D., Valdes, P. J., Shellwood, B. W., 1997. Prediction of modern bauxite occurence: implications for the climate reconstruction. Palaeogeogr. Paleoclimatol. Palaeoecol. Volume 131, Page: 1-14.

Price, G., 1999. The evidence and implications of polar ice during the Mesozoic, Earth-Science Reviews, Volume 48, Issue 3, Page: 183-210.

Price, G., D., Ruffell, A., H., Jones, C. E., Kalin , R. M. and Mutterlose, J., 2000. Isotopic evidence for temperature variation during the early Cretaceous (late Ryazanian–mid-Hauterivian). Journal of the Geological Society, Volume 157, No. 2, Page: 335-343.

Puceat, E., Lecuyer, C., Donnadieu, Y., Naveau, P., Cappetta, H., Ramstein, G., Huber, B. T., and Kriwet, J., 2007. Fish tooth {delta}18O revising Late Cretaceous meridional upper ocean water temperature gradients: Geology, Volume 35, Page: 107-110, doi: 10.1130/G23103A.1.

Raup, D., Sepkoski Jr, J., 1982. "Mass extinctions in the marine fossil record". Science Volume 215 (No.4539), Page: 1501–1503. doi:10.1126/science.215.4539.1501

Rees, P. M. A., Noto, C. R., Parrish, J. M., and Parrish, J. T., 2004. Late Jurassic climates, vegetation, and dinosaur distributions: The Journal of Geology, Volume 112, Page: 643-653.

Retallack G. J., 2002. Carbon dioxide and climate over the past 300 Myr. Philosophical Transactions of the Royal Society of London Volume 360, Page: 659–673.

Retallack, G. J. 2001. A 300-million-year record of atmospheric carbon dioxide from fossil plant cuticles. Nature Volume 411, Page: 287–290.

Retallack, G. J., 1990. Soils of the Past: an Introduction to Paleopedology. London: Unwin-Hyman. Page: 520

Retallack, G. J., 1999. Postapocalyptic greenhouse paleoclimate revealed by Earliest Triassic Paleosols in the Sydney Basin, Australia. GSA Bulletin Volume 111, Page: 52–70.

Retallack, G. J., 2009. and Krull, E. S. 1999. Landscape ecological shift at the Permian-Triassic boundary in Antarctica. Aust. J. Earth Sci. Volume 46, Page: 786–812.

Retallack, G. J., Krull, E. S., 1999. Landscape ecological shift at the Permian-Triassic boundary in Antarctica. Australian Journal of Earth Sciences, Volume 46, Page: 785-812.

Retallack, G. J.,: Refining a pedogenic-carbonate CO_2 paleobarometer to quantify a middle Miocene greenhouse spike, Palaeogeogr., Palaeoclimatol., Palaeoecol., Volume 281, Page: 57–65.

Retallack, G., 1986. Reappraisal of a 2200 Ma-old paleosol near Waterval Onder, South Africa: Precambrian Research, Volume 32, Page: 195-232.

Retallack, G., and Feakes, C., 1987. Trace fossil evidence for Late Ordovician animals on land, Science, Volume 235, Pages: 61-63.

Robinson, P. L., 1973. Paleoclimatology and continental drift. In: Tarling, D. H., Runcorn, S. K., (Eds.), Implications of continental drift to the Earth Sciences. Academic Press, London, Page: 449–476.

Rutter, N., Zhongli, D., Evans, M., and Yuchun, W., 1990. Magnetostratigraphy of the Baoji loess-paleosol section in the north-central China Loess Plateau: Quaternary International, Volume 7, Page: 97-102.

Rye, R., and Holland, H. D., 1998. Paleosols and the evolution of atmospheric oxygen: a critical review: American Journal of Science, Volume 298, Page: 621-672.

Sackmann, I. J., & Boothroyd, A I., 2003. Our Sun. V. A Bright Young Sun Consistent with Helioseismology and Warm Temperatures on Ancient Earth and Mars, The Astrophysical Journal, 583 (2): 1024-1039.

Sackmann, I. J., and Boothroyd, A. I., 2003. Our Sun. V. A Bright Young Sun Consistent with Helioseismology and Warm Temperatures on Ancient Earth and Mars, The Astrophysical Journal, Volume 583 (2), Page: 1024-1039.

Savin, S., 1977. The history of the Earth's surface temperature during the past 100 million years. A. Rev. Earth planet. Sci. Volume 5, Page: 319-355.

Schlanger, S. O., Arthur, M. A., Jenkyns, H. C., Scholle, P. A., 1987. The Cenomanian–Turonian Oceanic Anoxic Event, I. stratigraphy and distribution of organic carbonrich

beds and the marine ?13C excursion. In: Brooks, J., Fleet, A. J. (Eds.), Marine Petroleum Source Rocks: Spec. Publ. Geol. Soc. London, Volume 26, Page: 371–399.

Schlanger, S. O., Jenkyns, H. C., 1976. Cretaceous oceanic anoxic events: causes and consequences. Geol. Mijnbouw Volume 55, Page: 179–184.

Schlanger, S. O., Jenkyns, H. C., Premoli Silva, I., 1981. Volcanism and vertical tectonics in the Pacific basin related to the global Cretaceous transgressions. Earth Planet. Sci. Lett. Volume 52, Page: 435-449.

Scotese, C. R., Boucot, A. J., McKerrow, W. S., 1999. Gondwanan palaeogeography and palaeoclimatology, Journal of African Earth Science, Volume 28, Page:99–114.

Scotese, C.R., Illich, H., Zumberge, J, and Brown, S., and Moore, T.,2008. The GANDOLPH Project: Year Two Report: Paleogeographic and Paleoclimatic Controls on Hydrocarbon Source Rock Deposition, A Report on the Methods Employed, the Results of the Paleoclimate Simulations (FOAM), and Oils/Source Rock Compilation for the Miocene (10 Ma), Early Cretaceous (Aptian/Albian; 120 Ma and Berriasian/Barremian (140 Ma), Late Triassic (220 Ma), and Early Silurian (430 Ma), Conclusions at the End of Year Two, July, 2008. GeoMark Research Ltd, Houston, Texas, 177 pp.

Scotese, C.R., Illich, H., Zumberge, J, and Brown, S., and Moore, T.,2009. The GANDOLPH Project: Year Three Report: Paleogeographic and Paleoclimatic Controls on Hydrocarbon Source Rock Deposition, A Report on the Methods Employed, the Results of the Paleoclimate Simulations (FOAM), and Oils/Source Rock Compilation for the Eocene (45 Ma), Early/Middle Jurassic (180 Ma), Mississippian (340 Ma), and Neoproterozoic (600 Ma), Conclusions at the End of Year Three, August, 2009. GeoMark Research Ltd, Houston, Texas, 154 pp.

Scotese, C.R., Illich, H., Zumberge, J, and Brown, S., and Moore, T.,2011. The GANDOLPH Project: Year Four Report: Paleogeographic and Paleoclimatic Controls on Hydrocarbon Source Rock Deposition, A Report on the Methods Employed, the Results of the Paleoclimate Simulations (FOAM), and Oils/Source Rock Compilation for the

Oligocene (30 Ma), Cretaceous/Tertiary (70 Ma), Permian/Triassic (250 Ma), Silurian/Devonian (400 Ma), and Cambrian/Ordovician (480 Ma), Conclusions at the End of Year Four, April 2011. GeoMark Research Ltd, Houston, Texas, 219 pp.

Scotese, C.R., Illich, H., Zumberge, J, and Brown, S.,2007. The GANDOLPH Project: Year One Report: Paleogeographic and Paleoclimatic Controls on Hydrocarbon Source Rock Deposition, A Report on the Methods Employed, the Results of the Paleoclimate Simulations (FOAM), and Oils/Source Rock Compilation for the Late Cretaceous (Cenomanian/Turonian; 93.5 Ma), Late Jurassic (Kimmeridgian/Tithonioan; 151 Ma), Early Permian (Sakmarian/Artinskian; 284 Ma), and Late Devonian (Frasnian/Femennian; 372 Ma), Conclusions at the End of Year One, February, 2007. GeoMark Research Ltd, Houston, Texas, 142 pp.

Sellwood, B. W., Price, G. D., and Valdes, P. J., 1994. Cooler estimates of Cretaceous temperatures: Nature, Volume 370, Page: 453–455.

Seward, A. C., 1898. FossilPlants, Vol. 1. Cambridgeuniversity Press, Cambridge (facsimile edn Hafner, New York, 1963).

Sheldon, N. D., Retallack, G. J.,2004. Regional paleoprecipitation records from the late Eocene and Oligocene of North America, J. Geol. Volume 112 Page: 487–494.

Sheldon, N.D., Retallack, G.J., Tanaka, S., 2002. Geochemical climofunctions from North American soils and application to paleosols across the Eocene–Oligocene boundary in Oregon. Journal of Geology Volume 110, Page: 687–696.

Sinha, R., Tandon, S. K., Sanyal, P., Gibling, M. R., Stuben, D., Berner, Z., Ghazanfari, P., 2006. Calcretes from a Late Quaternary interfluve in the Ganga Plains, India: carbonate types and isotopic systems in a monsoonal setting. Palaeogeography, Palaeoclimatology, Palaeoecology Volume 242, Page: 214–239.

Srivastava, P., 2001. Paleoclimatic implications of pedogenic carbonates in Holocene soils of the Gangetic Plains, India: Palaeogeography, Palaeoclimatology, Palaeoecology, Volume 172, Page: 207–222.

Staub, B., and Rosenzweig. C.,1987. Global digital data sets of soil type, soil texture, surface slope, and other properties, NASA Technical Memorandum 100685.

Steuber, T., Rauch, M., Masse, J. P., Graaf, J, Malkoc, M., Low-latitude seasonality of Cretaceous temperatures in warm and cold episodes. Nature 2005. Volume 437(No.7063), Page:1341-1344.

Steuber, T., Rauch, M., Masse, J., P., Graaf, J., and Malko, M., 2005. Low-latitude seasonality of Cretaceous temperatures in warm and cold episodes. Nature, Volume 437, Page 1341-1344

Stevens, G. R., 1971. Oxygen isotope shtdies on Jmassic and Cretaceous belemnites from New Zealand and their biogeographic significance. NZ. J. Geol. Geophys. Volume 14, (No.4), Page: 829-897.

Stoll, H. M., and Schrag, D. P., 1996. Evidence for glacial control of rapid sea level changes in the Early Cretaceous. Science Volume 272, Page: 1171-1174.

Stoll, H. M., and Schrag, D. P., 2000. High-resolution stable isotope records from the Upper Cretaceous rocks of Italy and Spain: Glacial episodes in a greenhouse planet? Geological Society of America, Bulletin Volume 112,(No.2), Page: 308-319

Tabor, N. J., Montañez, I. P., Scotese, C. R., Poulsen, C. J., and Mack, G. H., 2008. Paleosol archives of environmental and climatic history in paleotropical western Pangea during the latest Pennsylvanian through Early Permian: Geological Society of America Special Papers, Volume 441, Page: 291-303, doi: 10.1130/2008.2441(20).

Taylor, E. L., 1989. Tree-ring structure in woody axes from the central Transantarctic Mountains, Antarctica. Proceedings of the International Symposium on Antarctic Research (Hangzhou, P.R. China, May, 1989). China Ocean Press, Tianjin, Page: 109–113.

Upchurch, G. R., Kiehl, J., Shields, C., Scherer, J., and Scotese, C. R., 2011. atitudinal temperature gradients and high latitude temperatures during the latest Cretaceous: Congruence of geologic data and climate models (in press).

Vakhrameev, V. A., 1987. Cretaceous paleogeography of the USSR Palaeogeogr., Palaeoclimatol., Palaeoecol. Volume 59, (No.1), Page: 57-67.

Vakhrameev, V. A., Dobruskina, I. A., Meyen, S. V. & Zaklinskaya, E. D., 1978. Palaozoische und mesozoische Floren Eurasiens und die Phytogeographdiei dieser Zeit. (300 pages.) Jena: VEB Gustav Fischer Verlag.

Verosub, K. L., Fine, P., Singer, M. J., and TenPas, J., 1993. Pedogenesis and paleoclimate: Interpretation of the magnetic susceptibility record of Chinese loess-paleosol sequences: Geology, Volume 21, Page: 1011

Walker, P. A., and Cocks, K. D., 1991. HABITAT: a procedure for modelling a disjoint environmental envelope for a plant or animal species, Global Ecol. Biogeog. Lett., Volume 1, Page: 108-118.

Wang, H., Follmer, L. R., and Liu, J. C., 2000. Isotope evidence of paleo–El Niño–Southern Oscillation cycles in loess-paleosol record in the central United States: Geology, Volume 28, Page: 771.

Wang, P. X., 2009. Global monsoon in a geological perspective. Chinese Science Bulletin Volume 54, Page: 1113–1136

Wang, Y., and Zheng, S. H., 1989. Paleosol nodules as Pleistocene paleoclimatic indicators, Luochuan, PR China: Palaeogeography, Palaeoclimatology, Palaeoecology, Volume 76, Page: 39-44.

Webster, T., 1826. Observations on the Purbeck and Portland Beds. GeologicdSociety of London Transactions Volume 2, Page: 37-44.

Weishampel, D. B., Barrett, P. M., Coria, R. A., Le Loueff, J., Xu, X., Zhao, X., Sahni, A., Gomani, E. M. P., and Noto, C. N., 2004. Dinosaur distribution, in: Weishampel, D. B., Dodson, P., and Osmólska, H. (eds.), The Dinosauria, University of California Press, Berkeley (2nd ed.), ISBN 0-520-24209-2, Page: 517-606.

Weissert, H., and Mohr, H., 1996. Late Jurassic climate and its impact on carbon cycling: Palaeogeography, Palaeoclimatology, Palaeoecology, Volume 122, Page: 27-43.

Weissert, H., and Mohr, H., 1996. Late Jurassic climate and its impact on carbon cycling, Palaeogeography, Palaeoclimatology, Palaeoecology, Volume 122, Issues 1-4, Page: 27-43.

Wesley, A., 1973. Jurassic plants. In: Hallam, A. (Ed.), Atlas of Palaeobiogeography. Elsevier, Amsterdam, Page: 329–338.

Wiedmann, J., Neugebauer, J., 1978. Lower Cretaceous ammonites from the South Atlantic Leg 40 (DSDP), their stratigraphic value and sedimentologic properties. Initial Reports of the Deep Sea Drilling Project 40, 709–734.

Wilson, A. C., 1980. The Devonian sedimentation and tectonism of a rapidly subsiding, semi-arid fluvial basin in the Midland Valley of Scotland, Scottish Journal of Geology, Volume 16, Pages: 291-313.

Wilson, P. A., Norris, R. D., Cooper, M. J., 2002. Testing the Cretaceous greenhouse hypothesis using glassy foraminiferal calcite from the core of the Turonian tropics on Demerara Rise. Geology Volume 30, Page: 607–610.

Wright, J. D., Miller, K. G., and Fairbanks, R. G., 1992. Early and middle Miocene stable isotopes: implications for deepwater circulation and climate: Paleoceanography, Volume 7, Page: 357-389.

Xiao, J., and An, Z., 1999. Three large shifts in East Asian monsoon circulation indicated by loess-paleosol sequences in China and late Cenozoic deposits in Japan: Palaeogeography, Palaeoclimatology, Palaeoecology, Volume 154, Page: 179-189

Zachos, J., Pagani, M., Sloan, L., Thomas, E., and Billups, K., 2001. Trends, rhythms, and aberrations in global climate 65 Ma to present: Science, Volume 292, Page: 686.

Zakharov, Y. D., Smyshlyaeva, O. P., Tanabe, K., Shigeta, Y., Maeda, H., Ignatiev, A. V., Velivetskaya, T. A., et al. 2005. Seasonal temperature fluctuations in the high northern latitudes during the Cretaceous Period: isotopic evidence from Albian and Coniacian shallow-water invertebrates of the Talovka River Basin, Koryak Upland, Russian Far East. Cretac. Res. Volume 26, Page: 113–132.

Zharkov, M. A., Murdmaa, I. O., Filatova, N. I., 1998. Paleogeography of the Coniacian–Maastrichtian time of the Late Cretaceous. Stratigr. Geol. Correl. Volume 6, Page: 3–16.

Zhisheng, A., Tungsheng, L., Yizhi, Z., Fuqing, S., and Zhongly, D., 1987. The paleosol complex S 5 in the China Loess Plateau—A record of climatic optimum during the last 1.2 Ma: GeoJournal, Volume 15, Page: 141-143.

Zobler, L., 1986. A World Soil File for Global Climate Modeling, NASA Technical Memorandum: 87802, Page: 32.

Zobler, L., 1999. Global soil types, 1-degree grid (Zobler): Data Set. Available on-Line [http://www.daac.ornl.gov] from Oak Ridge National Laboratory Distributed Active Archive Center, Oak Ridge, Tennessee, USA DOI, Volume 10.

BIOGRAPHICAL INFORMATION

Arghya Goswami was born in West Bengal, India. He completed his Bachelor of Science degree with Geology honors from Presidency College, Kolkata, West Bengal, India in 1997. He graduated with his Master of Science in 1999 with Geology from the same institution. His Master's thesis was titled "Sedimentary Facies Analysis of a Permo-Carboniferous Termino-Glacial Succession, Saharjuri Basin, Bihar, India". After that he worked as a Photogrammetrist for couple of years. In 2004, he joined the University of Texas at Arlington as a Master's student where he started working with Dr. Christopher R. Scotese. Dr. Scotese's research on paleogeography, paleoclimate had a profound impact on the author's career as well as his research interest. From 2005 he was working under Dr. Scotese's supervision in the Department of Earth & Environmental Sciences, University of Texas at Arlington on his Doctoral dissertation.